

**UNCONSTRAINED MOTION
AND
CONSTRAINED FORCE AND MOTION
CONTROL OF
ROBOTS WITH FLEXIBLE LINKS**

**A THESIS SUBMITTED TO
THE GRADUATE SCHOOL OF NATURAL AND APPLIED SCIENCES
OF
MIDDLE EAST TECHNICAL UNIVERSITY**

BY

SINAN KILICASLAN

**IN PARTIAL FULFILLMENT OF THE REQUIREMENTS
FOR
THE DEGREE OF DOCTOR OF PHILOSOPHY
IN
MECHANICAL ENGINEERING**

FEBRUARY 2005

Approval of the Graduate School of Natural and Applied Sciences

Prof. Dr. Canan Ozgen
Director

I certify that thesis satisfies all the requirements as a thesis for the degree of Doctor of Philosophy.

Prof. Dr. S. Kemal Ider
Head of Department

This is to certify that we have read this thesis and that in our opinion it is fully adequate, in scope and quality, as a thesis for the degree of Doctor of Philosophy.

Prof. Dr. M. Kemal Ozgoren
Co-Supervisor

Prof. Dr. S. Kemal Ider
Supervisor

Examining Committee Members

Prof. Dr. Resit Soylu (METU, ME) _____

Prof. Dr. S. Kemal Ider (METU, ME) _____

Prof. Dr. M. Kemal Ozgoren (METU, ME) _____

Prof. Dr. Aydan Erkmen (METU, EE) _____

Prof. Dr. Omer Morgul (Bilkent U., EE) _____

I hereby declare that all information in this document has been obtained and presented in accordance with academic rules and ethical conduct. I also declare that, as required by these rules and conduct, I have fully cited and referenced all material and results that are not original to this work.

Name, Last name : Sinan Kilicaslan

Signature :

ABSTRACT

UNCONSTRAINED MOTION AND CONSTRAINED FORCE AND MOTION CONTROL OF ROBOTS WITH FLEXIBLE LINKS

Kilicaslan, Sinan

Ph.D., Department of Mechanical Engineering

Supervisor : Prof. Dr. S. Kemal Ider

Co-Supervisor : Prof. Dr. M. Kemal Ozgoren

February 2005, 412 pages

New control methods are developed for the unconstrained motion and constrained force and motion control of flexible robots. The dynamic equations of the flexible robots are partitioned as pseudostatic equilibrium equations and deviations from them. The pseudostatic equilibrium considered here is defined as a hypothetical state where the tip point variables have their desired values while the modal variables are instantaneously constant. Then, the control torques for the pseudostatic equilibrium and for the stabilization of the deviation equations are formed in terms of tip point coordinates, modal variables and contact force components. The performances of the proposed methods are illustrated on a planar two-link robot and on a spatial three-link robot. Unmodeled dynamics and measurement noises are also taken into consideration. Performance of the proposed motion control method is compared with the computed torque method.

Keywords: Motion Control, Trajectory Tracking Control, Force and Motion Control, Flexible Robots, Flexible Manipulators, Pseudostatic Dynamic Equations, Unmodeled Dynamics, Measurement Noises.

ÖZ

ESNEK KOLLU ROBOTLARIN SINIRLANDIRILMAMIŞ HAREKET VE SINIRLANDIRILMIŞ KUVVET VE HAREKET DENETİMİ

Kılıçaslan, Sinan

Doktora, Makina Mühendisliği Bölümü

Tez Yöneticisi : Prof. Dr. S. Kemal İder

Ortak Tez Yöneticisi : Prof. Dr. M. Kemal Özgören

Şubat 2005, 412 sayfa

Esnek robotların sınırlandırılmamış hareket ve sınırlandırılmış kuvvet ve hareket denetimi için yeni denetim yöntemleri geliştirilmiştir. Dinamik denklemler sanal statik denge denklemleri ve bunlardan sapma denklemleri olarak ayrıştırılmıştır. Burada gözönüne alınan sanal statik denge, uç nokta değişkenlerinin istenen değerleri aldığı, bu sırada da modal değişkenlerin anlık sabit olduğu varsayımsal bir durumdur. Sonra, denetim torkları sanal statik denge ve sapma denklemlerinin kararlılığı için uç nokta koordinatları, modal değişkenler ve temas kuvveti bileşenleri cinsinden oluşturulmuştur. Önerilen yöntemlerin başarıları düzlemsel iki kollu bir esnek robot ve uzaysal üç kollu bir esnek robot üzerinde gösterilmiştir. Modellenmemiş dinamik ve ölçüm gürültüleri de gözönüne alınmıştır. Önerilen hareket denetim metodunun başarısı hesaplanmış torklar metodu ile karşılaştırılmıştır.

Anahtar Kelimeler: Hareket Denetimi, Yörünge İzleme Denetimi, Kuvvet ve Hareket Denetimi, Esnek Robotlar, Esnek Manipulatörler, Sanal Statik Dinamik Denklemler, Modellenmemiş Dinamik, Ölçüm Gürültüleri.

ACKNOWLEDGEMENTS

I would like to express my deep appreciation to Professor S. Kemal Ider and Professor M. Kemal Ozgoren for their supports, guidances, friendships and expertises throughout the thesis. Their suggestions and motivations during this study were invaluable. It would always be my pleasure to work with them again in other research projects.

I would like to express my special thanks to Professor Aydan Erkmen, Professor Resit Soylu and Professor Omer Morgul for their valuable comments and suggestions.

Mr. Serkan Kilicaslan who helped me typing the manuscript of the thesis deserves special thanks.

Finally, I would like to express my deepest thanks to my family for their support, encouragement and unattainable understanding.

TABLE OF CONTENTS

ABSTRACT.....	iv
ÖZ.....	vi
ACKNOWLEDGMENTS.....	viii
TABLE OF CONTENTS.....	ix
LIST OF TABLES.....	xii
LIST OF FIGURES.....	xiii
LIST OF SYMBOLS.....	xxxiv
CHAPTER	
1. INTRODUCTION.....	1
1.1 An Example to Nonminimum Phase Systems.....	2
1.2 Literature Review on Motion Control of Flexible Robots.....	6
1.3 Literature Review on Force and Motion Control of Flexible Robots.....	15
1.4 Discussions on Previous Studies.....	19
1.5 The Outline of the Thesis.....	21
2. CONTROLLER DESIGNS FOR UNCONSTRAINED MOTION AND CONSTRAINED FORCE AND MOTION OF FLEXIBLE ROBOTS.....	24
2.1 Motion Control Method for Flexible Robots.....	24
2.2 Force and Motion Control Method for Flexible Robots.....	31
2.3 Measuring Systems.....	37
2.4 Stability Considerations.....	39
2.5 Controllability Considerations.....	42
3. MODELING OF FLEXIBLE MULTIBODY SYSTEMS.....	44

3.1 Introduction.....	44
3.2 Dynamic Modeling of Planar Two Link Manipulator with Flexible Forearm by Using Relative Coordinates.....	45
3.2.1 Position Vectors of Arbitrary Points of Each Body.....	46
3.2.2 Velocities of Arbitrary Points of Each Body.....	48
3.2.3 Accelerations of Arbitrary Points of Each Body.....	51
3.2.4 Equations of Motion.....	54
3.2.5 Generalized Inertia Forces.....	54
3.2.6 Generalized External Forces.....	58
3.2.7 Generalized Structural Stiffness Forces.....	62
3.3 Dynamic Modeling of Spatial Three Link Manipulator with Two Flexible Arms by Using Absolute Coordinates.....	63
3.3.1 Kinematic and Dynamic Equations of Each Body.....	65
3.3.2 Constraint Equations.....	109
3.3.3 Equations of Motion.....	114
3.4 An Alternative Form of Dynamic Equations for Controller Design.....	116
4. NUMERICAL SIMULATIONS FOR PLANAR ROBOT.....	122
4.1 Numerical Simulation of Uncontrolled Motion of Planar Robot.....	123
4.2 Numerical Simulation of Motion Control of Planar Robot.....	129
4.3 Numerical Simulation of Motion Control of Planar Robot with Unmodeled Dynamics.....	145
4.4 Numerical Simulation of Motion Control of Planar Robot by Using Computed Torque Method.....	160
4.5 Numerical Simulation of Force and Motion Control of Planar Robot.....	170
4.6 Numerical Simulation of Force and Motion Control of Planar Robot with Unmodeled Dynamics	186

5. NUMERICAL SIMULATIONS FOR SPATIAL ROBOT.....	203
5.1 Numerical Simulation of Uncontrolled Motion of Spatial Robot.....	203
5.2 Numerical Simulation of Motion Control of Spatial Robot.....	216
5.3 Numerical Simulation of Motion Control of Spatial Robot with Measurement Noises.....	254
5.4 Numerical Simulation of Force and Motion Control of Spatial Robot.....	303
5.5 Numerical Simulation of Force and Motion Control of Spatial Robot with Measurement Noises.....	339
6. CONCLUSIONS AND FURTHER WORKS.....	387
REFERENCES.....	391
APPENDICES	
A. BEAM ELEMENT SHAPE FUNCTIONS.....	396
B. INERTIA PROPERTIES OF SPATIAL ROBOT.....	399
C. INERTIA PROPERTIES OF PLANAR ROBOT.....	410
CURRICULUM VITAE.....	412

LIST OF TABLES

TABLES

4.1 Physical parameters of the planar robot.....	125
4.2 Closed loop poles used in motion control of planar robot.....	130
4.3 Closed loop poles used in motion control of planar robot with unmodeled dynamics.....	145
4.4 Closed loop poles used in motion control of planar robot by using computed torque method.....	162
4.5 Closed loop poles used in force and motion control of planar robot.....	172
4.6 Closed loop poles used in force and motion control of planar robot with unmodeled dynamics.....	188
5.1 Physical parameters of the spatial robot used in uncontrolled motion.....	204
5.2 Physical parameters of the spatial robot used in controlled motion.....	217
5.3 Closed loop poles used in motion control of spatial robot.....	218
5.4 Closed loop poles used in motion control of spatial robot with measurement noise.....	256
5.5 Closed loop poles used in force and motion control of spatial robot.....	304

LIST OF FIGURES

FIGURES

1.1 Distributed parameter model of the flexible single link manipulator in translational motion.....	3
3.1 Planar two link manipulator with flexible forearm.....	45
3.2 Spatial three link manipulator with two flexible arms.....	65
4.1 Angular position of joint 1.....	125
4.2 Angular position of joint 2.....	126
4.3 Angular velocity of joint 1.....	126
4.4 Angular velocity of joint 2.....	127
4.5 First modal coordinate.....	127
4.6 Second modal coordinate.....	128
4.7 Derivative first modal coordinate.....	128
4.8 Derivative second modal coordinate.....	129
4.9 Tip point position component in n_1 direction.....	131
4.10 Tip point position component in n_2 direction.....	131
4.11 Workspace and tip point position.....	132
4.12 Tip point velocity component in n_1 direction.....	132
4.13 Tip point velocity component in n_2 direction.....	133
4.14 Deviation of tip point position component in n_1 direction.....	133
4.15 Deviation of tip point position component in n_2 direction.....	134
4.16 Deviation of tip point velocity component in n_1 direction.....	134
4.17 Deviation of tip point velocity component in n_2 direction.....	135
4.18 First modal coordinate.....	135
4.19 Second modal coordinate.....	136
4.20 Derivative of first modal coordinate.....	136
4.21 Derivative of second modal coordinate.....	137
4.22 Pseudostatic value of first modal coordinate.....	137
4.23 Pseudostatic value of second modal coordinate.....	138

4.24 Derivative of pseudostatic value of first modal coordinate.....	138
4.25 Derivative of pseudostatic value of second modal coordinate.....	139
4.26 Deviation from pseudostatic value of first modal coordinate.....	139
4.27 Deviation from pseudostatic value of second modal coordinate.....	140
4.28 Deviation from derivative of pseudostatic value of first modal coordinate.....	140
4.29 Deviation from derivative of pseudostatic value of second modal coordinate.....	141
4.30 Pseudostatic torque applied at joint 1.....	141
4.31 Pseudostatic torque applied at joint 2.....	142
4.32 Stabilization torque applied at joint 1.....	142
4.33 Stabilization torque applied at joint 2.....	143
4.34 Overall torque applied at joint 1.....	143
4.35 Overall torque applied at joint 2.....	144
4.36 Tip point position component in n_1 direction.....	146
4.37 Tip point position component in n_2 direction.....	146
4.38 Workspace and tip point position.....	147
4.39 Tip point velocity component in n_1 direction.....	147
4.40 Tip point velocity component in n_2 direction.....	148
4.41 Deviation of tip point position component in n_1 direction.....	148
4.42 Deviation of tip point position component in n_2 direction.....	149
4.43 Deviation of tip point velocity component in n_1 direction.....	149
4.44 Deviation of tip point velocity component in n_2 direction.....	150
4.45 First modal coordinate.....	150
4.46 Second modal coordinate.....	151
4.47 Derivative of first modal coordinate.....	151
4.48 Derivative of second modal coordinate.....	152
4.49 Pseudostatic value of first modal coordinate.....	152
4.50 Pseudostatic value of second modal coordinate.....	153
4.51 Derivative of pseudostatic value of first modal coordinate.....	153
4.52 Derivative of pseudostatic value of second modal coordinate.....	154
4.53 Deviation from pseudostatic value of first modal coordinate.....	154
4.54 Deviation from pseudostatic value of second modal coordinate.....	155

4.55 Deviation from derivative of pseudostatic value of first modal coordinate.....	155
4.56 Deviation from derivative of pseudostatic value of second modal coordinate.....	156
4.57 Pseudostatic torque applied at joint 1.....	156
4.58 Pseudostatic torque applied at joint 2.....	157
4.59 Stabilization torque applied at joint 1.....	157
4.60 Stabilization torque applied at joint 2.....	158
4.61 Overall torque applied at joint 1.....	158
4.62 Overall torque applied at joint 2.....	159
4.63 Tip point position component in n_1 direction.....	162
4.64 Tip point position component in n_2 direction.....	163
4.65 Workspace and tip point position.....	163
4.66 Tip point velocity component in n_1 direction.....	164
4.67 Tip point velocity component in n_2 direction.....	164
4.68 Deviation of tip point position component in n_1 direction.....	165
4.69 Deviation of tip point position component in n_2 direction.....	165
4.70 Deviation of tip point velocity component in n_1 direction.....	166
4.71 Deviation of tip point velocity component in n_2 direction.....	166
4.72 First modal coordinate.....	167
4.73 Second modal coordinate.....	167
4.74 Derivative of first modal coordinate.....	168
4.75 Derivative of second modal coordinate.....	168
4.76 Torque applied at joint 1.....	169
4.77 Torque applied at joint 2.....	169
4.78 Tip point position on the constraint surface.....	172
4.79 Workspace and tip point position.....	173
4.80 Tip point velocity on the constraint surface.....	173
4.81 Impulse of Lagrange multiplier.....	174
4.82 Lagrange multiplier.....	174
4.83 Deviation of tip point position on the constraint surface.....	175
4.84 Deviation of tip point velocity on the constraint surface.....	175
4.85 Deviation of impulse of Lagrange multiplier.....	176

4.86 Deviation of Lagrange multiplier.....	176
4.87 First modal coordinate.....	177
4.88 Second modal coordinate.....	177
4.89 Derivative of first modal coordinate.....	178
4.90 Derivative of second modal coordinate.....	178
4.91 Pseudostatic value of first modal coordinate.....	179
4.92 Pseudostatic value of second modal coordinate.....	179
4.93 Derivative of pseudostatic value of first modal coordinate.....	180
4.94 Derivative of pseudostatic value of second modal coordinate.....	180
4.95 Deviation from pseudostatic value of first modal coordinate.....	181
4.96 Deviation from pseudostatic value of second modal coordinate.....	181
4.97 Deviation from derivative of pseudostatic value of first modal coordinate.....	182
4.98 Deviation from derivative of pseudostatic value of second modal coordinate.....	182
4.99 Pseudostatic torque applied at joint 1.....	183
4.100 Pseudostatic torque applied at joint 2.....	183
4.101 Stabilization torque applied at joint 1.....	184
4.102 Stabilization torque applied at joint 2.....	184
4.103 Overall torque applied at joint 1.....	185
4.104 Overall torque applied at joint 2.....	185
4.105 Tip point position on the constraint surface.....	188
4.106 Workspace and tip point position.....	189
4.107 Tip velocity on the constraint surface.....	189
4.108 Impulse of Lagrange multiplier.....	190
4.109 Lagrange multiplier.....	190
4.110 Deviation of tip point position on the constraint surface.....	191
4.111 Deviation of tip point velocity on the constraint surface.....	191
4.112 Deviation of impulse of Lagrange multiplier.....	192
4.113 Deviation of Lagrange multiplier.....	192
4.114 First modal coordinate.....	193
4.115 Second modal coordinate.....	193
4.116 Derivative of first modal coordinate.....	194

4.117 Derivative of second modal coordinate.....	194
4.118 Pseudostatic value of first modal coordinate.....	195
4.119 Pseudostatic value of second modal coordinate.....	195
4.120 Derivative of pseudostatic value of first modal coordinate.....	196
4.121 Derivative of pseudostatic value of second modal coordinate.....	196
4.122 Deviation from pseudostatic value of first modal coordinate.....	197
4.123 Deviation from pseudostatic value of second modal coordinate.....	197
4.124 Deviation from derivative of pseudostatic value of first modal coordinate.....	198
4.125 Deviation from derivative of pseudostatic value of second modal coordinate.....	198
4.126 Pseudostatic torque applied at joint 1.....	199
4.127 Pseudostatic torque applied at joint 2.....	199
4.128 Stabilization torque applied at joint 1.....	200
4.129 Stabilization torque applied at joint 2.....	200
4.130 Overall torque applied at joint 1.....	201
4.131 Overall torque applied at joint 2.....	201
5.1 Angular position of joint 2.....	205
5.2 Angular position of joint 3.....	206
5.3 Angular velocity of joint 2.....	206
5.4 Angular velocity of joint 3.....	207
5.5 First modal coordinate of body 2.....	207
5.6 Second modal coordinate of body 2.....	208
5.7 First modal coordinate of body 3.....	208
5.8 Second modal coordinate of body 3.....	209
5.9 Derivative of first modal coordinate of body 2.....	209
5.10 Derivative of second modal coordinate of body 2.....	210
5.11 Derivative of first modal coordinate of body 3.....	210
5.12 Derivative of second modal coordinate of body 3.....	211
5.13 Tip point position component in n_1 direction.....	211
5.14 Tip point position component in n_2 direction.....	212
5.15 Tip point velocity component in n_1 direction.....	212
5.16 Tip point velocity component in n_2 direction.....	213

5.17 Euler angle γ_2	213
5.18 Euler angle γ_3	214
5.19 Derivative of Euler angle γ_2	214
5.20 Derivative of Euler angle γ_3	215
5.21 Deformation displacement component of point B of body 2 in $n_2^{(2)}$ direction.....	215
5.22 Deformation displacement component of point B of body 2 in $n_2^{(3)}$ direction.....	216
5.23 Tip point position component in n_1 direction.....	219
5.24 Tip point position component in n_2 direction.....	219
5.25 Tip point position component in n_3 direction.....	220
5.26 Tip point velocity component in n_1 direction.....	220
5.27 Tip point velocity component in n_2 direction.....	221
5.28 Tip point velocity component in n_3 direction.....	221
5.29 Deviation of tip point position component in n_1 direction.....	222
5.30 Deviation of tip point position component in n_2 direction.....	222
5.31 Deviation of tip point position component in n_3 direction.....	223
5.32 Deviation of tip point velocity component in n_1 direction.....	223
5.33 Deviation of tip point velocity component in n_2 direction.....	224
5.34 Deviation of tip point velocity component in n_3 direction.....	224
5.35 First modal coordinate of body 2 for bending in xy plane.....	225
5.36 Second modal coordinate of body 2 for bending in xy plane.....	225
5.37 First modal coordinate of body 2 for bending in xz plane.....	226
5.38 Second modal coordinate of body 2 for bending in xz plane.....	226
5.39 First modal coordinate of body 3 for bending in xy plane.....	227
5.40 Second modal coordinate of body 3 for bending in xy plane.....	227
5.41 First modal coordinate of body 3 for bending in xz plane.....	228
5.42 Second modal coordinate of body 3 for bending in xz plane.....	228
5.43 Derivative of first modal coordinate of body 2 for bending in xy plane.....	229
5.44 Derivative of second modal coordinate of body 2 for bending in xy plane.....	229
5.45 Derivative of first modal coordinate of body 2	

for bending in xz plane.....	230
5.46 Derivative of second modal coordinate of body 2	
for bending in xz plane.....	230
5.47 Derivative of first modal coordinate of body 3	
for bending in xy plane.....	231
5.48 Derivative of second modal coordinate of body 3	
for bending in xy plane.....	231
5.49 Derivative of first modal coordinate of body 3	
for bending in xz plane.....	232
5.50 Derivative of second modal coordinate of body 3	
for bending in xz plane.....	232
5.51 Pseudostatic value of first modal coordinate of body 2	
for bending in xy plane.....	233
5.52 Pseudostatic value of second modal coordinate of body 2	
for bending in xy plane.....	233
5.53 Pseudostatic value of first modal coordinate of body 2	
for bending in xz plane.....	234
5.54 Pseudostatic value of second modal coordinate of body 2	
for bending in xz plane.	234
5.55 Pseudostatic value of first modal coordinate of body 3.....	235
5.56 Pseudostatic value of second modal coordinate of body 3	
for bending in xy plane.....	235
5.57 Pseudostatic value of first modal coordinate of body 3	
for bending in xz plane.....	236
5.58 Pseudostatic value of second modal coordinate of body 3	
for bending in xz plane.....	236
5.59 Derivative of pseudostatic value of first modal coordinate	
of body 2 for bending in xy plane.....	237
5.60 Derivative of pseudostatic value of second modal coordinate	
of body 2 for bending in xy plane.....	237
5.61 Derivative of pseudostatic value of first modal coordinate	
of body 2 for bending in xz plane.....	238
5.62 Derivative of pseudostatic value of second modal coordinate	

of body 2 for bending in xz plane.....	238
5.63 Derivative of pseudostatic value of first modal coordinate	
of body 3 for bending in xy plane.....	239
5.64 Derivative of pseudostatic value of second modal coordinate	
of body 3 for bending in xy plane.....	239
5.65 Derivative of pseudostatic value of first modal coordinate	
of body 3 for bending in xz plane.....	240
5.66 Derivative of pseudostatic value of second modal coordinate	
of body 3 for bending in xz plane.....	240
5.67 Deviation from pseudostatic value of first modal coordinate	
of body 2 for bending in xy plane.....	241
5.68 Deviation from pseudostatic value of second modal coordinate	
of body 2 for bending in xy plane.....	241
5.69 Deviation from pseudostatic value of first modal coordinate	
of body 2 for bending in xz plane.....	242
5.70 Deviation from pseudostatic value of second modal coordinate	
of body 2 for bending in xz plane.....	242
5.71 Deviation from pseudostatic value of first modal coordinate	
of body 3 for bending in xy plane.....	243
5.72 Deviation from pseudostatic value of second modal coordinate	
of body 3 for bending in xy plane.....	243
5.73 Deviation from pseudostatic value of first modal coordinate	
of body 3 for bending in xz plane.....	244
5.74 Deviation from pseudostatic value of second modal coordinate	
of body 3 for bending in xz plane.....	244
5.75 Deviation from derivative of pseudostatic value of first modal	
coordinate of body 2 for bending in xy plane.....	245
5.76 Deviation from derivative of pseudostatic value of second modal	
coordinate of body 2 for bending in xy plane.....	245
5.77 Deviation from derivative of pseudostatic value of first modal	
coordinate of body 2 for bending in xz plane.....	246
5.78 Deviation from derivative of pseudostatic value of second modal	
coordinate of body 2 for bending in xz plane.....	246

5.79 Deviation from derivative of pseudostatic value of first modal	
coordinate of body 3 for bending in xy plane.....	247
5.80 Deviation from derivative of pseudostatic value of second modal	
coordinate of body 3 for bending in xy plane.....	247
5.81 Deviation from derivative of pseudostatic value of first modal	
coordinate of body 3 for bending in xz plane.....	248
5.82 Deviation from derivative of pseudostatic value of second modal	
coordinate of body 3 for bending in xz plane.....	248
5.83 Pseudostatic torque applied at joint 1.....	249
5.84 Pseudostatic torque applied at joint 2.....	249
5.85 Pseudostatic torque applied at joint 3.....	250
5.86 Stabilization torque applied at joint 1.....	250
5.87 Stabilization torque applied at joint 2.....	251
5.88 Stabilization torque applied at joint 3.....	251
5.89 Overall torque applied at joint 1.....	252
5.90 Overall torque applied at joint 2.....	252
5.91 Overall torque applied at joint 3.....	253
5.92 Tip point position component in n_1 direction.....	257
5.93 Tip point position component in n_2 direction.....	257
5.94 Tip point position component in n_3 direction.....	258
5.95 Tip point velocity component in n_1 direction.....	258
5.96 Tip point velocity component in n_2 direction.....	259
5.97 Tip point velocity component in n_3 direction.....	259
5.98 Deviation of tip point position component in n_1 direction.....	260
5.99 Deviation of tip point position component in n_2 direction.....	260
5.100 Deviation of tip point position component in n_3 direction.....	261
5.101 Deviation of tip point velocity component in n_1 direction.....	261
5.102 Deviation of tip point velocity component in n_2 direction.....	262
5.103 Deviation of tip point velocity component in n_3 direction.....	262
5.104 First modal coordinate of body 2 for bending in xy plane.....	263
5.105 Second modal coordinate of body 2 for bending in xy plane.....	263
5.106 First modal coordinate of body 2 for bending in xz plane.....	264
5.107 Second modal coordinate of body 2 for bending in xz plane.....	264

5.108	First modal coordinate of body 3 for bending in xy plane.....	265
5.109	Second modal coordinate of body 3 for bending in xy plane.....	265
5.110	First modal coordinate of body 3 for bending in xz plane.....	266
5.111	Second modal coordinate of body 3 for bending in xz plane.....	266
5.112	Derivative of first modal coordinate of body 2 for bending in xy plane.....	267
5.113	Derivative of second modal coordinate of body 2 for bending in xy plane.....	267
5.114	Derivative of first modal coordinate of body 2 for bending in xz plane.....	268
5.115	Derivative of second modal coordinate of body 2 for bending in xz plane.....	268
5.116	Derivative of first modal coordinate of body 3 for bending in xy plane.....	269
5.117	Derivative of second modal coordinate of body 3 for bending in xy plane.....	269
5.118	Derivative of first modal coordinate of body 3 for bending in xz plane.....	270
5.119	Derivative of second modal coordinate of body 3 for bending in xz plane.....	270
5.120	Pseudostatic value of first modal coordinate of body 2 for bending in xy plane.....	271
5.121	Pseudostatic value of second modal coordinate of body 2 for bending in xy plane.....	271
5.122	Pseudostatic value of first modal coordinate of body 2 for bending in xz plane.....	272
5.123	Pseudostatic value of second modal coordinate of body 2 for bending in xz plane.....	272
5.124	Pseudostatic value of first modal coordinate of body 3 for bending in xy plane.....	273
5.125	Pseudostatic value of second modal coordinate of body 3 for bending in xy plane.....	273
5.126	Pseudostatic value of first modal coordinate of body 3	

for bending in xz plane.....	274
5.127 Pseudostatic value of second modal coordinate of body 3	
for bending in xz plane.....	274
5.128 Derivative of pseudostatic value of first modal coordinate	
of body 2 for bending in xy plane.....	275
5.129 Derivative of pseudostatic value of second modal coordinate	
of body 2 for bending in xy plane.....	275
5.130 Derivative of pseudostatic value of first modal coordinate	
of body 2 for bending in xz plane.....	276
5.131 Derivative of pseudostatic value of second modal coordinate	
of body 2 for bending in xz plane.....	276
5.132 Derivative of pseudostatic value of first modal coordinate	
of body 3 for bending in xy plane.....	277
5.133 Derivative of pseudostatic value of second modal coordinate	
of body 3 for bending in xy plane.....	277
5.134 Derivative of pseudostatic value of first modal coordinate	
of body 3 for bending in xz plane.....	278
5.135 Derivative of pseudostatic value of second modal coordinate	
of body 3 for bending in xz plane.....	278
5.136 Deviation from pseudostatic value of first modal coordinate	
of body 2 for bending in xy plane.....	279
5.137 Deviation from pseudostatic value of second modal coordinate	
of body 2 for bending in xy plane.....	279
5.138 Deviation from pseudostatic value of first modal coordinate of	
body 2 for bending in xz plane.....	280
5.139 Deviation from pseudostatic value of second modal coordinate	
of body 2 for bending in xz plane.....	280
5.140 Deviation from pseudostatic value of first modal coordinate	
of body 3 for bending in xy plane.....	281
5.141 Deviation from pseudostatic value of second modal coordinate	
of body 3 for bending in xy plane.....	281
5.142 Deviation from pseudostatic value of first modal coordinate	
of body 3 for bending in xz plane.....	282

5.143 Deviation from pseudostatic value of second modal coordinate of body 3 for bending in xz plane.....	282
5.144 Deviation from derivative of pseudostatic value of first modal coordinate of body 2 for bending in xy plane.....	283
5.145 Deviation from derivative of pseudostatic value of second modal coordinate of body 2 for bending in xy plane.....	283
5.146 Deviation from derivative of pseudostatic value of first modal coordinate of body 2 for bending in xz plane.....	284
5.147 Deviation from derivative of pseudostatic value of second modal coordinate of body 2 for bending in xz plane.....	284
5.148 Deviation from derivative of pseudostatic value of first modal coordinate of body 3 for bending in xy plane.....	285
5.149 Deviation from derivative of pseudostatic value of second modal coordinate of body 3 for bending in xy plane.....	285
5.150 Deviation from derivative of pseudostatic value of first modal coordinate of body 3 for bending in xz plane.....	286
5.151 Deviation from derivative of pseudostatic value of second modal coordinate of body 3 for bending in xz plane.....	286
5.152 Pseudostatic torque applied at joint 1.....	287
5.153 Pseudostatic torque applied at joint 2.....	287
5.154 Pseudostatic torque applied at joint 3.....	288
5.155 Stabilization torque applied at joint	288
5.156 Stabilization torque applied at joint 2.....	289
5.157 Stabilization torque applied at joint 3.....	289
5.158 Overall torque applied at joint 1.....	290
5.159 Overall torque applied at joint 2.....	290
5.160 Overall torque applied at joint 3.....	291
5.161 Measurement noise of tip point position component in n_1 direction.....	291
5.162 Measurement noise of tip point position component in n_2 direction.....	292
5.163 Measurement noise of tip point position component in n_3 direction.....	292
5.164 Measurement noise of tip point velocity component in n_1 direction.....	293
5.165 Measurement noise of tip point velocity component in n_2 direction.....	293
5.166 Measurement noise of tip point velocity component in n_3 direction.....	294

5.167 Measurement noise of first modal coordinate of body 2	
for bending in xy plane.....	294
5.168 Measurement noise of second modal coordinate of body 2	
for bending in xy plane.....	295
5.169 Measurement noise of first modal coordinate of body 2	
for bending in xz plane.....	295
5.170 Measurement noise of second modal coordinate of body 2	
for bending in xz plane.....	296
5.171 Measurement noise of first modal coordinate of body 3	
for bending in xy plane.....	296
5.172 Measurement noise of second modal coordinate of body 3	
for bending in xy plane.....	297
5.173 Measurement noise of first modal coordinate of body 3	
for bending in xz plane.....	297
5.174 Measurement noise of second modal coordinate of body 3	
for bending in xz plane.....	298
5.175 Measurement noise of derivative of first modal coordinate	
of body 2 for bending in xy plane.....	298
5.176 Measurement noise of derivative of second modal coordinate	
of body 2 for bending in xy plane.....	299
5.177 Measurement noise of derivative of first modal coordinate	
of body 2 for bending in xz plane.....	299
5.178 Measurement noise of derivative of second modal coordinate	
of body 2 for bending in xz plane.....	300
5.179 Measurement noise of derivative of first modal coordinate	
of body 3 for bending in xy plane.....	300
5.180 Measurement noise of derivative of second modal coordinate	
of body 3 for bending in xy plane.....	301
5.181 Measurement noise of derivative of first modal coordinate	
of body 3 for bending in xz plane.....	301
5.182 Measurement noise of derivative of second modal coordinate	
of body 3 for bending in xz plane.....	302
5.183 Azimuth angle coordinate of tip point.....	305

5.184 Elevation angle coordinate of tip point.....	305
5.185 Derivative of azimuth angle coordinate of tip point.....	306
5.186 Derivative of elevation angle coordinate of tip point.....	306
5.187 Impulse of Lagrange multiplier.....	307
5.188 Lagrange multiplier.....	307
5.189 Deviation of azimuth angle coordinate of tip point.....	308
5.190 Deviation of elevation angle coordinate of tip point.....	308
5.191 Deviation of derivative of azimuth angle coordinate of tip point.....	309
5.192 Deviation of derivative of elevation angle coordinate of tip point.....	309
5.193 Deviation of impulse of Lagrange multiplier.....	310
5.194 Deviation of Lagrange multiplier.....	310
5.195 First modal coordinate of body 2 for bending in xy plane.....	311
5.196 Second modal coordinate of body 2 for bending in xy plane.....	311
5.197 First modal coordinate of body 2 for bending in xz plane.....	312
5.198 Second modal coordinate of body 2 for bending in xz plane.....	312
5.199 First modal coordinate of body 3 for bending in xy plane.....	313
5.200 Second modal coordinate of body 3 for bending in xy plane.....	313
5.201 First modal coordinate of body 3 for bending in xz plane.....	314
5.202 Second modal coordinate of body 3 for bending in xz plane.....	314
5.203 Derivative of first modal coordinate of body 2 for bending in xy plane.....	315
5.204 Derivative of second modal coordinate of body 2 for bending in xy plane.....	315
5.205 Derivative of first modal coordinate of body 2 for bending in xz plane.....	316
5.206 Derivative of second modal coordinate of body 2 for bending in xz plane.....	316
5.207 Derivative of first modal coordinate of body 3 for bending in xy plane.....	317
5.208 Derivative of second modal coordinate of body 3 for bending in xy plane.....	317
5.209 Derivative of first modal coordinate of body 3 for bending in xz plane.....	318

5.210 Derivative of second modal coordinate of body 3	
for bending in xz plane.....	318
5.211 Pseudostatic value of first modal coordinate of body 2	
for bending in xy plane.....	319
5.212 Pseudostatic value of second modal coordinate of body 2	
for bending in xy plane.....	319
5.213 Pseudostatic value of first modal coordinate of body 2	
for bending in xz plane.....	320
5.214 Pseudostatic value of second modal coordinate of body 2	
for bending in xz plane.....	320
5.215 Pseudostatic value of first modal coordinate of body 3	
for bending in xy plane.....	321
5.216 Pseudostatic value of second modal coordinate of body 3	
for bending in xy plane.....	321
5.217 Pseudostatic value of first modal coordinate of body 3	
or bending in xz plane.....	322
5.218 Pseudostatic value of second modal coordinate of body 3	
for bending in xz plane.....	322
5.219 Derivative of pseudostatic value of first modal coordinate	
of body 2 for bending in xy plane.....	323
5.220 Derivative of pseudostatic value of second modal coordinate	
of body 2 for bending in xy plane.....	323
5.221 Derivative of pseudostatic value of first modal coordinate	
of body 2 for bending in xz plane.....	324
5.222 Derivative of pseudostatic value of second modal coordinate	
of body 2 for bending in xz plane.....	324
5.223 Derivative of pseudostatic value of first modal coordinate	
of body 3 for bending in xy plane.....	325
5.224 Derivative of pseudostatic value of second modal coordinate	
of body 3 for bending in xy plane.....	325
5.225 Derivative of pseudostatic value of first modal coordinate	
of body 3 for bending in xz plane.....	326
5.226 Derivative of pseudostatic value of second modal coordinate	

of body 3 for bending in xz plane.....	326
5.227 Deviation from pseudostatic value of first modal coordinate of body 2 for bending in xy plane.....	327
5.228 Deviation from pseudostatic value of second modal coordinate of body 2 for bending in xy plane.....	327
5.229 Deviation from pseudostatic value of first modal coordinate of body 2 for bending in xz plane.....	328
5.230 Deviation from pseudostatic value of second modal coordinate of body 2 for bending in xz plane.....	328
5.231 Deviation from pseudostatic value of first modal coordinate of body 3 for bending in xy plane.....	329
5.232 Deviation from pseudostatic value of second modal coordinate of body 3 for bending in xy plane.....	329
5.233 Deviation from pseudostatic value of first modal coordinate of body 3 for bending in xz plane.....	330
5.234 Deviation from pseudostatic value of second modal coordinate of body 3 for bending in xz plane.....	330
5.235 Deviation from derivative of pseudostatic value of first modal coordinate of body 2 for bending in xy plane.....	331
5.236 Deviation from derivative of pseudostatic value of second modal coordinate of body 2 for bending in xy plane.....	331
5.237 Deviation from derivative of pseudostatic value of first modal coordinate of body 2 for bending in xz plane.....	332
5.238 Deviation from derivative of pseudostatic value of second modal coordinate of body 2 for bending in xz plane.....	332
5.239 Deviation from derivative of pseudostatic value of first modal coordinate of body 3 for bending in xy plane.....	333
5.240 Deviation from derivative of pseudostatic value of second modal coordinate of body 3 for bending in xy plane.....	333
5.241 Deviation from derivative of pseudostatic value of first modal coordinate of body 3 for bending in xz plane.....	334
5.242 Deviation from derivative of pseudostatic value of second modal coordinate of body 3 for bending in xz plane.....	334

5.243 Pseudostatic torque applied at joint 1.....	335
5.244 Pseudostatic torque applied at joint 2.....	335
5.245 Pseudostatic torque applied at joint 3.....	336
5.246 Stabilization torque applied at joint 1.....	336
5.247 Stabilization torque applied at joint 2.....	337
5.248 Stabilization torque applied at joint 3.....	337
5.249 Overall torque applied at joint 1.....	338
5.250 Overall torque applied at joint 2.....	338
5.251 Overall torque applied at joint 3.....	339
5.252 Azimuth angle coordinate of tip point.....	341
5.253 Elevation angle coordinate of tip point.....	341
5.254 Derivative of azimuth angle coordinate of tip point.....	342
5.255 Derivative of elevation angle coordinate of tip point.....	342
5.256 Impulse of Lagrange multiplier.....	343
5.257 Lagrange multiplier.....	343
5.258 Deviation of azimuth angle coordinate of tip point.....	344
5.259 Deviation of elevation angle coordinate of tip point.....	344
5.260 Deviation of derivative of azimuth angle coordinate of tip point.....	345
5.261 Deviation of derivative of elevation angle coordinate of tip point.....	345
5.262 Deviation of impulse of Lagrange multiplier.....	346
5.263 Deviation of Lagrange multiplier.....	346
5.264 First modal coordinate of body 2 for bending in xy plane.....	347
5.265 Second modal coordinate of body 2 for bending in xy plane.....	347
5.266 First modal coordinate of body 2 for bending in xz plane.....	348
5.267 Second modal coordinate of body 2 for bending in xz plane.....	348
5.268 First modal coordinate of body 3 for bending in xy plane.....	349
5.269 Second modal coordinate of body 3 for bending in xy plane.....	349
5.270 First modal coordinate of body 3 for bending in xz plane.....	350
5.271 Second modal coordinate of body 3 for bending in xz plane.....	350
5.272 Derivative of first modal coordinate of body 2 for bending in xy plane.....	351
5.273 Derivative of second modal coordinate of body 2 for bending in xy plane.....	351

5.274 Derivative of first modal coordinate of body 2	
for bending in xz plane.....	352
5.275 Derivative of second modal coordinate of body 2	
for bending in xz plane.....	352
5.276 Derivative of first modal coordinate of body 3	
for bending in xy plane.....	353
5.277 Derivative of second modal coordinate of body 3	
for bending in xy plane.....	353
5.278 Derivative of first modal coordinate of body 3	
for bending in xz plane.....	354
5.279 Derivative of second modal coordinate of body 3	
for bending in xz plane.....	354
5.280 Pseudostatic value of first modal coordinate of body 2	
for bending in xy plane.....	355
5.281 Pseudostatic value of second modal coordinate of body 2	
for bending in xy plane.....	355
5.282 Pseudostatic value of first modal coordinate of body 2	
for bending in xz plane.....	356
5.283 Pseudostatic value of second modal coordinate of body 2	
for bending in xz plane.....	356
5.284 Pseudostatic value of first modal coordinate of body 3	
for bending in xy plane.....	357
5.285 Pseudostatic value of second modal coordinate of body 3	
for bending in xy plane.....	357
5.286 Pseudostatic value of first modal coordinate of body 3	
for bending in xz plane.....	358
5.287 Pseudostatic value of second modal coordinate of body 3	
for bending in xz plane.....	358
5.288 Derivative of pseudostatic value of first modal coordinate of body 2 for bending in xy plane.....	359
5.289 Derivative of pseudostatic value of second modal coordinate of body 2 for bending in xy plane.....	359
5.290 Derivative of pseudostatic value of first modal coordinate	

of body 2 for bending in xz plane.....	360
5.291 Derivative of pseudostatic value of second modal coordinate of body 2 for bending in xz plane.....	360
5.292 Derivative of pseudostatic value of first modal coordinate of body 3 for bending in xy plane.....	361
5.293 Derivative of pseudostatic value of second modal coordinate of body 3 for bending in xy plane.....	361
5.294 Derivative of pseudostatic value of first modal coordinate of body 3 for bending in xz plane.....	362
5.295 Derivative of pseudostatic value of second modal coordinate of body 3 for bending in xz plane.....	362
5.296 Deviation from pseudostatic value of first modal coordinate of body 2 for bending in xy plane.....	363
5.297 Deviation from pseudostatic value of second modal coordinate of body 2 for bending in xy plane.....	363
5.298 Deviation from pseudostatic value of first modal coordinate of body 2 for bending in xz plane.....	364
5.299 Deviation from pseudostatic value of second modal coordinate of body 2 for bending in xz plane.....	364
5.300 Deviation from pseudostatic value of first modal coordinate of body 3 for bending in xy plane.....	365
5.301 Deviation from pseudostatic value of second modal coordinate of body 3 for bending in xy plane.....	365
5.302 Deviation from pseudostatic value of first modal coordinate of body 3 for bending in xz plane.....	366
5.303 Deviation from pseudostatic value of second modal coordinate of body 3 for bending in xz plane.....	366
5.304 Deviation from derivative of pseudostatic value of first modal coordinate of body 2 for bending in xy plane.....	367
5.305 Deviation from derivative of pseudostatic value of second modal coordinate of body 2 for bending in xy plane.....	367
5.306 Deviation from derivative of pseudostatic value of first modal coordinate of body 2 for bending in xz plane.....	368

5.307 Deviation from derivative of pseudostatic value of second modal coordinate of body 2 for bending in xz plane.....	368
5.308 Deviation from derivative of pseudostatic value of first modal coordinate of body 3 for bending in xy plane.....	369
5.309 Deviation from derivative of pseudostatic value of second modal coordinate of body 3 for bending in xy plane.....	369
5.310 Deviation from derivative of pseudostatic value of first modal coordinate of body 3 for bending in xz plane.....	370
5.311 Deviation from derivative of pseudostatic value of second modal coordinate of body 3 for bending in xz plane.....	370
5.312 Pseudostatic torque applied at joint 1.....	371
5.313 Pseudostatic torque applied at joint 2.....	371
5.314 Pseudostatic torque applied at joint 3.....	372
5.315 Stabilization torque applied at joint 1.....	372
5.316 Stabilization torque applied at joint 2.....	373
5.317 Stabilization torque applied at joint 3.....	373
5.318 Overall torque applied at joint 1.....	374
5.319 Overall torque applied at joint 2.....	374
5.320 Overall torque applied at joint 3.....	375
5.321 Measurement noise of azimuth angle coordinate of tip point.....	375
5.322 Measurement noise of elevation angle coordinate of tip point.....	376
5.323 Measurement noise of derivative of azimuth angle coordinate of tip point.....	376
5.324 Measurement noise of derivative of elevation angle coordinate of tip point.....	377
5.325 Measurement noise of first modal coordinate of body 2 for bending in xy plane.....	377
5.326 Measurement noise of second modal coordinate of body 2 for bending in xy plane.....	378
5.327 Measurement noise of first modal coordinate of body 2 for bending in xz plane.....	378
5.328 Measurement noise of second modal coordinate of body 2 for bending in xz plane.....	379

5.329 Measurement noise of first modal coordinate of body 3	
for bending in xy plane.....	379
5.330 Measurement noise of second modal coordinate of body 3	
for bending in xy plane.....	380
5.331 Measurement noise of first modal coordinate of body 3	
for bending in xz plane.....	380
5.332 Measurement noise of second modal coordinate of body 3	
for bending in xz plane.....	381
5.333 Measurement noise of derivative of first modal	
coordinate of body 2 for bending in xy plane.....	381
5.334 Measurement noise of derivative of second modal	
coordinate of body 2 for bending in xy plane.....	382
5.335 Measurement noise of derivative of first modal	
coordinate of body 2 for bending in xz plane.....	382
5.336 Measurement noise of derivative of second modal	
coordinate of body 2 for bending in xz plane.....	383
5.337 Measurement noise of derivative of first modal	
coordinate of body 3 for bending in xy plane.....	383
5.338 Measurement noise of derivative of second modal	
coordinate of body 3 for bending in xy plane.....	384
5.339 Measurement noise of derivative of first modal	
coordinate of body 3 for bending in xz plane.....	384
5.340 Measurement noise of derivative of second modal	
coordinate of body 3 for bending in xz plane.....	385
5.341 Measurement noise of impulse of Lagrange multiplier.....	385

LIST OF SYMBOLS

Chapter 1

\mathbf{f}	Generalized force matrix
F	Applied force
\mathbf{K}	Generalized stiffness matrix
L	Length of the link
m	Mass of the link
\mathbf{M}	Generalized mass matrix
$\bar{\mathbf{u}}$	Deformation displacement vector of point P
x	Tip position of the link defined in base frame
\mathbf{y}	Vector of generalized coordinates
$Y(L)$	Shape function matrix of the link evaluated at the end of the link
ζ	Translational displacement of the link
η	Elastic (modal) coordinate of the link

Chapter 2

b	Dimension of the tip point position vector
$\mathbf{C}(\boldsymbol{\beta}, \dot{\boldsymbol{\beta}})$	Matrix corresponding to the generalized Coriolis and centrifugal force vector
\mathbf{D}	Solution of the Riccati equation
\mathbf{E}	System matrix
$\mathbf{f}^c(\boldsymbol{\beta})$	Generalized constraint force vector
$\mathbf{f}^e(\boldsymbol{\beta})$	Generalized external force vector
$\mathbf{f}^g(\boldsymbol{\beta})$	Generalized gravitational force vector
$\mathbf{f}^s(\boldsymbol{\eta})$	Generalized structural stiffness force vector
\mathbf{F}	Input matrix
g	gravitational acceleration

h	Corresponding eigenvectors of the eigenvalues κ
J	Performance index
k	Number of constraint equations
K	Matrix corresponding to the structural stiffnesses of the links
L	Matrix corresponding to T
m	Number of the modal variables
M(β)	Generalized mass matrix
n	Number of joint variables
P	Tip point position of the manipulator
P'	Deviation from the desired tip point position
P*	Desired tip point position
q	Vector of joint variables
Q	Appropriate positive definite symmetric matrix
R	Appropriate positive definite symmetric matrix
s	Trajectory variable
s'	Deviation from the desired trajectory variable
s*	Desired trajectory variable
S	Gain matrix
T	Vector of external forces and torques
T'	Stabilization torque for the deviation from the desired tip point trajectory
T*	Pseudostatic torque
x'	Deviation state vector
W	Bias vector
Z	Matrix corresponding to λ
β	Vector of generalized coordinates of the system
η	Vector of the elastic (modal) variables
η'	Deviation from the pseudostatic modal variables
η^*	Pseudostatic modal variables
κ	Closed loop eigenvalues of the system
κ_1	Most dominant eigenvalue
λ	Vector of Lagrange multipliers

λ'	Deviation from the desired Lagrange multipliers
λ^*	Desired Lagrange multipliers
μ'	Impulse of λ'
ϕ	Constraint equations

Section 3.2

$\mathbf{a}^{(1)}$	Acceleration of an arbitrary point P of Body 1
$\mathbf{a}^{(2)}$	Acceleration of an arbitrary point P of Body 2
\mathbf{a}^k	Acceleration of an arbitrary point P of Body k
$c(\cdot)$	$\cos(\cdot)$
$\mathbf{d}^{(1)}$	Position vector from A to B
E^k	Modulus of elasticity of Body k
\mathbf{f}	Generalized external force
\mathbf{f}^*	Generalized inertia force
\mathbf{f}^e	Total generalized external forces due to external forces
$\mathbf{f}^{e(T_1)}$	Generalized external force due to torque T_1
$\mathbf{f}^{e(T_2)}$	Generalized external force due to torque T_2
\mathbf{f}^g	Total generalized gravitational force due to weight of the whole system
$\mathbf{f}^{g(1)}$	Generalized gravitational force due to weight of Body 1
$\mathbf{f}^{g(2)}$	Generalized gravitational force due to weight of Body 2
\mathbf{f}^{gk}	Generalized gravitational force due to weight of Body k
\mathbf{f}^s	Generalized structural stiffness force
$\mathbf{f}^{s(2)}$	Generalized structural stiffness matrix of Body 2
g	Gravitational acceleration
I_3^k	Second moment of area of the cross section of Body k about \mathbf{n}_3^k
$\mathbf{K}^{(2)}$	Structural stiffness matrix of Body 2
L_1	Length of Body 1
\mathbf{M}	Generalized mass matrix of the whole system
\mathbf{M}^k	Generalized mass matrix of Body k

\mathbf{n}	Fixed frame
$\mathbf{n}^{(1)}$	Body 1 reference frame
$\mathbf{n}^{(2)}$	Body 2 reference frame
$\mathbf{P}^{(1)}$	Position vector of an arbitrary point P of Body 1
$\mathbf{P}^{(2)}$	Position vector of an arbitrary point P of Body 2
$\mathbf{q}^{(2)}$	Position vector of point P of Body 2 with respect to Body 2 reference frame
\mathbf{Q}	Generalized Coriolis and centrifugal force vector of the whole system
\mathbf{Q}^k	Generalized Coriolis and centrifugal force matrix of Body k
$\mathbf{r}^{(1)}$	Position vector of point P of Body 1 with respect to Body 1 reference frame at undeformed state
$\bar{\mathbf{r}}^{(1)}$	Position of point P of Body 1 with respect to Body 1 reference frame at undeformed state
$\mathbf{r}^{(2)}$	Position vector of point P of Body 2 with respect to Body 2 reference frame at undeformed state
$\bar{\mathbf{r}}^{(2)}$	Position of point P of Body 2 with respect to Body 2 reference frame at undeformed state
$\bar{r}_1^{(1)}, x^{(1)}$	Position component of point P of Body 1 in $\mathbf{n}_1^{(1)}$ direction
$\bar{r}_2^{(1)}, y^{(1)}$	Position component of point P of Body 1 in $\mathbf{n}_2^{(1)}$ direction
$\bar{r}_1^{(2)}, x^{(2)}$	Position component of point P of Body 2 at undeformed state in $\mathbf{n}_1^{(2)}$ direction
$\bar{r}_2^{(2)}, y^{(2)}$	Position component of point P of Body 2 at undeformed state in $\mathbf{n}_2^{(2)}$ direction
\mathbf{s}	Unit vector along gravitational acceleration in fixed frame
$s(\cdot)$	$\sin(\cdot)$
$\mathbf{T}^{(1)}$	Transformation matrix from Body 1 reference frame to fixed frame
$\mathbf{T}^{(2)}$	Transformation matrix from Body 2 reference frame to fixed frame
$\mathbf{T}^{(1-2)}$	Transformation matrix from Body 2 reference frame to Body 1 reference frame
$\mathbf{T}_1, \mathbf{T}_2$	Actuator torques applied to Body 1 and Body 2, respectively

T_1, T_2	Magnitudes of the actuator torques applied to Body 1 and Body 2, respectively
$\mathbf{u}^{(2)}$	Deformation displacement vector of Body 2 with respect to Body 2 reference frame
$\bar{\mathbf{u}}^{(2)}$	Deformation displacement of Body 2 with respect to Body 2 reference frame
$\mathbf{v}^{(1)}$	Velocity of an arbitrary point P of Body 1
$\mathbf{v}^{(2)}$	Velocity of an arbitrary point P of Body 2
\mathbf{v}^k	Velocity of an arbitrary point P of Body k
V_k	Volume of Body k
W_s^k	Negative of the strain energy
\mathbf{x}	Generalized coordinates
$\dot{\mathbf{x}}$	Time derivative of the generalized coordinates
Y_i	i th bending mode of Body k
δ_2^k	Bending of centerline of Body k
$\boldsymbol{\eta}^{(2)}$	Vector modal variables of Body 2
$\dot{\boldsymbol{\eta}}$	Derivative of vector of modal variables
$\ddot{\boldsymbol{\eta}}$	Second derivative of the vector of modal variables
θ_1	Joint angle of Body 1
θ_2	Joint angle of Body 2
$\theta_3^k(x, t)$	Rotation of the centerline of Body k in its frame
$\boldsymbol{\mu}^k$	Velocity influence coefficient matrix of Body k
$\boldsymbol{\xi}^{(1)}$	Influence coefficient matrix related to the rigid body motion of Body 1
$\boldsymbol{\xi}^{(2)}$	Influence coefficient matrix related to the rigid body motion of Body 2
$\boldsymbol{\xi}^k$	Influence coefficient matrix related to the rigid body motion of Body k
$\dot{\boldsymbol{\xi}}^{(1)}$	Rate of the influence coefficient matrix related to the rigid body motion of Body 1

$\dot{\xi}^{(2)}$	Rate of the influence coefficient matrix related to the rigid body motion of Body 2
ρ_k	Density of Body k material
$\mathbf{v}^{(2)}$	Influence coefficient matrix related to the elastic motion of Body 2
\mathbf{v}^k	Influence coefficient matrix related to the elastic motion of Body k
$\dot{\mathbf{v}}^{(2)}$	Rate of the influence coefficient matrix related to the elastic motion of Body 2
$\phi^{(2)}$	Shape function matrix of Body 2
$\dot{\Omega}$	Generalized speeds vector related to the rigid body motion
$\ddot{\Omega}$	Rate of the generalized speeds vector related to the rigid body motion

Section 3.3

$\mathbf{a}^{(1)}$	Acceleration of point P of Body 1
\mathbf{a}^{2i}	Acceleration of point P of element i of Body 2
\mathbf{a}^{3i}	Acceleration of point P of element i of Body 3
\mathbf{a}^A	Acceleration of point A of Body 1
\mathbf{a}^B	Acceleration of point B of Body 2
\mathbf{a}^C	Acceleration of point C of Body 3
$\bar{\mathbf{b}}^{2i}$	Position vector from Body 2 reference frame to element i reference frame expressed in Body 2 reference frame
$\bar{\mathbf{b}}^{3i}$	Position vector from Body 3 reference frame to element i reference frame in expressed Body 3 reference frame
\mathbf{B}	Constraint Jacobian matrix
\mathbf{B}^{2i}	Boolean matrix of element i of Body 2
\mathbf{B}^{2r}	Boolean matrix of the element r of Body 2 that includes specific point
\mathbf{B}^{3i}	Boolean matrix of element i of Body 3
\mathbf{B}^{3r}	Boolean matrix of the element r of Body 3 that includes specific point

c	Number of constraint equations
$c(\cdot)$	$\cos(\cdot)$
$\bar{\mathbf{D}}^{(1)}$	Transformation matrix from derivative of Euler angles of Body 1 reference frame to the angular velocity of Body 1 reference frame
$\bar{\mathbf{D}}^{(2)}$	Transformation matrix from derivative of Euler angles of Body 2 reference frame to the angular velocity of Body 2 reference frame
$\bar{\mathbf{D}}^{(3)}$	Transformation matrix from derivative of Euler angles of Body 3 reference frame to the angular velocity of Body 3 reference frame
$\mathbf{f}^{(1)}$	Generalized external force of Body 1
$\mathbf{f}_{m_A}^{(1)}$	Generalized external force of lumped mass m_A at point A of Body 1
$\mathbf{f}^{(2)}$	Generalized external force of Body 2
$\mathbf{f}_{m_B}^{(2)}$	Generalized external force of lumped mass m_B at point B of Body 2
$\mathbf{f}^{(3)}$	Generalized external force of Body 3
$\mathbf{f}_{m_C}^{(3)}$	Generalized external force of lumped mass m_C at point C of Body 3
$\mathbf{f}^{*(1)}$	Generalized inertia force of Body 1
$\mathbf{f}_{m_A}^{*(1)}$	Generalized inertia force of lumped mass m_A at point A of Body 1
$\mathbf{f}^{*(2)}$	Generalized inertia force of Body 2
$\mathbf{f}_{m_B}^{*(2)}$	Generalized inertia force of lumped mass m_B at point B of Body 2
$\mathbf{f}^{*(3)}$	Generalized inertia force of Body 3
$\mathbf{f}_{m_C}^{*(3)}$	Generalized inertia force of lumped mass m_C at point C of Body 3
\mathbf{f}^c	Generalized constraint force due to joint forces
\mathbf{f}^e	Generalized external force vector of the system
$\mathbf{f}^{e(T_1)(1)}$	Generalized external force of Body 1 due to torque \mathbf{T}_1
$\mathbf{f}^{e(T_2)(1)}$	Generalized external force of Body 1 due to torque \mathbf{T}_2
$\mathbf{f}^{e(T_2)(2)}$	Generalized external force of Body 2 due to torque \mathbf{T}_2

$\mathbf{f}^{e(T_3)(2)}$	Generalized external force of Body 2 due to torque \mathbf{T}_3
$\mathbf{f}^{e(T_3)(3)}$	Generalized external force of Body 3 due to torque \mathbf{T}_3
\mathbf{f}^g	Generalized gravitational force vector of the system
$\mathbf{f}^{g(1)}$	Generalized external force due to weight of Body 1
$\mathbf{f}_{m_A}^{g(1)}$	Generalized external force due weight of lumped mass m_A
$\mathbf{f}^{g(2)}$	Generalized external force due to weight of Body 2
$\mathbf{f}_{m_B}^{g(2)}$	Generalized external force due to weight of lumped mass m_B
$\mathbf{f}^{g(3)}$	Generalized external force due to weight of Body 3
$\mathbf{f}_{m_C}^{g(3)}$	Generalized external force due to weight of lumped mass m_C
\mathbf{f}^s	Generalized structural stiffness force vector of the system
$\mathbf{f}^{s(2)}$	Generalized structural stiffness force of Body 2
$\mathbf{f}^{s(3)}$	Generalized structural stiffness force of Body 3
g	Gravitational acceleration
\mathbf{H}^{2i}	Structural stiffness matrix of element i of Body 2 expressed in element i frame
\mathbf{H}^{3i}	Structural stiffness matrix of element i of Body 3 expressed in element i frame
\mathbf{I}	Identity matrix
$\mathbf{I}^{(1)}$	Moment of inertia of Body 1 about its reference frame
$\mathbf{K}^{(2)}$	Structural stiffness matrix of Body 2
\mathbf{K}^{2i}	Structural stiffness matrix of element i of Body 2 expressed in Body 2 reference frame
$\mathbf{K}^{(3)}$	Structural stiffness matrix of Body 3
\mathbf{K}^{3i}	Structural stiffness matrix of element i of Body 3 expressed in Body 3 reference frame
L_1	Length of Body 1
m_A	Lumped mass at point A
m_B	Lumped mass at point B

m_C	Lumped mass at point C
\mathbf{M}	Generalized mass matrix of the system
$\mathbf{M}^{(1)}$	Generalized mass matrix of Body 1
$\mathbf{M}_{m_A}^{(1)}$	Generalized mass matrix of lumped mass m_A
$\mathbf{M}^{(2)}$	Generalized mass matrix of Body 2
$\mathbf{M}_{m_B}^{(2)}$	Generalized mass matrix of lumped mass m_B
$\mathbf{M}^{(3)}$	Generalized mass matrix of Body 3
$\mathbf{M}_{m_C}^{(3)}$	Generalized mass matrix of lumped mass m_C
n	Dimension of vector \mathbf{y}
N_2	Number of finite elements in Body 2
N_3	Number of finite elements in Body 3
$\bar{\mathbf{q}}^{2i}$	Position vector from Body 2 reference frame to point P of element i of Body 2 at deformed state expressed in Body 2 reference frame
$\tilde{\mathbf{q}}^{2i}$	Skew symmetric matrix of vector $\bar{\mathbf{q}}^{2i}$
$\bar{\mathbf{q}}^{3i}$	Position vector from Body 3 reference frame to point P of element i of Body 3 at deformed state expressed in Body 3 reference frame
$\tilde{\mathbf{q}}^{3i}$	Skew symmetric matrix of vector $\bar{\mathbf{q}}^{3i}$
$\bar{\mathbf{q}}^{B_2}$	Position vector from Body 2 reference frame to point B of Body 2 at deformed state expressed in Body 2 reference frame
$\tilde{\mathbf{q}}^{B_2}$	Skew symmetric matrix of the vector $\bar{\mathbf{q}}^{B_2}$
$\bar{\mathbf{q}}^{B_3}$	Position vector from Body 3 reference frame to point B of Body 3 at deformed state expressed in Body 3 reference frame
$\tilde{\mathbf{q}}^{B_3}$	Skew symmetric matrix of the vector $\bar{\mathbf{q}}^{B_3}$
$\bar{\mathbf{q}}^{C_3}$	Position vector from Body 3 reference frame to point C of Body 3 at deformed state expressed in Body 3 reference frame
$\tilde{\mathbf{q}}^{C_3}$	Skew symmetric matrix of the vector $\bar{\mathbf{q}}^{C_3}$
\mathbf{Q}	Generalized Coriolis and centrifugal force vector of the system
$\mathbf{Q}^{(1)}$	Generalized Coriolis and centrifugal force vector of Body 1

$\mathbf{Q}_{m_A}^{(1)}$	Generalized Coriolis and centrifugal force vector of lumped mass m_A
$\mathbf{Q}^{(2)}$	Generalized Coriolis and centrifugal force vector of Body 2
$\mathbf{Q}_{m_B}^{(2)}$	Generalized Coriolis and centrifugal force vector of lumped mass m_B
$\mathbf{Q}^{(3)}$	Generalized Coriolis and centrifugal force vector of Body 3
$\mathbf{Q}_{m_C}^{(3)}$	Generalized Coriolis and centrifugal force vector of lumped mass m_C
$\mathbf{r}^{(1)}$	Position of point P of Body 1 expressed in fixed frame
$\bar{\mathbf{r}}^{(1)}$	Position of point P of Body 1 expressed in Body 1 reference frame
$\bar{r}_1^{(1)}, x^{(1)}$	Position component of point P of Body 1 in $\mathbf{n}_1^{(1)}$ direction
$\bar{r}_2^{(1)}, y^{(1)}$	Position component of point P of Body 1 in $\mathbf{n}_2^{(1)}$ direction
$\bar{r}_3^{(1)}, z^{(1)}$	Position component of point P of Body 1 in $\mathbf{n}_3^{(1)}$ direction
$\tilde{\mathbf{r}}^{(1)}$	Skew symmetric matrix of the vector $\bar{\mathbf{r}}^{(1)}$
$\bar{\mathbf{r}}^{2i}$	Position vector from element i frame to point P at undeformed state expressed in Body 2 reference frame
$\bar{\mathbf{r}}^{3i}$	Position vector from element i frame to point P at undeformed state expressed in Body 3 reference frame
$\bar{\mathbf{r}}^{A_1}$	Position vector of point A of Body 1
$\tilde{\mathbf{r}}^{A_1}$	Skew symmetric matrix of the vector $\bar{\mathbf{r}}^{A_1}$
$\mathbf{R}^{(1)}$	Position vector to arbitrary point P of Body 1
\mathbf{R}^{2i}	Position vector to arbitrary point P of element i of Body 2
\mathbf{R}^{3i}	Position vector to arbitrary point P of element i of Body 3
\mathbf{s}	Unit vector along gravitational acceleration in fixed frame
$s(\cdot)$	$\sin(\cdot)$
\mathbf{s}^{2i}	Shape function matrix of element i of Body 2
$\mathbf{s}_{\text{rot}}^{2i}$	Rotation shape function matrix of element i of Body 2
\mathbf{s}^{3i}	Shape function matrix of element i of Body 3
$\mathbf{s}_{\text{rot}}^{3i}$	Rotation shape function matrix of element i of Body 3

T_1	Magnitude of the torque generated by the actuator at point O
T_2	Magnitude of the torque generated by the actuator at point A
T_3	Magnitude of the torque generated at actuator at point B
$\mathbf{T}^{(1)}$	Transformation matrix from Body 1 reference frame to fixed frame
$\bar{\mathbf{T}}_1^{(1)}$	Torque vector applied to Body 1 due to actuator at point O expressed in Body 1 reference frame
$\bar{\mathbf{T}}_2^{(1)}$	Torque vector applied to Body 1 due to actuator at point A expressed in Body 1 reference frame
$\mathbf{T}^{(2)}$	Transformation matrix from Body 2 reference frame to fixed frame
\mathbf{T}^{2i}	Transformation matrix from element i of Body 2 frame to Body 2 reference frame
$\mathbf{T}^{(3)}$	Transformation matrix from Body 3 reference frame to fixed frame
\mathbf{T}^{3i}	Transformation matrix from element i of Body 3 frame to Body 3 reference frame
${}^{A_2}\mathbf{T}_2$	Torque vector applied to Body 2 due to actuator at point A expressed in joint frame A_2
${}^{B_2}\mathbf{T}_3$	Torque vector applied to Body 2 due to actuator at point B expressed in joint frame B_2
${}^{B_3}\mathbf{T}_3$	Torque vector applied to Body 3 due to actuator at point B expressed in joint frame B_3
$\mathbf{T}^{A_1-A_2}$	Transformation matrix from the joint frame at point A of Body 2 to the joint frame at point A of Body 1
\mathbf{T}^{A_2-2}	Transformation matrix from Body 2 reference frame to the joint frame at A_2 due to angular deformation of Body 2
\mathbf{T}^{B_2-2}	Transformation matrix from Body 2 reference frame to the joint frame at B_2 due to angular deformation of Body 2
$\mathbf{T}^{B_2-B_3}$	Transformation matrix from the joint frame at point B of Body 3 to the joint frame at point B of Body 2
\mathbf{T}^{B_3-3}	Transformation matrix from Body 3 reference frame to the joint frame at B_3 due to angular deformation of Body 3

$\bar{\mathbf{u}}^{2i}$	Deformation displacement vector of point P of element i of Body 2 expressed in Body 2 reference frame
$\bar{\mathbf{u}}^{3i}$	Deformation displacement vector of point P of element i of Body 3 expressed in Body 3 reference frame
$\mathbf{v}^{(1)}$	Velocity of point P of Body 1
\mathbf{v}^{2i}	Velocity of point P of element i of Body 2
\mathbf{v}^{3i}	Velocity of point P of element i of Body 3
\mathbf{v}^{B_2}	Velocity vector of point B of Body 2
\mathbf{v}^{B_3}	Velocity vector of point B of Body 3
V_1	Volume of Body 1
V_{2i}	Volume of element i of Body 2
V_{3i}	Volume of element i of Body 3
$\mathbf{x}^{(1)}$	Generalized coordinates of Body 1
$\mathbf{x}^{(2)}$	Generalized coordinates of Body 2
$\mathbf{x}^{(3)}$	Generalized coordinates of Body 3
\mathbf{y}	Generalized speed vector of the system
$\mathbf{y}^{(1)}$	Generalized speed vector of Body 1
$\mathbf{y}^{(2)}$	Generalized speed vector of Body 2
$\mathbf{y}^{(3)}$	Generalized speed vector of Body 3
$\dot{\mathbf{y}}^{(1)}$	Generalized acceleration vector of Body 1
$\dot{\mathbf{y}}^{(2)}$	Generalized acceleration vector of Body 2
$\dot{\mathbf{y}}^{(3)}$	Generalized acceleration vector of Body 3
$\alpha_1, \beta_1, \gamma_1$	Roll, pitch, yaw Euler angles of Body 1 reference frame, respectively
$\alpha_2, \beta_2, \gamma_2$	Roll, pitch, yaw Euler angles of Body 2 reference frame, respectively
$\alpha_3, \beta_3, \gamma_3$	Roll, pitch, yaw Euler angles of Body 3 reference frame, respectively
$\boldsymbol{\alpha}^{(1)}$	Euler angles of Body 1 reference frame in columnwise form

$\dot{\alpha}^{(1)}$	Derivative of Euler angles of Body 1 reference frame in columnwise form
$\alpha^{(2)}$	Euler angles of Body 2 reference frame in columnwise form
$\dot{\alpha}^{(2)}$	Derivative of Euler angles of Body 2 reference frame in columnwise form
$\bar{\alpha}^{(2)}$	Vector of nodal variables of Body 2 expressed in Body 2 reference frame
$\bar{\alpha}^{2i}$	Vector of nodal variables of element i of Body 2 expressed in Body 2 reference frame
$\alpha^{(3)}$	Euler angles of Body 3 reference frame in columnwise form
$\dot{\alpha}^{(3)}$	Derivative of Euler angles of Body 3 reference frame in columnwise form
$\bar{\alpha}^{(3)}$	Vector of nodal variables of Body 3 expressed in Body 3 reference frame
$\bar{\alpha}^{3i}$	Vector of nodal variables of element i of Body 3 expressed in Body 3 reference frame
$\bar{\gamma}^{2i}$	Angular deformation of element i of Body 2 expressed in Body 2 reference frame
$\bar{\gamma}^{3i}$	Angular deformation of element i of Body 3 expressed in Body 3 reference frame
$\bar{\gamma}^{A_2}$	Value of $\bar{\gamma}^{2i}$ evaluated at point A_2
$\bar{\gamma}^{B_2}$	Value of $\bar{\gamma}^{2i}$ evaluated at point B_2
$\bar{\gamma}^{B_3}$	Value of $\bar{\gamma}^{3i}$ evaluated at point B_3
$\zeta^{(2)}$	Position vector from fixed frame to Body 2 reference frame
$\dot{\zeta}^{(2)}$	Derivative of the position vector from fixed frame to Body 2 reference frame
$\zeta^{(3)}$	Position vector from fixed frame to Body 3 reference frame
$\dot{\zeta}^{(3)}$	Derivative of the position vector from fixed frame to Body 3 reference frame
$\eta^{(2)}$	Vector of modal variables of Body 2

$\dot{\eta}^{(2)}$	Derivative of vector of modal variables of Body 2
$\eta^{(3)}$	Vector of modal variables of Body 3
$\dot{\eta}^{(3)}$	Derivative of vector of modal variables of Body 3
θ_3	Joint angle of Body 3
λ	c dimensional vector of constraint forces at the joints
$\mu^{(1)}$	Velocity influence coefficient matrix of Body 1
μ^{2i}	Velocity influence coefficient matrix of Body 2
μ^{3i}	Velocity influence coefficient matrix of Body 3
μ^A	Velocity influence coefficient matrix of point A of Body 1
μ^B	Velocity influence coefficient matrix of point B of Body 2
μ^C	Velocity influence coefficient matrix of point C of Body 3
ρ_1	Density of Body 1 material
ρ_{2i}	Density of element i of Body 2 material
ρ_{3i}	Density of element i of Body 3 material
ϕ^{B_2}	Value of ϕ^{2i} at point B of Body 2
ϕ^{B_3}	Value of ϕ^{3i} at point B of Body 3
ϕ^{C_3}	Value of ϕ^{3i} at point C of Body 3
$\chi^{(2)}$	Modal matrix of Body 2
$\chi^{(3)}$	Modal matrix of Body 3
Ψ^{A_2}	Value of Ψ^{2i} evaluated at point A_2
Ψ^{B_2}	Value of Ψ^{2i} evaluated at point B_2
Ψ^{B_3}	Value of Ψ^{3i} evaluated at point B_3
$\bar{\omega}^{(1)}$	Angular velocity of Body 1 reference frame expressed in the same frame
$\bar{\omega}^{(2)}$	Angular velocity of Body 2 reference frame expressed in the same frame
$\bar{\omega}^{(3)}$	Angular velocity of Body 3 reference frame expressed in the same frame

ω^{A_1}	Angular velocity vector of point A of Body 1
ω^{A_2}	Angular velocity vector of point A of Body 2
ω^{B_2}	Angular velocity vector of point B of Body 2
ω^{B_3}	Angular velocity vector of point B of Body 3
${}^{A_1}\omega^{A_1}$	Angular velocity of joint frame at point A of Body 1 expressed in the same frame
${}^{A_2}\omega^{A_2}$	Angular velocity of joint frame at point A of Body 2 expressed in the same frame
${}^{A_1}\omega^{A_2}$	Angular velocity of joint frame at point A of Body 2 expressed in joint frame at point A of Body 1
${}^{B_2}\omega^{B_2}$	Angular velocity of joint frame at point B of Body 2 expressed in the same frame
${}^{B_3}\omega^{B_3}$	Angular velocity of joint frame at point B of Body 3 expressed in the same frame
${}^{B_2}\omega^{B_3}$	Angular velocity of joint frame at point B of Body 3 expressed in joint frame at point B of Body 2
$\Omega^{(1)}$	Angular velocity influence coefficient matrix of Body 1
${}^{A_2}\Omega^{A_2}$	Influence coefficient matrix of angular velocity of joint frame at point A of Body 2 expressed in the same frame
${}^{B_2}\Omega^{B_2}$	Influence coefficient matrix of angular velocity of joint frame at point B of Body 2 expressed in the same frame
${}^{B_3}\Omega^{B_3}$	Influence coefficient matrix of angular velocity of joint frame at point B of Body 3 expressed in the same frame

Section 3.4

c	Number of constraint equations
$m^{(2)}, m^{(3)}$	Number of modal coordinates for Body 2 and Body 3, respectively
$\zeta, \dot{\eta}$	Vectors of primary variables
κ	Vector of secondary variables
λ	Vector of constraint forces

Chapter 4

k	Constant coefficient of the exponential expression
p_i	Desired closed loop poles
P_1, P_2	Tip point position coordinates
P_{1c}, P_{2c}	Center coordinates of the circle with respect to fixed frame
\mathbf{P}^*	Desired tip point position vector
\mathbf{P}_0^*	Desired initial tip point position vector
\mathbf{P}_f^*	Desired final tip point position vector
R	Radius of the circle
s	Trajectory variable
t_1	Time for the end of cycloidal rise motion
t_2	Time for the beginning of the cycloidal return motion
t_f	Time to complete motion
Y_i	Mode shape functions
ε	Error
ε_m	Initial error in absolute value
$\boldsymbol{\lambda}^*$	Desired Lagrange multiplier vector
$\boldsymbol{\lambda}_0^*$	Desired constant value of the Lagrange multiplier vector
$\phi(P_1, P_2)$	Constraint equations in terms of tip point variables
ω_{ni}	Natural frequency associated with natural mode
$\omega_{ni}(\varepsilon)$	Closed loop natural frequency that is scheduled at an instant
$\omega_{ni}^s, \omega_{ni}^f$	Smallest and largest values of the closed loop natural frequency

Chapter 5

p_i	Desired closed loop poles
P_1, P_2, P_3	Tip point position coordinates
P_{1c}, P_{2c}, P_{3c}	Center coordinates of the sphere with respect to fixed frame

R	Radius of the sphere
s_1, s_2	Trajectory variables
ω_c	Crossover frequency

CHAPTER 1

INTRODUCTION

Conventional industrial manipulators are usually made stiff and bulky to avoid vibrations and hence to achieve precision in motion control. Several considerations such as lower arm cost, higher motion speeds, higher accuracy in operations, better energy efficiency, safer operation and improved mobility resulted in a new generation of manipulators with lightweight, flexible links.

Robot manipulators with flexible links include lightweight manipulators and/or large articulated structures that are encountered in a variety of conventional and nonconventional settings. Very long arms needed for accessing hostile environments such as nuclear sites, underground waste deposits, deep sea, space, etc. or automated crane devices for building construction can be considered as actual applications in the real life. The ultimate challenge is the design of mechanical arms made of light materials that are suitable for complex industrial manipulation tasks, such as pick-and-place, arc welding, spray painting, laser cutting, grinding, deburring, assembly, or surface finishing.

In complex industrial tasks (e.g., grinding, deburring, assembly) robots usually operate in a constrained environment. Good control performance in these applications can hardly be achieved using conventional point-to-point control strategies. Thus, simultaneous motion tracking and force control are required in this type of applications.

Robot manipulators will play an important role in future space missions as the important demand for low-energy consumption and limitation of carrying capacity of space rockets, links of the space manipulators, as well as other space

structures, are required to be light. However, as a result of the elasticity of the arms and the structures, undesirable low frequency vibrations may occur. In the case of constructing large space structures, for example, a space station, using space robot manipulators, it is necessary to control not only the position and vibration of the manipulators but also the force exerted by the hand on the working surface.

Robot arms with flexible links have an infinite number of degrees of freedom. A reduced-order model, which is still highly nonlinear and complex, is typically used for purposes of simulation and controller design. The inherent difficulty of the control problem can be ascribed to the fact that the number of controlled variables is strictly less than the number of mechanical degrees of freedom. Moreover, the dynamic relation between the input torques of the joint actuators and the tip position reveals a behavior which is the nonlinear counterpart of the nonminimum phase phenomenon of linear systems. Hence, inversion-based control strategies would normally lead to instability in the closed loop. This is shown on a simple example in the next section.

A brief review of the studies related to the motion control and force and motion control of robots with flexible links is given in sections 1.2 and 1.3, respectively. Discussions on these studies are presented in section 1.4.

1.1 An Example to Nonminimum Phase Systems

To show that the trajectory tracking of the manipulator is non-minimum phase, distributed parameter model of a flexible single link manipulator in translational motion is taken into consideration.

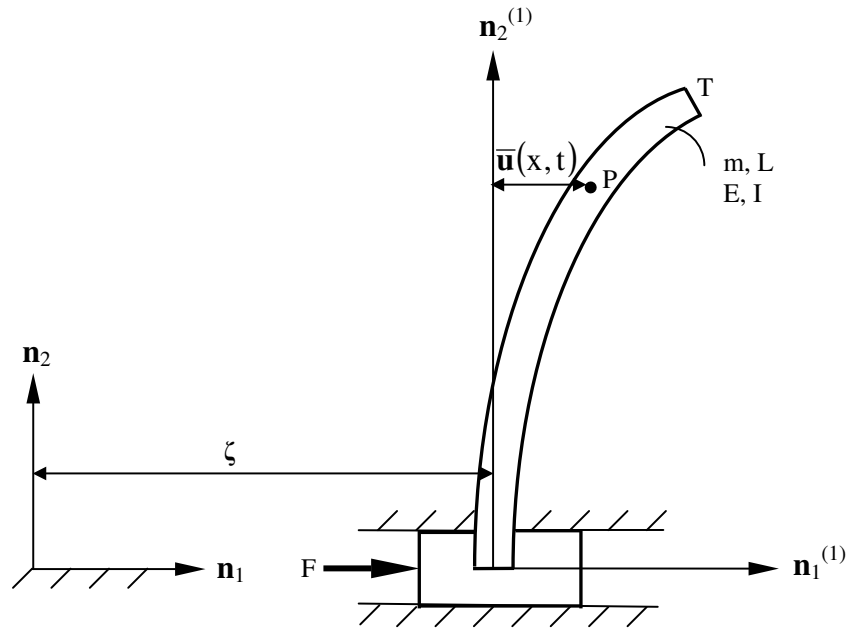


Figure 1.1 Distributed parameter model of the flexible single link manipulator in translational motion.

Figure 1.1 represents the distributed parameter model of the manipulator. In the figure, m is the mass, L is the length, F is the applied force, ζ is the translational displacement of the beam, \bar{u} is the deformation displacement vector of point P . The first fixed free bending mode will be used here to represent the vibration of the beam. The dynamic equations of the model have the form

$$\mathbf{M}\ddot{\mathbf{y}} + \mathbf{K}\mathbf{y} = \mathbf{f} \quad (1.1)$$

where \mathbf{M} is the generalized mass matrix, \mathbf{K} is the generalized stiffness matrix, \mathbf{y} is the vector of generalized coordinates, \mathbf{f} is the vector of generalized forces and they are given as

$$\mathbf{y} = \begin{bmatrix} \zeta \\ \eta \end{bmatrix} \quad (1.2)$$

$$\mathbf{M} = \begin{bmatrix} m & 2.38m \\ 2.38m & 9.23m \end{bmatrix} \quad (1.3)$$

$$\mathbf{K} = \begin{bmatrix} 0 & 0 \\ 0 & 114.06 \frac{EI}{L^3} \end{bmatrix} \quad (1.4)$$

$$\mathbf{f} = \begin{bmatrix} F \\ 0 \end{bmatrix} \quad (1.5)$$

where η is the elastic (modal) coordinate of the link. The dynamic equations of the manipulator can be written as

$$m\ddot{\zeta}(t) + 2.38m\ddot{\eta}(t) = F(t) \quad (1.6)$$

$$2.38m\ddot{\zeta}(t) + 9.23m\ddot{\eta}(t) + 114.06 \frac{EI}{L^3} \eta(t) = 0 \quad (1.7)$$

If the Laplace transform of the Equations (1.6) and (1.7) are taken, the following equations are obtained as

$$ms^2\zeta(s) + 2.38ms^2\eta(s) = F(s) \quad (1.8)$$

$$2.38ms^2\zeta(s) + 9.23ms^2\eta(s) + 114.06 \frac{EI}{L^3} \eta(s) = 0 \quad (1.9)$$

From Equation (1.8), $\eta(s)$ can be written as

$$\eta(s) = \frac{-\zeta + \frac{F}{ms^2}}{2.38} \quad (1.10)$$

If Equation (1.10) is substituted into Equation (1.9) and the necessary arrangements are done, the following equation is obtained

$$\left(1.5ms^4 + 47.92 \frac{EI}{L^3} s^2 \right) \zeta(s) = \left(3.88s^2 + 47.92 \frac{EI}{mL^3} \right) F(s) \quad (1.11)$$

Equation (1.11) can be written as

$$\frac{\zeta(s)}{F(s)} = \frac{3.88s^2 + 47.92 \frac{EI}{mL^3}}{s^2 \left(1.5ms^2 + 47.92 \frac{EI}{L^3} \right)} \quad (1.12)$$

If Equation (1.11) is substituted into Equation (1.10) one obtains the following equation

$$\frac{\eta(s)}{F(s)} = \frac{-1}{\left(1.5ms^2 + 47.92 \frac{EI}{L^3} \right)} \quad (1.13)$$

The tip position of the manipulator defined in the base frame can be written as

$$x = \zeta + \bar{u}(L) \quad (1.14)$$

which can be expressed as

$$x = \zeta + Y(L)\eta \quad (1.15)$$

where $Y(L)$ is shape function matrix of the link evaluated at the end of the link. If the first fixed-free bending mode shape function is evaluated at the end of the link, $Y(L)$ is found as 6.075. Therefore, Equation (1.15) becomes

$$x = \zeta + 6.075\eta \quad (1.16)$$

If Equations (1.12) and (1.13) are substituted into Equation (1.16), Equation (1.16) becomes

$$\frac{x(s)}{F(s)} = \frac{-2.189s^2 + 47.92 \frac{EI}{mL^3}}{s^2 \left(1.5ms^2 + 47.92 \frac{EI}{L^3} \right)} \quad (1.17)$$

Equation (1.17) represents the forward dynamics transfer function of the manipulator. In other words, for given force input, the end position of the manipulator is found. It is seen from the equation that forward dynamics transfer function has a positive zero. When the inverse dynamics of this manipulator is taken into consideration, the input becomes the desired end point trajectory and the output becomes the force that satisfies this trajectory. In other words, the forward dynamics transfer function is reversed in the case of inverse dynamics. Therefore, in this case, positive zero of the forward dynamics becomes the positive pole of inverse dynamics. Thus, inverse dynamics problem becomes unstable. This means that trajectory tracking control of flexible link manipulator has non-minimum phase property.

1.2 Literature Review on Motion Control of Flexible Robots

Some researchers considered point-to-point position control or regulation of single link and multilink robots in which the main task is to suppress the residue vibrations. It was shown that independent joint control is stable for positioning and that stability does not depend on explicitly on the system parameters. However it can be shown that when the trajectory tracking is concerned independent joint control may become unstable. In many applications, however, tip trajectory tracking is required. Tip tracking control of flexible link manipulators has the difficulty of the non-minimum phase property due to the finite speed of propagation of the mechanical wave along the links since the joint actuators are non-collocated. In the literature, various modeling and controller design schemes have been proposed for motion of the manipulator. A brief review of them is given in the following paragraphs.

Goldenberg and Rakhsha [1] utilized the computed torque technique to control a single-link flexible robot. It was assumed that the arm could rotate in a horizontal plane and the link flexibility produced in-plane bending. The single flexible link was modeled as a continuous beam by using Euler-Bernoulli formulation with small deflections (relative to length) and all terms involving the square of joint

variable were neglected. The technique was implemented by calculating, for a given trajectory, the nominal torque from the rigid body model of the robot. The technique provided feedforward compensation which introduces an additional zero of the closed-loop system transfer function. Using a PD feedback compensator in addition to the feedforward one almost pole-zero cancellation of the dominant closed-loop poles of the system was done. Luca and Siciliano [2] considered the trajectory tracking control problem for a one link flexible arm described by a nonlinear model. The arm was assumed to move on a horizontal plane. The link was modeled as Euler-Bernoulli beam. Two system outputs were chosen; namely, the joint angle and the angular position of a suitable point along the link. Based on the input-output inversion algorithm, a state-feedback control law was designed that enabled tracking of any smooth trajectory specified for the output. In the closed loop an unobservable dynamics naturally arised, related to the variables describing the arm's distributed flexibility. Kwon and Book [3] addressed inverse dynamic trajectory planning issues of a single-link flexible manipulator. To derive the equations of motion of the manipulator, they described the position of a point on the beam with virtual rigid-body motion and deflection with respect to the rigid-body coordinate by using Euler-Bernoulli beam model. The virtual rigid body motion was represented by the motion of the moving coordinate attached to the beam. The inverse dynamic equation of a single-link flexible manipulator was solved in the time-domain. The inverse dynamic method calculated the feedforward torque and the trajectories of all state variables that did not excite structural vibrations for a given end-point trajectory. Zhu et al. [4] studied tip tracking control of a single-link flexible robot. The controller investigated was of a two-loop PD type, which was deduced from a control approach originally developed for elastic joint robots. A very simple model, with the flexible link of the robot being lumped to a spring-mass unit, was employed for the controller design. Bounded Input and Bounded Output (BIBO) stable tip tracking was obtained. Parameter uncertainty was also taken into consideration. The design of feedforward controllers to control the position of single-link flexible arms was developed by Feliu and Rattan [5]. The dynamic inversion of the single-link flexible arm was studied from a discrete point of view. A method to obtain a feedforward controller was developed, even in the case when the

system transfer function was of non-minimum phase. Ge et al. [6] derived a nonlinear dynamic model of a flexible manipulator through finite element method associated with Lagrange approach. The single link flexible manipulator was modeled as an Euler-Bernoulli beam driven by a motor at its base and with a point mass tip payload. The generalized coordinates of the system were selected to be the displacements and rotations of the nodes on the considered flexible beam, and such that a state space model was obtained. Based on this model, a nonlinear feedback controller was developed to control the tip position. Yeung and Chen [7] designed the controller of a single-link flexible manipulator moving in a vertical plane. The equations of the manipulator were obtained by using Lagrangian formulation. The controller was designed in two steps: linearization of the rigid part of its dynamic equation, and stabilization of the overall linearized system with conventional linear techniques. For the linearization, they employed the sliding-mode technique to arrive at a desired linear equation. To avoid chattering, a sliding layer function was used to replace the sign function. In the stabilization step, PD/PID compensations were used to stabilize the system. The parameters of the PD/PID compensators were determined from pole placement. The locations of the poles have to be carefully selected in order to arrive at adequate insensitivity against payload variations. A controller design for controlling a flexible one link manipulator based on variable structure theory was presented by Qian and Ma [8]. The link was assumed to move on a horizontal plane and governing partial differential equation was obtained by applying Hamilton's principle. The discontinuous control law based on the variable structure system theory for the non-collocated manipulator tip position control was designed. The position state variables were obtained directly from the inversion of the output submatrix multiplied by the sensor measurements. The velocity state variables were estimated through decoupled estimators -a separate first-order observer for each of the system's modes under consideration.

Luca et al. [9] gave a framework for computing the torques that were needed for moving a flexible arm along a given trajectory. This torque computation required a dynamic generator system and could be accomplished both in an open- or in a closed-loop fashion. In the open-loop case, the dynamic generator was the full or

reduced order inverse system associated to the arm dynamics and outputs. In order to successfully invert the arm dynamics, the torque generator should be a stable system. The stability properties depended on the chosen system output, that was on the robot variables (e.g., joint or end effector) to be controlled. The same inversion technique could be applied for closed-loop trajectory control of flexible robots. A simple nonlinear dynamic model of a one link flexible arm was used to illustrate the control strategies. A technique was presented for solving the inverse dynamics and kinematics of multilink flexible robots by Bayo et al. [10]. The proposed method found the joint torques necessary to produce a specified end effector motion. Since the inverse dynamic problem in elastic manipulators was closely coupled to the inverse kinematic problem, the solution of the first also rendered the displacements and rotations at any point of the manipulator, including the joints. The Timoshenko beam theory was used to model the elastic characteristics, and the resulting equations of motion were discretized using the finite element method. An iterative solution scheme was proposed that relies on local linearization of the problem. The solution of each linearization was carried out in the frequency domain. A two link flexible manipulator which was on a horizontal plane was used as an example. Experimental study was also conducted. The inverse dynamics of robot manipulators based on flexible arm models were also considered by Asada et al. [11]. Actuator torques required for a flexible arm to track a given trajectory were formulated and computed by using special moving coordinate systems, called virtual rigid link coordinates. Dynamic deformations of the flexible arm can be represented in a simple and compact form with use of the virtual coordinate systems. They focused on the feedforward compensation based on inverse dynamics of flexible arm models. The formulation was applied to a two link arm which was constrained in a horizontal plane. Xi [12] combined the kinematics of a flexible link manipulator with its dynamics. Based on this combination, a numerical method was proposed for analyzing the inverse dynamics of a spatial two link flexible manipulator. The manipulator was modeled as Euler-Bernoulli beam. A linearized solution of flexible manipulator dynamics was demonstrated by Gawronski et al. [13]. Based on this approach, the inverse dynamics problem was defined and solved. The forward compensation torques were determined, with the joint angles in the flexible body configuration were matched to the angles in the

rigid body configuration. The combined feedforward compensation and feedback control was used. A two link flexible manipulator was considered as an example. Moallem et al. [14] presented an inverse dynamics control strategy for a class of multilink structurally flexible manipulators. This was done by defining new outputs near the end points of the arms as well as by augmenting the control inputs by terms that ensure stable operation of the closed loop system under specific conditions. The controller was designed in a two-step process. First, an output was defined such that the zero dynamics of the original system were stabilized. Next, the control input was modified such that stable asymptotic tracking of the new output or approximate tracking of the actual output might be obtained. This was illustrated for the case of single link and two link flexible manipulators.

A rigid and flexible motion controller based on integral plus state feedback controller was derived by Chalhoub and Ulsoy [15]. In the controller, they introduced additional damping into the flexible motion. This was done by using additional sensors to measure the compliant link vibrations and fed them back to the controller. The performance of the controller was tested on a dynamic model for a spherical coordinate two link robot arm which had two revolute joints and one prismatic joint. The last link of the robot only was considered to be flexible. Baruh and Tadikonda [16] presented an approach similar to the component mode and substructure synthesis methods to derive the equations of motion, and both open loop and closed loop control of the manipulator arm considered, where in the latter the feedback quantities were calculated by using the output of spatially distributed sensors. A two link manipulator that had three degree of freedom was taken as an illustration. Carusone and D'Eleuterio [17] presented a feedback control strategy for the end effector position and orientation tracking of structurally flexible manipulators free of external forces as in space applications. The fully feedback-driven approach employed an augmented dynamical description in which derivatives of the control inputs were included in the state. The feedback law used gain scheduling of a series of steady-state regulators derived by considering the manipulator at intermediate (nominally rigid and stationary) configurations along the desired trajectory. The performance of the control method was demonstrated in simulations of a planar three link manipulator

system. Ider et al. [18] developed a method for end effector trajectory tracking control of robots with flexible links. In order to cope with the non-minimum phase property of the system, the closed-loop poles were placed at desired locations using full state feedback. The dynamic equations were linearized about the rigid motion. A composite control law was designed to track the desired trajectory while at the same time the internal dynamics was stabilized. A two link planar manipulator was considered whose upperarm was rigid and forearm was flexible.

A reference-oriented procedure for controlling elastic robots was presented by Pfeiffer [19]. This afforded, in a first step, an optimal path planning method generating the reference trajectory. It was realized by a classical feedforward decoupling scheme. The elastic deviations from this reference were corrected within the feedforward loop by calculation of the joint correction angles putting back the endpoint to its nominal position. In a final step, elastic vibrations of the arms were damped by an additional joint output control system, which used as an input joint kinematics and strain gauge measurements of the elastic curvatures. Three link robot with two flexible arm was used. The design of inversion-based nonlinear control laws solving the problem of trajectory tracking for robot arms having flexible links was considered by Luca and Siciliano [20]. Links were modeled as Euler-Bernoulli beams. The interaction between the Lagrangian/assumed modes modeling approach and the complexity of the resulting inversion control laws was stressed. The control was composed of a nonlinear state feedback compensation term and of a linear feedback stabilization term. A feedforward strategy for the nonlinear part was also investigated. Simulation results were presented for a planar manipulator with two flexible links. Li [21] presented a control design for the tip position trajectory tracking of a two link manipulator arm with a flexible forearm. The control design was based on two steps. First, input-output linearization was applied to decouple the shoulder arm dynamics from the forearm dynamics, which transformed the trajectory tracking control of the nonlinear non-minimum phase system into the trajectory tracking control of two linear subsystems. Then trajectory tracking control design of each subsystem was carried out in the second design step. Yim [22] treated the end point trajectory control of a flexible manipulator based on the nonlinear

inversion technique. The manipulator had two rigid links and the third link was elastic. A parameterization of the Cartesian coordinates of a point close to the end effector position was suggested. Using these coordinates as output variables, an inverse feedback control law was derived for tracking reference Cartesian trajectories. The stability of the zero dynamics associated with the end point motion control was examined. It was shown that inverse control of the end point caused divergent oscillatory flexible modes. In addition, for regulating the end point to a fixed position, a linear stabilizer was designed to damp the elastic vibration. Zhao and Chen [23] developed a tracking control strategy for a two link flexible manipulator. The Euler-Bernoulli beam was assumed. Horizontal planar maneuver of the manipulator was assumed. The controller used a feedforward signal generated by stable inversion and a stabilizing signal from a feedback stabilizer.

Chen and Yeung [24] presented a work which was a continuation of the Yeung and Chen [7] studies. This work presented an extension of the sliding-mode control design method to multilink flexible manipulators. As for the dynamic analysis, a clamped loaded Euler-Bernoulli beam was selected as an approximate model for each link in the presence of lateral deformation. Coupling effects caused by flexibilities between the two links were neglected. There were two main steps in the design procedure, linearization and stabilization. In the linearization step, the sliding-mode technique was used to replace the rigid part of the dynamic equations by a set of linear equations which were determined by the switching surfaces. In the stabilization step, conventional PD/PID compensations were adopted to stabilize the linearized time-invariant system. Two link flexible manipulator was used in simulations. Nathan and Singh [25] treated the question of control of an elastic robotic arm of two links based on variable structure system (VSS) theory and pole assignment technique for stabilization. A discontinuous joint angle control law, based on variable structure system theory, was designed for the asymptotic decoupled joint angle trajectory tracking. In the closed-loop system, the trajectories were attracted toward a chosen hypersurface in the state space and then slid along it. Although, joint angles were controlled using variable structure control law, the flexible modes of the links were excited. Using

center manifold theory, it was shown that the closed-loop system, including the sliding mode controller, was stable. Based on a linearized model about the terminal state, a stabilizer was designed using pole assignment technique to control the elastic oscillations of the links. A control logic was included which switched the stabilizer at the instant when the joint angle trajectory entered a specified neighborhood of the terminal state. Moallem et al. [26] considered a control strategy based on nonlinear inversion for a class of multilink, structurally flexible manipulators. New outputs near the end points of the arms were defined. By using the concept of a sliding surface in variable structure control (VSC), the nonlinear plant's error dynamics were driven onto a sliding surface. In order to avoid over-excitation of higher frequency flexural modes due to control chattering, the discontinuous functions normally used in classical variable structure control were replaced by saturation

A nonlinear tracking controller for the link tip positions and velocities of a multilink flexible robot arm was designed by Vandegrift et al. [27]. The controller had three parts: a model-based trajectory generator, an inner loop based on input-output feedback linearization, and an outer loop that stabilized the internal dynamics (e.g., the flexible modes) using a singular perturbation design. A two link spatial arm whose second link was modeled by using Euler-Bernoulli beam model was taken into consideration. A robust control strategy for the trajectory tracking control of elastic robot manipulators was proposed by Morita et al. [28]. The controller was designed to be robust against both of the structured uncertainty and the unstructured uncertainty arising from modeling errors. The model consisting of the rigid-body modes and the elastic modes was decomposed into the slow model and the fast model by using an integral manifold approach. By using the slow model, slow controller was designed based on the VSS theory and the stability of the closed loop system was shown via Liapunov theory. On the other hand, the fast controller was designed for the fast model on the basis of H-infinity control theory. A two link flexible robot manipulator moving on a vertical plane was used. Moallem et al. [29] developed a nonlinear control strategy for tip position trajectory tracking of a class of structurally flexible multilink manipulators. Using the concept of integral manifolds and singular perturbation

theory, the full-order flexible system was decomposed into corrected slow and fast subsystems. The tip-position vector was similarly partitioned into corrected slow and fast outputs. The corrected slow subsystem was augmented by a dynamical controller in such a way that the resulting closed-loop zero dynamics were linear and asymptotically stable. The tracking problem was then redefined as tracking the slow output and stabilizing the corrected fast subsystem by using dynamic output feedback. A two link planar manipulator with flexible forearm was considered as an example.

An adaptive self-tuning control scheme was developed for end-point position control of flexible manipulators by Bodur and Sezer [30]. The effect of flexibility was included in the dynamic model by approximating flexible links with a number of rigid sublinks connected at fictitious joints. The relatively high stiffness of the fictitious joints was shown to result in a decomposition of the model into two subsystems operating at different rates. This allowed for stabilization of the oscillatory modes associated with the flexible links by a fast feedback control in addition to a slower control for trajectory tracking. The control was constructed from measurements of the end-point position and deformations of the flexible links, with the manipulator parameters required to form the control obtained using a recursive least-squares estimation algorithm. The control scheme was tested by digital simulation of a two link manipulator with flexible first link. Pham et al. [31] presented a nonlinear, model-based control of flexible link robots. The control task was formulated requiring rigid joints variables to track reference time-varying trajectory and elastic deflection to be damped. The stability and robustness properties of the control scheme were analyzed from a passive energy consideration. A direct adaptive version was also proposed. This approach was performed using a single-flexible-link and a two-flexible-link horizontal robot. Another controller for solving the tracking problem of flexible robot arms was presented by Arteaga and Siciliano [32]. In order to achieve this goal, the desired trajectory for the link (flexible) coordinates was computed from the dynamic model of the robot arm and was guaranteed to be bounded, and the desired trajectory for the joint (rigid) coordinates could be assigned arbitrarily. The proposed control law based on the well-known approach

with filtered reference velocity at the basis of passivity-based and adaptive controllers. The case of no internal damping was also considered, and a robust control technique was used to enhance the damping of the system. In order to test the controllers, a planar two link flexible robot modeled as Euler-Bernoulli beam was used.

Morgul [33] considered a flexible beam clamped to a rigid base at one point and free at the other end. He assumed that the rigid base rotated with a constant angular frequency and that the motion of the flexible beam took place on a plane. To stabilize the beam vibrations, he proposed a dynamic boundary force control applied to the free end of the beam. He showed that, with the proposed control, when the rigid base angular frequency was sufficiently small, the beam vibrations exponentially decayed to zero. Morgul [34] again considered a flexible structure modeled as a rigid body which rotated in inertial space; a flexible beam was clamped to the rigid body at one end and free at the other. He assumed that the flexible beam performed only planar motion. He posed two control problems, namely, the orientation and stabilization of the system. It was shown that suitable boundary controls applied to the free end of the beam and suitable control torques applied to the rigid body solved the problems posed above. The proofs were obtained by using the energy of the system as a Lyapunov functional.

1.3 Literature Review on Force and Motion Control of Flexible Robots

A limited number of studies for simultaneous force and motion control of robots with flexible links has been found in the literature. A brief review of them is given in the following paragraphs.

Unconstrained and constrained motion control of a planar two link structurally flexible robotic manipulator were considered by Choi and Krishnamurthy [35]. The dynamic model was obtained by using the extended Hamilton's principle and the Galerkin criterion. A method was presented to obtain the linearized equations of motion in Cartesian space for use in designing the control system. The

approach to solving the control problem was to use feedforward and feedback control torques. The feedforward torques maneuvered the flexible manipulator along a nominal trajectory and the feedback torques minimized any deviations from the nominal trajectory. The feedforward and feedback torques were obtained by solving the inverse dynamics problem for the rigid manipulator and designing linear quadratic Gaussian with loop transfer recovery (LQG/LTR) compensators, respectively. The LQG/LTR design methodology was exploited to design a robust feedback control system that could handle modeling errors and sensor noise, and operate on Cartesian space trajectory errors. Matsuno et al. [36] have considered the problem of hybrid position/force control of a planar two link flexible manipulator. They derived the dynamic model of the constrained flexible manipulator by introducing the Lagrange multiplier. They assumed that the elastic deformations of the links were small compared to their lengths; the densities of the links materials and tip point lumped mass so small that rigid body variables in the equations of the vibrations of the flexible links could be neglected and the angular rotation of link 2 due to deformation of the link was negligibly small compared to the rigid body rotation of link 2. On the basis of these assumptions they derived the quasi-static equation and designed the hybrid position/force controller by using these quasi-static equations. PD type control plus force feedback control was used. An implicit force control scheme for flexible link manipulators was considered by Borowiec and Tzes [37]. The control output was composed of a feedforward and a feedback term. The feedforward torque component compensated the underlying rigid arm dynamics along the desired trajectory. The feedback component regulated the joint coordinate error perturbations. The minimization of a linear quadratic frequency-shaped cost functional yielded the time-varying feedback controller gains. The frequency shaping dependence was included to eliminate undesirable effects associated with control and observation spillover. The proposed control scheme was employed in simulation studies on a planar two link rigid flexible manipulator. Shi et al. [38] proposed a multivariable controller for the force and motion control of a planar two link rigid-flexible manipulator moving in a horizontal plane. The static tip deflection of the flexible link was allowed in order to maintain the contact force between the end effector and the constrained path. The controller consisted of a

feedforward term which contributed the torque for the expected joint angles and the contact force, and a feedback term with the time varying optimal gains obtained from the Matrix Riccati equation. A two-stage interaction control scheme for a flexible arm whose tip was in contact with a compliant surface has been proposed by Siciliano and Villani [39]. The first stage was in charge of solving the inverse kinematics problem to compute the desired vectors of the joint and the deflection variables that placed the flexible arm tip at the desired position with the desired contact force. The solution was based on the transpose of a suitably modified arm Jacobian so as to account for the static effects due to gravity and contact force. The computed variables were used as the set-points for the second stage, which was a simple PD joint regulator. The scheme was tested in a simulation case study for a planar two link flexible manipulator.

Hu and Ulsoy [40] reported the results of a study of the combined joint motion control, vibration control, and force control of a spatial two link rigid-flexible constrained robot arm. A robust controller design technique was proposed by Corless and Leitmann, and further developed by Corless, for the tracking control of uncertain mechanical systems. This technique, incorporating contact force, feedback, was used as the first method of design for a nonlinear controller. This method assumed that only information on the rigid-body motion is available, and treated the effects of flexible motion as uncertainties on the rigid system. A second method, a modified version of the Corless-Leitmann technique suggested by Yigit and Ulsoy, includes the feedback of the flexible-body motion of a robot arm, but utilizes no control actuator for the degree of freedom of the flexible-body motion. This second method (modified Corless-Leitmann controller) was employed, to design a controller for improving the suppression of the flexible vibration. Yim and Singh [41] were considered the position and force control of a spatial three link rigid-rigid-flexible manipulator on a constraint surface based on nonlinear inversion of an input-output map and linear feedback stabilization. Unlike the rigid robots, the feedback linearizing control of end point motion gave rise to unstable zero dynamics. Instability of zero dynamics was avoided by controlling a parameterized output vector corresponding to a point close to the

end point of the arm. Zero dynamics were stable or almost stable as long as the parameter in the output vector did not exceed a critical value. Using the inverse controller, the control of the force and the position of the end point was possible while the end effector moved on the constraint surface. However, this excited the elastic modes. For the final capture of the terminal state and vibration suppression, a linear stabilizer was designed. Choi et al. [42] proposed an approach employing the framework of constraint Hamiltonian system for the compliant control of a planar two link rigid-flexible manipulator with surface constraints. Two nonlinear controllers consisting of force part and position part were derived from a constrained Hamiltonian system, followed by the formulation of corresponding linear feedback controllers that satisfied the Lyapunov stability of the total Hamiltonian system which possessed the nonlinear controllers. The compliant control strategy was accomplished by steering the end effector of the flexible manipulator onto the constraint surface with the linear controllers, and subsequently by executing imposed desired motion with the nonlinear controllers.

Kim et al. [43] presented a control strategy for the position and force control of flexible manipulators exploiting the characteristics of actuators fabricated from smart materials. The governing equations of motion of a planar two link flexible manipulator which featured piezoceramic actuators and piezofilm sensors bonded on each flexible link were derived via Hamilton's principle. A nominal control torque of the motor to command the desired position and force was determined by a sliding mode controller based on the rigid-mode dynamics. In order to take uncertainties into account, the sliding mode controller with perturbation estimation was adopted. The routine was then incorporated with the fuzzy technique to determine the appropriate control gains while maintaining the stability of the system. A set of fuzzy parameters and control rules was then obtained from the estimated perturbation. During the commanded motion, undesirable oscillations were suppressed by applying feedback control voltages to the piezoceramic actuators. These feedback voltages were determined by the sliding mode controller with perturbation estimation.

Matsuno and Yamamoto [44] have considered the problem of dynamic hybrid position/force control of a planar two link rigid-flexible manipulator. B-spline functions were used for an approximation of the elastic deformation of the flexible link. On the basis of the singular perturbation method, the model was reduced to a slow subsystem and a fast subsystem. A composite controller for the dynamic hybrid position/force control of the flexible manipulator was designed. Although the system matrices of the fast subsystem depended on the manipulator configuration, the controller for the fast subsystem was designed on the basis of the fixed matrices, which were obtained for a specific manipulator configuration. For the fast subsystem, state feedback control was used. For the slow subsystem, PD type control plus force feedback was used.

1.4 Discussions on Previous Studies

In this section, a discussion is made on previously mentioned studies and drawbacks of some of the studies are mentioned.

In the studies of Luca and Siciliano [2], Feliu and Rattan [5], Qian and Ma [8], Asada et al. [11], Gawronski et al. [13], Chalhoub and Ulsoy [15], Moallem et al. [26] and Bodur and Sezer [30], flexible one link was examined and most of them proposed the control strategies for this specific case. The flexible one link case is too simple to capture the coupling effects between rigid body and deformation dynamics.

Zhu et al. [4], Ge et al. [6], Luca et al. [9], Xi [12], Chalhoub and Ulsoy [15], Carusone and D'Eleuterio [17], Chen and Yeung [24], Nathan and Singh [25], Pham et al. [31], Choi and Krishnamurthy [35], Siciliano and Villani [39] and Hu and Ulsoy [40] designed the controllers based on joint variables. Joint space motion control of the manipulator may be easier, but for a flexible arm, it is more meaningful to directly control the end effector trajectory so that the tip position error will be minimum.

In the studies of Luca et al. [9], Bayo et al. [10], Ider et al. [18], Yim [22], Chen and Yeung [24], Nathan and Singh [25], Arteaga and Siciliano [32], Shi et al. [38], Yim and Singh [41] and Choi et al. [42], the rigid body dynamics and/or deformation dynamics linearization required. When the degree of freedom of the robot increases, linearization most probably becomes harder.

Actually tip positioning was taken into consideration by Siciliano and Villani [39]. When the desired tip position is time varying, a different Lyapunov argument should be worked out in the algorithms. In the algorithms, the inverse kinematics problem was formulated in differential terms by deriving a Jacobian that related the joint and deflection rates to the tip rate. In the solution algorithms, the Jacobian was employed, but it might not exactly be suitable for this case as it was originally developed for rigid manipulators even though the Jacobian employed in the algorithm was obtained by correcting it with two terms that accounted for the static deflection due to gravity and contact force.

In the study of Matsuno et al. [36], no controller was designed for the deviation from the quasi-static equations to guarantee the stability of the system. Link densities and tip point mass were assumed so small to simplify the equations, but this is not always the case. Derivation of the dynamic equations and the controller developed were very dependent to the robot taken into consideration. It was also assumed that tip deflection of link 1 was very small compared to the tip deflection of link 2. Tracking errors in the transient responses of the joint angles were observed in the case study results. The errors were most probably caused by this deflection approximation.

Singular perturbation approach was used by Ge et al. [6], Moallem et al. [14], Vandegrift et al. [27] and Matsuno and Yamamoto [44]. In this method, the link stiffness is assumed to be large enough so that a two-time scale model of the flexible manipulator is derived. In other words, the flexible motion of the link cannot affect the rigid motion of the link as the link stiffness is large. However, in flexible arms, the flexible motion of the link affects the rigid motion of the link.

1.5 The Outline of the Thesis

In this thesis, alternative control methods are developed for the unconstrained motion and constrained force and motion control of robots having flexible links.

The main advantage of the developed control methods is that no linearization of the dynamic equations is required but conventional linear control techniques are used based on the fact that the system can be rendered “slowly varying” with proper closed loop pole locations [49], [50]. Thus, implementation of the developed control methods are easy which is especially important for high degree of freedom robots having flexible arms. The developed control methods are designed based on the tip point variables, therefore better tracking quality is obtained compared to the control methods designed based on the joint variables assuming that the tip point variables are measured precisely.

The thesis is organized as five chapters. Contents of each chapter are summarized below.

Following Chapter 1, the control methods, their stability and controllability analyses are given in Chapter 2. The dynamic equations of a flexible robot are partitioned as pseudostatic equilibrium equations and deviations from them. The pseudostatic equilibrium considered here is defined as a hypothetical state where the tip point variables have their desired values while the modal variables are instantaneously constant. Then, the control torques for the pseudostatic equilibrium and for the stabilization of the deviation equations are formed in terms of tip point coordinates, modal variables and contact force components. In the constrained force and motion control method, the tip point coordinates are expressed in terms of the contact surface coordinates using the constraint equations. These coordinates describe the position of the tip point on the contact surface.

For the closed loop system to be asymptotically stable it must be slowly varying as defined in references [49], [50]. The stability condition is achieved by placing the poles at a sufficient distance from the imaginary axis [50].

Avoiding from the singularities is a necessary condition to obtain a controllable system. However, it may not be sufficient alone. Actually, the necessary and sufficient condition is that the controllability matrix be of full rank, where the controllability matrix is defined based on the state space representation of the system.

An incremental rotary optical encoder is the most popular sensor to monitor a joint variable of a robot. Typically, encoder angular resolutions ranging from 1.44 degrees down to 0.0036 degrees are achievable [45]. Strains are measured to calculate the modal variables. Probably the most sensitive strain gauge is the semiconductor gauge for this aim. A $\pm 1\%$ accuracy is typical, and this is a fundamental limit on accuracy in stress analysis applications [46]. On a flexible link, strains can be measured at those locations where the maximum stresses occur for each mode. These locations can be determined from the mode shapes of the flexible link. Contact force sensors generally placed between the end effector and last joint of the manipulator. Such a sensor consists of a mechanical structure instrumented with strain gauges which can measure the forces and torques acting on the end effector. Typically, these sensors also have $\pm 1\%$ accuracy [47]. Optical devices may also be used to measure the position of the tip point [48], [10]. It is recommended that they should be kept close to the tip point as much as possible. New technologies continue to improve the sensitivities of the sensors. The rates of the position and modal variables can be obtained by numerically differentiating their measured values.

Chapter 3 is devoted to model the flexible multibody systems. Different modeling approaches for flexible multibody systems and different discretization methods for flexible arms are used while modeling the planar and spatial robots. Planar two link robot with flexible forearm is modeled by using the relative coordinates approach and its flexible arm is discretized by using the assumed modes method.

On the other hand, spatial three link robot with two flexible arms is modeled by using the absolute coordinates approach and its flexible arms are discretized by using the finite element method. Then, an alternative form of dynamic equations, which has necessary and sufficient number of generalized coordinates and equations, is given for the controller design.

Applications of the control methods investigated in Chapter 2 are given in Chapters 4 and 5. A ninth order hermite polynomial is used to describe the reference motion trajectory and a cycloidal rise, a constant level and a cycloidal return constitute the reference variation for the contact force. Simulations are performed by programs written in MATLAB[®].

Planar robot simulations are presented in Chapter 4. Uncontrolled motion of the planar robot is simulated to verify the dynamic equations. In order to determine the effectiveness of the control methods the unconstrained motion and constrained force and motion control simulations are presented for the planar robot. Unmodeled dynamics of higher order is taken into consideration to illustrate the performance of the control method in such a case. Then, unconstrained motion and constrained force and motion control simulations are presented again. Motion control of the planar flexible robot by using the computed torque method with the rigidity assumption is also simulated for a comparison with the proposed method.

Spatial robot simulations are presented in Chapter 5. Uncontrolled motion of the spatial robot is simulated to verify the dynamic equations. After that, unconstrained motion and constrained force and motion control simulations are presented for the spatial robot. As a next step, measurement noises are taken into consideration. Then, by filtering the measured variables, unconstrained motion and constrained force and motion control simulations are presented again to illustrate the performance of the control method with the presence of measurement noises.

Finally, Chapter 6 gives the concluding remarks and also discusses possible further extensions of this work.

CHAPTER 2

CONTROLLER DESIGNS FOR UNCONSTRAINED MOTION AND CONSTRAINED FORCE AND MOTION OF FLEXIBLE ROBOTS

In this section, new control methods are proposed for the motion control and force and motion control of flexible robots. In these methods, the dynamic equations of a flexible robot are partitioned as pseudostatic equilibrium equations and deviations from them. The pseudostatic equilibrium considered here is defined as a hypothetical state where the tip point variables have their desired values while the modal variables are instantaneously constant. Then, the control torques for the pseudostatic equilibrium and for the stabilization of the deviation equations are formed in terms of tip point coordinates, modal variables and contact force components.

2.1 Motion Control Method for Flexible Robots

The dynamic equations of the unconstrained motion of a robotic manipulator with flexible links can be written as

$$\mathbf{M}(\boldsymbol{\beta})\ddot{\boldsymbol{\beta}} + \mathbf{C}(\boldsymbol{\beta}, \dot{\boldsymbol{\beta}})\dot{\boldsymbol{\beta}} + \mathbf{f}^s(\boldsymbol{\eta}) + \mathbf{f}^g(\boldsymbol{\beta}) = \mathbf{f}^e(\boldsymbol{\beta}) \quad (2.1)$$

where $\boldsymbol{\beta}$ is the vector of generalized coordinates of the system and is given more explicitly as

$$\boldsymbol{\beta} = \begin{bmatrix} \mathbf{q} \\ \boldsymbol{\eta} \end{bmatrix} \quad (2.2)$$

\mathbf{q} is the vector of joint variables and is expressed as

$$\mathbf{q} = \begin{bmatrix} \theta_1 \\ \theta_2 \\ \vdots \\ \theta_n \end{bmatrix} \quad (2.3)$$

where n is the number of joint variables. $\boldsymbol{\eta}$ is the vector of the elastic deflection variables (also called as modal variables) of all the links and is expressed as

$$\boldsymbol{\eta} = \begin{bmatrix} \eta_1 \\ \eta_2 \\ \vdots \\ \eta_m \end{bmatrix} \quad (2.4)$$

where m is the number of the modal variables. $\mathbf{M}(\boldsymbol{\beta})$ is the generalized mass matrix, $\mathbf{C}(\boldsymbol{\beta}, \dot{\boldsymbol{\beta}})$ is the matrix corresponding to the generalized Coriolis and centrifugal force vector, $\mathbf{f}^s(\boldsymbol{\eta})$, $\mathbf{f}^g(\boldsymbol{\beta})$ and $\mathbf{f}^e(\boldsymbol{\beta})$ are the generalized structural stiffness, gravitational and external force vectors, respectively. The dynamic equations of the unconstrained motion of the robotic system can be partitioned in the form of

$$\begin{bmatrix} \mathbf{M}_{rr}(\mathbf{q}, \boldsymbol{\eta}) & \mathbf{M}_{re}(\mathbf{q}, \boldsymbol{\eta}) \\ \mathbf{M}_{er}(\mathbf{q}, \boldsymbol{\eta}) & \mathbf{M}_{ee}(\mathbf{q}, \boldsymbol{\eta}) \end{bmatrix} \begin{bmatrix} \ddot{\mathbf{q}} \\ \ddot{\boldsymbol{\eta}} \end{bmatrix} + \begin{bmatrix} \mathbf{C}_{rr}(\mathbf{q}, \dot{\mathbf{q}}, \boldsymbol{\eta}, \dot{\boldsymbol{\eta}}) & \mathbf{C}_{re}(\mathbf{q}, \dot{\mathbf{q}}, \boldsymbol{\eta}, \dot{\boldsymbol{\eta}}) \\ \mathbf{C}_{er}(\mathbf{q}, \dot{\mathbf{q}}, \boldsymbol{\eta}, \dot{\boldsymbol{\eta}}) & \mathbf{C}_{ee}(\mathbf{q}, \dot{\mathbf{q}}, \boldsymbol{\eta}, \dot{\boldsymbol{\eta}}) \end{bmatrix} \begin{bmatrix} \dot{\mathbf{q}} \\ \dot{\boldsymbol{\eta}} \end{bmatrix} + \begin{bmatrix} \mathbf{0} & \mathbf{0} \\ \mathbf{0} & \mathbf{K}_{ee} \end{bmatrix} \begin{bmatrix} \mathbf{q} \\ \boldsymbol{\eta} \end{bmatrix} + \begin{bmatrix} \mathbf{G}_r(\mathbf{q}, \boldsymbol{\eta}) \\ \mathbf{G}_e(\mathbf{q}, \boldsymbol{\eta}) \end{bmatrix} = \begin{bmatrix} \mathbf{L}_r(\mathbf{q}, \boldsymbol{\eta}) \\ \mathbf{L}_e(\mathbf{q}, \boldsymbol{\eta}) \end{bmatrix} \mathbf{T} \quad (2.5)$$

where subscripts r and e refer to the rigid and elastic partitions, respectively, \mathbf{K} is the matrix corresponding to the structural stiffnesses of the links, \mathbf{T} is the vector of the actuating forces and torques, \mathbf{L} is the matrix corresponding to \mathbf{T} and \mathbf{T} is expressed as

$$\mathbf{T} = \begin{bmatrix} \mathbf{T}_1 \\ \mathbf{T}_2 \\ \vdots \\ \mathbf{T}_n \end{bmatrix} \quad (2.6)$$

The tip point position of the manipulator can be written in terms of the joint and elastic deflection variables as

$$\mathbf{P} = \mathbf{P}(\mathbf{q}, \boldsymbol{\eta}) \quad (2.7)$$

The derivative of the above equation can be expressed as

$$\dot{\mathbf{P}} = \mathbf{J}\dot{\mathbf{q}} + \mathbf{H}\dot{\boldsymbol{\eta}} \quad (2.8)$$

where the Jacobian matrices \mathbf{J} and \mathbf{H} are given as

$$\mathbf{J} = \frac{\partial \mathbf{P}}{\partial \mathbf{q}} \quad (2.9)$$

$$\mathbf{H} = \frac{\partial \mathbf{P}}{\partial \boldsymbol{\eta}} \quad (2.10)$$

As long as $\det(\mathbf{J}) \neq 0$, i.e. in the absence of any kinematic singularity, $\dot{\mathbf{q}}$ can be obtained from Equation (2.8) as follows

$$\dot{\mathbf{q}} = \mathbf{J}^{-1}(\dot{\mathbf{P}} - \mathbf{H}\dot{\boldsymbol{\eta}}) \quad (2.11)$$

The second derivative of Equation (2.7) can be expressed as

$$\ddot{\mathbf{P}} = \mathbf{J}\ddot{\mathbf{q}} + \mathbf{H}\ddot{\boldsymbol{\eta}} + \dot{\mathbf{J}}\dot{\mathbf{q}} + \dot{\mathbf{H}}\dot{\boldsymbol{\eta}} \quad (2.12)$$

By using Equations (2.12) and (2.11), $\ddot{\mathbf{q}}$ can be obtained as

$$\ddot{\mathbf{q}} = \mathbf{J}^{-1}\ddot{\mathbf{P}} - \mathbf{J}^{-1}\mathbf{H}\ddot{\boldsymbol{\eta}} - \mathbf{J}^{-1}\dot{\mathbf{J}}\mathbf{J}^{-1}\dot{\mathbf{P}} + \mathbf{J}^{-1}(\dot{\mathbf{J}}\mathbf{J}^{-1}\mathbf{H} - \dot{\mathbf{H}})\dot{\boldsymbol{\eta}} \quad (2.13)$$

If Equations (2.11) and (2.13) are substituted into Equation (2.5), the dynamic equations of the unconstrained motion of the robotic system are obtained in terms of the tip point position and modal variables as

$$\mathbf{N}_{rr}\ddot{\mathbf{P}} + \mathbf{N}_{re}\ddot{\boldsymbol{\eta}} + \mathbf{V}_{rr}\dot{\mathbf{P}} + \mathbf{V}_{re}\dot{\boldsymbol{\eta}} + \mathbf{G}_r = \mathbf{L}_r\mathbf{T} \quad (2.14)$$

$$\mathbf{N}_{er}\ddot{\mathbf{P}} + \mathbf{N}_{ee}\ddot{\boldsymbol{\eta}} + \mathbf{V}_{er}\dot{\mathbf{P}} + \mathbf{V}_{ee}\dot{\boldsymbol{\eta}} + \mathbf{K}_{ee}\boldsymbol{\eta} + \mathbf{G}_e = \mathbf{L}_e\mathbf{T} \quad (2.15)$$

where \mathbf{N}_{rr} , \mathbf{N}_{re} , \mathbf{N}_{er} , \mathbf{N}_{ee} , \mathbf{V}_{rr} , \mathbf{V}_{re} , \mathbf{V}_{er} and \mathbf{V}_{ee} are expressed as

$$\mathbf{N}_{rr} = \mathbf{M}_{rr}\mathbf{J}^{-1} \quad (2.16)$$

$$\mathbf{N}_{re} = -\mathbf{M}_{rr}\mathbf{J}^{-1}\mathbf{H} + \mathbf{M}_{re} \quad (2.17)$$

$$\mathbf{N}_{er} = \mathbf{M}_{er}\mathbf{J}^{-1} \quad (2.18)$$

$$\mathbf{N}_{ee} = -\mathbf{M}_{er}\mathbf{J}^{-1}\mathbf{H} + \mathbf{M}_{ee} \quad (2.19)$$

$$\mathbf{V}_{rr} = -\mathbf{M}_{rr}\mathbf{J}^{-1}\dot{\mathbf{J}}\mathbf{J}^{-1} + \mathbf{C}_{rr}\mathbf{J}^{-1} \quad (2.20)$$

$$\mathbf{V}_{re} = \mathbf{M}_{rr}\mathbf{J}^{-1}(\dot{\mathbf{J}}\mathbf{J}^{-1}\mathbf{H} - \dot{\mathbf{H}}) - \mathbf{C}_{rr}\mathbf{J}^{-1}\mathbf{H} + \mathbf{C}_{re} \quad (2.21)$$

$$\mathbf{V}_{er} = -\mathbf{M}_{er}\mathbf{J}^{-1}\dot{\mathbf{J}}\mathbf{J}^{-1} + \mathbf{C}_{er}\mathbf{J}^{-1} \quad (2.22)$$

$$\mathbf{V}_{ee} = \mathbf{M}_{er}\mathbf{J}^{-1}(\dot{\mathbf{J}}\mathbf{J}^{-1}\mathbf{H} - \dot{\mathbf{H}}) - \mathbf{C}_{er}\mathbf{J}^{-1}\mathbf{H} + \mathbf{C}_{ee} \quad (2.23)$$

The tip point position, the modal and the actuating input variables can be partitioned as

$$\mathbf{P} = \mathbf{P}^* + \mathbf{P}' \quad (2.24)$$

$$\boldsymbol{\eta} = \boldsymbol{\eta}^* + \boldsymbol{\eta}' \quad (2.25)$$

$$\mathbf{T} = \mathbf{T}^* + \mathbf{T}' \quad (2.26)$$

where \mathbf{P}^* denotes the desired tip point position, \mathbf{P}' denotes the deviation from the desired tip point position, $\boldsymbol{\eta}^*$ consists of the pseudostatic modal variables, $\boldsymbol{\eta}'$ denotes the deviation from the pseudostatic modal variables, \mathbf{T}^* is the vector of

pseudostatic torques and \mathbf{T}' is the vector of stabilization torques applied to minimize the deviation from the desired tip point trajectory.

The pseudostatic equilibrium is defined as a state such that \mathbf{N}_{ij} , \mathbf{V}_{ij} , \mathbf{K}_{ii} , \mathbf{G}_i , and \mathbf{L}_i are assumed to be frozen at their instantaneous values and $\boldsymbol{\eta}^*$ is determined as the instantaneously constant elastic deflection vector corresponding to $\ddot{\mathbf{P}}^*$, $\dot{\mathbf{P}}^*$, and gravitational acceleration, g . Thus, the following equations can be written at the pseudostatic equilibrium:

$$\boldsymbol{\eta} = \boldsymbol{\eta}^* \quad (2.27)$$

$$\dot{\boldsymbol{\eta}} \cong \mathbf{0} \quad (2.28)$$

$$\ddot{\boldsymbol{\eta}} \cong \mathbf{0} \quad (2.29)$$

Therefore, at the pseudostatic equilibrium, the dynamic equations given in Equations (2.14) and (2.15) take the following form

$$\mathbf{N}_{rr} \ddot{\mathbf{P}}^* + \mathbf{V}_{rr} \dot{\mathbf{P}}^* + \mathbf{G}_r = \mathbf{L}_r \mathbf{T}^* \quad (2.30)$$

$$\mathbf{N}_{er} \ddot{\mathbf{P}}^* + \mathbf{V}_{er} \dot{\mathbf{P}}^* + \mathbf{K}_{ee} \boldsymbol{\eta}^* + \mathbf{G}_e = \mathbf{L}_e \mathbf{T}^* \quad (2.31)$$

\mathbf{T}^* and $\boldsymbol{\eta}^*$ can be expressed in terms of $\ddot{\mathbf{P}}^*$, $\dot{\mathbf{P}}^*$, and g from Equations (2.30) and (2.31) as

$$\begin{bmatrix} \mathbf{T}^* \\ \boldsymbol{\eta}^* \end{bmatrix} = \begin{bmatrix} \mathbf{L}_r & \mathbf{0} \\ \mathbf{L}_e & -\mathbf{K}_{ee} \end{bmatrix}^{-1} \begin{bmatrix} \mathbf{N}_{rr} \ddot{\mathbf{P}}^* + \mathbf{V}_{rr} \dot{\mathbf{P}}^* + \mathbf{G}_r \\ \mathbf{N}_{er} \ddot{\mathbf{P}}^* + \mathbf{V}_{er} \dot{\mathbf{P}}^* + \mathbf{G}_e \end{bmatrix} \quad (2.32)$$

provided that the indicated inverse matrix exists. Otherwise, the manipulator will be in an actuation singularity. If Equation (2.30) is subtracted from Equation (2.14) and Equation (2.31) is subtracted from Equation (2.15), the following deviation equations are obtained

$$\mathbf{N}_{rr} \ddot{\mathbf{P}}' + \mathbf{N}_{re} \ddot{\boldsymbol{\eta}}' + \mathbf{V}_{rr} \dot{\mathbf{P}}' + \mathbf{V}_{re} \dot{\boldsymbol{\eta}}' = \mathbf{L}_r \mathbf{T}' - (\mathbf{N}_{re} \ddot{\boldsymbol{\eta}}^* + \mathbf{V}_{re} \dot{\boldsymbol{\eta}}^*) \quad (2.33)$$

$$\mathbf{N}_{er}\ddot{\mathbf{P}}' + \mathbf{N}_{ce}\ddot{\boldsymbol{\eta}}' + \mathbf{V}_{er}\dot{\mathbf{P}}' + \mathbf{V}_{ce}\dot{\boldsymbol{\eta}}' + \mathbf{K}_{ce}\boldsymbol{\eta}' = \mathbf{L}_e\mathbf{T}' - (\mathbf{N}_{ce}\ddot{\boldsymbol{\eta}}^* + \mathbf{V}_{ce}\dot{\boldsymbol{\eta}}^*) \quad (2.34)$$

The above equations can be called as the deviation equations from the pseudostatic equilibrium. The terms in parentheses can be considered as the disturbances. Therefore, \mathbf{T}' is selected to stabilize the deviation equations (Equations (2.33) and (2.34)) according to the following feedback control action:

$$\mathbf{T}' = -\mathbf{S} \begin{bmatrix} \mathbf{P}' \\ \dot{\mathbf{P}}' \\ \boldsymbol{\eta}' \\ \dot{\boldsymbol{\eta}}' \end{bmatrix} \quad (2.35)$$

By using this input vector with a properly determined gain matrix \mathbf{S} , a stable solution can be obtained for the deviation equations (Equations (2.33) and (2.34)). \mathbf{S} may be determined either by minimizing a performance index or by using the pole placement method, which is preferred here. Equations (2.33) and (2.34) can also be written as

$$\begin{bmatrix} \ddot{\mathbf{P}}' \\ \ddot{\boldsymbol{\eta}}' \end{bmatrix} = \begin{bmatrix} \mathbf{A}_v & \mathbf{C}_v \\ \mathbf{B}_v & \mathbf{D}_v \end{bmatrix} \begin{bmatrix} \dot{\mathbf{P}}' \\ \dot{\boldsymbol{\eta}}' \end{bmatrix} + \begin{bmatrix} \mathbf{0} & \mathbf{C}_k \\ \mathbf{0} & \mathbf{D}_k \end{bmatrix} \begin{bmatrix} \mathbf{P}' \\ \boldsymbol{\eta}' \end{bmatrix} + \begin{bmatrix} \mathbf{A}_L \\ \mathbf{B}_L \end{bmatrix} \mathbf{T}' + \begin{bmatrix} \mathbf{A}_w \\ \mathbf{B}_w \end{bmatrix} \quad (2.36)$$

Hence, the state space representation of the deviation equations can be obtained as

$$\dot{\mathbf{x}}' = \mathbf{E}\mathbf{x}' + \mathbf{F}\mathbf{T}' + \mathbf{W} \quad (2.37)$$

where $\mathbf{x}' \in \mathfrak{R}^{2(n+m)}$ is the state vector, $\mathbf{E} \in \mathfrak{R}^{2(n+m) \times 2(n+m)}$ is the system matrix, $\mathbf{F} \in \mathfrak{R}^{2(n+m) \times n}$ is the input matrix, $\mathbf{T}' \in \mathfrak{R}^n$ is the control vector and $\mathbf{W} \in \mathfrak{R}^{2(n+m)}$ is the bias vector. They are defined as

$$\mathbf{x}' = \begin{bmatrix} \mathbf{P}' \\ \dot{\mathbf{P}}' \\ \boldsymbol{\eta}' \\ \dot{\boldsymbol{\eta}}' \end{bmatrix} \quad (2.38)$$

$$\mathbf{E} = \begin{bmatrix} \mathbf{0} & \mathbf{I} & \mathbf{0} & \mathbf{0} \\ \mathbf{0} & \mathbf{A}_v & \mathbf{C}_k & \mathbf{C}_v \\ \mathbf{0} & \mathbf{0} & \mathbf{0} & \mathbf{I} \\ \mathbf{0} & \mathbf{B}_v & \mathbf{D}_k & \mathbf{D}_v \end{bmatrix} \quad (2.39)$$

$$\mathbf{F} = \begin{bmatrix} \mathbf{0} \\ \mathbf{A}_L \\ \mathbf{0} \\ \mathbf{B}_L \end{bmatrix} \quad (2.40)$$

$$\mathbf{W} = \begin{bmatrix} \mathbf{0} \\ \mathbf{A}_w \\ \mathbf{0} \\ \mathbf{B}_w \end{bmatrix} \quad (2.41)$$

If Equation (2.35) is substituted into Equation (2.37), the following equation is obtained

$$\dot{\mathbf{x}}' = (\mathbf{E} - \mathbf{FS})\mathbf{x}' + \mathbf{W} \quad (2.42)$$

Therefore, \mathbf{S} has to be chosen such that the poles of Equation (2.42) are placed properly for stability.

In the first method, a pole placement algorithm is utilized in order to determine \mathbf{S} that corresponds to the selected pole locations.

In the other method, \mathbf{S} is found by using the optimal control theory. The performance index to be minimized may be selected as

$$J = \int_0^{\infty} (\mathbf{x}'^T \mathbf{Q} \mathbf{x}' + \mathbf{T}'^T \mathbf{R} \mathbf{T}') dt \quad (2.43)$$

where \mathbf{Q} and \mathbf{R} are appropriate positive definite symmetric matrices. The feedback control law is given by

$$\mathbf{T}' = -\mathbf{R}^{-1}\mathbf{F}^T\mathbf{D}\mathbf{x}' \quad (2.44)$$

where \mathbf{D} is the solution of the associated Riccati equation given as

$$\dot{\mathbf{D}} + \mathbf{D}\mathbf{E} - \mathbf{D}\mathbf{F}\mathbf{R}^{-1}\mathbf{F}^T\mathbf{D} + \mathbf{Q} + \mathbf{E}^T\mathbf{D} = \mathbf{0} \quad (2.45)$$

Equation (2.44) can be written as

$$\mathbf{T}' = -\mathbf{S}\mathbf{x}' \quad (2.46)$$

where \mathbf{S} is given as

$$\mathbf{S} = \mathbf{R}^{-1}\mathbf{F}^T\mathbf{D} \quad (2.47)$$

2.2 Force and Motion Control Method for Flexible Robots

The dynamic equations of the constrained motion of a robotic system with flexible links can be written as

$$\mathbf{M}(\boldsymbol{\beta})\ddot{\boldsymbol{\beta}} + \mathbf{C}(\boldsymbol{\beta}, \dot{\boldsymbol{\beta}})\dot{\boldsymbol{\beta}} + \mathbf{f}^s(\boldsymbol{\eta}) + \mathbf{f}^g(\boldsymbol{\beta}) = \mathbf{f}^e(\boldsymbol{\beta}) + \mathbf{f}^c(\boldsymbol{\beta}) \quad (2.48)$$

where $\mathbf{f}^c(\boldsymbol{\beta})$ is the generalized constraint force vector. The dynamic equations of the constrained motion of the robotic system can be partitioned in the following form

$$\begin{bmatrix} \mathbf{M}_{rr}(\mathbf{q}, \boldsymbol{\eta}) & \mathbf{M}_{re}(\mathbf{q}, \boldsymbol{\eta}) \\ \mathbf{M}_{er}(\mathbf{q}, \boldsymbol{\eta}) & \mathbf{M}_{ee}(\mathbf{q}, \boldsymbol{\eta}) \end{bmatrix} \begin{bmatrix} \ddot{\mathbf{q}} \\ \ddot{\boldsymbol{\eta}} \end{bmatrix} + \begin{bmatrix} \mathbf{C}_{rr}(\mathbf{q}, \dot{\mathbf{q}}, \boldsymbol{\eta}, \dot{\boldsymbol{\eta}}) & \mathbf{C}_{re}(\mathbf{q}, \dot{\mathbf{q}}, \boldsymbol{\eta}, \dot{\boldsymbol{\eta}}) \\ \mathbf{C}_{er}(\mathbf{q}, \dot{\mathbf{q}}, \boldsymbol{\eta}, \dot{\boldsymbol{\eta}}) & \mathbf{C}_{ee}(\mathbf{q}, \dot{\mathbf{q}}, \boldsymbol{\eta}, \dot{\boldsymbol{\eta}}) \end{bmatrix} \begin{bmatrix} \dot{\mathbf{q}} \\ \dot{\boldsymbol{\eta}} \end{bmatrix} + \begin{bmatrix} \mathbf{0} & \mathbf{0} \\ \mathbf{0} & \mathbf{K}_{ee} \end{bmatrix} \begin{bmatrix} \mathbf{q} \\ \boldsymbol{\eta} \end{bmatrix} + \begin{bmatrix} \mathbf{G}_r(\mathbf{q}, \boldsymbol{\eta}) \\ \mathbf{G}_e(\mathbf{q}, \boldsymbol{\eta}) \end{bmatrix} = \begin{bmatrix} \mathbf{L}_r(\mathbf{q}, \boldsymbol{\eta}) \\ \mathbf{L}_e(\mathbf{q}, \boldsymbol{\eta}) \end{bmatrix} \mathbf{T} + \begin{bmatrix} \mathbf{Z}_r(\mathbf{q}, \boldsymbol{\eta}) \\ \mathbf{Z}_e(\mathbf{q}, \boldsymbol{\eta}) \end{bmatrix} \boldsymbol{\lambda} \quad (2.49)$$

where $\boldsymbol{\lambda}$ is the vector of Lagrange multipliers which are perpendicular to the constraint surface and \mathbf{Z} is the matrix corresponding to $\boldsymbol{\lambda}$.

Similar to the unconstrained motion control, the dynamic equations of the constrained motion of the robotic system are obtained in terms of the tip point position and modal variables as

$$\mathbf{N}_{rr}\ddot{\mathbf{P}} + \mathbf{N}_{re}\ddot{\boldsymbol{\eta}} + \mathbf{V}_{rr}\dot{\mathbf{P}} + \mathbf{V}_{re}\dot{\boldsymbol{\eta}} + \mathbf{G}_r = \mathbf{L}_r\mathbf{T} + \mathbf{Z}_r\boldsymbol{\lambda} \quad (2.50)$$

$$\mathbf{N}_{er}\ddot{\mathbf{P}} + \mathbf{N}_{ee}\ddot{\boldsymbol{\eta}} + \mathbf{V}_{er}\dot{\mathbf{P}} + \mathbf{V}_{ee}\dot{\boldsymbol{\eta}} + \mathbf{K}_{ee}\boldsymbol{\eta} + \mathbf{G}_e = \mathbf{L}_e\mathbf{T} + \mathbf{Z}_e\boldsymbol{\lambda} \quad (2.51)$$

where \mathbf{N}_{rr} , \mathbf{N}_{re} , \mathbf{N}_{er} , \mathbf{N}_{ee} , \mathbf{V}_{rr} , \mathbf{V}_{re} , \mathbf{V}_{er} and \mathbf{V}_{ee} are expressed as

$$\mathbf{N}_{rr} = \mathbf{M}_{rr}\mathbf{J}^{-1} \quad (2.52)$$

$$\mathbf{N}_{re} = -\mathbf{M}_{rr}\mathbf{J}^{-1}\mathbf{H} + \mathbf{M}_{re} \quad (2.53)$$

$$\mathbf{N}_{er} = \mathbf{M}_{er}\mathbf{J}^{-1} \quad (2.54)$$

$$\mathbf{N}_{ee} = -\mathbf{M}_{er}\mathbf{J}^{-1}\mathbf{H} + \mathbf{M}_{ee} \quad (2.55)$$

$$\mathbf{V}_{rr} = -\mathbf{M}_{rr}\mathbf{J}^{-1}\dot{\mathbf{J}}\mathbf{J}^{-1} + \mathbf{C}_{rr}\mathbf{J}^{-1} \quad (2.56)$$

$$\mathbf{V}_{re} = \mathbf{M}_{rr}\mathbf{J}^{-1}(\dot{\mathbf{J}}\mathbf{J}^{-1}\mathbf{H} - \dot{\mathbf{H}}) - \mathbf{C}_{rr}\mathbf{J}^{-1}\mathbf{H} + \mathbf{C}_{re} \quad (2.57)$$

$$\mathbf{V}_{er} = -\mathbf{M}_{er}\mathbf{J}^{-1}\dot{\mathbf{J}}\mathbf{J}^{-1} + \mathbf{C}_{er}\mathbf{J}^{-1} \quad (2.58)$$

$$\mathbf{V}_{ee} = \mathbf{M}_{er}\mathbf{J}^{-1}(\dot{\mathbf{J}}\mathbf{J}^{-1}\mathbf{H} - \dot{\mathbf{H}}) - \mathbf{C}_{er}\mathbf{J}^{-1}\mathbf{H} + \mathbf{C}_{ee} \quad (2.59)$$

Constraint equations can be written in terms of tip point position variables as

$$\boldsymbol{\phi}(\mathbf{P}) = \mathbf{0} \quad (2.60)$$

where $\boldsymbol{\phi} \in \mathfrak{R}^k$, k is the number of constraint equations and $\mathbf{P} \in \mathfrak{R}^b$, b is the dimension of the tip point position vector. The derivative of Equation (2.60) can be expressed as

$$\boldsymbol{\Phi}\dot{\mathbf{P}} = \mathbf{0} \quad (2.61)$$

where $\Phi \in \mathfrak{R}^{k \times b}$ is given as

$$\Phi = \frac{\partial \phi}{\partial \mathbf{P}} \quad (2.62)$$

The tip point velocity components can be related to the rates of the contact surface coordinates as

$$\dot{\mathbf{P}} = \Psi \dot{\mathbf{s}} \quad (2.63)$$

where $\dot{\mathbf{s}} \in \mathfrak{R}^{b-k}$ represents the velocity vector tangent to the contact surface and $\Psi \in \mathfrak{R}^{b \times (b-k)}$. If Equation (2.63) is substituted into Equation (2.61), the following equation is obtained.

$$\Phi \Psi \dot{\mathbf{s}} = \mathbf{0} \quad (2.64)$$

Since $\dot{\mathbf{s}}$ is not identically equal to zero, Equation (2.64) is satisfied iff

$$\Phi \Psi = \mathbf{0} \quad (2.65)$$

The derivative of Equation (2.63) gives $\ddot{\mathbf{P}}$ as

$$\ddot{\mathbf{P}} = \Psi \ddot{\mathbf{s}} + \dot{\Psi} \dot{\mathbf{s}} \quad (2.66)$$

If Equations (2.63) and (2.66) are substituted into Equations (2.50) and (2.51), the following equations are obtained

$$\mathbf{R}_{rr} \ddot{\mathbf{s}} + \mathbf{R}_{re} \ddot{\boldsymbol{\eta}} + \mathbf{Y}_{rr} \dot{\mathbf{s}} + \mathbf{Y}_{re} \dot{\boldsymbol{\eta}} + \mathbf{G}_r = \mathbf{L}_r \mathbf{T} + \mathbf{Z}_r \boldsymbol{\lambda} \quad (2.67)$$

$$\mathbf{R}_{er} \ddot{\mathbf{s}} + \mathbf{R}_{ee} \ddot{\boldsymbol{\eta}} + \mathbf{Y}_{er} \dot{\mathbf{s}} + \mathbf{Y}_{ee} \dot{\boldsymbol{\eta}} + \mathbf{K}_{ee} \boldsymbol{\eta} + \mathbf{G}_e = \mathbf{L}_e \mathbf{T} + \mathbf{Z}_e \boldsymbol{\lambda} \quad (2.68)$$

where \mathbf{R}_{rr} , \mathbf{R}_{re} , \mathbf{R}_{er} , \mathbf{R}_{ee} , \mathbf{Y}_{rr} , \mathbf{Y}_{re} , \mathbf{Y}_{er} and \mathbf{Y}_{ee} are expressed as

$$\mathbf{R}_{rr} = \mathbf{N}_{rr} \Psi \quad (2.69)$$

$$\mathbf{R}_{re} = \mathbf{N}_{re} \quad (2.70)$$

$$\mathbf{R}_{er} = \mathbf{N}_{er} \Psi \quad (2.71)$$

$$\mathbf{R}_{ee} = \mathbf{N}_{ee} \quad (2.72)$$

$$\mathbf{Y}_{rr} = \mathbf{N}_{rr} \dot{\Psi} + \mathbf{V}_{rr} \Psi \quad (2.73)$$

$$\mathbf{Y}_{re} = \mathbf{V}_{re} \quad (2.74)$$

$$\mathbf{Y}_{er} = \mathbf{N}_{er} \dot{\Psi} + \mathbf{V}_{er} \Psi \quad (2.75)$$

$$\mathbf{Y}_{ee} = \mathbf{V}_{ee} \quad (2.76)$$

The vectors of contact surface coordinates, the modal variables, the actuating inputs and the Lagrange multipliers can be partitioned as

$$\mathbf{s} = \mathbf{s}^* + \mathbf{s}' \quad (2.77)$$

$$\boldsymbol{\eta} = \boldsymbol{\eta}^* + \boldsymbol{\eta}' \quad (2.78)$$

$$\mathbf{T} = \mathbf{T}^* + \mathbf{T}' \quad (2.79)$$

$$\boldsymbol{\lambda} = \boldsymbol{\lambda}^* + \boldsymbol{\lambda}' \quad (2.80)$$

where \mathbf{s}^* denotes the desired trajectory, \mathbf{s}' denotes the deviation from the desired trajectory, $\boldsymbol{\eta}^*$ is the vector of pseudostatic modal variables, $\boldsymbol{\eta}'$ is the deviation from $\boldsymbol{\eta}^*$, \mathbf{T}^* is the vector of pseudostatic torques and \mathbf{T}' is the vector of deviational stabilization torques, $\boldsymbol{\lambda}^*$ is the vector of desired Lagrange multipliers and $\boldsymbol{\lambda}'$ is the deviation from $\boldsymbol{\lambda}^*$.

As before, at the pseudostatic equilibrium, the following equations can be written:

$$\boldsymbol{\eta} = \boldsymbol{\eta}^* \quad (2.81)$$

$$\dot{\boldsymbol{\eta}} \cong \mathbf{0} \quad (2.82)$$

$$\ddot{\boldsymbol{\eta}} \cong \mathbf{0} \quad (2.83)$$

Therefore, at the pseudostatic equilibrium, the dynamic equations given in Equations (2.67) and (2.68) take the following form

$$\mathbf{R}_{rr}\ddot{\mathbf{s}}^* + \mathbf{Y}_{rr}\dot{\mathbf{s}}^* + \mathbf{G}_r = \mathbf{L}_r\mathbf{T}^* + \mathbf{Z}_r\boldsymbol{\lambda}^* \quad (2.84)$$

$$\mathbf{R}_{er}\ddot{\mathbf{s}}^* + \mathbf{Y}_{er}\dot{\mathbf{s}}^* + \mathbf{K}_{ee}\boldsymbol{\eta}^* + \mathbf{G}_e = \mathbf{L}_e\mathbf{T}^* + \mathbf{Z}_e\boldsymbol{\lambda}^* \quad (2.85)$$

\mathbf{T}^* and $\boldsymbol{\eta}^*$ can be expressed in terms of $\ddot{\mathbf{s}}^*$, $\dot{\mathbf{s}}^*$, $\boldsymbol{\lambda}^*$ and \mathbf{g} from Equations (2.84) and (2.85) as

$$\begin{bmatrix} \mathbf{T}^* \\ \boldsymbol{\eta}^* \end{bmatrix} = \begin{bmatrix} \mathbf{L}_r & \mathbf{0} \\ \mathbf{L}_e & -\mathbf{K}_{ee} \end{bmatrix}^{-1} \begin{bmatrix} \mathbf{R}_{rr}\ddot{\mathbf{s}}^* + \mathbf{Y}_{rr}\dot{\mathbf{s}}^* + \mathbf{G}_r - \mathbf{Z}_r\boldsymbol{\lambda}^* \\ \mathbf{R}_{er}\ddot{\mathbf{s}}^* + \mathbf{Y}_{er}\dot{\mathbf{s}}^* + \mathbf{G}_e - \mathbf{Z}_e\boldsymbol{\lambda}^* \end{bmatrix} \quad (2.86)$$

provided that the indicated inverse matrix exists. If Equation (2.84) is subtracted from Equation (2.67) and Equation (2.85) is subtracted from Equation (2.68), the following equations are obtained

$$\mathbf{R}_{rr}\dot{\mathbf{s}}' + \mathbf{R}_{re}\ddot{\boldsymbol{\eta}}' + \mathbf{Y}_{rr}\dot{\mathbf{s}}' + \mathbf{Y}_{re}\dot{\boldsymbol{\eta}}' = \mathbf{L}_r\mathbf{T}' + \mathbf{Z}_r\boldsymbol{\lambda}' - (\mathbf{R}_{re}\ddot{\boldsymbol{\eta}}^* + \mathbf{Y}_{re}\dot{\boldsymbol{\eta}}^*) \quad (2.87)$$

$$\mathbf{R}_{er}\dot{\mathbf{s}}' + \mathbf{R}_{ee}\ddot{\boldsymbol{\eta}}' + \mathbf{Y}_{er}\dot{\mathbf{s}}' + \mathbf{Y}_{ee}\dot{\boldsymbol{\eta}}' + \mathbf{K}_{ee}\boldsymbol{\eta}' = \mathbf{L}_e\mathbf{T}' + \mathbf{Z}_e\boldsymbol{\lambda}' - (\mathbf{R}_{ee}\ddot{\boldsymbol{\eta}}^* + \mathbf{Y}_{ee}\dot{\boldsymbol{\eta}}^*) \quad (2.88)$$

The above equations can be called as deviation equations from the pseudostatic equilibrium. The terms in parentheses can be considered as the disturbances. Therefore, \mathbf{T}' is selected to stabilize the deviation equations (Equations (2.87) and (2.88)). For the determination of \mathbf{T}' , methods similar to those given in the previous section can be used.

Equations (2.87) and (2.88) can be written in augmented form as

$$\begin{bmatrix} \mathbf{R}_{rr} & \mathbf{R}_{re} & -\mathbf{Z}_r \\ \mathbf{R}_{er} & \mathbf{R}_{ee} & -\mathbf{Z}_e \end{bmatrix} \begin{bmatrix} \ddot{\mathbf{s}}' \\ \ddot{\boldsymbol{\eta}}' \\ \boldsymbol{\lambda}' \end{bmatrix} + \begin{bmatrix} \mathbf{Y}_{rr} & \mathbf{Y}_{re} \\ \mathbf{Y}_{er} & \mathbf{Y}_{ee} \end{bmatrix} \begin{bmatrix} \dot{\mathbf{s}}' \\ \dot{\boldsymbol{\eta}}' \end{bmatrix} + \begin{bmatrix} \mathbf{0} & \mathbf{0} \\ \mathbf{0} & \mathbf{K}_{ee} \end{bmatrix} \begin{bmatrix} \mathbf{s}' \\ \boldsymbol{\eta}' \end{bmatrix} =$$

$$\begin{bmatrix} \mathbf{L}_r \\ \mathbf{L}_e \end{bmatrix} \mathbf{T}' - \begin{bmatrix} \mathbf{R}_{re} \dot{\boldsymbol{\eta}}^* + \mathbf{Y}_{re} \boldsymbol{\eta}^* \\ \mathbf{R}_{ee} \dot{\boldsymbol{\eta}}^* + \mathbf{Y}_{ee} \boldsymbol{\eta}^* \end{bmatrix} \quad (2.89)$$

This equation can also be written as

$$\begin{bmatrix} \ddot{\mathbf{s}}' \\ \ddot{\boldsymbol{\eta}}' \\ \boldsymbol{\lambda}' \end{bmatrix} = \begin{bmatrix} \mathbf{A}_v & \mathbf{D}_v \\ \mathbf{B}_v & \mathbf{E}_v \\ \mathbf{C}_v & \mathbf{F}_v \end{bmatrix} \begin{bmatrix} \dot{\mathbf{s}}' \\ \dot{\boldsymbol{\eta}}' \end{bmatrix} + \begin{bmatrix} \mathbf{0} & \mathbf{D}_k \\ \mathbf{0} & \mathbf{E}_k \\ \mathbf{0} & \mathbf{F}_k \end{bmatrix} \begin{bmatrix} \mathbf{s}' \\ \boldsymbol{\eta}' \end{bmatrix} + \begin{bmatrix} \mathbf{A}_L \\ \mathbf{B}_L \\ \mathbf{C}_L \end{bmatrix} \mathbf{T}' + \begin{bmatrix} \mathbf{A}_w \\ \mathbf{B}_w \\ \mathbf{C}_w \end{bmatrix} \quad (2.90)$$

Therefore, the state space representation of the deviation equations can be obtained as

$$\dot{\mathbf{x}}' = \mathbf{E}\mathbf{x}' + \mathbf{F}\mathbf{T}' + \mathbf{W} \quad (2.91)$$

where $\mathbf{x}' \in \mathfrak{R}^{(2(n+m)-k)}$ is the state vector, $\mathbf{E} \in \mathfrak{R}^{(2(n+m)-k) \times (2(n+m)-k)}$ is the system matrix, $\mathbf{F} \in \mathfrak{R}^{(2(n+m)-k) \times n}$ is the input matrix, $\mathbf{T}' \in \mathfrak{R}^n$ is the control vector and $\mathbf{W} \in \mathfrak{R}^{(2(n+m)-k)}$ is the bias vector. They are defined as follows:

$$\mathbf{x}' = \begin{bmatrix} \mathbf{s}' \\ \dot{\mathbf{s}}' \\ \boldsymbol{\eta}' \\ \dot{\boldsymbol{\eta}}' \\ \boldsymbol{\mu}' \end{bmatrix} \quad (2.92)$$

where $\boldsymbol{\mu}'$ is the impulse of $\boldsymbol{\lambda}'$, i.e.

$$\dot{\boldsymbol{\mu}}' = \boldsymbol{\lambda}' \quad (2.93)$$

$$\mathbf{E} = \begin{bmatrix} \mathbf{0} & \mathbf{I} & \mathbf{0} & \mathbf{0} & \mathbf{0} \\ \mathbf{0} & \mathbf{A}_v & \mathbf{D}_k & \mathbf{D}_v & \mathbf{0} \\ \mathbf{0} & \mathbf{0} & \mathbf{0} & \mathbf{I} & \mathbf{0} \\ \mathbf{0} & \mathbf{B}_v & \mathbf{E}_k & \mathbf{E}_v & \mathbf{0} \\ \mathbf{0} & \mathbf{C}_v & \mathbf{F}_k & \mathbf{F}_v & \mathbf{0} \end{bmatrix} \quad (2.94)$$

$$\mathbf{F} = \begin{bmatrix} \mathbf{0} \\ \mathbf{A}_L \\ \mathbf{0} \\ \mathbf{B}_L \\ \mathbf{C}_L \end{bmatrix} \quad (2.95)$$

$$\mathbf{W} = \begin{bmatrix} \mathbf{0} \\ \mathbf{A}_w \\ \mathbf{0} \\ \mathbf{B}_w \\ \mathbf{C}_w \end{bmatrix} \quad (2.96)$$

2.3 Measuring Systems

The success of controlling robots effectively depends on being able to obtain precise position and velocity information about the joints and/or the end effector. It is therefore necessary to have devices that provide such information. In particular, position, velocity, modal variables and contact force in constrained motion (or at least analog or digital representations of these quantities) must be measured to ensure that the robotic manipulator moves and applies force in a desired manner.

An incremental rotary optical encoder is the most popular sensor to monitor a joint variable of a robot. As the encoder shaft turns, the device outputs two square wave pulse trains 90 degrees out of phase. The shaft angle is determined by counting the number of pulses, and the direction of rotation is determined by the relative phase of the two square waves. The incremental encoder in its simplest form consists of a disk, a light emitting diode (LED), and a corresponding set of light receivers (e.g., phototransistors). The resolution of an encoder containing such a disk is normally defined as the number of lines, N . This implies that the encoder can resolve an angular position equal to $360 \text{ degrees}/N$. Typically, encoders with resolutions of 250, 512, 1000, 1024, even up to 100000 lines are available, meaning that angular resolutions ranging from 1.44 degrees down to 0.0036 degrees are achievable [45].

Strains are measured to calculate the modal variables. Probably the most sensitive strain gauge is the semiconductor gauge for this aim. The principle underlying the operation of a strain gauge is that a mechanical deformation produces a change in resistance of strain gauge. A Wheatstone bridge circuit is used to sense the change in gauge resistance and produce a voltage output as a result. Gauge is one arm of a Wheatstone bridge. A difficulty with this type of sensor is that variations in ambient temperature to change the gauge resistance, thereby causing the bridge to become unbalanced. It is possible to overcome such a problem by either (automatically) rebalancing the bridge periodically or by utilizing two gauges (and two bridges) and using the difference of their outputs as the actual sensing signal. The latter technique requires more circuitry but makes temperature drift a second order effect. A ± 1 percent accuracy is typical, and this is a fundamental limit on accuracy in stress analysis applications [46]. On a flexible link, strains can be measured at those locations where the maximum stresses occur for each mode. These locations can be determined from the mode shapes of the flexible link.

Contact force sensors generally placed between the end effector and last joint of the manipulator. These sensors are usually referred to as wrist sensors. Such a sensor consists of a mechanical structure instrumented with strain gauges which can measure the forces and torques acting on the end effector. Generally, semiconductor strain gauges are used in place of the foil types in these sensors to provide increased sensitivity. These sensors are capable of measuring from three to six components of the force/torque vector acting on the end effector. Typically, these sensors also have ± 1 percent accuracy [47].

Optical devices may also be used to measure the position of the tip point [48], [10]. It is recommended that they should be kept close to the tip point as much as possible. For example, Bayo et al. [10] mount a small infrared LED emitter at the tip point of the robot. A photodetector (optical xy position encoder) is hung approximately one meter above the arm and gives xy position of the robot tip point, by monitoring the movements of the mounted infrared LED. The optical position encoder uses lateral effect photodiode technology to encode the xy position of an infrared (440 nm - 1100 nm) point source. The output of the encoder

is filtered by the circuit (OP - EYE) and gives a resulting accuracy of better than ± 0.025 mm.

New technologies continue to improve the sensitivities of the sensors. The rates of the position and modal variables can be obtained by numerically differentiating their measured values.

2.4 Stability Considerations

As seen in the preceding sections, the control systems considered in this thesis have linear structures with variable coefficient matrices. Therefore, the following stability analysis validates the proposed controller designs based on the pole placement method. To investigate the stability of a linear time varying control system, consider the homogeneous equation associated with Equations (2.37) and (2.91), which can be written as

$$\dot{\mathbf{E}} = \mathbf{\Gamma}(t)\mathbf{E} \quad (2.97)$$

where $\mathbf{\Gamma}$ is given as

$$\mathbf{\Gamma} \equiv \mathbf{E} - \mathbf{F}\mathbf{S} \quad (2.98)$$

It is known that stability is not ensured by having only $\sigma_0 > 0$ such that [49]

$$\text{Re } \kappa_i(t) \leq -\sigma_0 < 0 \quad \forall i, \forall t \geq 0 \quad (2.99)$$

where κ_i , $i = 1, \dots, 2n$ are the closed loop eigenvalues of the system. However it can be shown that such a system is asymptotically stable when the variation of $\mathbf{\Gamma}$ is sufficiently slow as described in [49]-[51]. Desoer [50] showed that a time varying system is asymptotically stable at large if

$$\dot{\Gamma}_M \leq \frac{\sigma_0^2}{3m_c^4} \quad (2.100)$$

where σ_0 is as given by Equation (2.99), $\dot{\Gamma}_M$ is given as

$$\dot{\Gamma}_M = \sup_{t \geq 0} \|\dot{\Gamma}(t)\| \quad (2.101)$$

and m_c is a constant that satisfies

$$\|e^{\tau(t)}\| \leq m_c e^{-\tau(\sigma_0/2)} \quad \forall t \geq 0, \forall \tau \geq 0 \quad (2.102)$$

To see how σ_0 affects Equation (2.100) consider how $\dot{\Gamma}_M$ varies with σ_0 . The eigenvalue problems of Equations (2.37) and (2.91) can be written as

$$(\mathbf{E} - \mathbf{FS})\mathbf{h}_i = \kappa_i \mathbf{h}_i \quad (2.103)$$

where \mathbf{h}_i are the corresponding eigenvectors of eigenvalues κ_i . Equation (2.103) can also be expressed in the form

$$(\mathbf{E} - \kappa_i \mathbf{I})\mathbf{h}_i = \mathbf{F}\boldsymbol{\gamma}_i \quad (2.104)$$

where $\boldsymbol{\gamma}_i$ stands for

$$\boldsymbol{\gamma}_i = (\mathbf{S}\mathbf{h}_i) \quad (2.105)$$

\mathbf{S} can then be expressed as $\mathbf{S} = \mathbf{f}(\boldsymbol{\kappa}, \boldsymbol{\gamma}, t)$ where \mathbf{f} is a function such that the effect of $\boldsymbol{\kappa}$ on \mathbf{S} is in the order of $\boldsymbol{\kappa}$. In order to express $\dot{\Gamma}_M$, one can write

$$\dot{\mathbf{S}} = \frac{\partial \mathbf{f}}{\partial \boldsymbol{\kappa}} \dot{\boldsymbol{\kappa}} + \frac{\partial \mathbf{f}}{\partial \boldsymbol{\gamma}} \dot{\boldsymbol{\gamma}} + \frac{\partial \mathbf{f}}{\partial t} \quad (2.106)$$

Like $\boldsymbol{\kappa}$, $\dot{\boldsymbol{\kappa}}$ is also arbitrary, hence it can be chosen so that its dependence on $\boldsymbol{\kappa}$ is in the order of $\boldsymbol{\kappa}$. Also since $\boldsymbol{\gamma}$ and $\dot{\boldsymbol{\gamma}}$ are arbitrary they can be chosen independently of $\boldsymbol{\kappa}$. Therefore the effect of $\boldsymbol{\kappa}$ on $\dot{\boldsymbol{S}}$ is also in the order of $\boldsymbol{\kappa}$. Then,

$$\dot{\boldsymbol{\Gamma}} = \dot{\boldsymbol{E}} - \dot{\boldsymbol{F}}\boldsymbol{S} - \boldsymbol{F}\dot{\boldsymbol{S}} \quad (2.107)$$

Equation (2.107) implies that the effect of $\boldsymbol{\kappa}$ on $\dot{\boldsymbol{\Gamma}}$ is in the order of $\boldsymbol{\kappa}$. On the other hand,

$$\sigma_0 = \min_{t \geq 0} |\operatorname{Re} \kappa_1| \quad (2.108)$$

where κ_1 is the most dominant eigenvalue. Therefore the effect of σ_0 on $\dot{\boldsymbol{\Gamma}}_M$ is in the order of σ_0 , while the effect of σ_0 on the right hand side of Equation (2.100) is in the order of σ_0^2 . Hence by choosing a sufficiently large σ_0 , one can achieve asymptotic stability in the large.

As for the disturbance-like bias terms \boldsymbol{W} in Equations (2.37) and (2.91), they involve $\dot{\boldsymbol{\eta}}^*$ and $\ddot{\boldsymbol{\eta}}^*$, i.e. the first and second derivatives of the pseudostatic modal variables. Referring to the defining equations (Equations (2.30), (2.31) and Equations (2.84), (2.85)), it is seen that the most critical term that affects the magnitude of $\dot{\boldsymbol{\eta}}^*$ is the acceleration of the desired motion ($\ddot{\boldsymbol{P}}^*$ or $\ddot{\boldsymbol{s}}^*$). This implies that the desired motion must be specified to be continuous up to its second order jerk (i.e. up to $d^4\boldsymbol{P}^*/dt^4$ or $d^4\boldsymbol{s}^*/dt^4$) so that even $\ddot{\boldsymbol{\eta}}^*$ becomes a smoothly varying function of time. In addition to this continuity condition, it is recommended that the desired motion be selected to be slowly varying so that

$$\left\| \frac{d^4\boldsymbol{P}^*}{dt^4} \right\| \leq k_0 \|\boldsymbol{\kappa}_1\|^4 \quad \text{for all } t_0 \leq t \leq t_f \quad (2.109)$$

or

$$\left\| \frac{d^4 \mathbf{s}^*}{dt^4} \right\| \leq k_0' \|\mathbf{k}_1\|^4 \quad \text{for all } t_0 \leq t \leq t_f \quad (2.110)$$

where k_0 and k_0' are suitably selected constants. Then, all what \mathbf{W} causes is a bounded offset which can be suppressed to a desired level by means of sufficiently large control gains.

2.5 Controllability Considerations

Equations (2.11) and (2.32) indicate that the system will be controllable under the following necessary conditions:

$$\det(\mathbf{J}) \neq 0 \quad (2.111)$$

$$\det(\mathbf{\Lambda}) \neq 0 \quad (2.112)$$

where

$$\mathbf{\Lambda} = \begin{bmatrix} \mathbf{L}_r & \mathbf{0} \\ \mathbf{L}_e & -\mathbf{K}_{ee} \end{bmatrix} \quad (2.113)$$

Here, $\det(\mathbf{J})=0$ occurs in the case of kinematic singularities and $\det(\mathbf{\Lambda})=0$ occurs in the case of actuating singularities. On the other hand, if the matrices \mathbf{J} and $\mathbf{\Lambda}$ are not singular, then the controllability of the system can only be checked by looking at the rank of the controllability matrix defined as

$$\mathbf{CM} = [\mathbf{F} \quad \mathbf{EF} \quad \dots \quad \mathbf{E}^{2(n+m)-1}\mathbf{F}] \quad (2.114)$$

If \mathbf{F} has full rank n , then instead of looking at the rank of \mathbf{CM} one may also check the controllability of the system by looking at the rank of the matrix \mathbf{CI} defined as [52]

$$\mathbf{CI} = [\mathbf{F} \quad \mathbf{EF} \quad \dots \quad \mathbf{E}^{2(n+m)-n}\mathbf{F}] \quad (2.115)$$

In other words, checking the rank of \mathbf{CM} or \mathbf{CI} is the necessary and sufficient condition for the controllability of the system. Note that the size of \mathbf{CI} is smaller than that of \mathbf{CM} . So, it is more convenient to use.

As done in this thesis, a practical way of trajectory planning is to propose a candidate trajectory that satisfies the necessary conditions given in Equations (2.111) and (2.112), which are much easier to satisfy than the necessary and sufficient condition on the matrix \mathbf{CM} or \mathbf{CI} . Then, during the simulation if all the poles are placed as desired and if the proposed trajectory is successfully tracked, it is concluded that \mathbf{CM} or \mathbf{CI} condition is also satisfied on that trajectory. Thus, it can be used in an actual application.

CHAPTER 3

MODELING OF FLEXIBLE MULTIBODY SYSTEMS

3.1 Introduction

There are two basic approaches to model a mechanical system composed of rigid and flexible bodies. In the first approach, the motion of each body is formulated separately with respect to a fixed frame in terms of its absolute rigid body and elastic degrees of freedom. Then, the interconnections of the bodies are defined through a set of constraint equations. The second approach involves a recursive modeling in terms of the joint coordinates and elastic deformation variables. The formulation using the second approach results in a fewer number of equations but the expressions become longer. In this thesis, the mathematical modeling of planar two link flexible manipulator and spatial three link flexible manipulator are derived. The planar manipulator is modeled by using the latter method while the spatial manipulator is modeled by using the former method. Therefore, the expressions obtained for spatial manipulator are not too long.

For each flexible body, the elastic deformations are described relative to a body reference frame. The elastic deformation can be modeled by using assumed modes method or finite element method. Here, assumed modes method is used for the modeling of elastic deformations of the planar manipulator, while finite element method is used for the modeling of elastic deformations of the spatial manipulator. By using finite element method, any types of link geometry can be modeled.

3.2 Dynamic Modeling of Planar Two Link Manipulator with Flexible Forearm by Using Relative Coordinates

The planar two link manipulator with revolute joints depicted in Figure 3.1 is composed of a rigid upper arm and a flexible forearm. \mathbf{n} is fixed frame, $\mathbf{n}^{(1)}$ is Body 1 reference frame and $\mathbf{n}^{(2)}$ is Body 2 reference frame.

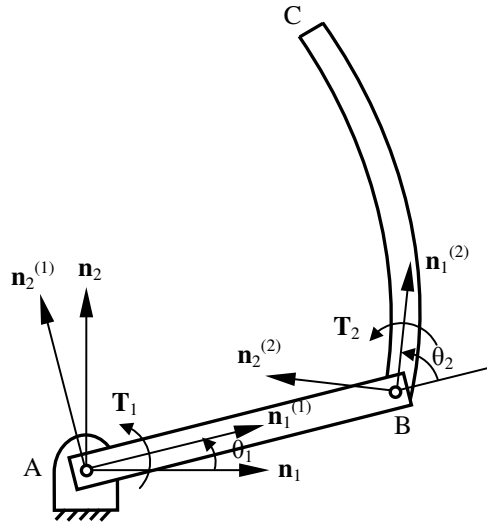


Figure 3.1 Planar two link manipulator with flexible forearm.

The dynamic equations are derived by using the relative coordinates approach. The flexible forearm is assumed to be Euler-Bernoulli beam (thin beam). By considering that the deformation displacement of the forearm is small enough to stay in the elastic range, it can be written as a sum of position dependent assumed mode shapes multiplied by the corresponding time dependent modal coordinates.

In the formulation, the numbers in parenthesis and the letter k as superscripts represent the body number. The overbar denotes that related variable is defined in related body reference frame. The vectors are column vectors. Boldface letters represent matrix or vector.

3.2.1 Position Vectors of Arbitrary Points of Each Body

The position vector of an arbitrary point of each body is obtained by summing the relative position vectors of the successive bodies. The position vector of an arbitrary point P of Body 1 can be written as

$$\mathbf{P}^{(1)} = \mathbf{r}^{(1)} \quad (3.1)$$

which can be written in the matrix form in Body 1 reference frame as

$$\bar{\mathbf{P}}^{(1)} = \bar{\mathbf{r}}^{(1)} = \begin{bmatrix} x^{(1)} \\ y^{(1)} \end{bmatrix} = \begin{bmatrix} \bar{r}_1^{(1)} \\ \bar{r}_2^{(1)} \end{bmatrix} \quad (3.2)$$

where $\bar{\mathbf{r}}^{(1)}$ is the position of point P of Body 1 with respect to Body 1 reference frame and $x^{(1)}$ and $y^{(1)}$ are the position components of point P of Body 1 in $\mathbf{n}_1^{(1)}$ and $\mathbf{n}_2^{(1)}$ axes, respectively. The position vector can be written in fixed frame as

$$\mathbf{P}^{(1)} = \mathbf{T}^{(1)} \bar{\mathbf{r}}^{(1)} \quad (3.3)$$

where $\mathbf{T}^{(1)}$ is the transformation matrix from Body 1 reference frame to fixed frame and it is given as

$$\mathbf{T}^{(1)} = \begin{bmatrix} c\theta_1 & -s\theta_1 \\ s\theta_1 & c\theta_1 \end{bmatrix} \quad (3.4)$$

where c stands for cosine and, s stands for sine and θ_1 is the joint angle of Body 1. The position vector of an arbitrary point P of Body 2 can be written as;

$$\mathbf{P}^{(2)} = \mathbf{d}^{(1)} + \mathbf{q}^{(2)} \quad (3.5)$$

$\mathbf{d}^{(1)}$ is the position vector from A to B. $\mathbf{q}^{(2)}$ is the position vector from B to P including undeformed position vector $\mathbf{r}^{(2)}$ and the deformation vector $\mathbf{u}^{(2)}$.

$$\mathbf{q}^{(2)} = \mathbf{r}^{(2)} + \mathbf{u}^{(2)} \quad (3.6)$$

Then, Equation (3.5) can be given in the following form in fixed frame

$$\mathbf{P}^{(2)} = \mathbf{T}^{(1)}\bar{\mathbf{d}}^{(1)} + \mathbf{T}^{(2)}\bar{\mathbf{q}}^{(2)} \quad (3.7)$$

where

$$\bar{\mathbf{d}}^{(1)} = \overline{\mathbf{AB}} = \begin{bmatrix} L_1 \\ 0 \end{bmatrix} \quad (3.8)$$

where L_1 is the length of Body 1.

$$\bar{\mathbf{q}}^{(2)} = \bar{\mathbf{r}}^{(2)} + \bar{\mathbf{u}}^{(2)} \quad (3.9)$$

where

$$\bar{\mathbf{r}}^{(2)} = \begin{bmatrix} x^{(2)} \\ y^{(2)} \end{bmatrix} = \begin{bmatrix} \bar{\mathbf{r}}_1^{(2)} \\ \bar{\mathbf{r}}_2^{(2)} \end{bmatrix} \quad (3.10)$$

where $\bar{\mathbf{r}}^{(2)}$ is the position of point P of Body 2 with respect to Body 2 reference frame at undeformed state and $x^{(2)}$ and $y^{(2)}$ are the position components of point P of Body 2 at undeformed state in $\mathbf{n}_1^{(2)}$ and $\mathbf{n}_2^{(2)}$ axes, respectively.

$$\bar{\mathbf{u}}^{(2)} = \boldsymbol{\phi}^{(2)}\boldsymbol{\eta}^{(2)} \quad (3.11)$$

where $\bar{\mathbf{u}}^{(2)}$ represents the deformation displacement of Body 2 with respect to Body 2 reference frame, $\boldsymbol{\phi}^{(2)}$ represents the shape function matrix of Body 2 and

$\boldsymbol{\eta}^{(2)}$ represents the vector of modal variables of Body 2. Thus, $\mathbf{P}^{(2)}$ can be written in the following form

$$\mathbf{P}^{(2)} = \mathbf{T}^{(1)}\bar{\mathbf{d}}^{(1)} + \mathbf{T}^{(2)}(\bar{\mathbf{r}}^{(2)} + \boldsymbol{\phi}^{(2)}\boldsymbol{\eta}^{(2)}) \quad (3.12)$$

where $\mathbf{T}^{(2)}$ represents the transformation matrix from Body 2 reference frame to fixed frame and is given by

$$\mathbf{T}^{(2)} = \mathbf{T}^{(1)}\mathbf{T}^{(1-2)} \quad (3.13)$$

where $\mathbf{T}^{(1-2)}$ is the transformation matrix from Body 2 reference frame to Body 1 reference frame and is denoted as

$$\mathbf{T}^{(1-2)} = \begin{bmatrix} c\theta_2 & -s\theta_2 \\ s\theta_2 & c\theta_2 \end{bmatrix} \quad (3.14)$$

where θ_2 is the joint angle of Body 2. Thus, $\mathbf{T}^{(2)}$ takes the following form

$$\mathbf{T}^{(2)} = \begin{bmatrix} c\theta_{12} & -s\theta_{12} \\ s\theta_{12} & c\theta_{12} \end{bmatrix} \quad (3.15)$$

where θ_{12} is given as

$$\theta_{12} = \theta_1 + \theta_2 \quad (3.16)$$

3.2.2 Velocities of Arbitrary Points of Each Body

Translational velocity of an arbitrary point P of Body k is obtained by taking the time derivative of position vector of point P. It can be represented in the following form

$$\mathbf{v}^k = \boldsymbol{\xi}^k \dot{\boldsymbol{\Omega}} + \mathbf{v}^k \dot{\boldsymbol{\eta}} \quad (3.17)$$

where $\boldsymbol{\xi}^k$ is the influence coefficient matrix related to the rigid body motion of Body k, $\dot{\boldsymbol{\Omega}}$ is the generalized speed vector related to the rigid body motion, \mathbf{v}^k is the influence coefficient matrix related to the elastic motion of Body k and $\dot{\boldsymbol{\eta}}$ is the derivative of vector of modal variables. Above equation can be written in the following form

$$\mathbf{v}^k = \boldsymbol{\mu}^k \dot{\mathbf{x}} \quad (3.18)$$

where $\boldsymbol{\mu}^k$ is the velocity influence coefficient matrix of Body k and given by

$$\boldsymbol{\mu}^k = \begin{bmatrix} \boldsymbol{\xi}^k & \mathbf{v}^k \end{bmatrix} \quad (3.19)$$

In Equation (3.18), $\dot{\mathbf{x}}$ is the time derivative of generalized coordinates \mathbf{x} which is given by

$$\mathbf{x} = \begin{bmatrix} \boldsymbol{\Omega} \\ \boldsymbol{\eta} \end{bmatrix} \quad (3.20)$$

Velocity of an arbitrary point P of Body 1 is obtained by taking the time derivative of position vector of the arbitrary point P of Body 1 (Equation (3.3)) as follows

$$\mathbf{v}^{(1)} = \dot{\mathbf{T}}^{(1)} \bar{\mathbf{r}}^{(1)} \quad (3.21)$$

$\dot{\mathbf{T}}^{(1)}$ can be written as

$$\dot{\mathbf{T}}^{(1)} = \mathbf{T}_\theta^{(1)} \dot{\boldsymbol{\theta}}_1 \quad (3.22)$$

where $\mathbf{T}_\theta^{(1)}$ is given as

$$\mathbf{T}_\theta^{(1)} = \begin{bmatrix} -s\theta_1 & -c\theta_1 \\ c\theta_1 & -s\theta_1 \end{bmatrix} \quad (3.23)$$

Therefore, $\mathbf{v}^{(1)}$ takes the following form

$$\mathbf{v}^{(1)} = \mathbf{T}_\theta^{(1)} \bar{\mathbf{r}}^{(1)} \dot{\theta}_1 \quad (3.24)$$

Equation (3.24) can be expressed as

$$\mathbf{v}^{(1)} = \boldsymbol{\xi}^{(1)} \dot{\boldsymbol{\Omega}} \quad (3.25)$$

where $\boldsymbol{\xi}^{(1)}$ is the influence coefficient matrix related to the rigid body motion of Body 1 and is given as

$$\boldsymbol{\xi}^{(1)} = \begin{bmatrix} \mathbf{T}_\theta^{(1)} \bar{\mathbf{r}}^{(1)} & \mathbf{0} \end{bmatrix} \quad (3.26)$$

$\dot{\boldsymbol{\Omega}}$ is given as

$$\dot{\boldsymbol{\Omega}} = \begin{bmatrix} \dot{\theta}_1 \\ \dot{\theta}_2 \end{bmatrix} \quad (3.27)$$

Velocity of an arbitrary point P of Body 2 is obtained by taking the time derivative of position vector Body 2 (Equation (3.12)) as follows

$$\mathbf{v}^{(2)} = \dot{\mathbf{T}}^{(1)} \bar{\mathbf{d}}^{(1)} + \dot{\mathbf{T}}^{(2)} \bar{\mathbf{q}}^{(2)} + \dot{\mathbf{T}}^{(2)} \boldsymbol{\phi}^{(2)} \dot{\boldsymbol{\eta}}^{(2)} \quad (3.28)$$

$\dot{\mathbf{T}}^{(2)}$ can be represented as

$$\dot{\mathbf{T}}^{(2)} = \mathbf{T}_\theta^{(2)} (\dot{\theta}_1 + \dot{\theta}_2) \quad (3.29)$$

where $\mathbf{T}_\theta^{(2)}$ is denoted as

$$\mathbf{T}_\theta^{(2)} = \begin{bmatrix} -s\theta_{12} & -c\theta_{12} \\ c\theta_{12} & -s\theta_{12} \end{bmatrix} \quad (3.30)$$

Thus, $\mathbf{v}^{(2)}$ becomes

$$\mathbf{v}^{(2)} = \mathbf{T}_\theta^{(1)} \bar{\mathbf{d}}^{(1)} \dot{\theta}_1 + \mathbf{T}_\theta^{(2)} \bar{\mathbf{q}}^{(2)} (\dot{\theta}_1 + \dot{\theta}_2) + \mathbf{T}^{(2)} \boldsymbol{\phi}^{(2)} \dot{\boldsymbol{\eta}}^{(2)} \quad (3.31)$$

Equation (3.31) can be denoted as

$$\mathbf{v}^{(2)} = \boldsymbol{\xi}^{(2)} \dot{\boldsymbol{\Omega}} + \mathbf{v}^{(2)} \dot{\boldsymbol{\eta}} \quad (3.32)$$

where $\boldsymbol{\xi}^{(2)}$ is the influence coefficient matrix related to the rigid body motion of Body 2 and is denoted as

$$\boldsymbol{\xi}^{(2)} = \left[\mathbf{T}_\theta^{(1)} \bar{\mathbf{d}}^{(1)} + \mathbf{T}_\theta^{(2)} \bar{\mathbf{q}}^{(2)} \quad \mathbf{T}_\theta^{(2)} \bar{\mathbf{q}}^{(2)} \right] \quad (3.33)$$

$\mathbf{v}^{(2)}$ is the influence coefficient matrix related to the elastic motion of Body 2 and is denoted as

$$\mathbf{v}^{(2)} = \mathbf{T}^{(2)} \boldsymbol{\phi}^{(2)} \quad (3.34)$$

$\dot{\boldsymbol{\eta}}$ is denoted as

$$\dot{\boldsymbol{\eta}} = \dot{\boldsymbol{\eta}}^{(2)} \quad (3.35)$$

3.2.3 Accelerations of Arbitrary Points of Each Body

Acceleration of an arbitrary point P of Body k is obtained by taking the time derivative of velocity vector of Body k. Acceleration of Body k can be represented in the following form

$$\mathbf{a}^k = \dot{\boldsymbol{\mu}}^k \dot{\mathbf{x}} + \boldsymbol{\mu}^k \ddot{\mathbf{x}} \quad (3.36)$$

where $\dot{\boldsymbol{\mu}}^k$ and $\ddot{\mathbf{x}}$ are given as

$$\dot{\boldsymbol{\mu}}^k = \begin{bmatrix} \dot{\boldsymbol{\xi}}^k & \dot{\mathbf{v}}^k \end{bmatrix} \quad (3.37)$$

$$\ddot{\mathbf{x}} = \begin{bmatrix} \ddot{\boldsymbol{\Omega}} \\ \ddot{\boldsymbol{\eta}} \end{bmatrix} \quad (3.38)$$

Acceleration of an arbitrary point P of Body 1 is obtained by taking the time derivative of Equation (3.25) as follows

$$\mathbf{a}^{(1)} = \begin{bmatrix} \dot{\mathbf{T}}_{\theta}^{(1)} \bar{\mathbf{r}}^{(1)} & \mathbf{0} \end{bmatrix} \begin{bmatrix} \dot{\theta}_1 \\ \dot{\theta}_2 \end{bmatrix} + \begin{bmatrix} \mathbf{T}_{\theta}^{(1)} \bar{\mathbf{r}}^{(1)} & \mathbf{0} \end{bmatrix} \begin{bmatrix} \ddot{\theta}_1 \\ \ddot{\theta}_2 \end{bmatrix} \quad (3.39)$$

$\dot{\mathbf{T}}_{\theta}^{(1)}$ is found as

$$\dot{\mathbf{T}}_{\theta}^{(1)} = -\mathbf{T}^{(1)} \dot{\boldsymbol{\theta}}_1 \quad (3.40)$$

Thus, Equation (3.39) can be represented as

$$\mathbf{a}^{(1)} = \dot{\boldsymbol{\xi}}^{(1)} \dot{\boldsymbol{\Omega}} + \boldsymbol{\xi}^{(1)} \ddot{\boldsymbol{\Omega}} \quad (3.41)$$

where $\dot{\boldsymbol{\xi}}^{(1)}$ is the rate of the influence coefficient matrix related to the rigid body motion of Body 1 and is given as

$$\dot{\boldsymbol{\xi}}^{(1)} = \begin{bmatrix} -\mathbf{T}^{(1)} \bar{\mathbf{r}}^{(1)} \dot{\boldsymbol{\theta}}_1 & \mathbf{0} \end{bmatrix} \quad (3.42)$$

$\ddot{\boldsymbol{\Omega}}$ is the rate of the generalized speeds vector related to the rigid body motion and is given as

$$\ddot{\mathbf{\Omega}} = \begin{bmatrix} \ddot{\theta}_1 \\ \ddot{\theta}_2 \end{bmatrix} \quad (3.43)$$

Acceleration of an arbitrary point P of Body 2 is obtained by taking the time derivative of Equation (3.32) as follows

$$\begin{aligned} \mathbf{a}^{(2)} = & \left[\dot{\mathbf{T}}_{\theta}^{(1)} \bar{\mathbf{d}}^{(1)} + \dot{\mathbf{T}}_{\theta}^{(2)} \bar{\mathbf{q}}^{(2)} + \mathbf{T}_{\theta}^{(2)} \boldsymbol{\phi}^{(2)} \dot{\boldsymbol{\eta}}^{(2)} \quad \dot{\mathbf{T}}_{\theta}^{(2)} \bar{\mathbf{q}}^{(2)} + \mathbf{T}_{\theta}^{(2)} \boldsymbol{\phi}^{(2)} \dot{\boldsymbol{\eta}}^{(2)} \right] \begin{bmatrix} \dot{\theta}_1 \\ \dot{\theta}_2 \end{bmatrix} + \\ & \left[\dot{\mathbf{T}}^{(2)} \boldsymbol{\phi}^{(2)} \right] \left[\dot{\boldsymbol{\eta}}^{(2)} \right] + \left[\mathbf{T}_{\theta}^{(1)} \bar{\mathbf{d}}^{(1)} + \mathbf{T}_{\theta}^{(2)} \bar{\mathbf{q}}^{(2)} \quad \mathbf{T}_{\theta}^{(2)} \bar{\mathbf{q}}^{(2)} \right] \begin{bmatrix} \ddot{\theta}_1 \\ \ddot{\theta}_2 \end{bmatrix} + \left[\mathbf{T}^{(2)} \boldsymbol{\phi}^{(2)} \right] \left[\ddot{\boldsymbol{\eta}}^{(2)} \right] \end{aligned} \quad (3.44)$$

$\dot{\mathbf{T}}_{\theta}^{(2)}$ can be written as

$$\dot{\mathbf{T}}_{\theta}^{(2)} = -\mathbf{T}^{(2)} (\dot{\theta}_1 + \dot{\theta}_2) \quad (3.45)$$

Hence, Equation (3.44) can be written as

$$\mathbf{a}^{(2)} = \boldsymbol{\xi}^{(2)} \dot{\mathbf{\Omega}} + \mathbf{v}^{(2)} \dot{\boldsymbol{\eta}} + \boldsymbol{\xi}^{(2)} \ddot{\mathbf{\Omega}} + \mathbf{v}^{(2)} \ddot{\boldsymbol{\eta}} \quad (3.46)$$

where $\boldsymbol{\xi}^{(2)}$ is the rate of the influence coefficient matrix related to the rigid body motion of Body 2 and is given as

$$\begin{aligned} \boldsymbol{\xi}^{(2)} = & \left[-\mathbf{T}^{(1)} \bar{\mathbf{d}}^{(1)} \dot{\theta}_1 - \mathbf{T}^{(2)} \bar{\mathbf{q}}^{(2)} (\dot{\theta}_1 + \dot{\theta}_2) + \mathbf{T}_{\theta}^{(2)} \boldsymbol{\phi}^{(2)} \dot{\boldsymbol{\eta}}^{(2)} \right. \\ & \left. - \mathbf{T}^{(2)} \bar{\mathbf{q}}^{(2)} (\dot{\theta}_1 + \dot{\theta}_2) + \mathbf{T}_{\theta}^{(2)} \boldsymbol{\phi}^{(2)} \dot{\boldsymbol{\eta}}^{(2)} \right] \end{aligned} \quad (3.47)$$

$\mathbf{v}^{(2)}$ is the rate of the influence coefficient matrix related to the elastic motion of Body 2 and is given as

$$\mathbf{v}^{(2)} = \mathbf{T}_{\theta}^{(2)} \boldsymbol{\phi}^{(2)} (\dot{\theta}_1 + \dot{\theta}_2) \quad (3.48)$$

$\ddot{\eta}$ is the second derivative of the vector of modal variables and is given as

$$\ddot{\eta} = \ddot{\eta}^{(2)} \quad (3.49)$$

3.2.4 Equations of Motion

The equations of motion of the flexible multibody system can be expressed by using the Kane's equations as follows [53]

$$\mathbf{f}^* + \mathbf{f} + \mathbf{f}^s = \mathbf{0} \quad (3.50)$$

where \mathbf{f}^* , \mathbf{f} and \mathbf{f}^s are the generalized inertia, external and structural stiffness forces, respectively. These terms are considered in detail in the following sections.

3.2.5 Generalized Inertia Forces

The generalized inertia forces due to inertias of the bodies are

$$\mathbf{f}^* = \sum_{k=1}^2 \int_{V_k} \boldsymbol{\mu}^{kT} (-\rho_k \mathbf{a}^k) dV \quad (3.51)$$

where ρ_k represents the density of Body k and V_k stands for the volume of Body k . By using Equation (3.36), the above equation can be expressed in the following form

$$\mathbf{f}^* = -\mathbf{M}\ddot{\mathbf{x}} + \mathbf{Q} \quad (3.52)$$

where \mathbf{M} is the generalized mass matrix of the whole system given by

$$\mathbf{M} = \sum_{k=1}^2 \mathbf{M}^k \quad (3.53)$$

where \mathbf{M}^k is the generalized mass matrix of Body k,

$$\mathbf{M}^k = \int_{V_k} \rho_k \boldsymbol{\mu}^{kT} \boldsymbol{\mu}^k dV \quad (3.54)$$

and \mathbf{Q} is the generalized Coriolis and centrifugal force vector of the whole system given by

$$\mathbf{Q} = \sum_{k=1}^2 \mathbf{Q}^k \quad (3.55)$$

where \mathbf{Q}^k is the generalized Coriolis and centrifugal force matrix of Body k,

$$\mathbf{Q}^k = - \int_{V_k} \rho_k \boldsymbol{\mu}^{kT} \dot{\boldsymbol{\mu}}^k \dot{\mathbf{x}} dV \quad (3.56)$$

Equation (3.54) can be written as

$$\mathbf{M}^k = \int_{V_k} \rho_k \begin{bmatrix} \boldsymbol{\xi}^{kT} \boldsymbol{\xi}^k & \boldsymbol{\xi}^{kT} \mathbf{v}^k \\ \mathbf{v}^{kT} \boldsymbol{\xi}^k & \mathbf{v}^{kT} \mathbf{v}^k \end{bmatrix} dV \quad (3.57)$$

In order to deal with each term separately, the submatrices of \mathbf{M}^k are labeled as below

$$\mathbf{M}^k = \begin{bmatrix} \mathbf{M}_{ir}^k & \mathbf{M}_{re}^k \\ \mathbf{M}_{re}^{kT} & \mathbf{M}_{ee}^k \end{bmatrix} \quad (3.58)$$

The submatrices of \mathbf{M}^k for each body are obtained as follows:

The submatrices of Body 1 are as follows

$$\mathbf{M}_{rr}^{(1)} = \int_{V_1} \rho_1 \begin{bmatrix} \bar{\mathbf{r}}^{(1)T} \bar{\mathbf{r}}^{(1)} & 0 \\ 0 & 0 \end{bmatrix} dV \quad (3.59)$$

$$\mathbf{M}_{re}^{(1)} = \mathbf{0} \quad (3.60)$$

$$\mathbf{M}_{ee}^{(1)} = \mathbf{0} \quad (3.61)$$

The submatrices of Body 2 are as follows

$$\mathbf{M}_{rr}^{(2)} = \begin{bmatrix} \mathbf{M}_{rr_{11}}^{(2)} & \mathbf{M}_{rr_{12}}^{(2)} \\ \mathbf{M}_{rr_{21}}^{(2)} & \mathbf{M}_{rr_{22}}^{(2)} \end{bmatrix} \quad (3.62)$$

$$\begin{aligned} \mathbf{M}_{rr_{11}}^{(2)} = & \left(\int_{V_2} \rho_2 dV \right) \bar{\mathbf{d}}^{(1)T} \bar{\mathbf{d}}^{(1)} + \bar{\mathbf{d}}^{(1)T} \mathbf{T}_\theta^{(1)T} \mathbf{T}_\theta^{(2)} \left(\int_{V_2} \rho_2 \bar{\mathbf{q}}^{(2)} dV \right) + \\ & \left(\int_{V_2} \rho_2 \bar{\mathbf{q}}^{(2)T} dV \right) \mathbf{T}_\theta^{(2)T} \mathbf{T}_\theta^{(1)} \bar{\mathbf{d}}^{(1)} + \int_{V_2} \rho_2 \bar{\mathbf{q}}^{(2)T} \bar{\mathbf{q}}^{(2)} dV \end{aligned} \quad (3.63)$$

$$\mathbf{M}_{rr_{12}}^{(2)} = \bar{\mathbf{d}}^{(1)T} \mathbf{T}_\theta^{(1)T} \mathbf{T}_\theta^{(2)} \left(\int_{V_2} \rho_2 \bar{\mathbf{q}}^{(2)} dV \right) + \int_{V_2} \rho_2 \bar{\mathbf{q}}^{(2)T} \bar{\mathbf{q}}^{(2)} dV \quad (3.64)$$

$$\mathbf{M}_{rr_{21}}^{(2)} = \left(\mathbf{M}_{rr_{12}}^{(2)} \right)^T \quad (3.65)$$

$$\mathbf{M}_{rr_{22}}^{(2)} = \int_{V_2} \rho_2 \bar{\mathbf{q}}^{(2)T} \bar{\mathbf{q}}^{(2)} dV \quad (3.66)$$

$$\mathbf{M}_{re}^{(2)} = \begin{bmatrix} \mathbf{M}_{re_1}^{(2)} \\ \mathbf{M}_{re_2}^{(2)} \end{bmatrix} \quad (3.67)$$

$$\mathbf{M}_{re_1}^{(2)} = \bar{\mathbf{d}}^{(1)T} \mathbf{T}_\theta^{(1)T} \mathbf{T}^{(2)} \left(\int_{V_2} \rho_2 \phi^{(2)} dV \right) + \int_{V_2} \rho_2 \bar{\mathbf{q}}^{(2)T} \mathbf{T}_\theta^{(2)T} \mathbf{T}^{(2)} \phi^{(2)} dV \quad (3.68)$$

$$\mathbf{M}_{re_2}^{(2)} = \int_{V_2} \rho_2 \bar{\mathbf{q}}^{(2)T} \mathbf{T}_\theta^{(2)T} \mathbf{T}^{(2)} \phi^{(2)} dV \quad (3.69)$$

$$\mathbf{M}_{ee}^{(2)} = \int_{V_2} \rho_2 \phi^{(2)T} \phi^{(2)} dV \quad (3.70)$$

Equation (3.56) can be written as

$$\mathbf{Q}^k = - \int_{V_k} \rho_k \begin{bmatrix} \boldsymbol{\xi}^{kT} \dot{\boldsymbol{\mu}}^k \dot{\mathbf{x}} \\ \mathbf{v}^{kT} \dot{\boldsymbol{\mu}}^k \dot{\mathbf{x}} \end{bmatrix} dV \quad (3.71)$$

In order to deal with each term separately, the submatrices of \mathbf{Q}^k are labeled as follows

$$\mathbf{Q}^k = \begin{bmatrix} \mathbf{Q}_r^k \\ \mathbf{Q}_e^k \end{bmatrix} \quad (3.72)$$

The submatrices of \mathbf{Q}^k for each body are obtained as follows:

The submatrices of Body 1 are as follows

$$\mathbf{Q}_r^{(1)} = \begin{bmatrix} \left(\int_{V_1} \rho \bar{\mathbf{r}}^{(1)T} \mathbf{T}_\theta^{(1)T} \mathbf{T}^{(1)} \bar{\mathbf{r}}^{(1)} dV \right) \dot{\boldsymbol{\theta}}_1 & 0 \\ 0 & \dot{\boldsymbol{\Omega}} \end{bmatrix} \quad (3.73)$$

$$\mathbf{Q}_e^{(1)} = \mathbf{0} \quad (3.74)$$

The submatrices of Body 2 are given by

$$\mathbf{Q}_r^{(2)} = \begin{bmatrix} \mathbf{Q}_{r_1}^{(2)} \\ \mathbf{Q}_{r_2}^{(2)} \end{bmatrix} \quad (3.75)$$

$$\begin{aligned} \mathbf{Q}_{r_1}^{(2)} = & \left[\left(\int_{V_2} \rho_2 dV \right) \bar{\mathbf{d}}^{(1)T} \mathbf{T}_\theta^{(1)T} \mathbf{T}^{(1)} \bar{\mathbf{d}}^{(1)} \dot{\boldsymbol{\theta}}_1 + \bar{\mathbf{d}}^{(1)T} \mathbf{T}_\theta^{(1)T} \mathbf{T}^{(2)} \left(\int_{V_2} \rho_2 \bar{\mathbf{q}}^{(2)} dV \right) (\dot{\boldsymbol{\theta}}_1 + \dot{\boldsymbol{\theta}}_2) - \right. \\ & \bar{\mathbf{d}}^{(1)T} \mathbf{T}_\theta^{(1)T} \mathbf{T}_\theta^{(2)} \left(\int_{V_2} \rho_2 \boldsymbol{\phi}^{(2)} dV \right) \dot{\boldsymbol{\eta}}^{(2)} + \left(\int_{V_2} \rho_2 \bar{\mathbf{q}}^{(2)T} dV \right) \mathbf{T}_\theta^{(2)T} \mathbf{T}^{(1)} \bar{\mathbf{d}}^{(1)} \dot{\boldsymbol{\theta}}_1 + \\ & \left. \left(\int_{V_2} \rho_2 \bar{\mathbf{q}}^{(2)T} \mathbf{T}_\theta^{(2)T} \mathbf{T}^{(2)} \bar{\mathbf{q}}^{(2)} dV \right) (\dot{\boldsymbol{\theta}}_1 + \dot{\boldsymbol{\theta}}_2) - \left(\int_{V_2} \rho_2 \bar{\mathbf{q}}^{(2)T} \boldsymbol{\phi}^{(2)} dV \right) \dot{\boldsymbol{\eta}}^{(2)} \right. \\ & \left. \bar{\mathbf{d}}^{(1)T} \mathbf{T}_\theta^{(1)T} \mathbf{T}^{(2)} \left(\int_{V_2} \rho_2 \bar{\mathbf{q}}^{(2)} dV \right) (\dot{\boldsymbol{\theta}}_1 + \dot{\boldsymbol{\theta}}_2) - \bar{\mathbf{d}}^{(1)T} \mathbf{T}_\theta^{(1)T} \mathbf{T}_\theta^{(2)} \left(\int_{V_2} \rho_2 \boldsymbol{\phi}^{(2)} dV \right) \dot{\boldsymbol{\eta}}^{(2)} + \right. \end{aligned}$$

$$\begin{aligned}
& \left(\int_{V_2} \rho_2 \bar{\mathbf{q}}^{(2)T} \mathbf{T}_\theta^{(2)T} \mathbf{T}^{(2)} \bar{\mathbf{q}}^{(2)} dV \right) (\dot{\theta}_1 + \dot{\theta}_2) - \left(\int_{V_2} \rho_2 \bar{\mathbf{q}}^{(2)T} \boldsymbol{\phi}^{(2)} dV \right) \dot{\boldsymbol{\eta}}^{(2)} \Big] \dot{\boldsymbol{\Omega}} + \\
& \left[-\bar{\mathbf{d}}^{(1)T} \mathbf{T}_\theta^{(1)T} \mathbf{T}_\theta^{(2)} \left(\int_{V_2} \rho_2 \boldsymbol{\phi}^{(2)} dV \right) (\dot{\theta}_1 + \dot{\theta}_2) - \left(\int_{V_2} \rho_2 \bar{\mathbf{q}}^{(2)T} \boldsymbol{\phi}^{(2)} dV \right) (\dot{\theta}_1 + \dot{\theta}_2) \right] \dot{\boldsymbol{\eta}}
\end{aligned} \tag{3.76}$$

$$\begin{aligned}
\mathbf{Q}_{I_2}^{(2)} = & \left[\left(\int_{V_2} \rho_2 \bar{\mathbf{q}}^{(2)T} dV \right) \mathbf{T}_\theta^{(2)T} \mathbf{T}^{(1)} \bar{\mathbf{d}}^{(1)} \dot{\theta}_1 + \left(\int_{V_2} \rho_2 \bar{\mathbf{q}}^{(2)T} \mathbf{T}_\theta^{(2)T} \mathbf{T}^{(2)} \bar{\mathbf{q}}^{(2)} dV \right) (\dot{\theta}_1 + \dot{\theta}_2) - \right. \\
& \left. \left(\int_{V_2} \rho_2 \bar{\mathbf{q}}^{(2)T} \boldsymbol{\phi}^{(2)} dV \right) \dot{\boldsymbol{\eta}}^{(2)} \left(\int_{V_2} \rho_2 \bar{\mathbf{q}}^{(2)T} \mathbf{T}_\theta^{(2)T} \mathbf{T}^{(2)} \bar{\mathbf{q}}^{(2)} dV \right) (\dot{\theta}_1 + \dot{\theta}_2) - \right. \\
& \left. \left(\int_{V_2} \rho_2 \bar{\mathbf{q}}^{(2)T} \boldsymbol{\phi}^{(2)} dV \right) \dot{\boldsymbol{\eta}}^{(2)} \right] \dot{\boldsymbol{\Omega}} + \left[- \left(\int_{V_2} \rho_2 \bar{\mathbf{q}}^{(2)T} \boldsymbol{\phi}^{(2)} dV \right) (\dot{\theta}_1 + \dot{\theta}_2) \right] \dot{\boldsymbol{\eta}}
\end{aligned} \tag{3.77}$$

$$\begin{aligned}
\mathbf{Q}_e^{(2)} = & \left[\left(\int_{V_2} \rho_2 \boldsymbol{\phi}^{(2)T} dV \right) \mathbf{T}^{(2)T} \mathbf{T}^{(1)} \bar{\mathbf{d}}^{(1)} \dot{\theta}_1 + \left(\int_{V_2} \rho_2 \boldsymbol{\phi}^{(2)T} \bar{\mathbf{q}}^{(2)} dV \right) (\dot{\theta}_1 + \dot{\theta}_2) - \right. \\
& \left. \left(\int_{V_2} \rho_2 \boldsymbol{\phi}^{(2)T} \mathbf{T}^{(2)T} \mathbf{T}_\theta^{(2)} \boldsymbol{\phi}^{(2)} dV \right) \dot{\boldsymbol{\eta}}^{(2)} \left(\int_{V_2} \rho_2 \boldsymbol{\phi}^{(2)T} \bar{\mathbf{q}}^{(2)} dV \right) (\dot{\theta}_1 + \dot{\theta}_2) - \right. \\
& \left. \left(\int_{V_2} \rho_2 \boldsymbol{\phi}^{(2)T} \mathbf{T}^{(2)T} \mathbf{T}_\theta^{(2)} \boldsymbol{\phi}^{(2)} dV \right) \dot{\boldsymbol{\eta}}^{(2)} \right] \dot{\boldsymbol{\Omega}} + \\
& \left[- \left(\int_{V_2} \rho_2 \boldsymbol{\phi}^{(2)T} \mathbf{T}^{(2)T} \mathbf{T}_\theta^{(2)} \boldsymbol{\phi}^{(2)} dV \right) (\dot{\theta}_1 + \dot{\theta}_2) \right] \dot{\boldsymbol{\eta}}
\end{aligned} \tag{3.78}$$

3.2.6 Generalized External Forces

The external forces applied to the body are classified in two groups:

a) Consider a torque acting on Body k. Then, the generalized forces due to external torque \mathbf{T} are

$$\mathbf{f}_i^{e^k} = \frac{\partial \boldsymbol{\omega}^k}{\partial x_i} \mathbf{T} \quad i = 1, 2, \dots, n+m \tag{3.79}$$

where n is the number of rigid generalized coordinates, m is the number elastic coordinates and $\boldsymbol{\omega}^k$ is the angular velocity of the frame attached to the point of application of torque \mathbf{T} . \mathbf{T}_1 and \mathbf{T}_2 are considered to be actuator torques applied to Body 1 and Body 2, respectively.

Generalized external force due to torque \mathbf{T}_1 is

$$f_i^e = \frac{\partial \boldsymbol{\omega}^{(1)T}}{\partial x_i} \mathbf{T}_1 \quad (3.80)$$

Equation (3.80) becomes

$$f_i^e = \frac{\partial \dot{\theta}_1}{\partial x_i} T_1 \quad (3.81)$$

In matrix form the following equation is obtained

$$\mathbf{f}^{e(T_1)} = \begin{bmatrix} T_1 \\ 0 \\ \mathbf{0} \end{bmatrix} \quad (3.82)$$

Generalized external force due to torque \mathbf{T}_2 is

$$f_i^e = \frac{\partial \boldsymbol{\omega}^{(2)T}}{\partial x_i} \mathbf{T}_2 - \frac{\partial \boldsymbol{\omega}^{(1)T}}{\partial x_i} \mathbf{T}_2 \quad (3.83)$$

This equation leads to

$$f_i^e = \frac{\partial \dot{\theta}_2}{\partial x_i} T_2 \quad (3.84)$$

Equation (3.84) yields the following equation

$$\mathbf{f}^{e(T_2)} = \begin{bmatrix} 0 \\ T_2 \\ \mathbf{0} \end{bmatrix} \quad (3.85)$$

Thus, total generalized external forces due to external forces are the summation of $\mathbf{f}^{e(T_1)}$ and $\mathbf{f}^{e(T_2)}$ which leads to

$$\mathbf{f}^e = \begin{bmatrix} T_1 \\ T_2 \\ \mathbf{0} \end{bmatrix} \quad (3.86)$$

b) Consider the gravitational force (body force). As the gravitational force applied to Body k, the total force on Body k is found to be

$$\mathbf{f}^{g^k} = \int_{V_k} \boldsymbol{\mu}^{kT} (\rho_k \mathbf{g} \mathbf{s}) dV \quad (3.87)$$

where \mathbf{g} is gravitational acceleration and \mathbf{s} is the unit vector along gravitational acceleration in fixed frame, i.e.,

$$\mathbf{s} = \begin{bmatrix} 0 \\ -1 \end{bmatrix} \quad (3.88)$$

As submatrices, Equation (3.87) can be obtained as

$$\mathbf{f}^{g^k} = \begin{bmatrix} \mathbf{g} \int_{V_k} \rho_k \boldsymbol{\xi}^{kT} dV \mathbf{s} \\ \mathbf{g} \int_{V_k} \rho_k \mathbf{v}^{kT} dV \mathbf{s} \end{bmatrix} \quad (3.89)$$

In order to deal with each term separately, the submatrices of \mathbf{f}^{g^k} are labelled as follows

$$\mathbf{f}^{g^k} = \begin{bmatrix} \mathbf{f}_r^{g^k} \\ \mathbf{f}_e^{g^k} \end{bmatrix} \quad (3.90)$$

The submatrices of generalized external forces of each body due to gravitational force are as follows:

The submatrices of Body 1 are as follows

$$\mathbf{f}_r^{g^{(1)}} = \begin{bmatrix} \mathbf{f}_{r_1}^{g^{(1)}} \\ \mathbf{f}_{r_2}^{g^{(1)}} \end{bmatrix} \quad (3.91)$$

$$\mathbf{f}_{r_1}^{g^{(1)}} = g \int_{V_1} \rho_1 \bar{\mathbf{r}}^{(1)T} dV \mathbf{T}_\theta^{(1)T} \mathbf{s} \quad (3.92)$$

$$\mathbf{f}_{r_2}^{g^{(1)}} = 0 \quad (3.93)$$

$$\mathbf{f}_e^{g^{(1)}} = \mathbf{0} \quad (3.94)$$

The submatrices of Body 2 are as follows

$$\mathbf{f}_r^{g^{(2)}} = \begin{bmatrix} \mathbf{f}_{r_1}^{g^{(2)}} \\ \mathbf{f}_{r_2}^{g^{(2)}} \end{bmatrix} \quad (3.95)$$

$$\mathbf{f}_{r_1}^{g^{(2)}} = g \left(\int_{V_2} \rho_2 dV \right) \bar{\mathbf{d}}^{(1)T} \mathbf{T}_\theta^{(1)T} \mathbf{s} + g \left(\int_{V_2} \rho_2 \bar{\mathbf{q}}^{(2)T} dV \right) \mathbf{T}_\theta^{(2)T} \mathbf{s} \quad (3.96)$$

$$\mathbf{f}_{r_2}^{g^{(2)}} = g \left(\int_{V_2} \rho_2 \bar{\mathbf{q}}^{(2)T} dV \right) \mathbf{T}_\theta^{(2)T} \mathbf{s} \quad (3.97)$$

$$\mathbf{f}_e^{g^{(2)}} = g \left(\int_{V_2} \rho_2 \bar{\boldsymbol{\phi}}^{(2)T} dV \right) \mathbf{T}^{(2)T} \mathbf{s} \quad (3.98)$$

Thus, total generalized external force due to gravitational force is the summation of each body contribution which can be represented as

$$\mathbf{f}^g = \sum_{k=1}^2 \mathbf{f}^{g^k} \quad (3.99)$$

3.2.7 Generalized Structural Stiffness Forces

Generalized structural stiffness forces are found from the work done by the stiffness forces which is equal to the negative of the strain energy of the Body k. Negative of the strain energy is written as

$$W_s^k = -\frac{1}{2} \int_0^L \left(\frac{\partial \theta_3^k}{\partial x} \right)^2 E^k I_3^k dx \quad (3.100)$$

where E^k is the modulus of elasticity of Body k, I_3^k is the second moment of area of the cross section of Body k about \mathbf{n}_3^k and $\theta_3^k(x, t)$ refers to the rotation of the centerline of Body k in its frame, which is given by

$$\theta_3^k = \frac{\partial}{\partial t} \delta_2^k \quad (3.101)$$

where δ_2^k is the bending of centerline of Body k which can be expressed as

$$\delta_2^k = Y_1 \eta_1 + Y_2 \eta_2 + \dots + Y_m \eta_m \quad (3.102)$$

where Y_i ($i = 1, \dots, m$) is the i th bending mode of Body k. Hence, $f^{s(2)}$ takes the following form

$$\mathbf{f}^{s(2)} = \begin{bmatrix} 0 \\ 0 \\ \frac{\partial W_s^{(2)}}{\partial \eta_1} \\ \frac{\partial W_s^{(2)}}{\partial \eta_2} \\ \vdots \\ \frac{\partial W_s^{(2)}}{\partial \eta_m} \end{bmatrix} \quad (3.103)$$

Equation (3.103) can be written as

$$\mathbf{f}^{s(2)} = \begin{bmatrix} 0 \\ 0 \\ f_{\eta_1}^{s(2)} \\ f_{\eta_2}^{s(2)} \\ \vdots \\ f_{\eta_m}^{s(2)} \end{bmatrix} = - \begin{bmatrix} 0 \\ 0 \\ \mathbf{K}^{(2)} \boldsymbol{\eta}^{(2)} \end{bmatrix} \quad (3.104)$$

where $\mathbf{K}^{(2)}$ represents the structural stiffness matrix of Body 2.

3.3 Dynamic Modeling of Spatial Three Link Manipulator with Two Flexible Arms by Using Absolute Coordinates

The spatial three link manipulator is depicted in Figure 3.2. Body 1 (or Link 1) is assumed to be rigid while Body 2 and Body 3 are taken as flexible. Lumped masses m_A , m_B and m_C are considered at points A, B and C, respectively. They represent actuators at points A and B and end effector and payload at point C.

The dynamic equations are derived by using the absolute coordinate approach. The flexible bodies are assumed to be Euler-Bernoulli beam. The deformation displacements of the flexible bodies are considered small so that they stay in the elastic range. The finite element method is used for the modeling of elastic deformation of the flexible bodies. The beams are discretized by two node beam

elements. The nodal variables are centerline deformation displacements and deformation rotations. The element axis frame \mathbf{n}^{ki} is located at one of the nodes. Since the beams are straight, the body reference frame and the element frames have same orientation at the undeformed state. Beam element shape functions are given in Appendix A.

In the formulation, the numbers in parenthesis and the letter k as superscripts represent the body number. The overbar and double overbar denote that related variable is defined in related body reference frame and related element frame, respectively. The vectors are column vectors. Boldface letters represent matrix or vector.

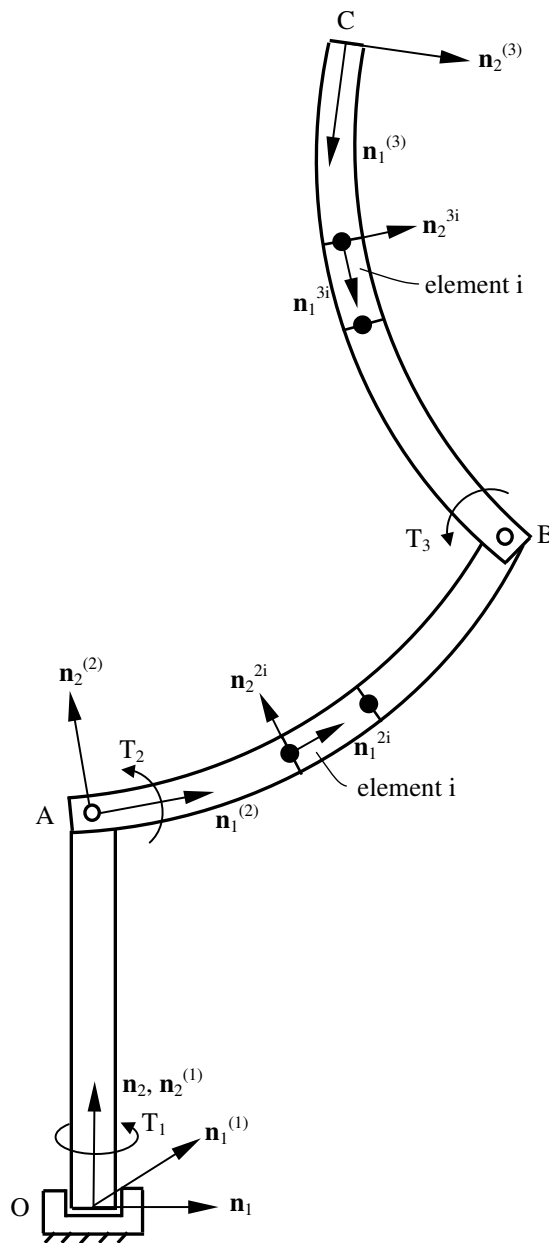


Figure 3.2 Spatial three link manipulator with two flexible arms.

3.3.1 Kinematic and Dynamic Equations of Each Body

Body 1

Position vector to arbitrary point P of Body 1 can be written as

$$\mathbf{R}^{(1)} = \mathbf{r}^{(1)} \tag{3.105}$$

Using components in fixed frame, $\mathbf{R}^{(1)}$ can be written as

$$\mathbf{R}^{(1)} = \mathbf{r}^{(1)} = \mathbf{T}^{(1)} \bar{\mathbf{r}}^{(1)} \quad (3.106)$$

where $\mathbf{r}^{(1)}$ is the position of point P of Body 1 expressed in fixed frame and $\bar{\mathbf{r}}^{(1)}$ is the position of point P of Body 1 expressed in Body 1 reference frame and is given as

$$\bar{\mathbf{r}}^{(1)} = \begin{bmatrix} \bar{r}_1^{(1)} \\ \bar{r}_2^{(1)} \\ \bar{r}_3^{(1)} \end{bmatrix} = \begin{bmatrix} x^{(1)} \\ y^{(1)} \\ z^{(1)} \end{bmatrix} \quad (3.107)$$

where $\bar{r}_1^{(1)}$, $\bar{r}_2^{(1)}$ and $\bar{r}_3^{(1)}$ and $x^{(1)}$, $y^{(1)}$ and $z^{(1)}$ are the position components of point P of Body 1 in $\mathbf{n}_1^{(1)}$, $\mathbf{n}_2^{(1)}$ and $\mathbf{n}_3^{(1)}$ axes, respectively. $\mathbf{T}^{(1)}$ is the transformation matrix from Body 1 reference frame to fixed frame. It can be expressed in terms of Euler angles, eg. by using the roll-pitch-yaw (1-2-3) sequence. Euler angles of Body 1 reference frame can be written in columnwise form as

$$\boldsymbol{\alpha}^{(1)} = \begin{bmatrix} \alpha_1 \\ \beta_1 \\ \gamma_1 \end{bmatrix} \quad (3.108)$$

where α_1 , β_1 and γ_1 are the roll, pitch, yaw Euler angles of Body 1 reference frame, respectively. It should be noted that roll and yaw motions do not occur for Body 1 reference frame. Therefore, $\mathbf{T}^{(1)}$ can be written as

$$\mathbf{T}^{(1)} = \begin{bmatrix} c\beta_1 & 0 & s\beta_1 \\ 0 & 1 & 0 \\ -s\beta_1 & 0 & c\beta_1 \end{bmatrix} \quad (3.109)$$

where c and s stand for cosine and sine, respectively. Generalized coordinates of Body 1, $\mathbf{x}^{(1)}$ can be chosen as Euler angles of Body 1 reference frame. Therefore, $\mathbf{x}^{(1)}$ can be written as

$$\mathbf{x}^{(1)} = \boldsymbol{\alpha}^{(1)} \quad (3.110)$$

Velocity of point P of Body 1 is obtained by taking the time derivative of position vector of point P of Body 1 as

$$\mathbf{v}^{(1)} = \dot{\mathbf{T}}^{(1)} \bar{\mathbf{r}}^{(1)} \quad (3.111)$$

Here $\dot{\mathbf{T}}^{(1)} \bar{\mathbf{r}}^{(1)}$ can be written in the following form

$$\dot{\mathbf{T}}^{(1)} \bar{\mathbf{r}}^{(1)} = \mathbf{T}^{(1)} \tilde{\mathbf{r}}^{(1)} \bar{\boldsymbol{\omega}}^{(1)} \quad (3.112)$$

where $\tilde{\mathbf{r}}^{(1)}$ is the skew symmetric matrix of the vector $\bar{\mathbf{r}}^{(1)}$, $\bar{\boldsymbol{\omega}}^{(1)}$ is the angular velocity of Body 1 reference frame expressed in the same frame and it can be written in terms of derivative of Euler angles of Body 1 reference frame as

$$\bar{\boldsymbol{\omega}}^{(1)} = \bar{\mathbf{D}}^{(1)} \dot{\boldsymbol{\alpha}}^{(1)} \quad (3.113)$$

where $\dot{\boldsymbol{\alpha}}^{(1)}$ is the derivative of Euler angles of Body 1 reference frame in columnwise form and is given as

$$\dot{\boldsymbol{\alpha}}^{(1)} = \begin{bmatrix} \dot{\alpha}_1 \\ \dot{\beta}_1 \\ \dot{\gamma}_1 \end{bmatrix} \quad (3.114)$$

$\bar{\mathbf{D}}^{(1)}$ is a transformation matrix from derivative of Euler angles of Body 1 reference frame to the angular velocity of Body 1 reference frame. It is expressed in Body 1 reference frame and is denoted as

$$\bar{\mathbf{D}}^{(1)} = \begin{bmatrix} c\beta_1 & 0 & 0 \\ 0 & 1 & 0 \\ s\beta_1 & 0 & 1 \end{bmatrix} \quad (3.115)$$

Therefore, Equation (3.112) can also be written as

$$\dot{\mathbf{T}}^{(1)}\bar{\mathbf{r}}^{(1)} = \mathbf{T}^{(1)}\tilde{\bar{\mathbf{r}}}^{(1)}\bar{\mathbf{D}}^{(1)}\dot{\boldsymbol{\alpha}}^{(1)} \quad (3.116)$$

One can choose a linear combination of the generalized coordinate derivatives as the generalized speeds of the body. For the rigid body rotation degrees of freedom, $\bar{\boldsymbol{\omega}}^{(1)}$ is the alternative to the Euler angle derivatives $\dot{\boldsymbol{\alpha}}^{(1)}$. Since $\bar{\boldsymbol{\omega}}^{(1)}$ yields simpler dynamic equations, it is chosen as the rotational generalized speeds. For this reason, $\mathbf{v}^{(1)}$ is written as below

$$\mathbf{v}^{(1)} = \mathbf{T}^{(1)}\tilde{\bar{\mathbf{r}}}^{(1)}\bar{\boldsymbol{\omega}}^{(1)} \quad (3.117)$$

Separating the coefficients of the generalized speeds, one has

$$\mathbf{v}^{(1)} = \boldsymbol{\mu}^{(1)}\mathbf{y}^{(1)} \quad (3.118)$$

where $\boldsymbol{\mu}^{(1)}$ is the velocity influence coefficient matrix of Body 1 and is given as

$$\boldsymbol{\mu}^{(1)} = \mathbf{T}^{(1)}\tilde{\bar{\mathbf{r}}}^{(1)} \quad (3.119)$$

$\mathbf{y}^{(1)}$ is the generalized speed vector of Body 1 and is given as

$$\mathbf{y}^{(1)} = \bar{\boldsymbol{\omega}}^{(1)} \quad (3.120)$$

Derivative of the generalized coordinates vector of Body 1 can be obtained from the generalized speed vector of Body 1 as

$$\dot{\boldsymbol{\alpha}}^{(1)} = \overline{\mathbf{D}}^{(1)-1} \overline{\boldsymbol{\omega}}^{(1)} \quad (3.121)$$

where inverse of the $\overline{\mathbf{D}}^{(1)}$ is given as

$$\overline{\mathbf{D}}^{(1)-1} = \begin{bmatrix} \frac{1}{c\beta_1} & 0 & 0 \\ 0 & 1 & 0 \\ -\frac{s\beta_1}{c\beta_1} & 0 & 1 \end{bmatrix} \quad (3.122)$$

$\beta_1 = \pm\pi/2$ and $\beta_1 = 3\pi/2$ are the singularities of the roll-pitch-yaw (1-2-3) sequence. At such positions, another sequence has to be used.

Acceleration of point P of Body 1 is obtained by taking the time derivative of the velocity vector of point P of Body 1 as

$$\mathbf{a}^{(1)} = \mathbf{T}^{(1)} \tilde{\mathbf{r}}^{(1)} \dot{\overline{\boldsymbol{\omega}}}^{(1)} + \dot{\mathbf{T}}^{(1)} \tilde{\mathbf{r}}^{(1)} \overline{\boldsymbol{\omega}}^{(1)} \quad (3.123)$$

which can be shortly written as

$$\mathbf{a}^{(1)} = \boldsymbol{\mu}^{(1)} \dot{\mathbf{y}}^{(1)} + \dot{\boldsymbol{\mu}}^{(1)} \mathbf{y}^{(1)} \quad (3.124)$$

where $\dot{\mathbf{y}}^{(1)}$ is the generalized acceleration vector of Body 1 and is given as

$$\dot{\mathbf{y}}^{(1)} = \dot{\overline{\boldsymbol{\omega}}}^{(1)} \quad (3.125)$$

$\boldsymbol{\mu}^{(1)} \dot{\mathbf{y}}^{(1)}$ consists of the terms involving the generalized accelerations as shown below

$$\boldsymbol{\mu}^{(1)} \dot{\mathbf{y}}^{(1)} = \mathbf{T}^{(1)} \tilde{\mathbf{r}}^{(1)} \dot{\overline{\boldsymbol{\omega}}}^{(1)} \quad (3.126)$$

$\dot{\boldsymbol{\mu}}^{(1)} \mathbf{y}^{(1)}$ involves the second order velocity terms, as shown below

$$\dot{\boldsymbol{\mu}}^{(1)} \mathbf{y}^{(1)} = -\mathbf{T}^{(1)} \tilde{\boldsymbol{\omega}}^{(1)} \tilde{\mathbf{r}}^{(1)} \bar{\boldsymbol{\omega}}^{(1)} \quad (3.127)$$

The dynamic equations of Body 1 can be derived by using the above kinematic expressions. Kane's equations are given as [53]

$$\mathbf{f}^{*(1)} + \mathbf{f}^{(1)} + \mathbf{f}_{m_A}^{*(1)} + \mathbf{f}_{m_A}^{(1)} = \mathbf{0} \quad (3.128)$$

where $\mathbf{f}^{*(1)}$ and $\mathbf{f}^{(1)}$ are the generalized inertia and external forces of Body 1, respectively. $\mathbf{f}_{m_A}^{*(1)}$ and $\mathbf{f}_{m_A}^{(1)}$ are the generalized inertia and external forces of lumped mass m_A at point A of Body 1, respectively.

The generalized inertia forces of Body 1 can be written as

$$\mathbf{f}^{*(1)} = \int_{V_1} \boldsymbol{\mu}^{(1)T} (-\rho_1 \mathbf{a}^{(1)}) dV \quad (3.129)$$

where ρ_1 represents the density of Body 1 material and V_1 stands for the volume of Body 1. Equation (3.129) can be expressed as the following form

$$\mathbf{f}^{*(1)} = -\mathbf{M}^{(1)} \dot{\mathbf{y}}^{(1)} + \mathbf{Q}^{(1)} \quad (3.130)$$

where $\mathbf{M}^{(1)}$ is the generalized mass matrix of Body 1 and is given as

$$\mathbf{M}^{(1)} = \int_{V_1} \rho_1 \boldsymbol{\mu}^{(1)T} \dot{\boldsymbol{\mu}}^{(1)} dV \quad (3.131)$$

$\mathbf{Q}^{(1)}$ is the generalized Coriolis and centrifugal force vector of Body 1 and is given as

$$\mathbf{Q}^{(1)} = -\int_{V_1} \rho_1 \boldsymbol{\mu}^{(1)T} \dot{\boldsymbol{\mu}}^{(1)} \mathbf{y}^{(1)} dV \quad (3.132)$$

$\mathbf{M}^{(1)}$ can be written in terms of the generalized coordinates of Body 1 by substituting the partitioned form of $\boldsymbol{\mu}^{(1)}$ into Equation (3.131) as follows

$$\mathbf{M}^{(1)} = \int_{V_1} \rho_1 \tilde{\mathbf{r}}^{(1)T} \tilde{\mathbf{r}}^{(1)} dV \quad (3.133)$$

which equals to

$$\mathbf{M}^{(1)} = \mathbf{I}^{(1)} \quad (3.134)$$

where $\mathbf{I}^{(1)}$ is the moment of inertia of Body 1 about its reference frame.

$\mathbf{Q}^{(1)}$ can be written in terms of the generalized coordinates and the generalized speeds by substituting the partitioned form of $\boldsymbol{\mu}^{(1)}$ into Equation (3.132) as follows

$$\mathbf{Q}^{(1)} = \int_{V_1} \rho_1 \tilde{\mathbf{r}}^{(1)T} \tilde{\boldsymbol{\omega}}^{(1)} \tilde{\mathbf{r}}^{(1)} dV \overline{\boldsymbol{\omega}}^{(1)} \quad (3.135)$$

It can be shown that by multiplying all matrices and rearranging terms, the above equation can be expressed as

$$\mathbf{Q}^{(1)} = \tilde{\boldsymbol{\omega}}^{(1)T} \mathbf{I}^{(1)} \overline{\boldsymbol{\omega}}^{(1)} \quad (3.136)$$

The generalized external force due to weight of Body 1 can be expressed as

$$\mathbf{f}^g{}^{(1)} = \int_{V_1} \boldsymbol{\mu}^{(1)T} (\rho_1 \mathbf{g} \mathbf{s}) dV \quad (3.137)$$

where g represents the gravitational acceleration and \mathbf{s} is a unit vector along gravitational acceleration in fixed frame and expressed as

$$\mathbf{s} = \begin{bmatrix} 0 \\ -1 \\ 0 \end{bmatrix} \quad (3.138)$$

After substituting $\boldsymbol{\mu}^{(1)}$ into Equation (3.137), it becomes

$$\mathbf{f}^{g(1)} = g \left(\int_{V_1} \rho_1 \tilde{\mathbf{r}}^{(1)T} dV \right) \mathbf{T}^{(1)T} \mathbf{s} \quad (3.139)$$

The generalized external force due to torque \mathbf{T}_1 can be expressed as

$$\mathbf{f}^{e(T_1)(1)} = \boldsymbol{\Omega}^{(1)T} \bar{\mathbf{T}}_1^{(1)} \quad (3.140)$$

where $\bar{\mathbf{T}}_1^{(1)}$ is the torque vector applied to Body 1 due to actuator at point O expressed in Body 1 reference frame and can be written as

$$\bar{\mathbf{T}}_1^{(1)} = \begin{bmatrix} 0 \\ T_1 \\ 0 \end{bmatrix} \quad (3.141)$$

where T_1 is the magnitude of the torque generated by the actuator at point O.

$\boldsymbol{\Omega}^{(1)}$ is the angular velocity influence coefficient matrix of Body 1 and it can be obtained as

$$\boldsymbol{\Omega}^{(1)} = \begin{bmatrix} 0 & 0 & 0 \\ 0 & 1 & 0 \\ 0 & 0 & 0 \end{bmatrix} \quad (3.142)$$

If Equations (3.141) and (3.142) are substituted into Equation (3.140), the following equation is obtained

$$\mathbf{f}^{e(T_1)^{(1)}} = \begin{bmatrix} 0 \\ T_1 \\ 0 \end{bmatrix} \quad (3.143)$$

The generalized external force due to torque T_2 can be expressed as

$$\mathbf{f}^{e(T_2)^{(1)}} = \boldsymbol{\Omega}^{(1)T} \bar{\mathbf{T}}_2^{(1)} \quad (3.144)$$

where $\bar{\mathbf{T}}_2^{(1)}$ is the torque vector applied to Body 1 due to actuator at point A expressed in Body 1 reference frame and can be written as

$$\bar{\mathbf{T}}_2^{(1)} = \begin{bmatrix} 0 \\ 0 \\ -T_2 \end{bmatrix} \quad (3.145)$$

where T_2 is the magnitude of the torque generated by the actuator at point A. If Equations (3.142) and (3.145) are substituted into Equation (3.144), the following equation is obtained

$$\mathbf{f}^{e(T_2)^{(1)}} = \begin{bmatrix} 0 \\ 0 \\ 0 \end{bmatrix} \quad (3.146)$$

The generalized inertia forces due to lumped mass m_A at point A of Body 1 can be written as

$$\mathbf{f}_{m_A}^{*(1)} = \boldsymbol{\mu}^A{}^T (-m_A \mathbf{a}^A) \quad (3.147)$$

where $\boldsymbol{\mu}^A$ is the velocity influence coefficient matrix of point A of Body 1 and \mathbf{a}^A is the acceleration of point A of Body 1. Equation (3.147) can be expressed as

$$\mathbf{f}_{m_A}^{*(1)} = -\mathbf{M}_{m_A}^{(1)} \dot{\mathbf{y}}^{(1)} + \mathbf{Q}_{m_A}^{(1)} \quad (3.148)$$

where $\mathbf{M}_{m_A}^{(1)}$ is the generalized mass matrix of lumped mass m_A and is given as

$$\mathbf{M}_{m_A}^{(1)} = m_A \tilde{\mathbf{r}}^{A_1 T} \tilde{\mathbf{r}}^{A_1} \quad (3.149)$$

where $\tilde{\mathbf{r}}^{A_1}$ is the position vector of point A of Body 1 and $\tilde{\mathbf{r}}^{A_1}$ is the skew symmetric matrix of the vector $\tilde{\mathbf{r}}^{A_1}$. $\mathbf{Q}_{m_A}^{(1)}$ is the generalized Coriolis and centrifugal force vector of lumped mass m_A and is given as

$$\mathbf{Q}_{m_A}^{(1)} = m_A \tilde{\mathbf{r}}^{A_1 T} \tilde{\boldsymbol{\omega}}^{(1)} \tilde{\mathbf{r}}^{A_1} \boldsymbol{\omega}^{(1)} \quad (3.150)$$

The generalized external force due weight of lumped mass m_A can be expressed as

$$\mathbf{f}_{m_A}^{g(1)} = \boldsymbol{\mu}^{A T} (m_A \mathbf{g} \mathbf{s}) \quad (3.151)$$

If $\boldsymbol{\mu}^A$ is substituted into above equation, the following equation is obtained

$$\mathbf{f}_{m_A}^{g(1)} = m_A \tilde{\mathbf{r}}^{A_1 T} \mathbf{T}^{(1) T} \mathbf{g} \mathbf{s} \quad (3.152)$$

Body 2

Position vector to arbitrary point P of element i of Body 2 can be written as

$$\mathbf{R}^{2i} = \boldsymbol{\zeta}^{(2)} + \mathbf{q}^{2i} \quad (3.153)$$

Using components in fixed frame, \mathbf{R}^{2i} can be written as

$$\mathbf{R}^{2i} = \boldsymbol{\zeta}^{(2)} + \mathbf{T}^{(2)}\bar{\mathbf{q}}^{2i} \quad (3.154)$$

where $\boldsymbol{\zeta}^{(2)}$ is the position vector from fixed frame to Body 2 reference frame. Here it is a constant vector and is denoted as

$$\boldsymbol{\zeta}^{(2)} = \begin{bmatrix} 0 \\ L_1 \\ 0 \end{bmatrix} \quad (3.155)$$

where L_1 stands for the length of Body 1. $\mathbf{T}^{(2)}$ is the transformation matrix from Body 2 reference frame to fixed frame. It can be expressed in terms of Euler angles, eg. by using the roll-pitch-yaw (1-2-3) sequence. Euler angles of Body 2 reference frame can be written in columnwise form as

$$\boldsymbol{\alpha}^{(2)} = \begin{bmatrix} \alpha_2 \\ \beta_2 \\ \gamma_2 \end{bmatrix} \quad (3.156)$$

where α_2 , β_2 and γ_2 are the roll, pitch, yaw Euler angles of Body 2 reference frame, respectively. It should be noted that roll motion is not required for Body 2 reference frame. Therefore, $\mathbf{T}^{(2)}$ takes the following form

$$\mathbf{T}^{(2)} = \begin{bmatrix} c\beta_2 c\gamma_2 & -c\beta_2 s\gamma_2 & s\beta_2 \\ s\gamma_2 & c\gamma_2 & 0 \\ -s\beta_2 c\gamma_2 & s\beta_2 s\gamma_2 & c\beta_2 \end{bmatrix} \quad (3.157)$$

$\bar{\mathbf{q}}^{2i}$ represents the position vector from Body 2 reference frame to point P of element i of Body 2 at deformed state expressed in Body 2 reference frame and is given as

$$\bar{\mathbf{q}}^{2i} = \bar{\mathbf{b}}^{2i} + \bar{\mathbf{r}}^{2i} + \bar{\mathbf{u}}^{2i} \quad (3.158)$$

where $\bar{\mathbf{b}}^{2i}$ represents the position vector from Body 2 reference frame to element i reference frame expressed in Body 2 reference frame, $\bar{\mathbf{r}}^{2i}$ represents the position vector from element i frame to point P at undeformed state expressed in Body 2 reference frame and $\bar{\mathbf{u}}^{2i}$ is the deformation displacement vector of point P of element i of Body 2 expressed in Body 2 reference frame and is given as

$$\bar{\mathbf{u}}^{2i} = \boldsymbol{\phi}^{2i} \bar{\boldsymbol{\alpha}}^{2i} \quad (3.159)$$

where $\boldsymbol{\phi}^{2i}$ is given as

$$\boldsymbol{\phi}^{2i} = \mathbf{T}^{2i} \mathbf{s}^{2i} \mathbf{R}^{2iT} \quad (3.160)$$

where \mathbf{T}^{2i} is the transformation matrix from element i of Body 2 frame to Body 2 reference frame and \mathbf{R}^{2i} is given as

$$\mathbf{R}^{2i} = \begin{bmatrix} \mathbf{T}^{2i} & & \mathbf{0} \\ & \ddots & \\ \mathbf{0} & & \mathbf{T}^{2i} \end{bmatrix} \quad (3.161)$$

Since all element frames and Body 2 reference frame are selected in the same orientation, at undeformed position \mathbf{T}^{2i} is 3 by 3 identity matrix and therefore \mathbf{R}^{2i} is 12 by 12 identity matrix. \mathbf{s}^{2i} is the shape function matrix of element i of Body 2. $\bar{\boldsymbol{\alpha}}^{2i}$ is the vector of nodal variables of element i of Body 2 expressed in Body 2 reference frame and it can be written as

$$\bar{\boldsymbol{\alpha}}^{2i} = \mathbf{B}^{2i} \bar{\boldsymbol{\alpha}}^{(2)} \quad (3.162)$$

where $\bar{\alpha}^{(2)}$ is the vector of nodal variables of Body 2 expressed in Body 2 reference frame and \mathbf{B}^{2i} is the Boolean matrix of element i of Body 2 that relates $\bar{\alpha}^{(2)}$ to $\bar{\alpha}^{2i}$. Therefore, Equation (3.159) can be written as

$$\bar{\mathbf{u}}^{2i} = \boldsymbol{\phi}^{2i} \mathbf{B}^{2i} \bar{\alpha}^{(2)} \quad (3.163)$$

To decrease the number of elastic coordinates of Body 2, nodal modal transformation can be done as follows

$$\bar{\alpha}^{(2)} = \boldsymbol{\chi}^{(2)} \boldsymbol{\eta}^{(2)} \quad (3.164)$$

where $\boldsymbol{\chi}^{(2)}$ is the modal matrix of Body 2. Each column of this matrix is the eigenvector of Body 2 and represents the mode shape of Body 2. $\boldsymbol{\eta}^{(2)}$ is the vector of modal variables of Body 2. Therefore, Equation (3.154) takes the following form

$$\mathbf{R}^{2i} = \boldsymbol{\zeta}^{(2)} + \mathbf{T}^{(2)} (\bar{\mathbf{b}}^{2i} + \bar{\mathbf{r}}^{2i} + \boldsymbol{\phi}^{2i} \mathbf{B}^{2i} \boldsymbol{\chi}^{(2)} \boldsymbol{\eta}^{(2)}) \quad (3.165)$$

Generalized coordinates of Body 2, $\mathbf{x}^{(2)}$, can be chosen as Euler angles of Body 2 reference frame and modal variables of Body 2. Therefore, $\mathbf{x}^{(2)}$ can be written as

$$\mathbf{x}^{(2)} = \begin{bmatrix} \boldsymbol{\alpha}^{(2)} \\ \boldsymbol{\eta}^{(2)} \end{bmatrix} \quad (3.166)$$

Velocity of point P of element i of Body 2 is obtained by taking the time derivative of the position vector of element i of Body 2 as

$$\mathbf{v}^{2i} = \mathbf{T}^{(2)} \tilde{\mathbf{q}}^{2i} \bar{\boldsymbol{\omega}}^{(2)} + \mathbf{T}^{(2)} \boldsymbol{\phi}^{2i} \mathbf{B}^{2i} \boldsymbol{\chi}^{(2)} \dot{\boldsymbol{\eta}}^{(2)} \quad (3.167)$$

where $\dot{\boldsymbol{\eta}}^{(2)}$ is the derivative of vector of modal variables of Body 2, $\tilde{\mathbf{q}}^{2i}$ is the skew symmetric matrix of vector $\bar{\mathbf{q}}^{2i}$ and $\bar{\boldsymbol{\omega}}^{(2)}$ is the angular velocity of Body 2

reference frame expressed in the same frame and it can be written in terms of derivative of Euler angles of Body 2 reference frame as

$$\bar{\boldsymbol{\omega}}^{(2)} = \bar{\mathbf{D}}^{(2)} \dot{\boldsymbol{\alpha}}^{(2)} \quad (3.168)$$

where $\dot{\boldsymbol{\alpha}}^{(2)}$ is the derivative of Euler angles of Body 2 reference frame in columnwise form and is given as

$$\dot{\boldsymbol{\alpha}}^{(2)} = \begin{bmatrix} \dot{\alpha}_2 \\ \dot{\beta}_2 \\ \dot{\gamma}_2 \end{bmatrix} \quad (3.169)$$

$\bar{\mathbf{D}}^{(2)}$ is a transformation matrix from derivative of Euler angles of Body 2 reference frame to the angular velocity of Body 2 reference frame. It is expressed in Body 2 reference frame and is denoted as

$$\bar{\mathbf{D}}^{(2)} = \begin{bmatrix} c\beta_2 c\gamma_2 & s\gamma_2 & 0 \\ -c\beta_2 s\gamma_2 & c\gamma_2 & 0 \\ s\beta_2 & 0 & 1 \end{bmatrix} \quad (3.170)$$

Choosing $\bar{\boldsymbol{\omega}}^{(2)}$ as the rotational generalized speeds of Body 2, v^{2i} is written as

$$\mathbf{v}^{2i} = \boldsymbol{\mu}^{2i} \mathbf{y}^{(2)} \quad (3.171)$$

where $\boldsymbol{\mu}^{2i}$ is the velocity influence coefficient matrix of Body 2 and is given as

$$\boldsymbol{\mu}^{2i} = \left[\mathbf{T}^{(2)} \tilde{\mathbf{q}}^{2i} \quad \mathbf{T}^{(2)} \boldsymbol{\phi}^{2i} \mathbf{B}^{2i} \boldsymbol{\chi}^{(2)} \right] \quad (3.172)$$

$\mathbf{y}^{(2)}$ is the generalized speed vector of Body 2 and is given as

$$\mathbf{y}^{(2)} = \begin{bmatrix} \bar{\boldsymbol{\omega}}^{(2)} \\ \dot{\boldsymbol{\eta}}^{(2)} \end{bmatrix} \quad (3.173)$$

Derivative of the generalized coordinates vector of Body 2 can be obtained from the generalized speeds vector of Body 2 as

$$\begin{bmatrix} \dot{\boldsymbol{\alpha}}^{(2)} \\ \dot{\boldsymbol{\eta}}^{(2)} \end{bmatrix} = \begin{bmatrix} \overline{\mathbf{D}}^{(2)-1} & \mathbf{0} \\ \mathbf{0} & \mathbf{I} \end{bmatrix} \begin{bmatrix} \dot{\boldsymbol{\omega}}^{(2)} \\ \dot{\boldsymbol{\eta}}^{(2)} \end{bmatrix} \quad (3.174)$$

where \mathbf{I} is an identity matrix and inverse of the $\overline{\mathbf{D}}^{(2)}$ is given as

$$\overline{\mathbf{D}}^{(2)-1} = \begin{bmatrix} \frac{c\gamma_2}{c\beta_2} & -\frac{s\gamma_2}{c\beta_2} & 0 \\ s\gamma_2 & c\gamma_2 & 0 \\ -\frac{s\beta_2 c\gamma_2}{c\beta_2} & \frac{s\beta_2 s\gamma_2}{c\beta_2} & 1 \end{bmatrix} \quad (3.175)$$

$\beta_2 = \pm\pi/2$ and $\beta_2 = 3\pi/2$ are the singularities of the roll-pitch-yaw (1-2-3) sequence. At such positions, another sequence has to be used.

Acceleration of point P of element i of Body 2 is obtained by taking the time derivative of the velocity vector of element i of Body 2 as

$$\begin{aligned} \mathbf{a}^{2i} = & \mathbf{T}^{(2)} \tilde{\mathbf{q}}^{2i} \dot{\boldsymbol{\omega}}^{(2)} + \mathbf{T}^{(2)} \boldsymbol{\phi}^{2i} \mathbf{B}^{2i} \boldsymbol{\chi}^{(2)} \ddot{\boldsymbol{\eta}}^{(2)} + \dot{\mathbf{T}}^{(2)} \tilde{\mathbf{q}}^{2i} \boldsymbol{\omega}^{(2)} + \\ & \mathbf{T}^{(2)} \dot{\tilde{\mathbf{q}}}^{2i} \boldsymbol{\omega}^{(2)} + \dot{\mathbf{T}}^{(2)} \boldsymbol{\phi}^{2i} \mathbf{B}^{2i} \boldsymbol{\chi}^{(2)} \dot{\boldsymbol{\eta}}^{(2)} \end{aligned} \quad (3.176)$$

which can be written shortly as

$$\mathbf{a}^{2i} = \boldsymbol{\mu}^{2i} \dot{\mathbf{y}}^{(2)} + \dot{\boldsymbol{\mu}}^{2i} \mathbf{y}^{(2)} \quad (3.177)$$

where $\dot{\mathbf{y}}^{(2)}$ is the generalized acceleration vector of Body 2 and is given as

$$\dot{\mathbf{y}}^{(2)} = \begin{bmatrix} \dot{\boldsymbol{\omega}}^{(2)} \\ \dot{\boldsymbol{\eta}}^{(2)} \end{bmatrix} \quad (3.178)$$

$\boldsymbol{\mu}^{2i} \dot{\mathbf{y}}^{(2)}$ consists of the terms involving the generalized accelerations as shown below

$$\boldsymbol{\mu}^{2i} \dot{\mathbf{y}}^{(2)} = \mathbf{T}^{(2)} \tilde{\mathbf{q}}^{2i} \dot{\tilde{\boldsymbol{\omega}}}^{(2)} + \mathbf{T}^{(2)} \boldsymbol{\phi}^{2i} \mathbf{B}^{2i} \boldsymbol{\chi}^{(2)} \dot{\boldsymbol{\eta}}^{(2)} \quad (3.179)$$

$\dot{\boldsymbol{\mu}}^{2i} \mathbf{y}^{(2)}$ includes the Coriolis and centripetal accelerations as shown below

$$\dot{\boldsymbol{\mu}}^{2i} \mathbf{y}^{(2)} = -\mathbf{T}^{(2)} \tilde{\boldsymbol{\omega}}^{(2)} \tilde{\mathbf{q}}^{2i} \tilde{\boldsymbol{\omega}}^{(2)} - 2\mathbf{T}^{(2)} \tilde{\boldsymbol{\omega}}^{(2)} \boldsymbol{\phi}^{2i} \mathbf{B}^{2i} \boldsymbol{\chi}^{(2)} \dot{\boldsymbol{\eta}}^{(2)} \quad (3.180)$$

The dynamic equations of Body 2 can be derived by using the above kinematic expressions. Kane's equations are given as [53]

$$\mathbf{f}^{*(2)} + \mathbf{f}^{(2)} + \mathbf{f}^s(2) + \mathbf{f}_{m_B}^{*(2)} + \mathbf{f}_{m_B}^{(2)} = \mathbf{0} \quad (3.181)$$

where $\mathbf{f}^{*(2)}$, $\mathbf{f}^{(2)}$ and $\mathbf{f}^s(2)$ are the generalized inertia, external, and stiffness forces of Body 2, respectively. $\mathbf{f}_{m_B}^{*(2)}$ and $\mathbf{f}_{m_B}^{(2)}$ are the generalized inertia and external forces of lumped mass m_B at point B of Body 2, respectively.

The generalized inertia forces of Body 2 can be written as

$$\mathbf{f}^{*(2)} = \int_{V_{2i}} \boldsymbol{\mu}^{2iT} (-\rho_{2i} \mathbf{a}^{2i}) dV \quad (3.182)$$

where ρ_{2i} represents the density of element i of Body 2 material and V_{2i} stands for the volume of element i of Body 2. Equation (3.182) can be expressed as the following form

$$\mathbf{f}^{*(2)} = -\mathbf{M}^{(2)} \dot{\mathbf{y}}^{(2)} + \mathbf{Q}^{(2)} \quad (3.183)$$

where $\mathbf{M}^{(2)}$ is the generalized mass matrix of Body 2 and is given as

$$\mathbf{M}^{(2)} = \sum_{i=1}^{N_2} \int_{V_{2i}} \rho_{2i} \boldsymbol{\mu}^{2iT} \boldsymbol{\mu}^{2i} dV \quad (3.184)$$

where N_2 is the number of finite elements in Body 2. $\mathbf{Q}^{(2)}$ is the generalized Coriolis and centrifugal force vector of Body 2 and is given as

$$\mathbf{Q}^{(2)} = -\sum_{i=1}^{N_2} \int_{V_{2i}} \rho_{2i} \boldsymbol{\mu}^{2iT} \ddot{\boldsymbol{\mu}}^{2i} \mathbf{y}^{(2)} dV \quad (3.185)$$

$\mathbf{M}^{(2)}$ can be written in terms of the generalized coordinates of Body 2 by substituting the partitioned form of $\boldsymbol{\mu}^{2i}$ into Equation (3.184) as follows

$$\mathbf{M}^{(2)} = \sum_{i=1}^{N_2} \int_{V_{2i}} \rho_{2i} \begin{bmatrix} \tilde{\mathbf{q}}^{2iT} \tilde{\mathbf{q}}^{2i} & \tilde{\mathbf{q}}^{2iT} \boldsymbol{\phi}^{2iT} \mathbf{B}^{2i} \boldsymbol{\chi}^{(2)} \\ \boldsymbol{\chi}^{(2)T} \mathbf{B}^{2iT} \boldsymbol{\phi}^{2iT} \tilde{\mathbf{q}}^{2i} & \boldsymbol{\chi}^{(2)T} \mathbf{B}^{2iT} \boldsymbol{\phi}^{2iT} \boldsymbol{\phi}^{2i} \mathbf{B}^{2i} \boldsymbol{\chi}^{(2)} \end{bmatrix} dV \quad (3.186)$$

In order to deal with each term separately, the submatrices of $\mathbf{M}^{(2)}$ corresponding to rotation and elastic deformation are labelled as below

$$\mathbf{M}^{(2)} = \begin{bmatrix} \mathbf{M}_{rr}^{(2)} & \mathbf{M}_{re}^{(2)} \\ \mathbf{M}_{re}^{(2)T} & \mathbf{M}_{ee}^{(2)} \end{bmatrix} \quad (3.187)$$

The submatrices of $\mathbf{M}^{(2)}$ can be obtained in the following forms

$$\mathbf{M}_{rr}^{(2)} = \sum_{i=1}^{N_2} \int_{V_{2i}} \rho_{2i} \tilde{\mathbf{q}}^{2iT} \tilde{\mathbf{q}}^{2i} dV \quad (3.188)$$

$$\mathbf{M}_{re}^{(2)} = \left\{ \sum_{i=1}^{N_2} \left(\int_{V_{2i}} \rho_{2i} \tilde{\mathbf{q}}^{2iT} \boldsymbol{\phi}^{2i} dV \right) \mathbf{B}^{2i} \right\} \boldsymbol{\chi}^{(2)} \quad (3.189)$$

$$\mathbf{M}_{ee}^{(2)} = \boldsymbol{\chi}^{(2)T} \left\{ \sum_{i=1}^{N_2} \mathbf{B}^{2iT} \left(\int_{V_{2i}} \rho_{2i} \boldsymbol{\phi}^{2iT} \boldsymbol{\phi}^{2i} dV \right) \mathbf{B}^{2i} \right\} \boldsymbol{\chi}^{(2)} \quad (3.190)$$

$\mathbf{Q}^{(2)}$ can be written in terms of the generalized coordinates and the generalized speeds by substituting the partitioned form of $\boldsymbol{\mu}^{2i}$ into Equation (3.185) as follows

$$\mathbf{Q}^{(2)} = \sum_{i=1}^{N_2} \int_{V_{2i}} \rho_{2i} \left[\begin{array}{c} \tilde{\mathbf{q}}^{2i\text{T}} \tilde{\boldsymbol{\omega}}^{(2)} \tilde{\mathbf{q}}^{2i} \tilde{\boldsymbol{\omega}}^{(2)} + 2\tilde{\mathbf{q}}^{2i\text{T}} \tilde{\boldsymbol{\omega}}^{(2)} \boldsymbol{\phi}^{2i} \mathbf{B}^{2i} \boldsymbol{\chi}^{(2)} \dot{\boldsymbol{\eta}}^{(2)} \\ \boldsymbol{\chi}^{(2)\text{T}} \mathbf{B}^{2i\text{T}} \boldsymbol{\phi}^{2i\text{T}} \tilde{\boldsymbol{\omega}}^{(2)} \tilde{\mathbf{q}}^{2i} \tilde{\boldsymbol{\omega}}^{(2)} + 2\boldsymbol{\chi}^{(2)\text{T}} \mathbf{B}^{2i\text{T}} \boldsymbol{\phi}^{2i\text{T}} \tilde{\boldsymbol{\omega}}^{(2)} \boldsymbol{\phi}^{2i} \mathbf{B}^{2i} \boldsymbol{\chi}^{(2)} \dot{\boldsymbol{\eta}}^{(2)} \end{array} \right] dV \quad (3.191)$$

In order to deal with each term separately, the subvectors of $\mathbf{Q}^{(2)}$ corresponding to rotation and elastic deformation are labelled as below

$$\mathbf{Q}^{(2)} = \begin{bmatrix} \mathbf{Q}_r^{(2)} \\ \mathbf{Q}_e^{(2)} \end{bmatrix} \quad (3.192)$$

The subvectors of $\mathbf{Q}^{(2)}$ can be obtained in the following forms

$$\mathbf{Q}_r^{(2)} = \left\{ \sum_{i=1}^{N_2} \int_{V_{2i}} \rho_{2i} \tilde{\mathbf{q}}^{2i\text{T}} \tilde{\boldsymbol{\omega}}^{(2)} \tilde{\mathbf{q}}^{2i} dV \right\} \tilde{\boldsymbol{\omega}}^{(2)} + 2 \left\{ \sum_{i=1}^{N_2} \left(\int_{V_{2i}} \rho_{2i} \tilde{\mathbf{q}}^{2i\text{T}} \tilde{\boldsymbol{\omega}}^{(2)} \boldsymbol{\phi}^{2i} dV \right) \mathbf{B}^{2i} \right\} \boldsymbol{\chi}^{(2)} \dot{\boldsymbol{\eta}}^{(2)} \quad (3.193)$$

$$\mathbf{Q}_e^{(2)} = \boldsymbol{\chi}^{(2)\text{T}} \left\{ \sum_{i=1}^{N_2} \mathbf{B}^{2i\text{T}} \left(\int_{V_{2i}} \rho_{2i} \boldsymbol{\phi}^{2i\text{T}} \tilde{\boldsymbol{\omega}}^{(2)} \tilde{\mathbf{q}}^{2i} dV \right) \right\} \tilde{\boldsymbol{\omega}}^{(2)} + 2\boldsymbol{\chi}^{(2)\text{T}} \left\{ \sum_{i=1}^{N_2} \mathbf{B}^{2i\text{T}} \left(\int_{V_{2i}} \rho_{2i} \boldsymbol{\phi}^{2i\text{T}} \tilde{\boldsymbol{\omega}}^{(2)} \boldsymbol{\phi}^{2i} dV \right) \mathbf{B}^{2i} \right\} \boldsymbol{\chi}^{(2)} \dot{\boldsymbol{\eta}}^{(2)} \quad (3.194)$$

The generalized external force due to weight of Body 2 can be expressed as

$$\mathbf{f}^g^{(2)} = \sum_{i=1}^{N_2} \int_{V_{2i}} \boldsymbol{\mu}^{2i\text{T}} (\rho_{2i} \mathbf{g}_s) dV \quad (3.195)$$

If $\boldsymbol{\mu}^{2i}$ is substituted into above equation, $\mathbf{f}^{g(2)}$ becomes

$$\mathbf{f}^{g(2)} = \sum_{i=1}^{N_2} \int_{V_{2i}} \rho_{2i} \begin{bmatrix} \tilde{\mathbf{q}}^{2iT} \mathbf{T}^{(2)T} \\ \boldsymbol{\chi}^{(2)T} \mathbf{B}^{2iT} \boldsymbol{\phi}^{2iT} \mathbf{T}^{(2)T} \end{bmatrix} \mathbf{g} s dV \quad (3.196)$$

In order to deal with each term separately, the subvectors of $\mathbf{f}^{g(2)}$ corresponding to rotation and elastic deformation are labelled as below

$$\mathbf{f}^{g(2)} = \begin{bmatrix} \mathbf{f}_r^{g(2)} \\ \mathbf{f}_e^{g(2)} \end{bmatrix} \quad (3.197)$$

The subvectors of $\mathbf{f}^{g(2)}$ can be obtained as follows

$$\mathbf{f}_r^{g(2)} = \left(\sum_{i=1}^{N_2} \int_{V_{2i}} \rho_{2i} \tilde{\mathbf{q}}^{2iT} dV \right) \mathbf{T}^{(2)T} \mathbf{g} s \quad (3.198)$$

$$\mathbf{f}_e^{g(2)} = \boldsymbol{\chi}^{(2)T} \left\{ \sum_{i=1}^{N_2} \mathbf{B}^{2iT} \left(\int_{V_{2i}} \rho_{2i} \boldsymbol{\phi}^{2iT} dV \right) \right\} \mathbf{T}^{(2)T} \mathbf{g} s \quad (3.199)$$

The generalized external force due to torque \mathbf{T}_2 can be expressed as

$$\mathbf{f}^{e(\mathbf{T}_2)(2)} = {}^{A_2} \boldsymbol{\Omega} {}^{A_2 T} {}^{A_2} \mathbf{T}_2 \quad (3.200)$$

where ${}^{A_2} \mathbf{T}_2$ is the torque vector applied to Body 2 due to actuator at point A expressed in joint frame A_2 and is written as

$${}^{A_2} \mathbf{T}_2 = \begin{bmatrix} 0 \\ 0 \\ \mathbf{T}_2 \end{bmatrix} \quad (3.201)$$

${}^{A_2}\boldsymbol{\Omega}^{A_2}$ is the influence coefficient matrix of angular velocity of joint frame at point A of Body 2 expressed in the same frame and it can be obtained as

$${}^{A_2}\boldsymbol{\Omega}^{A_2 T} = \left[\mathbf{T}^{A_2-2} \quad \mathbf{T}^{A_2-2} \boldsymbol{\Psi}^{A_2} \mathbf{B}^{2r} \boldsymbol{\chi}^{(2)} \right] \quad (3.202)$$

where \mathbf{T}^{A_2-2} is the transformation matrix from Body 2 reference frame to the joint frame at A_2 due to angular deformation of Body 2. Angular deformation of element i of Body 2 expressed in Body 2 reference frame, $\bar{\boldsymbol{\gamma}}^{2i}$, can be written as

$$\bar{\boldsymbol{\gamma}}^{2i} = \boldsymbol{\Psi}^{2i} \mathbf{B}^{2i} \boldsymbol{\chi}^{(2)} \boldsymbol{\eta}^{(2)} \quad (3.203)$$

where $\boldsymbol{\Psi}^{2i}$ is given as

$$\boldsymbol{\Psi}^{2i} = \mathbf{T}^{2i} \mathbf{s}_{\text{rot}}^{2i} \mathbf{R}^{2i T} \quad (3.204)$$

where $\mathbf{s}_{\text{rot}}^{2i}$ is the rotation shape function matrix of element i of Body 2. Since $\bar{\boldsymbol{\gamma}}^{2i}$ are small angles vector (therefore, $s\bar{\boldsymbol{\gamma}}_j^{2i} \approx \bar{\boldsymbol{\gamma}}_j^{2i}$, $c\bar{\boldsymbol{\gamma}}_j^{2i} \approx 1$ for $j=1,2,3$), \mathbf{T}^{A_2-2} can be expressed in terms of Euler angles by using the roll-pitch-yaw sequence as

$$\mathbf{T}^{A_2-2} = \begin{bmatrix} 1 & -\bar{\boldsymbol{\gamma}}_3^{A_2} & \bar{\boldsymbol{\gamma}}_2^{A_2} \\ \bar{\boldsymbol{\gamma}}_3^{A_2} & 1 & -\bar{\boldsymbol{\gamma}}_1^{A_2} \\ -\bar{\boldsymbol{\gamma}}_2^{A_2} & \bar{\boldsymbol{\gamma}}_1^{A_2} & 1 \end{bmatrix} \quad (3.205)$$

where $\bar{\boldsymbol{\gamma}}^{A_2}$ is the value of $\bar{\boldsymbol{\gamma}}^{2i}$ evaluated at point A_2 . $\boldsymbol{\Psi}^{A_2}$ is the value of $\boldsymbol{\Psi}^{2i}$ evaluated at point A_2 and \mathbf{B}^{2r} is the Boolean matrix of the element of Body 2 that includes point A.

Therefore, $\mathbf{f}^{e(T_2)(2)}$ can be written as

$$\mathbf{f}^{e(T_2)(2)} = \begin{bmatrix} \mathbf{T}^{A_2-2T} \\ \boldsymbol{\chi}^{(2)T} \mathbf{B}^{2rT} \boldsymbol{\Psi}^{A_2T} \mathbf{T}^{A_2-2T} \end{bmatrix}^{A_2} \mathbf{T}_2 \quad (3.206)$$

In order to deal with each term separately, the subvectors of $\mathbf{f}^{e(T_2)(2)}$ corresponding to rotation and elastic deformation are labelled as below

$$\mathbf{f}^{e(T_2)(2)} = \begin{bmatrix} \mathbf{f}_r^{e(T_2)(2)} \\ \mathbf{f}_e^{e(T_2)(2)} \end{bmatrix} \quad (3.207)$$

The subvectors of $\mathbf{f}^{e(T_2)(2)}$ can be obtained as follows

$$\mathbf{f}_r^{e(T_2)(2)} = \mathbf{T}^{A_2-2T} \mathbf{T}_2 \quad (3.208)$$

$$\mathbf{f}_e^{e(T_2)(2)} = \boldsymbol{\chi}^{(2)T} \mathbf{B}^{2rT} \boldsymbol{\Psi}^{A_2T} \mathbf{T}^{A_2-2T} \mathbf{T}_2 \quad (3.209)$$

The generalized external force due to torque \mathbf{T}_3 can be expressed as

$$\mathbf{f}^{e(T_3)(2)} = {}^{B_2} \boldsymbol{\Omega}^{B_2T} \mathbf{T}_3 \quad (3.210)$$

where ${}^{B_2} \mathbf{T}_3$ is the torque vector applied to Body 2 due to actuator at point B expressed in joint frame B_2 and is written as

$${}^{B_2} \mathbf{T}_3 = \begin{bmatrix} 0 \\ 0 \\ -T_3 \end{bmatrix} \quad (3.211)$$

where T_3 is the magnitude of the torque generated at actuator at point B. ${}^{B_2} \boldsymbol{\Omega}^{B_2}$ is the influence coefficient matrix of angular velocity of joint frame at point B of Body 2 expressed in the same frame and it can be obtained as

$${}^{B_2} \boldsymbol{\Omega}^{B_2} = \left[\mathbf{T}^{B_2-2} \quad \mathbf{T}^{B_2-2} \boldsymbol{\Psi}^{B_2} \mathbf{B}^{2r} \boldsymbol{\chi}^{(2)} \right] \quad (3.212)$$

where \mathbf{T}^{B_2-2} is the transformation matrix from Body 2 reference frame to the joint frame at B_2 due to angular deformation of Body 2 and it can be expressed as

$$\mathbf{T}^{B_2-2} = \begin{bmatrix} 1 & -\bar{\boldsymbol{\gamma}}_3^{B_2} & \bar{\boldsymbol{\gamma}}_2^{B_2} \\ \bar{\boldsymbol{\gamma}}_3^{B_2} & 1 & -\bar{\boldsymbol{\gamma}}_1^{B_2} \\ -\bar{\boldsymbol{\gamma}}_2^{B_2} & \bar{\boldsymbol{\gamma}}_1^{B_2} & 1 \end{bmatrix} \quad (3.213)$$

where $\bar{\boldsymbol{\gamma}}^{B_2}$ is the value of $\bar{\boldsymbol{\gamma}}^{2i}$ evaluated at point B_2 . $\boldsymbol{\Psi}^{B_2}$ is the value of $\boldsymbol{\Psi}^{2i}$ evaluated at point B_2 and \mathbf{B}^{2r} is the Boolean matrix of the element of Body 2 that includes point B.

Therefore, $\mathbf{f}^{e(T_3)(2)}$ can be written as

$$\mathbf{f}^{e(T_3)(2)} = \begin{bmatrix} \mathbf{T}^{B_2-2T} \\ \boldsymbol{\chi}^{(2)T} \mathbf{B}^{2rT} \boldsymbol{\Psi}^{B_2T} \mathbf{T}^{B_2-2T} \end{bmatrix}^{B_2} \mathbf{T}_3 \quad (3.214)$$

In order to deal with each term separately, the subvectors of $\mathbf{f}^{e(T_3)(2)}$ corresponding to rotation and elastic deformation are labelled as below

$$\mathbf{f}^{e(T_3)(2)} = \begin{bmatrix} \mathbf{f}_r^{e(T_3)(2)} \\ \mathbf{f}_e^{e(T_3)(2)} \end{bmatrix} \quad (3.215)$$

The subvectors of $\mathbf{f}^{e(T_3)(2)}$ can be obtained as follows

$$\mathbf{f}_r^{e(T_3)(2)} = \mathbf{T}^{B_2-2T} \mathbf{T}_3 \quad (3.216)$$

$$\mathbf{f}_e^{e(T_3)(2)} = \boldsymbol{\chi}^{(2)T} \mathbf{B}^{2rT} \boldsymbol{\Psi}^{B_2T} \mathbf{T}^{B_2-2T} \mathbf{T}_3 \quad (3.217)$$

Generalized structural stiffness forces of Body 2, $\mathbf{f}^{s(2)}$, are found from the work done by the stiffness forces of Body 2 which is equal to the negative of the strain energy of Body 2. Therefore, $\mathbf{f}^{s(2)}$ can be obtained as follows

$$\mathbf{f}^{s(2)} = - \begin{bmatrix} 0 \\ 0 \\ 0 \\ \boldsymbol{\chi}^{(2)\text{T}} \mathbf{K}^{(2)} \boldsymbol{\chi}^{(2)} \boldsymbol{\eta}^{(2)} \end{bmatrix} \quad (3.218)$$

where $\mathbf{K}^{(2)}$ is the structural stiffness matrix of Body 2 and it can be formed as

$$\mathbf{K}^{(2)} = \sum_{i=1}^{N_2} \mathbf{B}^{2i\text{T}} \mathbf{K}^{2i} \mathbf{B}^{2i} \quad (3.219)$$

where \mathbf{K}^{2i} is the structural stiffness matrix of element i of Body 2 expressed in Body 2 reference frame and is given as

$$\mathbf{K}^{2i} = \mathbf{R}^{2i} \mathbf{H}^{2i} \mathbf{R}^{2i\text{T}} \quad (3.220)$$

where \mathbf{H}^{2i} is the structural stiffness matrix of element i of Body 2 expressed in element i frame.

The generalized inertia forces due to lumped mass m_B at point B of Body 2 can be written as

$$\mathbf{f}_{m_B}^{*(2)} = \boldsymbol{\mu}^{\text{B}\text{T}} (-m_B \mathbf{a}^{\text{B}}) \quad (3.221)$$

where $\boldsymbol{\mu}^{\text{B}}$ is the velocity influence coefficient matrix of point B of Body 2 and \mathbf{a}^{B} is the acceleration of point B of Body 2. Equation (3.221) can be expressed as

$$\mathbf{f}_{m_B}^{*(2)} = -\mathbf{M}_{m_B}^{(2)} \dot{\mathbf{y}}^{(2)} + \mathbf{Q}_{m_B}^{(2)} \quad (3.222)$$

where $\mathbf{M}_{m_B}^{(2)}$ is the generalized mass matrix of lumped mass m_B and is given as

$$\mathbf{M}_{m_B}^{(2)} = m_B \boldsymbol{\mu}^{B^T} \boldsymbol{\mu}^B \quad (3.223)$$

$\mathbf{Q}_{m_B}^{(2)}$ is the generalized Coriolis and centrifugal force vector of lumped mass m_B and is given as

$$\mathbf{Q}_{m_B}^{(2)} = -m_B \boldsymbol{\mu}^{B^T} \dot{\boldsymbol{\mu}}^B \mathbf{y} \quad (3.224)$$

$\mathbf{M}_{m_B}^{(2)}$ can be written in terms of the generalized coordinates of Body 2 by substituting the partitioned form of $\boldsymbol{\mu}^B$ into Equation (3.223) as follows

$$\mathbf{M}_{m_B}^{(2)} = m_B \begin{bmatrix} \tilde{\mathbf{q}}^{B_2^T} \tilde{\mathbf{q}}^{B_2} & \tilde{\mathbf{q}}^{B_2^T} \boldsymbol{\phi}^{B_2} \mathbf{B}^{2r} \boldsymbol{\chi}^{(2)} \\ \boldsymbol{\chi}^{(2)T} \mathbf{B}^{2r^T} \boldsymbol{\phi}^{B_2^T} \tilde{\mathbf{q}}^{B_2} & \boldsymbol{\chi}^{(2)T} \mathbf{B}^{2r^T} \boldsymbol{\phi}^{B_2^T} \boldsymbol{\phi}^{B_2} \mathbf{B}^{2r} \boldsymbol{\chi}^{(2)} \end{bmatrix} \quad (3.225)$$

where $\tilde{\mathbf{q}}^{B_2}$ is the skew symmetric matrix of the vector $\bar{\mathbf{q}}^{B_2}$, $\bar{\mathbf{q}}^{B_2}$ is the position vector from Body 2 reference frame to point B of Body 2 at deformed state expressed in Body 2 reference frame, $\boldsymbol{\phi}^{B_2}$ is the value of $\boldsymbol{\phi}^{2i}$ at point B of Body 2 and \mathbf{B}^{2r} is the Boolean matrix of the element of Body 2 that includes point B.

In order to deal with each term separately, the submatrices of $\mathbf{M}_{m_B}^{(2)}$ corresponding to rotation and elastic deformation are labelled as below

$$\mathbf{M}_{m_B}^{(2)} = \begin{bmatrix} \mathbf{M}_{m_{Brr}}^{(2)} & \mathbf{M}_{m_{Bre}}^{(2)} \\ \mathbf{M}_{m_{Bre}}^{(2)T} & \mathbf{M}_{m_{Bee}}^{(2)} \end{bmatrix} \quad (3.226)$$

The submatrices of $\mathbf{M}_{m_B}^{(2)}$ can be obtained in the following forms

$$\mathbf{M}_{m_{B_r}}^{(2)} = m_B \tilde{\mathbf{q}}^{B_2 T} \tilde{\mathbf{q}}^{B_2} \quad (3.227)$$

$$\mathbf{M}_{m_{B_{re}}}^{(2)} = m_B \tilde{\mathbf{q}}^{B_2 T} \boldsymbol{\phi}^{B_2} \mathbf{B}^{2r} \boldsymbol{\chi}^{(2)} \quad (3.228)$$

$$\mathbf{M}_{m_{B_{ec}}}^{(2)} = m_B \boldsymbol{\chi}^{(2)T} \mathbf{B}^{2rT} \boldsymbol{\phi}^{B_2 T} \boldsymbol{\phi}^{B_2} \mathbf{B}^{2r} \boldsymbol{\chi}^{(2)} \quad (3.229)$$

$\mathbf{Q}_{m_B}^{(2)}$ can be written in terms of the generalized coordinates and the generalized speeds by substituting the partitioned form of $\boldsymbol{\mu}^B$ into Equation (3.224) as follows

$$\mathbf{Q}_{m_B}^{(2)} = m_B \begin{bmatrix} \tilde{\mathbf{q}}^{B_2 T} \tilde{\boldsymbol{\omega}}^{(2)} \tilde{\mathbf{q}}^{B_2} \tilde{\boldsymbol{\omega}}^{(2)} + 2 \tilde{\mathbf{q}}^{B_2 T} \tilde{\boldsymbol{\omega}}^{(2)} \boldsymbol{\phi}^{B_2} \mathbf{B}^{2r} \boldsymbol{\chi}^{(2)} \dot{\boldsymbol{\eta}}^{(2)} \\ \boldsymbol{\chi}^{(2)T} \mathbf{B}^{2rT} \boldsymbol{\phi}^{B_2 T} \tilde{\boldsymbol{\omega}}^{(2)} \tilde{\mathbf{q}}^{B_2} \tilde{\boldsymbol{\omega}}^{(2)} + 2 \boldsymbol{\chi}^{(2)T} \mathbf{B}^{2rT} \boldsymbol{\phi}^{B_2 T} \tilde{\boldsymbol{\omega}}^{(2)} \boldsymbol{\phi}^{B_2} \mathbf{B}^{2r} \boldsymbol{\chi}^{(2)} \dot{\boldsymbol{\eta}}^{(2)} \end{bmatrix} \quad (3.230)$$

In order to deal with each term separately, the subvectors of $\mathbf{Q}_{m_B}^{(2)}$ corresponding to rotation and elastic deformation are labelled as below

$$\mathbf{Q}_{m_B}^{(2)} = \begin{bmatrix} \mathbf{Q}_{m_{B_r}}^{(2)} \\ \mathbf{Q}_{m_{B_e}}^{(2)} \end{bmatrix} \quad (3.231)$$

The subvectors of $\mathbf{Q}_{m_{B_r}}^{(2)}$ can be obtained in the following forms

$$\mathbf{Q}_{m_{B_r}}^{(2)} = m_B \tilde{\mathbf{q}}^{B_2 T} \tilde{\boldsymbol{\omega}}^{(2)} \tilde{\mathbf{q}}^{B_2} \tilde{\boldsymbol{\omega}}^{(2)} + 2 m_B \tilde{\mathbf{q}}^{B_2 T} \tilde{\boldsymbol{\omega}}^{(2)} \boldsymbol{\phi}^{B_2} \mathbf{B}^{2r} \boldsymbol{\chi}^{(2)} \dot{\boldsymbol{\eta}}^{(2)} \quad (3.232)$$

$$\mathbf{Q}_{m_{B_e}}^{(2)} = m_B \boldsymbol{\chi}^{(2)T} \mathbf{B}^{2rT} \boldsymbol{\phi}^{B_2 T} \tilde{\boldsymbol{\omega}}^{(2)} \tilde{\mathbf{q}}^{B_2} \tilde{\boldsymbol{\omega}}^{(2)} + 2 m_B \boldsymbol{\chi}^{(2)T} \mathbf{B}^{2rT} \boldsymbol{\phi}^{B_2 T} \tilde{\boldsymbol{\omega}}^{(2)} \boldsymbol{\phi}^{B_2} \mathbf{B}^{2r} \boldsymbol{\chi}^{(2)} \dot{\boldsymbol{\eta}}^{(2)} \quad (3.233)$$

The generalized external force due to weight of lumped mass m_B can be expressed as

$$\mathbf{f}_{m_B}^{g(2)} = \boldsymbol{\mu}^{B T} (m_B \mathbf{g}) \quad (3.234)$$

If $\boldsymbol{\mu}^B$ is substituted into above equation $\mathbf{f}_{m_B}^{g(2)}$ becomes

$$\mathbf{f}_{m_B}^{g(2)} = m_B \begin{bmatrix} \tilde{\mathbf{q}}^{B_2^T} \mathbf{T}^{(2)T} \\ \boldsymbol{\chi}^{(2)T} \mathbf{B}^{2r^T} \boldsymbol{\phi}^{B_2^T} \mathbf{T}^{(2)T} \end{bmatrix} \mathbf{g} \mathbf{s} \quad (3.235)$$

In order to deal with each term separately, the subvectors of $\mathbf{f}_{m_B}^{g(2)}$ corresponding to rotation and elastic deformation are labelled as below

$$\mathbf{f}_{m_B}^{g(2)} = \begin{bmatrix} \mathbf{f}_{m_{B_r}}^{g(2)} \\ \mathbf{f}_{m_{B_e}}^{g(2)} \end{bmatrix} \quad (3.236)$$

The subvectors of $\mathbf{f}_{m_B}^{g(2)}$ can be obtained as follows

$$\mathbf{f}_{m_{B_r}}^{g(2)} = m_B \tilde{\mathbf{q}}^{B_2^T} \mathbf{T}^{(2)T} \mathbf{g} \mathbf{s} \quad (3.237)$$

$$\mathbf{f}_{m_{B_e}}^{g(2)} = m_B \boldsymbol{\chi}^{(2)T} \mathbf{B}^{2r^T} \boldsymbol{\phi}^{B_2^T} \mathbf{T}^{(2)T} \mathbf{g} \mathbf{s} \quad (3.238)$$

Body 3

Position vector to arbitrary point P of element i of Body 3 can be written as

$$\mathbf{R}^{3i} = \boldsymbol{\zeta}^{(3)} + \mathbf{q}^{3i} \quad (3.239)$$

Using components in fixed frame, \mathbf{R}^{3i} can be written as

$$\mathbf{R}^{3i} = \boldsymbol{\zeta}^{(3)} + \mathbf{T}^{(3)} \bar{\mathbf{q}}^{3i} \quad (3.240)$$

where $\boldsymbol{\zeta}^{(3)}$ is the position vector from fixed frame to Body 3 reference frame. $\mathbf{T}^{(3)}$ is the transformation matrix from Body 3 reference frame to fixed frame. It can be expressed in terms of Euler angles, eg. by using the roll-pitch-yaw (1-2-3)

sequence. Euler angles of Body 3 reference frame can be written in columnwise form as

$$\boldsymbol{\alpha}^{(3)} = \begin{bmatrix} \alpha_3 \\ \beta_3 \\ \gamma_3 \end{bmatrix} \quad (3.241)$$

where α_3 , β_3 and γ_3 are the roll-pitch-yaw Euler angles of Body 3 reference frame, respectively. Therefore, $\mathbf{T}^{(3)}$ takes the following form

$$\mathbf{T}^{(3)} = \begin{bmatrix} c\beta_3 c\gamma_3 & -c\beta_3 s\gamma_3 & s\beta_3 \\ c\alpha_3 s\gamma_3 + s\alpha_3 s\beta_3 c\gamma_3 & c\alpha_3 c\gamma_3 - s\alpha_3 s\beta_3 s\gamma_3 & -s\alpha_3 c\beta_3 \\ s\alpha_3 s\gamma_3 - c\alpha_3 s\beta_3 c\gamma_3 & c\alpha_3 s\beta_3 s\gamma_3 + s\alpha_3 c\gamma_3 & c\alpha_3 c\beta_3 \end{bmatrix} \quad (3.242)$$

$\bar{\mathbf{q}}^{3i}$ represents the position vector from Body 3 reference frame to point P of element i of Body 3 at deformed state expressed in Body 3 reference frame and is given as

$$\bar{\mathbf{q}}^{3i} = \bar{\mathbf{b}}^{3i} + \bar{\mathbf{r}}^{3i} + \bar{\mathbf{u}}^{3i} \quad (3.243)$$

where $\bar{\mathbf{b}}^{3i}$ represents the position vector from Body 3 reference frame to element i reference frame expressed in Body 3 reference frame, $\bar{\mathbf{r}}^{3i}$ represents the position vector from element i frame to point P at undeformed state expressed in Body 3 reference frame and $\bar{\mathbf{u}}^{3i}$ is the deformation displacement vector of point P of element i of Body 3 expressed in Body 3 reference frame and is given as

$$\bar{\mathbf{u}}^{3i} = \boldsymbol{\phi}^{3i} \bar{\boldsymbol{\alpha}}^{3i} \quad (3.244)$$

where $\boldsymbol{\phi}^{3i}$ is given as

$$\boldsymbol{\phi}^{3i} = \mathbf{T}^{3i} \mathbf{s}^{3i} \mathbf{R}^{3iT} \quad (3.245)$$

where \mathbf{T}^{3i} is the transformation matrix from element i of Body 3 frame to Body 3 reference frame and \mathbf{R}^{3i} is given as

$$\mathbf{R}^{3i} = \begin{bmatrix} \mathbf{T}^{3i} & \mathbf{0} \\ & \ddots \\ \mathbf{0} & \mathbf{T}^{3i} \end{bmatrix} \quad (3.246)$$

Since all element frames and Body 3 reference frame are in the same orientation, then \mathbf{T}^{3i} is 3 by 3 identity matrix and therefore \mathbf{R}^{3i} is 12 by 12 identity matrix. \mathbf{s}^{3i} is the shape function matrix of element i of Body 3. $\bar{\boldsymbol{\alpha}}^{3i}$ is the vector of nodal variables of element i of Body 3 expressed in Body 3 reference frame and it can be written as

$$\bar{\boldsymbol{\alpha}}^{3i} = \mathbf{B}^{3i} \bar{\boldsymbol{\alpha}}^{(3)} \quad (3.247)$$

where $\bar{\boldsymbol{\alpha}}^{(3)}$ is the vector of nodal variables of Body 3 expressed in Body 3 reference frame and \mathbf{B}^{3i} is the Boolean matrix of element i of Body 3 that relates $\bar{\boldsymbol{\alpha}}^{(3)}$ to $\bar{\boldsymbol{\alpha}}^{3i}$. Therefore, Equation (3.244) can be written as

$$\bar{\mathbf{u}}^{3i} = \boldsymbol{\phi}^{3i} \mathbf{B}^{3i} \bar{\boldsymbol{\alpha}}^{(3)} \quad (3.248)$$

To decrease the number of elastic coordinates of Body 3, nodal modal transformation can be done as follows

$$\bar{\boldsymbol{\alpha}}^{(3)} = \boldsymbol{\chi}^{(3)} \boldsymbol{\eta}^{(3)} \quad (3.249)$$

where $\boldsymbol{\chi}^{(3)}$ is the modal matrix of Body 3. Each column of this matrix is the eigenvector of Body 3 and represents the mode shape of Body 3. $\boldsymbol{\eta}^{(3)}$ is the vector of modal variables of Body 3. Therefore, Equation (3.240) takes the following form

$$\mathbf{R}^{3i} = \boldsymbol{\zeta}^{(3)} + \mathbf{T}^{(3)} (\bar{\mathbf{b}}^{3i} + \bar{\mathbf{r}}^{3i} + \boldsymbol{\phi}^{3i} \mathbf{B}^{3i} \boldsymbol{\chi}^{(3)} \boldsymbol{\eta}^{(3)}) \quad (3.250)$$

Generalized coordinates of Body 3, $\mathbf{x}^{(3)}$, can be chosen as position vector of Body 3 reference frame, Euler angles of Body 3 reference frame and modal variables of Body 3. Therefore, $\mathbf{x}^{(3)}$ can be written as

$$\mathbf{x}^{(3)} = \begin{bmatrix} \boldsymbol{\zeta}^{(3)} \\ \boldsymbol{\alpha}^{(3)} \\ \boldsymbol{\eta}^{(3)} \end{bmatrix} \quad (3.251)$$

Velocity of point P of element i of Body 3 is obtained by taking the time derivative of the position vector of element i of Body 3 as

$$\mathbf{v}^{3i} = \dot{\boldsymbol{\zeta}}^{(3)} + \mathbf{T}^{(3)} \tilde{\mathbf{q}}^{3i} \bar{\boldsymbol{\omega}}^{(3)} + \mathbf{T}^{(3)} \boldsymbol{\phi}^{3i} \mathbf{B}^{3i} \boldsymbol{\chi}^{(3)} \dot{\boldsymbol{\eta}}^{(3)} \quad (3.252)$$

where $\dot{\boldsymbol{\zeta}}^{(3)}$ is the derivative of the position vector from fixed frame to Body 3 reference frame, $\dot{\boldsymbol{\eta}}^{(3)}$ is the derivative of vector of modal variables of Body 3, $\tilde{\mathbf{q}}^{3i}$ is the skew symmetric matrix of vector $\bar{\mathbf{q}}^{3i}$ and $\bar{\boldsymbol{\omega}}^{(3)}$ is the angular velocity of Body 3 reference frame expressed in the same frame and it can be written in terms of derivative of Euler angles of Body 3 reference frame as

$$\bar{\boldsymbol{\omega}}^{(3)} = \bar{\mathbf{D}}^{(3)} \dot{\boldsymbol{\alpha}}^{(3)} \quad (3.253)$$

where $\dot{\boldsymbol{\alpha}}^{(3)}$ is the derivative of Euler angles of Body 3 reference frame in columnwise form and is given as

$$\dot{\boldsymbol{\alpha}}^{(3)} = \begin{bmatrix} \dot{\alpha}_3 \\ \dot{\beta}_3 \\ \dot{\gamma}_3 \end{bmatrix} \quad (3.254)$$

$\bar{\mathbf{D}}^{(3)}$ is a transformation matrix from derivative of Euler angles of Body 3 reference frame to the angular velocity of Body 3 reference frame. It is expressed in Body 3 reference frame and is denoted as

$$\bar{\mathbf{D}}^{(3)} = \begin{bmatrix} c\beta_3 c\gamma_3 & s\gamma_3 & 0 \\ -c\beta_3 s\gamma_3 & c\gamma_3 & 0 \\ s\beta_3 & 0 & 1 \end{bmatrix} \quad (3.255)$$

Choosing $\bar{\boldsymbol{\omega}}^{(3)}$ as the rotational generalized speeds of Body 3, \mathbf{v}^{3i} is written as

$$\mathbf{v}^{3i} = \boldsymbol{\mu}^{3i} \mathbf{y}^{(3)} \quad (3.256)$$

where $\boldsymbol{\mu}^{3i}$ is the velocity influence coefficient matrix of Body 3 and is given as

$$\boldsymbol{\mu}^{3i} = \begin{bmatrix} \mathbf{I} & \mathbf{T}^{(3)} \tilde{\mathbf{q}}^{3i} & \mathbf{T}^{(3)} \boldsymbol{\phi}^{3i} \mathbf{B}^{3i} \boldsymbol{\chi}^{(3)} \end{bmatrix} \quad (3.257)$$

where \mathbf{I} is an identity matrix. $\mathbf{y}^{(3)}$ is the generalized speed vector of Body 3 and is given as

$$\mathbf{y}^{(3)} = \begin{bmatrix} \dot{\boldsymbol{\zeta}}^{(3)} \\ \bar{\boldsymbol{\omega}}^{(3)} \\ \dot{\boldsymbol{\eta}}^{(3)} \end{bmatrix} \quad (3.258)$$

Derivative of the generalized coordinates vector of Body 3 can be obtained from the generalized speeds vector of Body 3 as

$$\begin{bmatrix} \dot{\boldsymbol{\zeta}}^{(3)} \\ \dot{\boldsymbol{\alpha}}^{(3)} \\ \dot{\boldsymbol{\eta}}^{(3)} \end{bmatrix} = \begin{bmatrix} \mathbf{I} & \mathbf{0} & \mathbf{0} \\ \mathbf{0} & \bar{\mathbf{D}}^{(3)-1} & \mathbf{0} \\ \mathbf{0} & \mathbf{0} & \mathbf{I} \end{bmatrix} \begin{bmatrix} \dot{\boldsymbol{\zeta}}^{(3)} \\ \bar{\boldsymbol{\omega}}^{(3)} \\ \dot{\boldsymbol{\eta}}^{(3)} \end{bmatrix} \quad (3.259)$$

where \mathbf{I} is an identity matrix and inverse of the $\bar{\mathbf{D}}^{(3)}$ is given as

$$\bar{\mathbf{D}}^{(3)-1} = \begin{bmatrix} \frac{c\gamma_3}{c\beta_3} & -\frac{s\gamma_3}{c\beta_3} & 0 \\ s\gamma_3 & c\gamma_3 & 0 \\ -\frac{s\beta_3 c\gamma_3}{c\beta_3} & \frac{s\beta_3 s\gamma_3}{c\beta_3} & 1 \end{bmatrix} \quad (3.260)$$

$\beta_3 = \pm\pi/2$ and $\beta_3 = 3\pi/2$ are the singularities of the roll-pitch-yaw (1-2-3) sequence. At such positions, another sequence has to be used.

Acceleration of point P of element i of Body 3 is obtained by taking the time derivative of the velocity vector of element i of Body 3 as

$$\mathbf{a}^{3i} = \ddot{\boldsymbol{\zeta}}^{(3)} + \mathbf{T}^{(3)} \tilde{\mathbf{q}}^{3i} \dot{\boldsymbol{\omega}}^{(3)} + \mathbf{T}^{(3)} \boldsymbol{\phi}^{3i} \mathbf{B}^{3i} \boldsymbol{\chi}^{(3)} \dot{\boldsymbol{\eta}}^{(3)} + \dot{\mathbf{T}}^{(3)} \tilde{\mathbf{q}}^{3i} \boldsymbol{\omega}^{(3)} + \mathbf{T}^{(3)} \dot{\tilde{\mathbf{q}}}^{3i} \boldsymbol{\omega}^{(3)} + \dot{\mathbf{T}}^{(3)} \boldsymbol{\phi}^{3i} \mathbf{B}^{3i} \boldsymbol{\chi}^{(3)} \dot{\boldsymbol{\eta}}^{(3)} \quad (3.261)$$

which can be written shortly as

$$\mathbf{a}^{3i} = \boldsymbol{\mu}^{3i} \dot{\mathbf{y}}^{(3)} + \dot{\boldsymbol{\mu}}^{3i} \mathbf{y}^{(3)} \quad (3.262)$$

where $\dot{\mathbf{y}}^{(3)}$ is the generalized acceleration vector of Body 3 and is given as

$$\dot{\mathbf{y}}^{(3)} = \begin{bmatrix} \ddot{\boldsymbol{\zeta}}^{(3)} \\ \dot{\boldsymbol{\omega}}^{(3)} \\ \ddot{\boldsymbol{\eta}}^{(3)} \end{bmatrix} \quad (3.263)$$

$\boldsymbol{\mu}^{3i} \dot{\mathbf{y}}^{(3)}$ consists of the terms involving the generalized accelerations as shown below

$$\boldsymbol{\mu}^{3i} \dot{\mathbf{y}}^{(3)} = \ddot{\boldsymbol{\zeta}}^{(3)} + \mathbf{T}^{(3)} \tilde{\mathbf{q}}^{3i} \dot{\boldsymbol{\omega}}^{(3)} + \mathbf{T}^{(3)} \boldsymbol{\phi}^{3i} \mathbf{B}^{3i} \boldsymbol{\chi}^{(3)} \dot{\boldsymbol{\eta}}^{(3)} \quad (3.264)$$

$\dot{\boldsymbol{\mu}}^{3i} \mathbf{y}^{(3)}$ includes the Coriolis and centripetal accelerations as shown below

$$\dot{\boldsymbol{\mu}}^{3i} \mathbf{y}^{(3)} = -\mathbf{T}^{(3)} \widetilde{\boldsymbol{\omega}}^{(3)} \widetilde{\mathbf{q}}^{3i} \widetilde{\boldsymbol{\omega}}^{(3)} - 2\mathbf{T}^{(3)} \widetilde{\boldsymbol{\omega}}^{(3)} \boldsymbol{\phi}^{3i} \mathbf{B}^{3i} \boldsymbol{\chi}^{(3)} \dot{\boldsymbol{\eta}}^{(3)} \quad (3.265)$$

The dynamic equations of Body 3 can be derived by using the above kinematic expressions. Kane's equations are given as [53]

$$\mathbf{f}^{*(3)} + \mathbf{f}^{(3)} + \mathbf{f}^s{}^{(3)} + \mathbf{f}_{m_c}{}^{*(3)} + \mathbf{f}_{m_c}{}^{(3)} = \mathbf{0} \quad (3.266)$$

where $\mathbf{f}^{*(3)}$, $\mathbf{f}^{(3)}$ and $\mathbf{f}^s{}^{(3)}$ are the generalized inertia, external and stiffness forces of Body 3, respectively. $\mathbf{f}_{m_c}{}^{*(3)}$ and $\mathbf{f}_{m_c}{}^{(3)}$ are the generalized inertia and external forces of lumped mass m_c at point C of Body 3, respectively.

The generalized inertia forces of Body 3 can be written as

$$\mathbf{f}^{*(3)} = \int_{V_{3i}} \boldsymbol{\mu}^{3iT} (-\rho_{3i} \mathbf{a}^{3i}) dV \quad (3.267)$$

where ρ_{3i} represents the density of element i of Body 3 material and V_{3i} stands for the volume of element i of Body 3. Equation (3.267) can be expressed as the following form

$$\mathbf{f}^{*(3)} = -\mathbf{M}^{(3)} \dot{\mathbf{y}}^{(3)} + \mathbf{Q}^{(3)} \quad (3.268)$$

where $\mathbf{M}^{(3)}$ is the generalized mass matrix of Body 3 and is given as

$$\mathbf{M}^{(3)} = -\sum_{i=1}^{N_3} \int_{V_{3i}} \rho_{3i} \boldsymbol{\mu}^{3iT} \boldsymbol{\mu}^{3i} dV \quad (3.269)$$

where N_3 is the number of finite elements in Body 3. $\mathbf{Q}^{(3)}$ is the generalized Coriolis and centrifugal force vector of Body 3 and is given as

$$\mathbf{Q}^{(3)} = -\sum_{i=1}^{N_3} \int_{V_{3i}} \rho_{3i} \boldsymbol{\mu}^{3iT} \dot{\boldsymbol{\mu}}^{3i} \mathbf{y}^{(3)} dV \quad (3.270)$$

$\mathbf{M}^{(3)}$ can be written in terms of the generalized coordinates of Body 3 by substituting the partitioned form of $\boldsymbol{\mu}^{3i}$ into Equation (3.269) as follows

$$\mathbf{M}^{(3)} = \sum_{i=1}^{N_3} \int_{V_{3i}} \rho_{3i} \begin{bmatrix} \mathbf{I} & \mathbf{T}^{(3)} \tilde{\mathbf{q}}^{3i} & \mathbf{T}^{(3)} \boldsymbol{\phi}^{3i} \mathbf{B}^{3i} \boldsymbol{\chi}^{(3)} \\ \tilde{\mathbf{q}}^{3iT} \mathbf{T}^{(3)T} & \tilde{\mathbf{q}}^{3iT} \tilde{\mathbf{q}}^{3i} & \tilde{\mathbf{q}}^{3iT} \boldsymbol{\phi}^{3i} \mathbf{B}^{3i} \boldsymbol{\chi}^{(3)} \\ \boldsymbol{\chi}^{(3)T} \mathbf{B}^{3iT} \boldsymbol{\phi}^{3iT} \mathbf{T}^{(3)T} & \boldsymbol{\chi}^{(3)T} \mathbf{B}^{3iT} \boldsymbol{\phi}^{3iT} \tilde{\mathbf{q}}^{3i} & \boldsymbol{\chi}^{(3)T} \mathbf{B}^{3iT} \boldsymbol{\phi}^{3iT} \boldsymbol{\phi}^{3i} \mathbf{B}^{3i} \boldsymbol{\chi}^{(3)} \end{bmatrix} \quad (3.271)$$

In order to deal with each term separately, the submatrices of $\mathbf{M}^{(3)}$ corresponding to translation, rotation and elastic deformation are labelled as below

$$\mathbf{M}^{(3)} = \begin{bmatrix} \mathbf{M}_{tt}^{(3)} & \mathbf{M}_{tr}^{(3)} & \mathbf{M}_{te}^{(3)} \\ \mathbf{M}_{tr}^{(3)T} & \mathbf{M}_{rr}^{(3)} & \mathbf{M}_{re}^{(3)} \\ \mathbf{M}_{te}^{(3)T} & \mathbf{M}_{re}^{(3)T} & \mathbf{M}_{ee}^{(3)} \end{bmatrix} \quad (3.272)$$

The submatrices of $\mathbf{M}^{(3)}$ can be obtained in the following forms

$$\mathbf{M}_{tt}^{(3)} = \sum_{i=1}^{N_3} \int_{V_{3i}} \rho_{3i} \mathbf{I} dV \quad (3.273)$$

$$\mathbf{M}_{tr}^{(3)} = \mathbf{T}^{(3)} \sum_{i=1}^{N_3} \int_{V_{3i}} \rho_{3i} \tilde{\mathbf{q}}^{3i} dV \quad (3.274)$$

$$\mathbf{M}_{te}^{(3)} = \mathbf{T}^{(3)} \left\{ \sum_{i=1}^{N_3} \left(\int_{V_{3i}} \rho_{3i} \boldsymbol{\phi}^{3i} dV \right) \mathbf{B}^{3i} \right\} \boldsymbol{\chi}^{(3)} \quad (3.275)$$

$$\mathbf{M}_{rr}^{(3)} = \sum_{i=1}^{N_3} \int_{V_{3i}} \rho_{3i} \tilde{\mathbf{q}}^{3iT} \tilde{\mathbf{q}}^{3i} dV \quad (3.276)$$

$$\mathbf{M}_{re}^{(3)} = \left\{ \sum_{i=1}^{N_3} \left(\int_{V_{3i}} \rho_{3i} \tilde{\mathbf{q}}^{3iT} \boldsymbol{\phi}^{3i} dV \right) \mathbf{B}^{3i} \right\} \boldsymbol{\chi}^{(3)} \quad (3.277)$$

$$\mathbf{M}_{ce}^{(3)} = \boldsymbol{\chi}^{(3)T} \left\{ \sum_{i=1}^{N_3} \mathbf{B}^{3iT} \left(\int_{V_{3i}} \rho_{3i} \boldsymbol{\phi}^{3iT} \boldsymbol{\phi}^{3i} dV \right) \mathbf{B}^{3i} \right\} \boldsymbol{\chi}^{(3)} \quad (3.278)$$

$\mathbf{Q}^{(3)}$ can be written in terms of generalized coordinates and the generalized speeds by substituting the partitioned form of $\boldsymbol{\mu}^{3i}$ into Equation (3.270) as follows

$$\mathbf{Q}^{(3)} = \sum_{i=1}^{N_3} \int_{V_{3i}} \rho_{3i} \left[\begin{array}{l} \mathbf{T}^{(3)} \tilde{\boldsymbol{\omega}}^{(3)} \tilde{\mathbf{q}}^{3i} \tilde{\boldsymbol{\omega}}^{(3)} + 2\mathbf{T}^{(3)} \tilde{\boldsymbol{\omega}}^{(3)} \boldsymbol{\phi}^{3i} \mathbf{B}^{3i} \boldsymbol{\chi}^{(3)} \dot{\boldsymbol{\eta}}^{(3)} \\ \tilde{\mathbf{q}}^{3iT} \tilde{\boldsymbol{\omega}}^{(3)} \tilde{\mathbf{q}}^{3i} \tilde{\boldsymbol{\omega}}^{(3)} + 2\tilde{\mathbf{q}}^{3iT} \tilde{\boldsymbol{\omega}}^{(3)} \boldsymbol{\phi}^{3i} \mathbf{B}^{3i} \boldsymbol{\chi}^{(3)} \dot{\boldsymbol{\eta}}^{(3)} \\ \boldsymbol{\chi}^{(3)T} \mathbf{B}^{3iT} \boldsymbol{\phi}^{3iT} \tilde{\boldsymbol{\omega}}^{(3)} \tilde{\mathbf{q}}^{3i} \tilde{\boldsymbol{\omega}}^{(3)} + 2\boldsymbol{\chi}^{(3)T} \mathbf{B}^{3iT} \boldsymbol{\phi}^{3iT} \tilde{\boldsymbol{\omega}}^{(3)} \boldsymbol{\phi}^{3i} \mathbf{B}^{3i} \boldsymbol{\chi}^{(3)} \dot{\boldsymbol{\eta}}^{(3)} \end{array} \right] dV \quad (3.279)$$

In order to deal with each term separately, the subvectors of $\mathbf{Q}^{(3)}$ corresponding to translation, rotation and elastic deformation are labelled as below

$$\mathbf{Q}^{(3)} = \begin{bmatrix} \mathbf{Q}_t^{(3)} \\ \mathbf{Q}_r^{(3)} \\ \mathbf{Q}_e^{(3)} \end{bmatrix} \quad (3.280)$$

The subvectors of $\mathbf{Q}^{(3)}$ can be obtained in the following forms

$$\begin{aligned} \mathbf{Q}_t^{(3)} &= \mathbf{T}^{(3)} \tilde{\boldsymbol{\omega}}^{(3)} \left\{ \sum_{i=1}^{N_3} \int_{V_{3i}} \rho_{3i} \tilde{\mathbf{q}}^{3i} dV \right\} \tilde{\boldsymbol{\omega}}^{(3)} + \\ & 2\mathbf{T}^{(3)} \tilde{\boldsymbol{\omega}}^{(3)} \left\{ \sum_{i=1}^{N_3} \left(\int_{V_{3i}} \rho_{3i} \boldsymbol{\phi}^{3i} dV \right) \mathbf{B}^{3i} \right\} \boldsymbol{\chi}^{(3)} \dot{\boldsymbol{\eta}}^{(3)} \end{aligned} \quad (3.281)$$

$$\begin{aligned} \mathbf{Q}_r^{(3)} &= \left\{ \sum_{i=1}^{N_3} \int_{V_{3i}} \rho_{3i} \tilde{\mathbf{q}}^{3iT} \tilde{\boldsymbol{\omega}}^{(3)} \tilde{\mathbf{q}}^{3i} dV \right\} \tilde{\boldsymbol{\omega}}^{(3)} + \\ & 2 \left\{ \sum_{i=1}^{N_3} \left(\int_{V_{3i}} \rho_{3i} \tilde{\mathbf{q}}^{3iT} \tilde{\boldsymbol{\omega}}^{(3)} \boldsymbol{\phi}^{3i} dV \right) \mathbf{B}^{3i} \right\} \boldsymbol{\chi}^{(3)} \dot{\boldsymbol{\eta}}^{(3)} \end{aligned} \quad (3.282)$$

$$\mathbf{Q}_e^{(3)} = \boldsymbol{\chi}^{(3)T} \left\{ \sum_{i=1}^{N_3} \mathbf{B}^{3iT} \left(\int_{V_{3i}} \rho_{3i} \boldsymbol{\phi}^{3iT} \tilde{\boldsymbol{\omega}}^{(3)} \tilde{\mathbf{q}}^{3i} dV \right) \right\} \tilde{\boldsymbol{\omega}}^{(3)} +$$

$$2\boldsymbol{\chi}^{(3)T} \left\{ \sum_{i=1}^{N_3} \mathbf{B}^{3iT} \left(\int_{V_{3i}} \rho_{3i} \boldsymbol{\phi}^{3iT} \tilde{\boldsymbol{\omega}}^{(3)} \boldsymbol{\phi}^{3i} dV \right) \mathbf{B}^{3i} \right\} \boldsymbol{\chi}^{(3)} \dot{\boldsymbol{\eta}}^{(3)} \quad (3.283)$$

The generalized external force due to weight of Body 3 can be expressed as

$$\mathbf{f}^{g(3)} = \sum_{i=1}^{N_3} \int_{V_{3i}} \boldsymbol{\mu}^{3iT} (\rho_{3i} \mathbf{g}) dV \quad (3.284)$$

If $\boldsymbol{\mu}^{3i}$ is substituted into above equation, $\mathbf{f}^{g(3)}$ becomes

$$\mathbf{f}^{g(3)} = \sum_{i=1}^{N_3} \int_{V_{3i}} \rho_{3i} \begin{bmatrix} \mathbf{I} \\ \tilde{\mathbf{q}}^{3iT} \mathbf{T}^{(3)T} \\ \boldsymbol{\chi}^{(3)T} \mathbf{B}^{3iT} \boldsymbol{\phi}^{3iT} \mathbf{T}^{(3)T} \end{bmatrix} \mathbf{g} dV \quad (3.285)$$

In order to deal with each term separately, the subvectors of $\mathbf{f}^{g(3)}$ corresponding to translation, rotation and elastic deformation are labelled as below

$$\mathbf{f}^{g(3)} = \begin{bmatrix} \mathbf{f}_t^{g(3)} \\ \mathbf{f}_r^{g(3)} \\ \mathbf{f}_e^{g(3)} \end{bmatrix} \quad (3.286)$$

The subvectors of $\mathbf{f}^{g(3)}$ can be obtained as follows

$$\mathbf{f}_t^{g(3)} = \left(\sum_{i=1}^{N_3} \int_{V_{3i}} \rho_{3i} \mathbf{I} dV \right) \mathbf{g} \quad (3.287)$$

$$\mathbf{f}_r^{g(3)} = \left\{ \sum_{i=1}^{N_3} \int_{V_{3i}} \rho_{3i} \tilde{\mathbf{q}}^{3iT} dV \right\} \mathbf{T}^{(3)T} \mathbf{g} \quad (3.288)$$

$$\mathbf{f}_e^{g(3)} = \boldsymbol{\chi}^{(3)T} \left\{ \sum_{i=1}^{N_3} \mathbf{B}^{3iT} \left(\int_{V_{3i}} \rho_{3i} \boldsymbol{\phi}^{3iT} dV \right) \right\} \mathbf{T}^{(3)T} \mathbf{g} \quad (3.289)$$

The generalized external force due to torque \mathbf{T}_3 can be expressed as

$$\mathbf{f}^{e(\mathbf{T}_3)^{(3)}} = {}^{B_3} \boldsymbol{\Omega}^{B_3 T} {}^{B_3} \mathbf{T}_3 \quad (3.290)$$

where ${}^{B_3} \mathbf{T}_3$ is the torque vector applied to Body 3 due to actuator at point B expressed in joint frame B_3 and is written as

$${}^{B_3} \mathbf{T}_3 = \begin{bmatrix} 0 \\ 0 \\ T_3 \end{bmatrix} \quad (3.291)$$

${}^{B_3} \boldsymbol{\Omega}^{B_3}$ is the influence coefficient matrix of angular velocity of joint frame at point B of Body 3 expressed in the same frame and it can be obtained as

$${}^{B_3} \boldsymbol{\Omega}^{B_3} = \begin{bmatrix} \mathbf{0} & \mathbf{T}^{B_3-3} & \mathbf{T}^{B_3-3} \boldsymbol{\Psi}^{B_3} \mathbf{B}^{3r} \boldsymbol{\chi}^{(3)} \end{bmatrix} \quad (3.292)$$

where \mathbf{T}^{B_3-3} is the transformation matrix from Body 3 reference frame to the joint frame at B_3 due to angular deformation of Body 3. Angular deformation of element i of Body 3 expressed in Body 3 reference frame, $\bar{\boldsymbol{\gamma}}^{3i}$, can be written as

$$\bar{\boldsymbol{\gamma}}^{3i} = \boldsymbol{\Psi}^{3i} \mathbf{B}^{3i} \boldsymbol{\chi}^{(3)} \boldsymbol{\eta}^{(3)} \quad (3.293)$$

where $\boldsymbol{\Psi}^{3i}$ is given as

$$\boldsymbol{\Psi}^{3i} = \mathbf{T}^{3i} \mathbf{s}_{\text{rot}}^{3i} \mathbf{R}^{3i T} \quad (3.294)$$

where $\mathbf{s}_{\text{rot}}^{3i}$ is the rotation shape function matrix of element i of Body 3. Since $\bar{\boldsymbol{\gamma}}^{3i}$ are small angles vector (therefore, $s\bar{\boldsymbol{\gamma}}_j^{3i} \approx \bar{\boldsymbol{\gamma}}_j^{3i}$, $c\bar{\boldsymbol{\gamma}}_j^{3i} \approx 1$ for $j=1,2,3$), \mathbf{T}^{B_3-3} can be expressed in terms of Euler angles by using the roll-pitch-yaw sequence as

$$\mathbf{T}^{B_3-3} = \begin{bmatrix} 1 & -\bar{\boldsymbol{\gamma}}_3^{B_3} & \bar{\boldsymbol{\gamma}}_2^{B_3} \\ \bar{\boldsymbol{\gamma}}_3^{B_3} & 1 & -\bar{\boldsymbol{\gamma}}_1^{B_3} \\ -\bar{\boldsymbol{\gamma}}_2^{B_3} & \bar{\boldsymbol{\gamma}}_1^{B_3} & 1 \end{bmatrix} \quad (3.295)$$

where $\bar{\boldsymbol{\gamma}}^{B_3}$ is the value of $\bar{\boldsymbol{\gamma}}^{3i}$ evaluated at point B_3 . $\boldsymbol{\Psi}^{B_3}$ is the value of $\boldsymbol{\Psi}^{3i}$ evaluated at point B_3 and \mathbf{B}^{3r} is the Boolean matrix of the element of Body 3 that includes point B.

Therefore, $\mathbf{f}^{e(T_3)^{(3)}}$ can be written as

$$\mathbf{f}^{e(T_3)^{(3)}} = \begin{bmatrix} \mathbf{0} \\ \mathbf{T}^{B_3-3T} \\ \boldsymbol{\chi}^{(3)T} \mathbf{B}^{3rT} \boldsymbol{\Psi}^{B_3T} \mathbf{T}^{B_3-3T} \end{bmatrix}_{B_3} \mathbf{T}_3 \quad (3.296)$$

In order to deal with each term separately, the subvectors of $\mathbf{f}^{e(T_3)^{(3)}}$ corresponding to translation, rotation and elastic deformation are labelled as below

$$\mathbf{f}^{e(T_3)^{(3)}} = \begin{bmatrix} \mathbf{f}_t^{e(T_3)^{(3)}} \\ \mathbf{f}_r^{e(T_3)^{(3)}} \\ \mathbf{f}_e^{e(T_3)^{(3)}} \end{bmatrix} \quad (3.297)$$

The subvectors of $\mathbf{f}^{e(T_3)^{(3)}}$ can be obtained as follows

$$\mathbf{f}_t^{e(T_3)^{(3)}} = \mathbf{0} \quad (3.298)$$

$$\mathbf{f}_r^{e(T_3)^{(3)}} = \mathbf{T}^{B_3-3T} \mathbf{T}_3 \quad (3.299)$$

$$\mathbf{f}_e^{e(T_3)^{(3)}} = \boldsymbol{\chi}^{(3)T} \mathbf{B}^{3rT} \boldsymbol{\Psi}^{B_3T} \mathbf{T}^{B_3-3T} \mathbf{T}_3 \quad (3.300)$$

Generalized structural stiffness forces of Body 3, $\mathbf{f}^{s(3)}$, are found from the work done by the stiffness forces of Body 3 which is equal to the negative of the strain energy of Body 3. Therefore, $\mathbf{f}^{s(3)}$ can be obtained as follows

$$\mathbf{f}^{s(3)} = - \begin{bmatrix} 0 \\ 0 \\ 0 \\ 0 \\ 0 \\ 0 \\ \boldsymbol{\chi}^{(3)T} \mathbf{K}^{(3)} \boldsymbol{\chi}^{(3)} \boldsymbol{\eta}^{(3)} \end{bmatrix} \quad (3.301)$$

where $\mathbf{K}^{(3)}$ is the structural stiffness matrix of Body 3 and it can be formed as

$$\mathbf{K}^{(3)} = \sum_{i=1}^{N_3} \mathbf{B}^{3iT} \mathbf{K}^{3i} \mathbf{B}^{3i} \quad (3.302)$$

where \mathbf{K}^{3i} is the structural stiffness matrix of element i of Body 3 expressed in Body 3 reference frame and is given as

$$\mathbf{K}^{3i} = \mathbf{R}^{3i} \mathbf{H}^{3i} \mathbf{R}^{3iT} \quad (3.303)$$

where \mathbf{H}^{3i} is the structural stiffness matrix of element i of Body 3 expressed in element i frame.

The generalized inertia forces due to lumped mass m_C at point C of Body 3 can be written as

$$\mathbf{f}_{m_C}^{*(3)} = \boldsymbol{\mu}^{CT} (-m_C \mathbf{a}^C) \quad (3.304)$$

where $\boldsymbol{\mu}^C$ is the velocity influence coefficient matrix of point C of Body 3 and \mathbf{a}^C is the acceleration of point C of Body 3. Equation (3.304) can be expressed as

$$\mathbf{f}_{m_c}^{*(3)} = -\mathbf{M}_{m_c}^{(3)} \dot{\mathbf{y}}^{(3)} + \mathbf{Q}_{m_c}^{(3)} \quad (3.305)$$

where $\mathbf{M}_{m_c}^{(3)}$ is the generalized mass matrix of lumped mass m_c and is given as

$$\mathbf{M}_{m_c}^{(3)} = m_c \boldsymbol{\mu}^{C^T} \boldsymbol{\mu}^C \quad (3.306)$$

$\mathbf{Q}_{m_c}^{(3)}$ is the generalized Coriolis and centrifugal force vector of lumped mass m_c and is given as

$$\mathbf{Q}_{m_c}^{(3)} = -m_c \boldsymbol{\mu}^{C^T} \dot{\boldsymbol{\mu}}^C \mathbf{y}^{(3)} \quad (3.307)$$

$\mathbf{M}_{m_c}^{(3)}$ can be written in terms of the generalized coordinates of Body 3 by substituting the partitioned form of $\boldsymbol{\mu}^C$ into Equation (3.306) as follows

$$\mathbf{M}_{m_c}^{(3)} = m_c \begin{bmatrix} \mathbf{I} & \mathbf{T}^{(3)} \tilde{\mathbf{q}}^{C_3} & \mathbf{T}^{(3)} \boldsymbol{\phi}^{C_3} \mathbf{B}^{3r} \boldsymbol{\chi}^{(3)} \\ \tilde{\mathbf{q}}^{C_3^T} \mathbf{T}^{(3)^T} & \tilde{\mathbf{q}}^{C_3^T} \tilde{\mathbf{q}}^{C_3} & \tilde{\mathbf{q}}^{C_3^T} \boldsymbol{\phi}^{C_3} \mathbf{B}^{3r} \boldsymbol{\chi}^{(3)} \\ \boldsymbol{\chi}^{(3)^T} \mathbf{B}^{3r^T} \boldsymbol{\phi}^{C_3^T} \mathbf{T}^{(3)^T} & \boldsymbol{\chi}^{(3)^T} \mathbf{B}^{3r^T} \boldsymbol{\phi}^{C_3^T} \tilde{\mathbf{q}}^{C_3} & \boldsymbol{\chi}^{(3)^T} \mathbf{B}^{3r^T} \boldsymbol{\phi}^{C_3^T} \boldsymbol{\phi}^{C_3} \mathbf{B}^{3r} \boldsymbol{\chi}^{(3)} \end{bmatrix} \quad (3.308)$$

where $\tilde{\mathbf{q}}^{C_3}$ is the skew symmetric matrix of the vector $\bar{\mathbf{q}}^{C_3}$, $\bar{\mathbf{q}}^{C_3}$ is the position vector from Body 3 reference frame to point C of Body 3 at deformed state expressed in Body 3 reference frame, $\boldsymbol{\phi}^{C_3}$ is the value of $\boldsymbol{\phi}^{3i}$ at point C of Body 3 and \mathbf{B}^{3r} is the Boolean matrix of the element of Body 3 that includes point C.

In order to deal with each term separately, the submatrices of $\mathbf{M}_{m_c}^{(3)}$ corresponding to translation, rotation and elastic deformation are labelled as below

$$\mathbf{M}_{m_c}^{(3)} = \begin{bmatrix} \mathbf{M}_{m_{C_{tt}}}^{(3)} & \mathbf{M}_{m_{C_{tr}}}^{(3)} & \mathbf{M}_{m_{C_{te}}}^{(3)} \\ \mathbf{M}_{m_{C_{tr}}}^{(3)T} & \mathbf{M}_{m_{C_{rr}}}^{(3)} & \mathbf{M}_{m_{C_{re}}}^{(3)} \\ \mathbf{M}_{m_{C_{te}}}^{(3)T} & \mathbf{M}_{m_{C_{re}}}^{(3)T} & \mathbf{M}_{m_{C_{ee}}}^{(3)} \end{bmatrix} \quad (3.309)$$

The submatrices of $\mathbf{M}_{m_c}^{(3)}$ can be obtained in the following forms

$$\mathbf{M}_{m_{C_{tt}}}^{(3)} = m_c \mathbf{I} \quad (3.310)$$

$$\mathbf{M}_{m_{C_{tr}}}^{(3)} = m_c \mathbf{T}^{(3)} \tilde{\mathbf{q}}^{C_3} \quad (3.311)$$

$$\mathbf{M}_{m_{C_{te}}}^{(3)} = m_c \mathbf{T}^{(3)} \phi^{C_3} \mathbf{B}^{3r} \chi^{(3)} \quad (3.312)$$

$$\mathbf{M}_{m_{C_{rr}}}^{(3)} = m_c \tilde{\mathbf{q}}^{C_3 T} \tilde{\mathbf{q}}^{C_3} \quad (3.313)$$

$$\mathbf{M}_{m_{C_{re}}}^{(3)} = m_c \tilde{\mathbf{q}}^{C_3 T} \phi^{C_3} \mathbf{B}^{3r} \chi^{(3)} \quad (3.314)$$

$$\mathbf{M}_{m_{C_{ee}}}^{(3)} = m_c \chi^{(3)T} \mathbf{B}^{3rT} \phi^{C_3 T} \phi^{C_3} \mathbf{B}^{3r} \chi^{(3)} \quad (3.315)$$

$\mathbf{Q}_{m_c}^{(3)}$ can be written in terms of the generalized coordinates and the generalized speeds by substituting the partitioned form of $\boldsymbol{\mu}^C$ into Equation (3.307) as follows

$$\mathbf{Q}_{m_c}^{(3)} = m_c \begin{bmatrix} \mathbf{T}^{(3)} \tilde{\boldsymbol{\omega}}^{(3)} \tilde{\mathbf{q}}^{C_3} \bar{\boldsymbol{\omega}}^{(3)} + 2\mathbf{T}^{(3)} \tilde{\boldsymbol{\omega}}^{(3)} \phi^{C_3} \mathbf{B}^{3r} \chi^{(3)} \dot{\boldsymbol{\eta}}^{(3)} \\ \tilde{\mathbf{q}}^{C_3 T} \tilde{\boldsymbol{\omega}}^{(3)} \tilde{\mathbf{q}}^{C_3} \bar{\boldsymbol{\omega}}^{(3)} + 2\tilde{\mathbf{q}}^{C_3 T} \tilde{\boldsymbol{\omega}}^{(3)} \phi^{C_3} \mathbf{B}^{3r} \chi^{(3)} \dot{\boldsymbol{\eta}}^{(3)} \\ \chi^{(3)T} \mathbf{B}^{3rT} \phi^{C_3 T} \tilde{\boldsymbol{\omega}}^{(3)} \tilde{\mathbf{q}}^{C_3} \bar{\boldsymbol{\omega}}^{(3)} + 2\chi^{(3)T} \mathbf{B}^{3rT} \phi^{C_3 T} \tilde{\boldsymbol{\omega}}^{(3)} \phi^{C_3} \mathbf{B}^{3r} \chi^{(3)} \dot{\boldsymbol{\eta}}^{(3)} \end{bmatrix} \quad (3.316)$$

In order to deal with each term separately, the subvectors of $\mathbf{Q}_{m_c}^{(3)}$ corresponding to translation, rotation and elastic deformation are labelled as below

$$\mathbf{Q}_{m_c}^{(3)} = \begin{bmatrix} \mathbf{Q}_{m_{C_t}}^{(3)} \\ \mathbf{Q}_{m_{C_r}}^{(3)} \\ \mathbf{Q}_{m_{C_e}}^{(3)} \end{bmatrix} \quad (3.317)$$

The subvectors of $\mathbf{Q}_{m_c}^{(3)}$ can be obtained in the following forms

$$\mathbf{Q}_{m_{C_t}}^{(3)} = m_C \mathbf{T}^{(3)} \tilde{\boldsymbol{\omega}}^{(3)} \tilde{\mathbf{q}}^{C_3} \overline{\boldsymbol{\omega}}^{(3)} + 2m_C \mathbf{T}^{(3)} \tilde{\boldsymbol{\omega}}^{(3)} \boldsymbol{\phi}^{C_3} \mathbf{B}^{3r} \boldsymbol{\chi}^{(3)} \dot{\boldsymbol{\eta}}^{(3)} \quad (3.318)$$

$$\mathbf{Q}_{m_{C_r}}^{(3)} = m_C \tilde{\mathbf{q}}^{C_3 T} \tilde{\boldsymbol{\omega}}^{(3)} \tilde{\mathbf{q}}^{C_3} \overline{\boldsymbol{\omega}}^{(3)} + 2m_C \tilde{\mathbf{q}}^{C_3 T} \tilde{\boldsymbol{\omega}}^{(3)} \boldsymbol{\phi}^{C_3} \mathbf{B}^{3r} \boldsymbol{\chi}^{(3)} \dot{\boldsymbol{\eta}}^{(3)} \quad (3.319)$$

$$\mathbf{Q}_{m_{C_e}}^{(3)} = m_C \boldsymbol{\chi}^{(3)T} \mathbf{B}^{3rT} \boldsymbol{\phi}^{C_3 T} \tilde{\boldsymbol{\omega}}^{(3)} \tilde{\mathbf{q}}^{C_3} \overline{\boldsymbol{\omega}}^{(3)} + 2m_C \boldsymbol{\chi}^{(3)T} \mathbf{B}^{3rT} \boldsymbol{\phi}^{C_3 T} \tilde{\boldsymbol{\omega}}^{(3)} \boldsymbol{\phi}^{C_3} \mathbf{B}^{3r} \boldsymbol{\chi}^{(3)} \dot{\boldsymbol{\eta}}^{(3)} \quad (3.320)$$

The generalized external force due to weight of lumped mass m_C can be expressed as

$$\mathbf{f}_{m_C}^{g(3)} = \boldsymbol{\mu}^{CT} (m_C \mathbf{g} \mathbf{s}) \quad (3.321)$$

If $\boldsymbol{\mu}^C$ is substituted into above equation $\mathbf{f}_{m_C}^{g(3)}$ becomes

$$\mathbf{f}_{m_C}^{g(3)} = m_C \begin{bmatrix} \mathbf{I} \\ \tilde{\mathbf{q}}^{C_3 T} \mathbf{T}^{(3)T} \\ \boldsymbol{\chi}^{(3)T} \mathbf{B}^{3rT} \boldsymbol{\phi}^{C_3 T} \mathbf{T}^{(3)T} \end{bmatrix} \mathbf{g} \mathbf{s} \quad (3.322)$$

In order to deal with each term separately, the subvectors of $\mathbf{f}_{m_C}^{g(3)}$ corresponding to translation, rotation and elastic deformation are labelled as

$$\mathbf{f}_{m_C}^{g(3)} = \begin{bmatrix} \mathbf{f}_{m_{C_t}}^{g(3)} \\ \mathbf{f}_{m_{C_r}}^{g(3)} \\ \mathbf{f}_{m_{C_e}}^{g(3)} \end{bmatrix} \quad (3.323)$$

The subvectors of $\mathbf{f}_{m_C}^{g(3)}$ can be obtained as follows

$$\mathbf{f}_{m_{C_t}}^{g(3)} = m_C \mathbf{I} \mathbf{g} \mathbf{s} \quad (3.324)$$

$$\mathbf{f}_{m_{C_r}}^{g(3)} = m_C \tilde{\mathbf{q}}^{C_3 T} \mathbf{T}^{(3)T} \mathbf{g} \mathbf{s} \quad (3.325)$$

$$\mathbf{f}_{m_{c_e}}^{g^{(3)}} = m_{c_e} \boldsymbol{\chi}^{(3)T} \mathbf{B}^{3rT} \boldsymbol{\phi}^{c_3T} \mathbf{T}^{(3)T} \mathbf{g} \mathbf{s} \quad (3.326)$$

The time and space dependent quantities have to be separated so that the space integrals can be evaluated. In the following equations superscript k refers to Body k.

$$\int_{V_{ki}} \rho_{ki} \tilde{\mathbf{q}}^{ki} dV = \begin{bmatrix} 0 & \int_{V_{ki}} \rho_{ki} \bar{\mathbf{q}}_3^{ki} dV & - \int_{V_{ki}} \rho_{ki} \bar{\mathbf{q}}_2^{ki} dV \\ - \int_{V_{ki}} \rho_{ki} \bar{\mathbf{q}}_3^{ki} dV & 0 & \int_{V_{ki}} \rho_{ki} \bar{\mathbf{q}}_1^{ki} dV \\ \int_{V_{ki}} \rho_{ki} \bar{\mathbf{q}}_2^{ki} dV & - \int_{V_{ki}} \rho_{ki} \bar{\mathbf{q}}_1^{ki} dV & 0 \end{bmatrix} \quad (3.327)$$

$$\int_{V_{ki}} \rho_{ki} \bar{\mathbf{q}}_j^{ki} dV = \int_{V_{ki}} \rho_{ki} (\bar{\mathbf{b}}_j^{ki} + \bar{\mathbf{r}}_j^{ki}) dV + \int_{V_{ki}} \rho_{ki} \boldsymbol{\phi}_j^{ki} dV \mathbf{B}^{ki} \boldsymbol{\chi}^k \boldsymbol{\eta}^k \quad j = 1,2,3 \quad (3.328)$$

where subscript j refers to the j th row of the corresponding matrix or vector.

$$\int_{V_{ki}} \rho_{ki} \tilde{\mathbf{q}}^{kiT} \tilde{\mathbf{q}}^{ki} dV = \begin{bmatrix} \int_{V_{ki}} \rho_{ki} \bar{\mathbf{q}}_3^{kiT} \bar{\mathbf{q}}_3^{ki} dV + \int_{V_{ki}} \rho_{ki} \bar{\mathbf{q}}_2^{kiT} \bar{\mathbf{q}}_2^{ki} dV \\ - \int_{V_{ki}} \rho_{ki} \bar{\mathbf{q}}_1^{kiT} \bar{\mathbf{q}}_2^{ki} dV \\ - \int_{V_{ki}} \rho_{ki} \bar{\mathbf{q}}_1^{kiT} \bar{\mathbf{q}}_3^{ki} dV \\ - \int_{V_{ki}} \rho_{ki} \bar{\mathbf{q}}_2^{kiT} \bar{\mathbf{q}}_1^{ki} dV \\ \int_{V_{ki}} \rho_{ki} \bar{\mathbf{q}}_3^{kiT} \bar{\mathbf{q}}_3^{ki} dV + \int_{V_{ki}} \rho_{ki} \bar{\mathbf{q}}_1^{kiT} \bar{\mathbf{q}}_1^{ki} dV \\ - \int_{V_{ki}} \rho_{ki} \bar{\mathbf{q}}_2^{kiT} \bar{\mathbf{q}}_3^{ki} dV \\ - \int_{V_{ki}} \rho_{ki} \bar{\mathbf{q}}_3^{kiT} \bar{\mathbf{q}}_1^{ki} dV \\ - \int_{V_{ki}} \rho_{ki} \bar{\mathbf{q}}_3^{kiT} \bar{\mathbf{q}}_2^{ki} dV \\ \int_{V_{ki}} \rho_{ki} \bar{\mathbf{q}}_2^{kiT} \bar{\mathbf{q}}_2^{ki} dV + \int_{V_{ki}} \rho_{ki} \bar{\mathbf{q}}_1^{kiT} \bar{\mathbf{q}}_1^{ki} dV \end{bmatrix} \quad (3.329)$$

$$\begin{aligned}
\int_{V_{ki}} \rho_{ki} \bar{q}_j^{kiT} \bar{q}_t^{ki} dV &= \int_{V_{ki}} \rho_{ki} (\bar{b}_j^{ki} + \bar{r}_j^{ki}) (\bar{b}_t^{ki} + \bar{r}_t^{ki}) dV + \\
&\int_{V_{ki}} \rho_{ki} (\bar{b}_j^{ki} + \bar{r}_j^{ki}) \phi_t^{ki} dV \mathbf{B}^{ki} \boldsymbol{\chi}^k \boldsymbol{\eta}^k + \\
&\boldsymbol{\eta}^{kT} \boldsymbol{\chi}^{kT} \mathbf{B}^{kiT} \int_{V_{ki}} \rho_{ki} \phi_j^{kiT} (\bar{b}_t^{ki} + \bar{r}_t^{ki}) dV + \\
&\boldsymbol{\eta}^{kT} \boldsymbol{\chi}^{kT} \mathbf{B}^{kiT} \int_{V_{ki}} \rho_{ki} \phi_j^{kiT} \phi_t^{ki} dV \mathbf{B}^{ki} \boldsymbol{\chi}^k \boldsymbol{\eta}^k \quad j, t = 1, 2, 3 \quad (3.330)
\end{aligned}$$

where subscript t refers to the t th row of corresponding matrix or vector.

$$\int_{V_{ki}} \rho_{ki} \tilde{\bar{q}}^{kiT} \phi^{ki} dV = \begin{bmatrix} - \int_{V_{ki}} \rho_{ki} \bar{q}_3^{kiT} \phi_2^{ki} dV + \int_{V_{ki}} \rho_{ki} \bar{q}_2^{kiT} \phi_3^{ki} dV \\ \int_{V_{ki}} \rho_{ki} \bar{q}_3^{kiT} \phi_1^{ki} dV - \int_{V_{ki}} \rho_{ki} \bar{q}_1^{kiT} \phi_3^{ki} dV \\ - \int_{V_{ki}} \rho_{ki} \bar{q}_2^{kiT} \phi_1^{ki} dV + \int_{V_{ki}} \rho_{ki} \bar{q}_1^{kiT} \phi_2^{ki} dV \end{bmatrix} \quad (3.331)$$

$$\begin{aligned}
\int_{V_{ki}} \rho_{ki} \bar{q}_j^{kiT} \phi_t^{ki} dV &= \int_{V_{ki}} \rho_{ki} (\bar{b}_j^{ki} + \bar{r}_j^{ki}) \phi_t^{ki} dV + \\
&\boldsymbol{\eta}^{kT} \boldsymbol{\chi}^{kT} \mathbf{B}^{kiT} \int_{V_{ki}} \rho_{ki} \phi_j^{kiT} \phi_t^{ki} dV \quad j, t = 1, 2, 3 \quad (3.332)
\end{aligned}$$

$$\int_{V_{ki}} \rho_{ki} \tilde{\bar{q}}^{kiT} \tilde{\bar{\omega}}^k \tilde{\bar{q}}^{ki} dV = \begin{bmatrix} \bar{\omega}_1^k \int_{V_{ki}} \rho_{ki} \bar{q}_2^{kiT} \bar{q}_3^{ki} dV - \bar{\omega}_1^k \int_{V_{ki}} \rho_{ki} \bar{q}_3^{kiT} \bar{q}_2^{ki} dV \\ - \bar{\omega}_3^k \int_{V_{ki}} \rho_{ki} \bar{q}_3^{kiT} \bar{q}_3^{ki} dV - \bar{\omega}_1^k \int_{V_{ki}} \rho_{ki} \bar{q}_1^{kiT} \bar{q}_3^{ki} dV - \bar{\omega}_2^k \int_{V_{ki}} \rho_{ki} \bar{q}_3^{kiT} \bar{q}_2^{ki} dV \\ \bar{\omega}_3^k \int_{V_{ki}} \rho_{ki} \bar{q}_2^{kiT} \bar{q}_3^{ki} dV + \bar{\omega}_2^k \int_{V_{ki}} \rho_{ki} \bar{q}_2^{kiT} \bar{q}_2^{ki} dV + \bar{\omega}_1^k \int_{V_{ki}} \rho_{ki} \bar{q}_1^{kiT} \bar{q}_2^{ki} dV \end{bmatrix}$$

$$\begin{aligned}
&\bar{\omega}_3^k \int_{V_{ki}} \rho_{ki} \bar{q}_3^{kiT} \bar{q}_3^{ki} dV + \bar{\omega}_2^k \int_{V_{ki}} \rho_{ki} \bar{q}_2^{kiT} \bar{q}_3^{ki} dV + \bar{\omega}_1^k \int_{V_{ki}} \rho_{ki} \bar{q}_3^{kiT} \bar{q}_1^{ki} dV \\
&- \bar{\omega}_2^k \int_{V_{ki}} \rho_{ki} \bar{q}_1^{kiT} \bar{q}_3^{ki} dV + \bar{\omega}_2^k \int_{V_{ki}} \rho_{ki} \bar{q}_3^{kiT} \bar{q}_1^{ki} dV \\
&- \bar{\omega}_3^k \int_{V_{ki}} \rho_{ki} \bar{q}_1^{kiT} \bar{q}_3^{ki} dV - \bar{\omega}_2^k \int_{V_{ki}} \rho_{ki} \bar{q}_2^{kiT} \bar{q}_1^{ki} dV - \bar{\omega}_1^k \int_{V_{ki}} \rho_{ki} \bar{q}_1^{kiT} \bar{q}_1^{ki} dV
\end{aligned}$$

$$\left. \begin{aligned}
& -\bar{\omega}_3^k \int_{V_{ki}} \rho_{ki} \bar{q}_3^{kiT} \bar{q}_2^{ki} dV - \bar{\omega}_2^k \int_{V_{ki}} \rho_{ki} \bar{q}_2^{kiT} \bar{q}_2^{ki} dV - \bar{\omega}_1^k \int_{V_{ki}} \rho_{ki} \bar{q}_2^{kiT} \bar{q}_1^{ki} dV \\
& \bar{\omega}_2^k \int_{V_{ki}} \rho_{ki} \bar{q}_1^{kiT} \bar{q}_2^{ki} dV + \bar{\omega}_3^k \int_{V_{ki}} \rho_{ki} \bar{q}_3^{kiT} \bar{q}_1^{ki} dV + \bar{\omega}_1^k \int_{V_{ki}} \rho_{ki} \bar{q}_1^{kiT} \bar{q}_1^{ki} dV \\
& \bar{\omega}_3^k \int_{V_{ki}} \rho_{ki} \bar{q}_1^{kiT} \bar{q}_2^{ki} dV - \bar{\omega}_3^k \int_{V_{ki}} \rho_{ki} \bar{q}_2^{kiT} \bar{q}_1^{ki} dV
\end{aligned} \right] \quad (3.333)$$

$$\int_{V_{ki}} \rho_{ki} \tilde{\mathbf{q}}^{kiT} \tilde{\boldsymbol{\omega}}^k \boldsymbol{\phi}^{ki} dV = \left[\begin{aligned}
& \bar{\omega}_3^k \int_{V_{ki}} \rho_{ki} \bar{q}_3^{kiT} \boldsymbol{\phi}_1^{ki} dV + \bar{\omega}_2^k \int_{V_{ki}} \rho_{ki} \bar{q}_2^{kiT} \boldsymbol{\phi}_1^{ki} dV - \\
& -\bar{\omega}_2^k \int_{V_{ki}} \rho_{ki} \bar{q}_1^{kiT} \boldsymbol{\phi}_1^{ki} dV + \bar{\omega}_3^k \int_{V_{ki}} \rho_{ki} \bar{q}_3^{kiT} \boldsymbol{\phi}_2^{ki} dV + \\
& -\bar{\omega}_3^k \int_{V_{ki}} \rho_{ki} \bar{q}_1^{kiT} \boldsymbol{\phi}_1^{ki} dV - \bar{\omega}_3^k \int_{V_{ki}} \rho_{ki} \bar{q}_2^{kiT} \boldsymbol{\phi}_2^{ki} dV + \\
& \bar{\omega}_1^k \int_{V_{ki}} \rho_{ki} \bar{q}_2^{kiT} \boldsymbol{\phi}_2^{ki} dV - \bar{\omega}_1^k \int_{V_{ki}} \rho_{ki} \bar{q}_3^{kiT} \boldsymbol{\phi}_3^{ki} dV \\
& \boldsymbol{\omega}_1^k \int_{V_{ki}} \rho_{ki} \bar{q}_1^{kiT} \boldsymbol{\phi}_2^{ki} dV - \bar{\omega}_2^k \int_{V_{ki}} \rho_{ki} \bar{q}_3^{kiT} \boldsymbol{\phi}_3^{ki} dV \\
& \bar{\omega}_2^k \int_{V_{ki}} \rho_{ki} \bar{q}_2^{kiT} \boldsymbol{\phi}_3^{ki} dV + \bar{\omega}_1^k \int_{V_{ki}} \rho_{ki} \bar{q}_1^{kiT} \boldsymbol{\phi}_3^{ki} dV
\end{aligned} \right] \quad (3.334)$$

$$\int_{V_{ki}} \rho_{ki} \bar{q}_j^{kiT} \boldsymbol{\phi}_t^{ki} dV = \int_{V_{ki}} \rho_{ki} (\bar{\mathbf{b}}_j^{ki} + \bar{\mathbf{r}}_j^{ki}) \boldsymbol{\phi}_t^{ki} dV + \boldsymbol{\eta}^{kT} \boldsymbol{\chi}^{kT} \mathbf{B}^{kiT} \int_{V_{ki}} \rho_{ki} \boldsymbol{\phi}_j^{kiT} \boldsymbol{\phi}_t^{ki} dV \quad j, t = 1,2,3 \quad (3.335)$$

$$\int_{V_{ki}} \rho_{ki} \boldsymbol{\phi}^{kiT} \tilde{\boldsymbol{\omega}}^k \tilde{\mathbf{q}}^{kiT} dV = \left[\begin{aligned}
& -\bar{\omega}_3^k \int_{V_{ki}} \rho_{ki} \boldsymbol{\phi}_1^{kiT} \bar{q}_3^{ki} dV + \bar{\omega}_1^k \int_{V_{ki}} \rho_{ki} \boldsymbol{\phi}_3^{kiT} \bar{q}_3^{ki} dV - \\
& \bar{\omega}_2^k \int_{V_{ki}} \rho_{ki} \boldsymbol{\phi}_1^{kiT} \bar{q}_2^{ki} dV + \bar{\omega}_1^k \int_{V_{ki}} \rho_{ki} \boldsymbol{\phi}_2^{kiT} \bar{q}_2^{ki} dV \\
& -\bar{\omega}_3^k \int_{V_{ki}} \rho_{ki} \boldsymbol{\phi}_2^{kiT} \bar{q}_3^{ki} dV + \bar{\omega}_2^k \int_{V_{ki}} \rho_{ki} \boldsymbol{\phi}_3^{kiT} \bar{q}_3^{ki} dV + \\
& \bar{\omega}_2^k \int_{V_{ki}} \rho_{ki} \boldsymbol{\phi}_1^{kiT} \bar{q}_1^{ki} dV - \bar{\omega}_1^k \int_{V_{ki}} \rho_{ki} \boldsymbol{\phi}_2^{kiT} \bar{q}_1^{ki} dV \\
& \bar{\omega}_3^k \int_{V_{ki}} \rho_{ki} \boldsymbol{\phi}_2^{kiT} \bar{q}_2^{ki} dV - \bar{\omega}_2^k \int_{V_{ki}} \rho_{ki} \boldsymbol{\phi}_3^{kiT} \bar{q}_2^{ki} dV + \\
& \bar{\omega}_3^k \int_{V_{ki}} \rho_{ki} \boldsymbol{\phi}_1^{kiT} \bar{q}_1^{ki} dV - \bar{\omega}_1^k \int_{V_{ki}} \rho_{ki} \boldsymbol{\phi}_3^{kiT} \bar{q}_1^{ki} dV
\end{aligned} \right] \quad (3.336)$$

$$\int_{V_{ki}} \rho_{ki} \phi_j^{kiT} \bar{q}_t^{ki} dV = \int_{V_{ki}} \rho_{ki} \phi_j^{kiT} (\bar{b}_t^{ki} + \bar{r}_t^{ki}) dV + \int_{V_{ki}} \rho_{ki} \phi_j^{kiT} \phi_t^{ki} dV \mathbf{B}^{ki} \boldsymbol{\chi}^k \boldsymbol{\eta}^k \quad j, t = 1, 2, 3 \quad (3.337)$$

$$\int_{V_{ki}} \rho_{ki} \phi^{kiT} \tilde{\boldsymbol{\omega}}^k \phi^{ki} dV = -\bar{\boldsymbol{\omega}}_3^k \int_{V_{ki}} \rho_{ki} \phi_2^{kiT} \phi_1^{ki} dV + \bar{\boldsymbol{\omega}}_2^k \int_{V_{ki}} \rho_{ki} \phi_3^{kiT} \phi_1^{ki} dV + \bar{\boldsymbol{\omega}}_3^k \int_{V_{ki}} \rho_{ki} \phi_1^{kiT} \phi_2^{ki} dV - \bar{\boldsymbol{\omega}}_1^k \int_{V_{ki}} \rho_{ki} \phi_3^{kiT} \phi_2^{ki} dV - \bar{\boldsymbol{\omega}}_2^k \int_{V_{ki}} \rho_{ki} \phi_1^{kiT} \phi_3^{ki} dV + \bar{\boldsymbol{\omega}}_1^k \int_{V_{ki}} \rho_{ki} \phi_2^{kiT} \phi_3^{ki} dV \quad (3.338)$$

The inertia properties of the beam element used for the spatial robot are given in Appendix B.

3.3.2 Constraint Equations

7 possible constraint equations can be written for the robot in consideration. The velocity level constraint equations can be written as follows:

Two scalar equations can be written for the revolute joint at point A by equating the first and second components of the angular velocity vector of point A of Body 1, $\boldsymbol{\omega}^{A_1}$, and the angular velocity vector of point A of Body 2, $\boldsymbol{\omega}^{A_2}$.

The angular velocity of joint frame at point A of Body 1 can be expressed in the same frame as follows

$${}^{A_1} \boldsymbol{\omega}^{A_1} = \begin{bmatrix} 0 \\ 1 \\ 0 \end{bmatrix} \dot{\beta}_1 \quad (3.339)$$

The angular velocity of joint frame at point A of Body 2 can be expressed in the same frame as follows

$${}^{A_2} \boldsymbol{\omega}^{A_2} = \mathbf{T}^{A_2-2} \overline{\boldsymbol{\omega}}^{(2)} + \mathbf{T}^{A_2-2} \boldsymbol{\psi}^{A_2} \mathbf{B}^{2r} \boldsymbol{\chi}^{(2)} \dot{\boldsymbol{\eta}}^{(2)} \quad (3.340)$$

On the other hand, the angular velocity of joint frame at point A of Body 2 can be expressed in joint frame at point A of Body 1 as follows

$${}^{A_1} \boldsymbol{\omega}^{A_2} = \mathbf{T}^{A_1-A_2} {}^{A_2} \boldsymbol{\omega}^{A_2} \quad (3.341)$$

where $\mathbf{T}^{A_1-A_2}$ is the transformation matrix from the joint frame at point A of Body 2 to the joint frame at point A of Body 1 and it can be expressed as

$$\mathbf{T}^{A_1-A_2} = \begin{bmatrix} c\gamma_2 & -s\gamma_2 & 0 \\ s\gamma_2 & c\gamma_2 & 0 \\ 0 & 0 & 1 \end{bmatrix} \quad (3.342)$$

Therefore, the following two constraint equations can be written

$${}^{A_1} \boldsymbol{\omega}_1^{A_1} = {}^{A_1} \boldsymbol{\omega}_1^{A_2} \quad \text{constraint equation (1)} \quad (3.343)$$

$${}^{A_1} \boldsymbol{\omega}_2^{A_1} = {}^{A_1} \boldsymbol{\omega}_2^{A_2} \quad \text{constraint equation (2)} \quad (3.344)$$

Three scalar equations can be written for the revolute joint at point B by equating the components of the velocity vector of point B of Body 2, \mathbf{v}^{B_2} , and the velocity vector of point B of Body 3, \mathbf{v}^{B_3} .

The velocity of point B of Body 2 can be expressed in fixed frame as

$$\mathbf{v}^{B_2} = \mathbf{T}^{(2)} \tilde{\mathbf{q}}^{B_2} \overline{\boldsymbol{\omega}}^{(2)} + \mathbf{T}^{(2)} \boldsymbol{\phi}^{B_2} \mathbf{B}^{2r} \boldsymbol{\chi}^{(2)} \dot{\boldsymbol{\eta}}^{(2)} \quad (3.345)$$

The velocity of point B of Body 3 can be expressed in fixed frame as

$$\mathbf{v}^{B_3} = \dot{\boldsymbol{\zeta}}^{(3)} + \mathbf{T}^{(3)} \tilde{\mathbf{q}}^{B_3} \overline{\boldsymbol{\omega}}^{(3)} + \mathbf{T}^{(3)} \boldsymbol{\phi}^{B_3} \mathbf{B}^{3r} \boldsymbol{\chi}^{(3)} \dot{\boldsymbol{\eta}}^{(3)} \quad (3.346)$$

where $\tilde{\mathbf{q}}^{B_3}$ is the skew symmetric matrix of the vector $\bar{\mathbf{q}}^{B_3}$, $\bar{\mathbf{q}}^{B_3}$ is the position vector from Body 3 reference frame to point B of Body 3 at deformed state expressed in Body 3 reference frame, ϕ^{B_3} is the value of ϕ^{3i} at point B of Body 3 and \mathbf{B}^{3r} is the Boolean matrix of the element of Body 3 that includes point B.

Therefore, the following three constraint equations can be written

$$v_1^{B_2} = v_1^{B_3} \quad \text{constraint equation (3)} \quad (3.347)$$

$$v_2^{B_2} = v_2^{B_3} \quad \text{constraint equation (4)} \quad (3.348)$$

$$v_3^{B_2} = v_3^{B_3} \quad \text{constraint equation (5)} \quad (3.349)$$

Two scalar equations can be written for the revolute joint at point B by equating the first and second components of the angular velocity vector of point B of Body 2, $\boldsymbol{\omega}^{B_2}$, and the angular velocity vector of point B of Body 3, $\boldsymbol{\omega}^{B_3}$.

The angular velocity of joint frame at point B of Body 2 can be expressed in the same frame as follows

$${}^{B_2} \boldsymbol{\omega}^{B_2} = \mathbf{T}^{B_2-2} \bar{\boldsymbol{\omega}}^{(2)} + \mathbf{T}^{B_2-2} \boldsymbol{\psi}^{B_2} \mathbf{B}^{2r} \boldsymbol{\chi}^{(2)} \dot{\eta}^{(2)} \quad (3.350)$$

The angular velocity of joint frame at point B of Body 3 can be expressed in the same frame as follows

$${}^{B_3} \boldsymbol{\omega}^{B_3} = \mathbf{T}^{B_3-3} \bar{\boldsymbol{\omega}}^{(3)} + \mathbf{T}^{B_3-3} \boldsymbol{\psi}^{B_3} \mathbf{B}^{3r} \boldsymbol{\chi}^{(3)} \dot{\eta}^{(3)} \quad (3.351)$$

On the other hand, the angular velocity of joint frame at point B of Body 3 can be expressed in joint frame at point B of Body 2 as follows

$${}^{B_2} \boldsymbol{\omega}^{B_3} = \mathbf{T}^{B_2-B_3} {}^{B_3} \boldsymbol{\omega}^{B_3} \quad (3.352)$$

where $\mathbf{T}^{B_2-B_3}$ is the transformation matrix from the joint frame at point B of Body 3 to the joint frame at point B of Body 2 and it can be expressed as

$$\mathbf{T}^{B_2-B_3} = \begin{bmatrix} c\theta_3 & -s\theta_3 & 0 \\ s\theta_3 & c\theta_3 & 0 \\ 0 & 0 & 1 \end{bmatrix} \quad (3.353)$$

where θ_3 is the joint angle of Body 3.

Therefore, the following two constraint equations can be written

$${}^{B_2}\boldsymbol{\omega}_1^{B_2} = {}^{B_2}\boldsymbol{\omega}_1^{B_3} \quad \text{constraint equation (6)} \quad (3.354)$$

$${}^{B_2}\boldsymbol{\omega}_2^{B_2} = {}^{B_2}\boldsymbol{\omega}_2^{B_3} \quad \text{constraint equation (7)} \quad (3.355)$$

The constraint equations at acceleration level can be obtained by taking the derivative of velocity level constraint equations as

$${}^{A_1}\dot{\boldsymbol{\omega}}_1^{A_1} = {}^{A_1}\dot{\boldsymbol{\omega}}_1^{A_2} \quad (3.356)$$

$${}^{A_1}\dot{\boldsymbol{\omega}}_2^{A_1} = {}^{A_1}\dot{\boldsymbol{\omega}}_2^{A_2} \quad (3.357)$$

$$\dot{\boldsymbol{v}}_1^{B_2} = \dot{\boldsymbol{v}}_1^{B_3} \quad (3.358)$$

$$\dot{\boldsymbol{v}}_2^{B_2} = \dot{\boldsymbol{v}}_2^{B_3} \quad (3.359)$$

$$\dot{\boldsymbol{v}}_3^{B_2} = \dot{\boldsymbol{v}}_3^{B_3} \quad (3.360)$$

$${}^{B_2}\dot{\boldsymbol{\omega}}_1^{B_2} = {}^{B_2}\dot{\boldsymbol{\omega}}_1^{B_3} \quad (3.361)$$

$${}^{B_2}\dot{\boldsymbol{\omega}}_2^{B_2} = {}^{B_2}\dot{\boldsymbol{\omega}}_2^{B_3} \quad (3.362)$$

The derivative of the necessary equations to form the acceleration level constraint equations can be obtained as

$${}^{A_1} \dot{\omega}^{A_1} = \begin{bmatrix} 0 \\ 1 \\ 0 \end{bmatrix} \ddot{\beta}_1 \quad (3.363)$$

$$\begin{aligned} {}^{A_1} \dot{\omega}^{A_2} = & \mathbf{T}^{A_1-A_2} \mathbf{T}^{A_2-2} \dot{\overline{\omega}}^{(2)} + \mathbf{T}^{A_1-A_2} \mathbf{T}^{A_2-2} \boldsymbol{\psi}^{A_2} \mathbf{B}^{2r} \boldsymbol{\chi}^{(2)} \dot{\boldsymbol{\eta}}^{(2)} + \\ & \dot{\mathbf{T}}^{A_1-A_2} \mathbf{T}^{A_2-2} \overline{\omega}^{(2)} + \mathbf{T}^{A_1-A_2} \dot{\mathbf{T}}^{A_2-2} \overline{\omega}^{(2)} + \\ & \dot{\mathbf{T}}^{A_1-A_2} \mathbf{T}^{A_2-2} \boldsymbol{\psi}^{A_2} \mathbf{B}^{2r} \boldsymbol{\chi}^{(2)} \dot{\boldsymbol{\eta}}^{(2)} + \mathbf{T}^{A_1-A_2} \dot{\mathbf{T}}^{A_2-2} \boldsymbol{\psi}^{A_2} \mathbf{B}^{2r} \boldsymbol{\chi}^{(2)} \dot{\boldsymbol{\eta}}^{(2)} \end{aligned} \quad (3.364)$$

where $\dot{\mathbf{T}}^{A_1-A_2}$ and $\dot{\mathbf{T}}^{A_2-2}$ are given as

$$\dot{\mathbf{T}}^{A_1-A_2} = \begin{bmatrix} -s\gamma_2 & -c\gamma_2 & 0 \\ c\gamma_2 & -s\gamma_2 & 0 \\ 0 & 0 & 0 \end{bmatrix} \dot{\gamma}_2 \quad (3.365)$$

$$\dot{\mathbf{T}}^{A_2-2} = \begin{bmatrix} 0 & -\dot{\gamma}_3^{A_2} & \dot{\gamma}_2^{A_2} \\ \dot{\gamma}_3^{A_2} & 0 & -\dot{\gamma}_1^{A_2} \\ -\dot{\gamma}_2^{A_2} & \dot{\gamma}_1^{A_2} & 0 \end{bmatrix} \quad (3.366)$$

where $\dot{\boldsymbol{\gamma}}^{A_2}$ is expressed as

$$\dot{\boldsymbol{\gamma}}^{A_2} = \boldsymbol{\psi}^{A_2} \mathbf{B}^{2r} \boldsymbol{\chi}^{(2)} \dot{\boldsymbol{\eta}}^{(2)} \quad (3.367)$$

$$\begin{aligned} \dot{\mathbf{v}}^{B_2} = & \mathbf{T}^{(2)} \tilde{\mathbf{q}}^{B_2} \dot{\overline{\omega}}^{(2)} + \mathbf{T}^{(2)} \boldsymbol{\phi}^{B_2} \mathbf{B}^{2r} \boldsymbol{\chi}^{(2)} \dot{\boldsymbol{\eta}}^{(2)} + \mathbf{T}^{(2)} \dot{\tilde{\mathbf{q}}}^{B_2} \overline{\omega}^{(2)} - \\ & \mathbf{T}^{(2)} \tilde{\overline{\omega}}^{(2)} \tilde{\mathbf{q}}^{B_2} \overline{\omega}^{(2)} - \mathbf{T}^{(2)} \tilde{\overline{\omega}}^{(2)} \boldsymbol{\phi}^{B_2} \mathbf{B}^{2r} \boldsymbol{\chi}^{(2)} \dot{\boldsymbol{\eta}}^{(2)} \end{aligned} \quad (3.368)$$

$$\begin{aligned} \dot{\mathbf{v}}^{B_3} = & \boldsymbol{\zeta}^{(3)} + \mathbf{T}^{(3)} \tilde{\mathbf{q}}^{B_3} \dot{\overline{\omega}}^{(3)} + \mathbf{T}^{(3)} \boldsymbol{\phi}^{B_3} \mathbf{B}^{3r} \boldsymbol{\chi}^{(3)} \dot{\boldsymbol{\eta}}^{(3)} + \mathbf{T}^{(3)} \dot{\tilde{\mathbf{q}}}^{B_3} \overline{\omega}^{(3)} - \\ & \mathbf{T}^{(3)} \tilde{\overline{\omega}}^{(3)} \tilde{\mathbf{q}}^{B_3} \overline{\omega}^{(3)} - \mathbf{T}^{(3)} \tilde{\overline{\omega}}^{(3)} \boldsymbol{\phi}^{B_3} \mathbf{B}^{3r} \boldsymbol{\chi}^{(3)} \dot{\boldsymbol{\eta}}^{(3)} \end{aligned} \quad (3.369)$$

$${}^{B_2} \dot{\omega}^{B_2} = \mathbf{T}^{B_2-2} \dot{\overline{\omega}}^{(2)} + \mathbf{T}^{B_2-2} \boldsymbol{\psi}^{B_2} \mathbf{B}^{2r} \boldsymbol{\chi}^{(2)} \dot{\boldsymbol{\eta}}^{(2)} + \dot{\mathbf{T}}^{B_2-2} \overline{\omega}^{(2)} + \dot{\mathbf{T}}^{B_2-2} \boldsymbol{\psi}^{B_2} \mathbf{B}^{2r} \boldsymbol{\chi}^{(2)} \dot{\boldsymbol{\eta}}^{(2)} \quad (3.370)$$

where $\dot{\mathbf{T}}^{B_2-2}$ is given as

$$\dot{\mathbf{T}}^{B_2-2} = \begin{bmatrix} 0 & -\dot{\gamma}_3^{B_2} & \dot{\gamma}_2^{B_2} \\ \dot{\gamma}_3^{B_2} & 0 & -\dot{\gamma}_1^{B_2} \\ -\dot{\gamma}_2^{B_2} & \dot{\gamma}_1^{B_2} & 0 \end{bmatrix} \quad (3.371)$$

where $\dot{\bar{\gamma}}^{B_2}$ is expressed as

$$\dot{\bar{\gamma}}^{B_2} = \Psi^{B_2} \mathbf{B}^{2r} \chi^{(2)} \dot{\eta}^{(2)} \quad (3.372)$$

$$\begin{aligned} {}^{B_2} \dot{\bar{\omega}}^{B_3} = & \mathbf{T}^{B_2-B_3} \mathbf{T}^{B_3-3} \dot{\bar{\omega}}^{(3)} + \mathbf{T}^{B_2-B_3} \mathbf{T}^{B_3-3} \Psi^{B_3} \mathbf{B}^{3r} \chi^{(3)} \dot{\eta}^{(3)} + \\ & \dot{\mathbf{T}}^{B_2-B_3} \mathbf{T}^{B_3-3} \bar{\omega}^{(3)} + \mathbf{T}^{B_2-B_3} \dot{\mathbf{T}}^{B_3-3} \bar{\omega}^{(3)} + \\ & \dot{\mathbf{T}}^{B_2-B_3} \mathbf{T}^{B_3-3} \Psi^{B_3} \mathbf{B}^{3r} \chi^{(3)} \dot{\eta}^{(3)} + \mathbf{T}^{B_2-B_3} \dot{\mathbf{T}}^{B_3-3} \Psi^{B_3} \mathbf{B}^{3r} \chi^{(3)} \dot{\eta}^{(3)} \end{aligned} \quad (3.373)$$

where $\dot{\mathbf{T}}^{B_2-B_3}$ and $\dot{\mathbf{T}}^{B_3-3}$ are given as

$$\dot{\mathbf{T}}^{B_2-B_3} = \begin{bmatrix} -s\theta_3 & -c\theta_3 & 0 \\ c\theta_3 & -s\theta_3 & 0 \\ 0 & 0 & 0 \end{bmatrix} \dot{\theta}_3 \quad (3.374)$$

$$\dot{\mathbf{T}}^{B_3-3} = \begin{bmatrix} 0 & -\dot{\gamma}_3^{B_3} & \dot{\gamma}_2^{B_3} \\ \dot{\gamma}_3^{B_3} & 0 & -\dot{\gamma}_1^{B_3} \\ -\dot{\gamma}_2^{B_3} & \dot{\gamma}_1^{B_3} & 0 \end{bmatrix} \quad (3.375)$$

where $\dot{\bar{\gamma}}^{B_3}$ is expressed as

$$\dot{\bar{\gamma}}^{B_3} = \Psi^{B_3} \mathbf{B}^{3r} \chi^{(3)} \dot{\eta}^{(3)} \quad (3.376)$$

3.3.3 Equations of Motion

Equations of motion of all bodies can be written considering the joint forces

$$\mathbf{M}\dot{\mathbf{y}} = \mathbf{Q} + \mathbf{f}^e + \mathbf{f}^g + \mathbf{f}^s + \mathbf{f}^c \quad (3.377)$$

where \mathbf{M} is the generalized mass matrix of the system, \mathbf{y} is the generalized speed vector of the system, \mathbf{Q} , \mathbf{f}^e , \mathbf{f}^g and \mathbf{f}^s are the generalized Coriolis and centrifugal, external, gravitational and structural stiffness force vectors of the system, respectively. They are formed as follows

$$\mathbf{M} = \begin{bmatrix} \mathbf{M}^{(1)} & & \mathbf{0} \\ & \mathbf{M}^{(2)} & \\ \mathbf{0} & & \mathbf{M}^{(3)} \end{bmatrix} \quad (3.378)$$

$$\mathbf{y} = \begin{bmatrix} \mathbf{y}^{(1)} \\ \mathbf{y}^{(2)} \\ \mathbf{y}^{(3)} \end{bmatrix} \quad (3.379)$$

$$\mathbf{Q} = \begin{bmatrix} \mathbf{Q}^{(1)} \\ \mathbf{Q}^{(2)} \\ \mathbf{Q}^{(3)} \end{bmatrix} \quad (3.380)$$

$$\mathbf{f}^e = \begin{bmatrix} \mathbf{f}^{e(1)} \\ \mathbf{f}^{e(2)} \\ \mathbf{f}^{e(3)} \end{bmatrix} \quad (3.381)$$

$$\mathbf{f}^g = \begin{bmatrix} \mathbf{f}^{g(1)} \\ \mathbf{f}^{g(2)} \\ \mathbf{f}^{g(3)} \end{bmatrix} \quad (3.382)$$

$$\mathbf{f}^s = \begin{bmatrix} \mathbf{f}^{s(1)} \\ \mathbf{f}^{s(2)} \\ \mathbf{f}^{s(3)} \end{bmatrix} \quad (3.383)$$

\mathbf{f}^c is the generalized constraint forces due to joint forces. In general, the constraint equations at velocity level can be written as

$$\sum_{m=1}^n \mathbf{B}_{pm} \mathbf{y}_m = \mathbf{0}_m \quad p = 1, \dots, c \quad (3.384)$$

where n is the dimension of vector \mathbf{y} and c is the number of constraint equations. Above equation can be written in matrix form as

$$\mathbf{B} \mathbf{y} = \mathbf{0} \quad (3.385)$$

Then \mathbf{f}^c can be expressed as

$$\mathbf{f}^c = \mathbf{B}^T \boldsymbol{\lambda} \quad (3.386)$$

where $\boldsymbol{\lambda}$ is c dimensional vector of constraint forces at the joints. If Equation (3.386) is substituted into Equation (3.377), the following equation is obtained

$$\mathbf{M}\dot{\mathbf{y}} - \mathbf{B}^T \boldsymbol{\lambda} = \mathbf{Q} + \mathbf{f}^e + \mathbf{f}^g + \mathbf{f}^s \quad (3.387)$$

Equation (3.387) has n scalar equations but n+c unknowns. Constraint equations can be written at acceleration level as

$$\mathbf{B}\ddot{\mathbf{y}} = -\dot{\mathbf{B}}\dot{\mathbf{y}} \quad (3.388)$$

Equation (3.388) has c scalar equations with the same n unknowns. If Equations (3.387) and (3.388) are augmented, the following system of equations are obtained

$$\begin{bmatrix} \mathbf{M} & -\mathbf{B}^T \\ \mathbf{B} & \mathbf{0} \end{bmatrix} \begin{bmatrix} \dot{\mathbf{y}} \\ \boldsymbol{\lambda} \end{bmatrix} = \begin{bmatrix} \mathbf{Q} + \mathbf{f}^e + \mathbf{f}^g + \mathbf{f}^s \\ -\dot{\mathbf{B}}\dot{\mathbf{y}} \end{bmatrix} \quad (3.389)$$

3.4 An Alternative Form of Dynamic Equations for Controller Design

The equations of motion of a multibody system derived by using absolute coordinates may have many equations especially when the number of body increases and body flexibilities are taken into consideration. The number of equations can be reduced from n+c to n by substituting velocity level constraint equations into the dynamic equations of the multibody system.

The tip point position vector and elastic variables of the bodies are sufficient to describe the dynamics of a flexible robotic system completely. The tip point position vector is the variable to be controlled for flexible robotic systems.

Therefore, by using the constraint equations, the remaining variables can be expressed in terms of tip point position vector and elastic variables of the bodies.

The system of equations of a multibody system is written here once more

$$\mathbf{M}\dot{\mathbf{y}} - \mathbf{B}^T \boldsymbol{\lambda} = \mathbf{Q} + \mathbf{f}^e + \mathbf{f}^g + \mathbf{f}^s \quad (3.390)$$

$$\mathbf{B}\dot{\mathbf{y}} = -\dot{\mathbf{B}}\mathbf{y} \quad (3.391)$$

The generalized speed vector can be rearranged in the following order

$$\mathbf{y}_m = \begin{bmatrix} \dot{\boldsymbol{\zeta}} \\ \dot{\boldsymbol{\eta}} \\ \dot{\boldsymbol{\kappa}} \end{bmatrix} \quad (3.392)$$

where $\dot{\boldsymbol{\zeta}} \in \mathfrak{R}^{3 \times 1}$, $\dot{\boldsymbol{\eta}} \in \mathfrak{R}^{m \times 1}$, $m = m^{(2)} + m^{(3)}$, $\dot{\boldsymbol{\kappa}} \in \mathfrak{R}^{c \times 1}$. $m^{(2)}$ and $m^{(3)}$ are the number of modal coordinates of Body 2 and Body 3, respectively. These variables are given as

$$\dot{\boldsymbol{\zeta}} = \dot{\boldsymbol{\zeta}}^{(3)} \quad (3.393)$$

$$\dot{\boldsymbol{\eta}} = \begin{bmatrix} \dot{\boldsymbol{\eta}}^{(2)} \\ \dot{\boldsymbol{\eta}}^{(3)} \end{bmatrix} \quad (3.394)$$

$$\dot{\boldsymbol{\kappa}} = \begin{bmatrix} \dot{\beta}_1 \\ \overline{\boldsymbol{\omega}}^{(2)} \\ \overline{\boldsymbol{\omega}}^{(3)} \end{bmatrix} \quad (3.395)$$

The vectors $\dot{\boldsymbol{\zeta}}$ and $\dot{\boldsymbol{\eta}}$ are called as primary variables and the vector $\dot{\boldsymbol{\kappa}}$ is called as secondary variables. The system of equations can be arranged according to the new ordered generalized speed vector as follows

$$\mathbf{M}_m \dot{\mathbf{y}}_m - \mathbf{B}_m^T \boldsymbol{\lambda}_m = \mathbf{Q}_m + \mathbf{f}_m^e + \mathbf{f}_m^g + \mathbf{f}_m^s \quad (3.396)$$

$$\mathbf{B}_m \dot{\mathbf{y}}_m = -\dot{\mathbf{B}}_m \mathbf{y}_m \quad (3.397)$$

where subscript m means that the order of the rows and/or columns of the related matrix or vector are modified. Equation (3.396) and (3.397) can be written in partitioned form as follows

$$\mathbf{M}_{m_{\zeta\zeta}} \ddot{\boldsymbol{\zeta}} + \mathbf{M}_{m_{\zeta\eta}} \ddot{\boldsymbol{\eta}} + \mathbf{M}_{m_{\zeta\kappa}} \dot{\boldsymbol{\kappa}} - \mathbf{B}_{m_{\zeta}}^T \boldsymbol{\lambda} = \mathbf{C}_{m_{\zeta\zeta}} \dot{\boldsymbol{\zeta}} + \mathbf{C}_{m_{\zeta\eta}} \dot{\boldsymbol{\eta}} + \mathbf{C}_{m_{\zeta\kappa}} \boldsymbol{\kappa} + \mathbf{H}_{m_{\zeta}} \mathbf{T} + \mathbf{f}_{m_{\zeta}}^g \quad (3.398)$$

$$\mathbf{M}_{m_{\eta\zeta}} \ddot{\boldsymbol{\zeta}} + \mathbf{M}_{m_{\eta\eta}} \ddot{\boldsymbol{\eta}} + \mathbf{M}_{m_{\eta\kappa}} \dot{\boldsymbol{\kappa}} - \mathbf{B}_{m_{\eta}}^T \boldsymbol{\lambda} = \mathbf{C}_{m_{\eta\zeta}} \dot{\boldsymbol{\zeta}} + \mathbf{C}_{m_{\eta\eta}} \dot{\boldsymbol{\eta}} + \mathbf{C}_{m_{\eta\kappa}} \boldsymbol{\kappa} + \mathbf{S}_{m_{\eta\eta}} \boldsymbol{\eta} + \mathbf{H}_{m_{\eta}} \mathbf{T} + \mathbf{f}_{m_{\eta}}^g \quad (3.399)$$

$$\mathbf{M}_{m_{\kappa\zeta}} \ddot{\boldsymbol{\zeta}} + \mathbf{M}_{m_{\kappa\eta}} \ddot{\boldsymbol{\eta}} + \mathbf{M}_{m_{\kappa\kappa}} \dot{\boldsymbol{\kappa}} - \mathbf{B}_{m_{\kappa}}^T \boldsymbol{\lambda} = \mathbf{C}_{m_{\kappa\zeta}} \dot{\boldsymbol{\zeta}} + \mathbf{C}_{m_{\kappa\eta}} \dot{\boldsymbol{\eta}} + \mathbf{C}_{m_{\kappa\kappa}} \boldsymbol{\kappa} + \mathbf{H}_{m_{\kappa}} \mathbf{T} + \mathbf{f}_{m_{\kappa}}^g \quad (3.400)$$

$$\mathbf{B}_{m_{\zeta}} \dot{\boldsymbol{\zeta}} + \mathbf{B}_{m_{\eta}} \dot{\boldsymbol{\eta}} + \mathbf{B}_{m_{\kappa}} \boldsymbol{\kappa} = \mathbf{0} \quad (3.401)$$

where matrices \mathbf{C}_m , \mathbf{S}_m and \mathbf{H}_m stand for the partitioned forms of \mathbf{Q}_m , \mathbf{f}_m^s and \mathbf{f}_m^e , respectively. \mathbf{T} is the vector of actuating input.

The secondary variables can be obtained in terms of primary variables by using Equation (3.401) as

$$\boldsymbol{\kappa} = \mathbf{B}_{m_{\kappa}}^{-1} \left(-\mathbf{B}_{m_{\zeta}} \dot{\boldsymbol{\zeta}} - \mathbf{B}_{m_{\eta}} \dot{\boldsymbol{\eta}} \right) \quad (3.402)$$

The acceleration level constraint equations can be partitioned as

$$\mathbf{B}_{m_{\zeta}} \ddot{\boldsymbol{\zeta}} + \mathbf{B}_{m_{\eta}} \ddot{\boldsymbol{\eta}} + \mathbf{B}_{m_{\kappa}} \dot{\boldsymbol{\kappa}} = -\dot{\mathbf{B}}_{m_{\zeta}} \dot{\boldsymbol{\zeta}} - \dot{\mathbf{B}}_{m_{\eta}} \dot{\boldsymbol{\eta}} - \dot{\mathbf{B}}_{m_{\kappa}} \boldsymbol{\kappa} \quad (3.403)$$

Rate of the secondary variables can be obtained in terms of primary variables and their rates by using Equations (3.403) and (3.402) as

$$\dot{\boldsymbol{\kappa}} = \mathbf{B}_{m_{\kappa}}^{-1} \left\{ -\mathbf{B}_{m_{\zeta}} \ddot{\boldsymbol{\zeta}} - \mathbf{B}_{m_{\eta}} \ddot{\boldsymbol{\eta}} - \left(\dot{\mathbf{B}}_{m_{\zeta}} - \dot{\mathbf{B}}_{m_{\kappa}} \mathbf{B}_{m_{\kappa}}^{-1} \mathbf{B}_{m_{\zeta}} \right) \dot{\boldsymbol{\zeta}} - \left(\dot{\mathbf{B}}_{m_{\eta}} - \dot{\mathbf{B}}_{m_{\kappa}} \mathbf{B}_{m_{\kappa}}^{-1} \mathbf{B}_{m_{\eta}} \right) \dot{\boldsymbol{\eta}} \right\} \quad (3.404)$$

By substituting Equations (3.402) and (3.404) into Equations (3.398), (3.399) and (3.400), the secondary variables and their rates can be eliminated from the dynamic equations. Therefore, the dynamic equations take the following form

$$\mathbf{N}_{\zeta\zeta}\ddot{\boldsymbol{\zeta}} + \mathbf{N}_{\zeta\eta}\ddot{\boldsymbol{\eta}} - \mathbf{B}_{m_\zeta}^T \boldsymbol{\lambda} + \mathbf{V}_{\zeta\zeta}\dot{\boldsymbol{\zeta}} + \mathbf{V}_{\zeta\eta}\dot{\boldsymbol{\eta}} + \mathbf{G}_\zeta = \mathbf{Y}_\zeta \mathbf{T} \quad (3.405)$$

$$\mathbf{N}_{\eta\zeta}\ddot{\boldsymbol{\zeta}} + \mathbf{N}_{\eta\eta}\ddot{\boldsymbol{\eta}} - \mathbf{B}_{m_\eta}^T \boldsymbol{\lambda} + \mathbf{V}_{\eta\zeta}\dot{\boldsymbol{\zeta}} + \mathbf{V}_{\eta\eta}\dot{\boldsymbol{\eta}} + \mathbf{K}_{\eta\eta}\boldsymbol{\eta} + \mathbf{G}_\eta = \mathbf{Y}_\eta \mathbf{T} \quad (3.406)$$

$$\mathbf{N}_{\kappa\zeta}\ddot{\boldsymbol{\zeta}} + \mathbf{N}_{\kappa\eta}\ddot{\boldsymbol{\eta}} - \mathbf{B}_{m_\kappa}^T \boldsymbol{\lambda} + \mathbf{V}_{\kappa\zeta}\dot{\boldsymbol{\zeta}} + \mathbf{V}_{\kappa\eta}\dot{\boldsymbol{\eta}} + \mathbf{G}_\kappa = \mathbf{Y}_\kappa \mathbf{T} \quad (3.407)$$

where $\mathbf{N}_{\zeta\zeta}$, $\mathbf{N}_{\zeta\eta}$, $\mathbf{N}_{\eta\zeta}$, $\mathbf{N}_{\eta\eta}$, $\mathbf{N}_{\kappa\zeta}$, $\mathbf{N}_{\kappa\eta}$, $\mathbf{V}_{\zeta\zeta}$, $\mathbf{V}_{\zeta\eta}$, $\mathbf{V}_{\eta\zeta}$, $\mathbf{V}_{\eta\eta}$, $\mathbf{V}_{\kappa\zeta}$, $\mathbf{V}_{\kappa\eta}$, $\mathbf{K}_{\eta\eta}$, \mathbf{G}_ζ , \mathbf{G}_η , \mathbf{G}_κ , \mathbf{Y}_ζ , \mathbf{Y}_η and \mathbf{Y}_κ are expressed as

$$\mathbf{N}_{\zeta\zeta} = \mathbf{M}_{m_{\zeta\zeta}} - \mathbf{M}_{m_{\zeta\kappa}} \mathbf{B}_{m_\kappa}^{-1} \mathbf{B}_{m_\zeta} \quad (3.408)$$

$$\mathbf{N}_{\zeta\eta} = \mathbf{M}_{m_{\zeta\eta}} - \mathbf{M}_{m_{\zeta\kappa}} \mathbf{B}_{m_\kappa}^{-1} \mathbf{B}_{m_\eta} \quad (3.409)$$

$$\mathbf{N}_{\eta\zeta} = \mathbf{M}_{m_{\eta\zeta}} - \mathbf{M}_{m_{\eta\kappa}} \mathbf{B}_{m_\kappa}^{-1} \mathbf{B}_{m_\zeta} \quad (3.410)$$

$$\mathbf{N}_{\eta\eta} = \mathbf{M}_{m_{\eta\eta}} - \mathbf{M}_{m_{\eta\kappa}} \mathbf{B}_{m_\kappa}^{-1} \mathbf{B}_{m_\eta} \quad (3.411)$$

$$\mathbf{N}_{\kappa\zeta} = \mathbf{M}_{m_{\kappa\zeta}} - \mathbf{M}_{m_{\kappa\kappa}} \mathbf{B}_{m_\kappa}^{-1} \mathbf{B}_{m_\zeta} \quad (3.412)$$

$$\mathbf{N}_{\kappa\eta} = \mathbf{M}_{m_{\kappa\eta}} - \mathbf{M}_{m_{\kappa\kappa}} \mathbf{B}_{m_\kappa}^{-1} \mathbf{B}_{m_\eta} \quad (3.413)$$

$$\mathbf{V}_{\zeta\zeta} = -\mathbf{M}_{m_{\zeta\kappa}} \mathbf{B}_{m_\kappa}^{-1} (\dot{\mathbf{B}}_{m_\zeta} - \dot{\mathbf{B}}_{m_\kappa} \mathbf{B}_{m_\kappa}^{-1} \mathbf{B}_{m_\zeta}) - \mathbf{C}_{m_{\zeta\zeta}} + \mathbf{C}_{m_{\zeta\kappa}} \mathbf{B}_{m_\kappa}^{-1} \mathbf{B}_{m_\zeta} \quad (3.414)$$

$$\mathbf{V}_{\zeta\eta} = -\mathbf{M}_{m_{\zeta\kappa}} \mathbf{B}_{m_\kappa}^{-1} (\dot{\mathbf{B}}_{m_\eta} - \dot{\mathbf{B}}_{m_\kappa} \mathbf{B}_{m_\kappa}^{-1} \mathbf{B}_{m_\eta}) - \mathbf{C}_{m_{\zeta\eta}} + \mathbf{C}_{m_{\zeta\kappa}} \mathbf{B}_{m_\kappa}^{-1} \mathbf{B}_{m_\eta} \quad (3.415)$$

$$\mathbf{V}_{\eta\zeta} = -\mathbf{M}_{m_{\eta\kappa}} \mathbf{B}_{m_\kappa}^{-1} (\dot{\mathbf{B}}_{m_\zeta} - \dot{\mathbf{B}}_{m_\kappa} \mathbf{B}_{m_\kappa}^{-1} \mathbf{B}_{m_\zeta}) - \mathbf{C}_{m_{\eta\zeta}} + \mathbf{C}_{m_{\eta\kappa}} \mathbf{B}_{m_\kappa}^{-1} \mathbf{B}_{m_\zeta} \quad (3.416)$$

$$\mathbf{V}_{\eta\eta} = -\mathbf{M}_{m_{\eta\kappa}} \mathbf{B}_{m_\kappa}^{-1} (\dot{\mathbf{B}}_{m_\eta} - \dot{\mathbf{B}}_{m_\kappa} \mathbf{B}_{m_\kappa}^{-1} \mathbf{B}_{m_\eta}) - \mathbf{C}_{m_{\eta\eta}} + \mathbf{C}_{m_{\eta\kappa}} \mathbf{B}_{m_\kappa}^{-1} \mathbf{B}_{m_\eta} \quad (3.417)$$

$$\mathbf{V}_{\kappa\zeta} = -\mathbf{M}_{m_{\kappa\kappa}} \mathbf{B}_{m_\kappa}^{-1} (\dot{\mathbf{B}}_{m_\zeta} - \dot{\mathbf{B}}_{m_\kappa} \mathbf{B}_{m_\kappa}^{-1} \mathbf{B}_{m_\zeta}) - \mathbf{C}_{m_{\kappa\zeta}} + \mathbf{C}_{m_{\kappa\kappa}} \mathbf{B}_{m_\kappa}^{-1} \mathbf{B}_{m_\zeta} \quad (3.418)$$

$$\mathbf{V}_{\kappa\eta} = -\mathbf{M}_{m_{\kappa\kappa}} \mathbf{B}_{m_\kappa}^{-1} (\dot{\mathbf{B}}_{m_\eta} - \dot{\mathbf{B}}_{m_\kappa} \mathbf{B}_{m_\kappa}^{-1} \mathbf{B}_{m_\eta}) - \mathbf{C}_{m_{\kappa\eta}} + \mathbf{C}_{m_{\kappa\kappa}} \mathbf{B}_{m_\kappa}^{-1} \mathbf{B}_{m_\eta} \quad (3.419)$$

$$\mathbf{K}_{\eta\eta} = -\mathbf{S}_{m_{\eta\eta}} \quad (3.420)$$

$$\mathbf{G}_\zeta = -\mathbf{f}_{m_\zeta}^g \quad (3.421)$$

$$\mathbf{G}_\eta = -\mathbf{f}_{m_\eta}^g \quad (3.422)$$

$$\mathbf{G}_\kappa = -\mathbf{f}_{m_\kappa}^{eg} \quad (3.423)$$

$$\mathbf{Y}_\zeta = \mathbf{H}_{m_\zeta} \quad (3.424)$$

$$\mathbf{Y}_\eta = \mathbf{H}_{m_\eta} \quad (3.425)$$

$$\mathbf{Y}_\kappa = \mathbf{H}_{m_\kappa} \quad (3.426)$$

Vector of constraint forces can be expressed in terms of primary variables and their rates by using Equation (3.407)

$$\boldsymbol{\lambda} = \left(\mathbf{B}_{m_\kappa}^T \right)^{-1} \left(\mathbf{N}_{\kappa\zeta} \ddot{\boldsymbol{\zeta}} + \mathbf{N}_{\kappa\eta} \ddot{\boldsymbol{\eta}} + \mathbf{V}_{\kappa\zeta} \dot{\boldsymbol{\zeta}} + \mathbf{V}_{\kappa\eta} \dot{\boldsymbol{\eta}} + \mathbf{G}_\kappa - \mathbf{Y}_\kappa \mathbf{T} \right) \quad (3.427)$$

By substituting Equation (3.427) in Equations (3.405) and (3.406), vector of constraint forces can be eliminated from the dynamic equations. Therefore, the dynamic equations take the following form

$$\mathbf{A}_{\zeta\zeta} \ddot{\boldsymbol{\zeta}} + \mathbf{A}_{\zeta\eta} \ddot{\boldsymbol{\eta}} + \mathbf{B}_{\zeta\zeta} \dot{\boldsymbol{\zeta}} + \mathbf{B}_{\zeta\eta} \dot{\boldsymbol{\eta}} + \mathbf{D}_\zeta = \mathbf{E}_\zeta \mathbf{T} \quad (3.428)$$

$$\mathbf{A}_{\eta\zeta} \ddot{\boldsymbol{\zeta}} + \mathbf{A}_{\eta\eta} \ddot{\boldsymbol{\eta}} + \mathbf{B}_{\eta\zeta} \dot{\boldsymbol{\zeta}} + \mathbf{B}_{\eta\eta} \dot{\boldsymbol{\eta}} + \mathbf{K}_{\eta\eta} \boldsymbol{\eta} + \mathbf{D}_\eta = \mathbf{E}_\eta \mathbf{T} \quad (3.429)$$

where $\mathbf{A}_{\zeta\zeta}$, $\mathbf{A}_{\zeta\eta}$, $\mathbf{A}_{\eta\zeta}$, $\mathbf{A}_{\eta\eta}$, $\mathbf{B}_{\zeta\zeta}$, $\mathbf{B}_{\zeta\eta}$, $\mathbf{B}_{\eta\zeta}$, $\mathbf{B}_{\eta\eta}$, \mathbf{D}_ζ , \mathbf{D}_η , \mathbf{E}_ζ and \mathbf{E}_η are expressed as

$$\mathbf{A}_{\zeta\zeta} = \mathbf{N}_{\zeta\zeta} - \mathbf{B}_{m_\zeta}^T \left(\mathbf{B}_{m_\kappa}^T \right)^{-1} \mathbf{N}_{\kappa\zeta} \quad (3.430)$$

$$\mathbf{A}_{\zeta\eta} = \mathbf{N}_{\zeta\eta} - \mathbf{B}_{m_\zeta}^T \left(\mathbf{B}_{m_\kappa}^T \right)^{-1} \mathbf{N}_{\kappa\eta} \quad (3.431)$$

$$\mathbf{A}_{\eta\zeta} = \mathbf{N}_{\eta\zeta} - \mathbf{B}_{m_\eta}^T \left(\mathbf{B}_{m_\kappa}^T \right)^{-1} \mathbf{N}_{\kappa\zeta} \quad (3.432)$$

$$\mathbf{A}_{\eta\eta} = \mathbf{N}_{\eta\eta} - \mathbf{B}_{m_\eta}^T \left(\mathbf{B}_{m_\kappa}^T \right)^{-1} \mathbf{N}_{\kappa\eta} \quad (3.433)$$

$$\mathbf{B}_{\zeta\zeta} = \mathbf{V}_{\zeta\zeta} - \mathbf{B}_{m_\zeta}^T \left(\mathbf{B}_{m_\kappa}^T \right)^{-1} \mathbf{V}_{\kappa\zeta} \quad (3.434)$$

$$\mathbf{B}_{\zeta\eta} = \mathbf{V}_{\zeta\eta} - \mathbf{B}_{m_\zeta}^T \left(\mathbf{B}_{m_\kappa}^T \right)^{-1} \mathbf{V}_{\kappa\eta} \quad (3.435)$$

$$\mathbf{B}_{\eta\zeta} = \mathbf{V}_{\eta\zeta} - \mathbf{B}_{m_\eta}^T \left(\mathbf{B}_{m_\kappa}^T \right)^{-1} \mathbf{V}_{\kappa\zeta} \quad (3.436)$$

$$\mathbf{B}_{\eta\eta} = \mathbf{V}_{\eta\eta} - \mathbf{B}_{m_\eta}^T (\mathbf{B}_{m_\kappa}^T)^{-1} \mathbf{V}_{\kappa\eta} \quad (3.437)$$

$$\mathbf{D}_\zeta = \mathbf{G}_\zeta - \mathbf{B}_{m_\zeta}^T (\mathbf{B}_{m_\kappa}^T)^{-1} \mathbf{G}_\kappa \quad (3.438)$$

$$\mathbf{D}_\eta = \mathbf{G}_\eta - \mathbf{B}_{m_\eta}^T (\mathbf{B}_{m_\kappa}^T)^{-1} \mathbf{G}_\kappa \quad (3.439)$$

$$\mathbf{E}_\zeta = \mathbf{H}_{m_\zeta} - \mathbf{B}_{m_\zeta}^T (\mathbf{B}_{m_\kappa}^T)^{-1} \mathbf{H}_{m_\kappa} \quad (3.440)$$

$$\mathbf{E}_\eta = \mathbf{H}_{m_\eta} - \mathbf{B}_{m_\eta}^T (\mathbf{B}_{m_\kappa}^T)^{-1} \mathbf{H}_{m_\kappa} \quad (3.441)$$

Therefore, Equations (3.428) and (3.429) describe the systems of equations of the multibody system in terms of only primary variables.

CHAPTER 4

NUMERICAL SIMULATIONS FOR PLANAR ROBOT

In this section, planar two degrees of freedom robot with flexible forearm is taken into consideration to test the performance of the proposed controllers. Numerical simulations are carried out in three parts. In the first part, uncontrolled motion of planar robot is simulated. In the second part, motion control of the tip point is simulated. In the third part, force and motion control of the tip point is simulated.

In the first part, the uncontrolled motion of the robot as a flexible double pendulum is simulated for the verification of the dynamic equations.

In the second part, firstly, the motion control of the tip point is simulated by using the proposed method. In this simulation, the same number of modes are used both in the dynamic equations and the controller. Secondly, unmodeled dynamics is taken into consideration to test the performance of the control method even as such. So, the motion control of the tip point with unmodeled dynamics is also simulated and compared with the previous simulation. After that, the motion control of the tip point is simulated by using the computed torque method applied as if the robot is rigid. This provides another comparison.

In the third part, firstly, the force and motion control of the tip point is simulated. In this simulation, the same number of modes are also used for both the dynamic equations and the controller. Then, as the next stage, the force and motion control of the tip point with unmodeled dynamics is simulated for similar reasons as in the second part.

In the simulations, Runge-Kutta fourth-order numerical integration method is used to solve the ordinary differential equations that describe the dynamics of the

system with suitable sampling frequency. Computer codes are written in MATLAB® [54].

The closed loop poles are classified as dominant poles and inherent poles. The dominant poles are selected based on the desired response of the system more or less like a robot with rigid links. The inherent poles are selected with norms close to the natural frequencies of the system due to the link flexibilities. However, their angles from the imaginary axis are increased so that artificial damping is added to the flexible modes of the system. A similar closed loop poles selection is made by Yeung and Chen [7], [24].

4.1 Numerical Simulation of Uncontrolled Motion of Planar Robot

The dynamic equations of the robot with flexible arms have long and complicated expressions. Therefore, it is very important to verify the dynamic equations before applying the proposed control methods to the robot.

To verify the derivation of the dynamic equations and the code written for them, the numerical simulation of the uncontrolled motion of the planar robot with flexible forearm is presented in this section. The numerical simulation is obtained for the uncontrolled motion of the flexible robot as a double pendulum.

In the simulations, the axial deformations are assumed to be negligible and the bending deformations are approximated by the first two bending modes for the forearm. Fixed-free boundary conditions are used. In fact a beam has an infinite number of mode shapes, all with different natural frequencies. However, typically the lowest frequency modes have the largest amplitudes and are the most effective to approximate the deflection of the forearm. The mode shape functions are as follows [55].

$$Y_i(x) = (\sin \beta_i L_2 - \sinh \beta_i L_2)(\sin \beta_i x - \sinh \beta_i x) + (\cos \beta_i L_2 + \cosh \beta_i L_2)(\cos \beta_i x - \cosh \beta_i x) \quad i=1,2 \quad (4.1)$$

where

$$\beta_1 = \frac{1.875}{L_2} \quad (4.2)$$

$$\beta_2 = \frac{4.694}{L_2} \quad (4.3)$$

The natural frequencies associated with the natural modes are

$$\omega_{ni} = (\beta_i L_2)^2 \sqrt{\frac{EI}{m_2 L_2^3}} \quad i=1,2 \quad (4.4)$$

Therefore, mode shape function matrix and vector of modal variables of Body 2 have the following form

$$\phi^{(2)} = \begin{bmatrix} 0 & 0 \\ Y_1(x) & Y_2(x) \end{bmatrix} \quad (4.5)$$

$$\eta^{(2)} = \begin{bmatrix} \eta_1 \\ \eta_2 \end{bmatrix} \quad (4.6)$$

As a result of this, the degree of the freedom of the system is four which is the total number of the joint angles and the modal variables. The inertia properties of the planar robot are given in Appendix C.

The physical parameters of the planar robot are given in Table 4.1.

Table 4.1 Physical parameters of the planar robot.

Parameter	Value
Length of link 1 (m)	1
Length of link 2 (m)	1.5
Mass of link 1 (kg)	1
Mass of link 2 (kg)	1
Elastic rigidity of link 2 (Nm ²)	50

The numerical values of the natural frequencies associated with natural modes are 13.5316 rad/s and 84.8075 rad/s, respectively. It is assumed that the robot starts its motion from rest with no initial deflections. The initial joint angular positions are taken as $\theta_1 = 80$ degrees and $\theta_2 = 5$ degrees. The sampling frequency is taken as 6000 Hz. The simulation results are given in Figures 4.1 - 4.8.

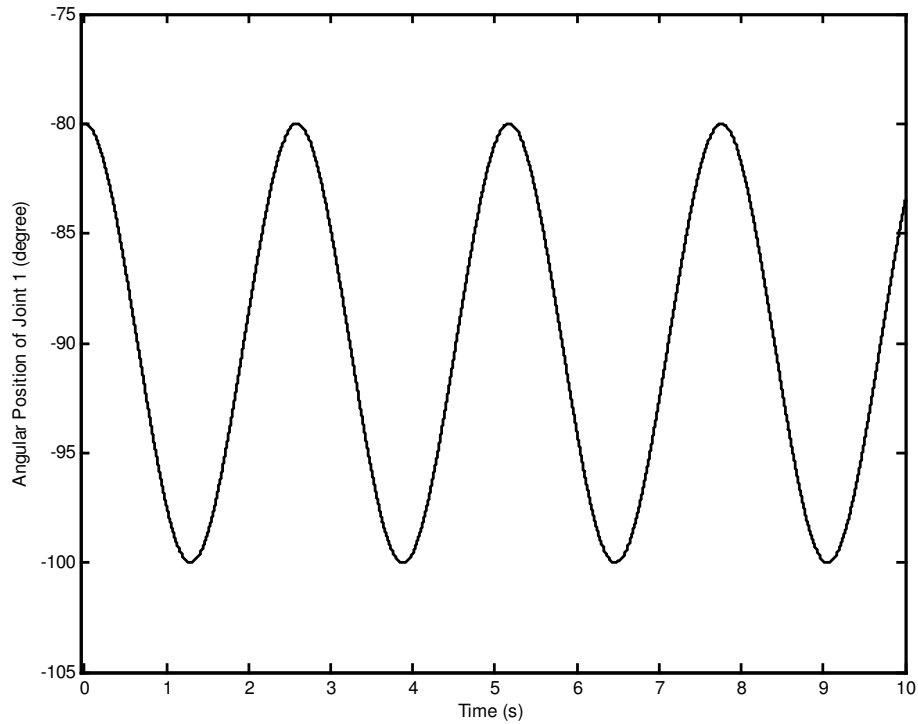


Figure 4.1 Angular position of joint 1.

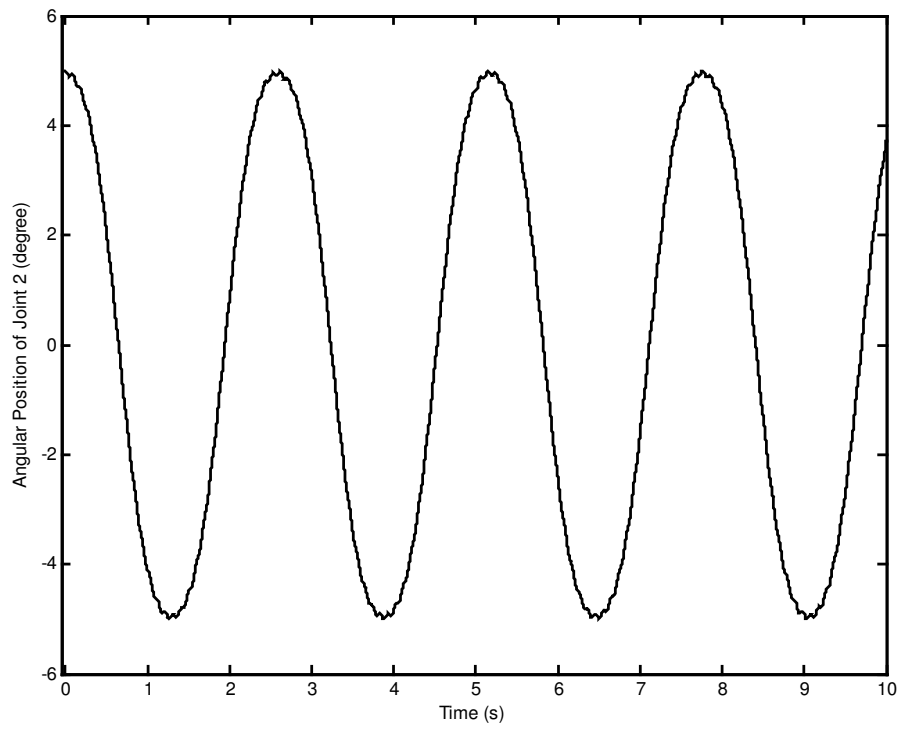


Figure 4.2 Angular position of joint 2.

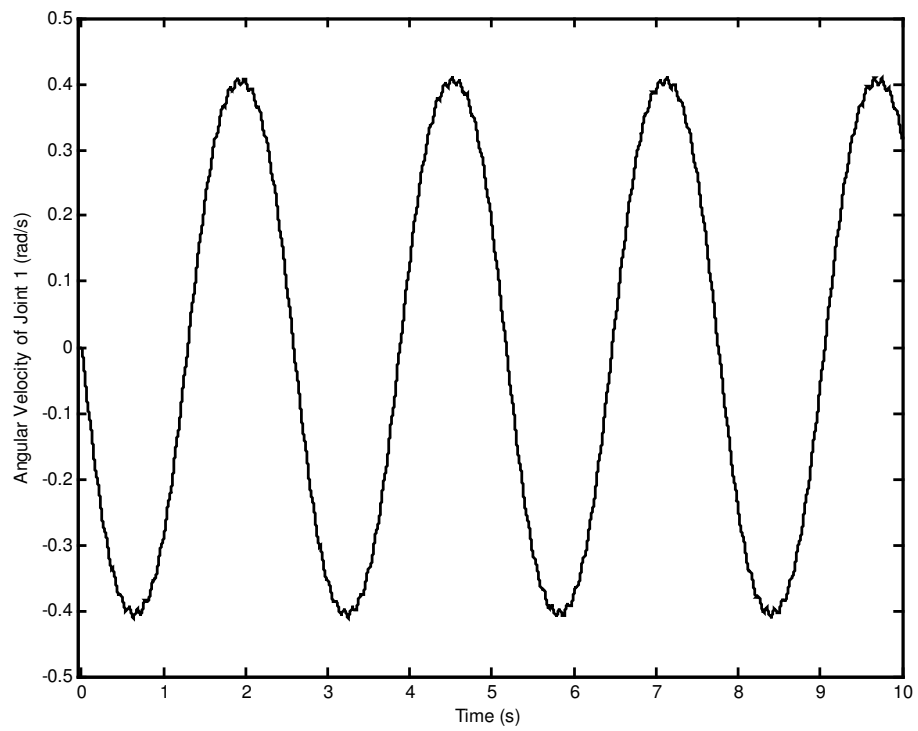


Figure 4.3 Angular velocity of joint 1.

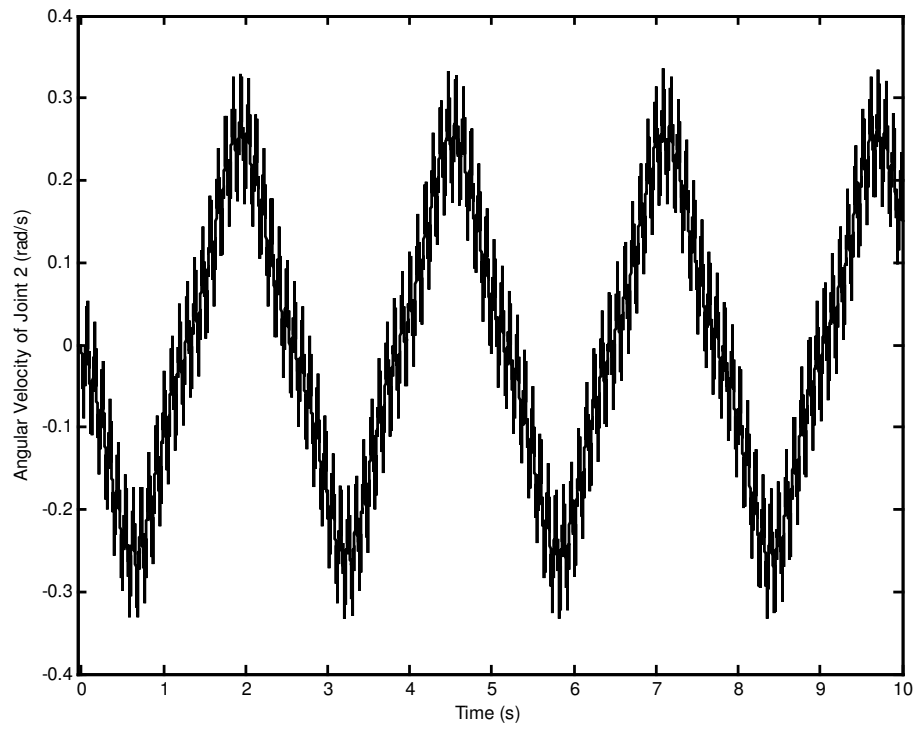


Figure 4.4 Angular velocity of joint 2.

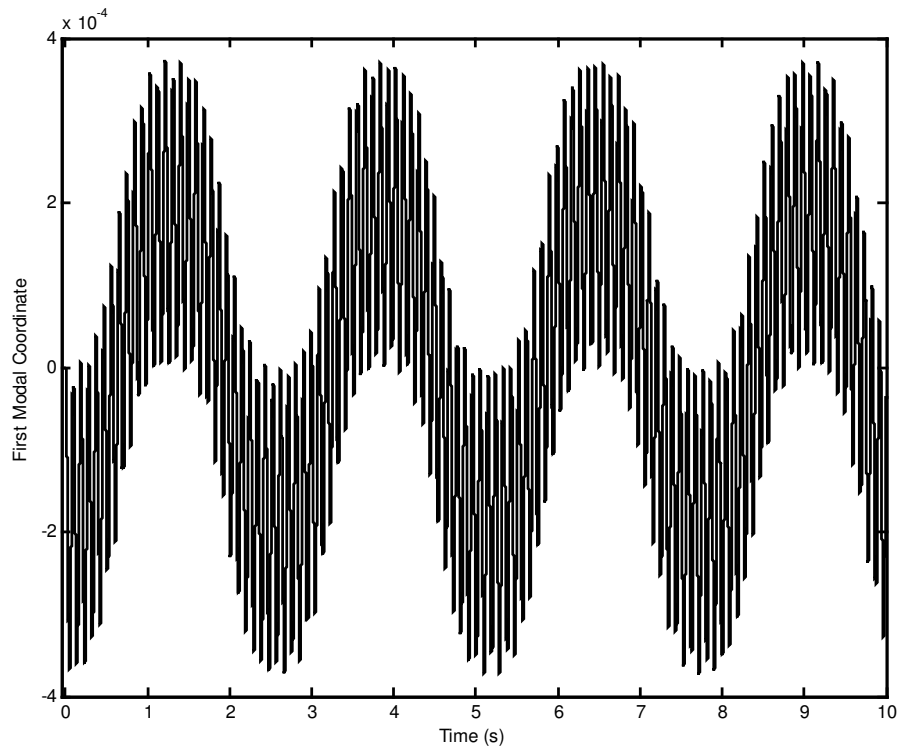


Figure 4.5 First modal coordinate.

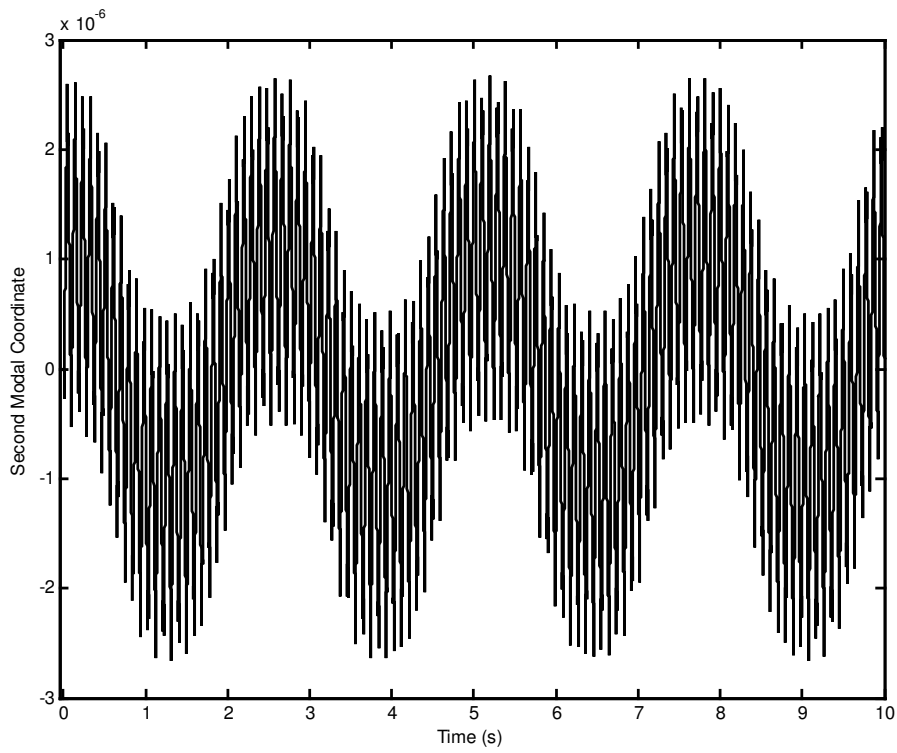


Figure 4.6 Second modal coordinate.

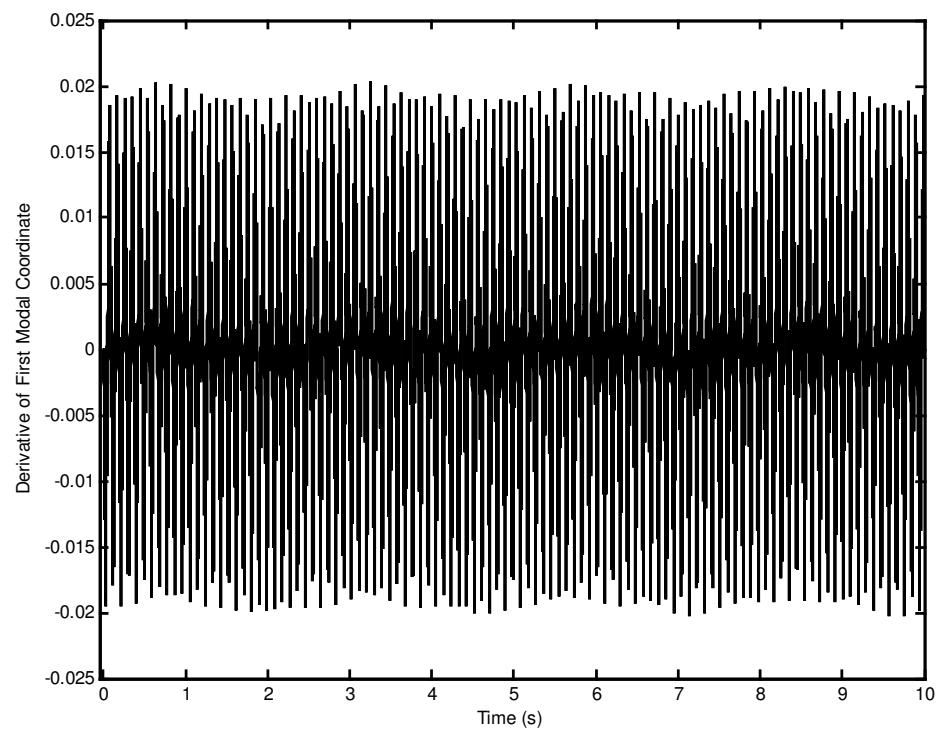


Figure 4.7 Derivative first modal coordinate.

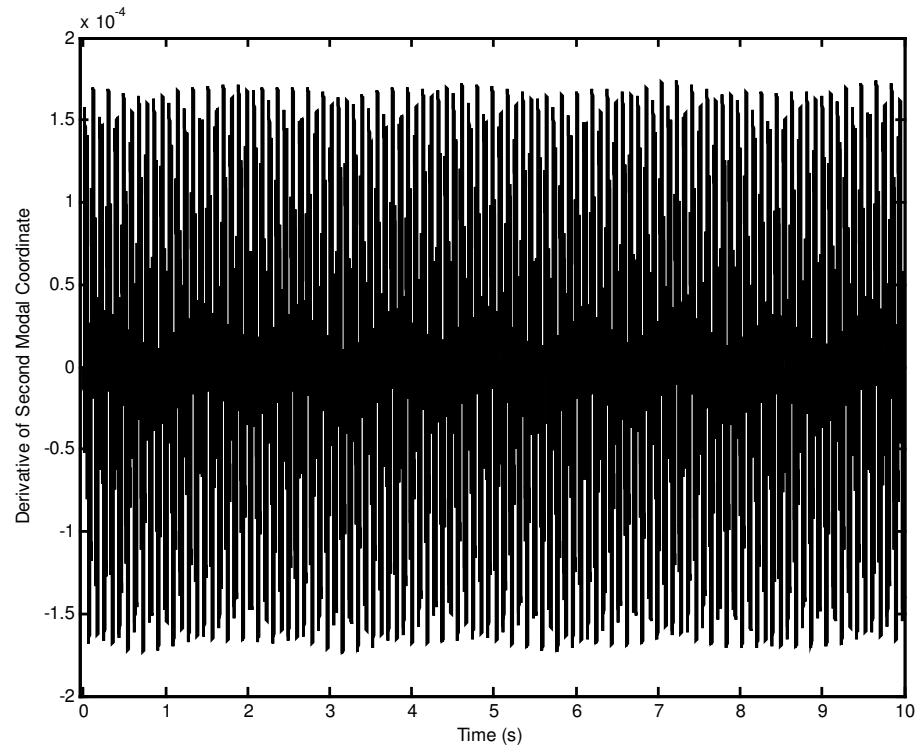


Figure 4.8 Derivative second modal coordinate.

When Figures 4.1 - 4.8 are examined, it is seen that they are as expected.

4.2 Numerical Simulation of Motion Control of Planar Robot

In this section, the numerical simulation of motion control of planar robot with flexible forearm is presented by using the motion control method proposed at Chapter 2. The tip point is required to track a straight line.

The reference motion on the required tip point trajectory is supposed to be described as a smooth time function. Here, it is formed by ninth-order Hermite polynomials providing the continuous boundary conditions for position, velocity, acceleration, jerk and snap (derivative of jerk). The position time history for such a motion is given by [56]

$$\mathbf{P}^*(t) = \mathbf{P}_0^* + (\mathbf{P}_f^* - \mathbf{P}_0^*) \left(\frac{70}{t_f^9} t^9 - \frac{315}{t_f^8} t^8 + \frac{540}{t_f^7} t^7 - \frac{420}{t_f^6} t^6 + \frac{126}{t_f^5} t^5 \right) \quad (4.7)$$

where \mathbf{P}^* is the desired tip point position vector, \mathbf{P}_0^* is the desired initial tip point position vector, \mathbf{P}_f^* is the desired final tip point position vector and t_f is the time to complete motion.

After a few trials, proper closed loop natural frequencies and damping ratios are obtained as 5 rad/s, 15 rad/s, 30 rad/s, 85 rad/s, 0.85, 0.85, 0.85 and 0.85. The corresponding closed loop poles are given in Table 4.2.

Table 4.2 Closed loop poles used in motion control of planar robot.

Closed Loop Poles
$p_1 = -4.2500 + 2.6339j$
$p_2 = -4.2500 - 2.6339j$
$p_3 = -12.7500 + 7.9017j$
$p_4 = -12.7500 - 7.9017j$
$p_5 = -25.5000 + 15.8035j$
$p_6 = -25.5000 - 15.8035j$
$p_7 = -72.2500 + 44.7765j$
$p_8 = -72.2500 - 44.7765j$

During the simulations, the sampling frequency can be taken as 200 Hz or above. Here the sampling frequency is taken as 2500 Hz to compare the simulation results with those obtained by using computed torque method. The simulation results are presented in Figures 4.9 - 4.35.

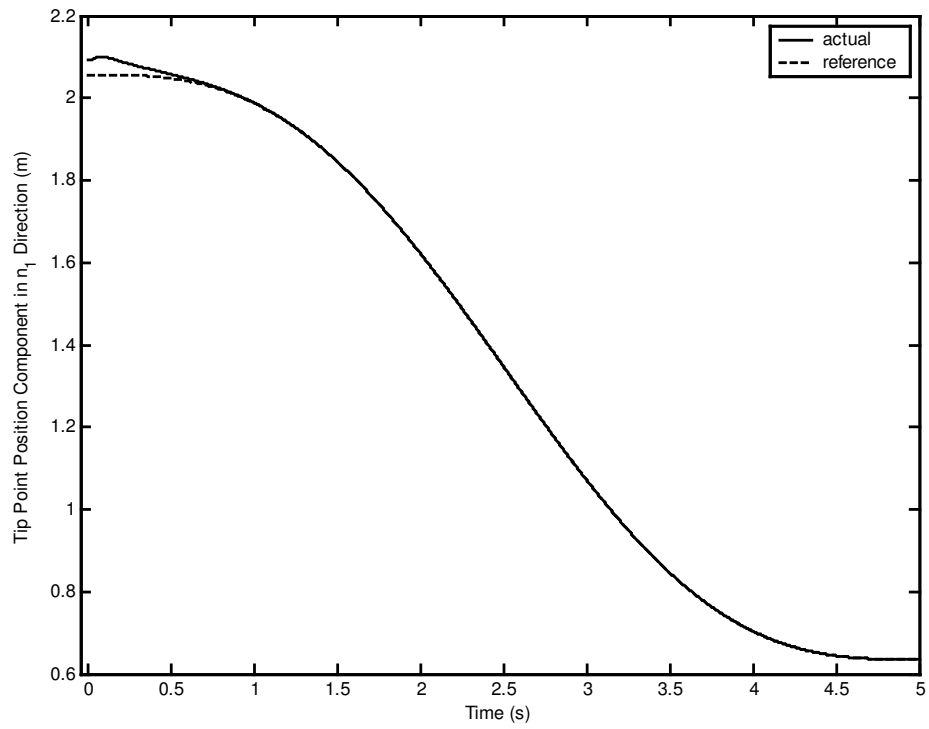


Figure 4.9 Tip point position component in n_1 direction.

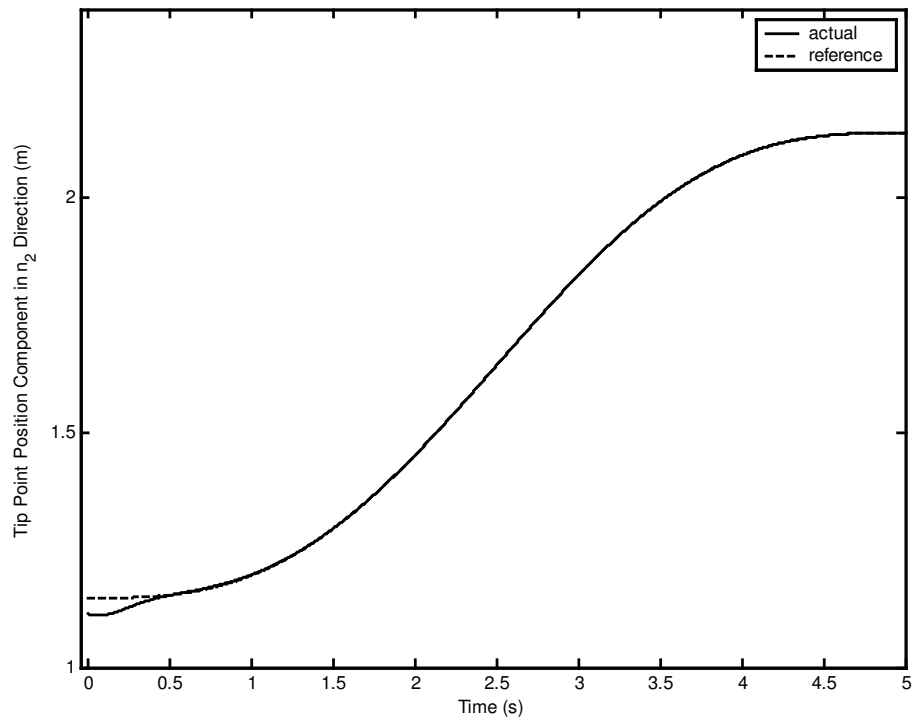


Figure 4.10 Tip point position component in n_2 direction.

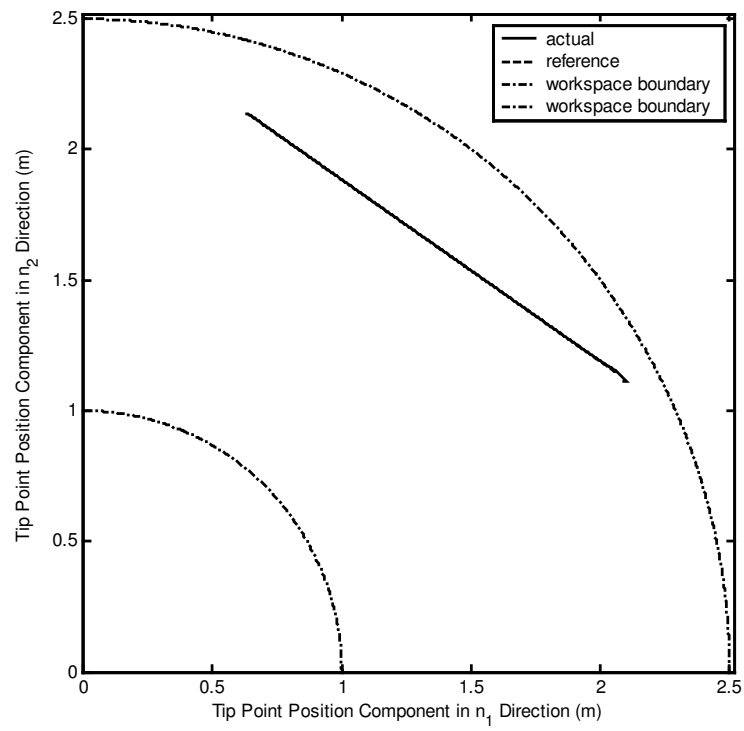


Figure 4.11 Workspace and tip point position.

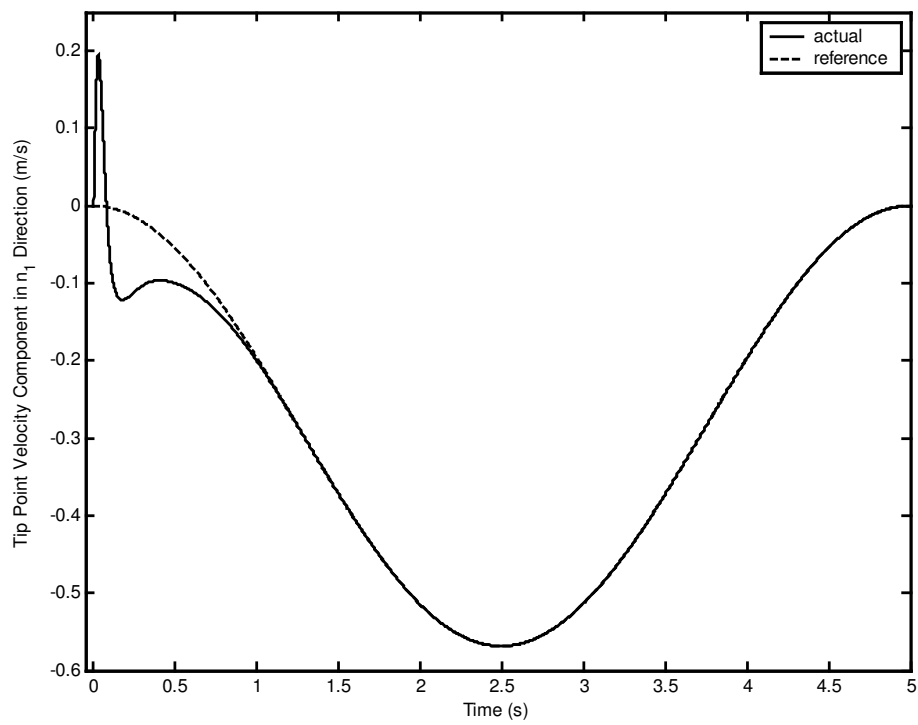


Figure 4.12 Tip point velocity component in n_1 direction.

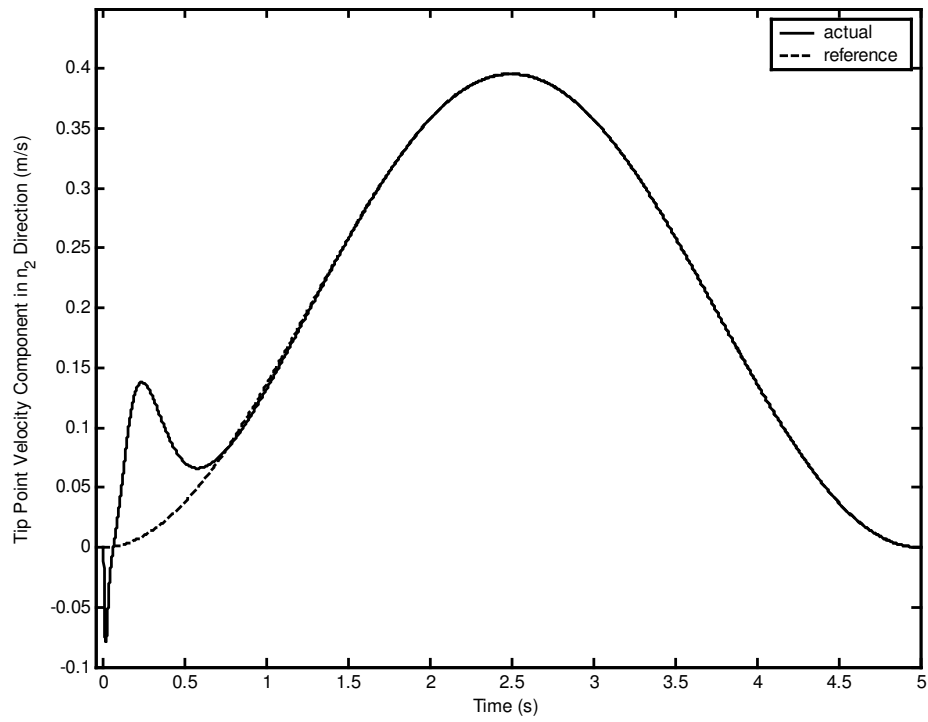


Figure 4.13 Tip point velocity component in n_2 direction.

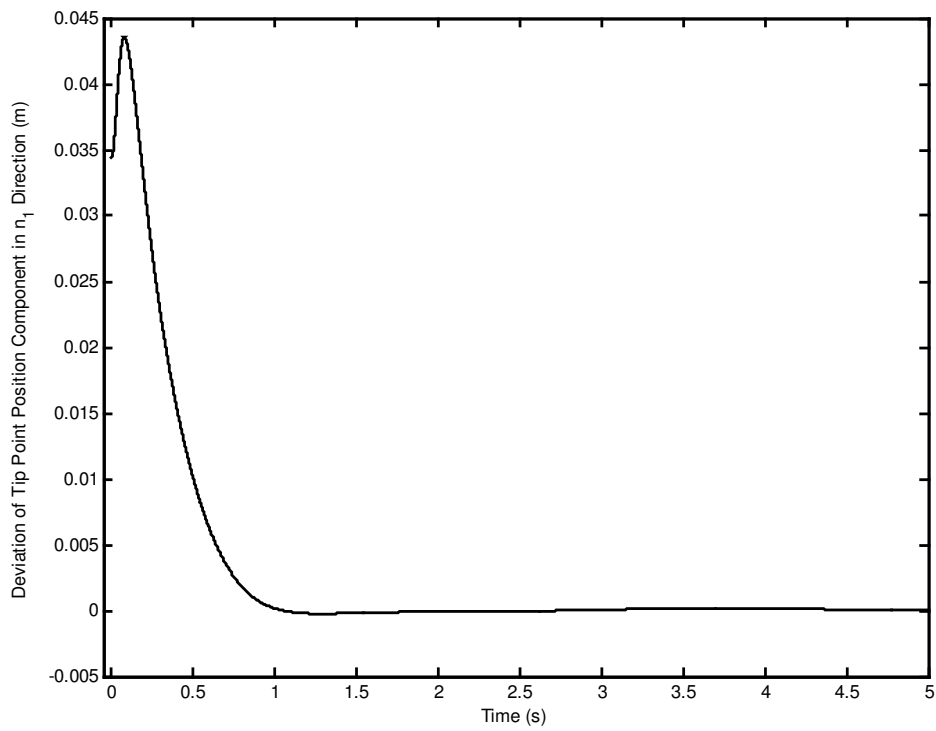


Figure 4.14 Deviation of tip point position component in n_1 direction.

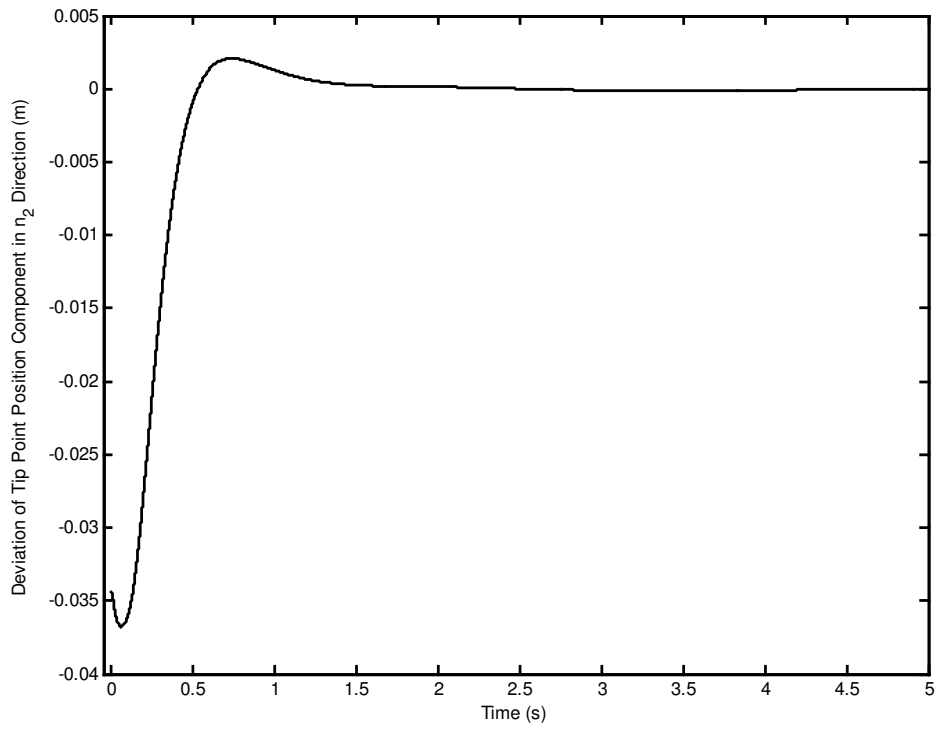


Figure 4.15 Deviation of tip point position component in n_2 direction.

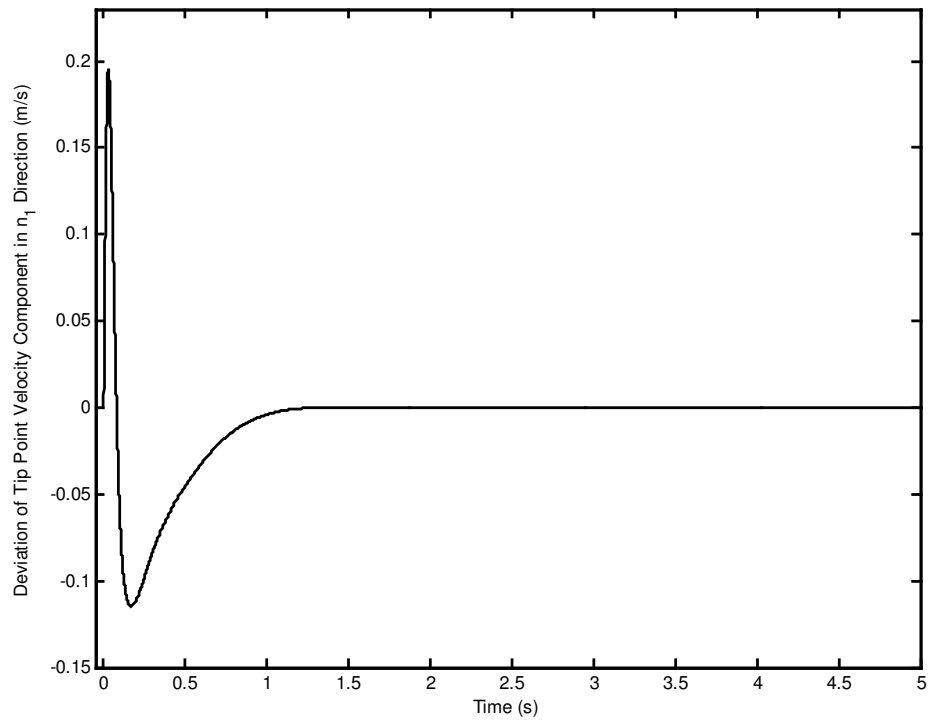


Figure 4.16 Deviation of tip point velocity component in n_1 direction.

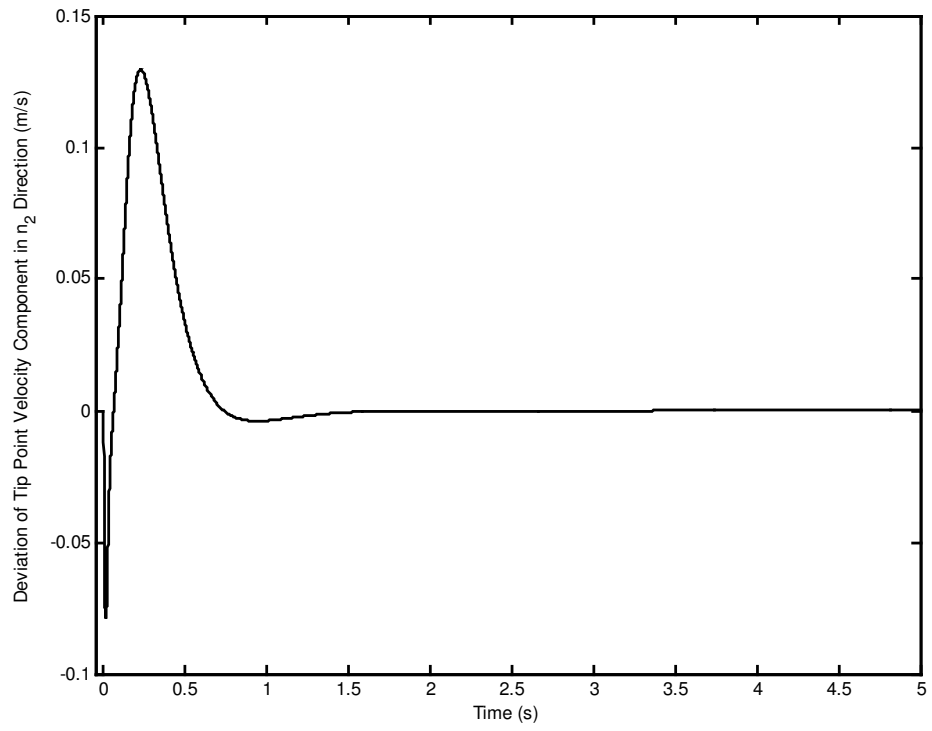


Figure 4.17 Deviation of tip point velocity component in n_2 direction.

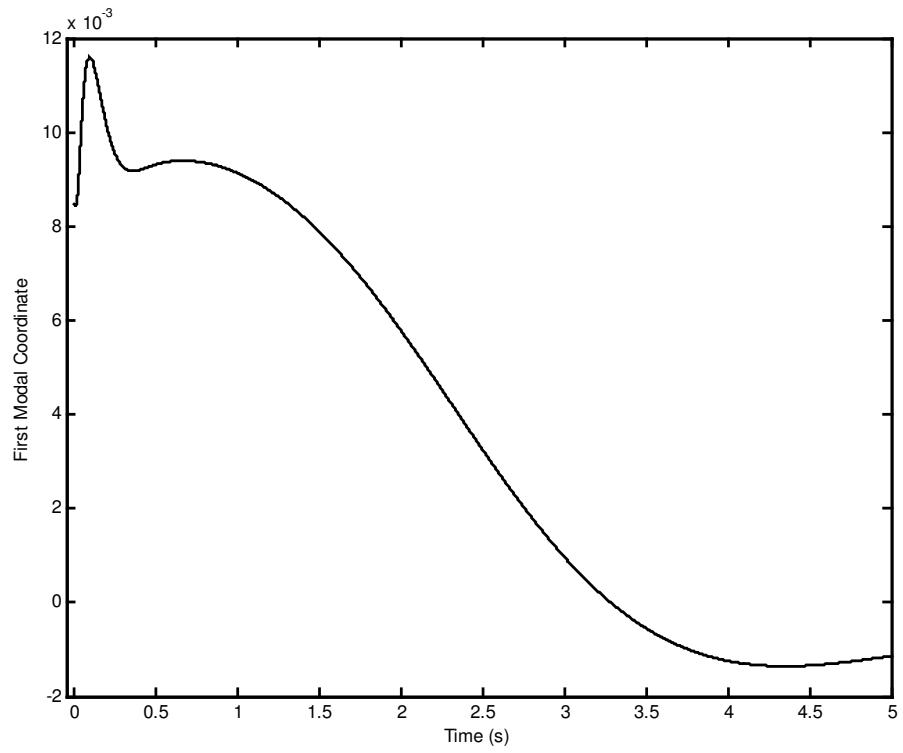


Figure 4.18 First modal coordinate.

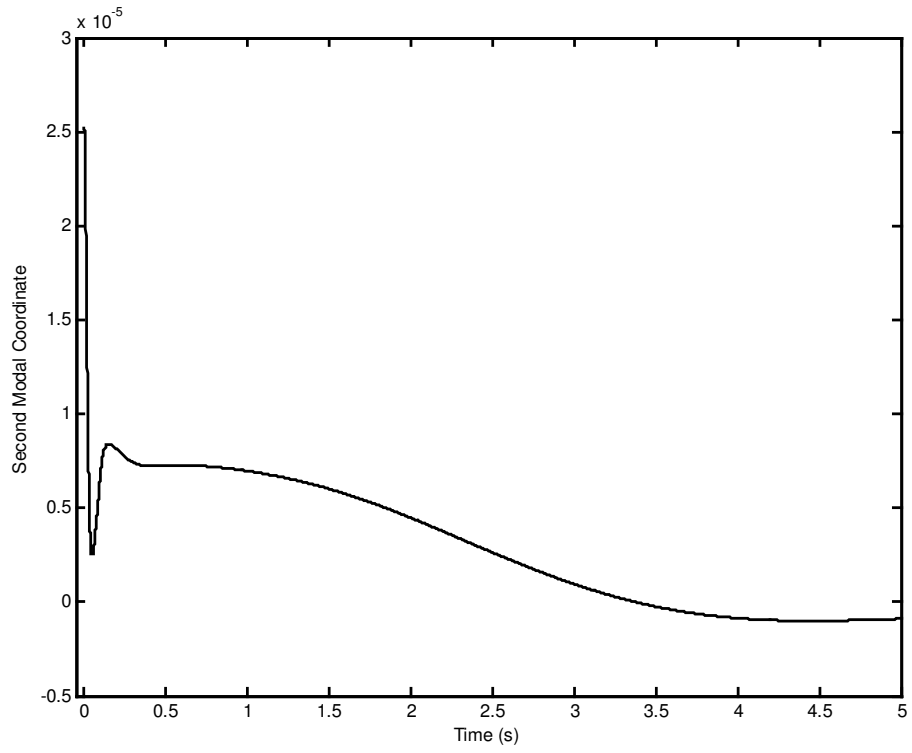


Figure 4.19 Second modal coordinate.

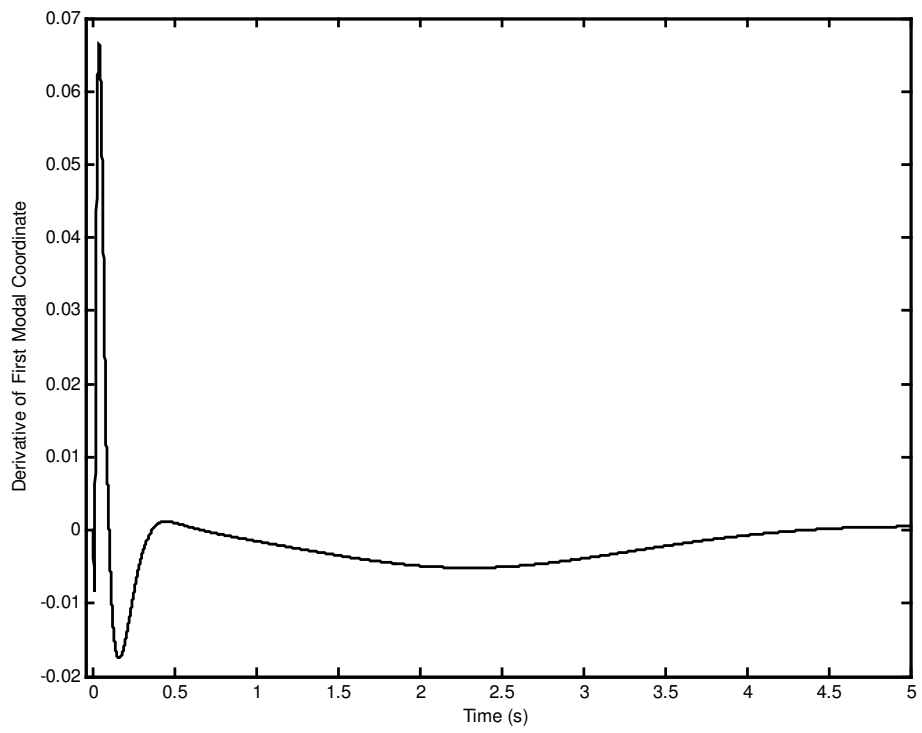


Figure 4.20 Derivative of first modal coordinate.

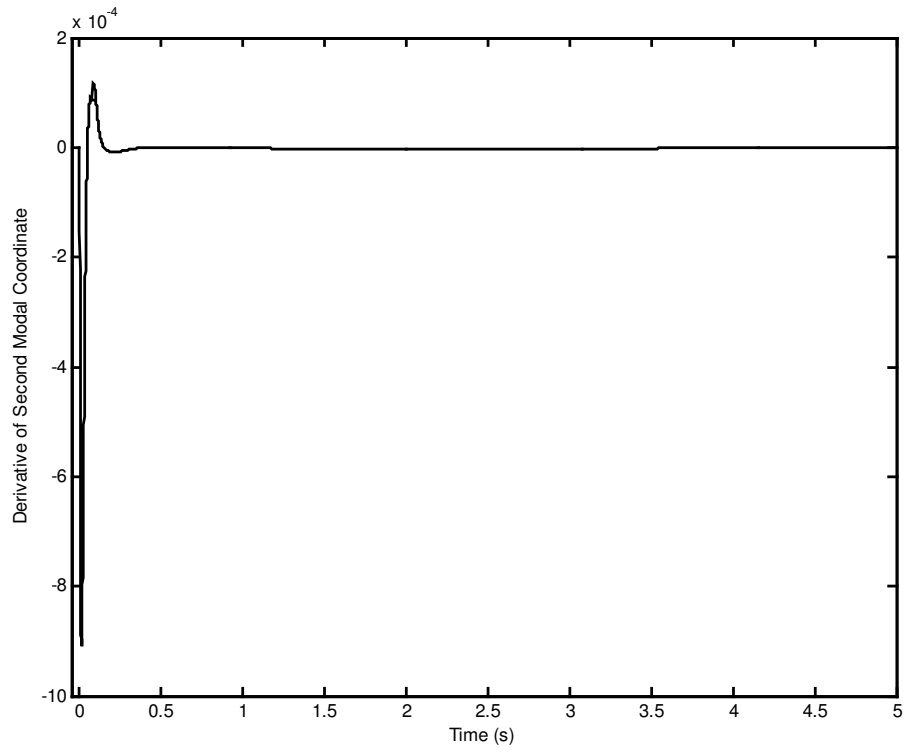


Figure 4.21 Derivative of second modal coordinate.

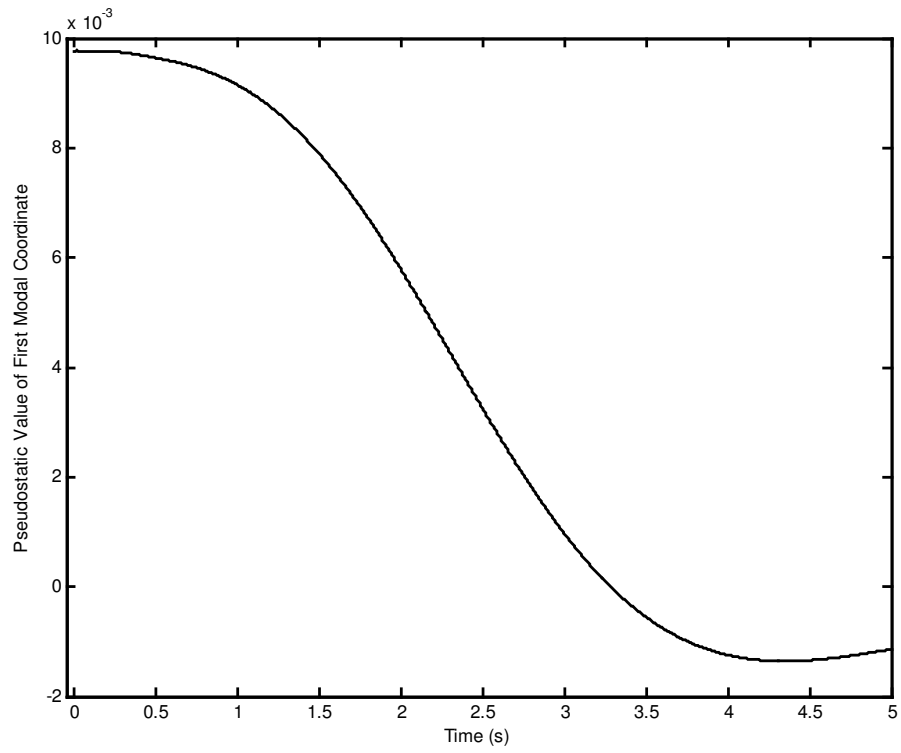


Figure 4.22 Pseudostatic value of first modal coordinate.

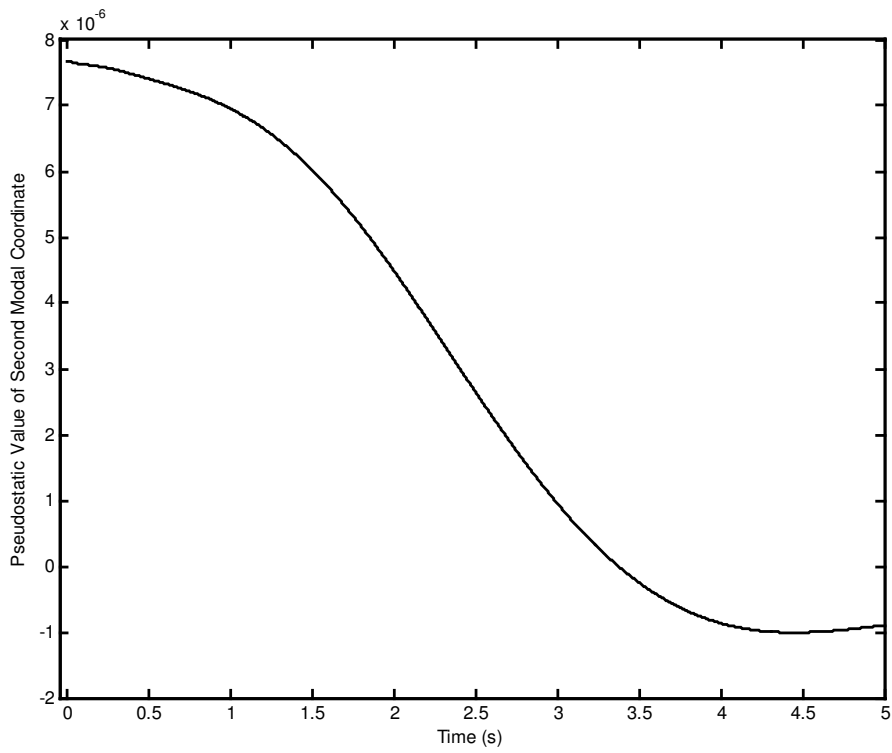


Figure 4.23 Pseudostatic value of second modal coordinate.

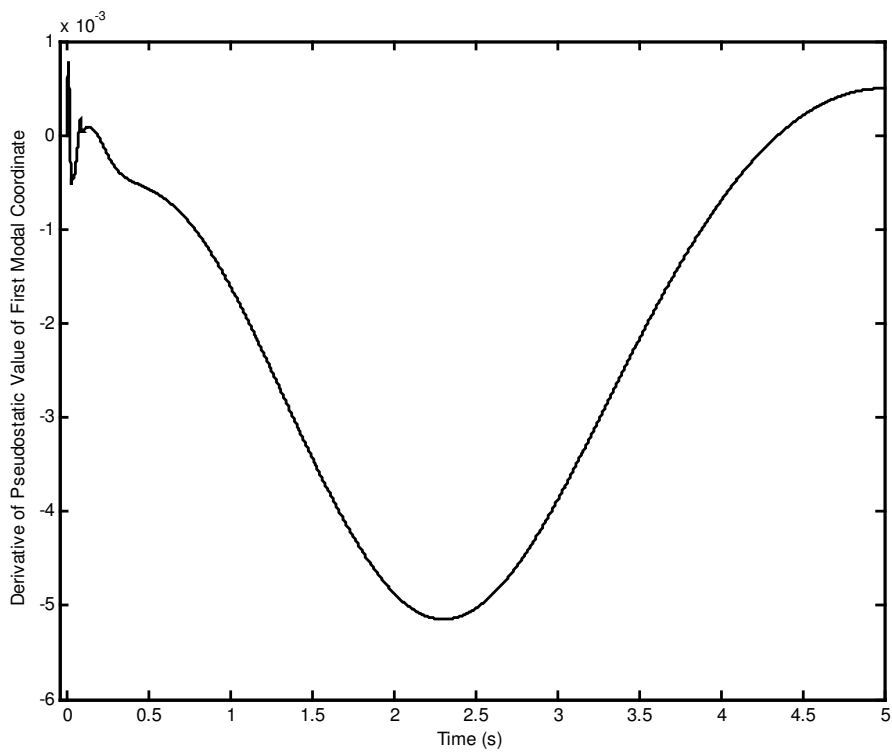


Figure 4.24 Derivative of pseudostatic value of first modal coordinate.

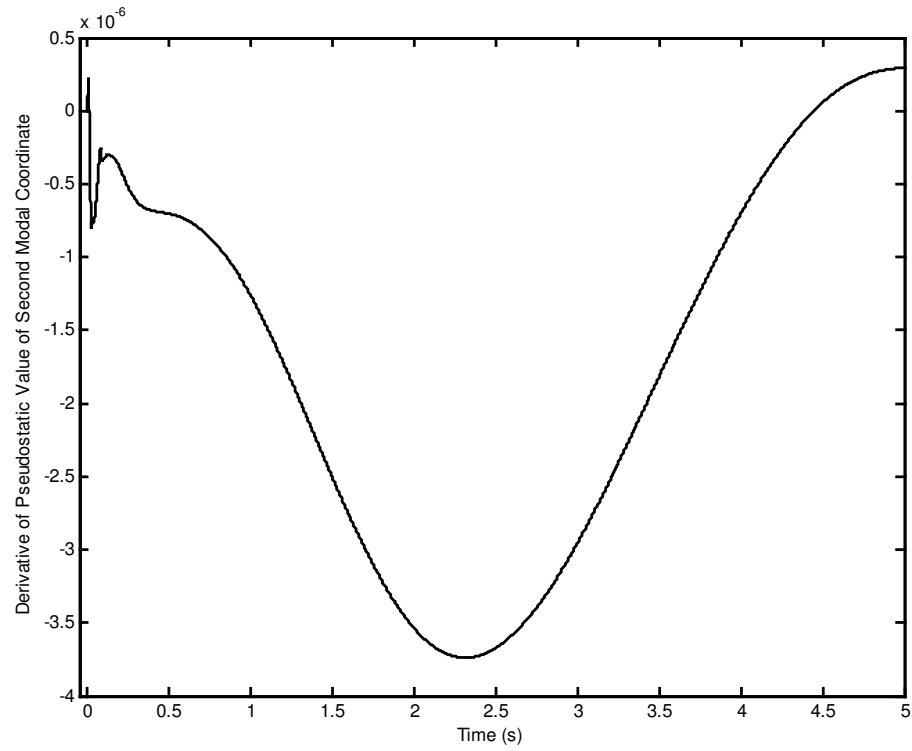


Figure 4.25 Derivative of pseudostatic value of second modal coordinate.

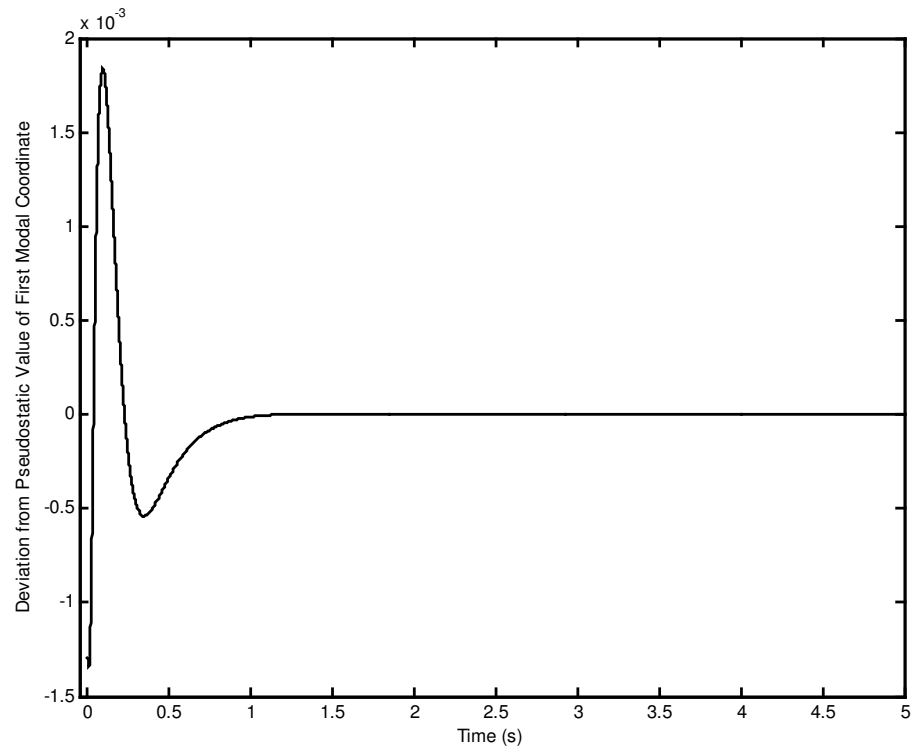


Figure 4.26 Deviation from pseudostatic value of first modal coordinate.

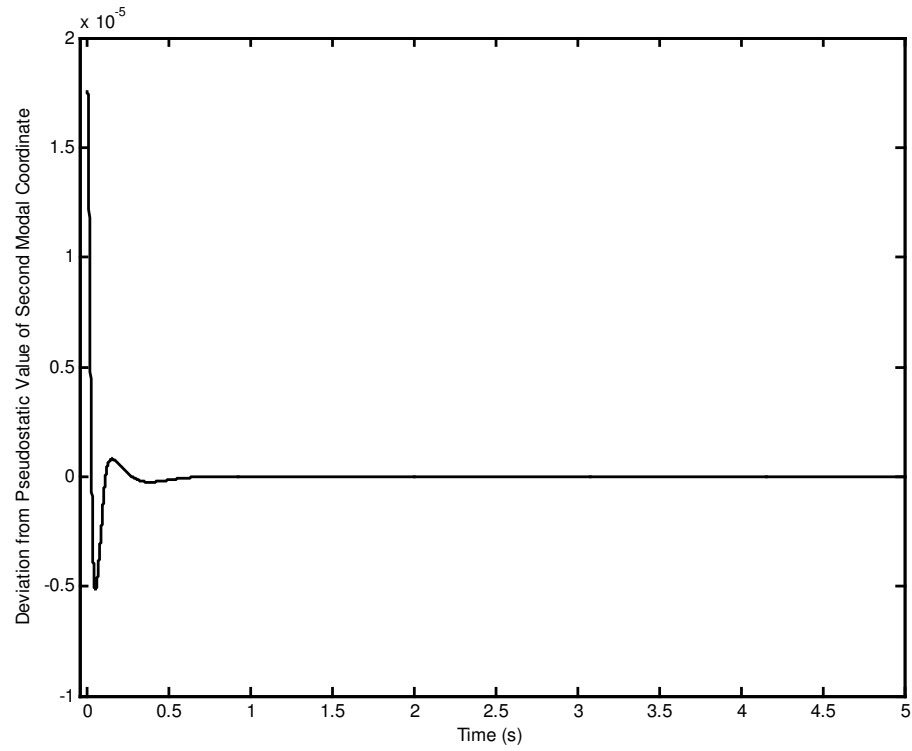


Figure 4.27 Deviation from pseudostatic value of second modal coordinate.

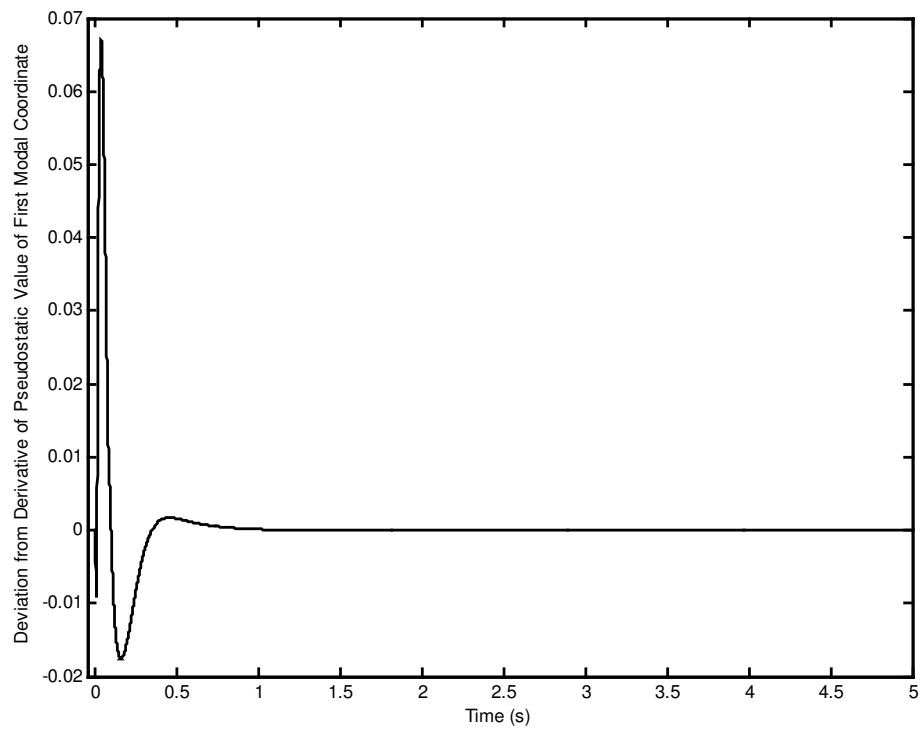


Figure 4.28 Deviation from derivative of pseudostatic value of first modal coordinate.

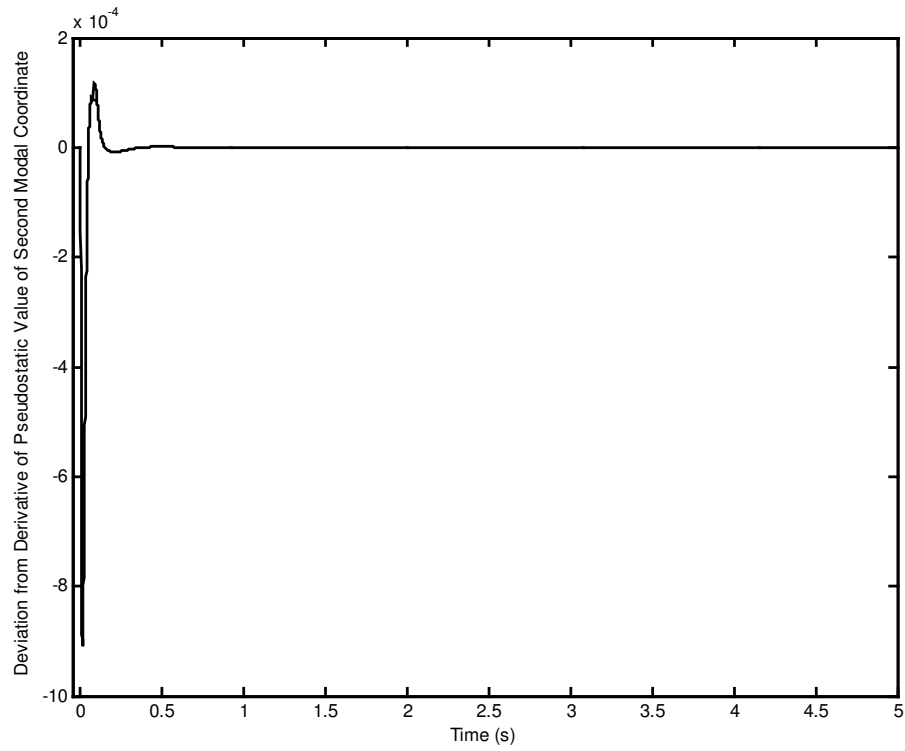


Figure 4.29 Deviation from derivative of pseudostatic value of second modal coordinate.

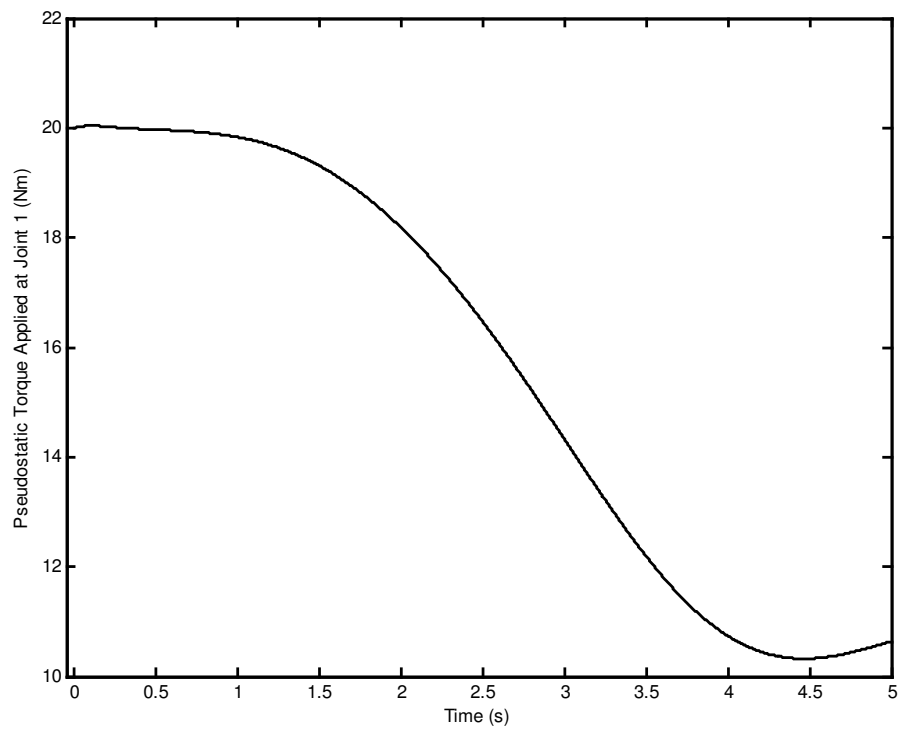


Figure 4.30 Pseudostatic torque applied at joint 1.

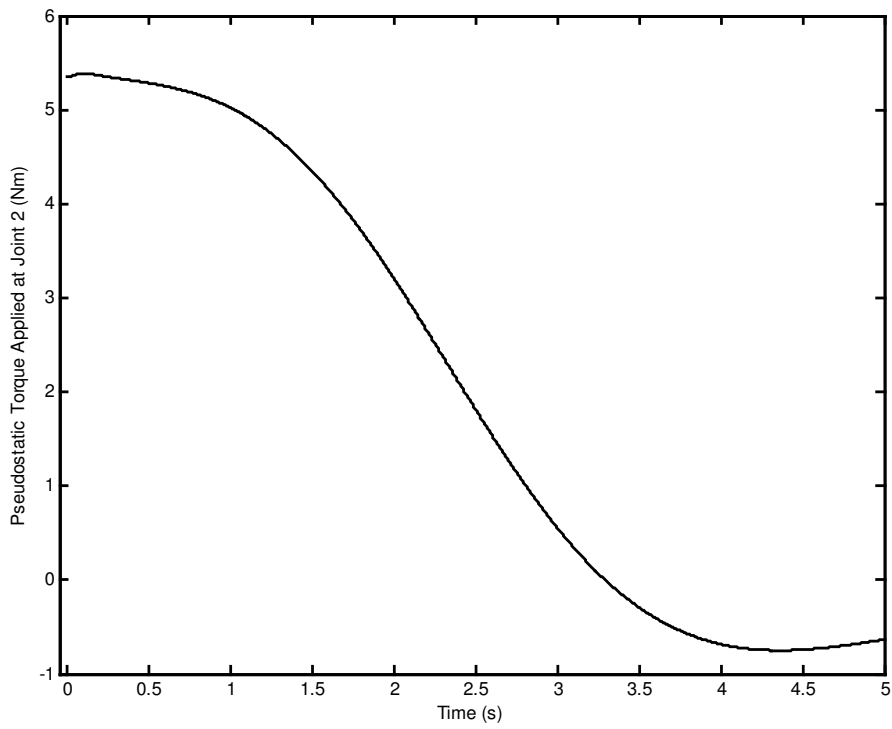


Figure 4.31 Pseudostatic torque applied at joint 2.

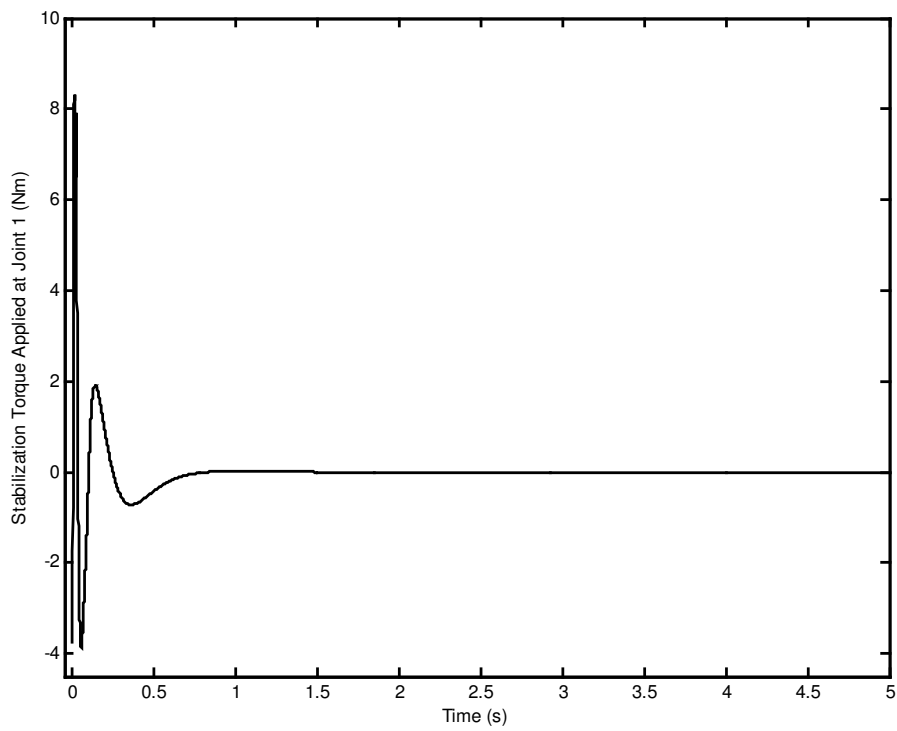


Figure 4.32 Stabilization torque applied at joint 1.

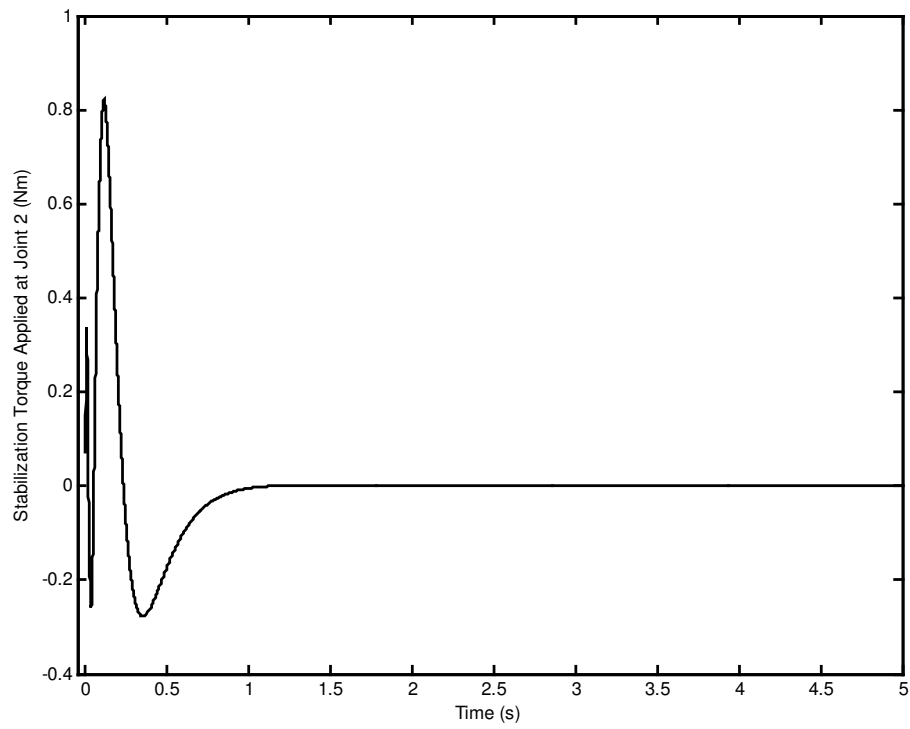


Figure 4.33 Stabilization torque applied at joint 2.

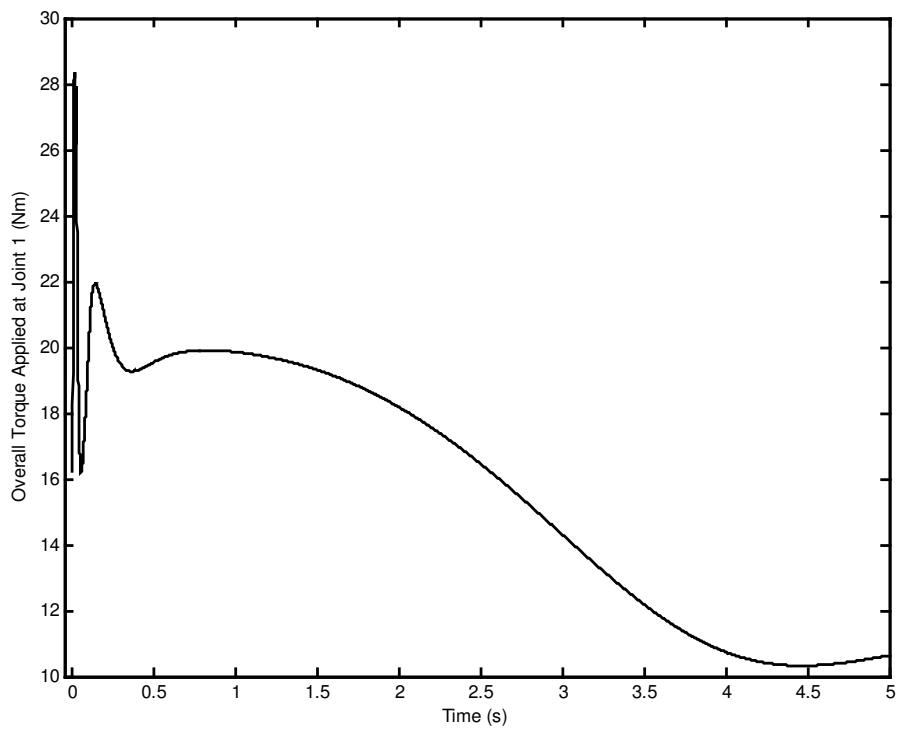


Figure 4.34 Overall torque applied at joint 1.

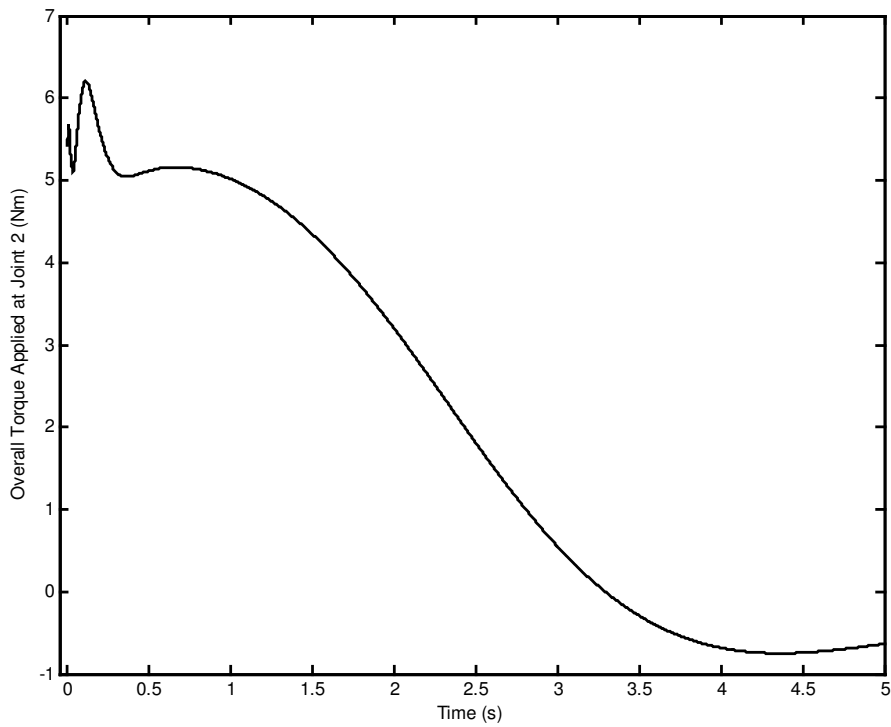


Figure 4.35 Overall torque applied at joint 2.

It is seen from Figures 4.9 and 4.10 that there is tip point position error due to the deflection of the forearm, but is compensated in about 1 s for the initial deviations of about 35 mm during the motion. There is a reverse action at the beginning of the motion as seen in the tip point position and velocity which are given in Figures 4.14 - 4.17. The maximum tip point position tracking error components along the trajectory after the tip point settles on the trajectory are 1.5935×10^{-4} m and -1.3340×10^{-4} m in \mathbf{n}_1 and \mathbf{n}_2 directions, respectively. The tip point position error components at the end of the motion are 3.6058×10^{-5} m and -9.6852×10^{-6} m in \mathbf{n}_1 and \mathbf{n}_2 directions, respectively. The maximum overall torques applied to the joints are in small magnitudes which is in the order of 28 Nm as seen from Figures 4.34 and 4.35.

4.3 Numerical Simulation of Motion Control of Planar Robot with Unmodeled Dynamics

To test the performance of the proposed control algorithm, unmodeled dynamics is taken into consideration. The dynamics of the robot is modeled by using the first two modes while the motion is simulated, but they are modeled by using only the first mode while the control torques are generated. In other words the plant dynamics is modeled by representing the link flexibility with the first two modes, while the controller is designed by representing the link flexibility with the first mode. The numerical simulation of motion control of the planar robot with unmodelled dynamics is obtained by using the motion control method proposed at Chapter 2. The same reference trajectory given in the previous section is used.

After a few trials, proper closed loop natural frequencies and damping ratios are obtained as 5 rad/s, 15 rad/s, 30 rad/s, 0.85, 0.85 and 0.85. The corresponding closed loop poles are given in Table 4.3.

Table 4.3 Closed loop poles used in motion control of planar robot with unmodeled dynamics.

Closed Loop Poles
$p_1 = -4.2500 + 2.6339j$
$p_2 = -4.2500 - 2.6339j$
$p_3 = -12.7500 + 7.9017j$
$p_4 = -12.7500 - 7.9017j$
$p_5 = -25.5000 + 15.8035j$
$p_6 = -25.5000 - 15.8035j$

The sampling frequency is taken as 2500 Hz. The simulation results are given in Figures 4.36 - 4.62.

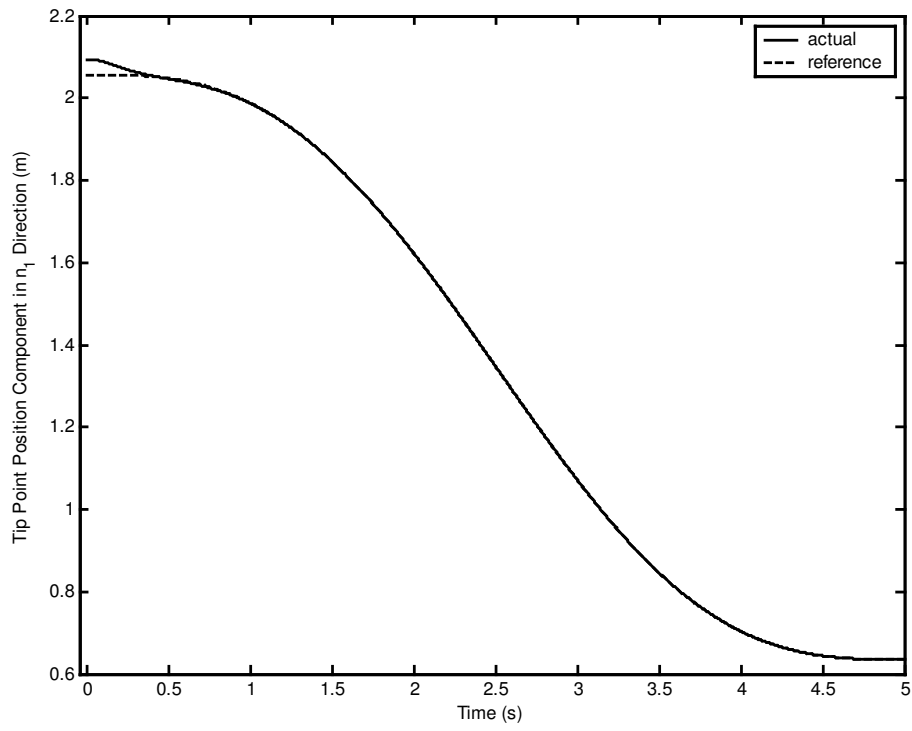


Figure 4.36 Tip point position component in n_1 direction.

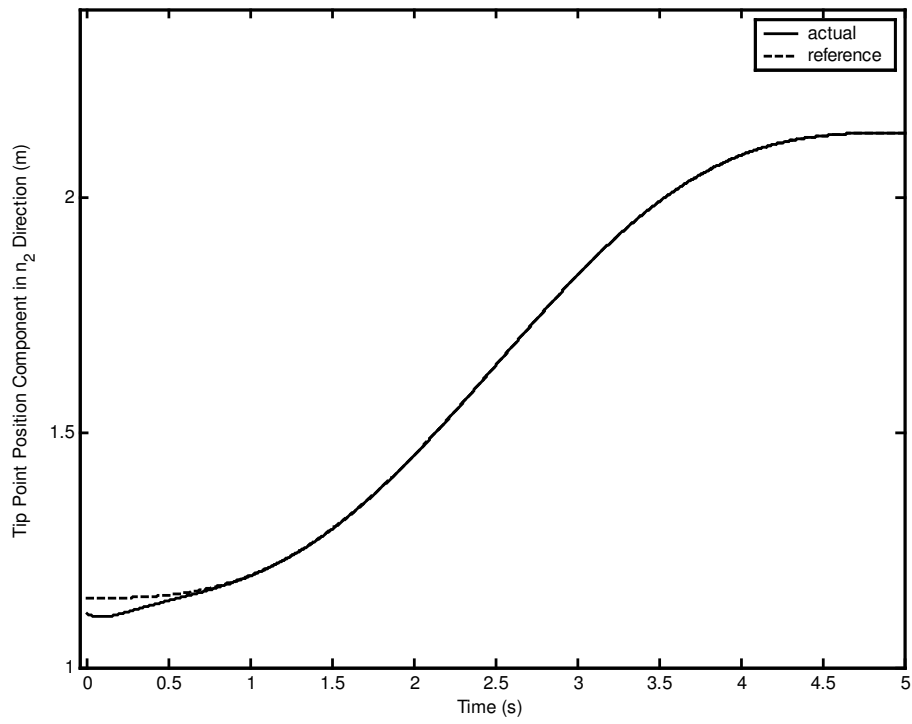


Figure 4.37 Tip point position component in n_2 direction.

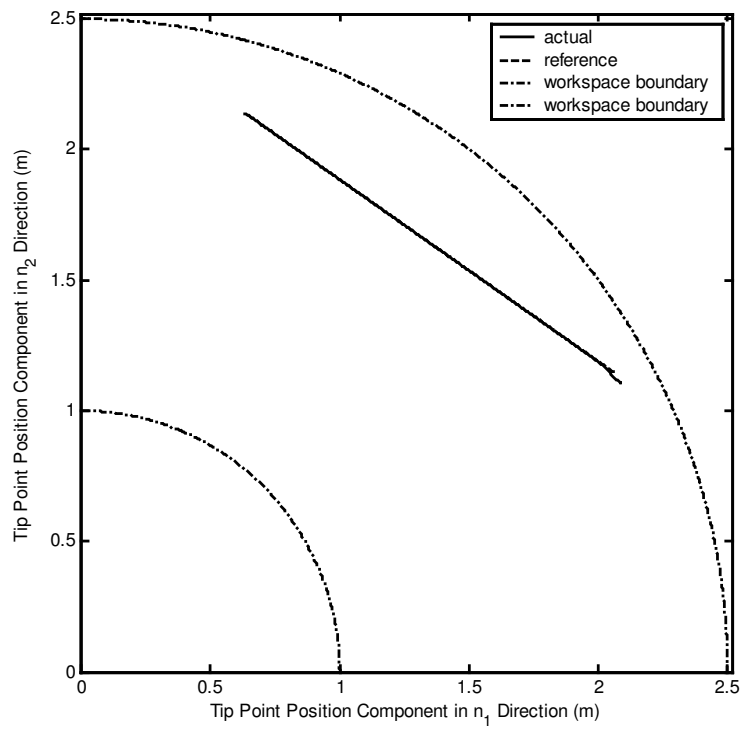


Figure 4.38 Workspace and tip point position.

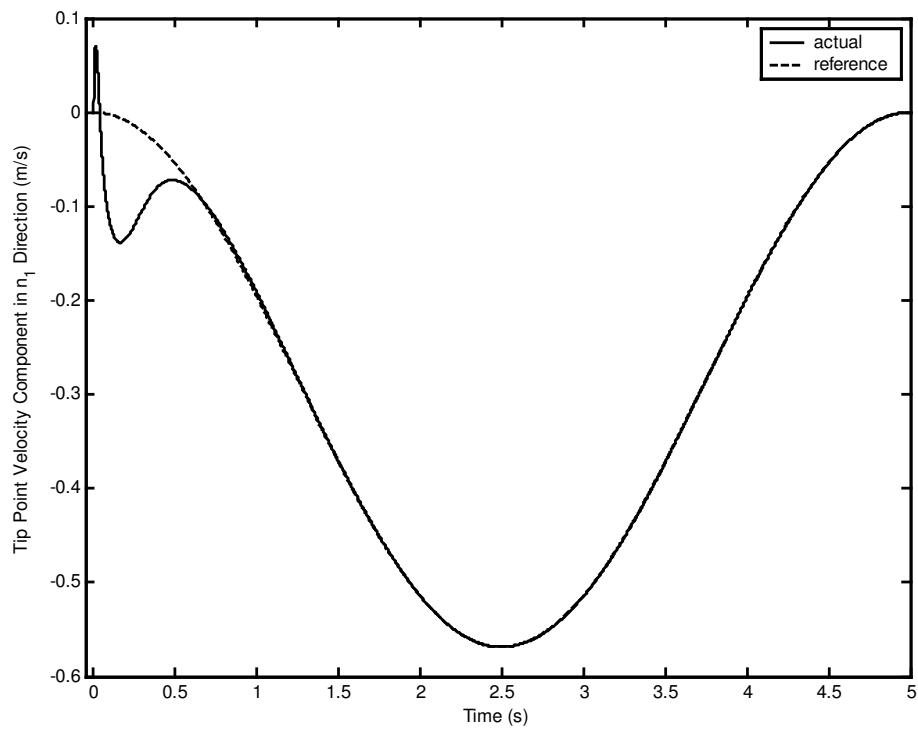


Figure 4.39 Tip point velocity component in n_1 direction.

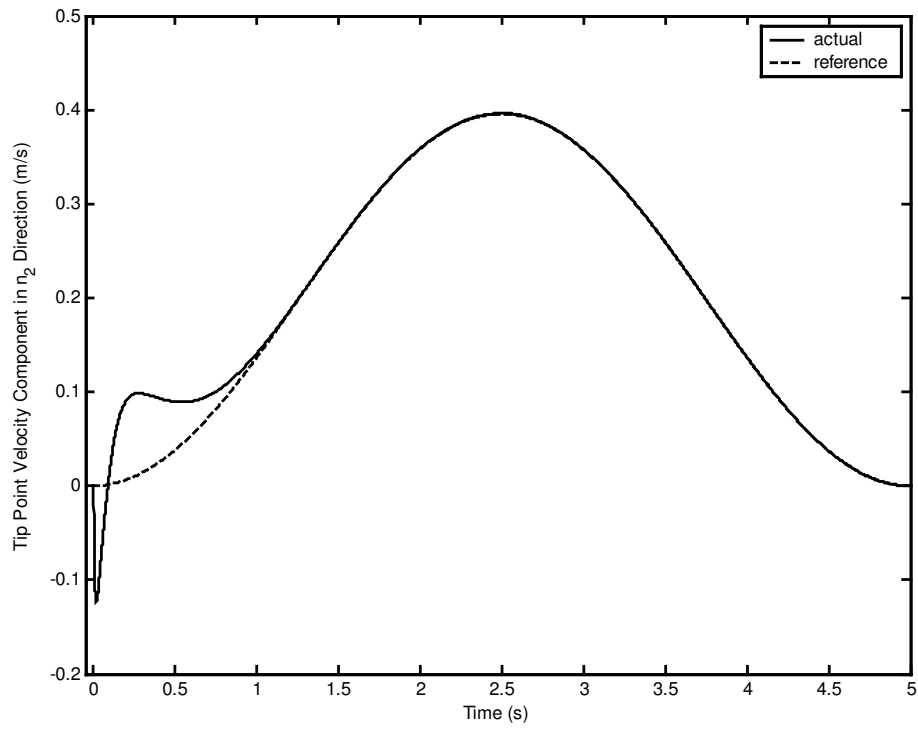


Figure 4.40 Tip point velocity component in n_2 direction.

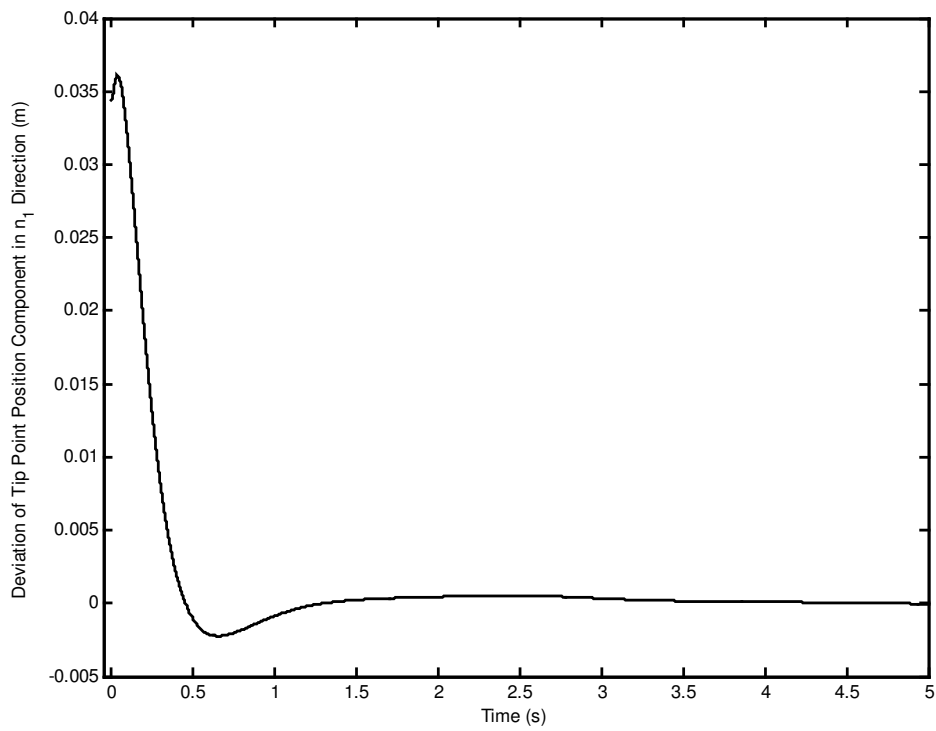


Figure 4.41 Deviation of tip point position component in n_1 direction.

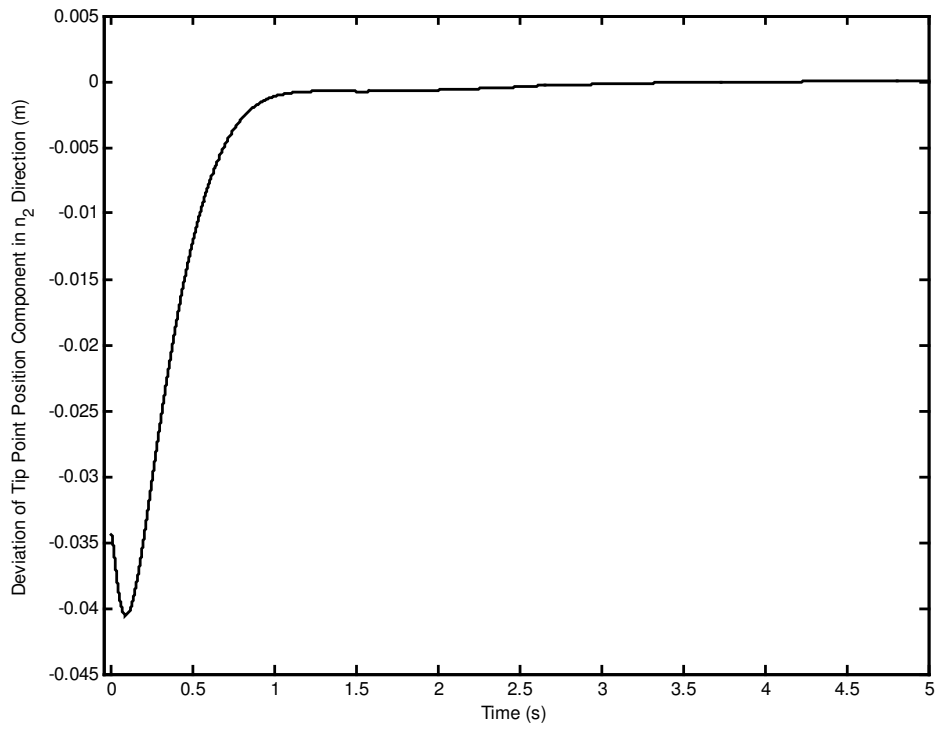


Figure 4.42 Deviation of tip point position component in n_2 direction.

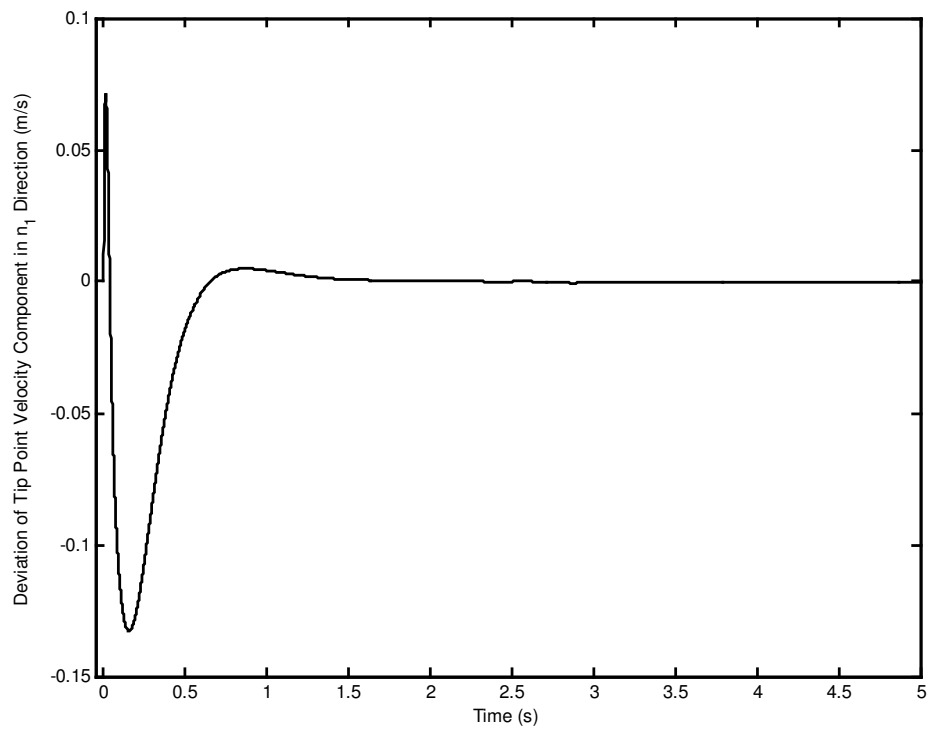


Figure 4.43 Deviation of tip point velocity component in n_1 direction.

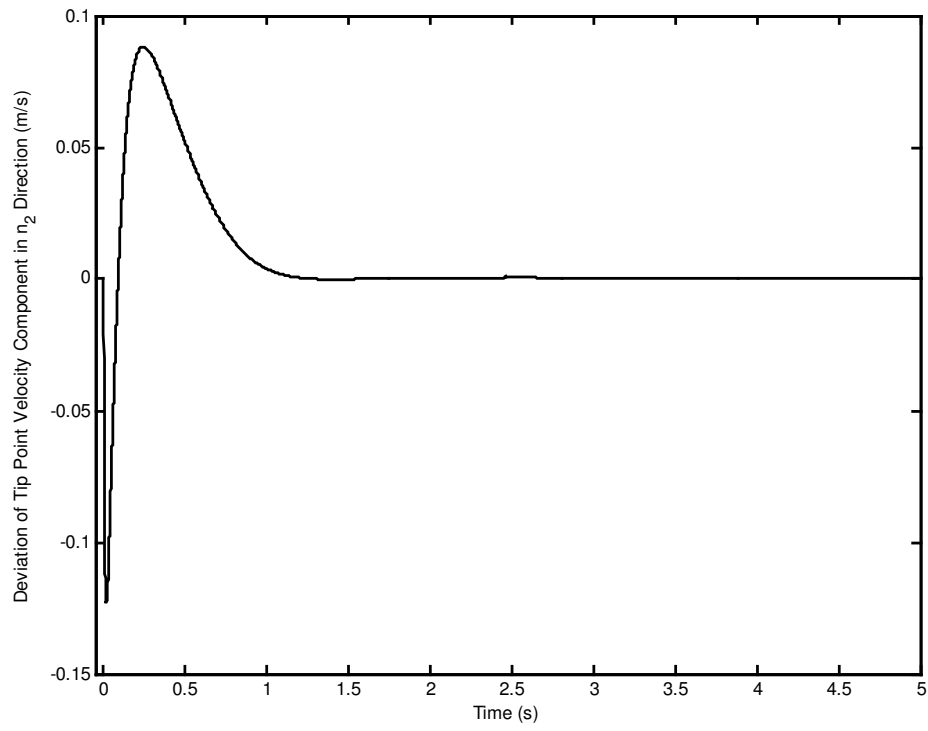


Figure 4.44 Deviation of tip point velocity component in n_2 direction.

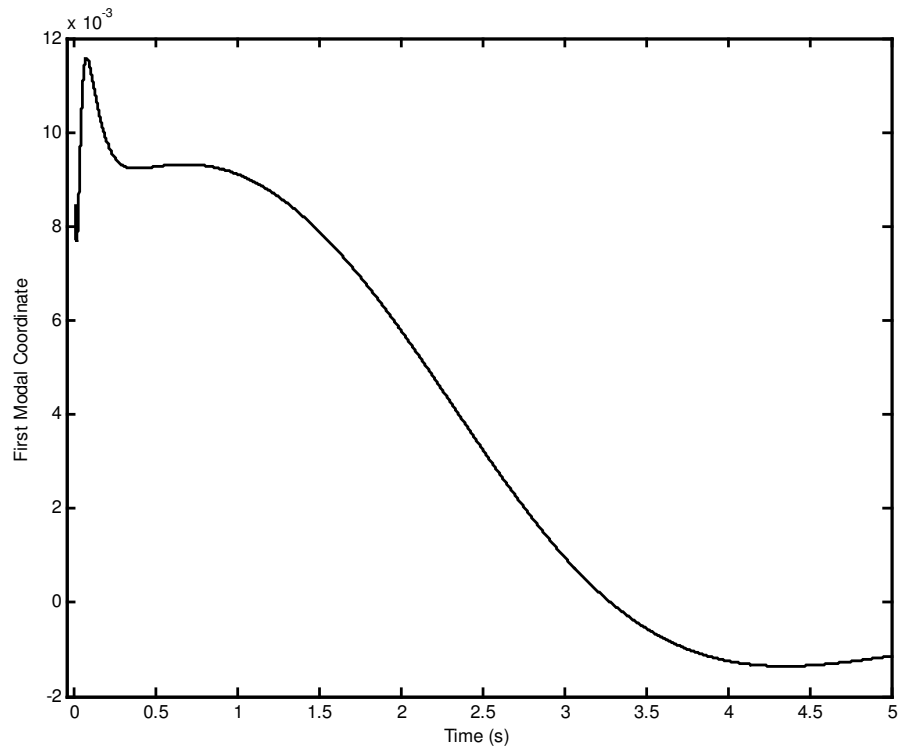


Figure 4.45 First modal coordinate.

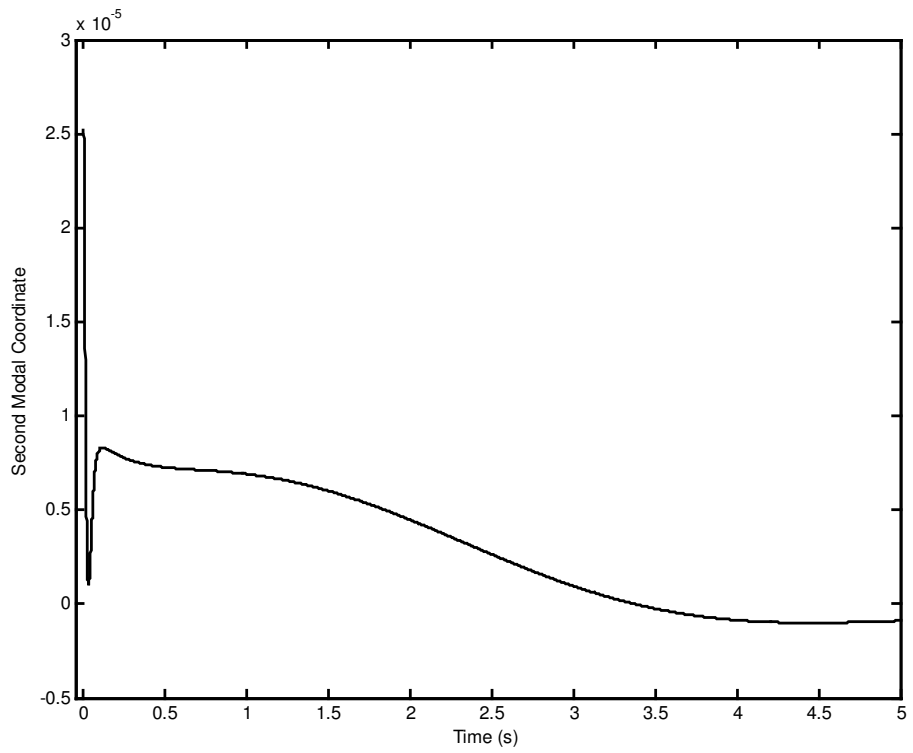


Figure 4.46 Second modal coordinate.

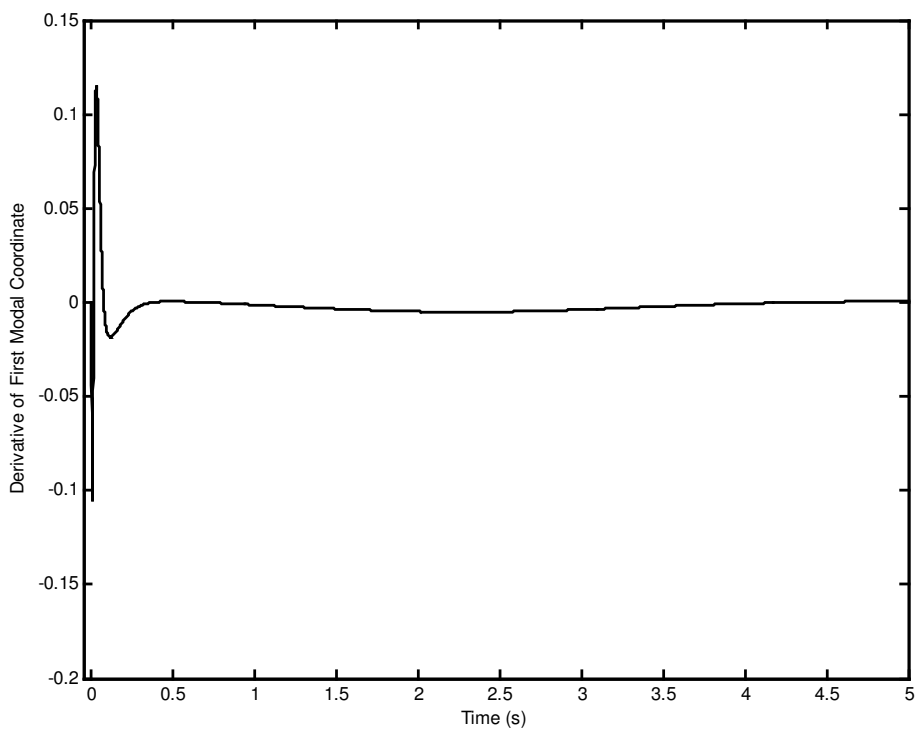


Figure 4.47 Derivative of first modal coordinate.

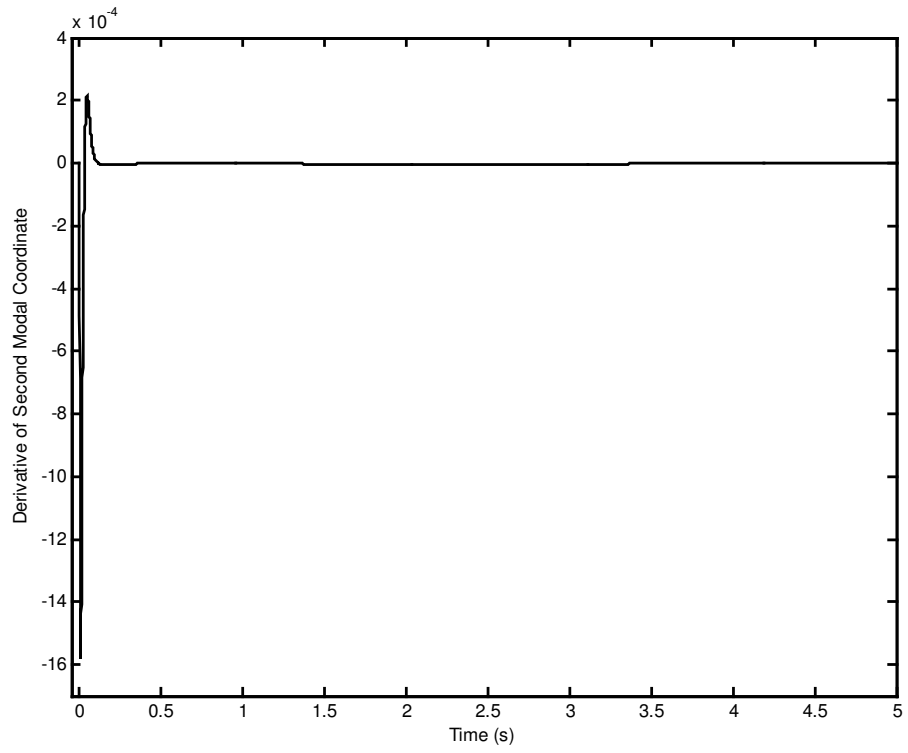


Figure 4.48 Derivative of second modal coordinate.

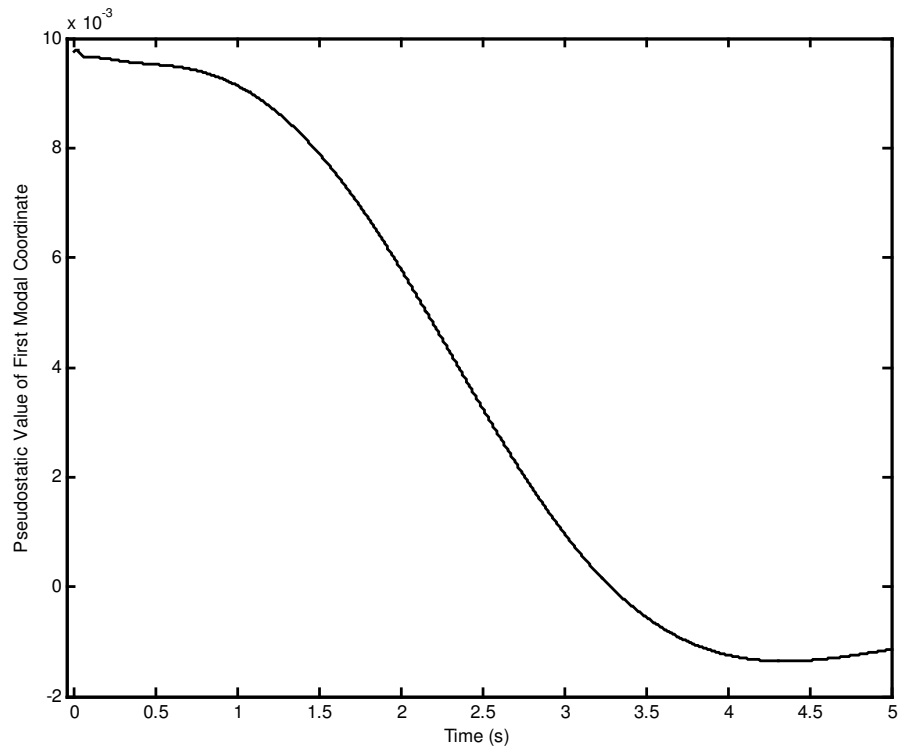


Figure 4.49 Pseudostatic value of first modal coordinate.

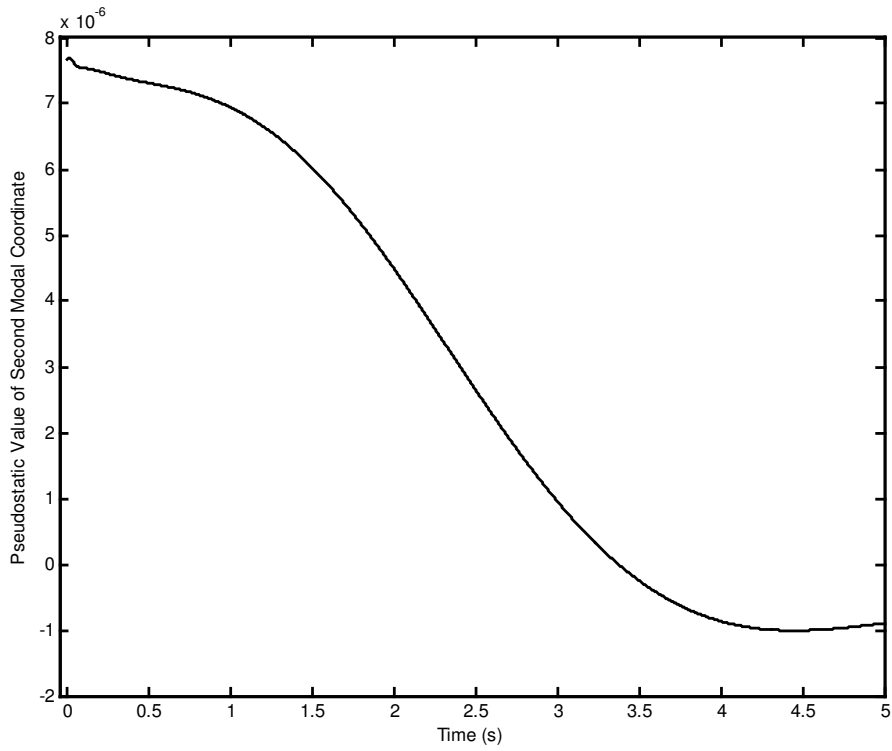


Figure 4.50 Pseudostatic value of second modal coordinate.

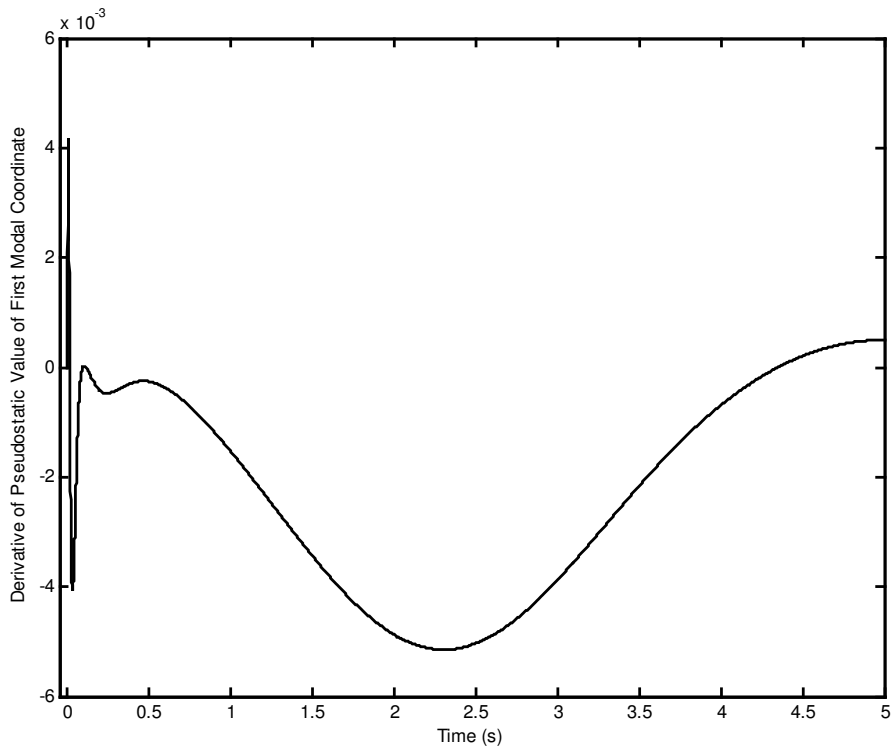


Figure 4.51 Derivative of pseudostatic value of first modal coordinate.

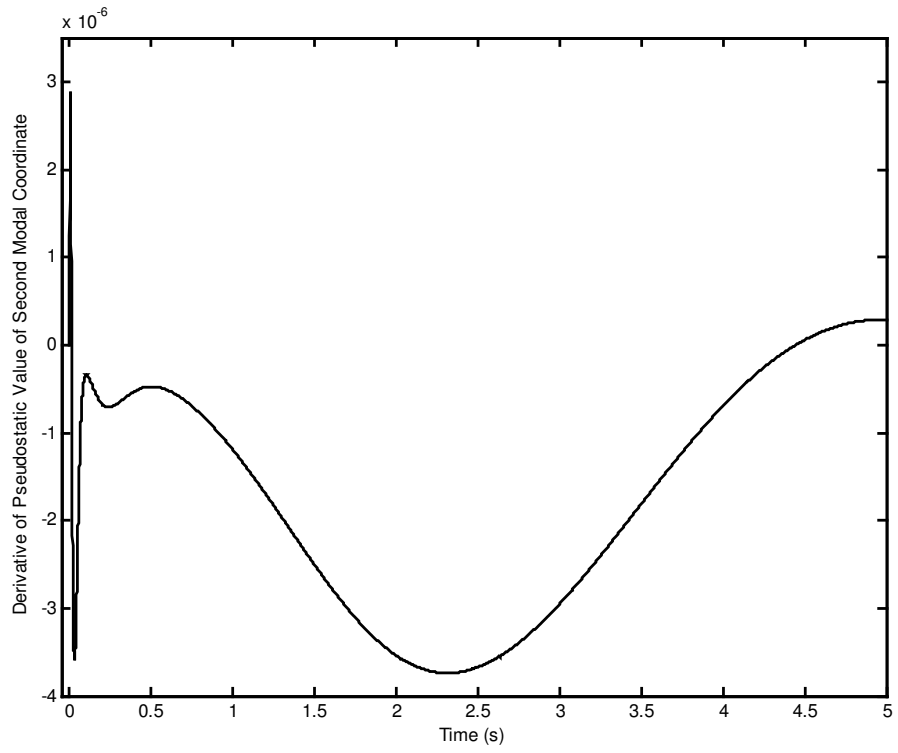


Figure 4.52 Derivative of pseudostatic value of second modal coordinate.

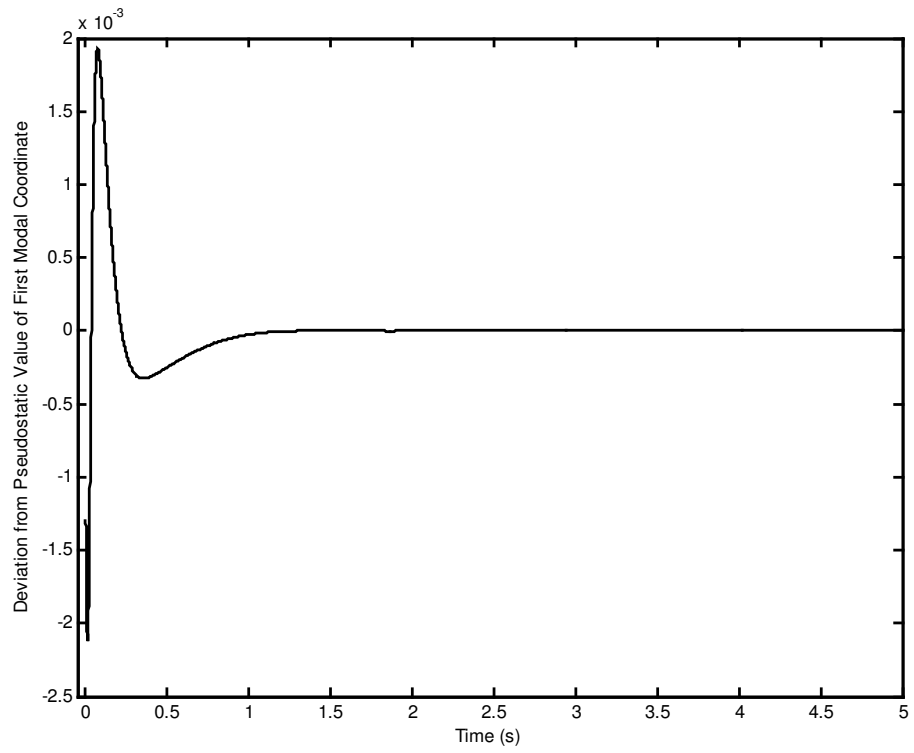


Figure 4.53 Deviation from pseudostatic value of first modal coordinate.

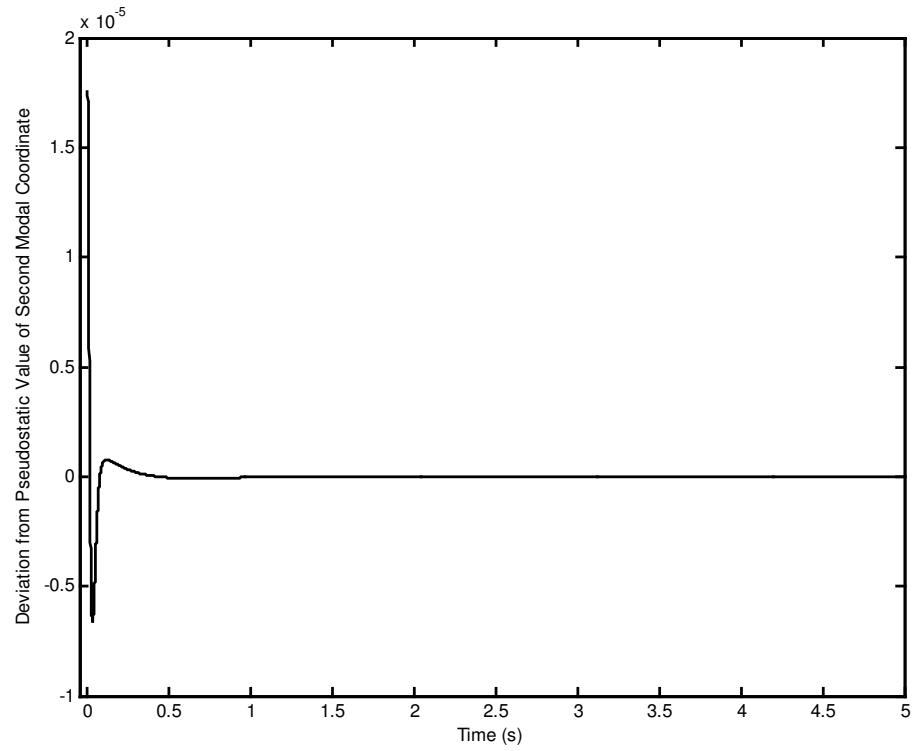


Figure 4.54 Deviation from pseudostatic value of second modal coordinate.

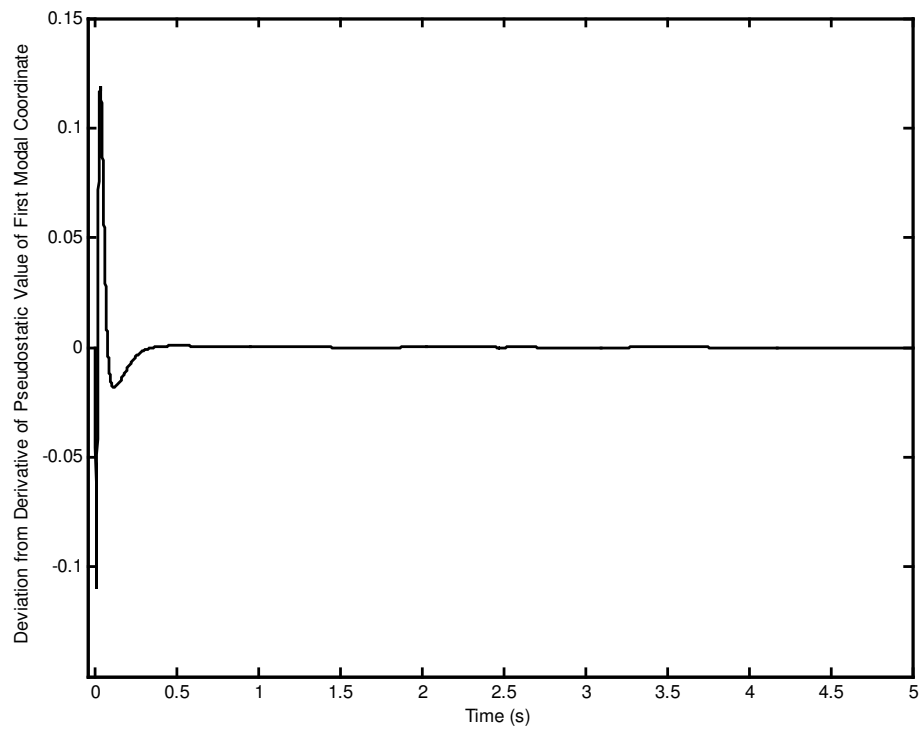


Figure 4.55 Deviation from derivative of pseudostatic value of first modal coordinate.

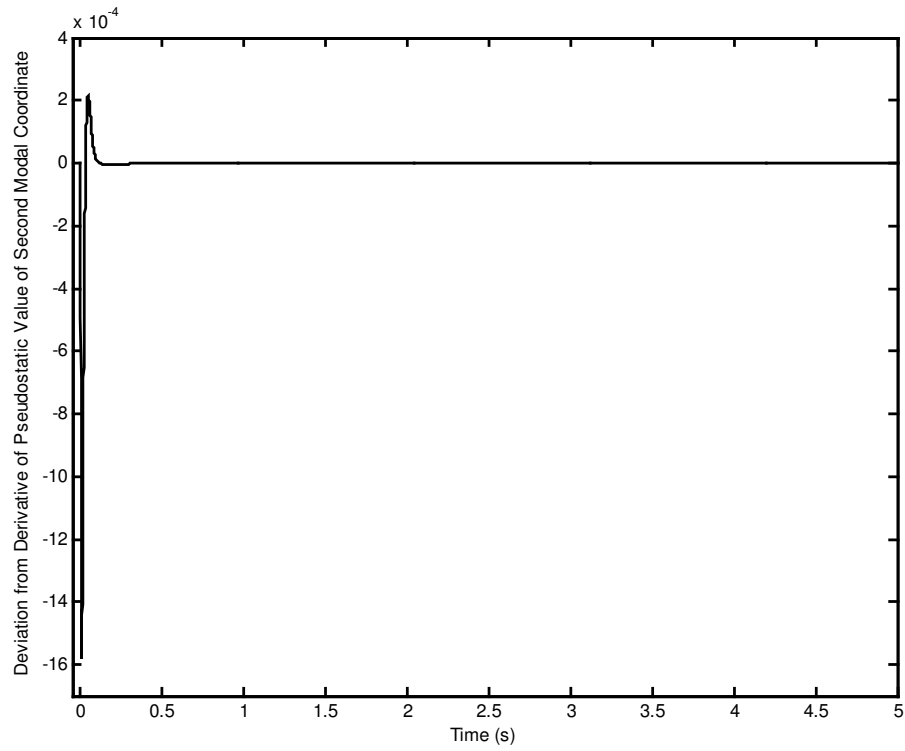


Figure 4.56 Deviation from derivative of pseudostatic value of second modal coordinate.

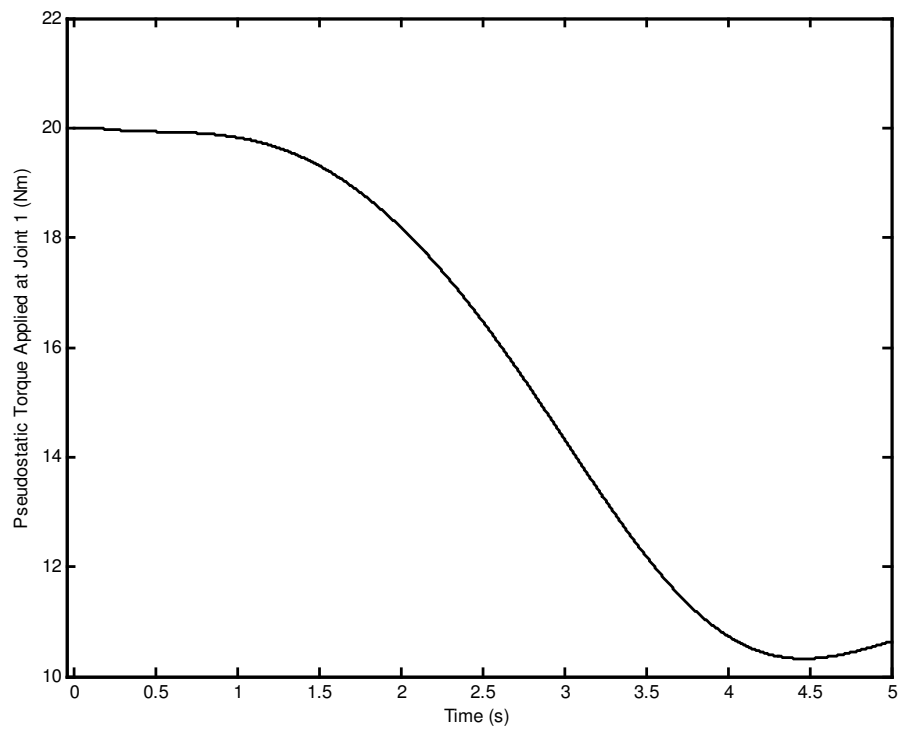


Figure 4.57 Pseudostatic torque applied at joint 1.

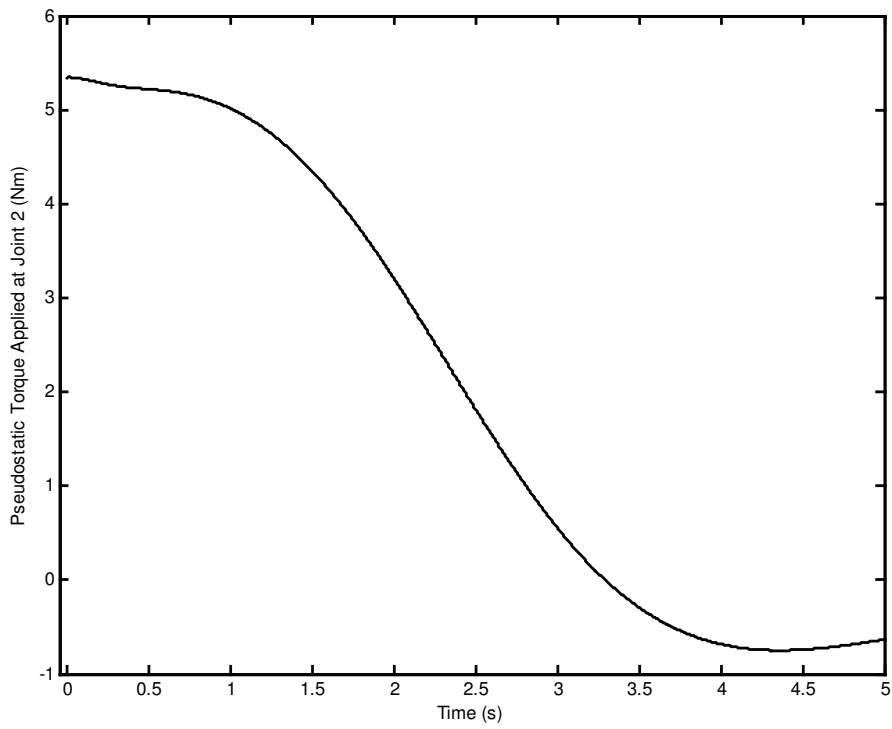


Figure 4.58 Pseudostatic torque applied at joint 2.

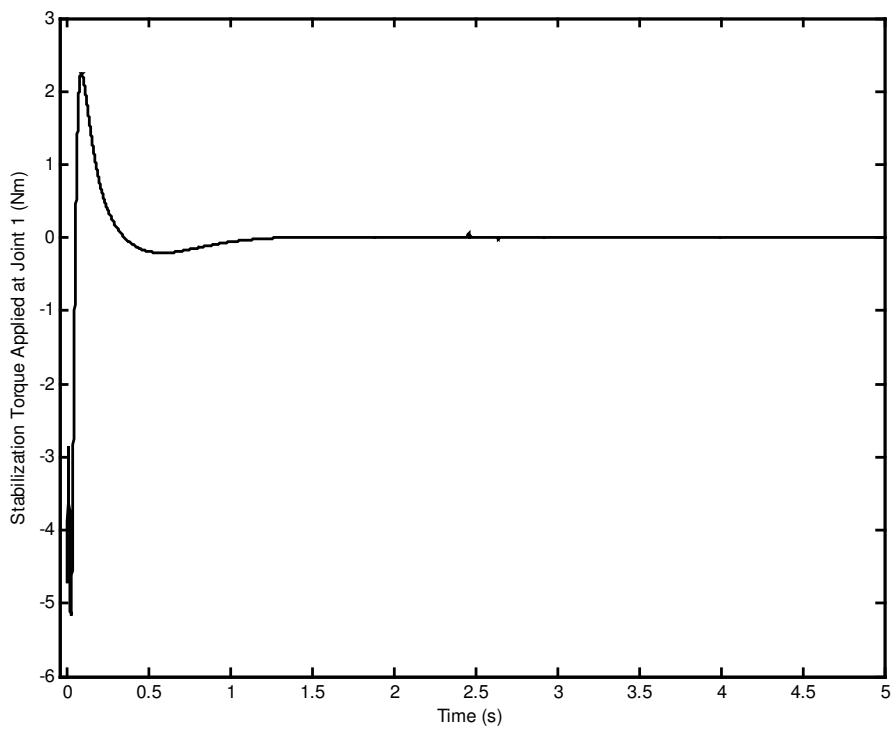


Figure 4.59 Stabilization torque applied at joint 1.

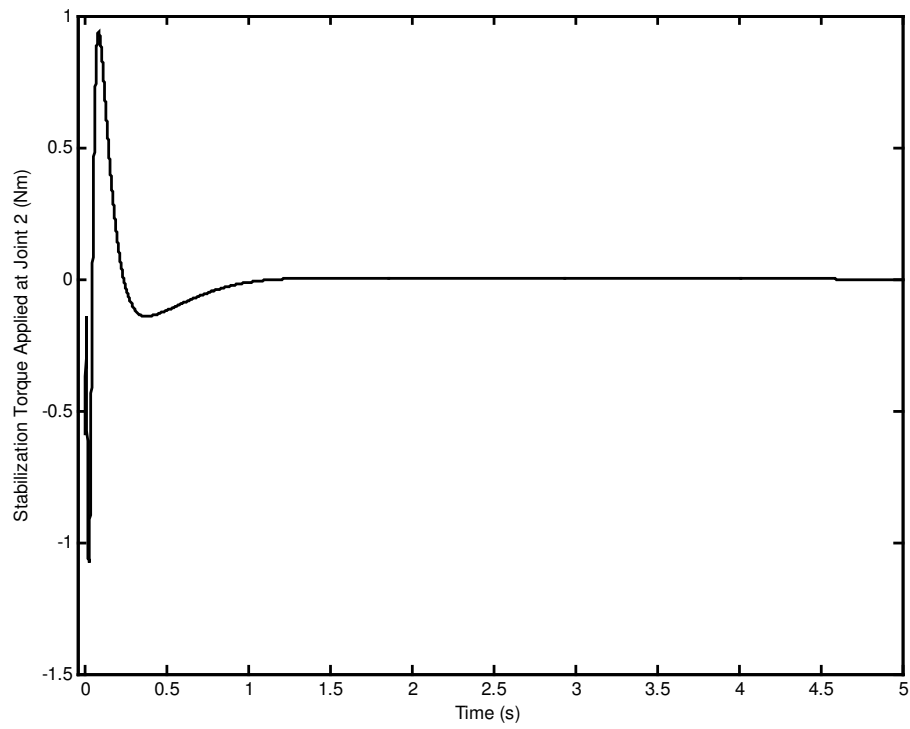


Figure 4.60 Stabilization torque applied at joint 2.

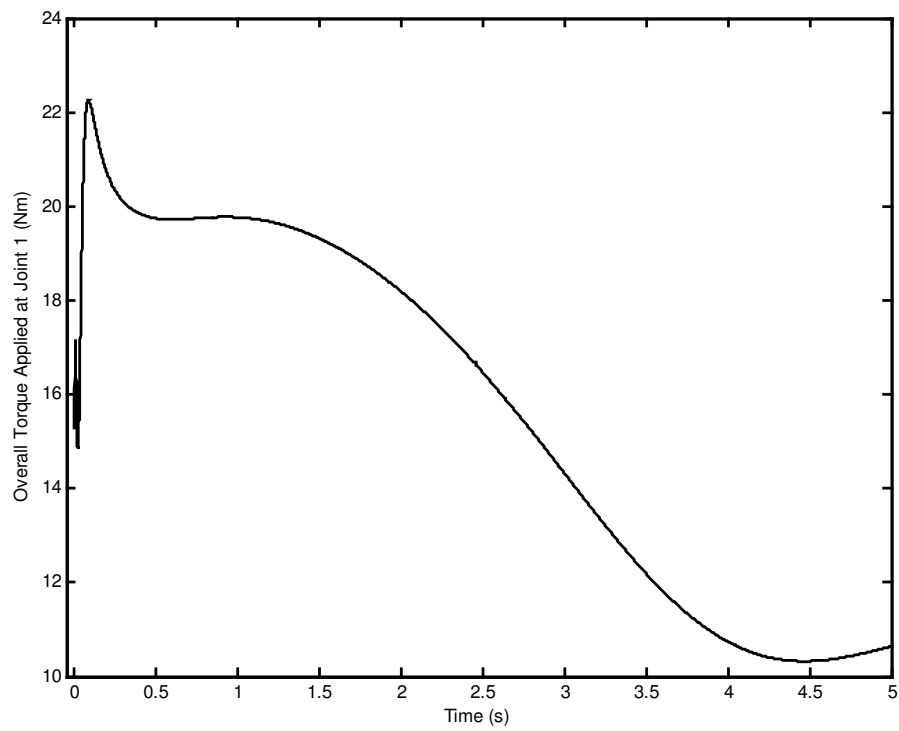


Figure 4.61 Overall torque applied at joint 1.

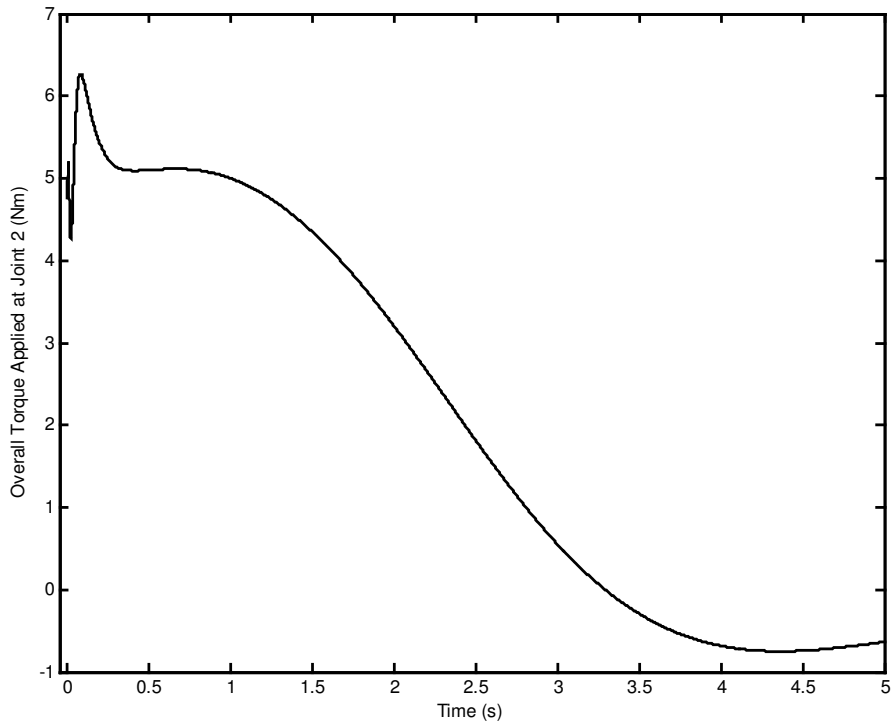


Figure 4.62 Overall torque applied at joint 2.

When the figures are examined, it is seen that it takes about 1 s in settling the tip point to the desired trajectory for the initial deviations of about 35 mm. There is reverse action at the beginning of the motion as seen in tip point position and velocity which are given in Figures 4.41 - 4.44. The maximum tip point position tracking error components along the trajectory after the tip point settles on the trajectory are 5.0190×10^{-4} m and -7.4560×10^{-4} m in \mathbf{n}_1 and \mathbf{n}_2 directions, respectively. The tip point position error components at the end of the motion are -3.5691×10^{-5} m and 2.2783×10^{-5} m in \mathbf{n}_1 and \mathbf{n}_2 directions, respectively. The maximum overall torques applied to the joints are in small magnitudes which is in the order of 22 Nm as seen from Figures 4.61 and 4.62. The results show that the proposed control method works satisfactorily even though only the first mode is taken into consideration in the controller design.

4.4 Numerical Simulation of Motion Control of Planar Robot by Using Computed Torque Method

The computed torque method (control) is one of the conventional control methods used in robot control. It is known also under the name of inverse dynamics control. In this section, numerical simulation of motion control of the planar robot with flexible forearm is presented by using the computed torque method designed as if the robot is rigid. In other words, the plant dynamics are modeled by using the flexible robot with two modes, while the controller is designed by the robot as if it is rigid.

The equations of motion of a rigid robot can be expressed as

$$\mathbf{M}(\mathbf{q})\ddot{\mathbf{q}} + \mathbf{C}(\mathbf{q}, \dot{\mathbf{q}})\dot{\mathbf{q}} + \mathbf{G}(\mathbf{q}) = \mathbf{T} \quad (4.8)$$

where $\mathbf{M}(\mathbf{q})$ is the mass matrix, $\mathbf{C}(\mathbf{q}, \dot{\mathbf{q}})$ is the Coriolis and centrifugal force term matrix, $\mathbf{G}(\mathbf{q})$ is the gravitational vector, \mathbf{T} is the external torque vector and \mathbf{q} is the vector of joint variables. Equation (4.8) can be written as

$$\mathbf{M}(\mathbf{q})\ddot{\mathbf{q}} + \mathbf{B}(\mathbf{q}, \dot{\mathbf{q}}) = \mathbf{T} \quad (4.9)$$

where $\mathbf{B}(\mathbf{q}, \dot{\mathbf{q}})$ is given as

$$\mathbf{B}(\mathbf{q}, \dot{\mathbf{q}}) = \mathbf{C}(\mathbf{q}, \dot{\mathbf{q}})\dot{\mathbf{q}} + \mathbf{G}(\mathbf{q}) \quad (4.10)$$

To cancel the nonlinear terms and to decouple the dynamics of each link computed torque control can be selected in the form of

$$\mathbf{T} = \mathbf{M}(\mathbf{q})\mathbf{u} + \mathbf{B}(\mathbf{q}, \dot{\mathbf{q}}) \quad (4.11)$$

where \mathbf{u} is an auxiliary control input to be designed. If Equation (4.11) is substituted into Equation (4.9), the following equation is obtained

$$\ddot{\mathbf{q}} = \mathbf{u} \quad (4.12)$$

A typical choice for \mathbf{u} is

$$\mathbf{u} = \ddot{\mathbf{q}}^* + \mathbf{K}_d (\dot{\mathbf{q}}^* - \dot{\mathbf{q}}) + \mathbf{K}_p (\mathbf{q}^* - \mathbf{q}) \quad (4.13)$$

where superscript * stands for the desired values, \mathbf{K}_p and \mathbf{K}_d are the proportional and derivative control gains. If Equation (4.12) is substituted into Equation (4.13) the following equation is obtained.

$$\ddot{\boldsymbol{\varepsilon}} + \mathbf{K}_d \dot{\boldsymbol{\varepsilon}} + \mathbf{K}_p \boldsymbol{\varepsilon} = \mathbf{0} \quad (4.14)$$

Where $\boldsymbol{\varepsilon}$ is given as

$$\boldsymbol{\varepsilon} = (\mathbf{q}^* - \mathbf{q}) \quad (4.15)$$

Equation (4.14) represents a set of second order differential equations. Therefore, \mathbf{K}_p and \mathbf{K}_d can be selected as

$$\mathbf{K}_p = \text{diag}(\omega_{ni}^2) \quad i = 1, \dots, n \quad (4.16)$$

$$\mathbf{K}_d = \text{diag}(2\zeta_i \omega_{ni}) \quad i = 1, \dots, n \quad (4.17)$$

where ω_{ni} and ζ_i are the desired natural frequencies and damping ratios of the closed loop system and n is the degree of the freedom of the robot.

The first two of the four closed loop natural frequencies and damping ratios given in Section 4.2 are used for the values required by the Equations (4.16) and (4.17). It is done so in order to obtain comparable responses. In other words, the closed loop natural frequencies and damping ratios are taken as 5 rad/s, 15 rad/s, 0.85 and

0.85 for this simulation. The corresponding closed loop poles are given in Table 4.4.

Table 4.4 Closed loop poles used in motion control of planar robot by using computed torque method.

Closed Loop Poles
$p_1 = -4.2500 + 2.6339j$
$p_2 = -4.2500 - 2.6339j$
$p_3 = -12.7500 + 7.9017j$
$p_4 = -12.7500 - 7.9017j$

The same reference trajectory given in Section 4.2 is used. The robot motion cannot be simulated when the sampling frequency is smaller than 2220 Hz. So, the sampling frequency is taken as 2500 Hz. The simulation results are given in Figures 4.63 - 4.77.

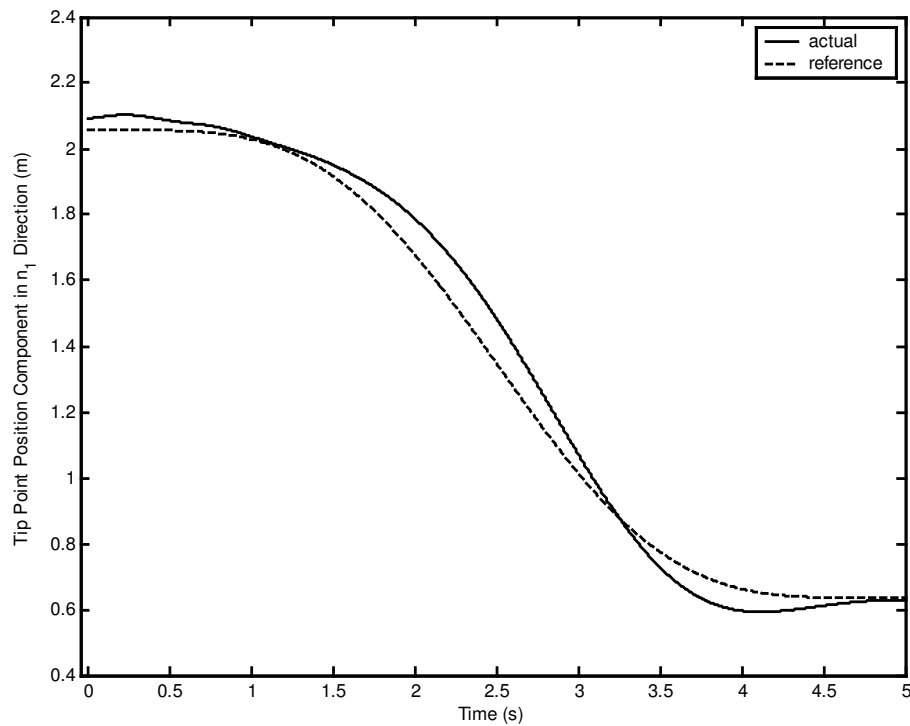


Figure 4.63 Tip point position component in n_1 direction.

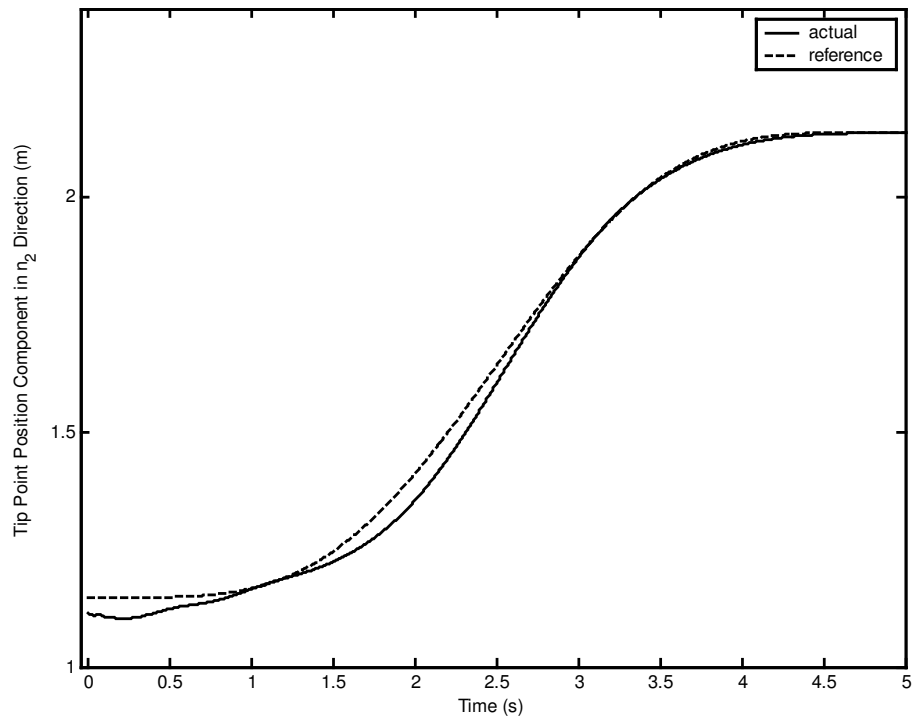


Figure 4.64 Tip point position component in n_2 direction.

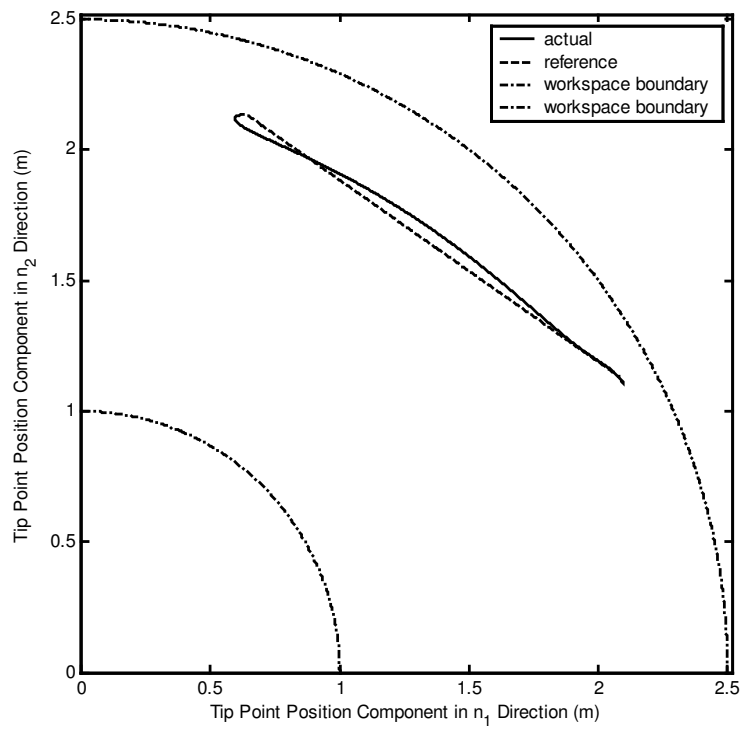


Figure 4.65 Workspace and tip point position.

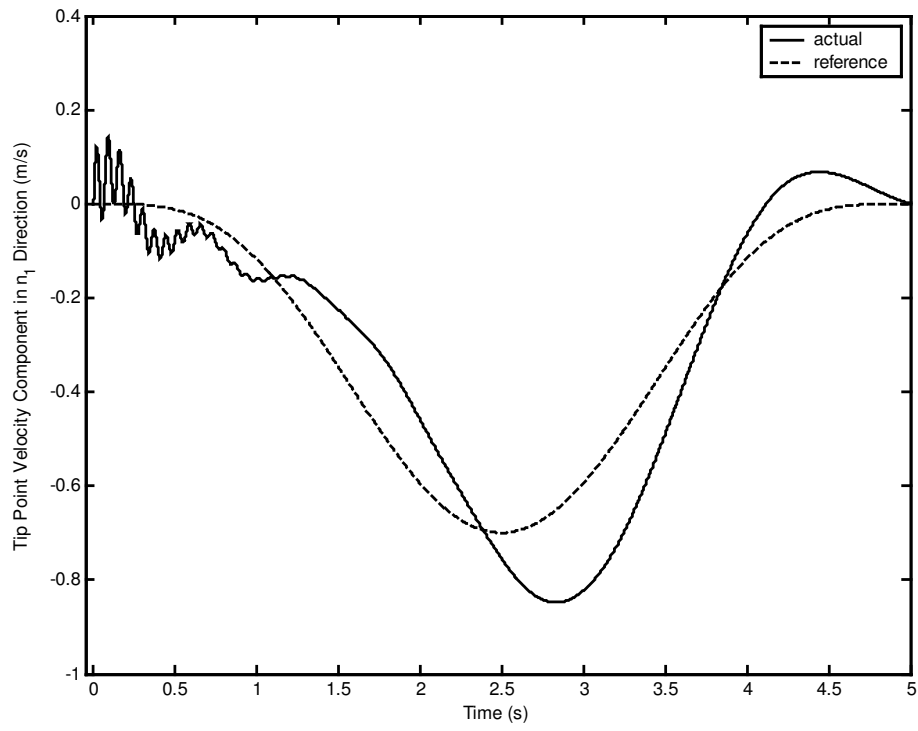


Figure 4.66 Tip point velocity component in n_1 direction.

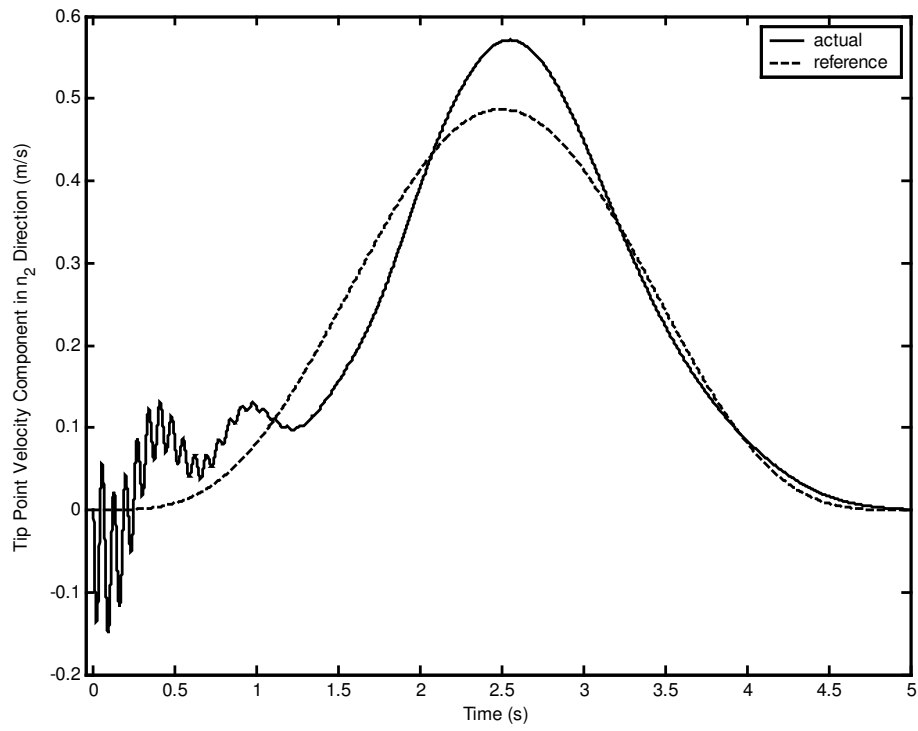


Figure 4.67 Tip point velocity component in n_2 direction.

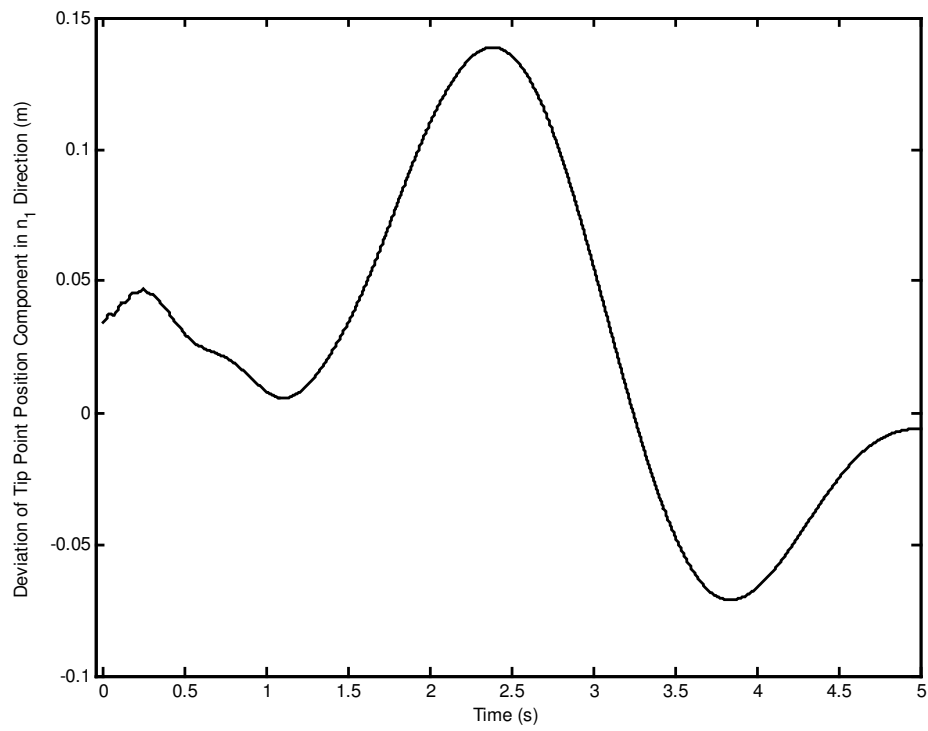


Figure 4.68 Deviation of tip point position component in n_1 direction.

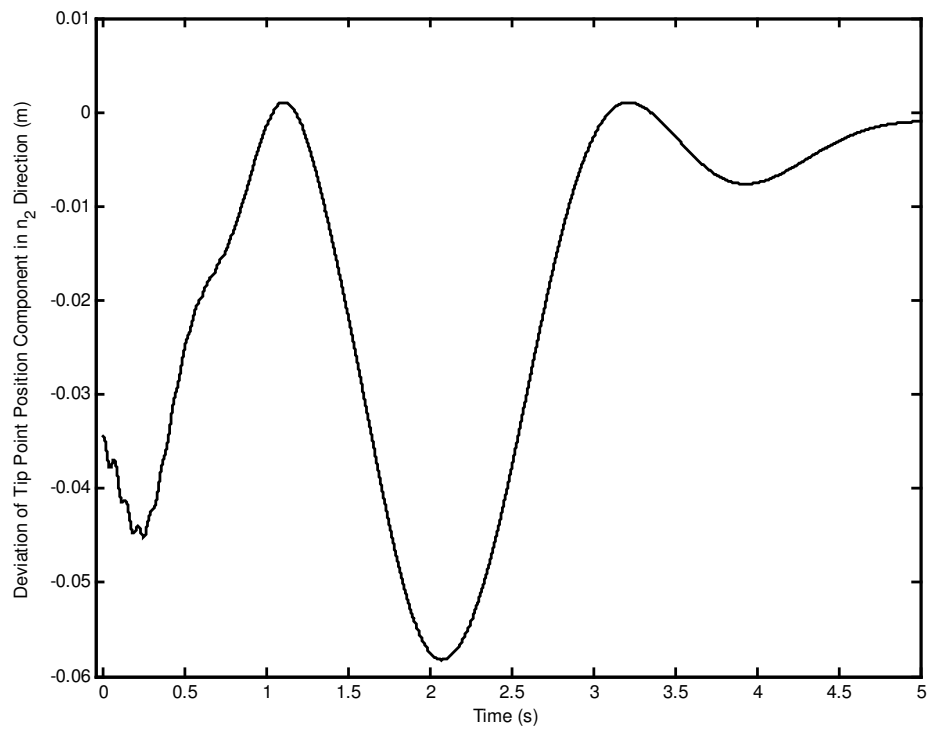


Figure 4.69 Deviation of tip point position component in n_2 direction.

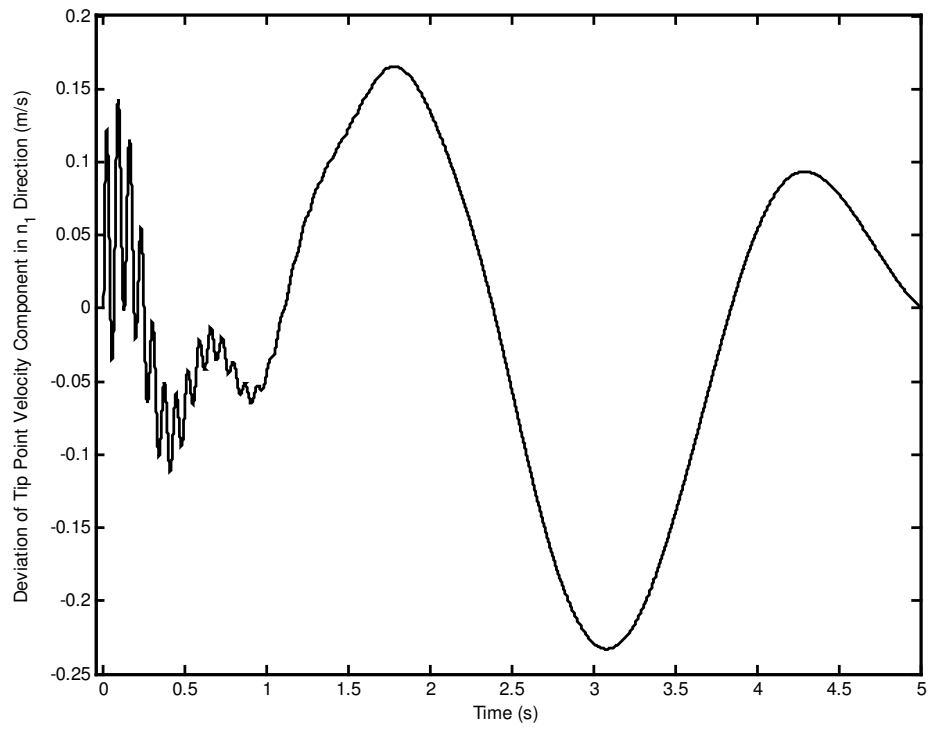


Figure 4.70 Deviation of tip point velocity component in n_1 direction.

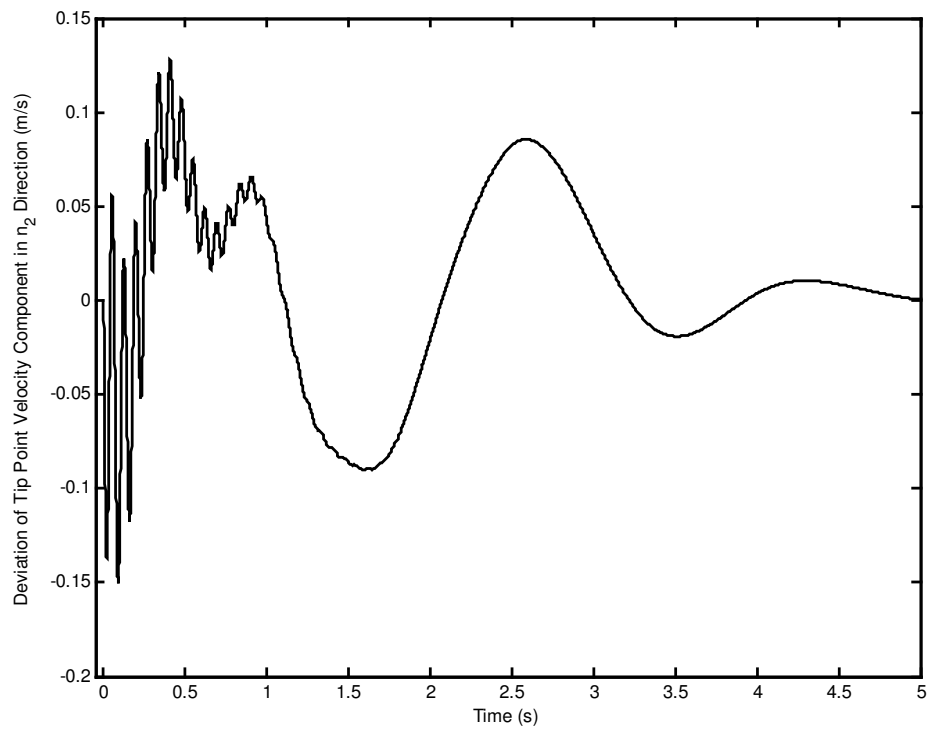


Figure 4.71 Deviation of tip point velocity component in n_2 direction.

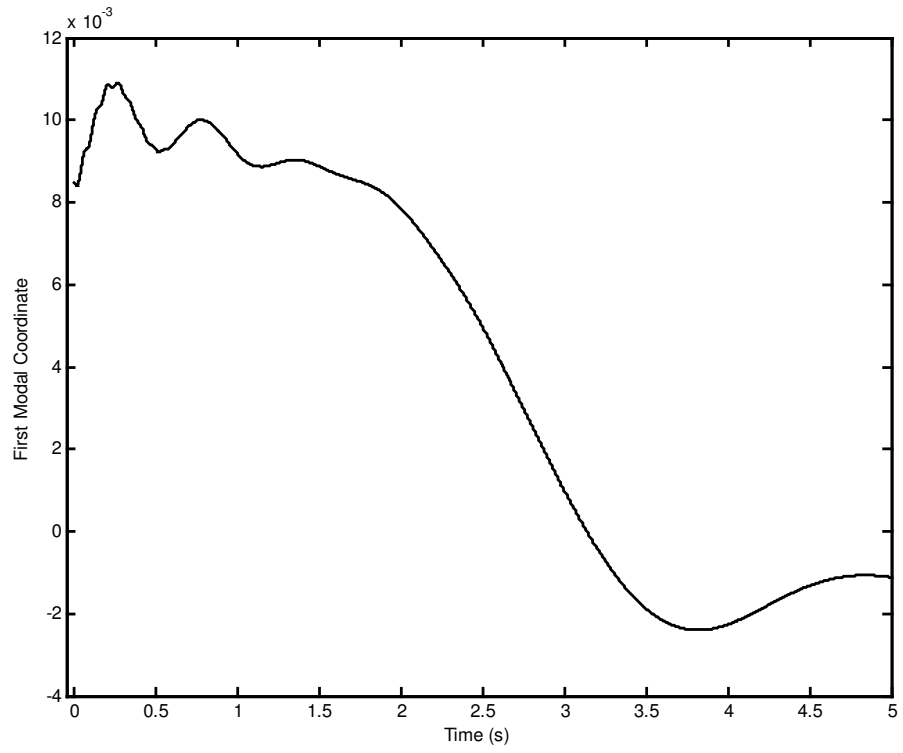


Figure 4.72 First modal coordinate.

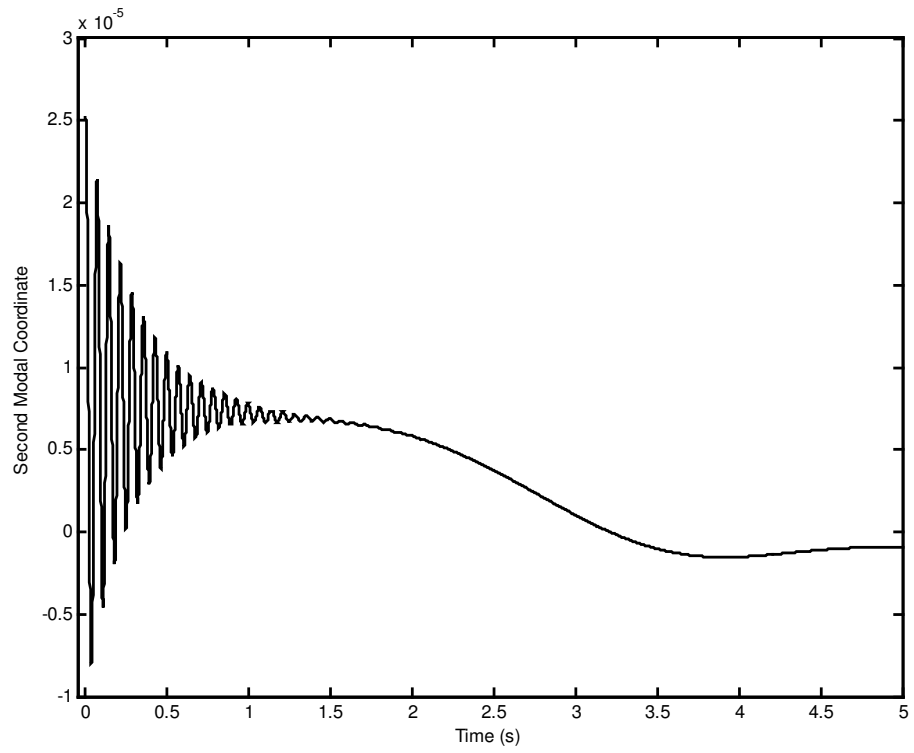


Figure 4.73 Second modal coordinate.

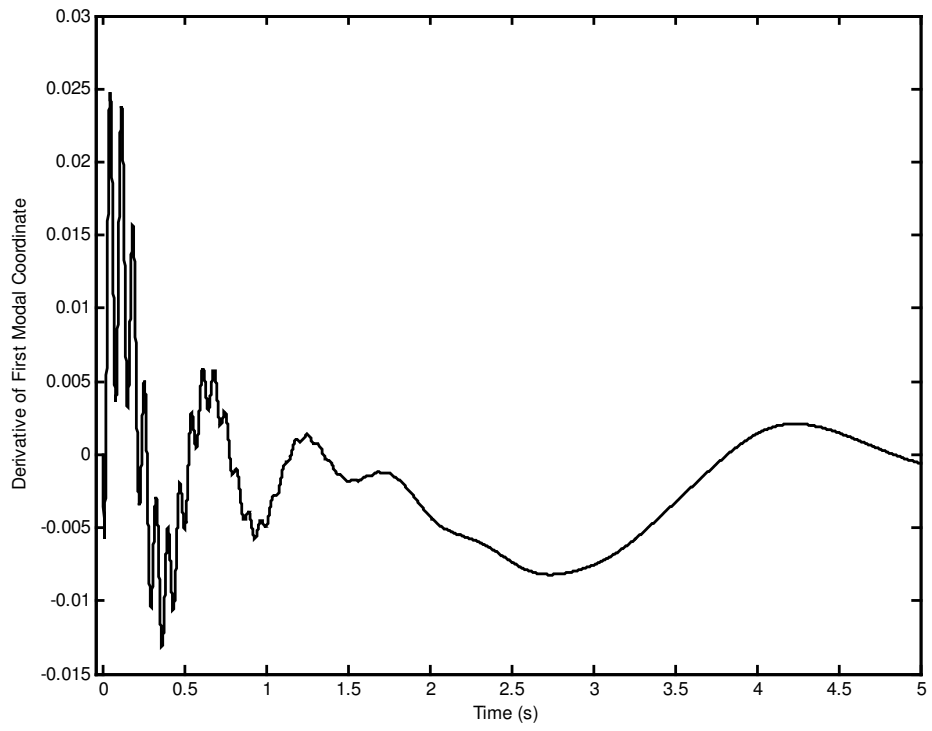


Figure 4.74 Derivative of first modal coordinate.

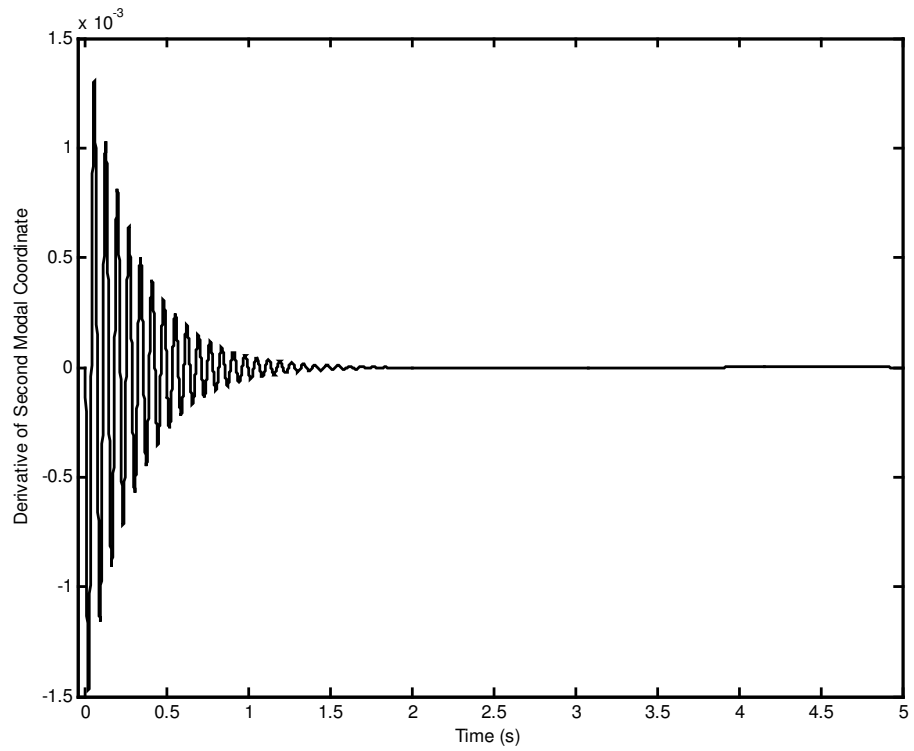


Figure 4.75 Derivative of second modal coordinate.

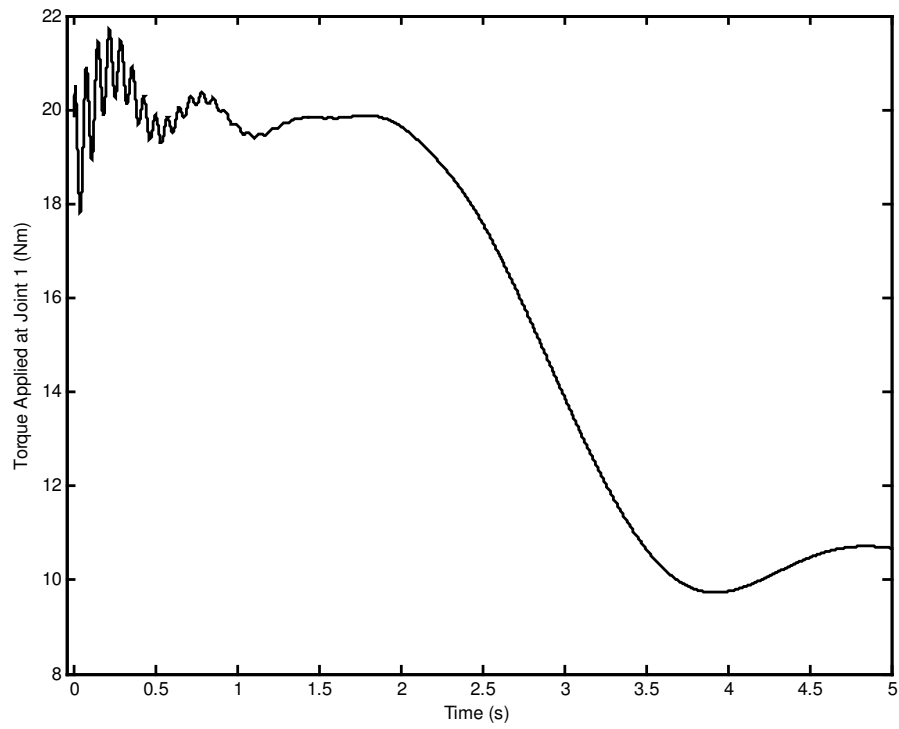


Figure 4.76 Torque applied at joint 1.

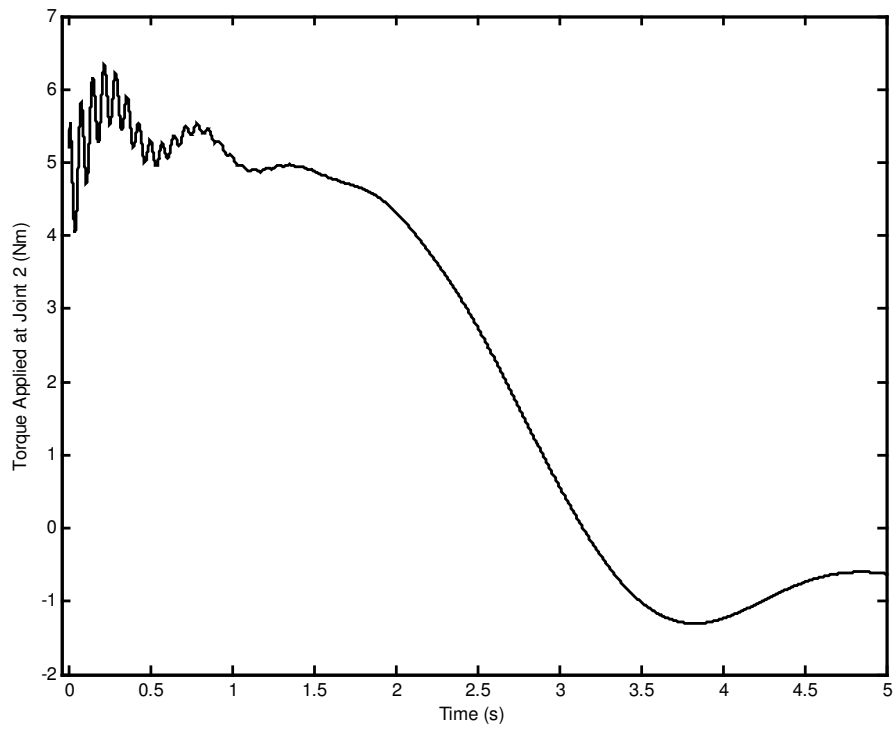


Figure 4.77 Torque applied at joint 2.

The maximum tip point position tracking error components along the trajectory are 0.1388 m and -0.0582 m in \mathbf{n}_1 and \mathbf{n}_2 directions, respectively. The tip point position error components at the end of the motion are -6.0119×10^{-3} m and -9.9180×10^{-4} m, respectively. The maximum overall torques applied to the joints are in the order of 22 Nm as seen from Figures 4.76 and 4.77.

When the Figures 4.14, 4.68 and 4.15, 4.69 are compared, it is seen that the tip point tracking performance is greatly improved when the proposed control method is used. It should be also noted that the proposed method can be simulated by taking the sampling frequency 200 Hz or above, but the computed torque method can be simulated by taking the sampling frequency 2220 Hz or above for the robot considered here.

4.5 Numerical Simulation of Force and Motion Control of Planar Robot

In this section, the numerical simulation of the force and motion control of planar robot with flexible forearm is presented by using the force and motion control method proposed at Chapter 2. The tip point is required to track a circular arc. The constraint equation can be written in terms of the tip point variables as

$$\phi(P_1, P_2) = (P_1 - P_{1c})^2 + (P_2 - P_{2c})^2 - R^2 = 0 \quad (4.18)$$

This equation represents a circular trajectory in the plane of motion. P_{1c} and P_{2c} represent the center coordinates of the circle in P_1 and P_2 directions respectively with respect to the fixed frame and R is the radius of the circle. Therefore, the tip point position components in fixed frame can be expressed in terms of a trajectory length variable (s) as follows:

$$P_1 = P_{1c} + R \cos\left(\frac{s}{R}\right) \quad (4.19)$$

$$P_2 = P_{2c} + R \sin\left(\frac{s}{R}\right) \quad (4.20)$$

Here, s is the distance covered on the trajectory. The required variation of the Lagrange multiplier (i.e. the contact force) is formed so that it is composed of a cycloidal rise, a constant level and a cycloidal return. This function also provides continuous boundary conditions and it is represented as

$$\lambda^*(t) = \begin{cases} \frac{\lambda_0^*}{t_1} \left(t - \frac{t_1}{2\pi} \sin \frac{2\pi}{t_1} t \right) & \text{for } 0 \leq t \leq t_1 \\ \lambda_0^* & \text{for } t_1 < t < t_2 \\ \lambda_0^* - \frac{\lambda_0^*}{(t_f - t_2)} \left[(t - t_2) - \frac{(t_f - t_2)}{2\pi} \sin \frac{2\pi(t - t_2)}{(t_f - t_2)} \right] & \text{for } t_2 \leq t \leq t_3 \end{cases} \quad (4.21)$$

where λ^* is the desired Lagrange multiplier, λ_0^* is its desired constant value, t_1 is the time for the end of cycloidal rise motion, t_2 is the time for the beginning of the cycloidal return motion and t_f is the time to complete the motion. The same function for the reference tip point trajectory given in Section 4.2 is used in this simulation, too.

After a few trials, proper closed loop natural frequencies and damping ratios are obtained as 15 rad/s, 20 rad/s, 30 rad/s, 85 rad/s, 0.85, 0.85, 0.85 and 1. The corresponding closed loop poles are given in Table 4.5.

Table 4.5 Closed loop poles used in force and motion control of planar robot.

Closed Loop Poles
$p_1 = -12.7500 + 7.9017j$
$p_2 = -12.7500 - 7.9017j$
$p_3 = -17.0000 + 10.5357j$
$p_4 = -17.0000 - 10.5357j$
$p_5 = -30.0000$
$p_6 = -72.2500 + 44.7765j$
$p_7 = -72.2500 - 44.7765j$

For the desired Lagrange multiplier profile, cycloidal rise and cycloidal return periods are taken as 1.5 s constant level period is taken as 7 s and the desired constant value of the Lagrange multiplier is taken as 50 N. The sampling frequency is taken as 500 Hz. The simulation results are given in Figures 4.78 - 4.104.

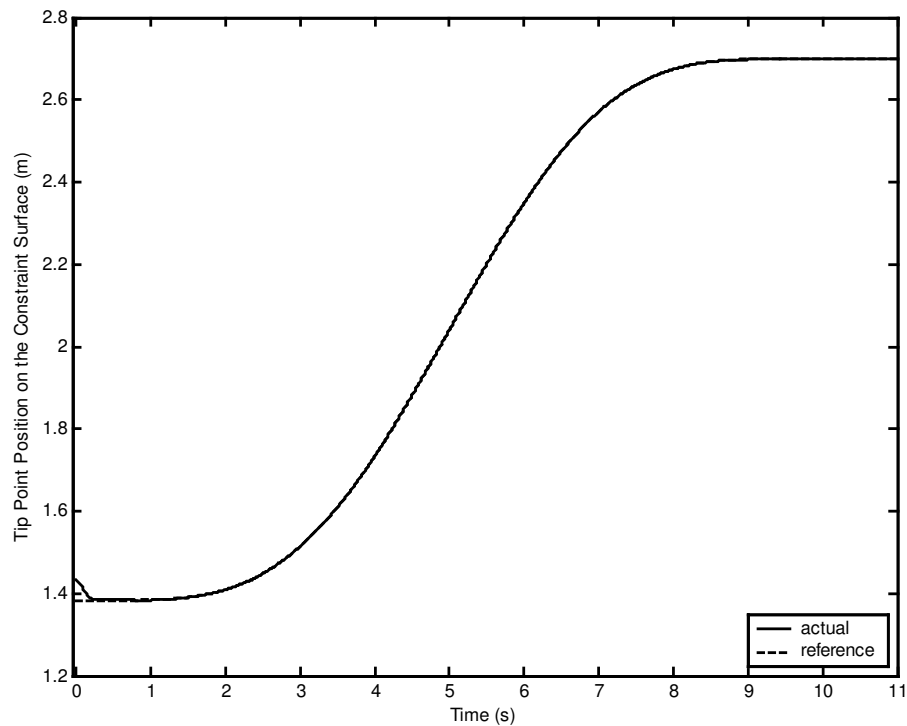


Figure 4.78 Tip point position on the constraint surface.

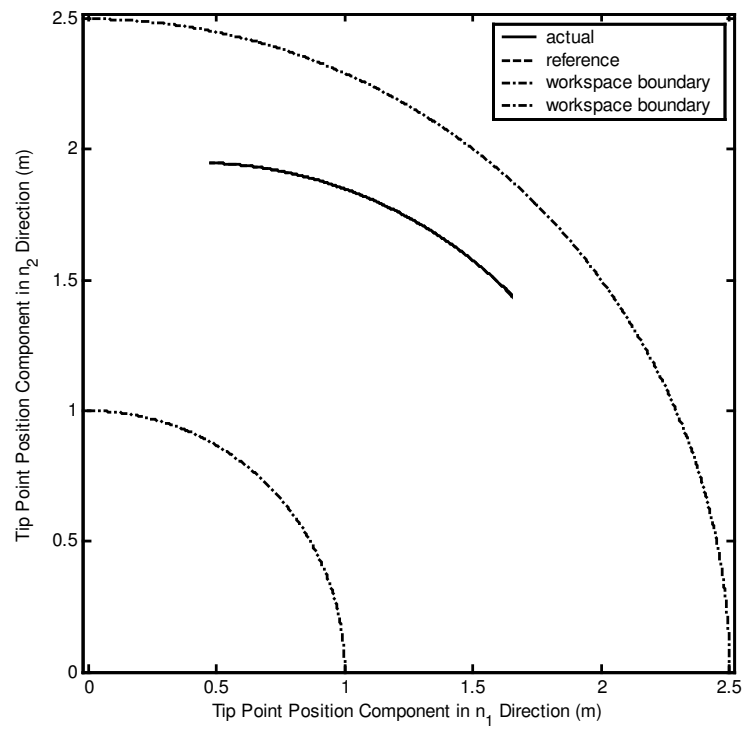


Figure 4.79 Workspace and tip point position.

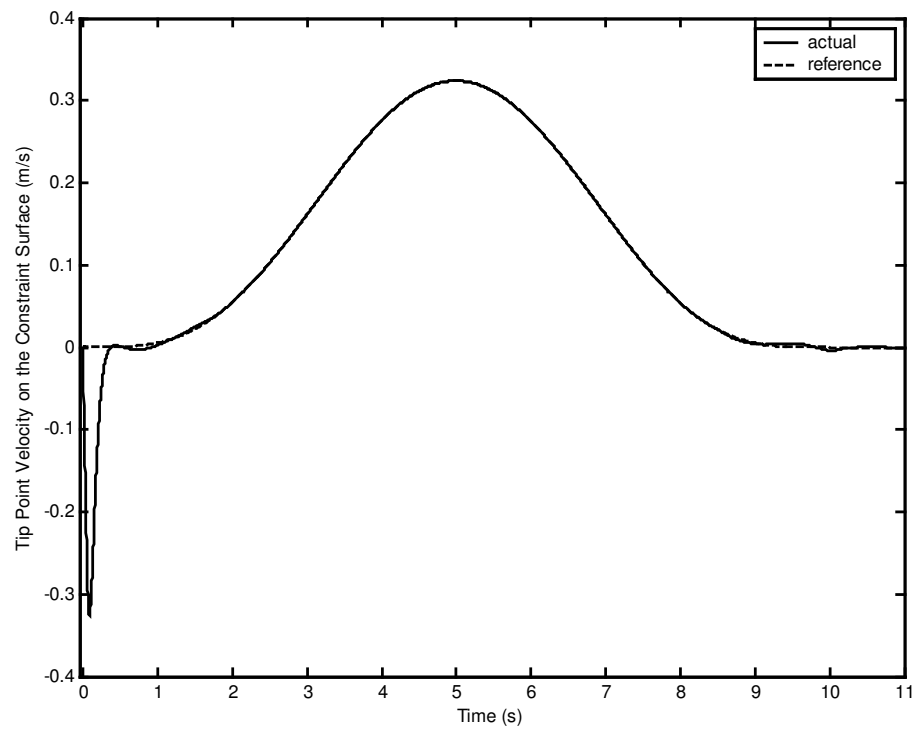


Figure 4.80 Tip point velocity on the constraint surface.

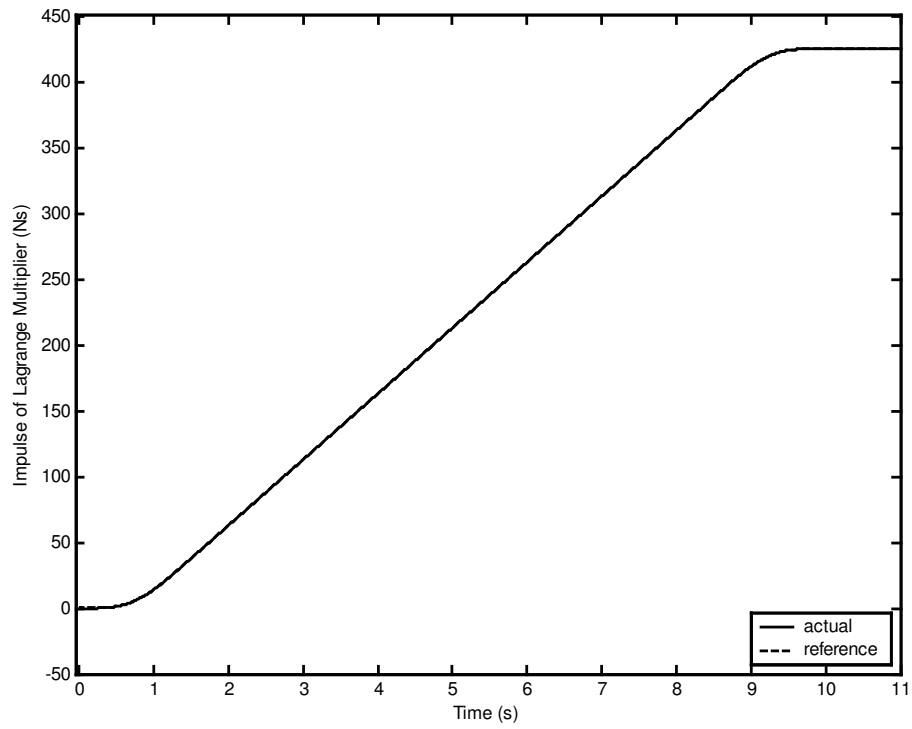


Figure 4.81 Impulse of Lagrange multiplier.

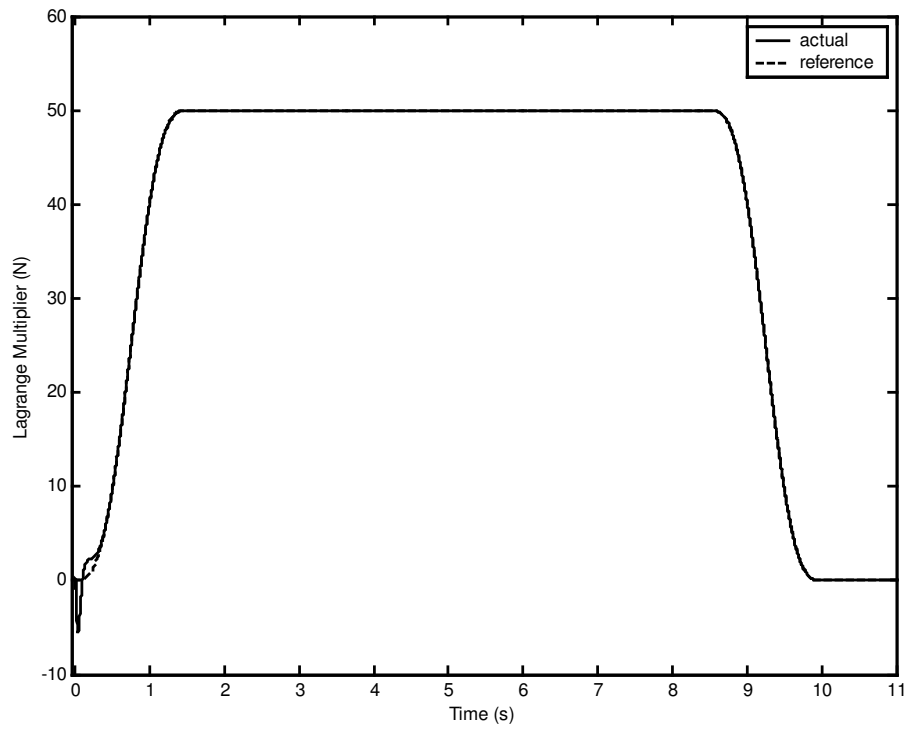


Figure 4.82 Lagrange multiplier.

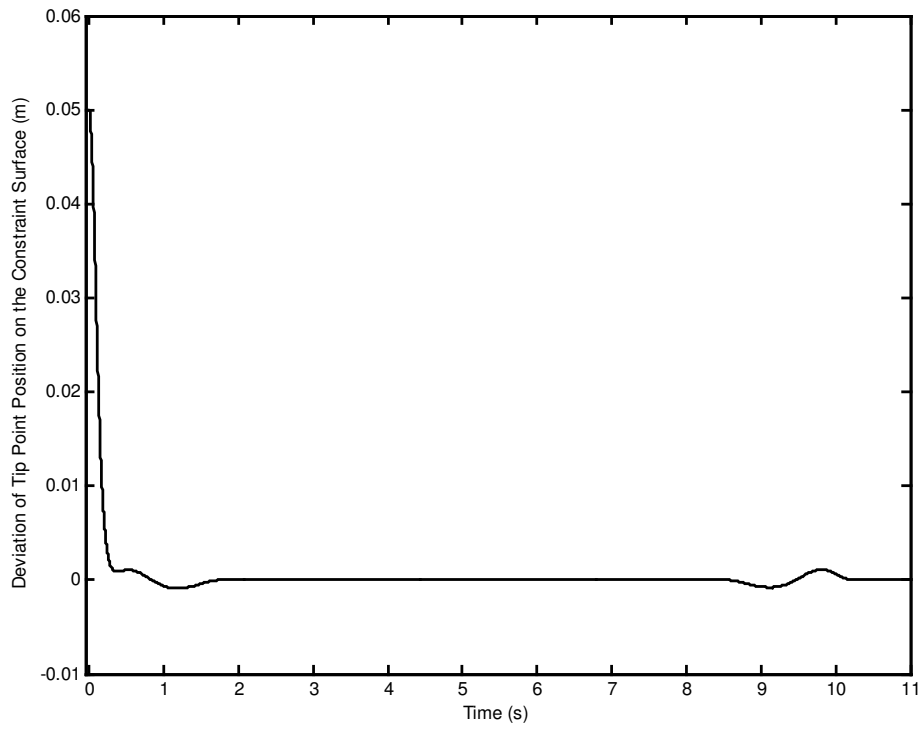


Figure 4.83 Deviation of tip point position on the constraint surface.

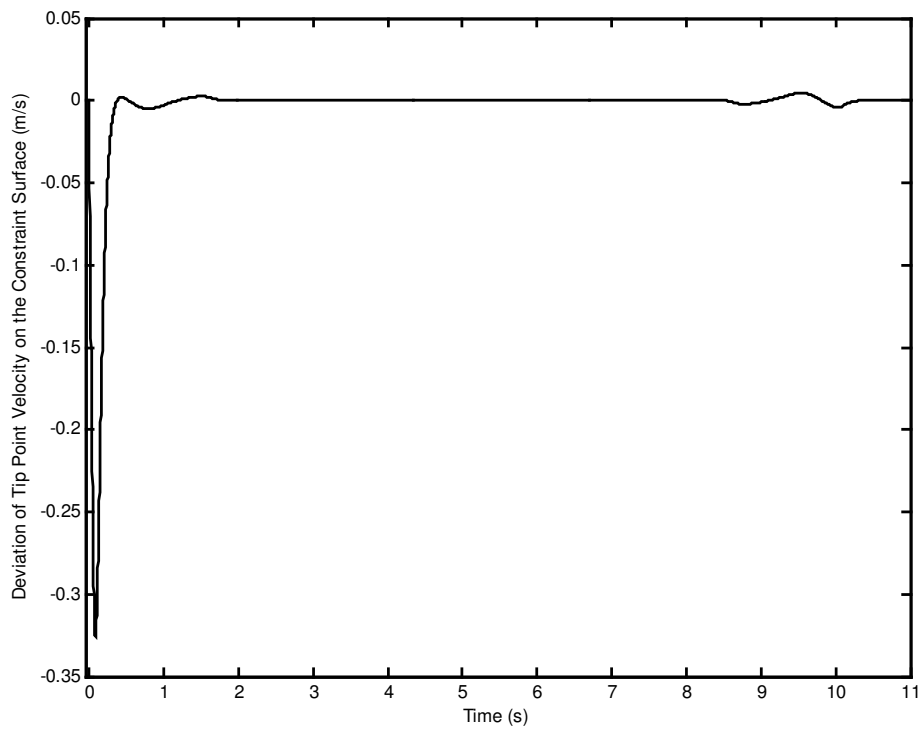


Figure 4.84 Deviation of tip point velocity on the constraint surface.

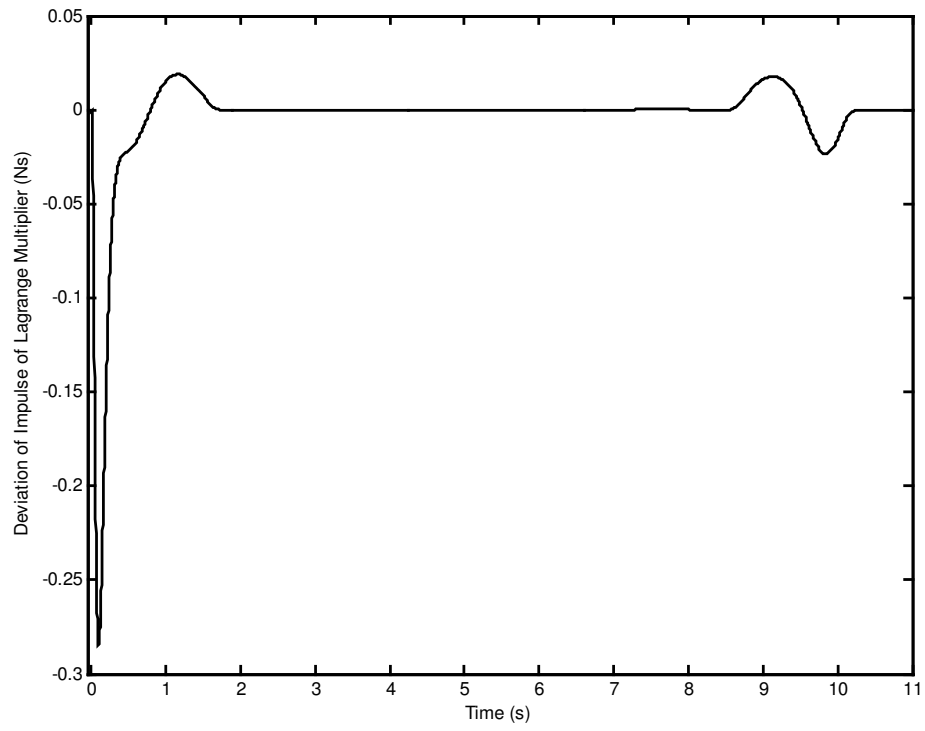


Figure 4.85 Deviation of impulse of Lagrange multiplier.

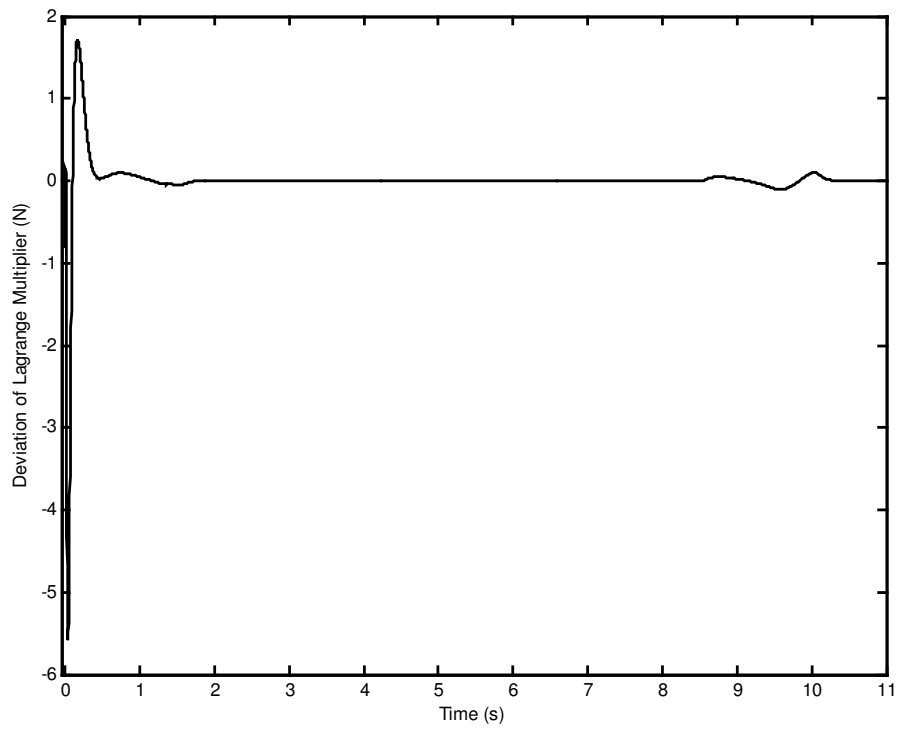


Figure 4.86 Deviation of Lagrange multiplier.

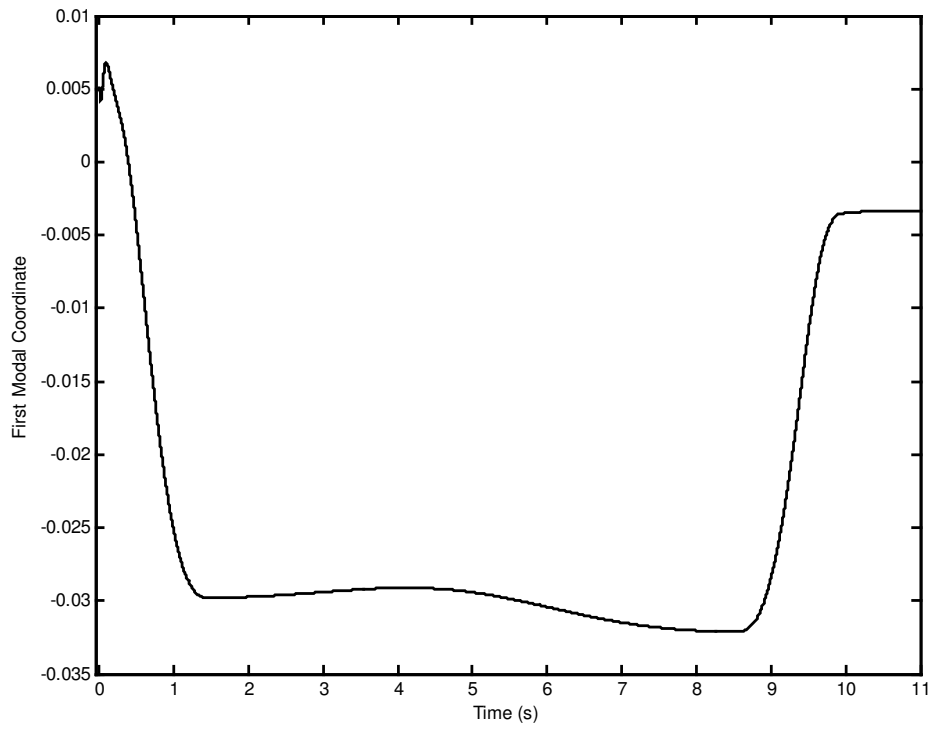


Figure 4.87 First modal coordinate.

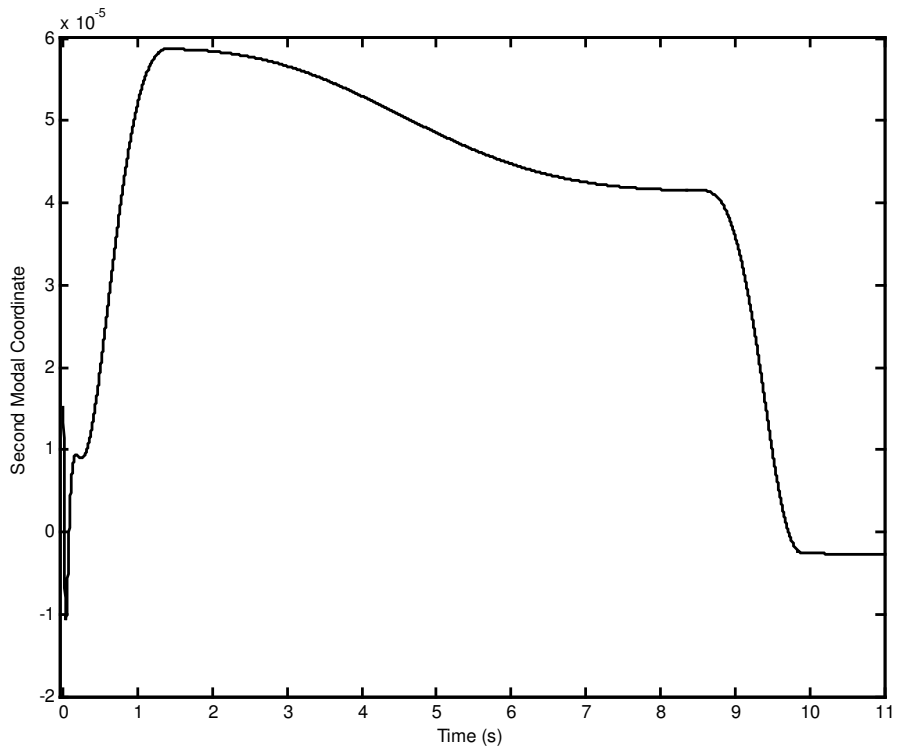


Figure 4.88 Second modal coordinate.

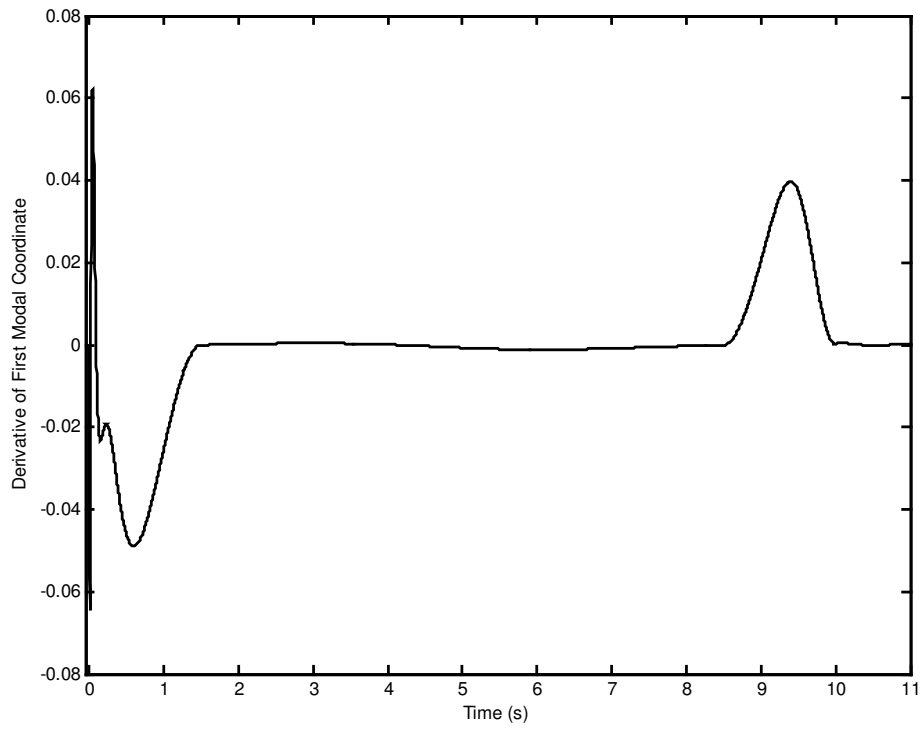


Figure 4.89 Derivative of first modal coordinate.

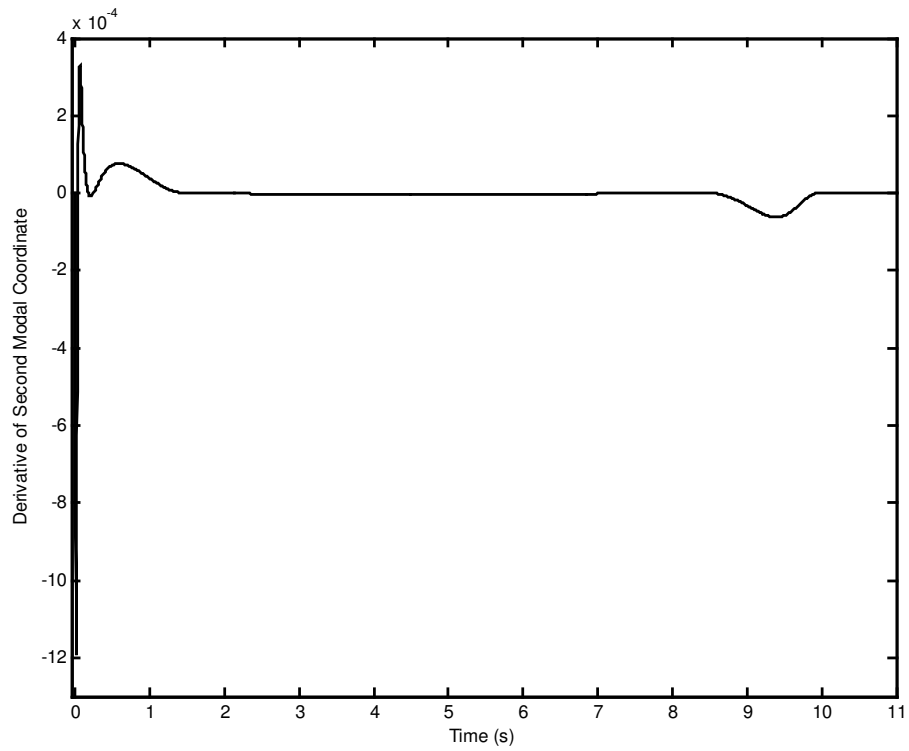


Figure 4.90 Derivative of second modal coordinate.

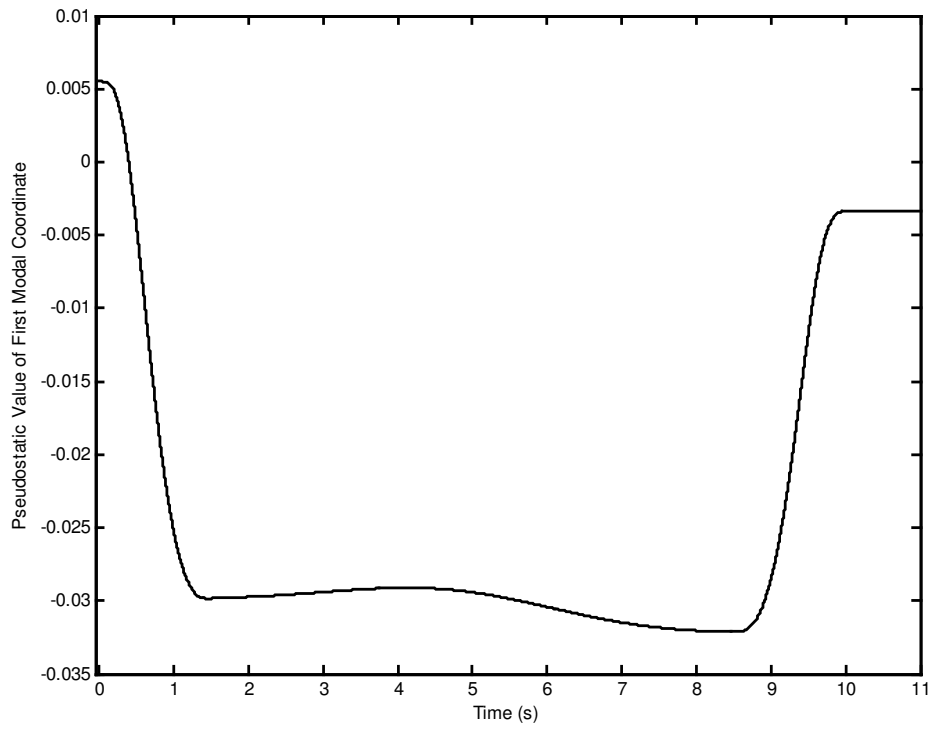


Figure 4.91 Pseudostatic value of first modal coordinate.

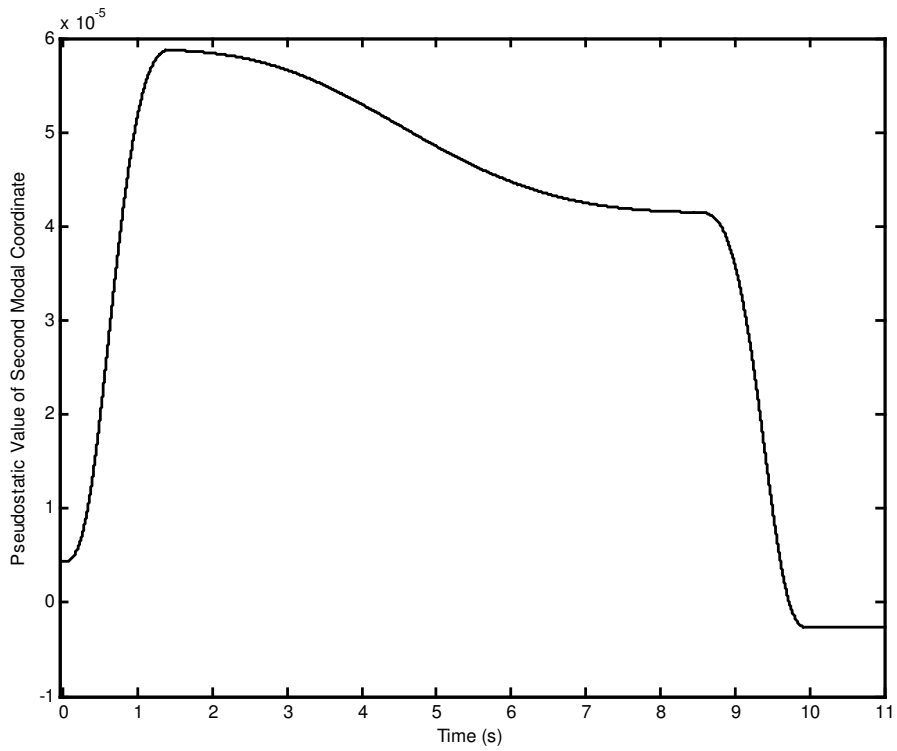


Figure 4.92 Pseudostatic value of second modal coordinate.

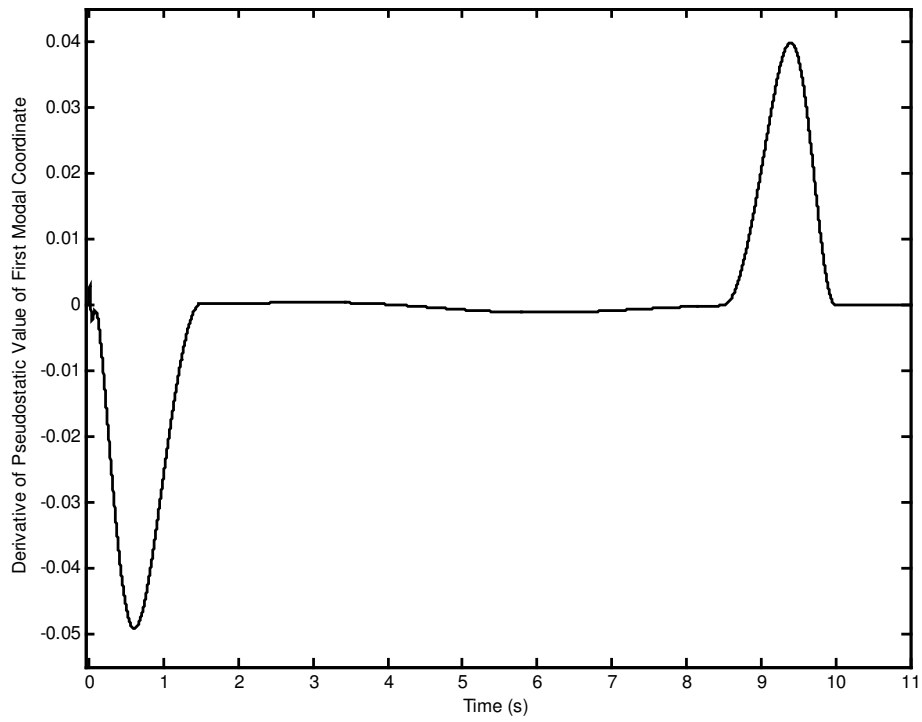


Figure 4.93 Derivative of pseudostatic value of first modal coordinate.

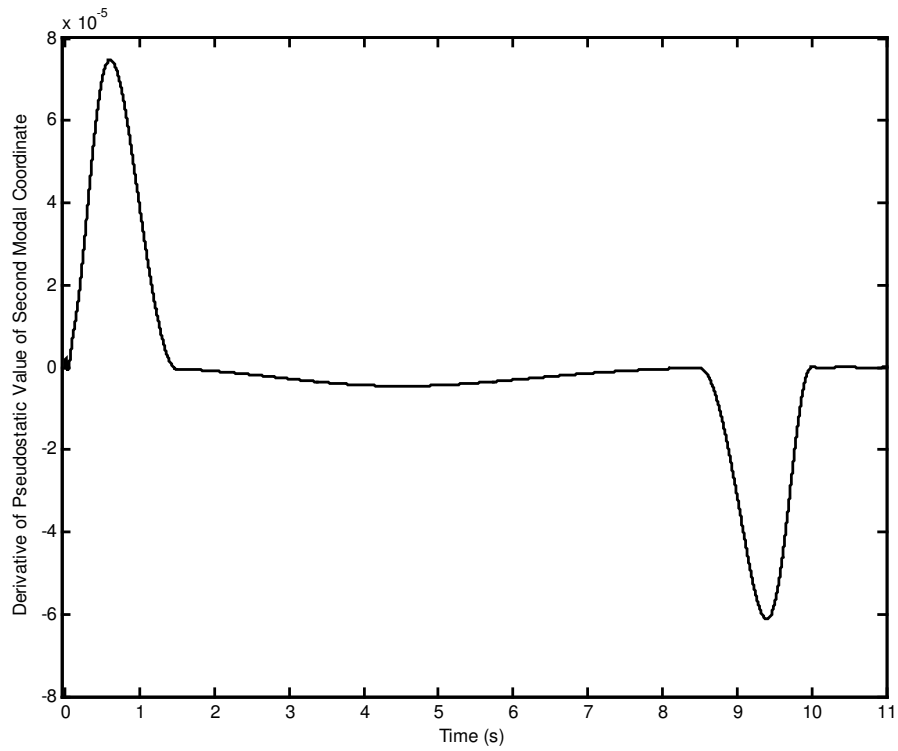


Figure 4.94 Derivative of pseudostatic value of second modal coordinate.

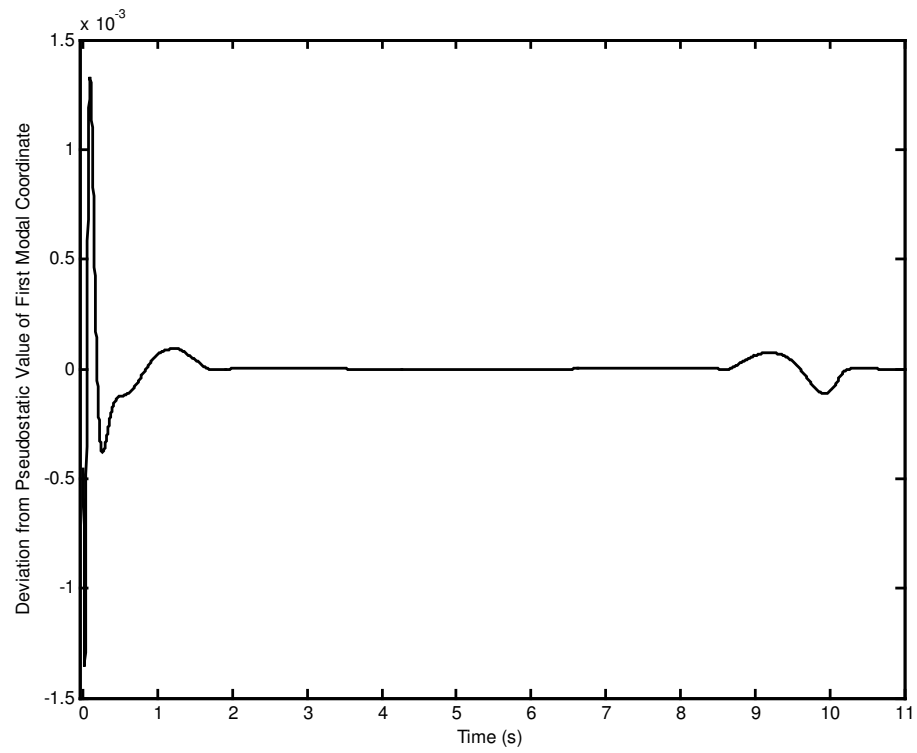


Figure 4.95 Deviation from pseudostatic value of first modal coordinate.

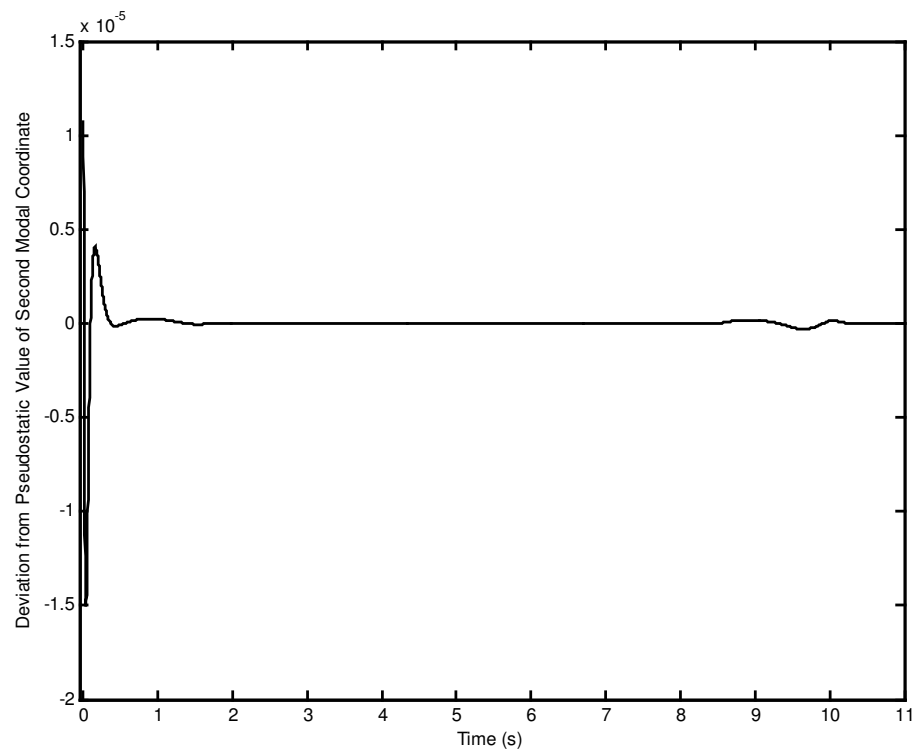


Figure 4.96 Deviation from pseudostatic value of second modal coordinate.

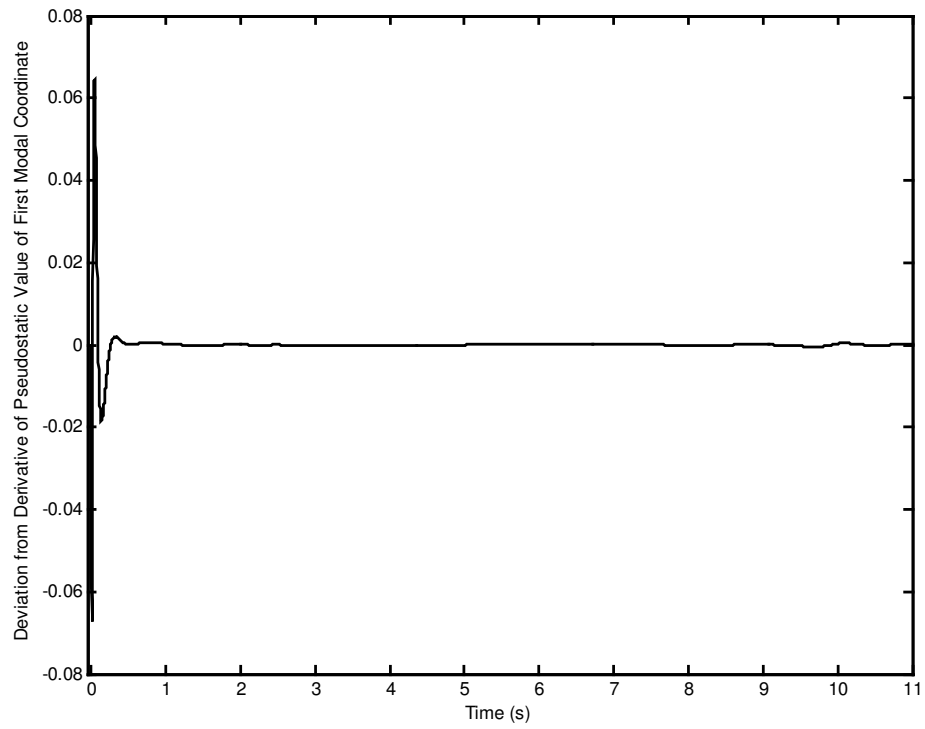


Figure 4.97 Deviation from derivative of pseudostatic value of first modal coordinate.

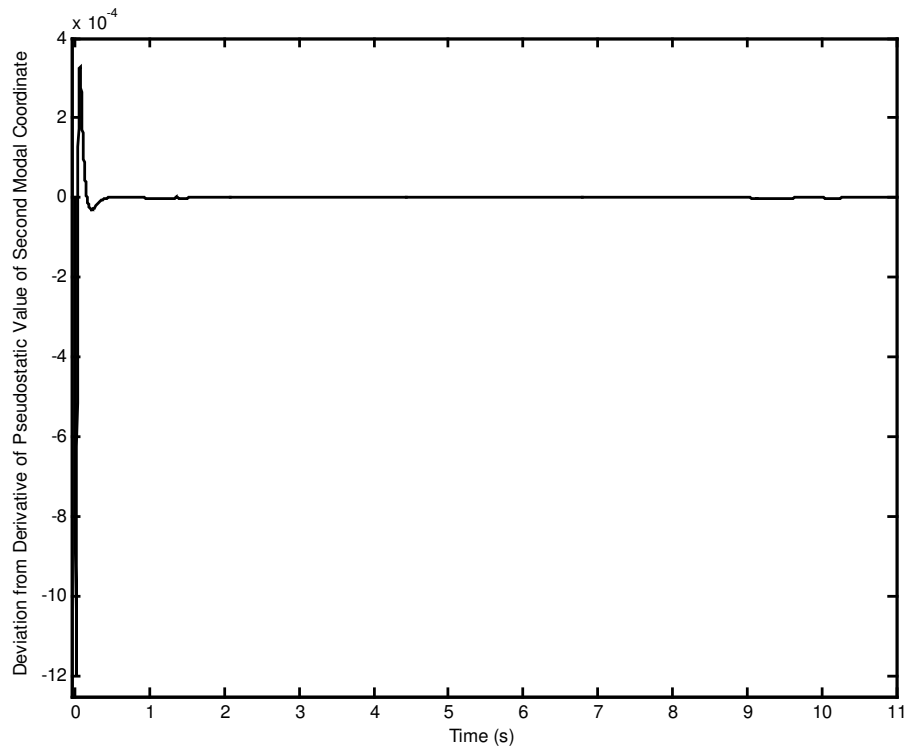


Figure 4.98 Deviation from derivative of pseudostatic value of second modal coordinate.

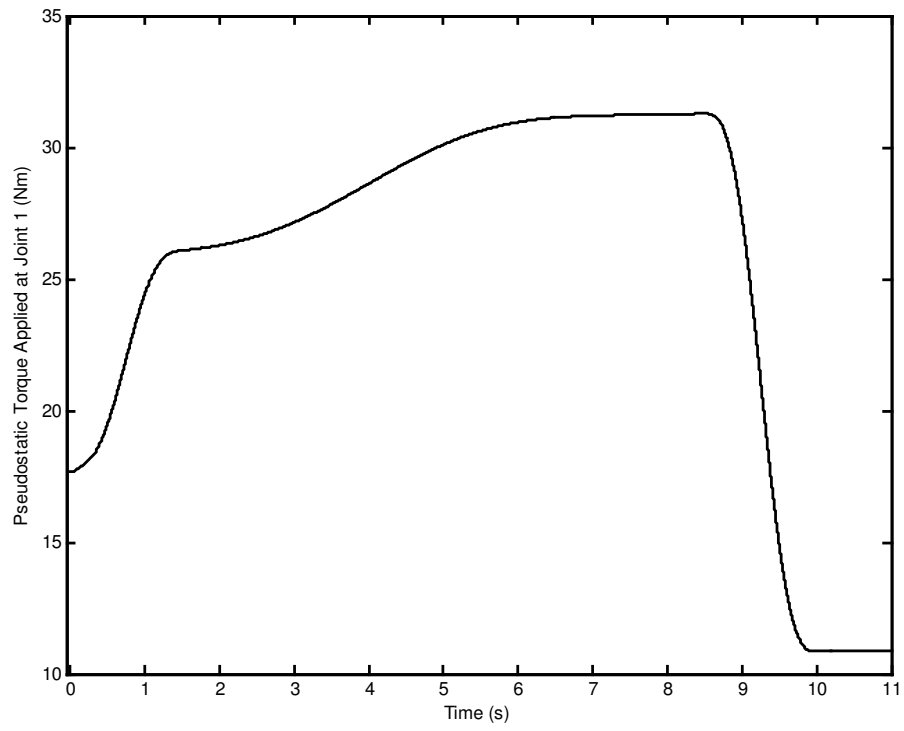


Figure 4.99 Pseudostatic torque applied at joint 1.

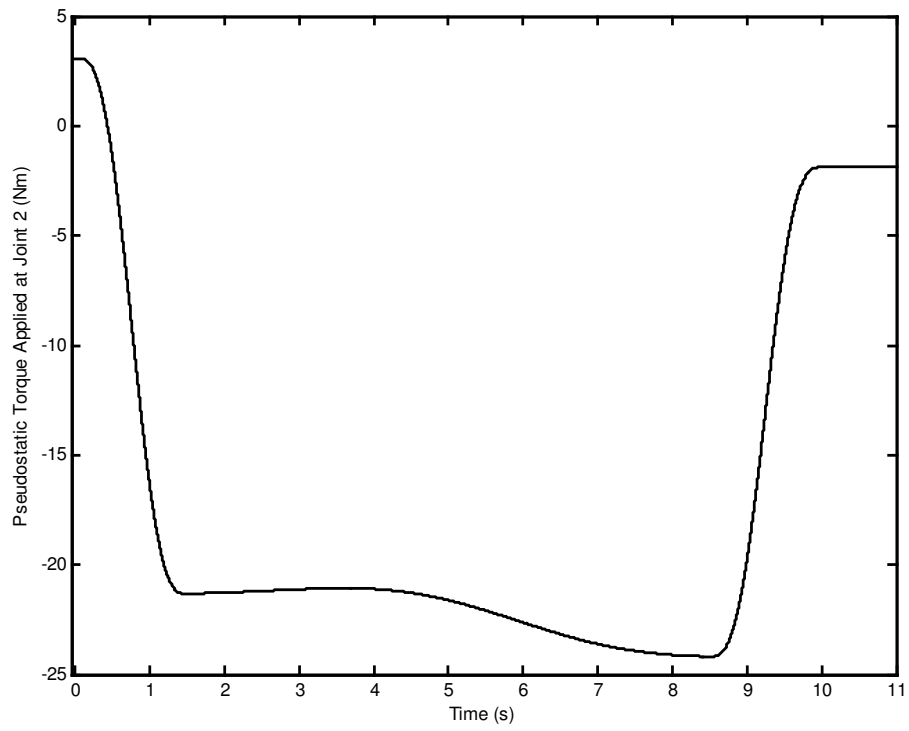


Figure 4.100 Pseudostatic torque applied at joint 2.

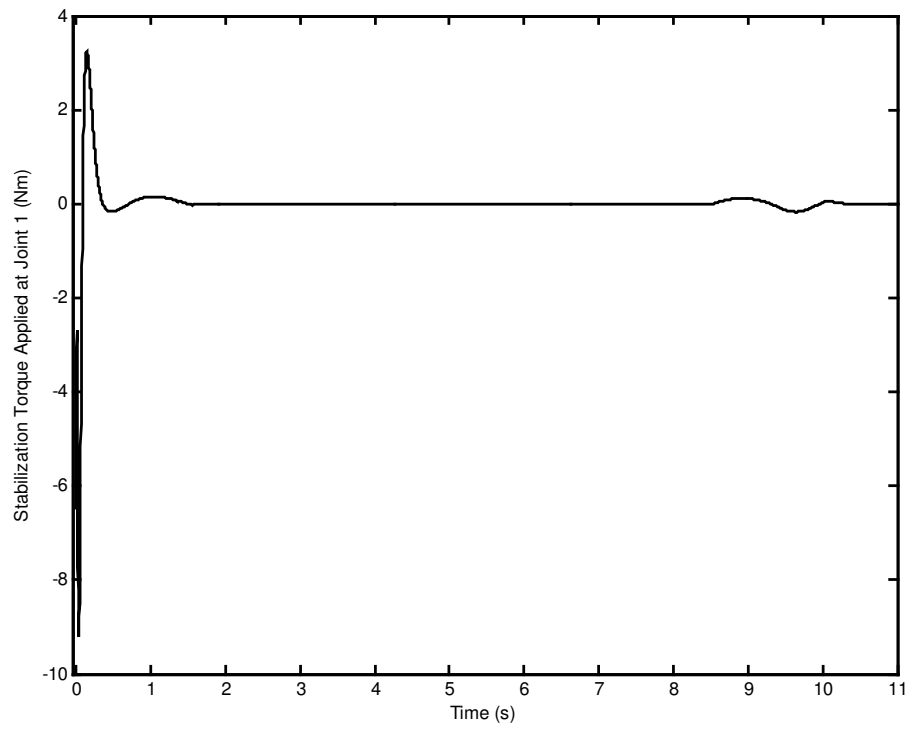


Figure 4.101 Stabilization torque applied at joint 1.

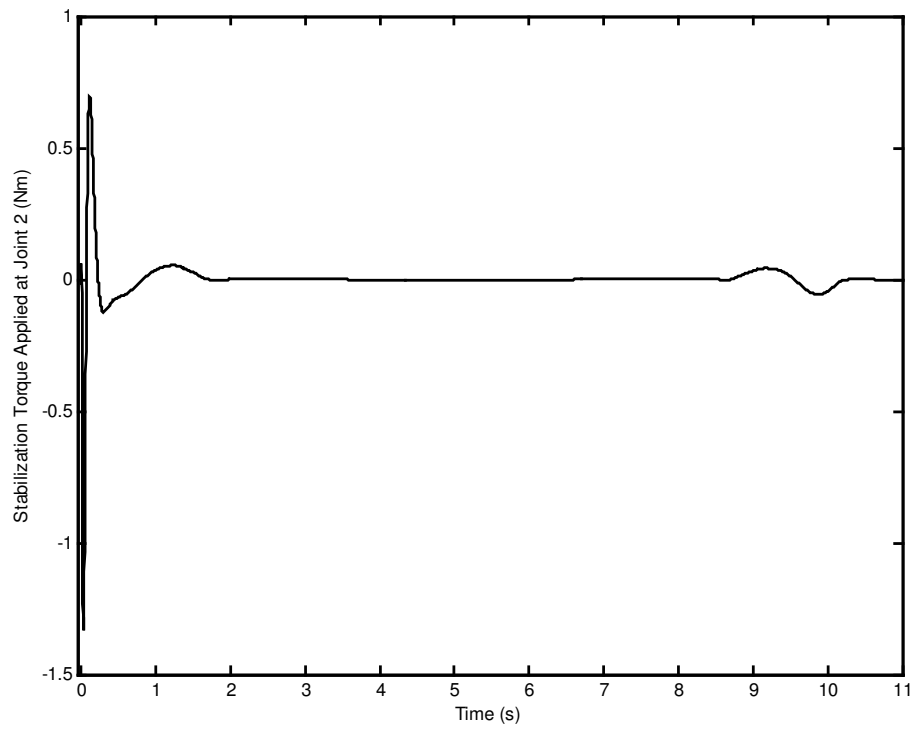


Figure 4.102 Stabilization torque applied at joint 2.

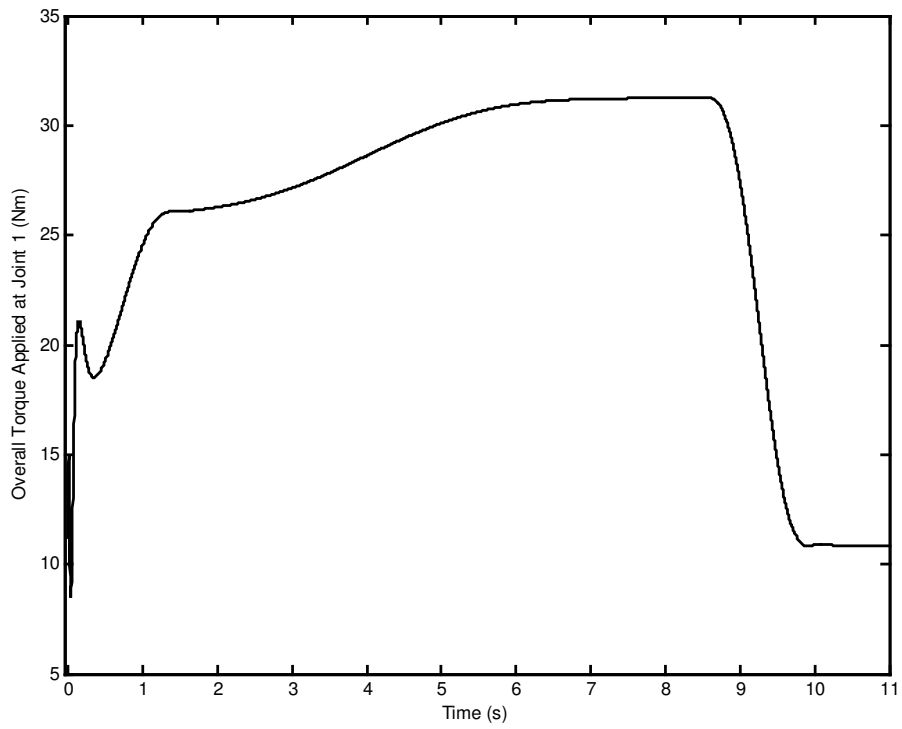


Figure 4.103 Overall torque applied at joint 1.

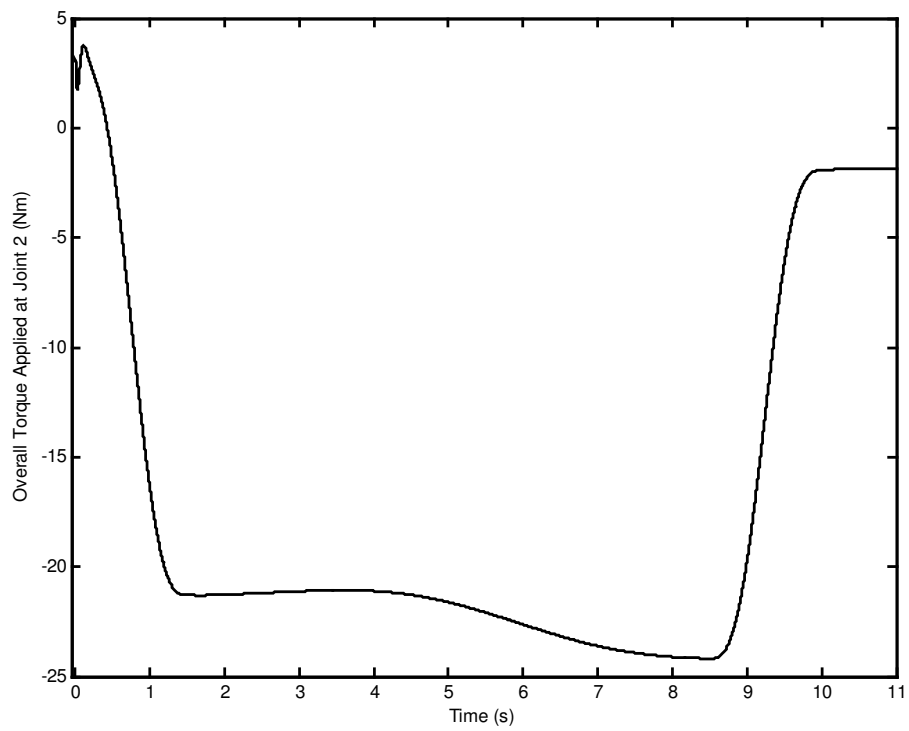


Figure 4.104 Overall torque applied at joint 2.

It is seen from Figure 4.83 that there is tip point position error on the constraint surface due to the mispositioning, but is compensated in about 2 s for the initial deviations of about 50 mm during the motion. There is a reverse action at the beginning of the motion in the tip point position and velocity on the constraint surface as well as the Lagrange multiplier and its impulse which are given in Figures 4.83 - 4.86. The maximum tip point position tracking error on the constraint surface along the trajectory after the settling time is 1.0952×10^{-3} m. The corresponding maximum tip point position tracking error components are -1.0944×10^{-3} m and 4.1090×10^{-5} m in \mathbf{n}_1 and \mathbf{n}_2 directions, respectively. The maximum Lagrange multiplier error after the settling time is 0.1046 N. The maximum overall torques applied to the joints are in small magnitudes in the order of 32 Nm as seen in Figures 4.103 and 4.104.

4.6 Numerical Simulation of Force and Motion Control of Planar Robot with Unmodeled Dynamics

The plant dynamics are modeled by representing the link flexibility with the first two modes, while the controller is designed by representing the link flexibility with the first mode. The numerical simulation of force and motion control of planar robot with unmodeled dynamics is obtained by using the force and motion control method proposed at Chapter 2. For the tip point, the same reference trajectory and reference Lagrange multiplier considered in the previous section are used.

After a few trials, closed loop natural frequencies and damping ratios that give acceptable response are obtained as 13.5 rad/s, 27 rad/s, 40 rad/s, 0.85, 0.85 and 1. However, the simulation results indicate that, although the steady state errors are reasonably small, the maximum Lagrange multiplier error and the maximum start up torque happen to be quite large in the order of 787 N and 5644 Nm, respectively.

In order to obtain smaller start up torques and smaller Lagrange multiplier error, gain scheduling is made for the closed loop natural frequencies by increasing them from small values to their final values as a function of tip point position tracking error according to the following exponential expression:

$$\omega_{ni}(\varepsilon) = \frac{\omega_{ni}^s - \omega_{ni}^f e^{-k}}{1 - e^{-k}} + \left(\frac{\omega_{ni}^f - \omega_{ni}^s}{1 - e^{-k}} \right) e^{-k\varepsilon/\varepsilon_m} \quad (4.22)$$

where $\omega_{ni}(\varepsilon)$ represents the closed loop natural frequency that is scheduled at an instant where error is ε , ω_{ni}^s and ω_{ni}^f represent the smallest and largest values of ω_{ni} , ε_m stands for the initial error in absolute value, k is the constant coefficient of the exponential expression. In the simulations, it is taken as 2.

Besides obtaining smaller start up torques and smaller initial Lagrange multiplier, smaller settling time and smaller maximum overshoot are also obtained as a result of the gain scheduling.

After a few trials, it has been found that reasonable Lagrange multiplier error and start up torques are obtained by the application of the gain scheduling even to only one of the dominant closed loop natural frequencies. Proper initial and final closed loop natural frequencies and damping ratios are obtained as $\omega_{n1} = 13.5$ rad/s, $\omega_{n2}^s = 5$ rad/s, $\omega_{n2}^f = 27$ rad/s, $\omega_{n3} = 40$ rad/s, $\zeta_{d1} = 0.85$, $\zeta_{d2} = 0.85$, $\zeta_{d3} = 1$. The corresponding closed loop poles are given in Table 4.6.

Table 4.6 Closed loop poles used in force and motion control of planar robot with unmodeled dynamics.

Closed Loop Poles
$p_1 = -11.4750 + 7.1116j$
$p_2 = -11.4750 - 7.1116j$
$p_3^s = -4.2500 + 2.6339j$
$p_3^f = -22.9500 + 14.2231j$
$p_4^s = -4.2500 - 2.6339j$
$p_4^f = -22.9500 - 14.2231j$
$p_5 = -40.0000$

The sampling frequency is taken as 500 Hz. The simulation results are given in Figures 4.105 - 4.131.

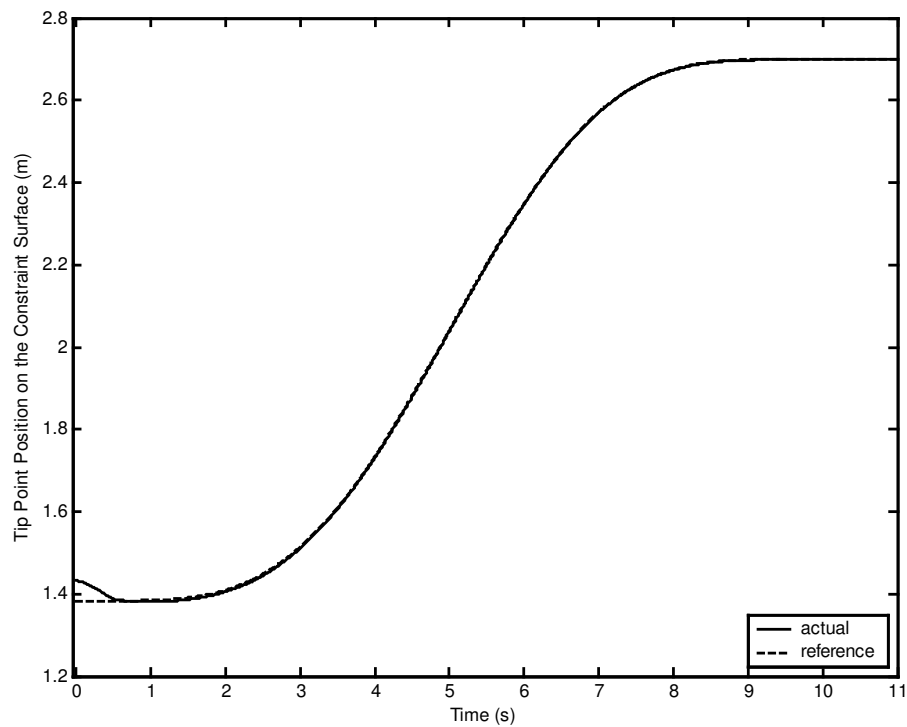


Figure 4.105 Tip point position on the constraint surface.

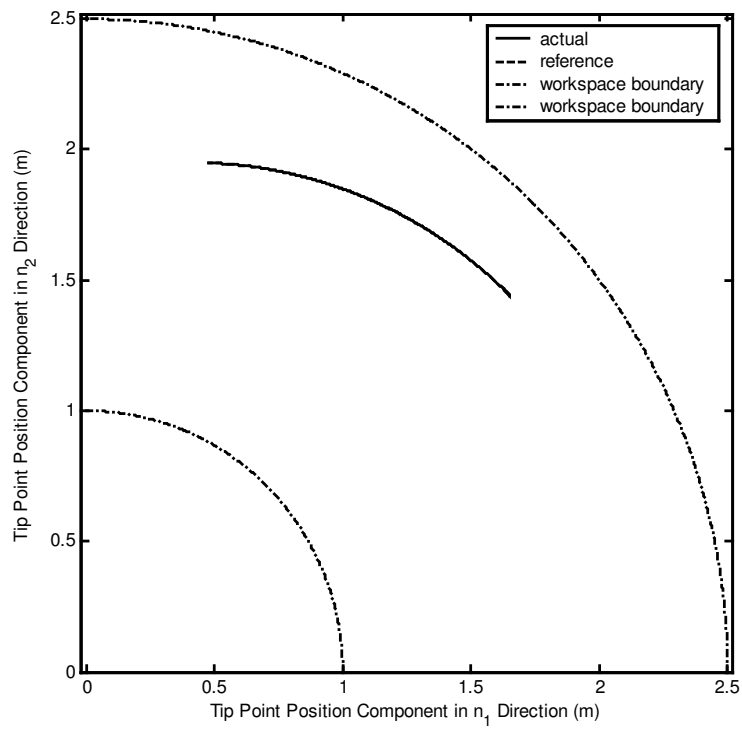


Figure 4.106 Workspace and tip point position.

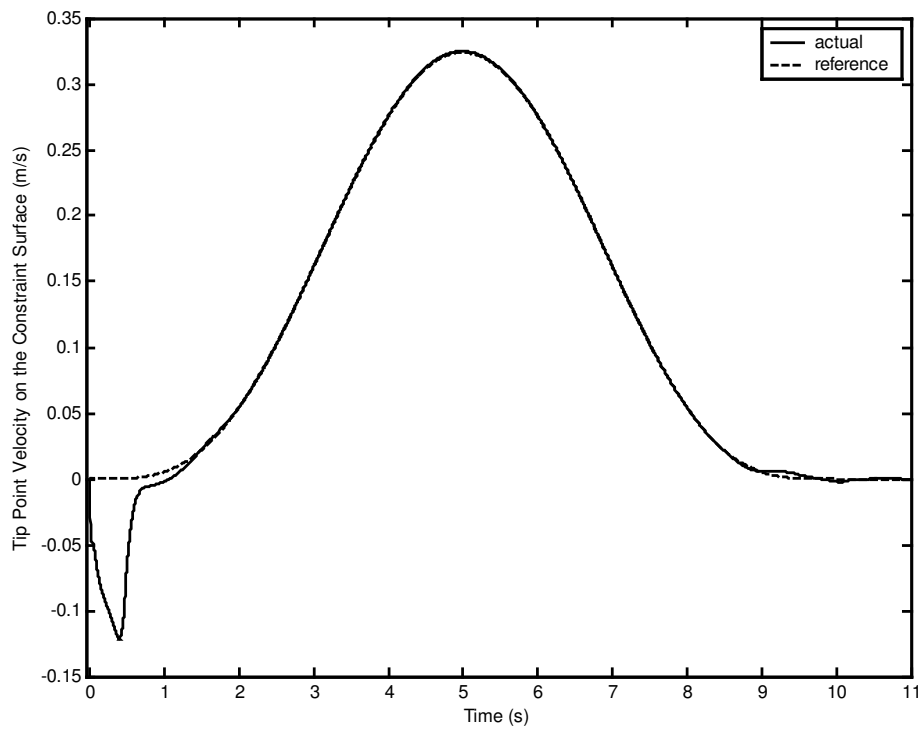


Figure 4.107 Tip velocity on the constraint surface.

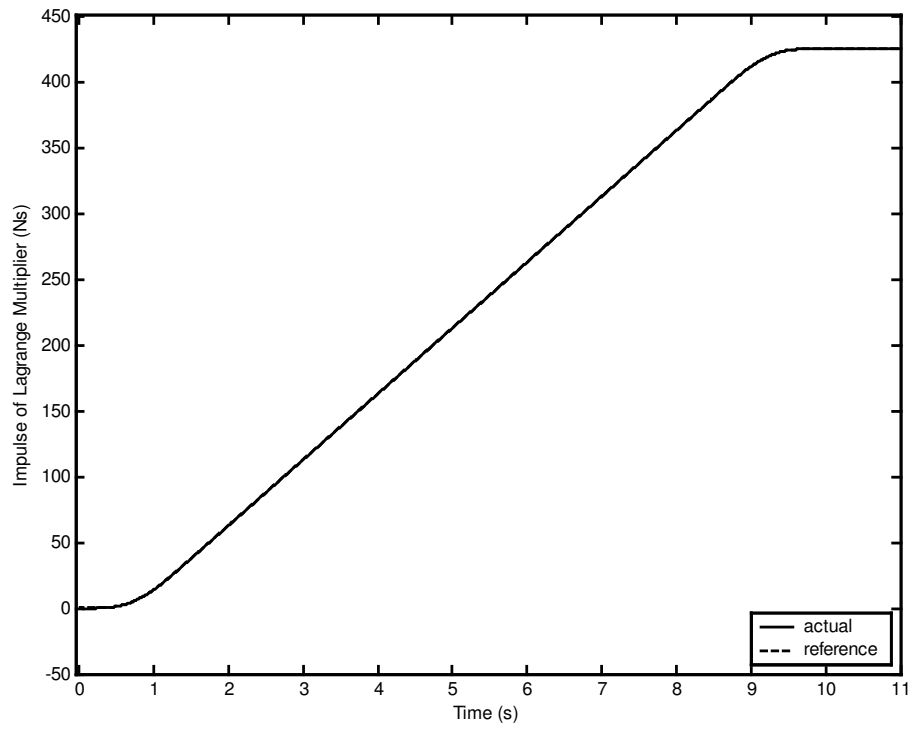


Figure 4.108 Impulse of Lagrange multiplier.

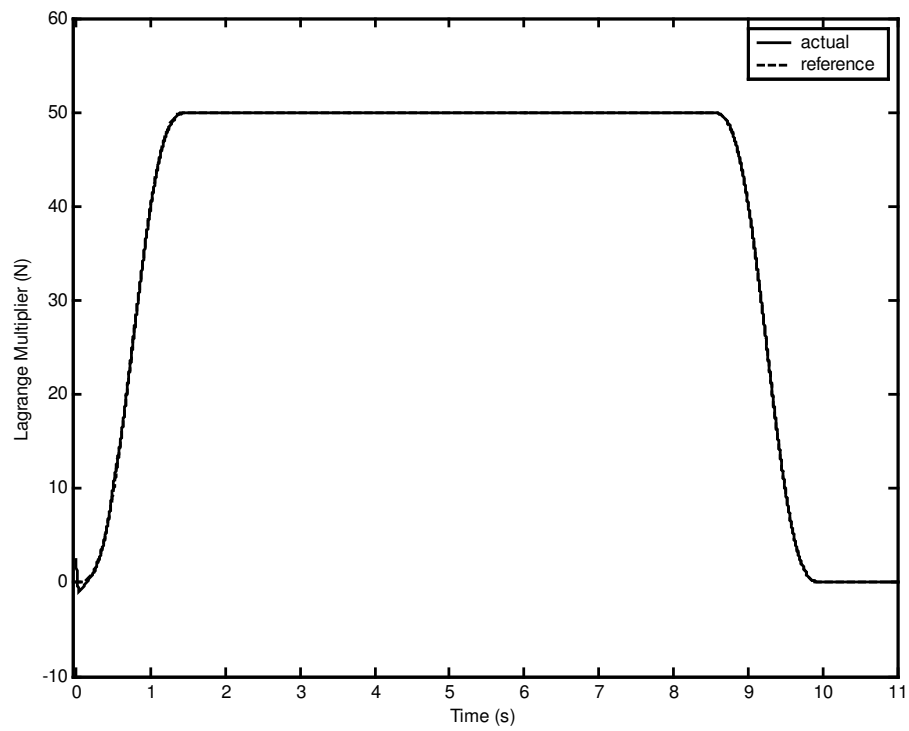


Figure 4.109 Lagrange multiplier.

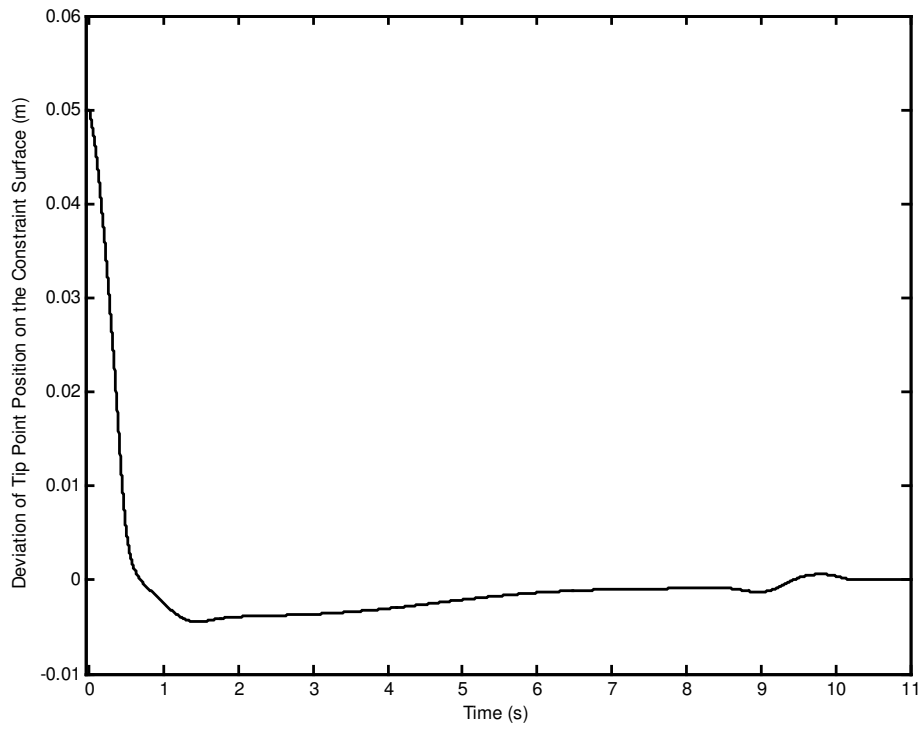


Figure 4.110 Deviation of tip point position on the constraint surface.

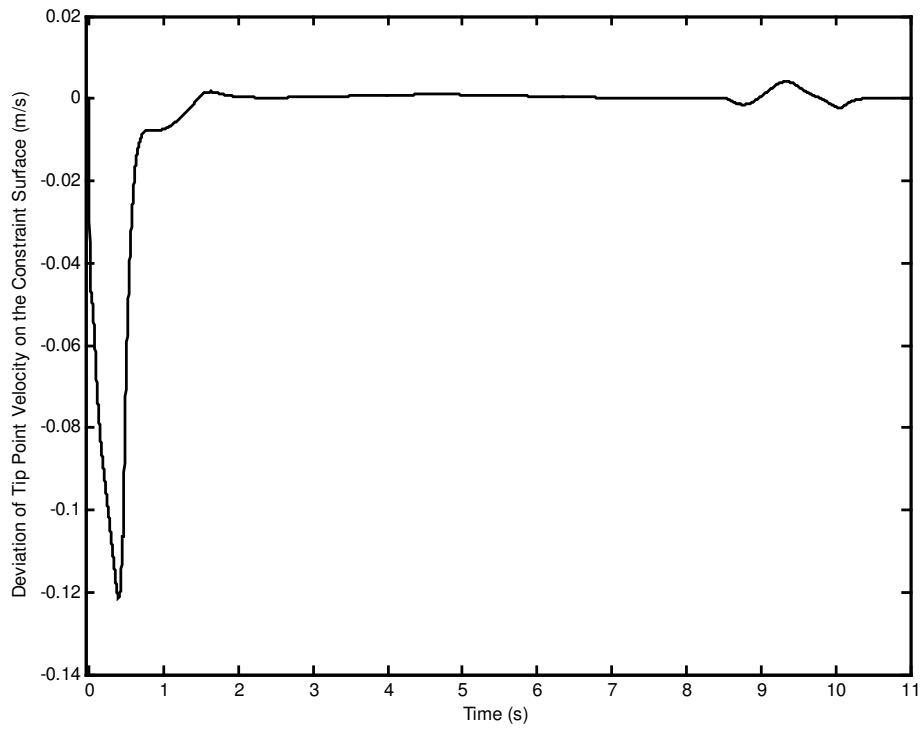


Figure 4.111 Deviation of tip point velocity on the constraint surface.

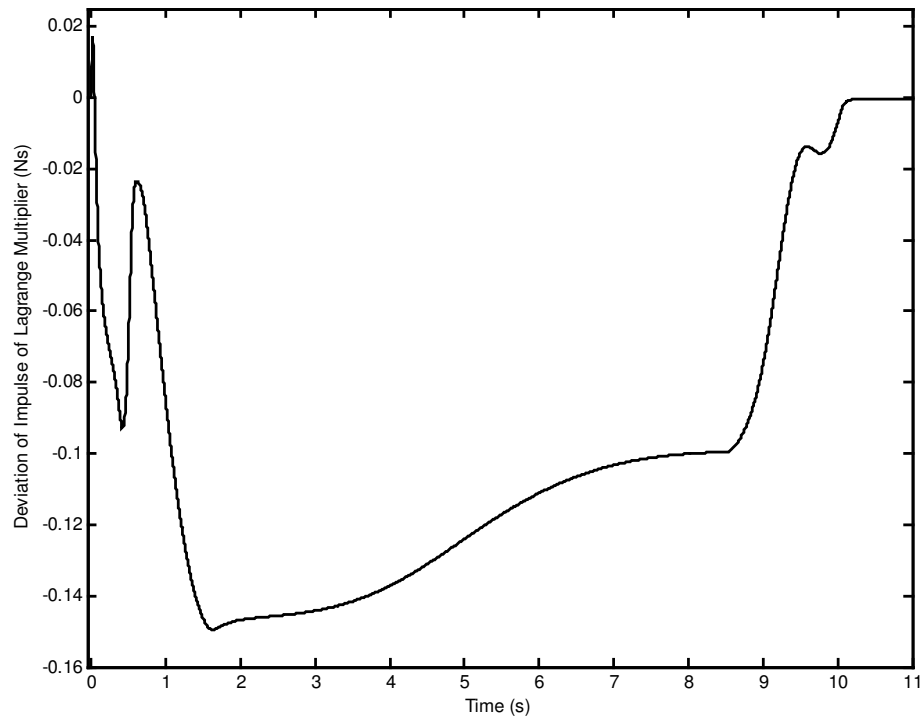


Figure 4.112 Deviation of impulse of Lagrange multiplier.

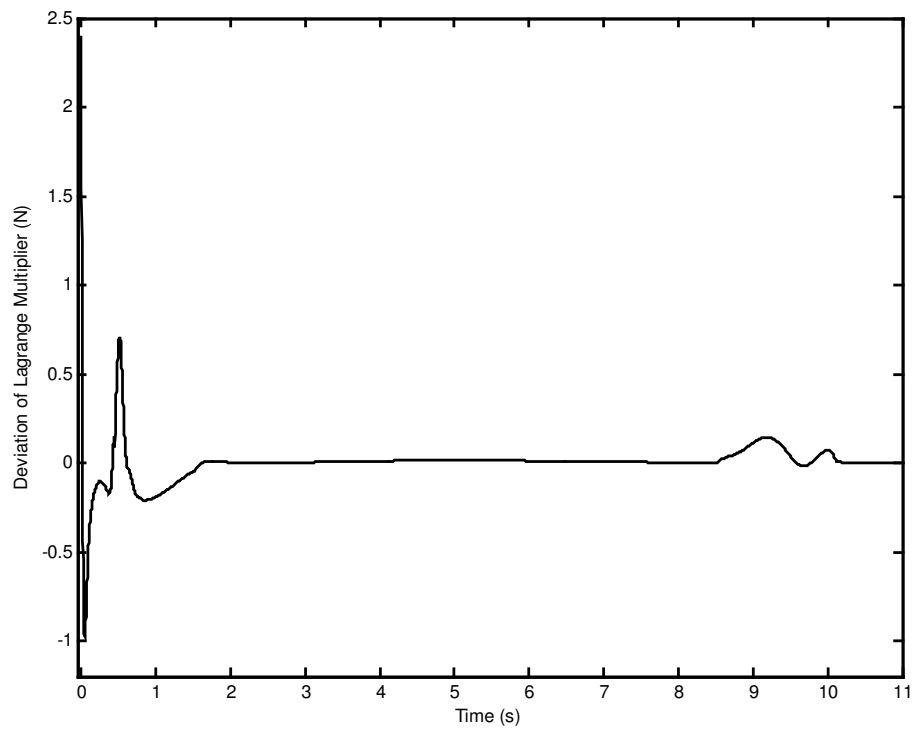


Figure 4.113 Deviation of Lagrange multiplier.

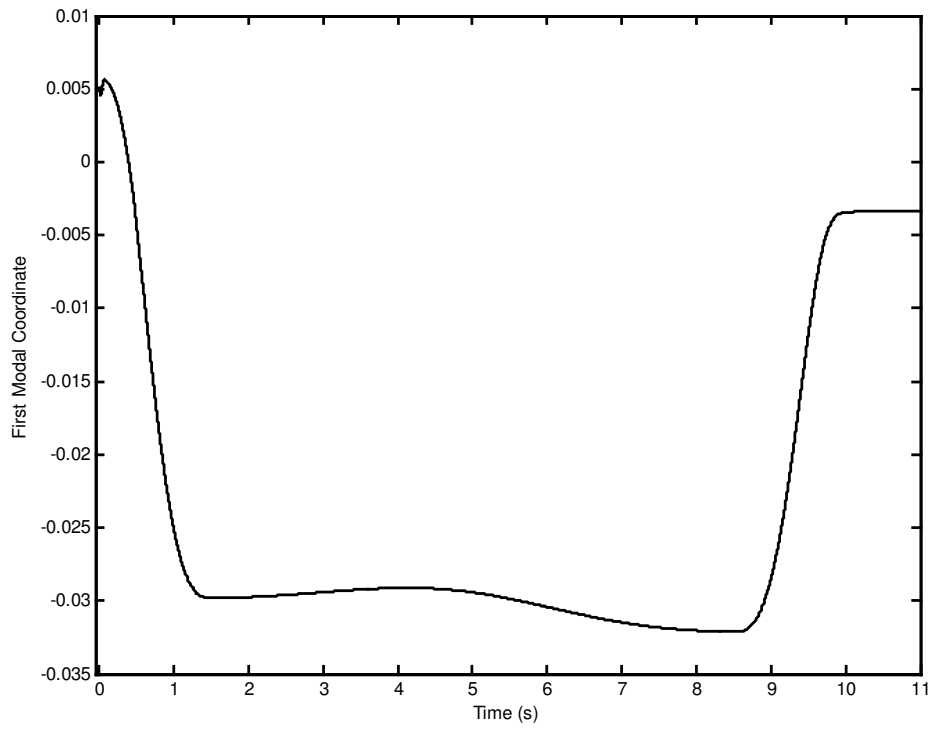


Figure 4.114 First modal coordinate.

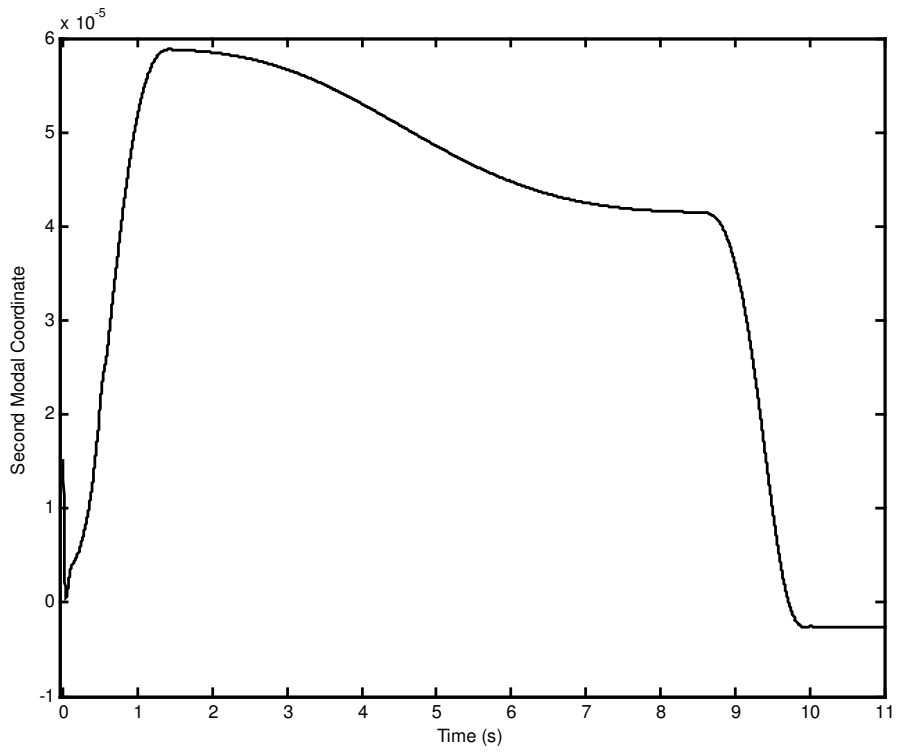


Figure 4.115 Second modal coordinate.

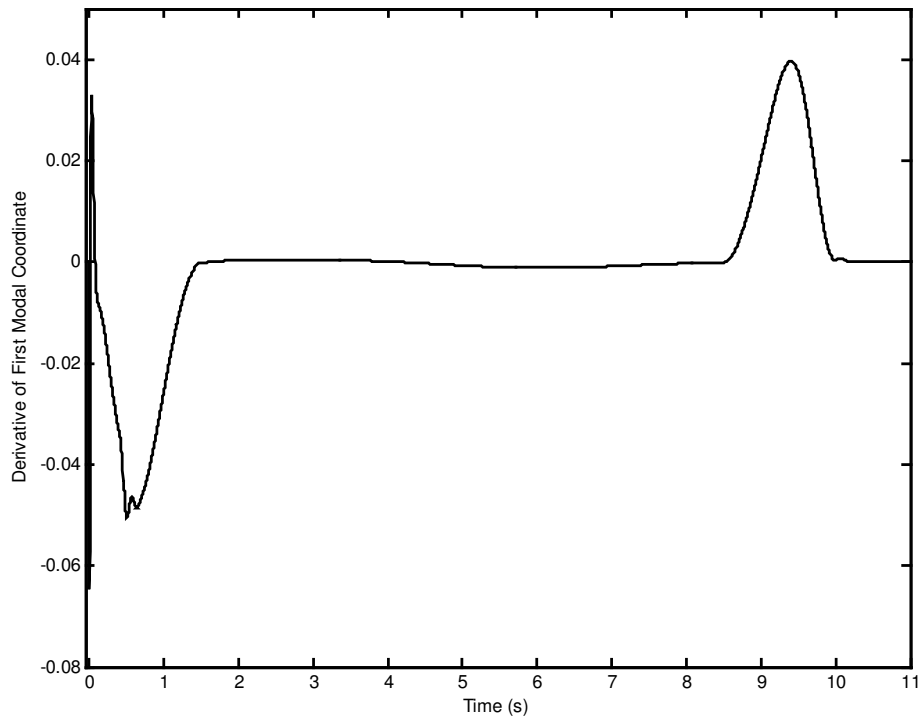


Figure 4.116 Derivative of first modal coordinate.

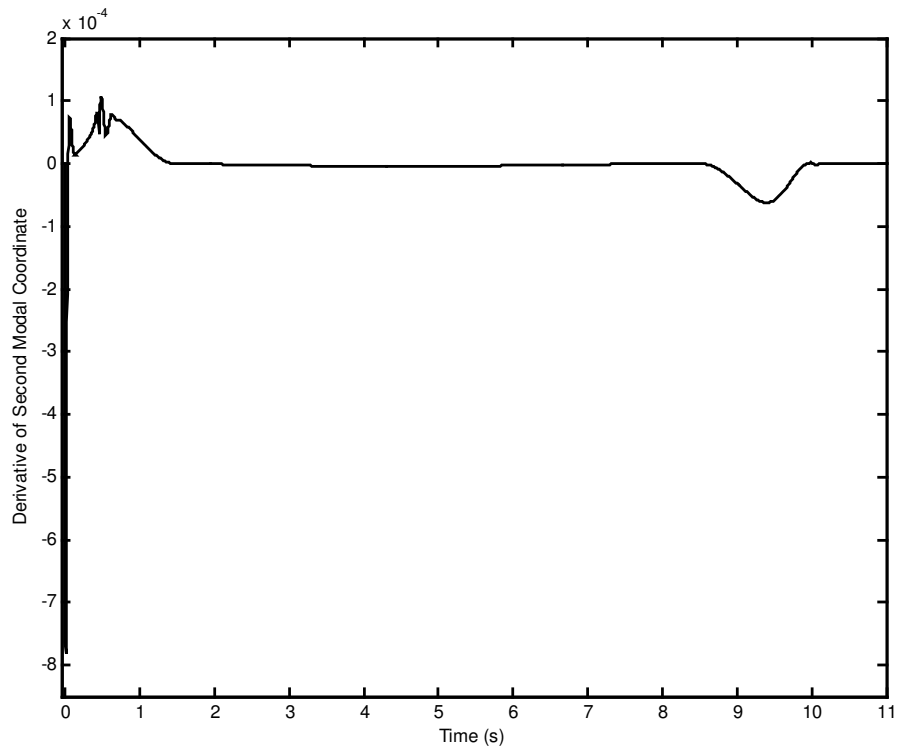


Figure 4.117 Derivative of second modal coordinate.

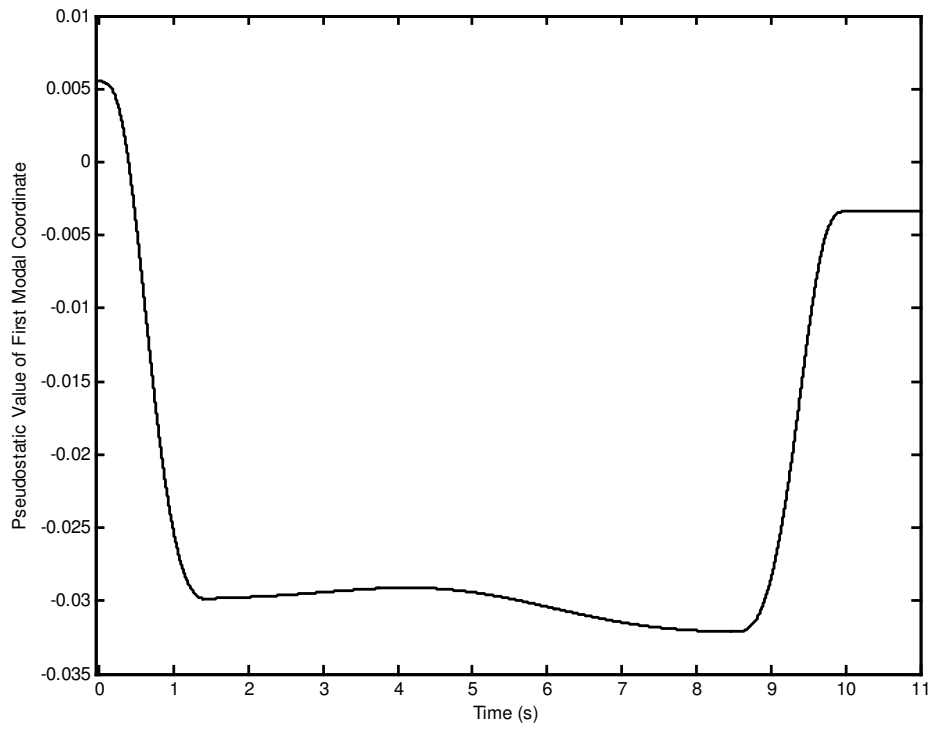


Figure 4.118 Pseudostatic value of first modal coordinate.

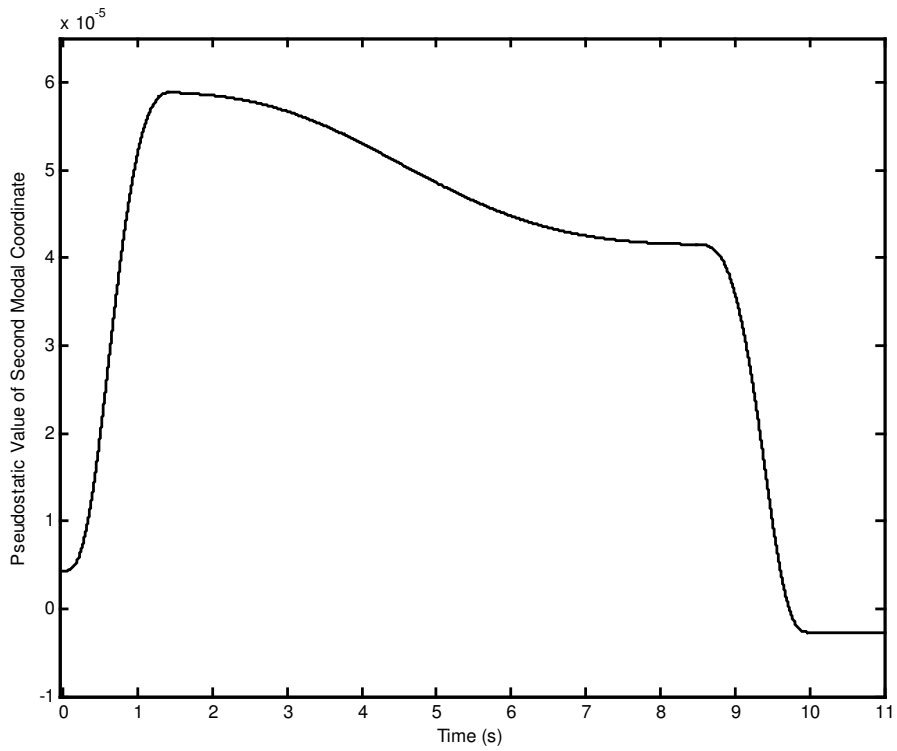


Figure 4.119 Pseudostatic value of second modal coordinate.

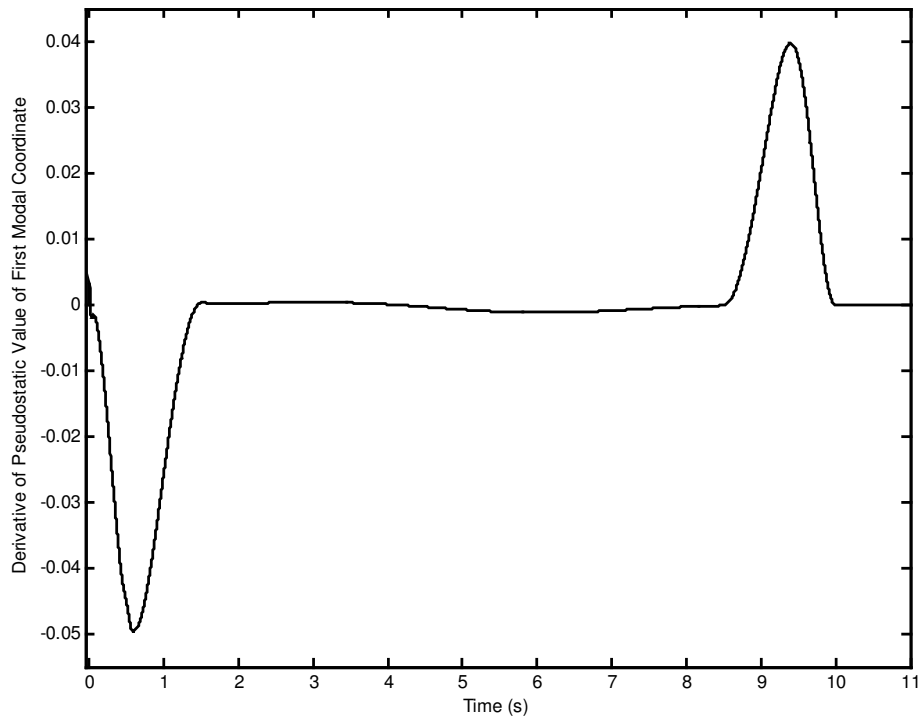


Figure 4.120 Derivative of pseudostatic value of first modal coordinate.

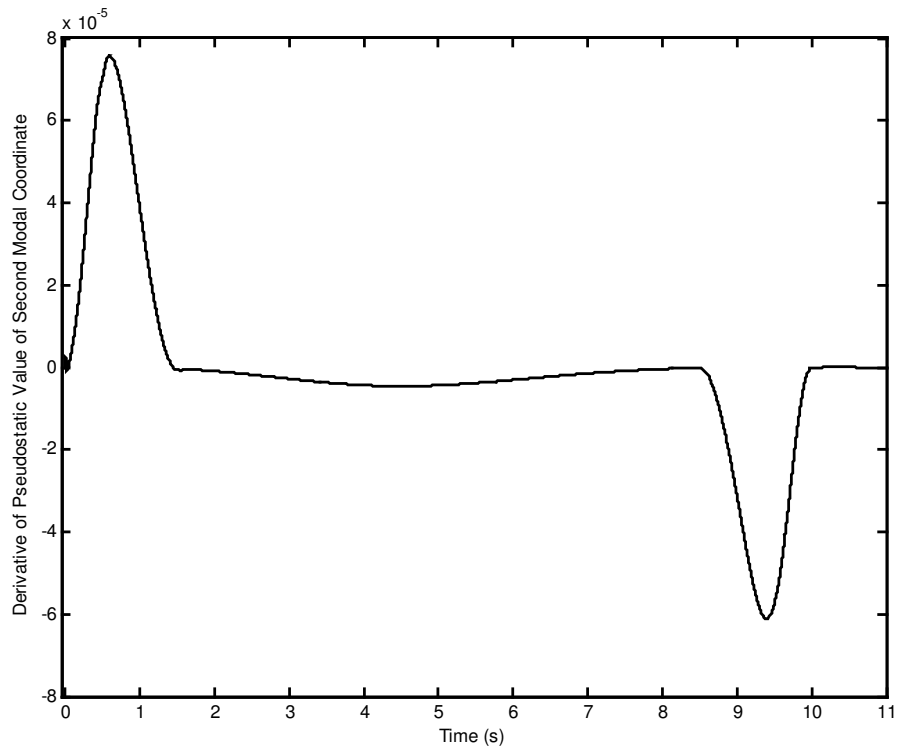


Figure 4.121 Derivative of pseudostatic value of second modal coordinate.

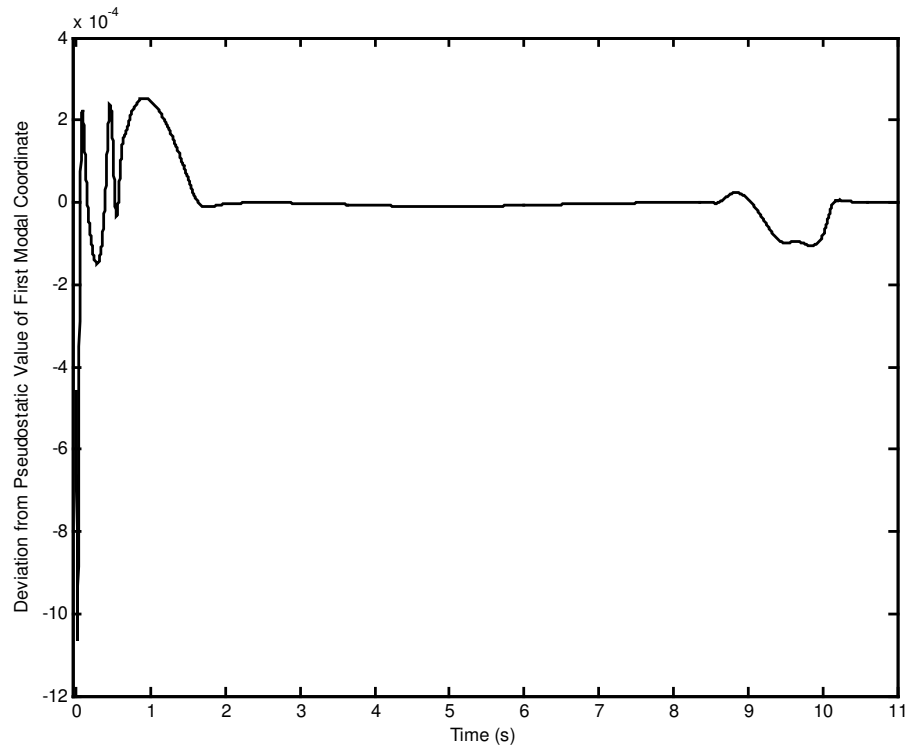


Figure 4.122 Deviation from pseudostatic value of first modal coordinate.

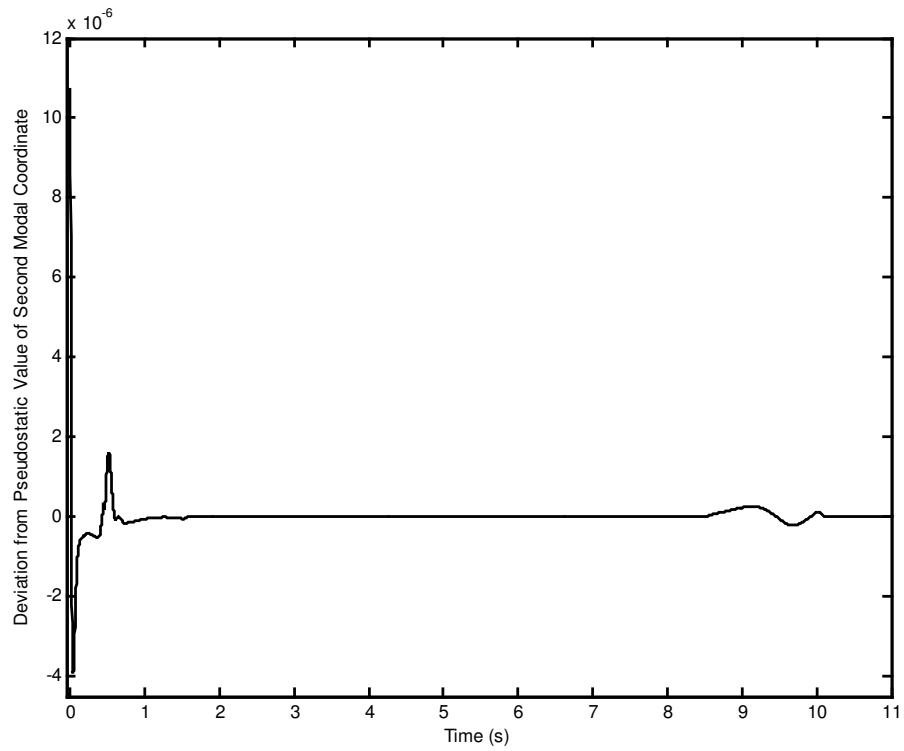


Figure 4.123 Deviation from pseudostatic value of second modal coordinate.

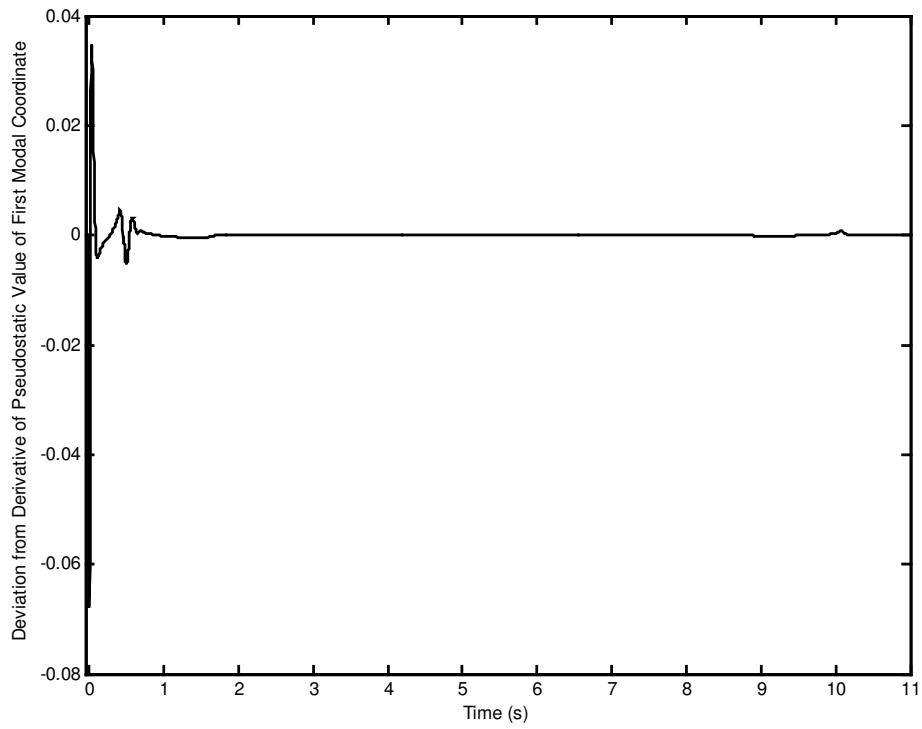


Figure 4.124 Deviation from derivative of pseudostatic value of first modal coordinate.

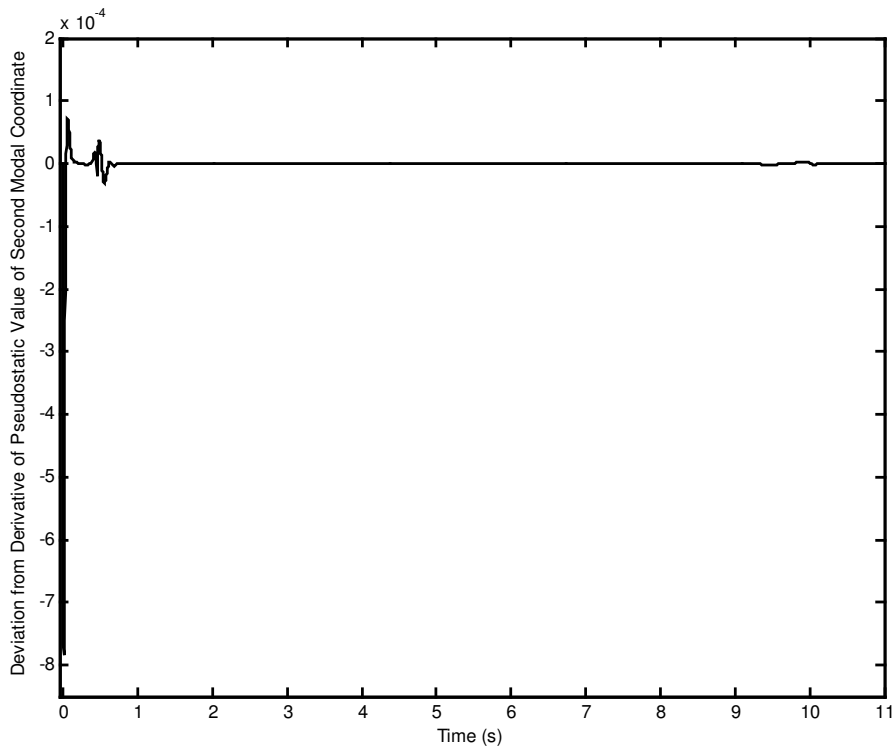


Figure 4.125 Deviation from derivative of pseudostatic value of second modal coordinate.

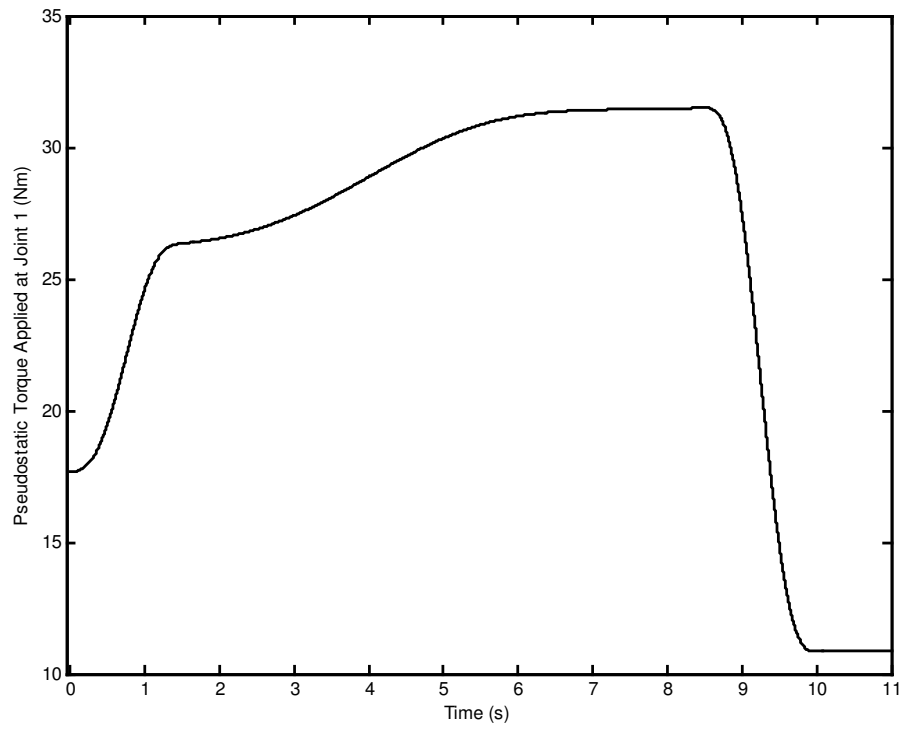


Figure 4.126 Pseudostatic torque applied at joint 1.

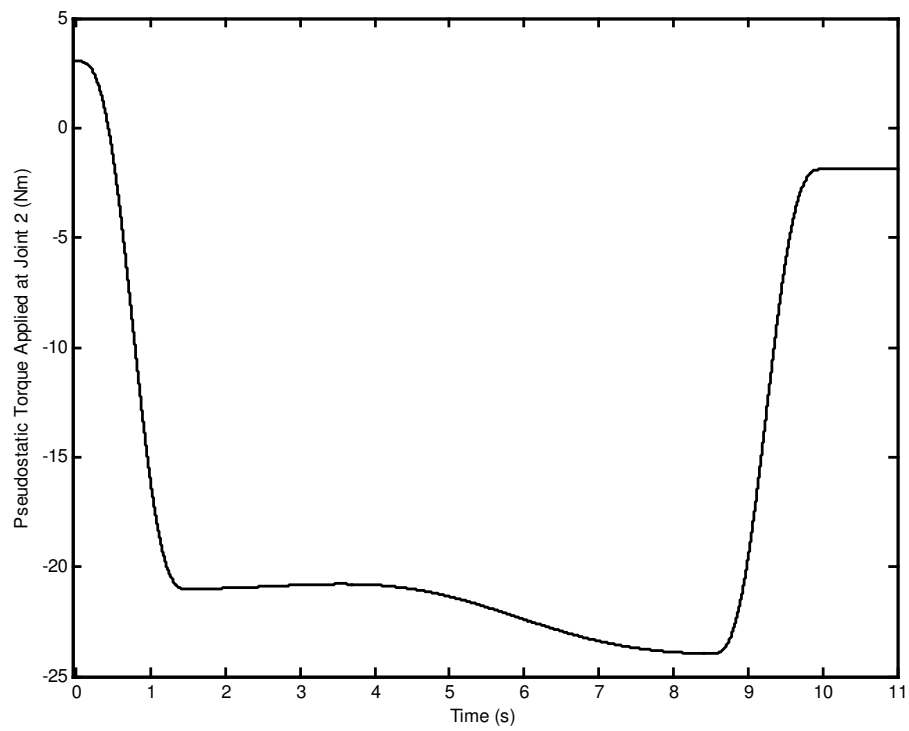


Figure 4.127 Pseudostatic torque applied at joint 2.

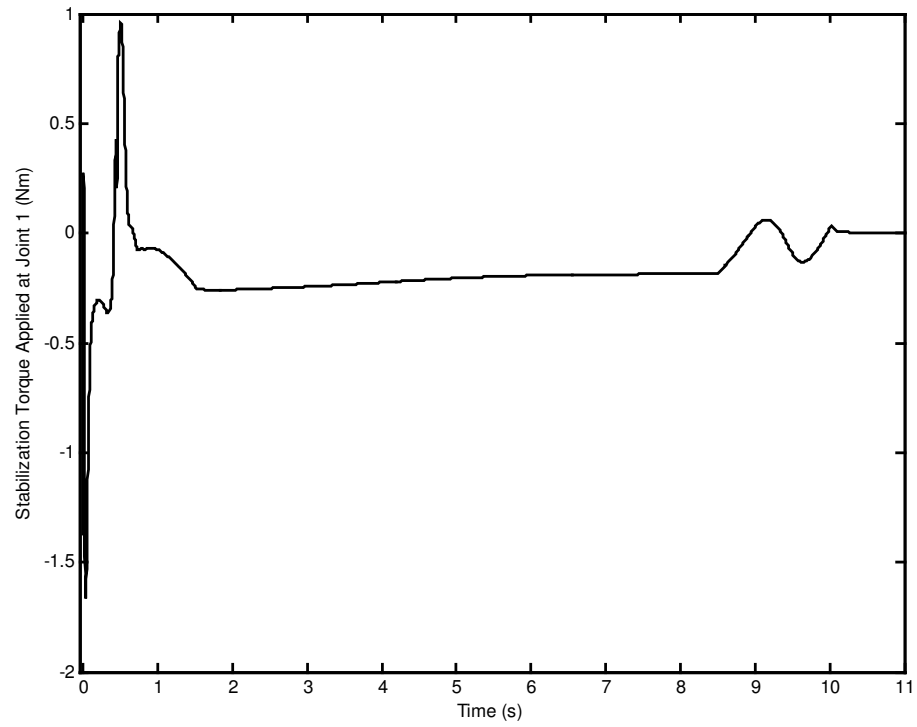


Figure 4.128 Stabilization torque applied at joint 1.

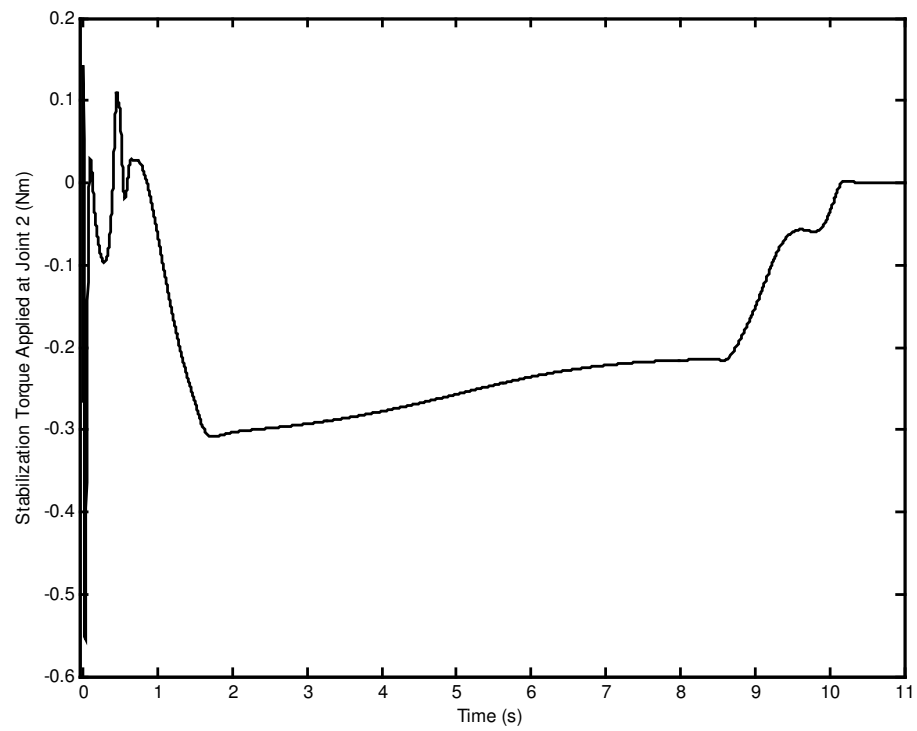


Figure 4.129 Stabilization torque applied at joint 2.

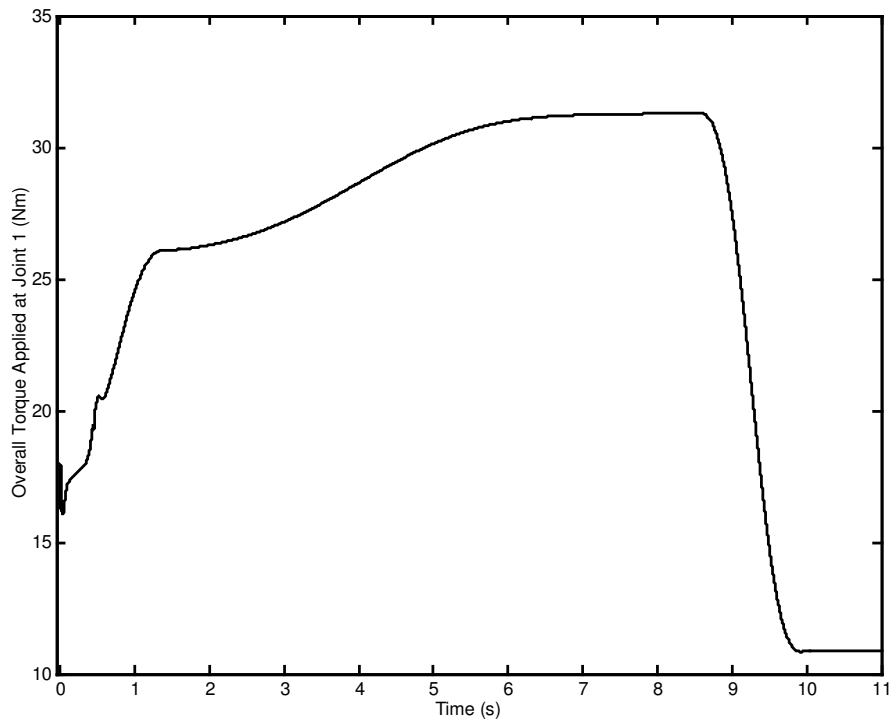


Figure 4.130 Overall torque applied at joint 1.

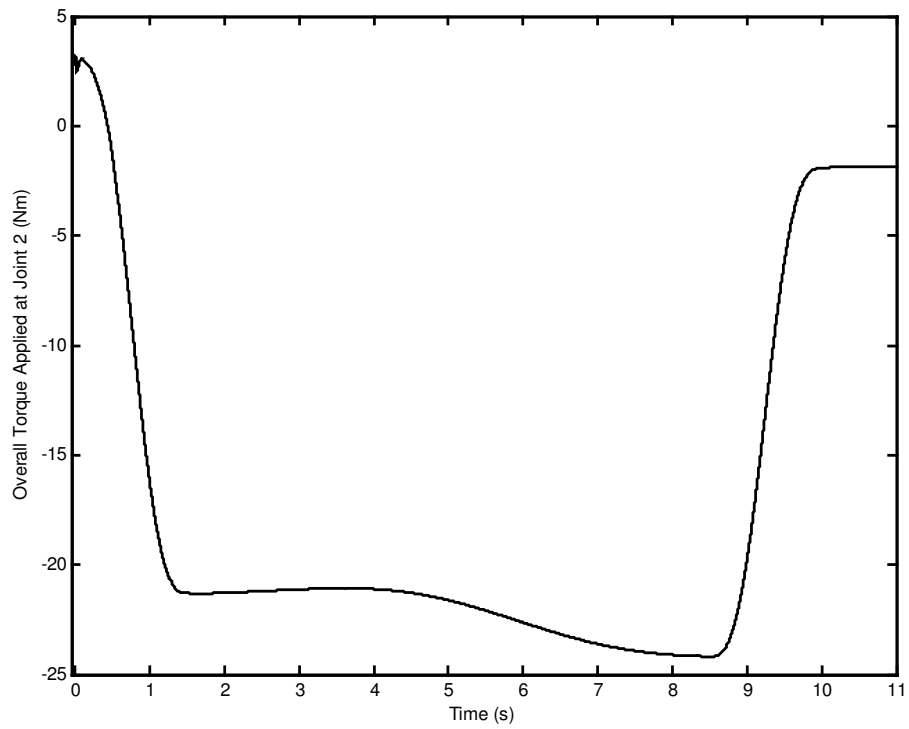


Figure 4.131 Overall torque applied at joint 2.

It is seen from the figures that there is a delay in settling to the desired trajectory compared to the previous simulation. The tip point position error on the constraint surface due to the mispositioning is about 50 mm as seen from Figure 4.83. There is a reverse action at the beginning of the motion as seen in the tip point position and velocity on the constraint surface and the Lagrange multiplier and its impulse which are given in Figures 4.110 - 4.113. The maximum tip point position tracking error on the constraint surface along the trajectory after the settling time is -3.9177×10^{-3} m. The corresponding maximum tip point position tracking error components are 2.8074×10^{-3} m and 2.7325×10^{-3} m in \mathbf{n}_1 and \mathbf{n}_2 directions, respectively. The maximum Lagrange multiplier error after the settling time is 0.145 N. The maximum overall torques applied to the joints are in small magnitudes in the order of 32 Nm as seen from Figures 4.130 and 4.131.

CHAPTER 5

NUMERICAL SIMULATIONS FOR SPATIAL ROBOT

In this section, a spatial three degrees of freedom robot with two flexible links is taken into consideration. Similar to the previous chapter, the numerical simulations are carried out in three parts.

In the first part, the uncontrolled motion of the robot as a flexible double pendulum is simulated for the verification of the dynamic equations.

In the second part, firstly, the motion control of the tip point is simulated by using the proposed method. Then, the measurement noises are taken into consideration and the motion control of the robot including measurement noises is simulated.

In the third part, firstly, the force and motion control of the tip point is simulated. Then, the measurement noises are again taken into consideration and the force and motion control of the robot including measurement noises is simulated.

5.1 Numerical Simulation of Uncontrolled Motion of Spatial Robot

The dynamic equations of the spatial robot with two flexible arms have very long and complicated expressions. Therefore, it is important to verify the dynamic equations before applying the proposed control methods to the robot. To verify the derivation of the dynamic equations and the code written for dynamic equations, the numerical simulation of the uncontrolled motion of the spatial robot with two flexible arms is presented in this section. The numerical simulation is obtained for the motion of the flexible robot as a double pendulum.

In the simulations, the axial, torsional and shear deformations are assumed to be negligible. The bending deformations are approximated by taking the first two bending modes in xy and xz planes for link 2 and link 3. Therefore, the vector of the modal variables has the following form

$$\boldsymbol{\eta}^{(2)} = \begin{bmatrix} \eta_1^{(2)} \\ \eta_2^{(2)} \end{bmatrix} \quad (5.1)$$

$$\boldsymbol{\eta}^{(3)} = \begin{bmatrix} \eta_1^{(3)} \\ \eta_2^{(3)} \end{bmatrix} \quad (5.2)$$

Fixed-free boundary conditions are used for both links. The links are assumed to have square cross section. Link 2 and link 3 are divided into five finite elements. The physical parameters of the three link spatial robot with flexible two arms considered here are given in Table 5.1.

Table 5.1 Physical parameters of the spatial robot used in uncontrolled motion.

Parameter	Value
Length of link 1 (m)	1
Length of link 2 (m)	1.5
Length of link 3 (m)	1.4
Mass of link 1 (kg)	1
Mass of link 2 (kg)	1
Mass of link 3 (kg)	1
Density of link 1 (kg/m ³)	7860
Density of link 2 (kg/m ³)	2710
Density of link 3 (kg/m ³)	2710
Modulus of elasticity of link 2 (Pa)	70x10 ⁹
Modulus of elasticity of link 3 (Pa)	70x10 ⁹
Lumped mass at point A (kg)	2
Lumped mass at point B (kg)	1.5
Lumped mass at point C (kg)	5

The numerical values of the natural frequencies associated with natural modes are 35.9598 rad/s, 225.4660 rad/s in xy plane and 35.9598 rad/s, 225.4660 rad/s in xz plane for Body 2 and 42.7293 rad/s, 267.9101rad/s in xy plane and 42.7293 rad/s, 267.9101 rad/s in xz plane for Body 3, respectively. It is assumed that the robot starts its motion from rest with no initial deflections. The initial joint angular positions are taken as $\theta_1 = 0$ degree, $\theta_2 = 280$ degrees and $\theta_3 = 5$ degrees. The sampling frequency is taken as 6000 Hz. The simulation results are given in Figures 5.1 - 5.22.

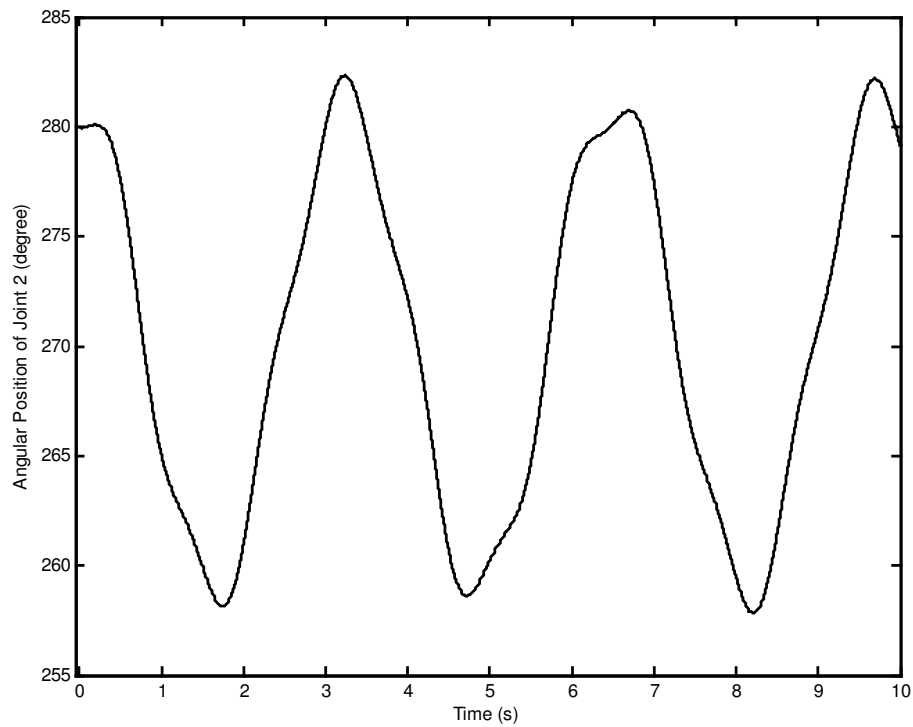


Figure 5.1 Angular position of joint 2.

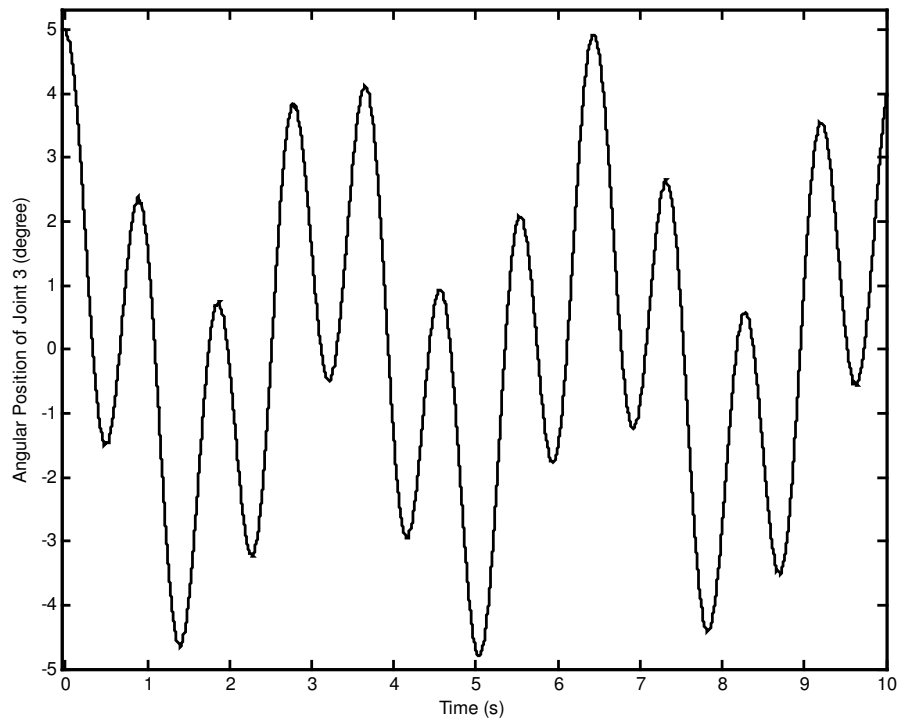


Figure 5.2 Angular position of joint 3.

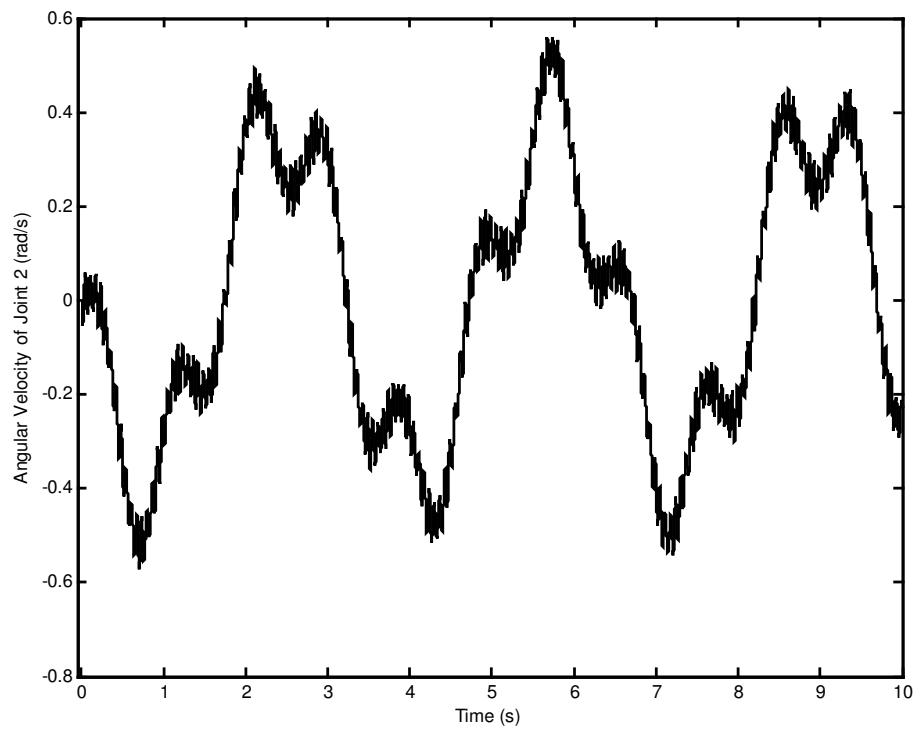


Figure 5.3 Angular velocity of joint 2.

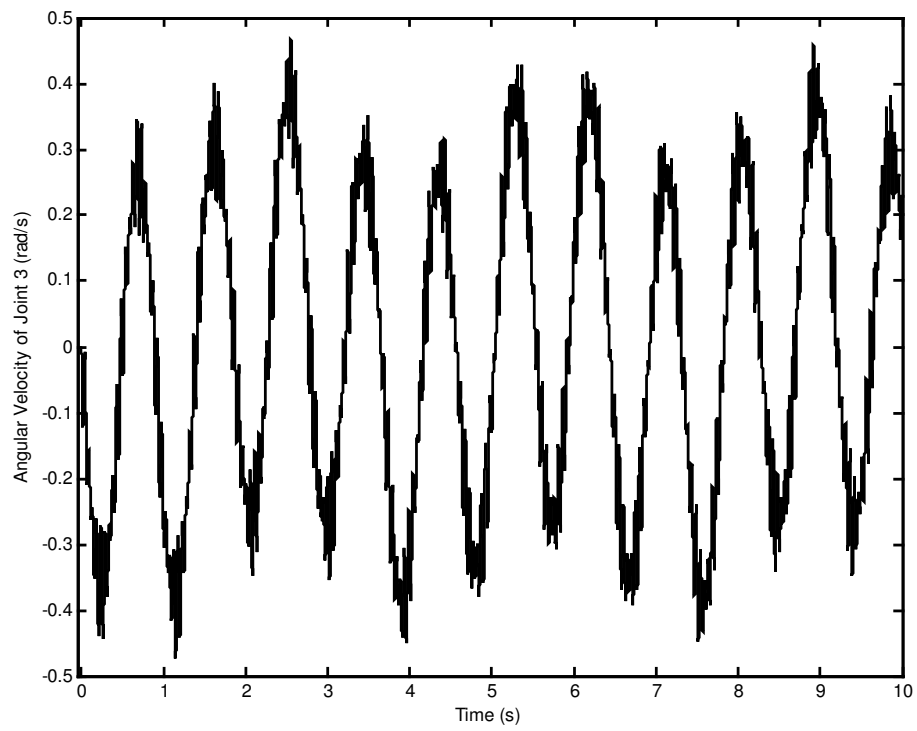


Figure 5.4 Angular velocity of joint 3.

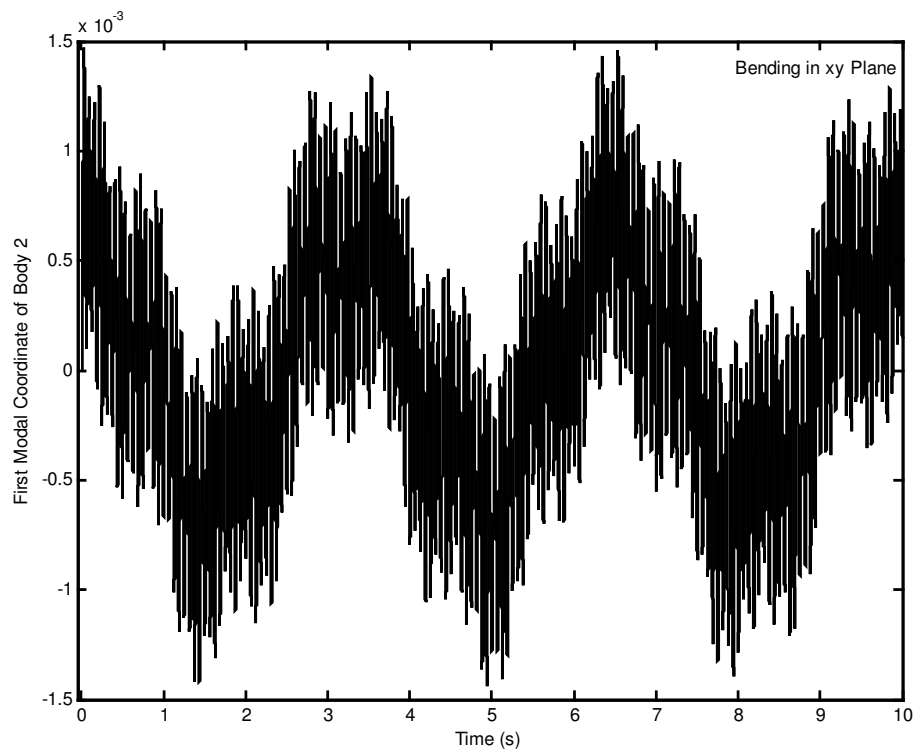


Figure 5.5 First modal coordinate of body 2.

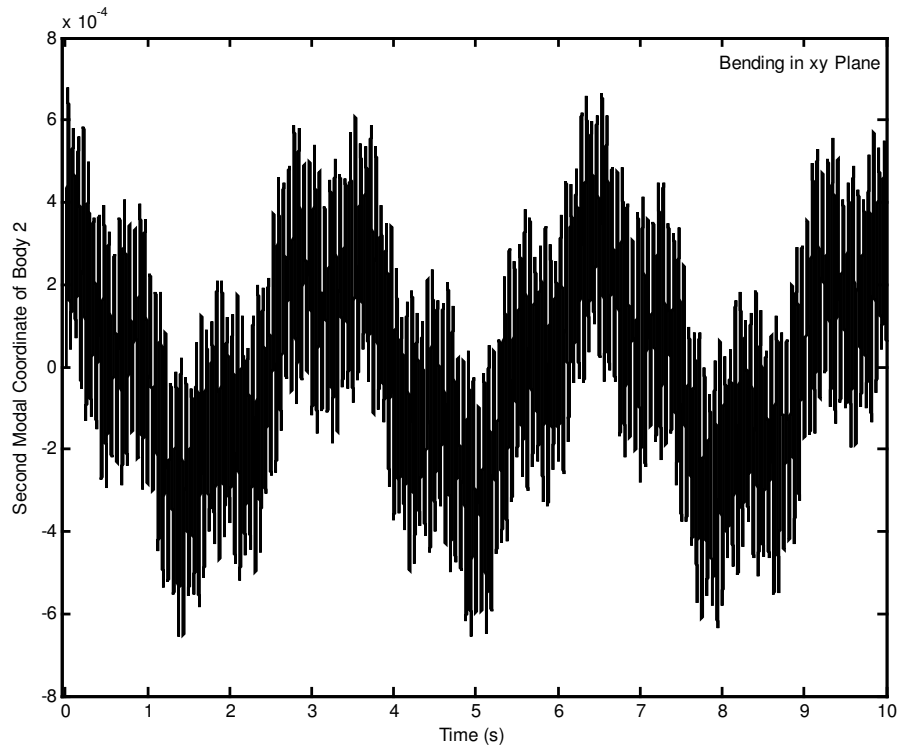


Figure 5.6 Second modal coordinate of body 2.

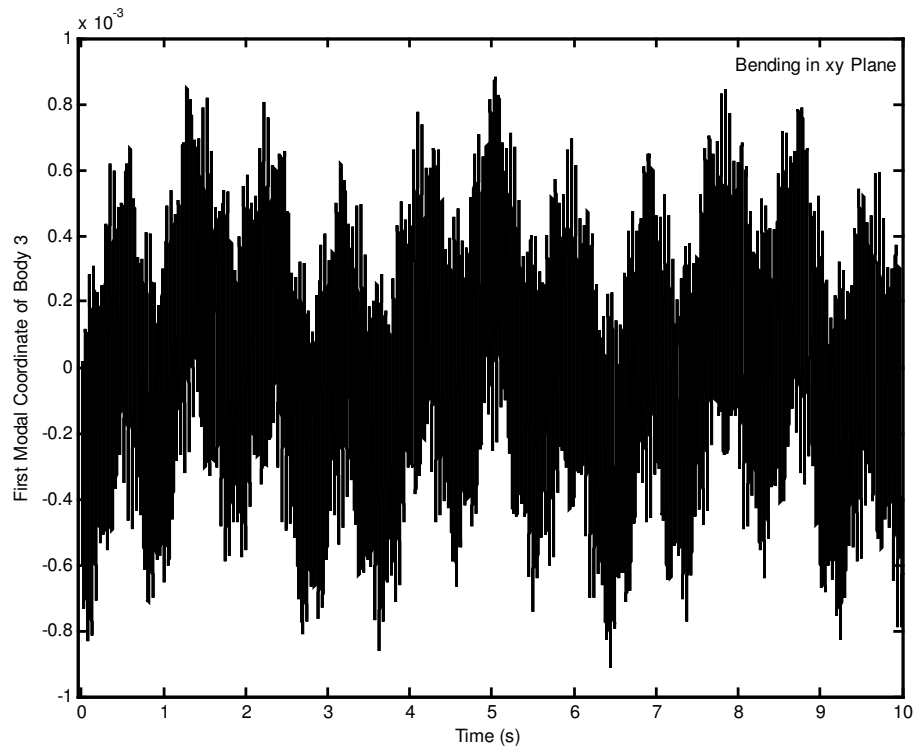


Figure 5.7 First modal coordinate of body 3.

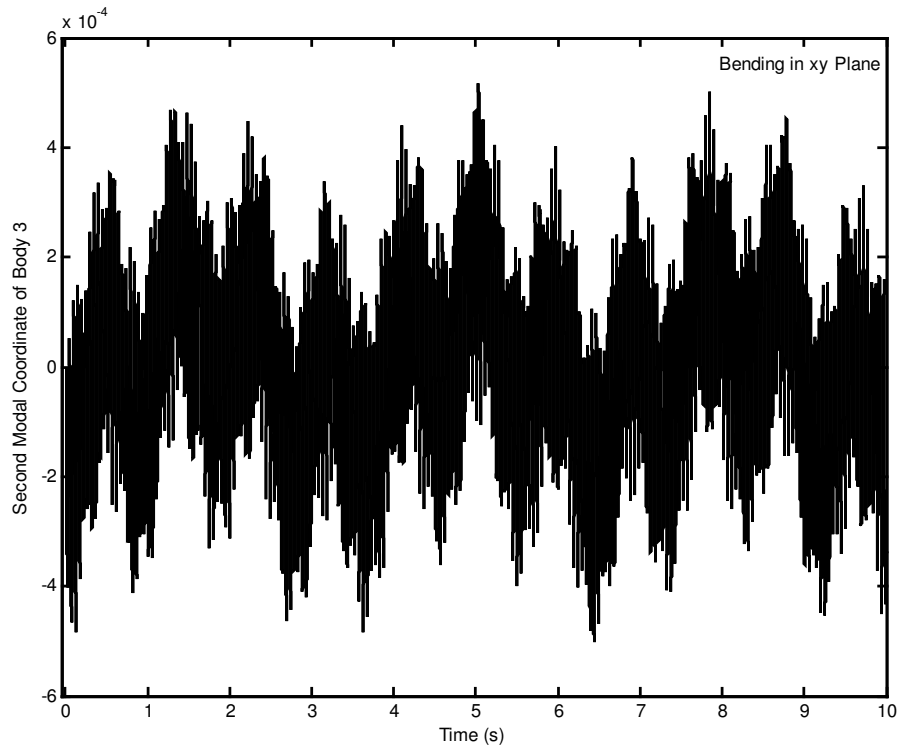


Figure 5.8 Second modal coordinate of body 3.

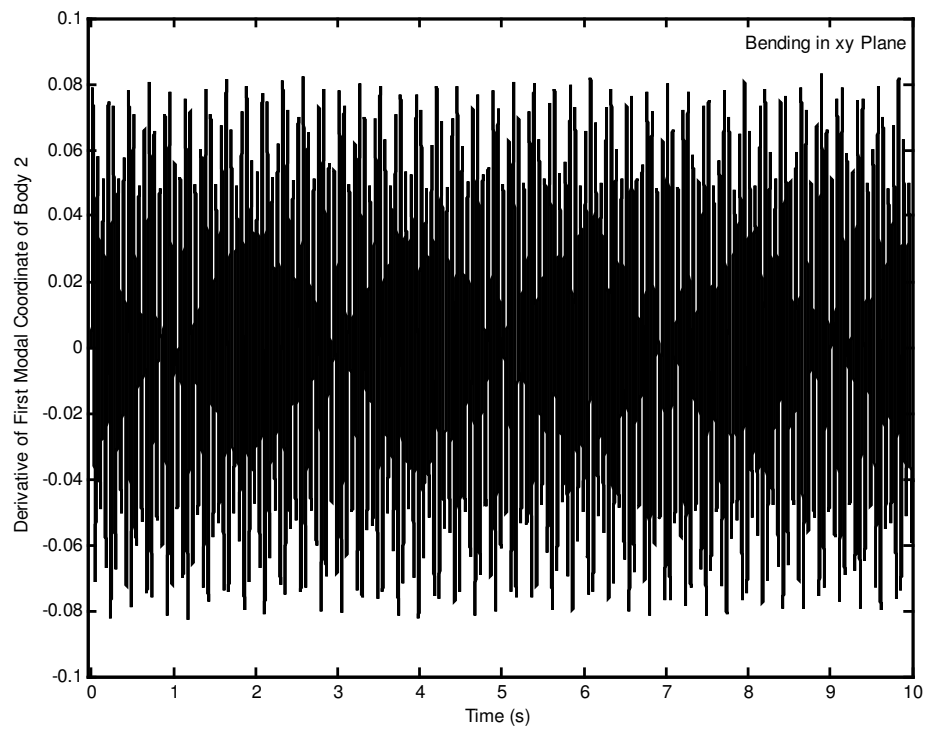


Figure 5.9 Derivative of first modal coordinate of body 2.

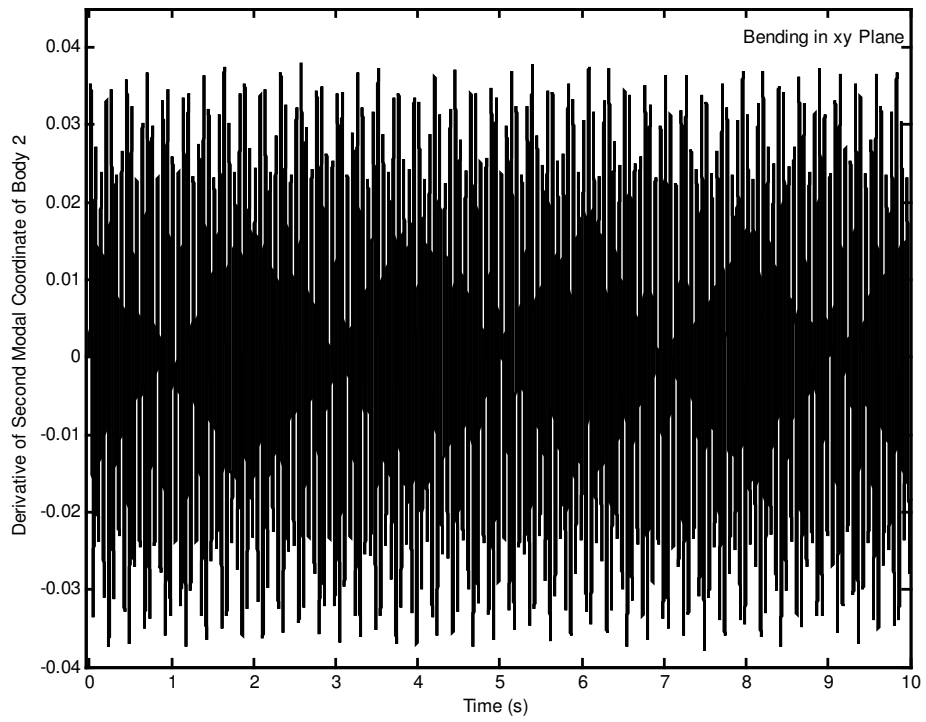


Figure 5.10 Derivative of second modal coordinate of body 2.

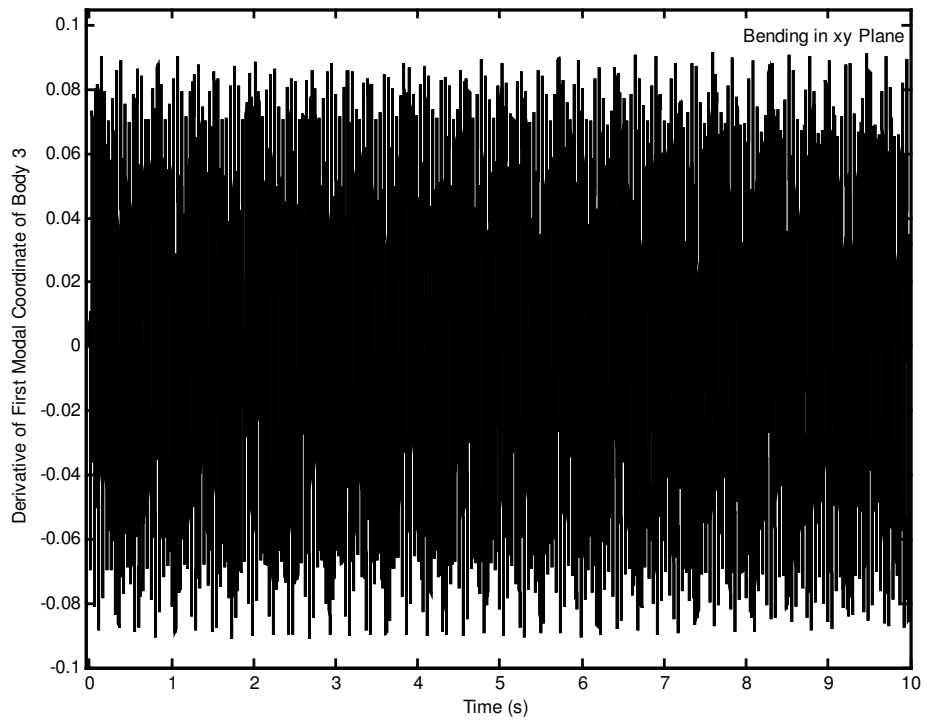


Figure 5.11 Derivative of first modal coordinate of body 3.

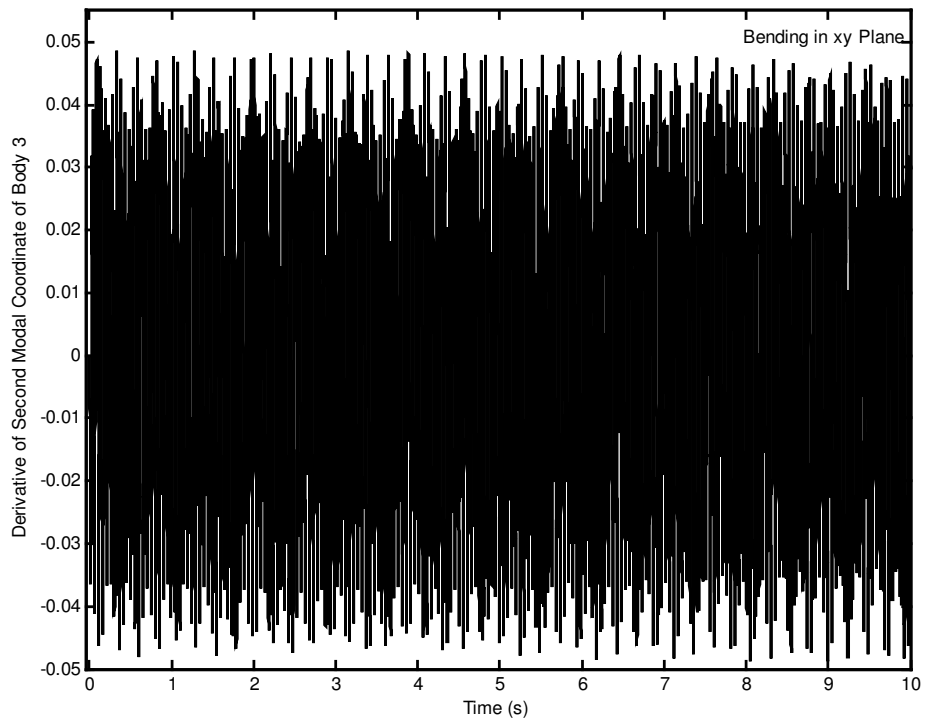


Figure 5.12 Derivative of second modal coordinate of body 3.

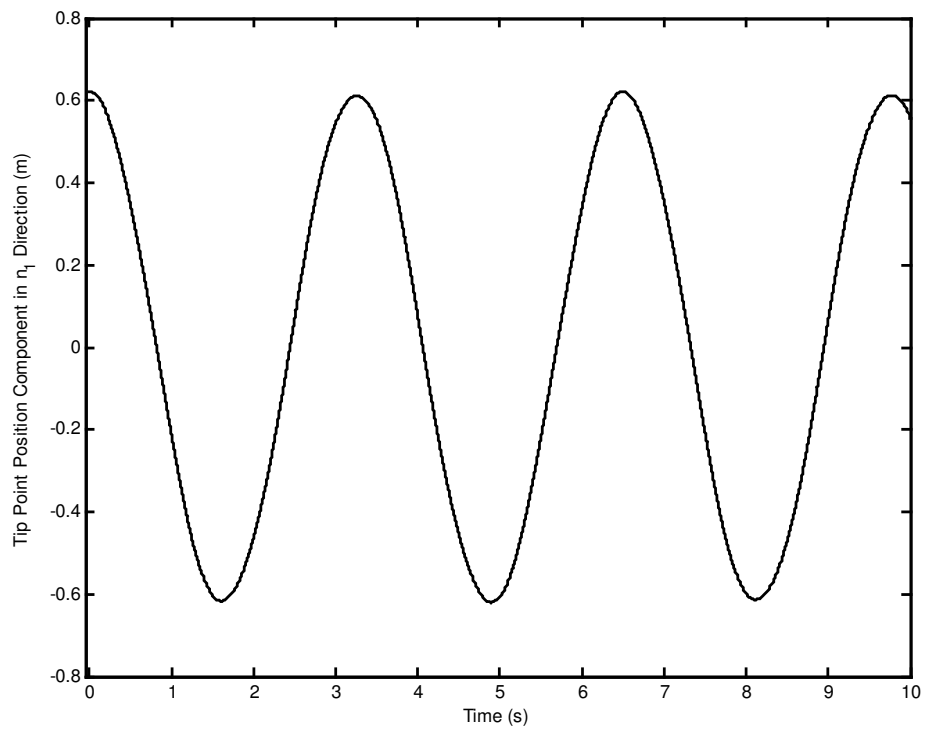


Figure 5.13 Tip point position component in n_1 direction.

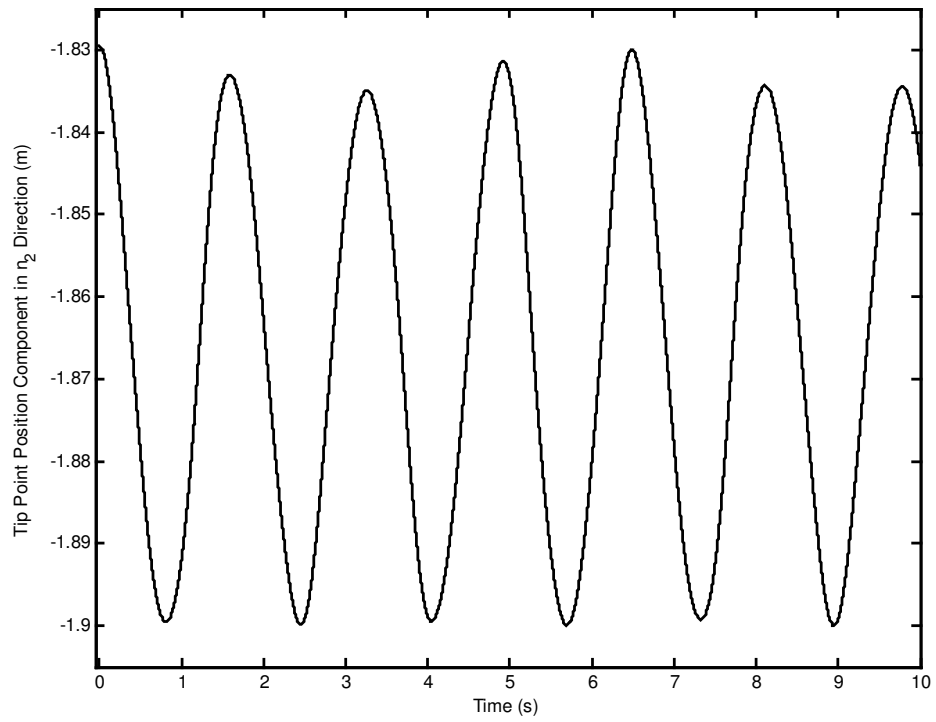


Figure 5.14 Tip point position component in n_2 direction.

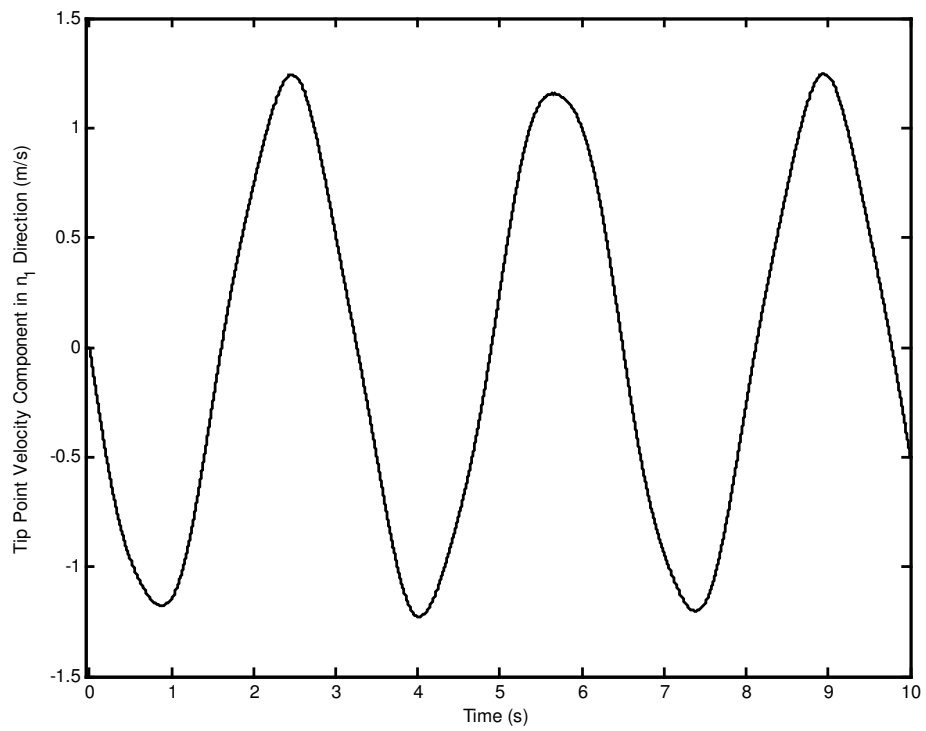


Figure 5.15 Tip point velocity component in n_1 direction.

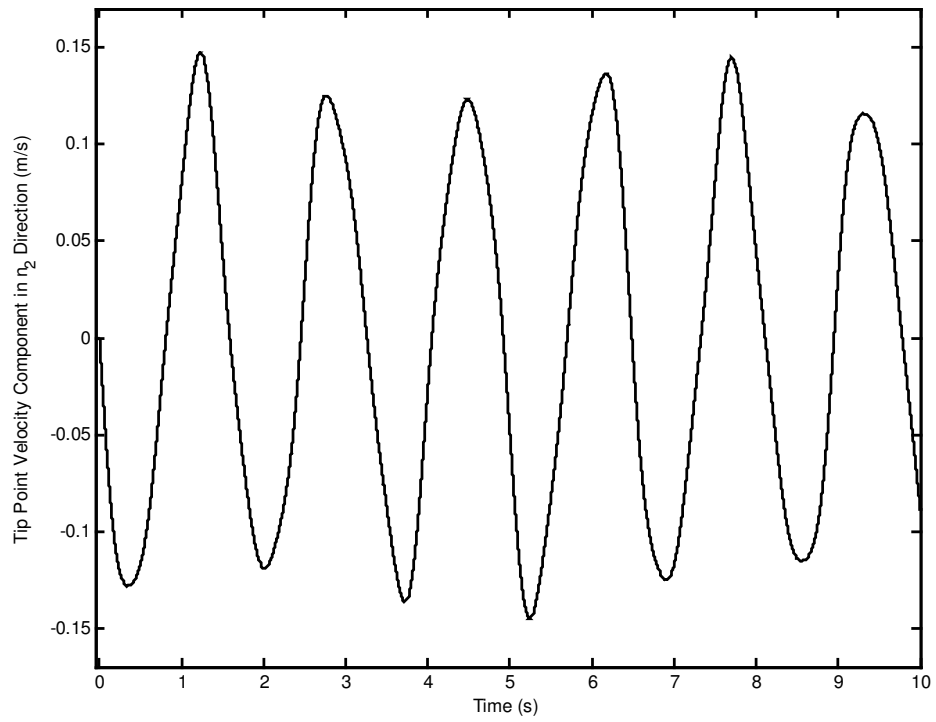


Figure 5.16 Tip point velocity component in n_2 direction.

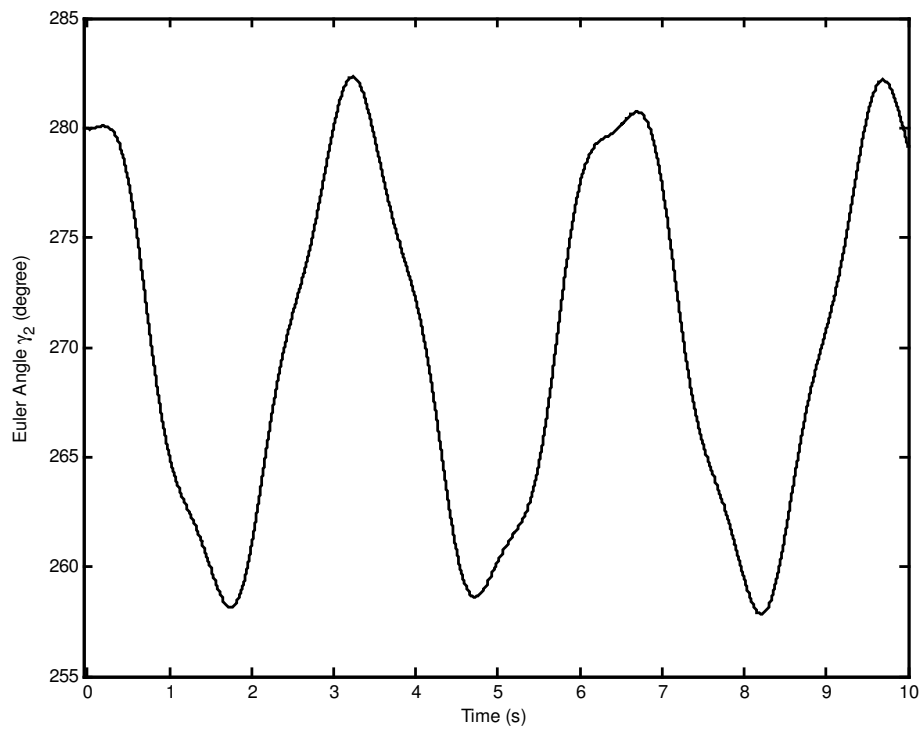


Figure 5.17 Euler angle γ_2 .

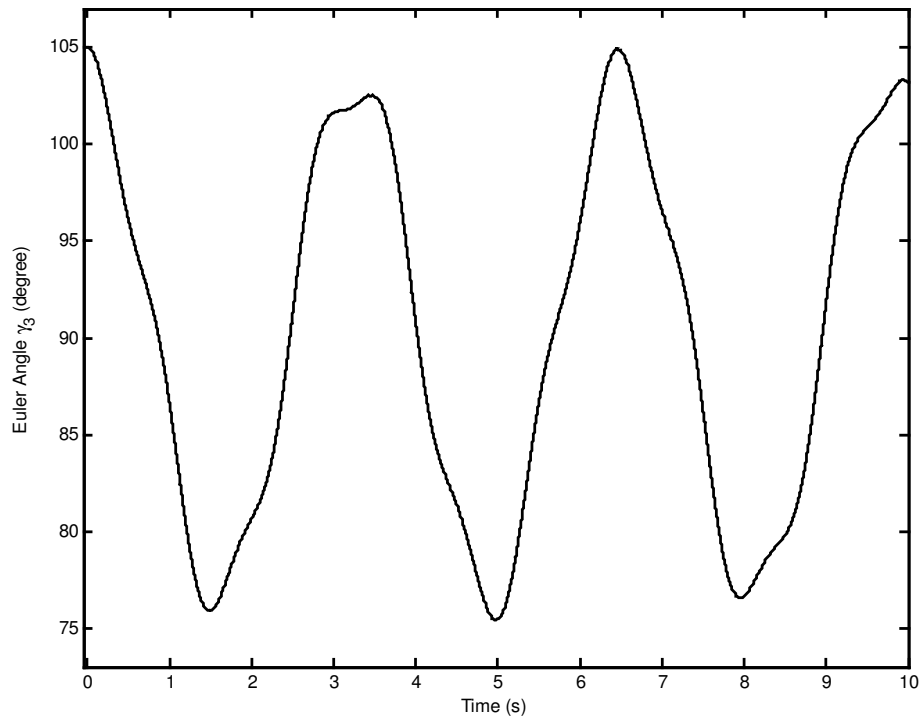


Figure 5.18 Euler angle γ_3 .

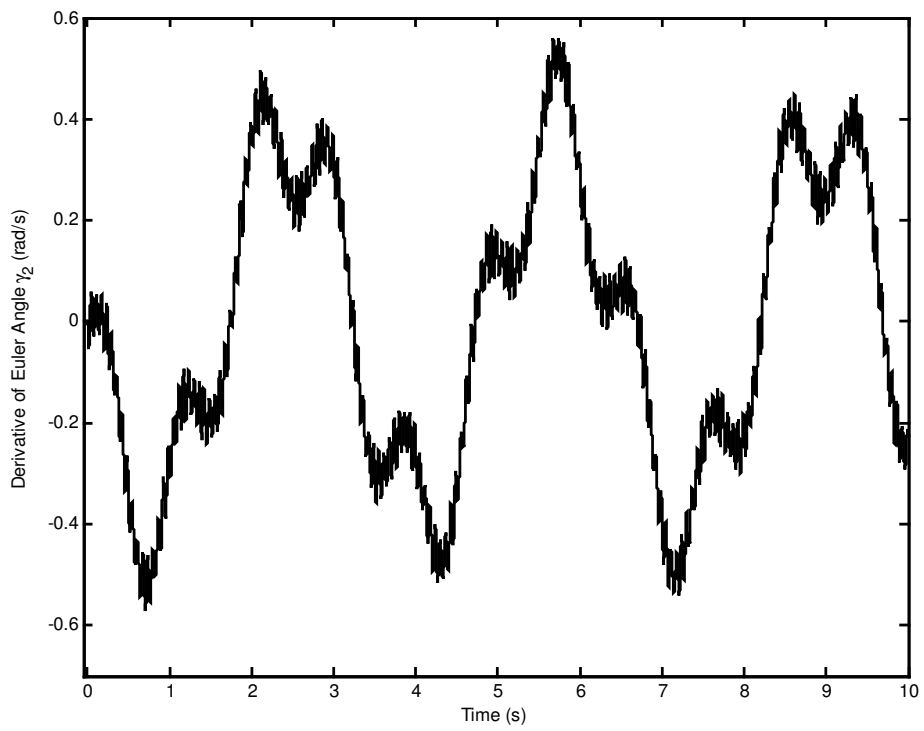


Figure 5.19 Derivative of Euler angle γ_2 .

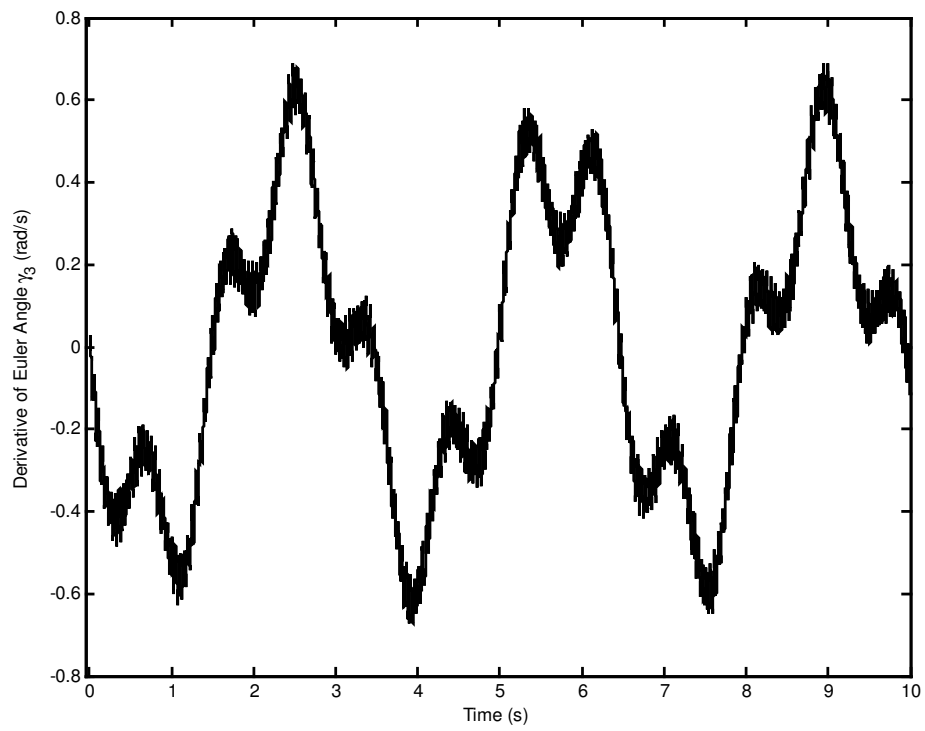


Figure 5.20 Derivative of Euler angle γ_3 .

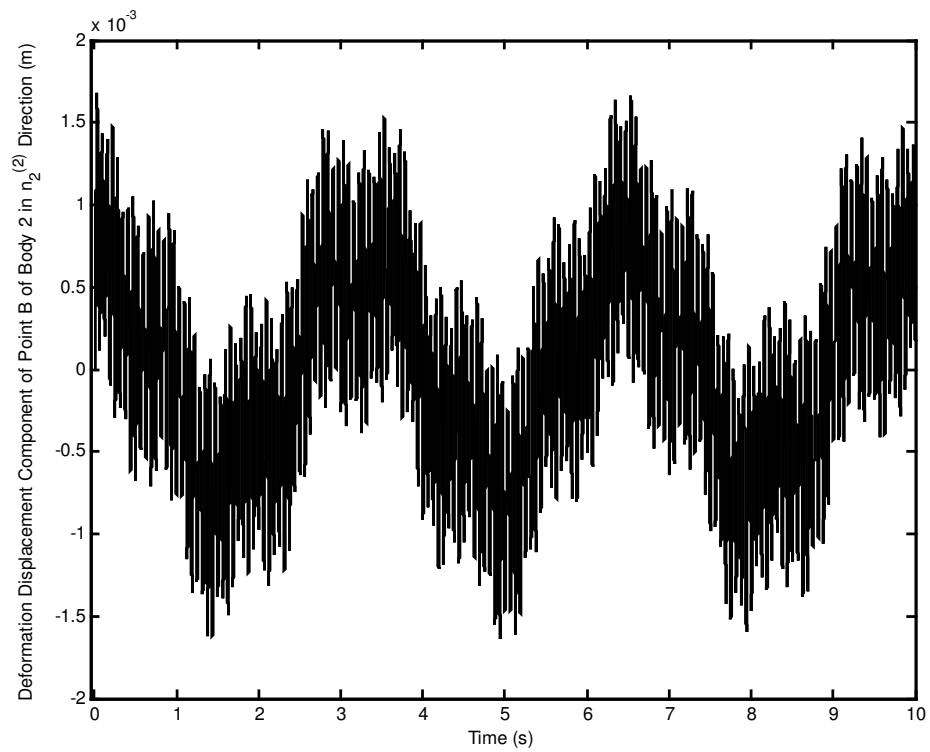


Figure 5.21 Deformation displacement component of point B of body 2 in $n_2^{(2)}$ direction.

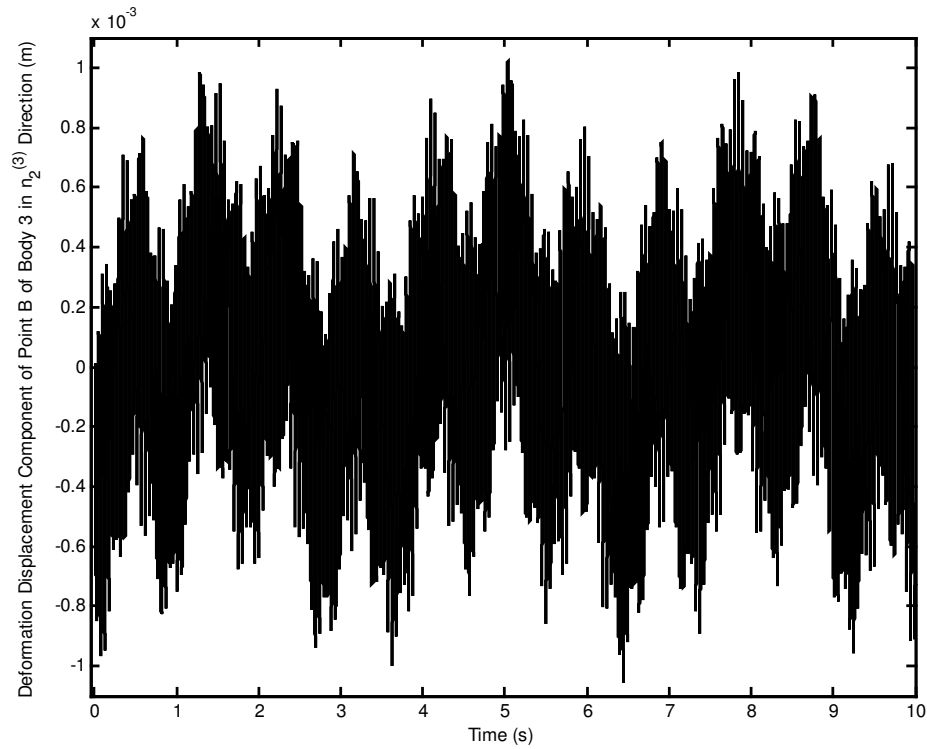


Figure 5.22 Deformation displacement component of point B of body 2 in $n_2^{(3)}$ direction.

When Figures 5.1 - 5.22 are examined, it is seen that they are as expected. Since the only external force on the robot is the gravitational force which is in xy plane, there is no motion in xz plane. Therefore, angular position of joint 1 remains constant and modal coordinates in xz plane for Body 2 and Body 3 are zero. The time derivatives of these variables are also zero. As a result of that the variables relating to these situations are not plotted.

5.2 Numerical Simulation of Motion Control of Spatial Robot

In this section, the numerical simulation of motion control of the spatial robot with flexible two arms is presented by using the motion control method proposed at Chapter 2. The tip point is required to track a straight line. The same function for the reference tip point trajectory given in Chapter 4 is used.

The physical parameters of the three link spatial robot with flexible two arms used in the controlled motion simulations are given in Table 5.2.

Table 5.2 Physical parameters of the spatial robot used in controlled motion.

Parameter	Value
Length of link 1 (m)	0.5
Length of link 2 (m)	1.5
Length of link 3 (m)	1.4
Mass of link 1 (kg)	1
Mass of link 2 (kg)	1.5
Mass of link 3 (kg)	1
Density of link 1 (kg/m ³)	7860
Density of link 2 (kg/m ³)	2710
Density of link 3 (kg/m ³)	2710
Modulus of elasticity of link 2 (Pa)	70x10 ⁹
Modulus of elasticity of link 3 (Pa)	70x10 ⁹
Lumped mass at point A (kg)	1.5
Lumped mass at point B (kg)	1
Lumped mass at point C (kg)	2

The numerical values of the natural frequencies associated with natural modes are 44.042 rad/s, 276.14 rad/s in xy plane and 44.042 rad/s, 276.14 rad/s rad/s in xz plane for Body 2 and 42.7293 rad/s, 267.9101rad/s in xy plane and 42.7293 rad/s, 267.9101 rad/s in xz plane for Body 3, respectively.

After a few trials, proper closed loop natural frequencies and damping ratios are obtained as 5 rad/s, 10 rad/s, 15 rad/s, 43 rad/s, 43 rad/s, 44 rad/s, 44 rad/s, 268 rad/s, 268 rad/s, 276 rad/s, 276 rad/s, 0.85, 0.85, 0.85, 0.85, 0.85, 0.85, 0.85, 0.85, 0.85, 0.85 and 0.85. The corresponding closed loop poles are given in Table 5.3.

Table 5.3 Closed loop poles used in motion control of spatial robot.

Closed Loop Poles
$p_1 = -4.2500 + 2.6339j$
$p_2 = -4.2500 - 2.6339j$
$p_3 = -8.5000 + 5.2678j$
$p_4 = -8.5000 - 5.2678j$
$p_5 = -12.7500 + 7.9017j$
$p_6 = -12.7500 - 7.9017j$
$p_{7,8} = -36.5500 + 22.6517j$
$p_{9,10} = -36.5500 - 22.6517j$
$p_{11,12} = -37.4000 + 23.1784j$
$p_{13,14} = -37.4000 - 23.1784j$
$p_{15,16} = -227.8000 + 141.1778j$
$p_{17,18} = -227.8000 - 141.1778j$
$p_{19,20} = -234.6000 + 145.3920j$
$p_{21,22} = -234.6000 - 145.3920j$

The sampling frequency is taken as 500 Hz. The simulation results are presented in Figures 5.23 - 5.91.

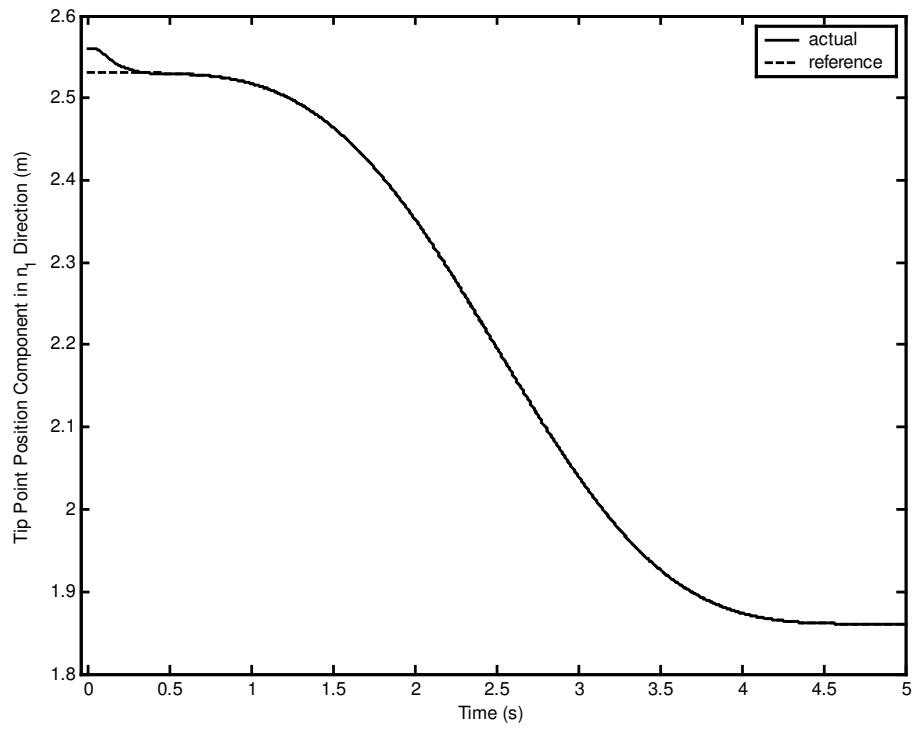


Figure 5.23 Tip point position component in n_1 direction.

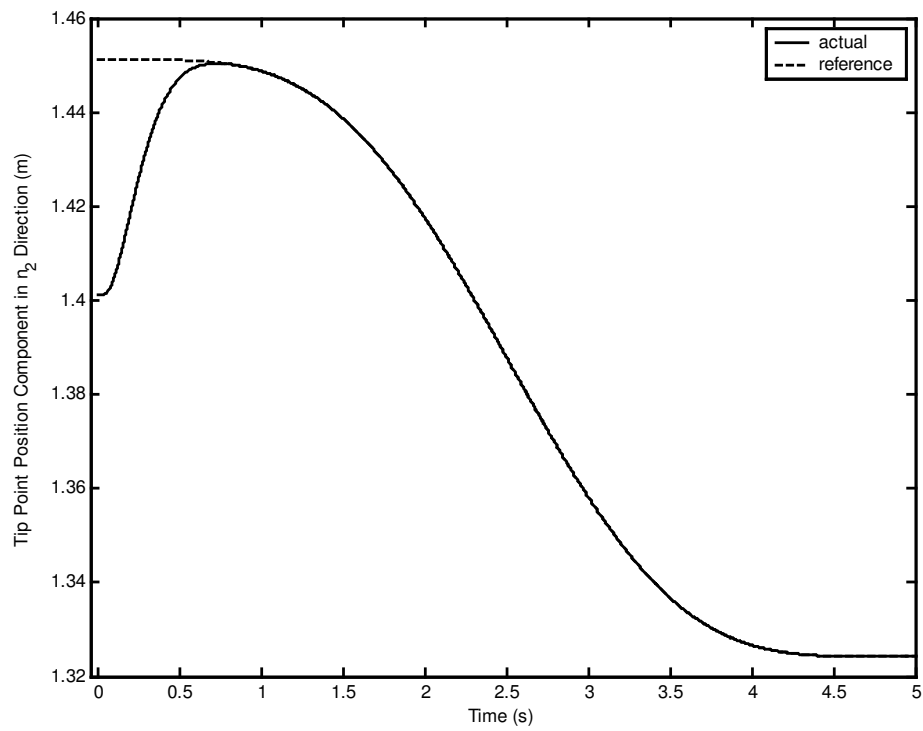


Figure 5.24 Tip point position component in n_2 direction.

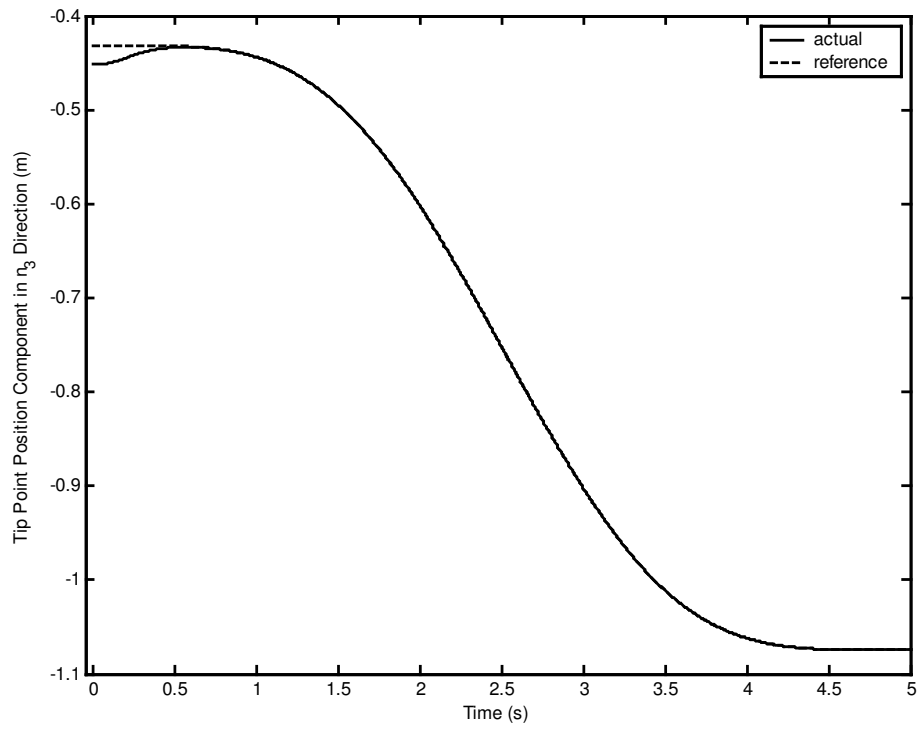


Figure 5.25 Tip point position component in n_3 direction.

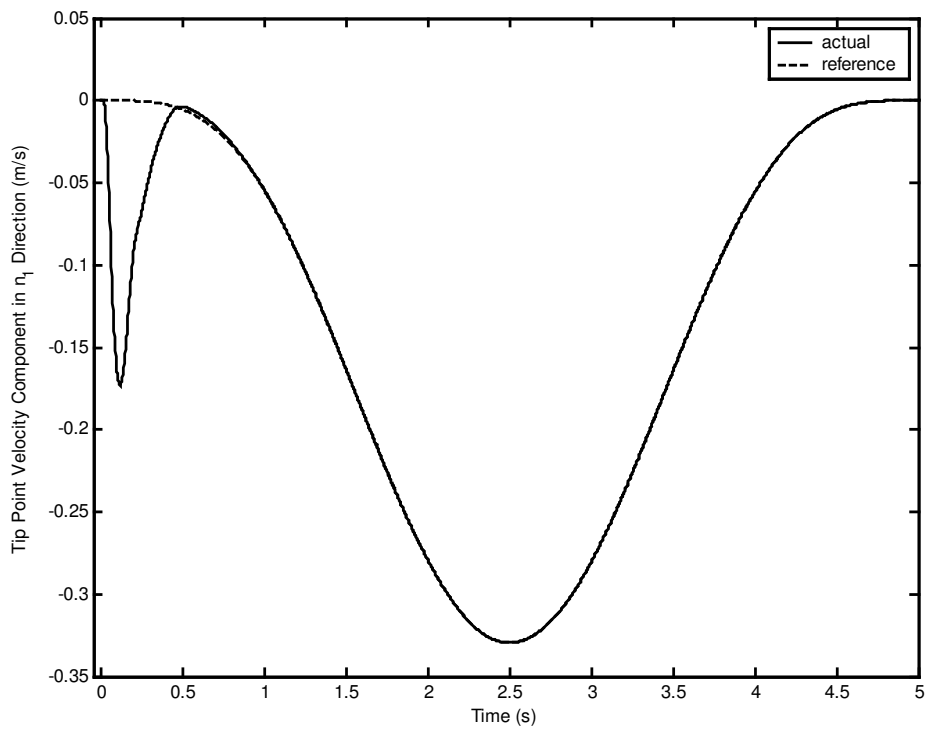


Figure 5.26 Tip point velocity component in n_1 direction.

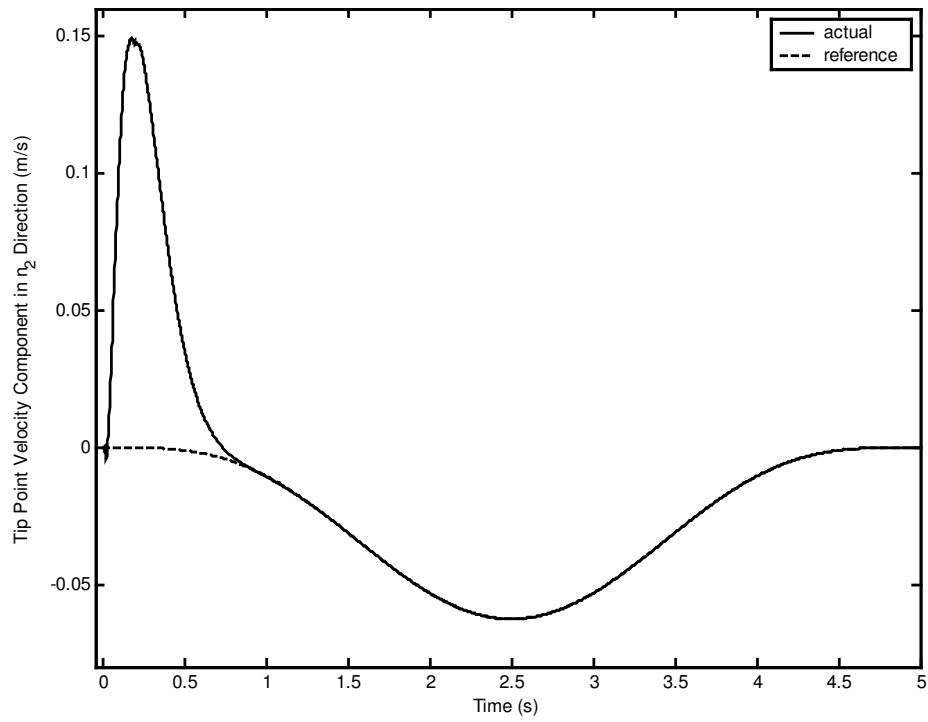


Figure 5.27 Tip point velocity component in n_2 direction.

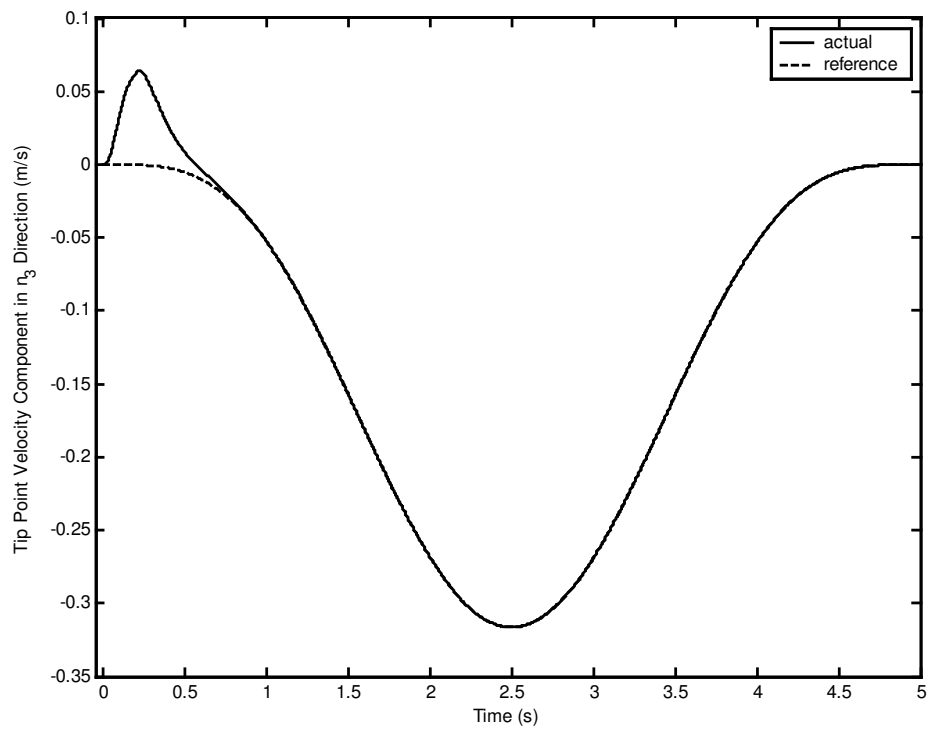


Figure 5.28 Tip point velocity component in n_3 direction.

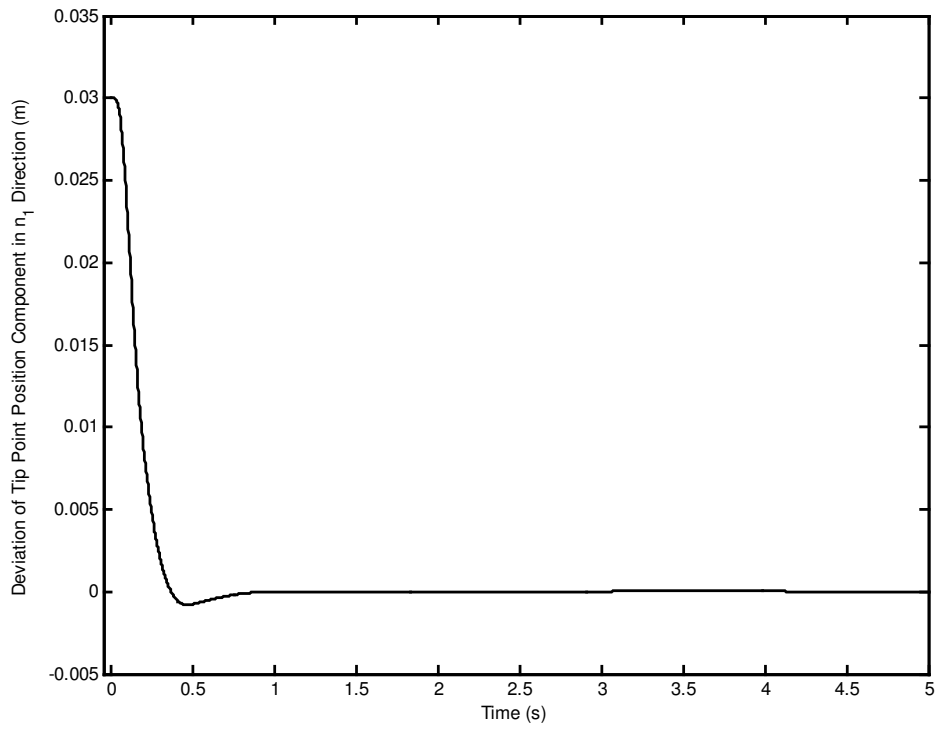


Figure 5.29 Deviation of tip point position component in n_1 direction.

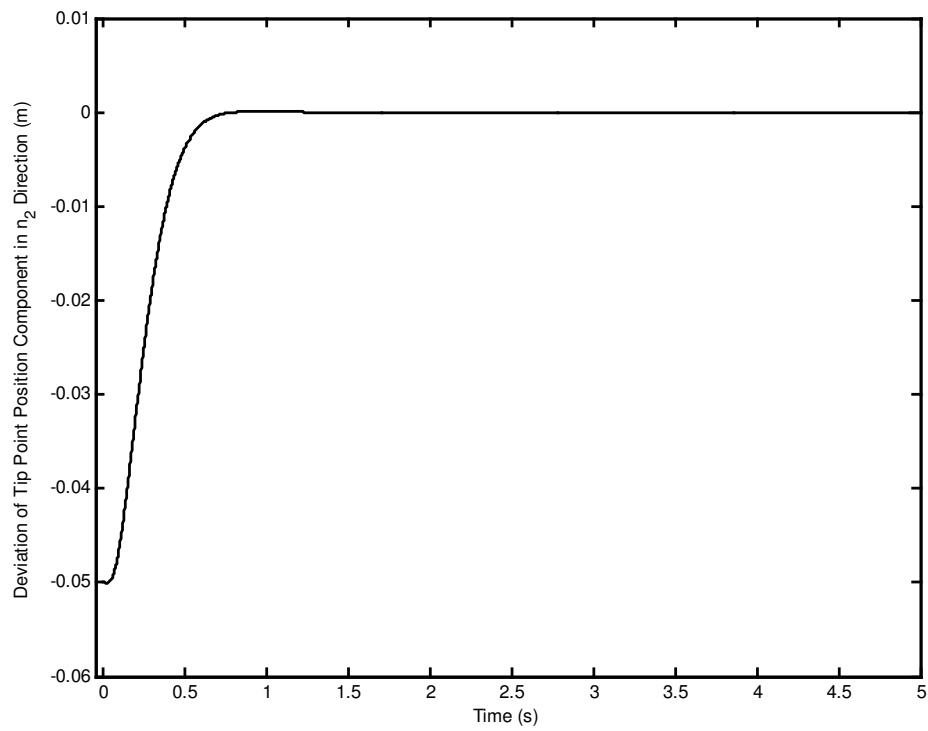


Figure 5.30 Deviation of tip point position component in n_2 direction.

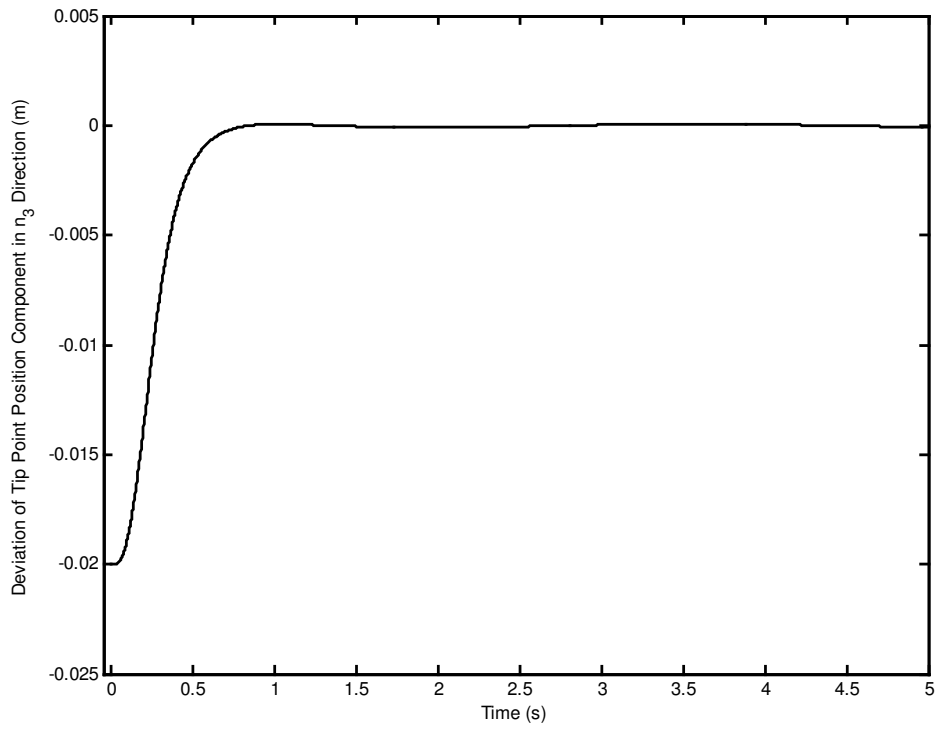


Figure 5.31 Deviation of tip point position component in n_3 direction.

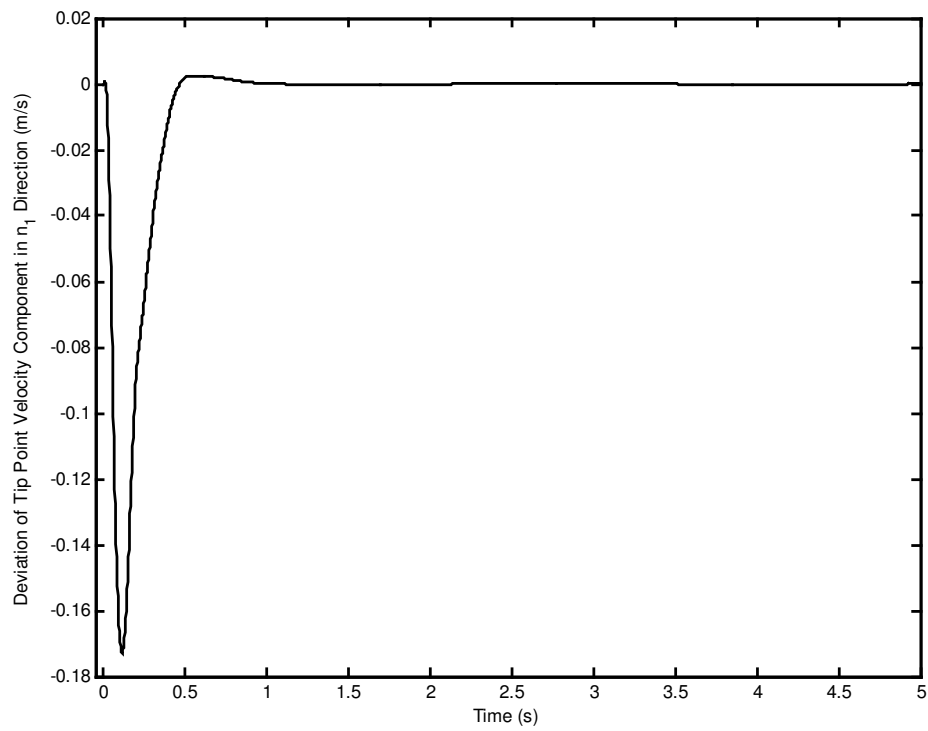


Figure 5.32 Deviation of tip point velocity component in n_1 direction.

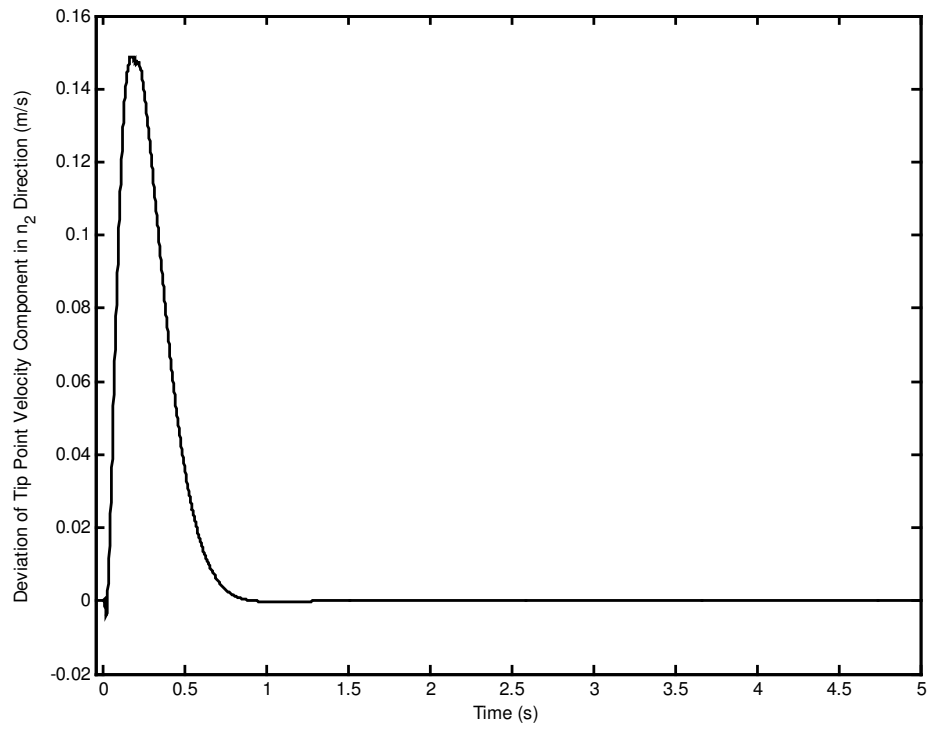


Figure 5.33 Deviation of tip point velocity component in n_2 direction.

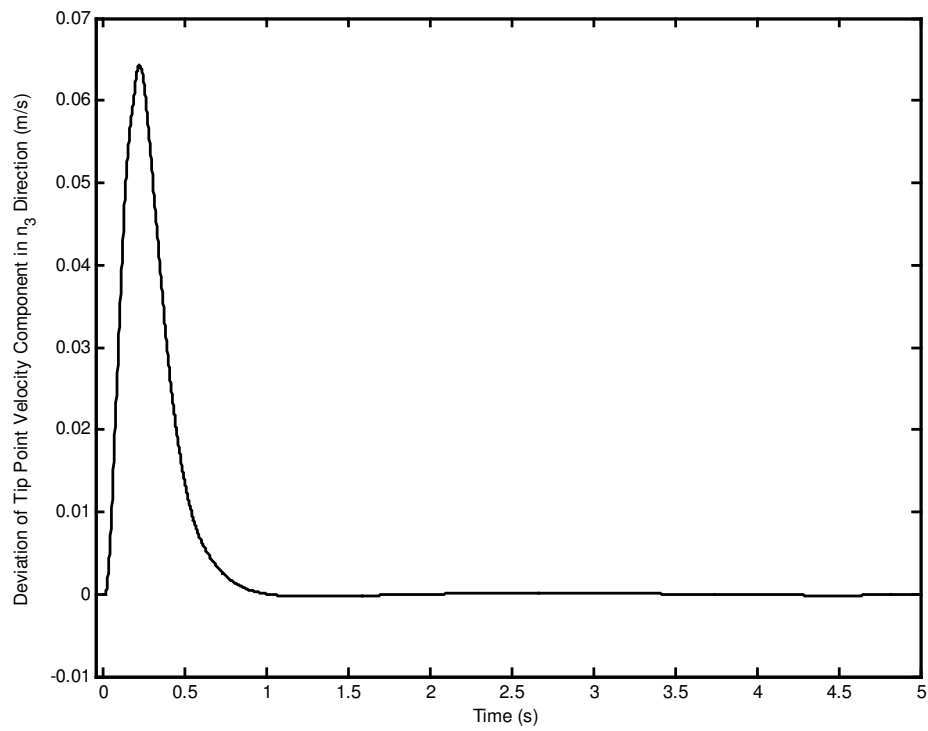


Figure 5.34 Deviation of tip point velocity component in n_3 direction.

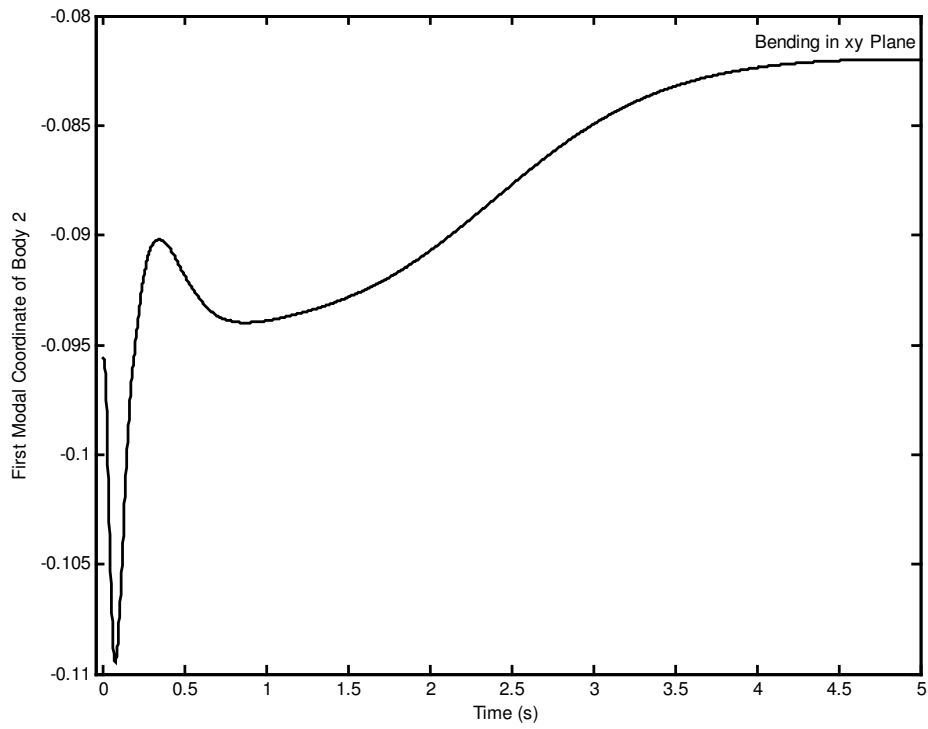


Figure 5.35 First modal coordinate of body 2 for bending in xy plane.

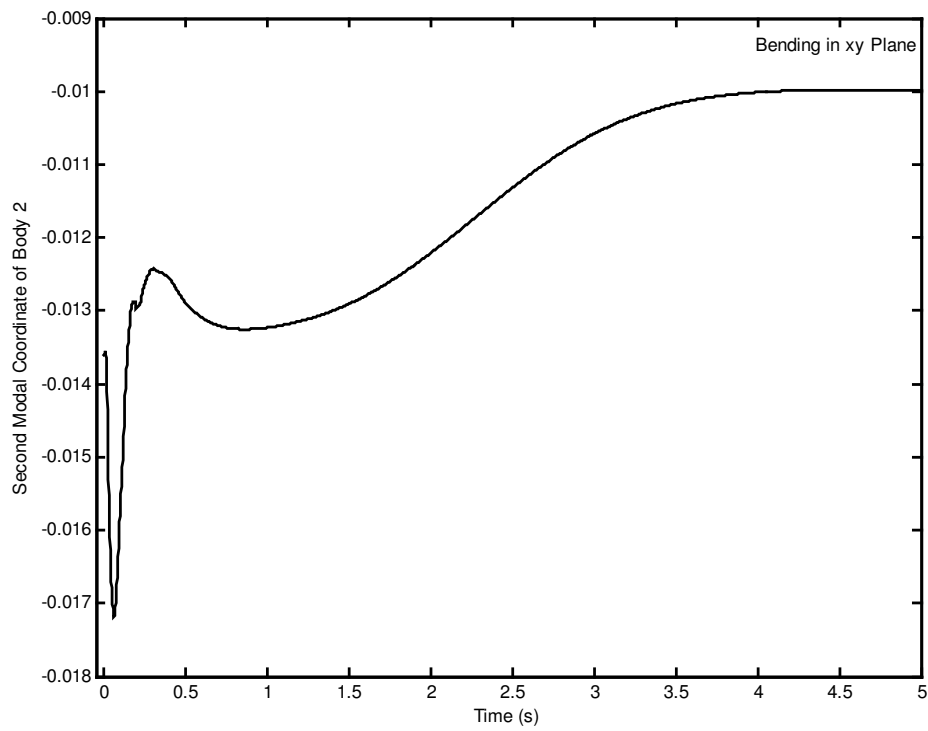


Figure 5.36 Second modal coordinate of body 2 for bending in xy plane.

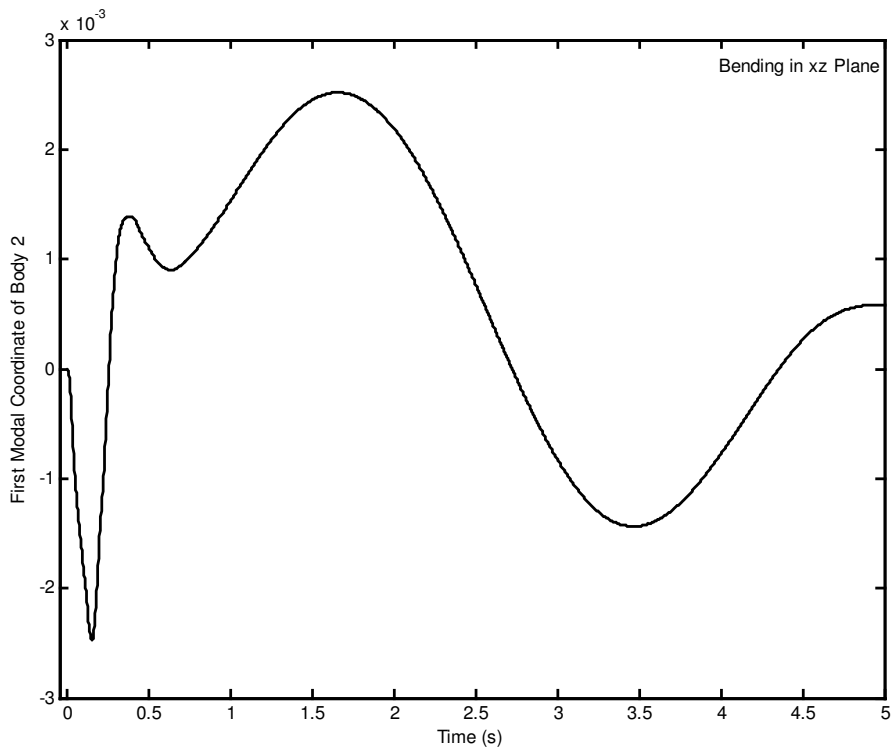


Figure 5.37 First modal coordinate of body 2 for bending in xz plane.

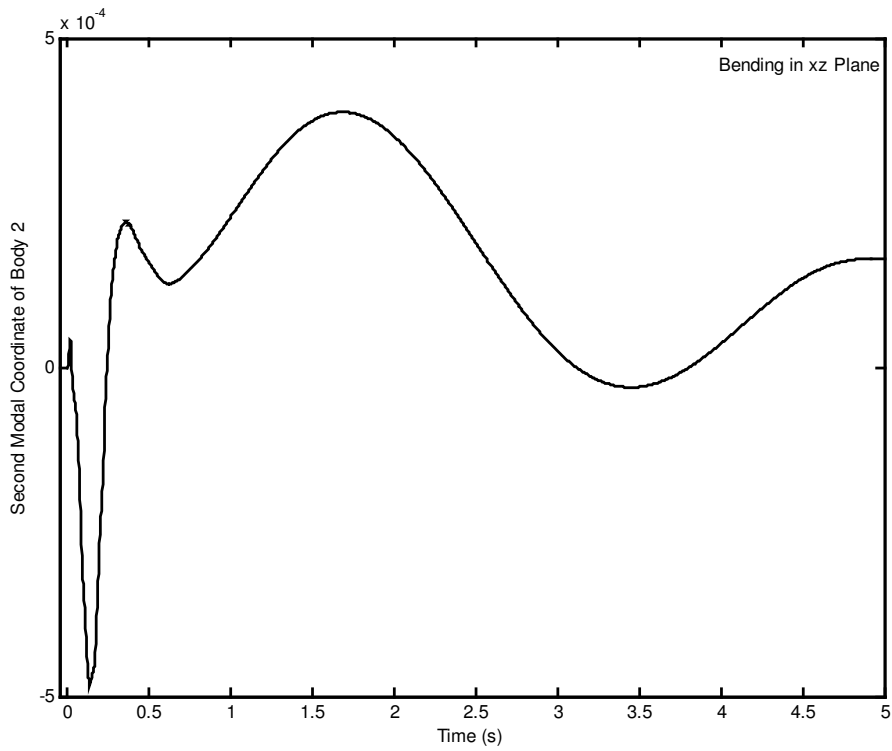


Figure 5.38 Second modal coordinate of body 2 for bending in xz plane.

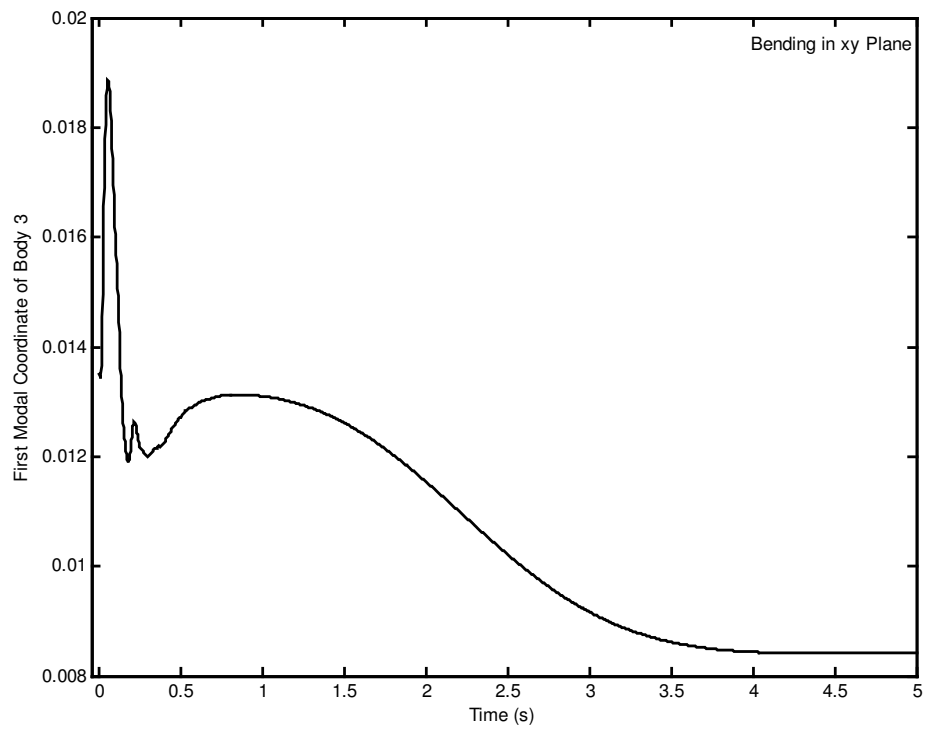


Figure 5.39 First modal coordinate of body 3 for bending in xy plane.

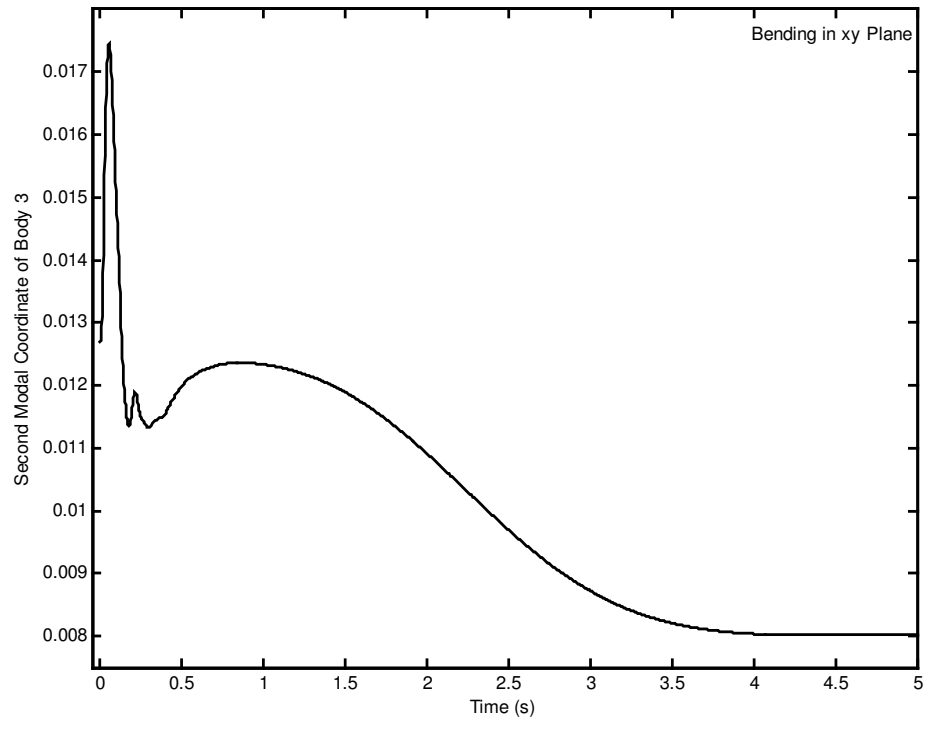


Figure 5.40 Second modal coordinate of body 3 for bending in xy plane.

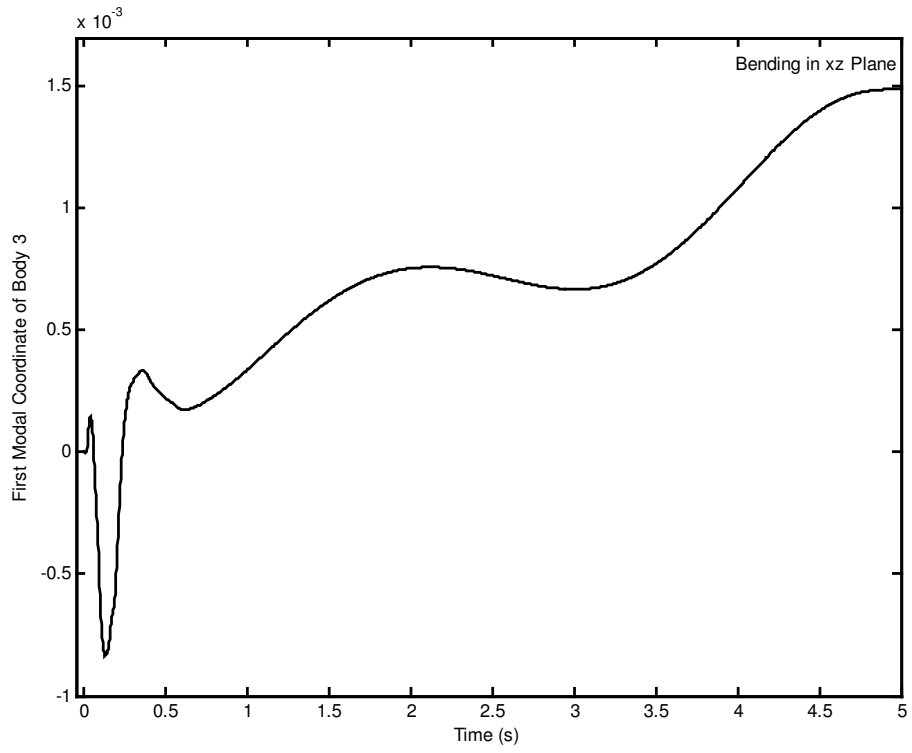


Figure 5.41 First modal coordinate of body 3 for bending in xz plane.

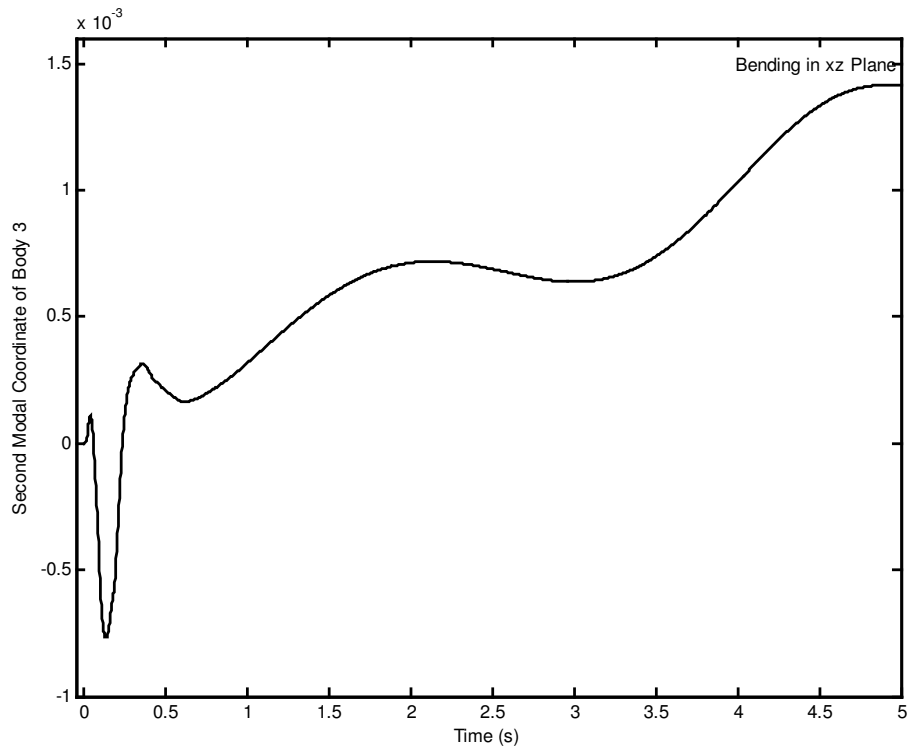


Figure 5.42 Second modal coordinate of body 3 for bending in xz plane.

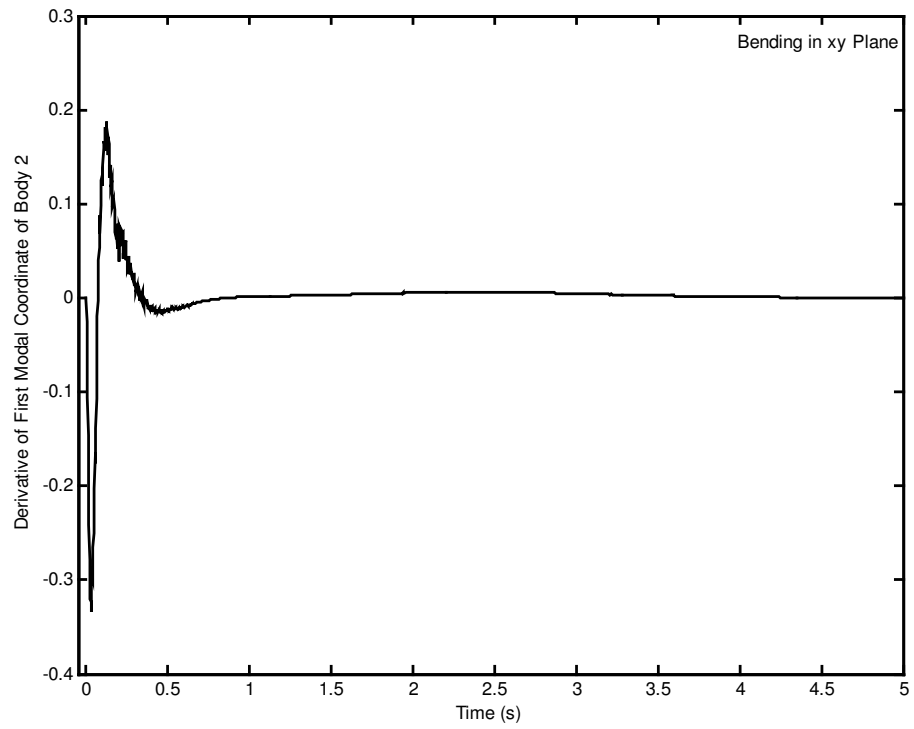


Figure 5.43 Derivative of first modal coordinate of body 2 for bending in xy plane.

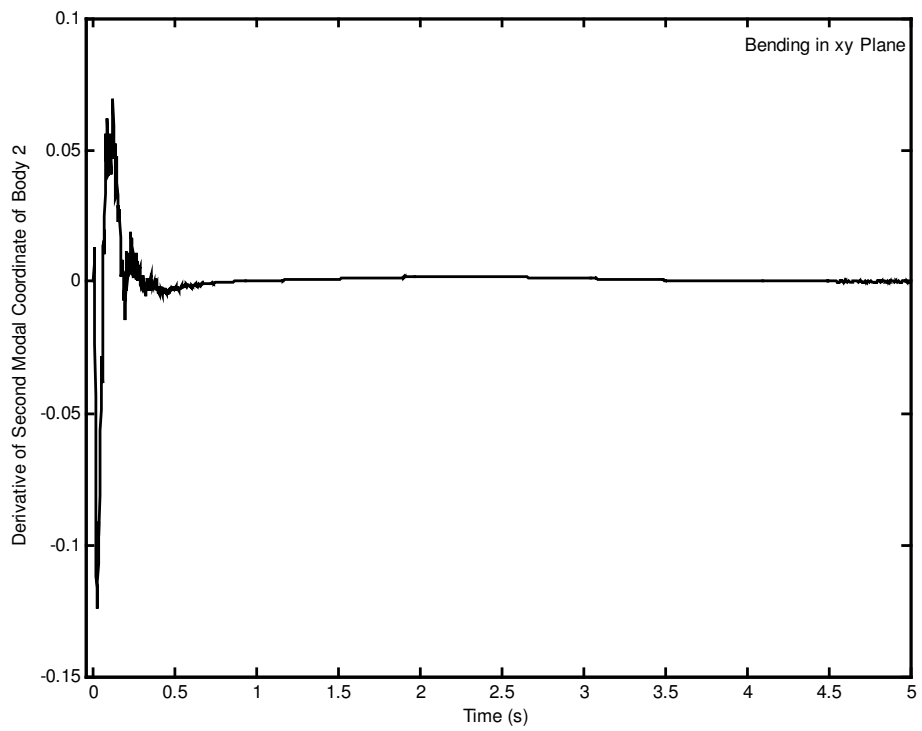


Figure 5.44 Derivative of second modal coordinate of body 2 for bending in xy plane.

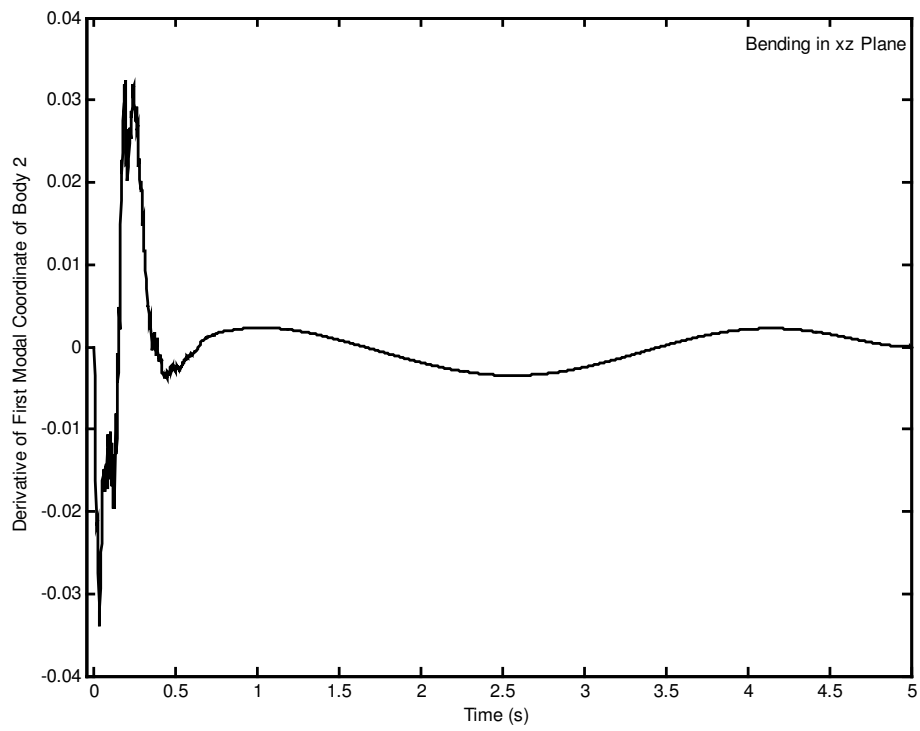


Figure 5.45 Derivative of first modal coordinate of body 2 for bending in xz plane.

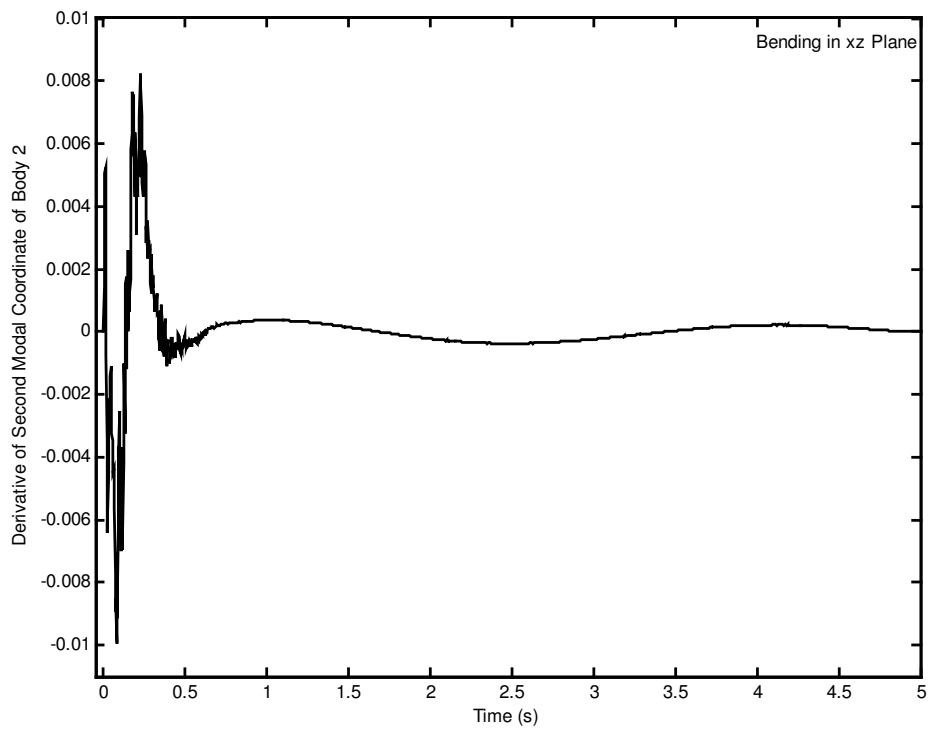


Figure 5.46 Derivative of second modal coordinate of body 2 for bending in xz plane.

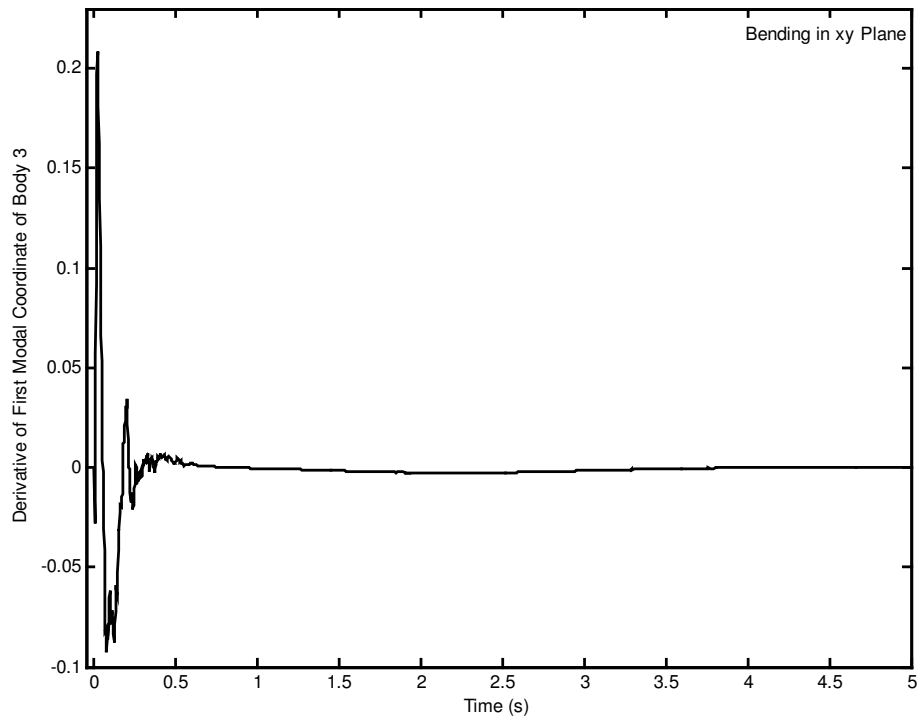


Figure 5.47 Derivative of first modal coordinate of body 3 for bending in xy plane.

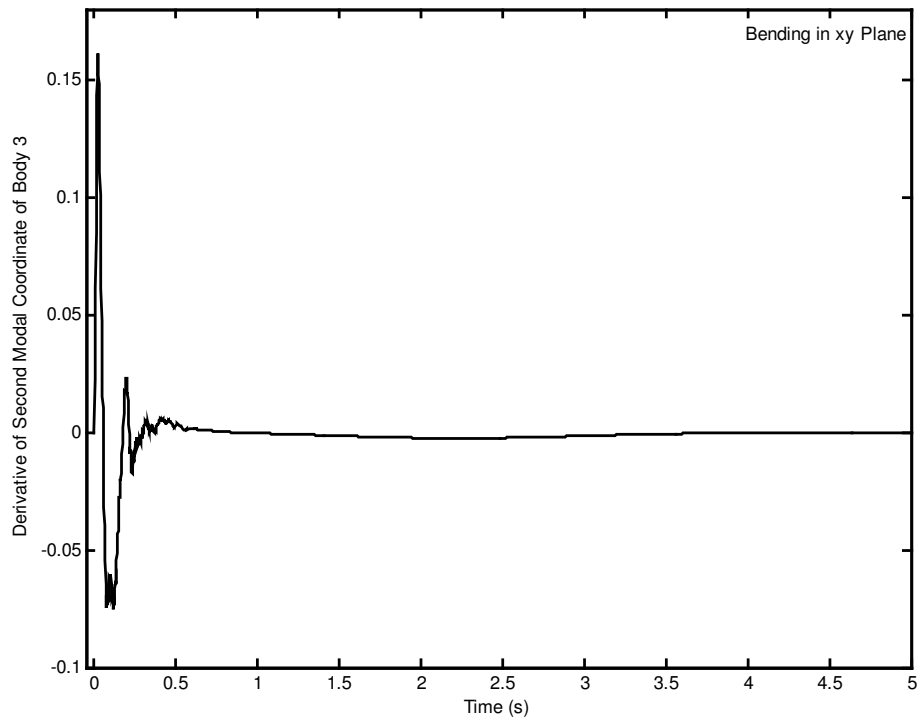


Figure 5.48 Derivative of second modal coordinate of body 3 for bending in xy plane.

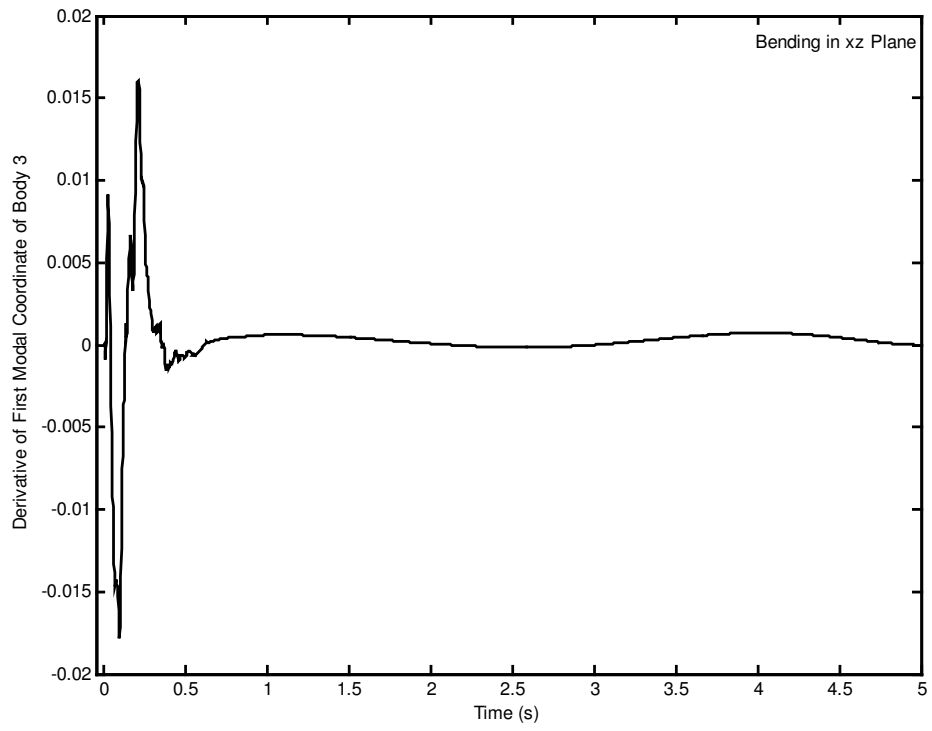


Figure 5.49 Derivative of first modal coordinate of body 3 for bending in xz plane.

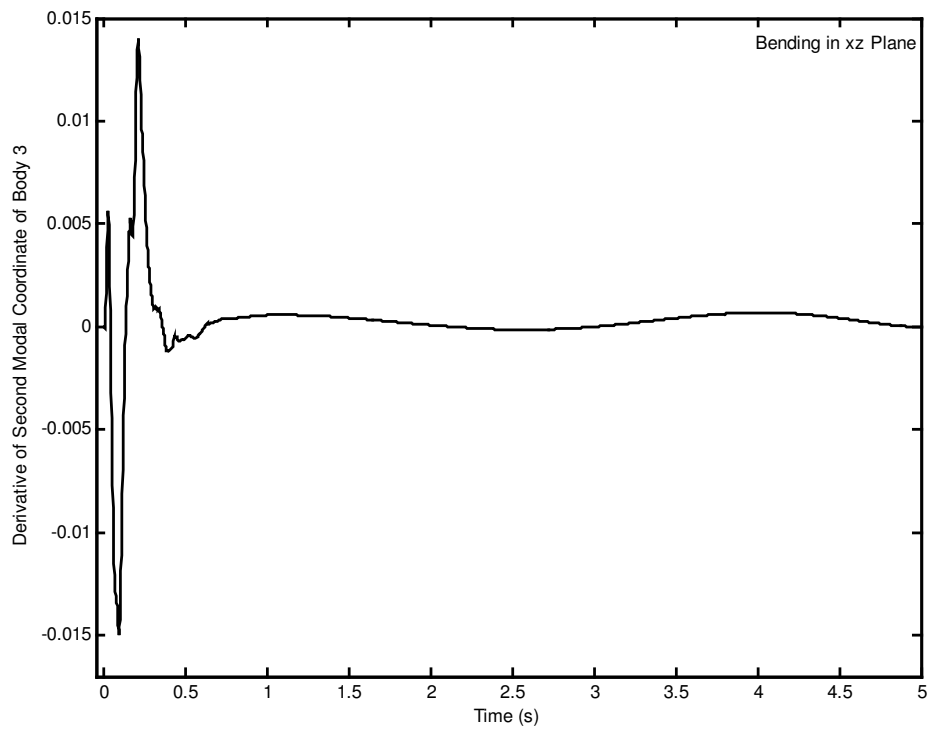


Figure 5.50 Derivative of second modal coordinate of body 3 for bending in xz plane.

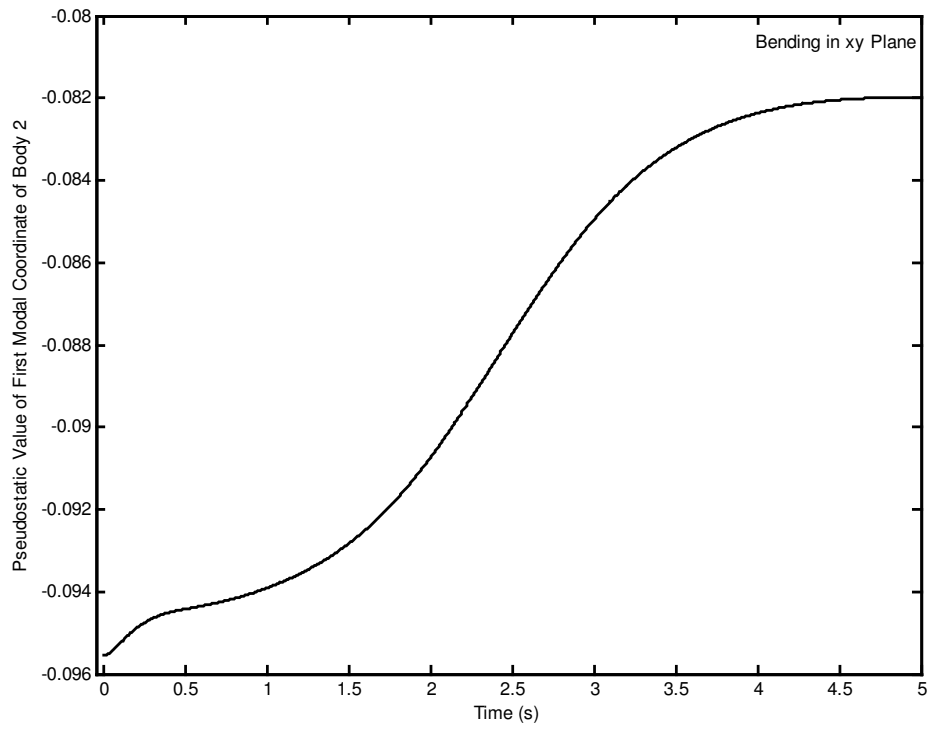


Figure 5.51 Pseudostatic value of first modal coordinate of body 2 for bending in xy plane.

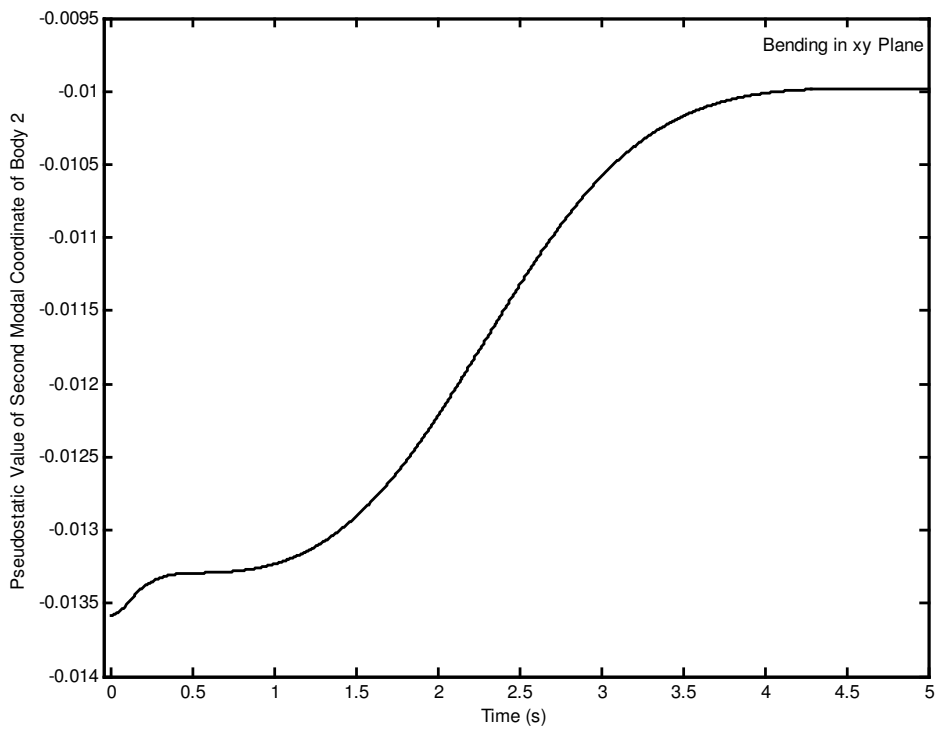


Figure 5.52 Pseudostatic value of second modal coordinate of body 2 for bending in xy plane.

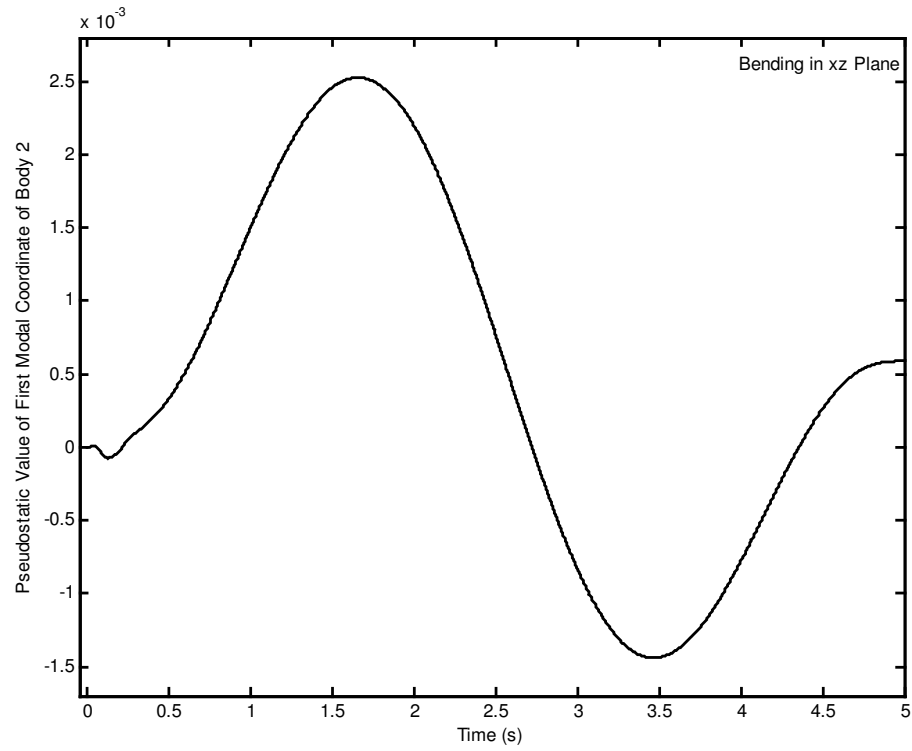


Figure 5.53 Pseudostatic value of first modal coordinate of body 2 for bending in xz plane.

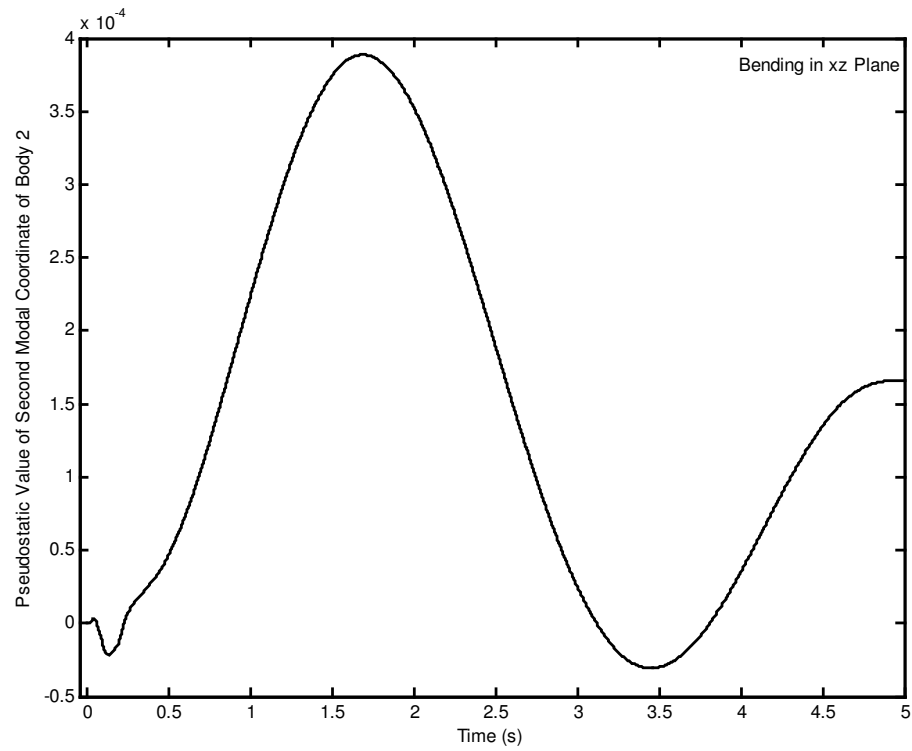


Figure 5.54 Pseudostatic value of second modal coordinate of body 2 for bending in xz plane.

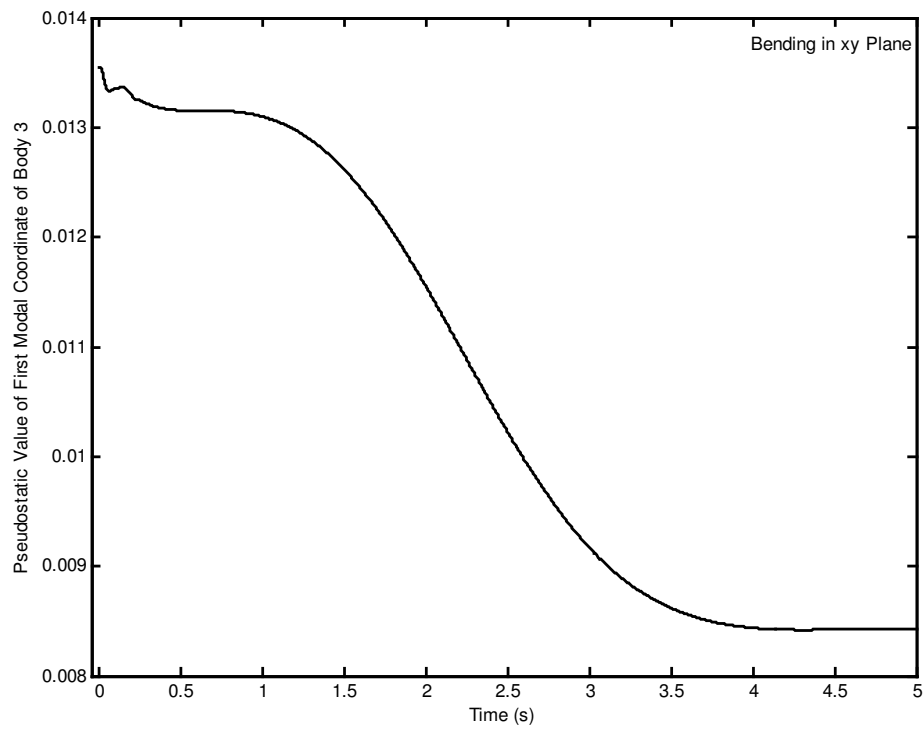


Figure 5.55 Pseudostatic value of first modal coordinate of body 3 for bending in xy plane.

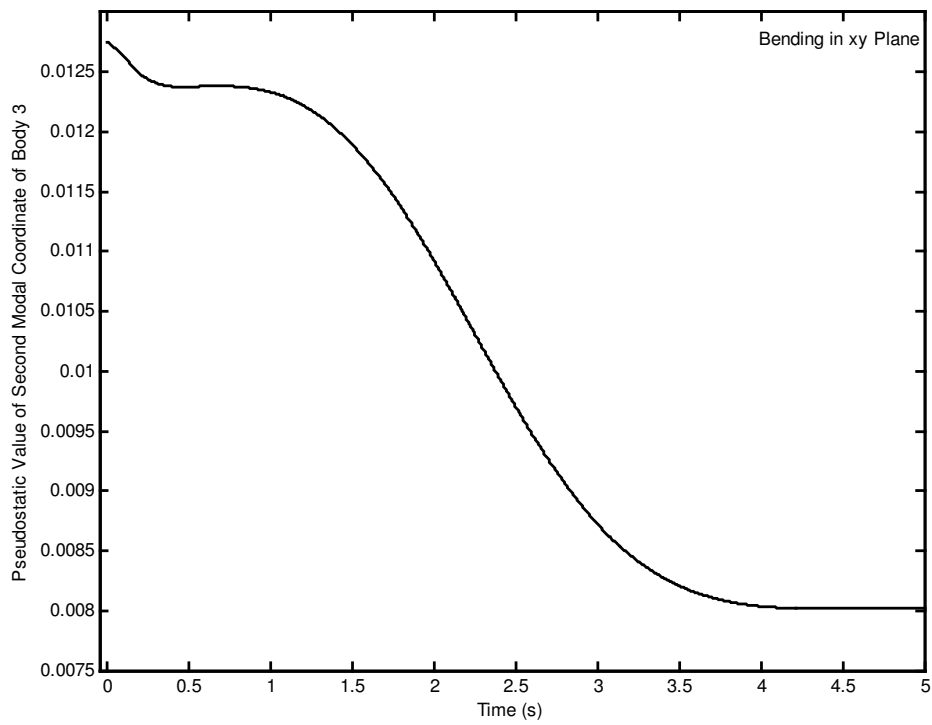


Figure 5.56 Pseudostatic value of second modal coordinate of body 3 for bending in xy plane.

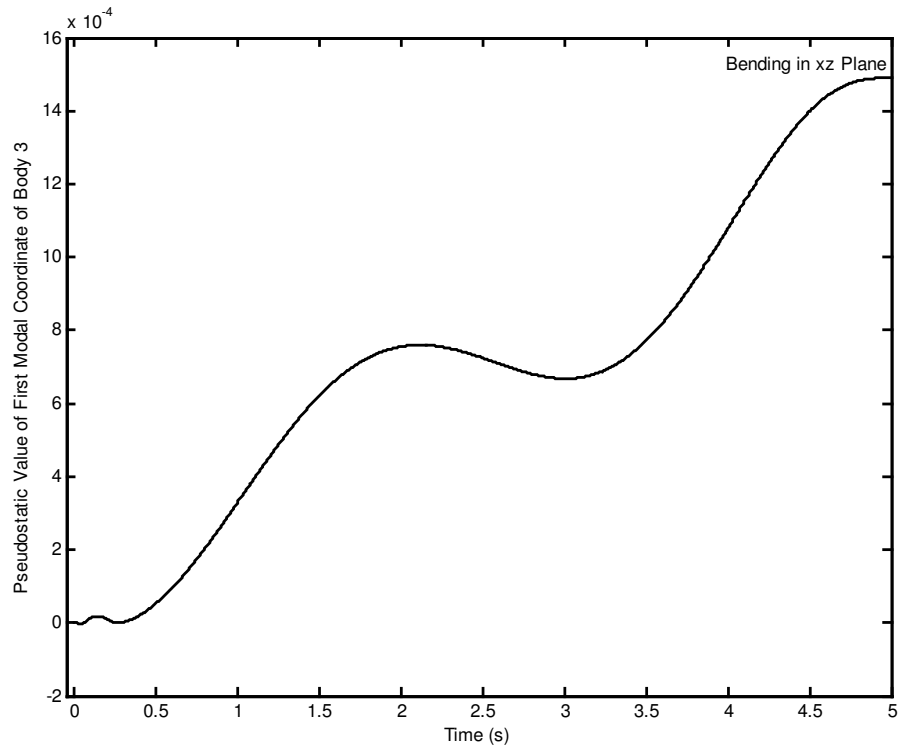


Figure 5.57 Pseudostatic value of first modal coordinate of body 3 for bending in xz plane.

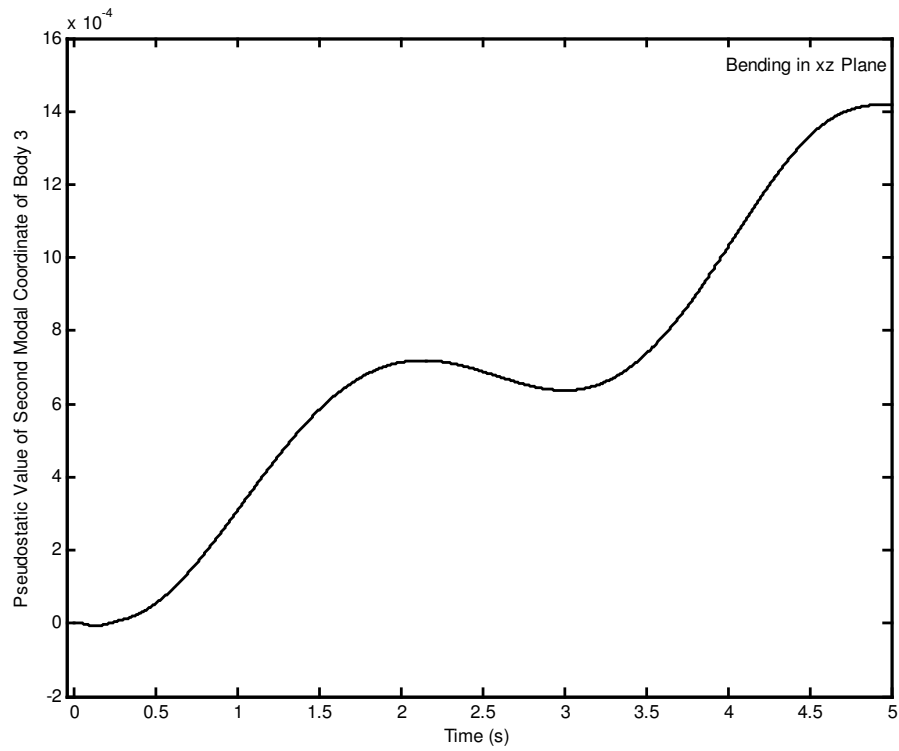


Figure 5.58 Pseudostatic value of second modal coordinate of body 3 for bending in xz plane.

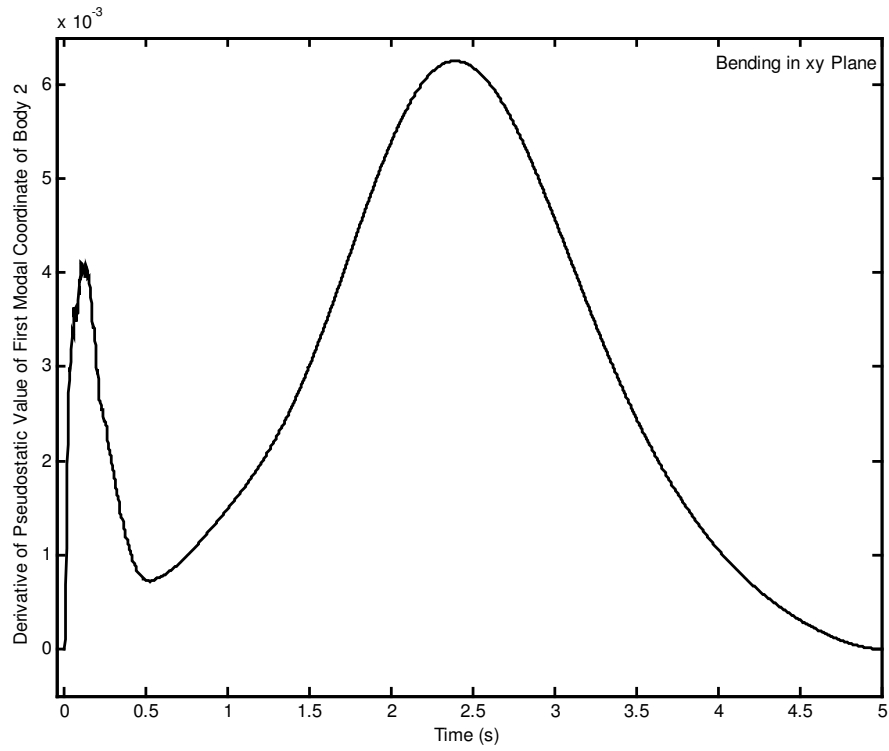


Figure 5.59 Derivative of pseudostatic value of first modal coordinate of body 2 for bending in xy plane.

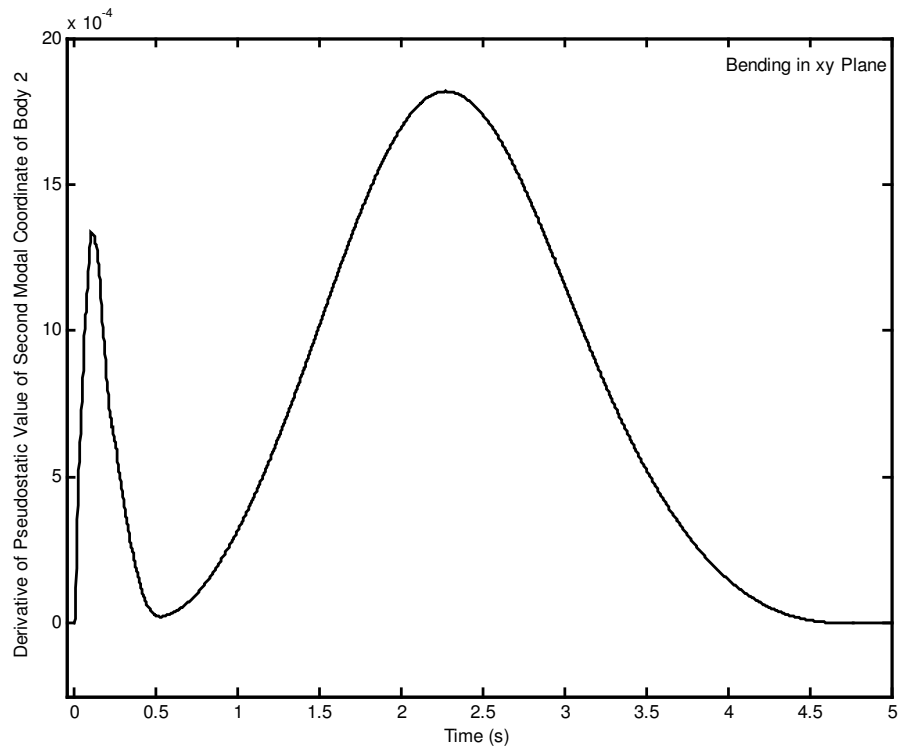


Figure 5.60 Derivative of pseudostatic value of second modal coordinate of body 2 for bending in xy plane.

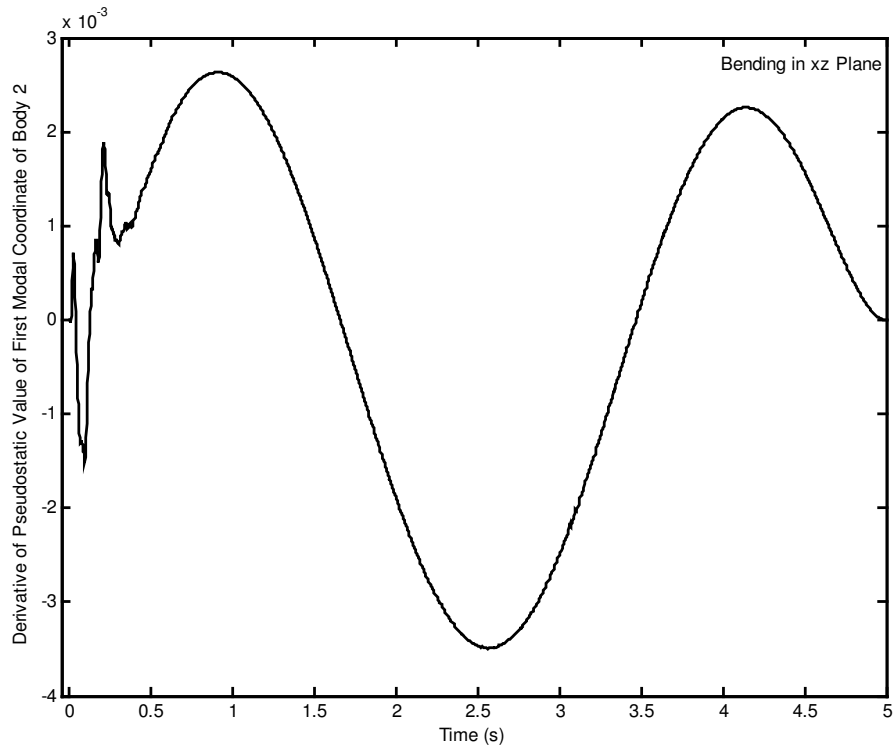


Figure 5.61 Derivative of pseudostatic value of first modal coordinate of body 2 for bending in xz plane.

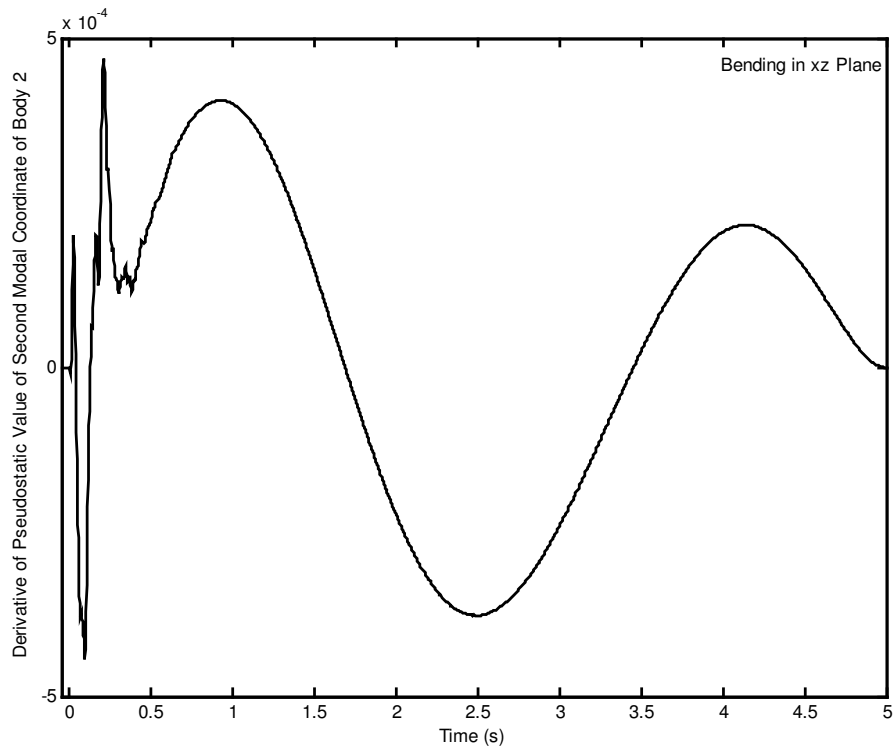


Figure 5.62 Derivative of pseudostatic value of second modal coordinate of body 2 for bending in xz plane.

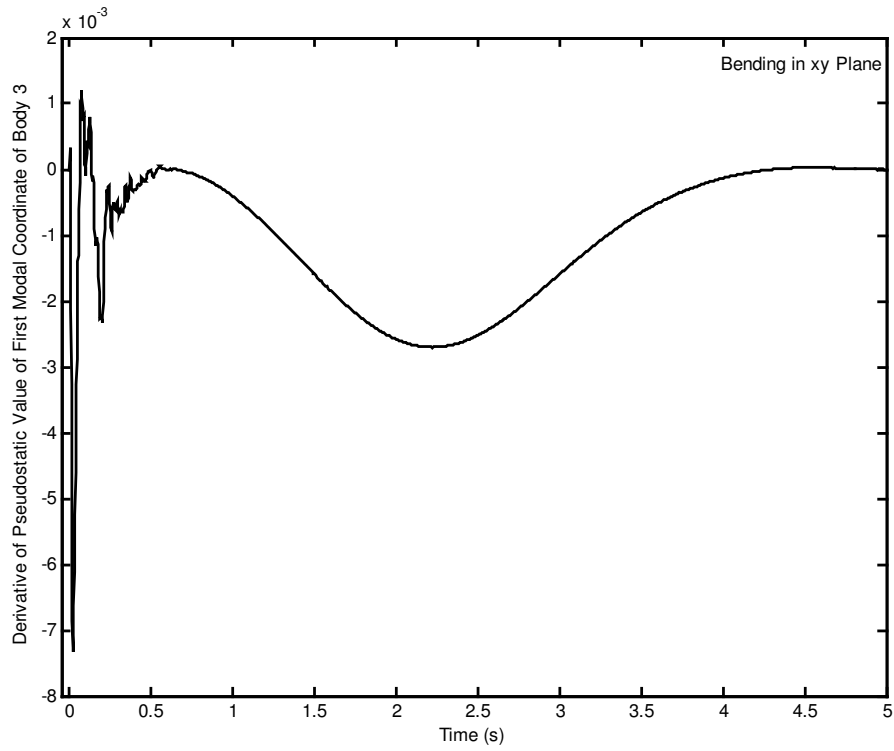


Figure 5.63 Derivative of pseudostatic value of first modal coordinate of body 3 for bending in xy plane.

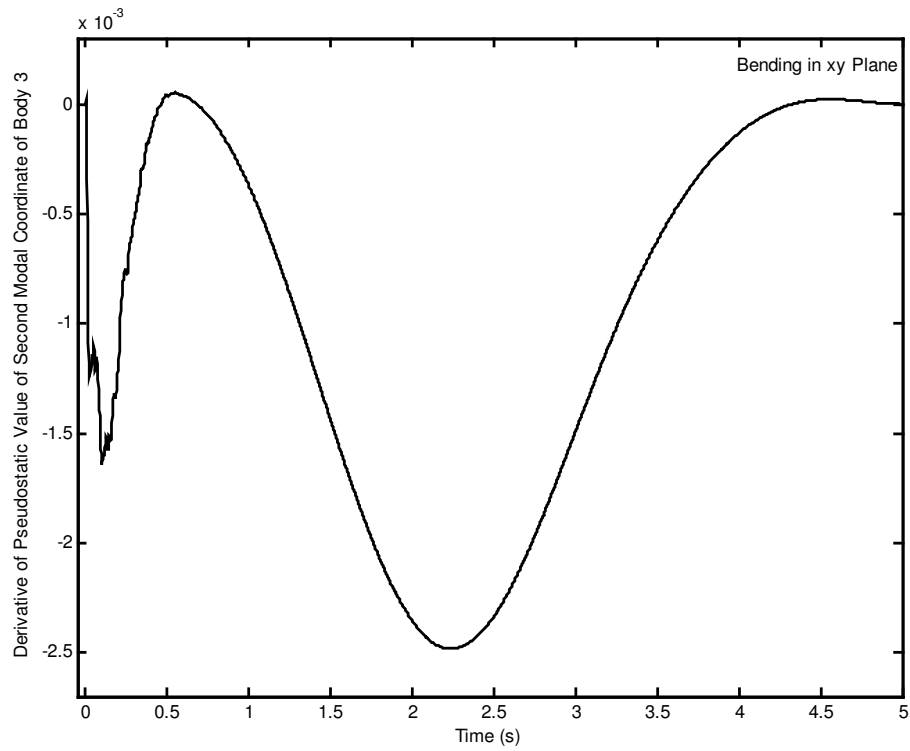


Figure 5.64 Derivative of pseudostatic value of second modal coordinate of body 3 for bending in xy plane.

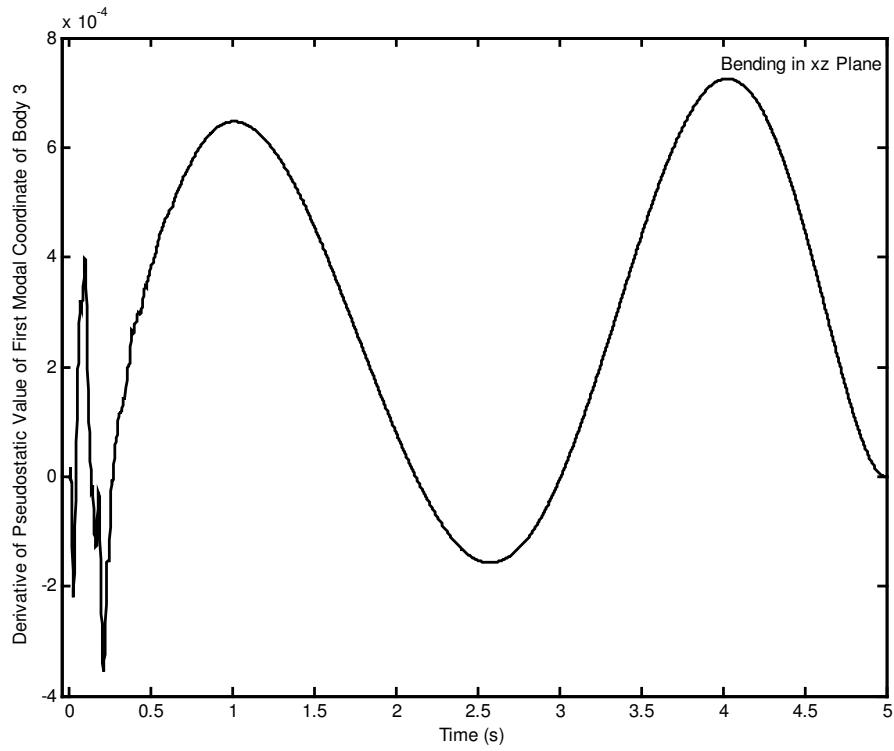


Figure 5.65 Derivative of pseudostatic value of first modal coordinate of body 3 for bending in xz plane.

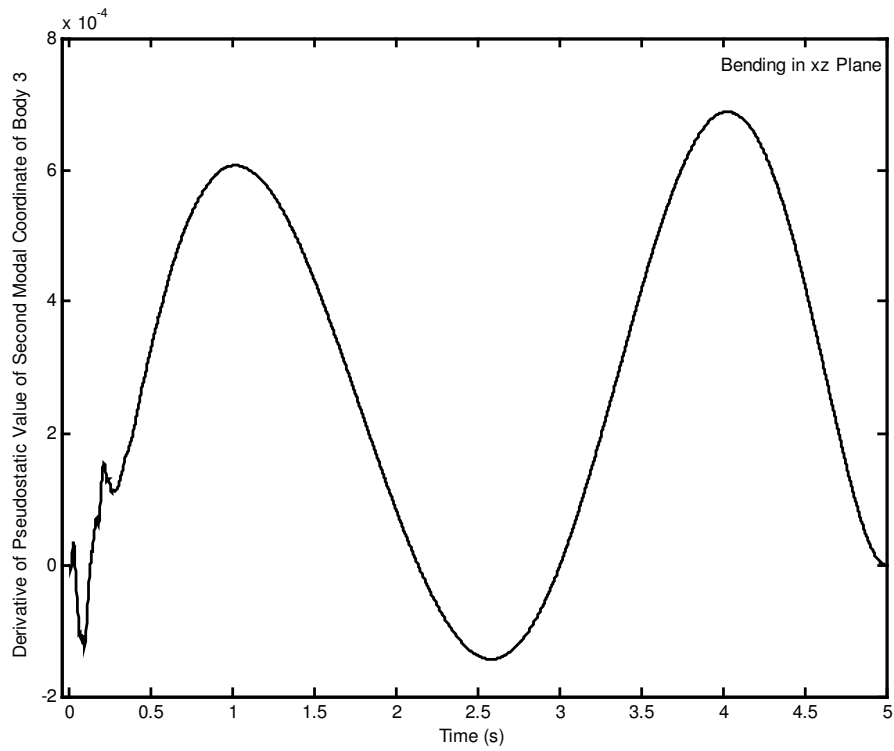


Figure 5.66 Derivative of pseudostatic value of second modal coordinate of body 3 for bending in xz plane.

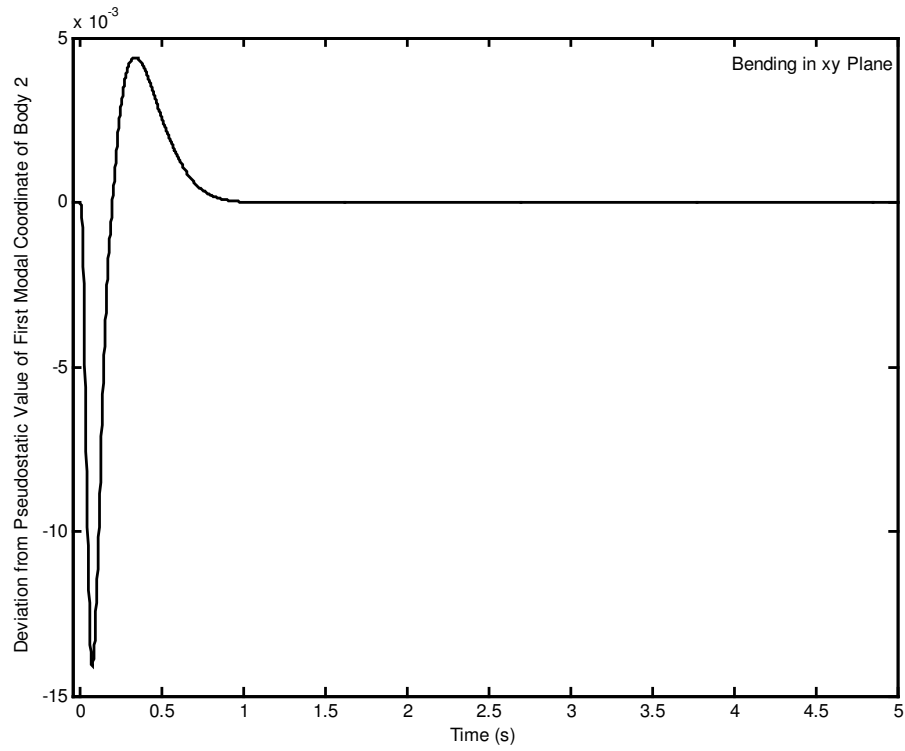


Figure 5.67 Deviation from pseudostatic value of first modal coordinate of body 2 for bending in xy plane.

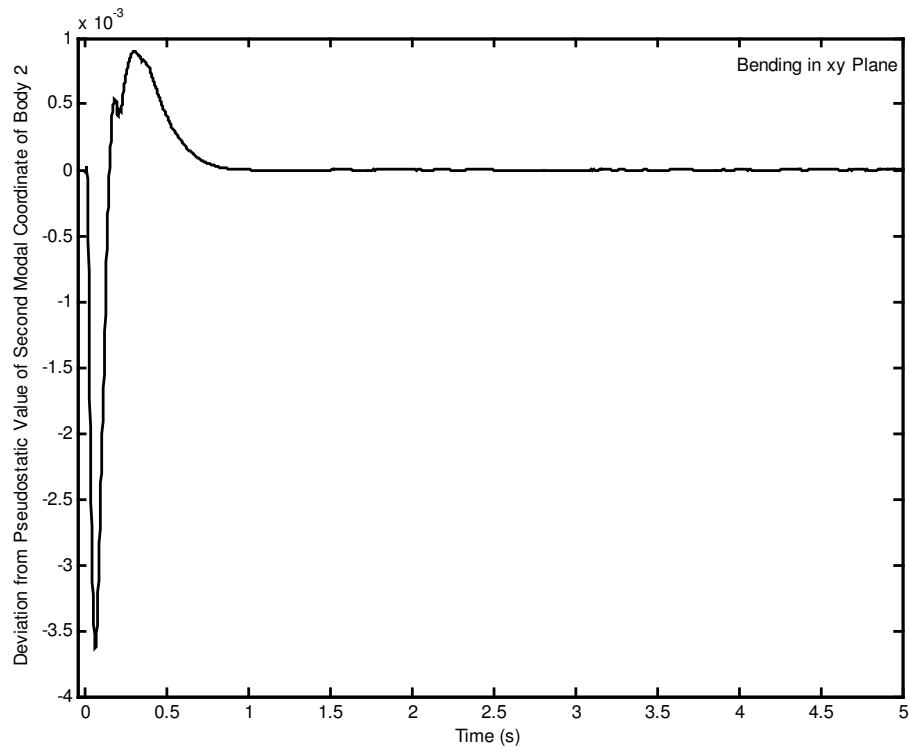


Figure 5.68 Deviation from pseudostatic value of second modal coordinate of body 2 for bending in xy plane.

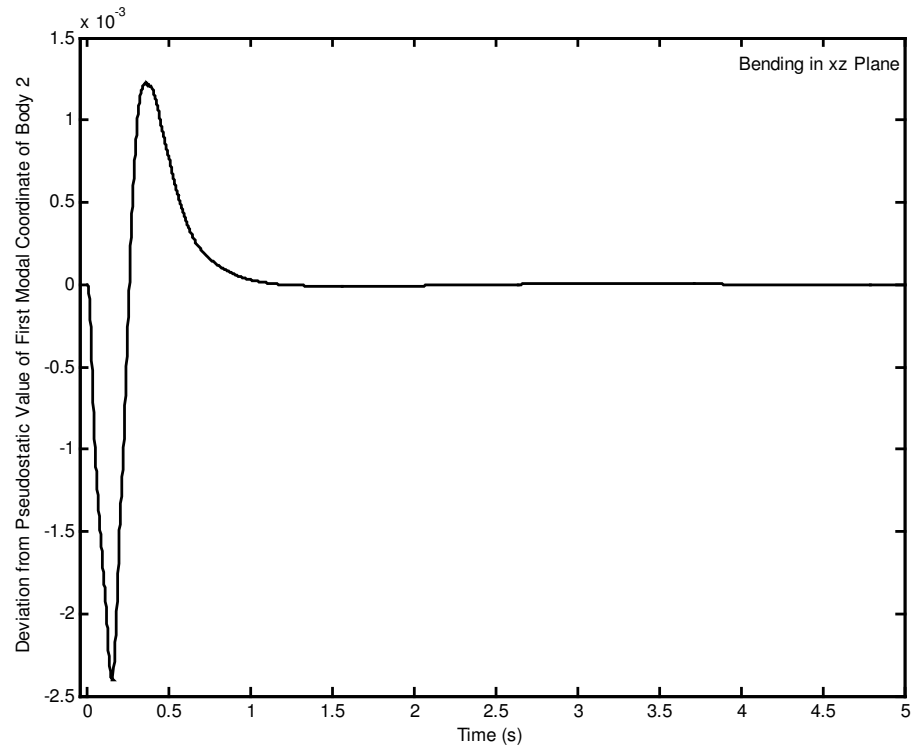


Figure 5.69 Deviation from pseudostatic value of first modal coordinate of body 2 for bending in xz plane.

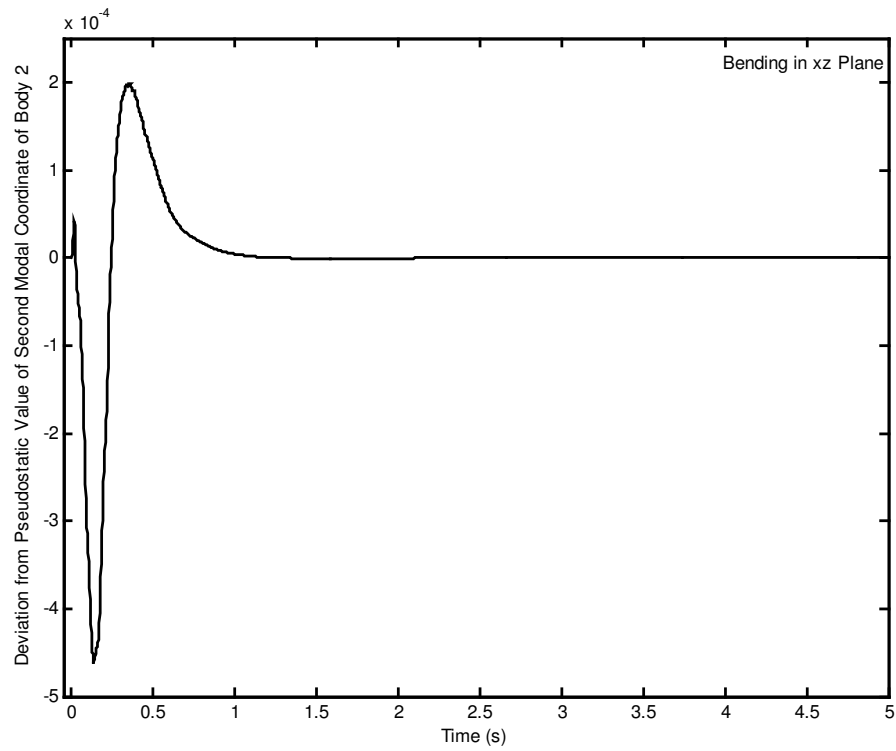


Figure 5.70 Deviation from pseudostatic value of second modal coordinate of body 2 for bending in xz plane.

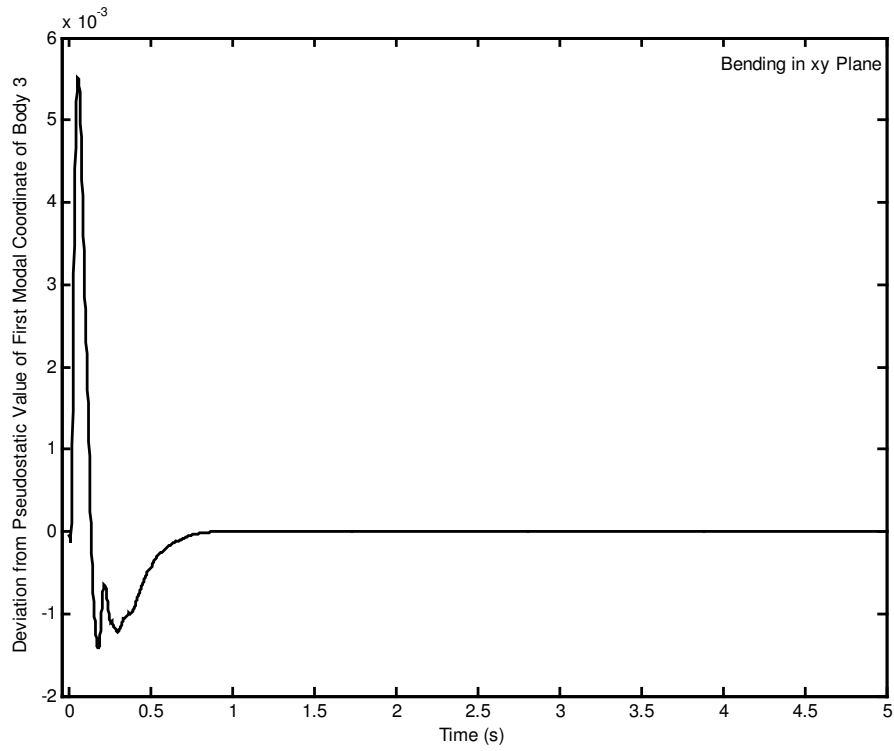


Figure 5.71 Deviation from pseudostatic value of first modal coordinate of body 3 for bending in xy plane.

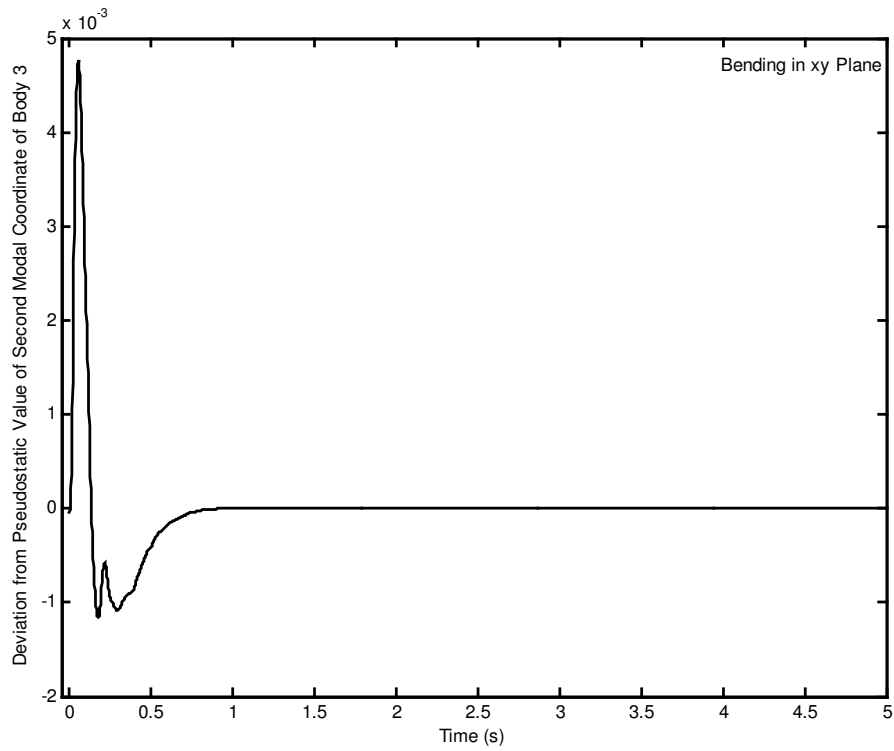


Figure 5.72 Deviation from pseudostatic value of second modal coordinate of body 3 for bending in xy plane.

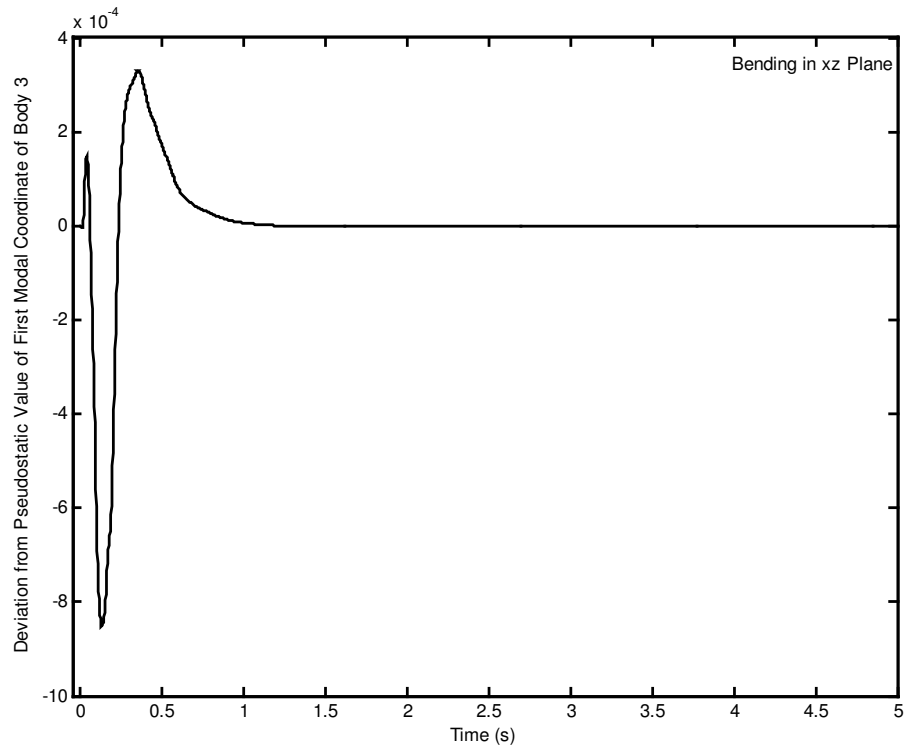


Figure 5.73 Deviation from pseudostatic value of first modal coordinate of body 3 for bending in xz plane.

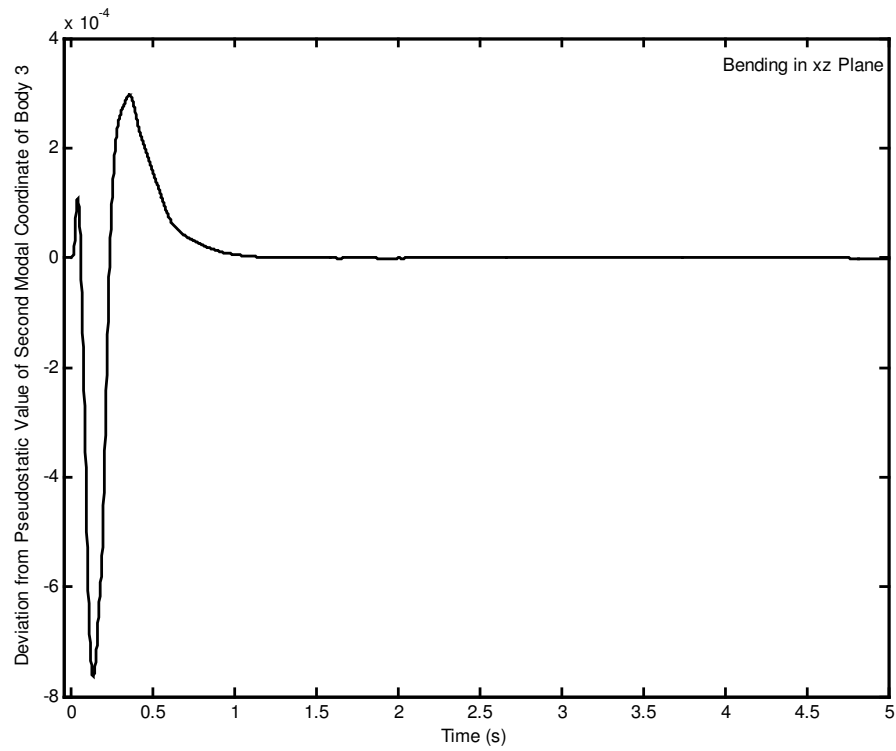


Figure 5.74 Deviation from pseudostatic value of second modal coordinate of body 3 for bending in xz plane.

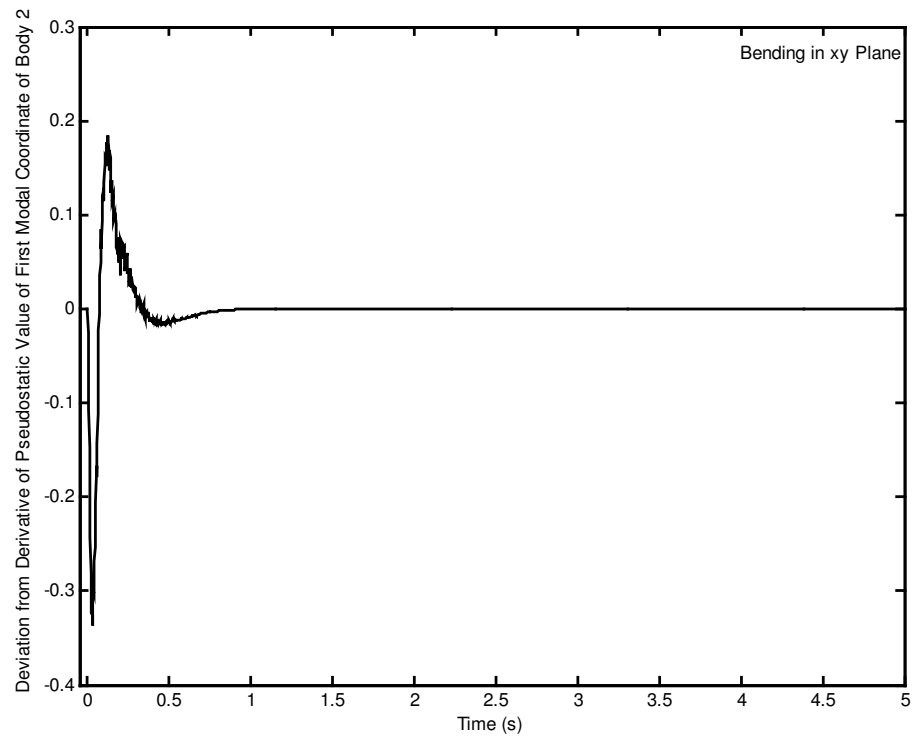


Figure 5.75 Deviation from derivative of pseudostatic value of first modal coordinate of body 2 for bending in xy plane.

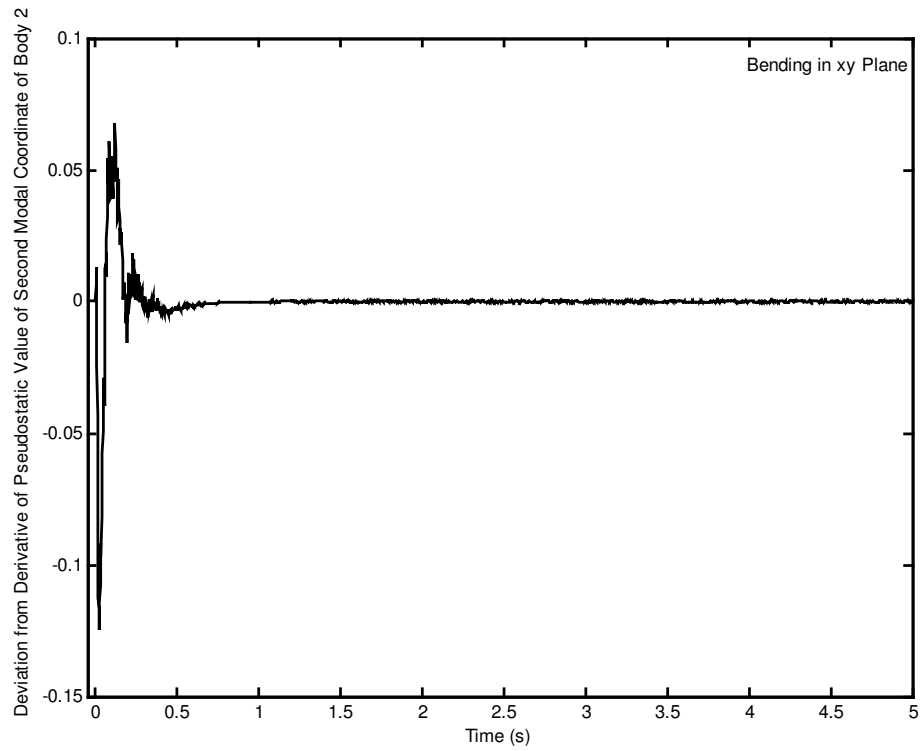


Figure 5.76 Deviation from derivative of pseudostatic value of second modal coordinate of body 2 for bending in xy plane.

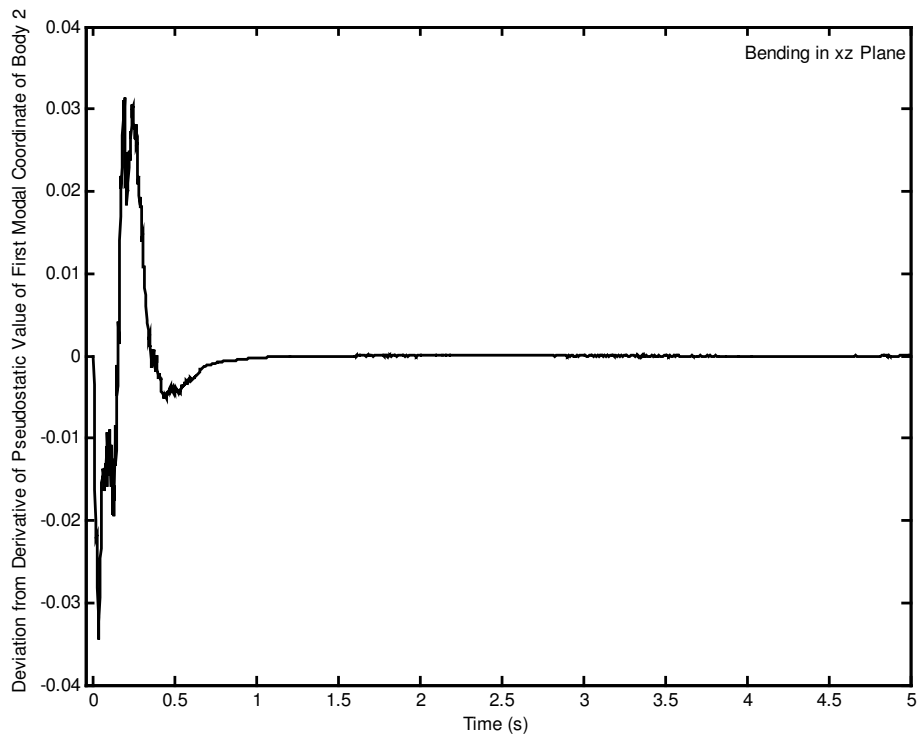


Figure 5.77 Deviation from derivative of pseudostatic value of first modal coordinate of body 2 for bending in xz plane.

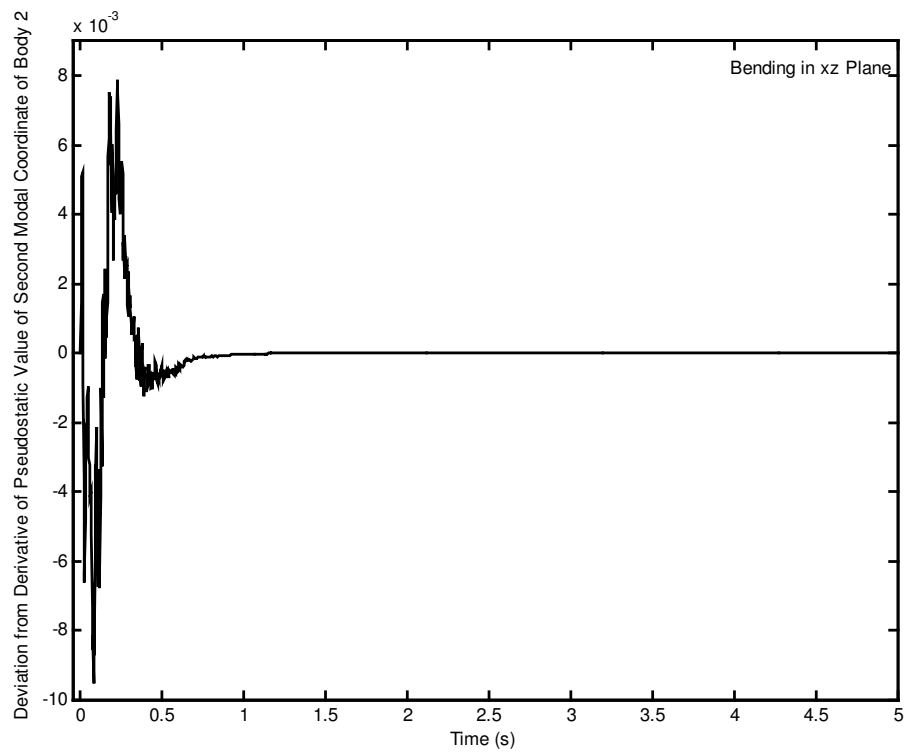


Figure 5.78 Deviation from derivative of pseudostatic value of second modal coordinate of body 2 for bending in xz plane.

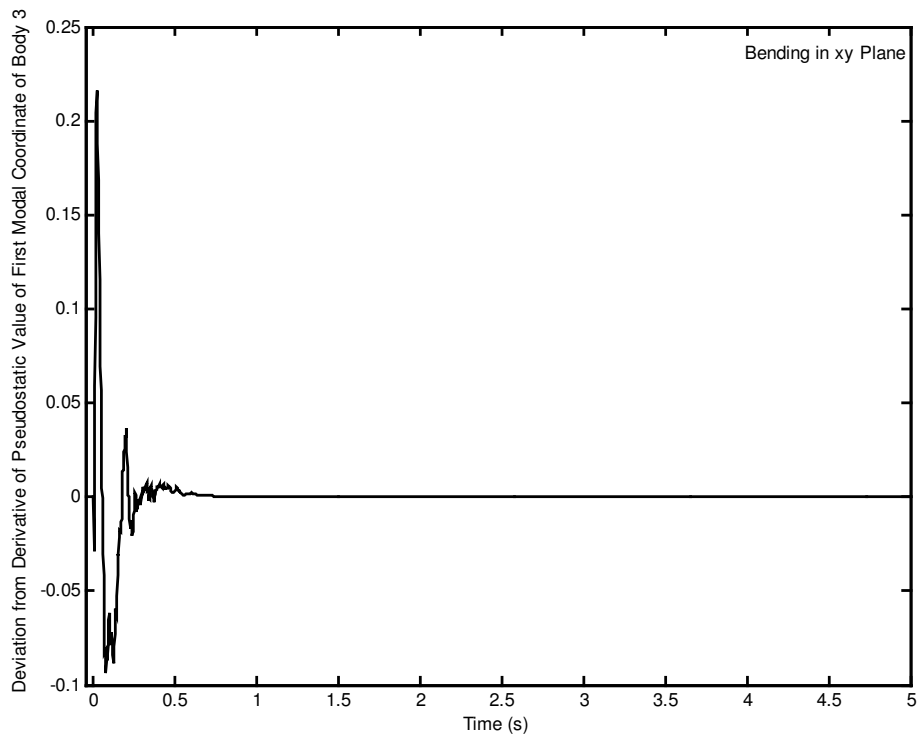


Figure 5.79 Deviation from derivative of pseudostatic value of first modal coordinate of body 3 for bending in xy plane.

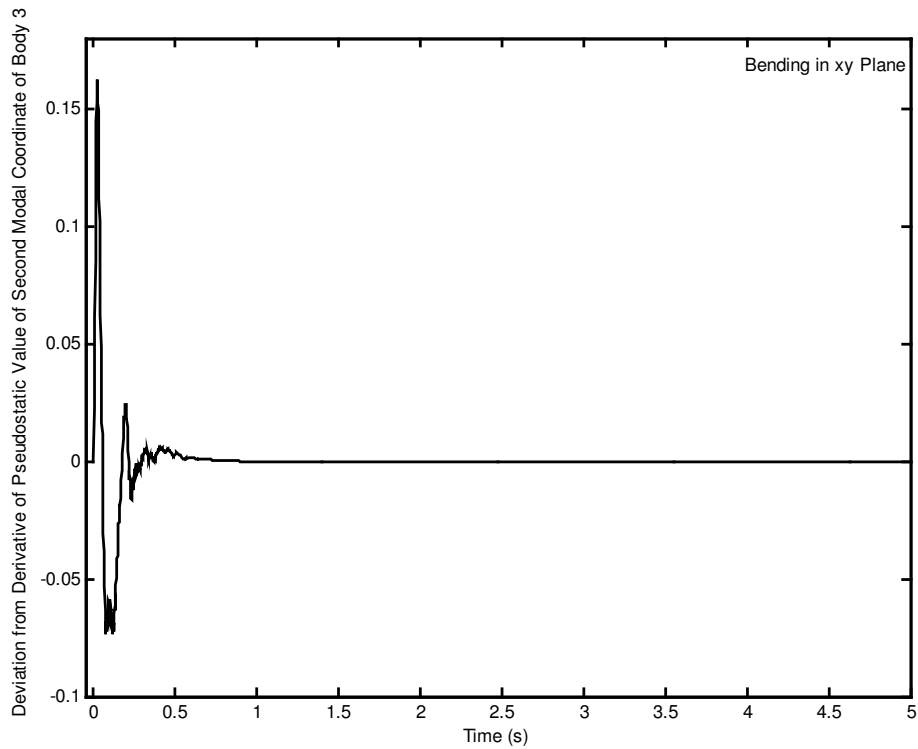


Figure 5.80 Deviation from derivative of pseudostatic value of second modal coordinate of body 3 for bending in xy plane.

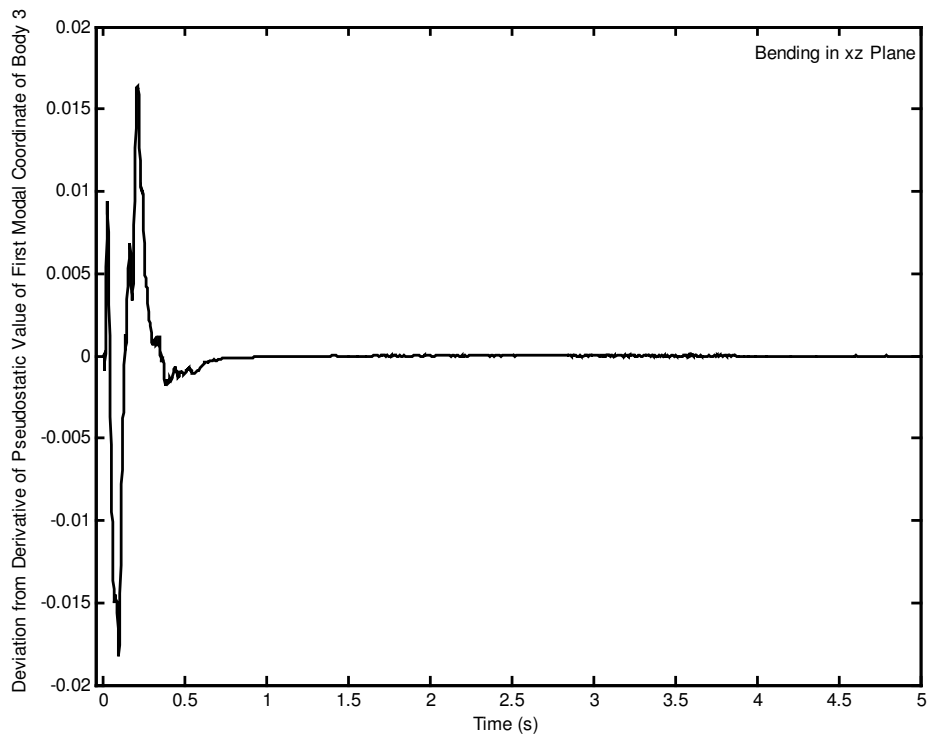


Figure 5.81 Deviation from derivative of pseudostatic value of first modal coordinate of body 3 for bending in xz plane.

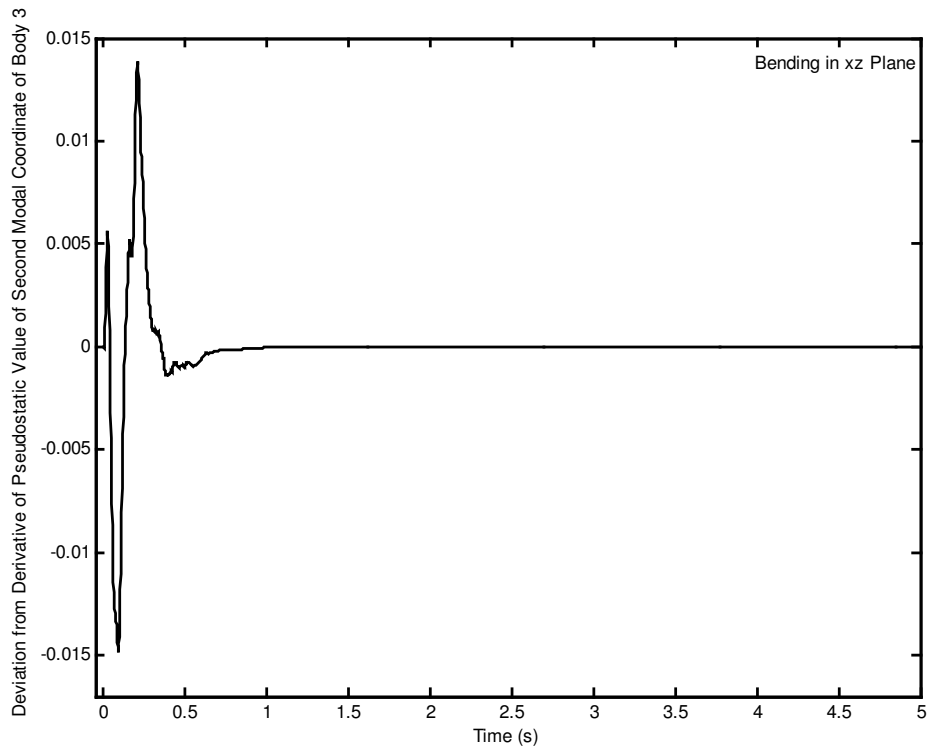


Figure 5.82 Deviation from derivative of pseudostatic value of second modal coordinate of body 3 for bending in xz plane.

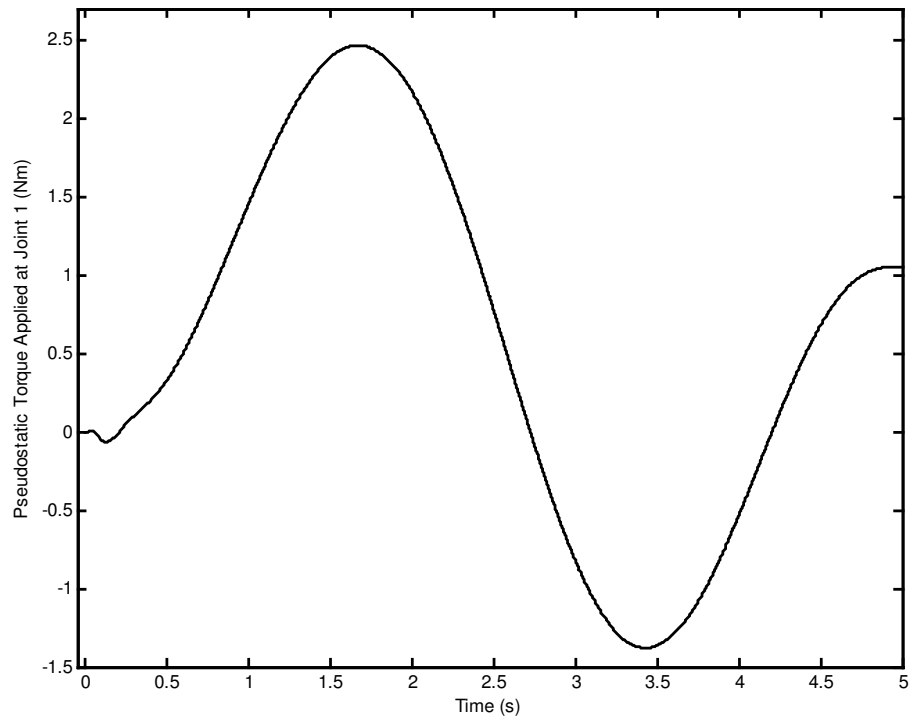


Figure 5.83 Pseudostatic torque applied at joint 1.

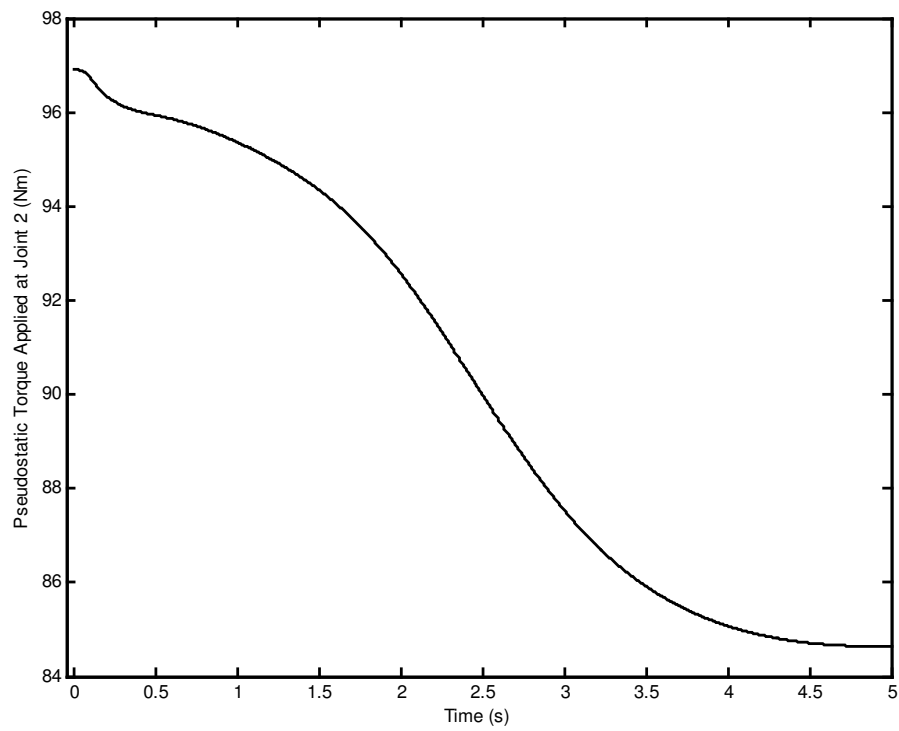


Figure 5.84 Pseudostatic torque applied at joint 2.

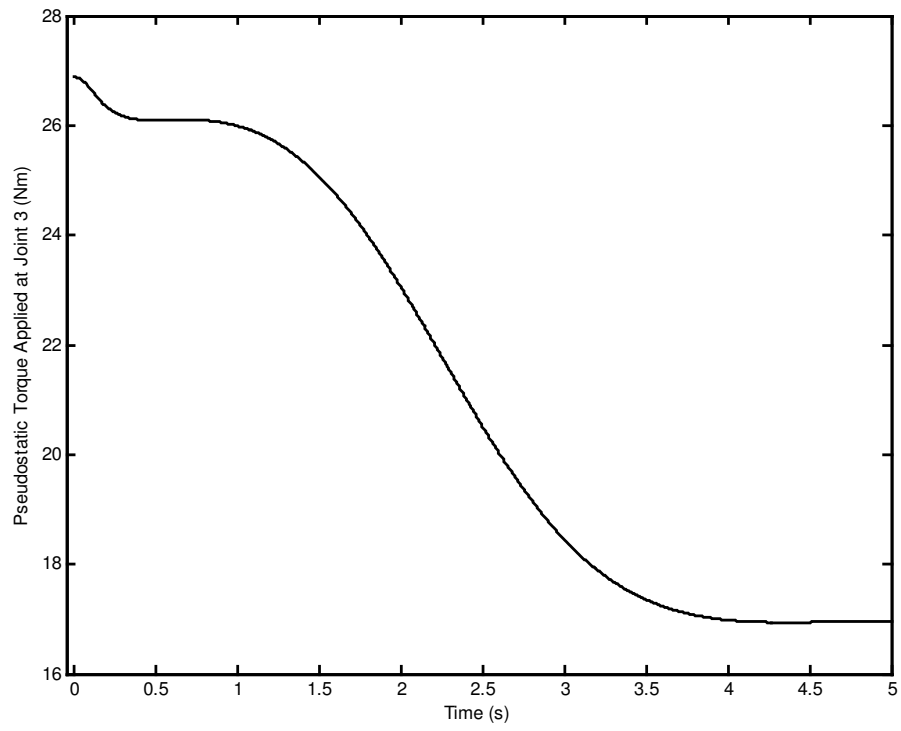


Figure 5.85 Pseudostatic torque applied at joint 3.

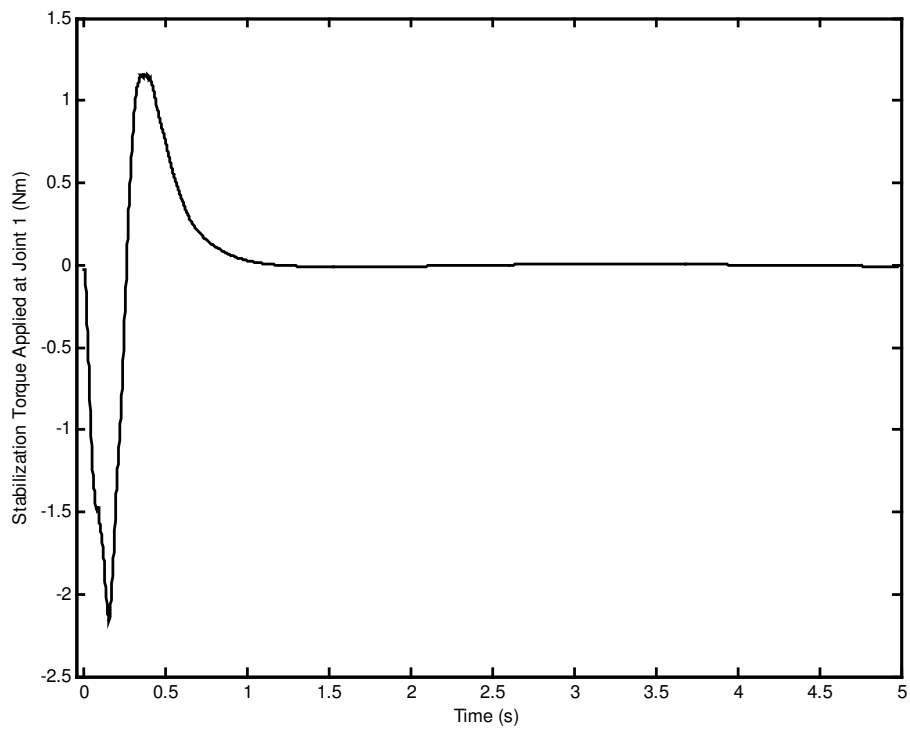


Figure 5.86 Stabilization torque applied at joint 1.

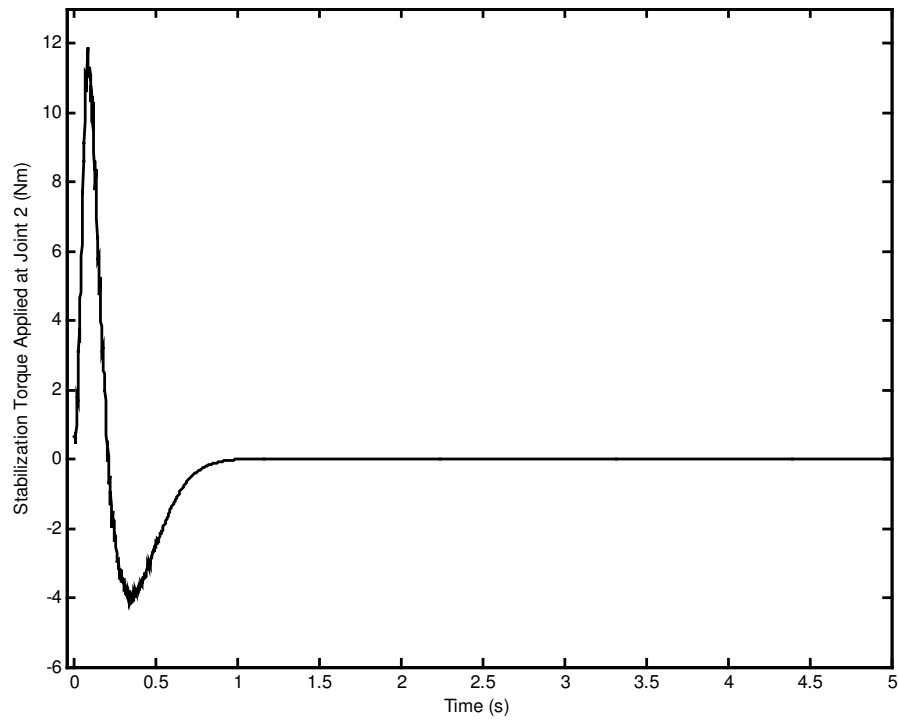


Figure 5.87 Stabilization torque applied at joint 2.

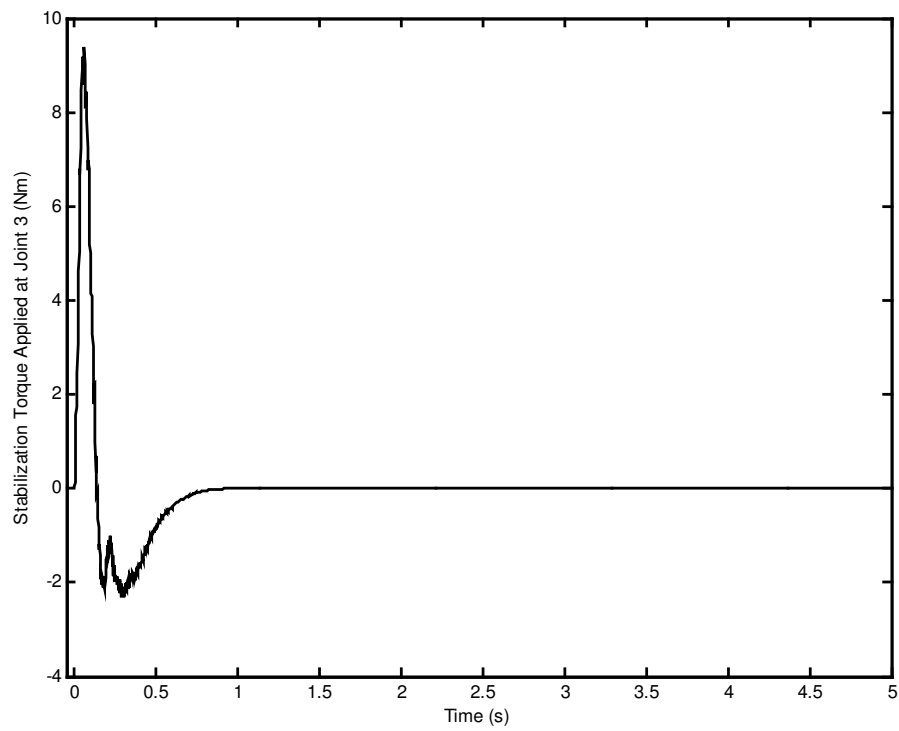


Figure 5.88 Stabilization torque applied at joint 3.

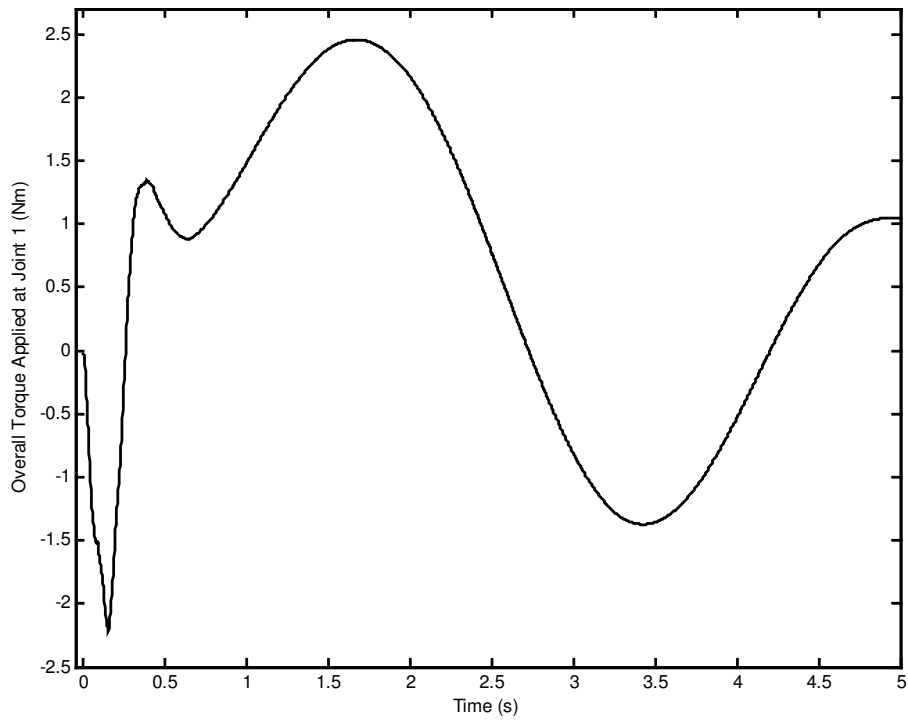


Figure 5.89 Overall torque applied at joint 1.

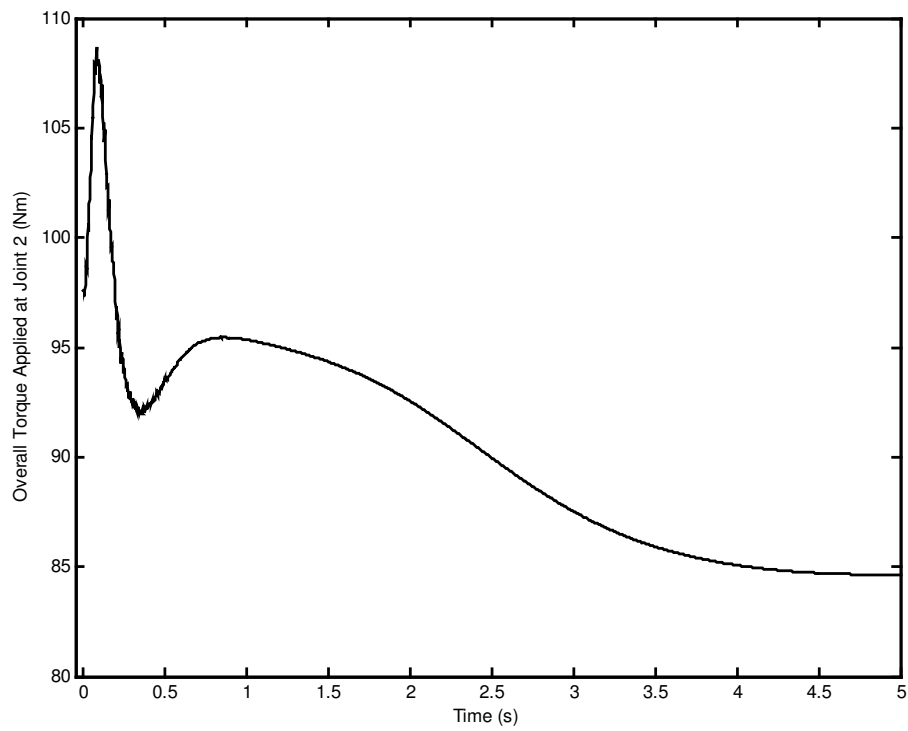


Figure 5.90 Overall torque applied at joint 2.

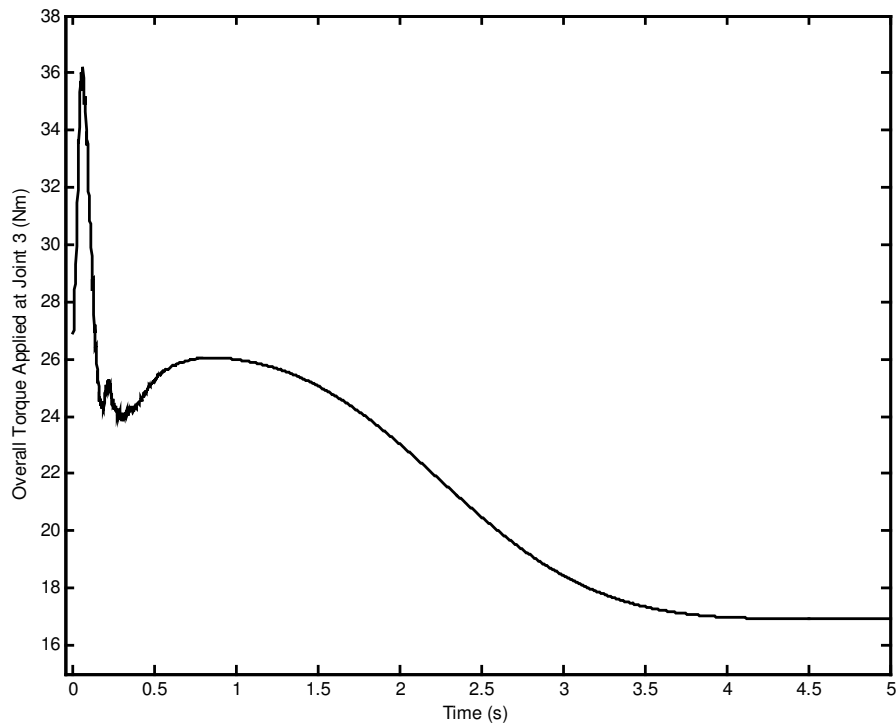


Figure 5.91 Overall torque applied at joint 3.

As seen from Figures 5.23 - 5.25 the initial error due to the mispositioning of the tip point is 0.03 m, -0.05 m and -0.02 m in \mathbf{n}_1 , \mathbf{n}_2 and \mathbf{n}_3 directions, respectively. However, the effect of initial mispositioning can be compensated in about 1 s. There is a reverse action at the beginning of the motion as seen in the tip point velocity which is given in Figures 5.32 - 5.34. The maximum tip point position tracking error components along the trajectory after the tip point settles on the trajectory are 4.2849×10^{-5} m, -8.6660×10^{-6} m and -9.5643×10^{-5} m in \mathbf{n}_1 , \mathbf{n}_2 and \mathbf{n}_3 directions, respectively. The tip point position error components at the end of the motion are -3.4359×10^{-5} m, 2.1104×10^{-6} m and -5.6728×10^{-5} m in \mathbf{n}_1 , \mathbf{n}_2 and \mathbf{n}_3 directions, respectively. The maximum overall torques applied to the joints are in the order of 109 Nm as seen from Figures 5.89 - 5.91.

5.3 Numerical Simulation of Motion Control of Spatial Robot with Measurement Noises

In this section, the numerical simulation of the motion control of the spatial robot including measurement noises is presented by using the motion control method proposed at Chapter 2. The measurement noises are considered for the state variables that are used for the generation of the stabilizing control torques (i.e., the measured variables). They are the tip point coordinates and their rates and the modal variables of Body 2 and Body 3 and their rates.

The measurement noises are generated by using normally distributed random numbers with zero mean and specific standard deviation. 1 % deviation from the mean value of each variable is assumed to obtain the standard deviation for each variable.

A first order low pass filter whose transfer function given below is used to filter the measured variables.

$$G(s) = \frac{\omega_c}{s + \omega_c} \quad (5.3)$$

Where ω_c stands for the crossover frequency. Other types of filters, eg. Kalman filters, can also be used to filter the measured variables.

The same reference tip point trajectory considered in the previous section is used. After a few trials, closed loop natural frequencies and damping ratios that give acceptable response are obtained as 20 rad/s, 25 rad/s, 30 rad/s, 43 rad/s, 43 rad/s, 44 rad/s, 44 rad/s, 268 rad/s, 268 rad/s, 276 rad/s, 276 rad/s, 0.85, 0.85, 0.85, 0.85, 0.85, 0.85, 0.85, 0.85, 0.85, 0.85, 0.85 and 0.85. The simulation results give the maximum start up torque in the order of 156 Nm and the order of 59 Nm of it is used for stabilization. Therefore, the maximum start up torque can be decreased by reducing the stabilization part of it.

In order to obtain smaller start up torque, gain scheduling is applied to all of the dominant natural frequencies. After a few trials, proper initial and final closed loop natural frequencies and damping ratios are obtained as $\omega_{n1}^s = 5$ rad/s, $\omega_{n1}^f = 20$ rad/s, $\omega_{n2}^s = 10$ rad/s, $\omega_{n2}^f = 25$ rad/s, $\omega_{n3}^s = 15$ rad/s, $\omega_{n3}^f = 30$ rad/s, $\omega_{n4,5} = 43$ rad/s, $\omega_{n6,7} = 44$ rad/s, $\omega_{n8,9} = 268$ rad/s, $\omega_{n10,11} = 276$ rad/s and $\zeta_{di} = 0.85$ ($i = 1, 2, \dots, 11$). The corresponding closed loop poles are given in Table 5.4.

Table 5.4 Closed loop poles used in motion control of spatial robot with measurement noises.

Closed Loop Poles
$p_1^s = -4.2500 + 2.6339j$
$p_1^f = -17.0000 + 10.5357j$
$p_2^s = -4.2500 - 2.6339j$
$p_2^f = -17.0000 - 10.5357j$
$p_3^s = -8.5000 + 5.2678j$
$p_3^f = -21.2500 + 13.1696j$
$p_4^s = -8.5000 - 5.2678j$
$p_4^f = -21.2500 - 13.1696j$
$p_5^s = -12.7500 + 7.9017j$
$p_5^f = -25.5000 + 15.8035j$
$p_6^s = -12.7500 - 7.9017j$
$p_6^f = -25.5000 - 15.8035j$
$p_{7,8} = -36.5500 + 22.6517j$
$p_{9,10} = -36.5500 - 22.6517j$
$p_{11,12} = -37.4000 + 23.1784j$
$p_{13,14} = -37.4000 - 23.1784j$
$p_{15,16} = -227.8000 + 141.1778j$
$p_{17,18} = -227.8000 - 141.1778j$
$p_{19,20} = -234.6000 + 145.3920j$
$p_{21,22} = -234.6000 - 145.3920j$

The sampling frequency is taken as 500 Hz. After a few trials, a proper crossover frequency for the filter is found as 276 rad/s. The simulation results are presented in Figures 5.92 - 5.182.

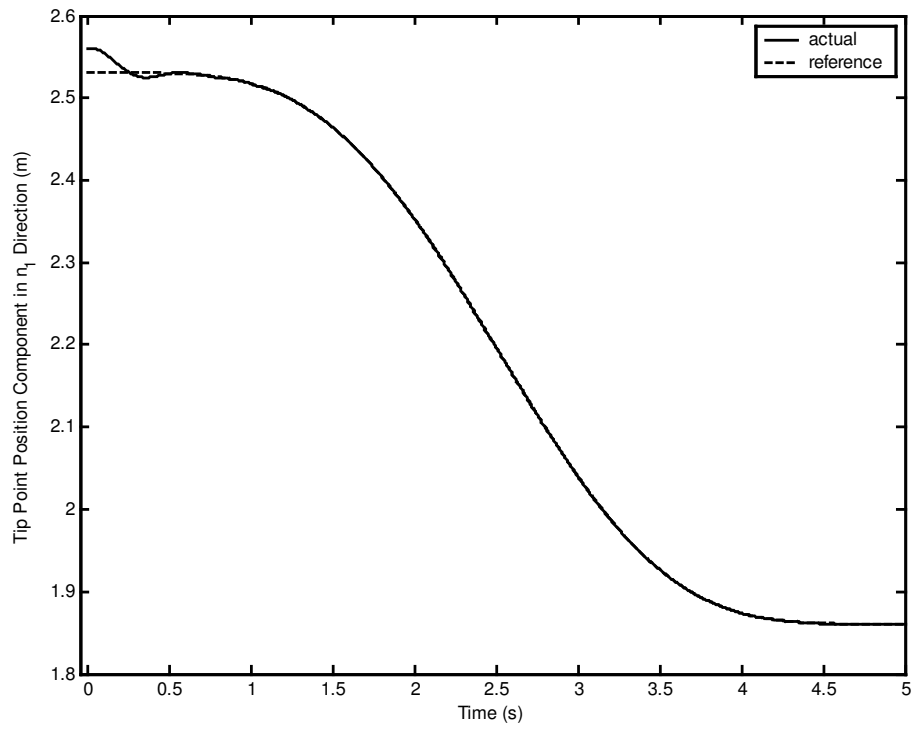


Figure 5.92 Tip point position component in n_1 direction.

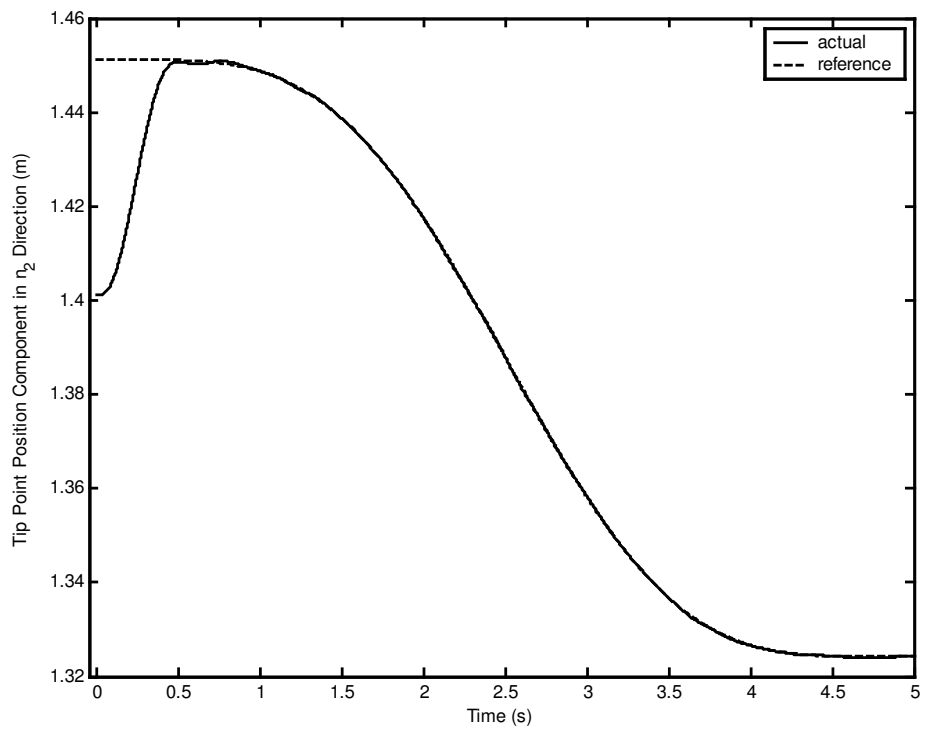


Figure 5.93 Tip point position component in n_2 direction.

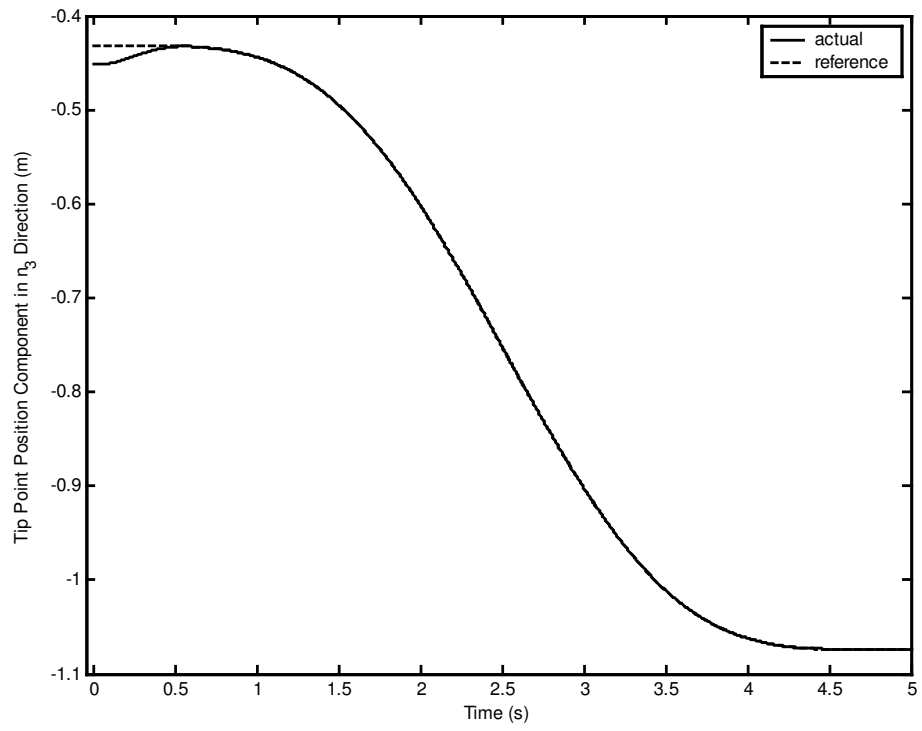


Figure 5.94 Tip point position component in n_3 direction.

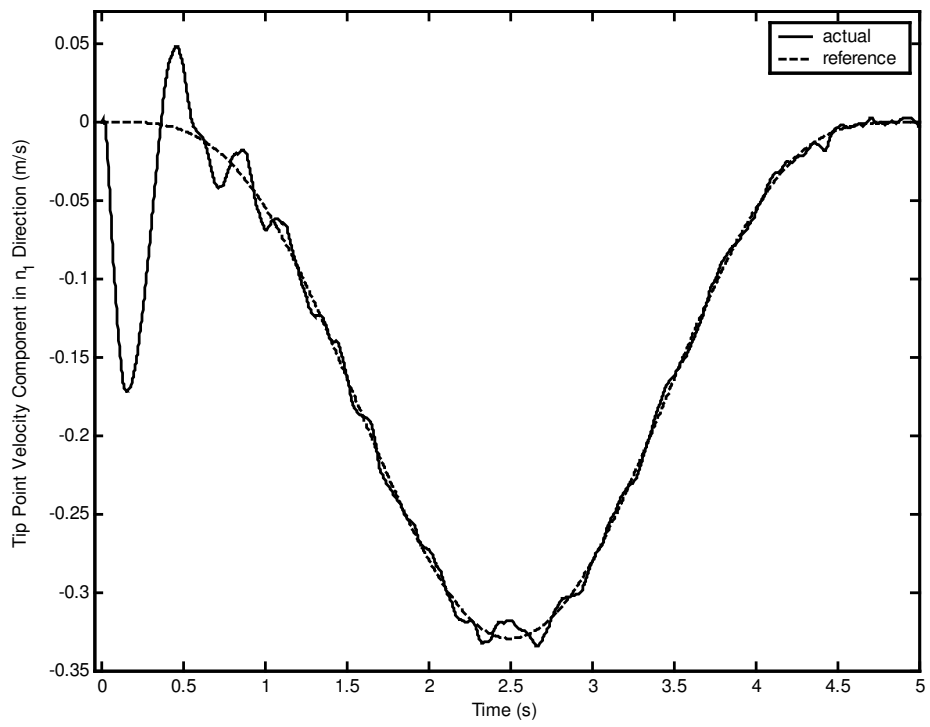


Figure 5.95 Tip point velocity component in n_1 direction.

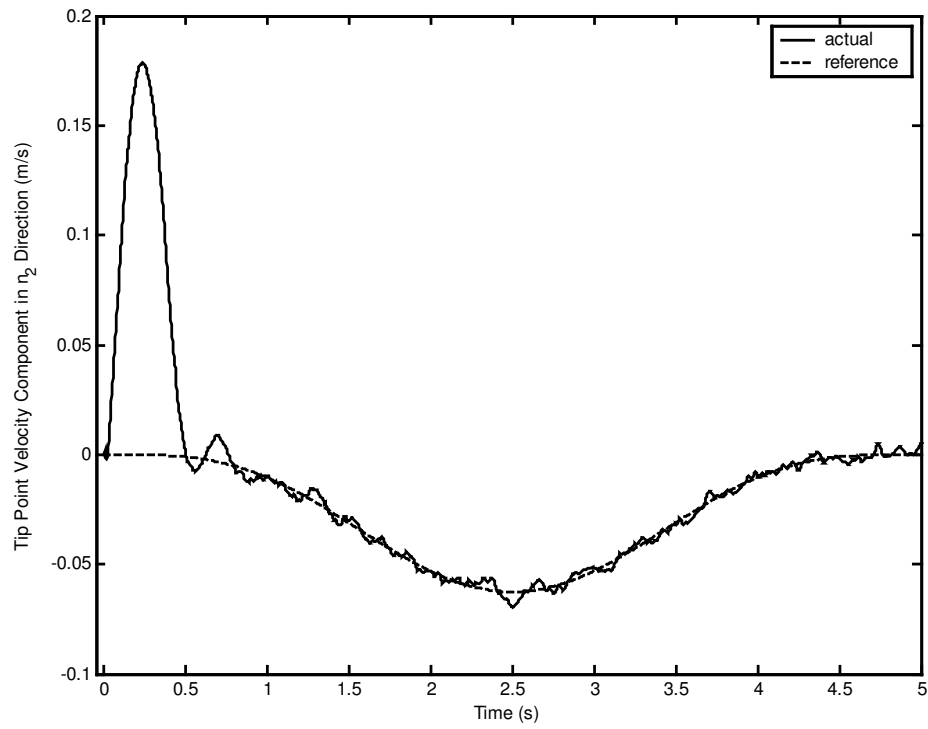


Figure 5.96 Tip point velocity component in n_2 direction.

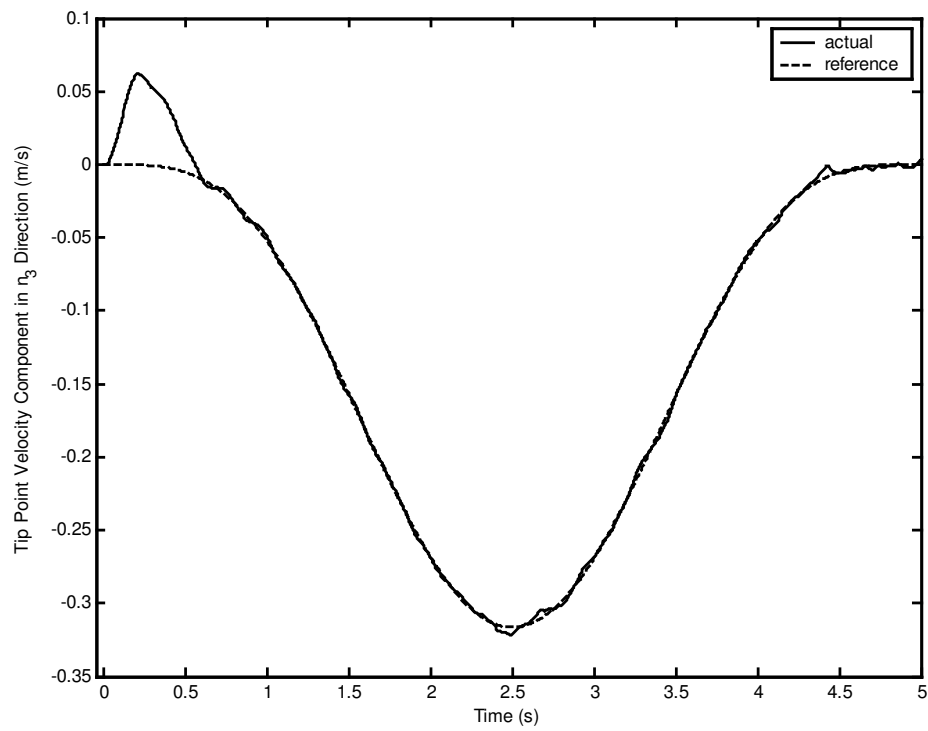


Figure 5.97 Tip point velocity component in n_3 direction.

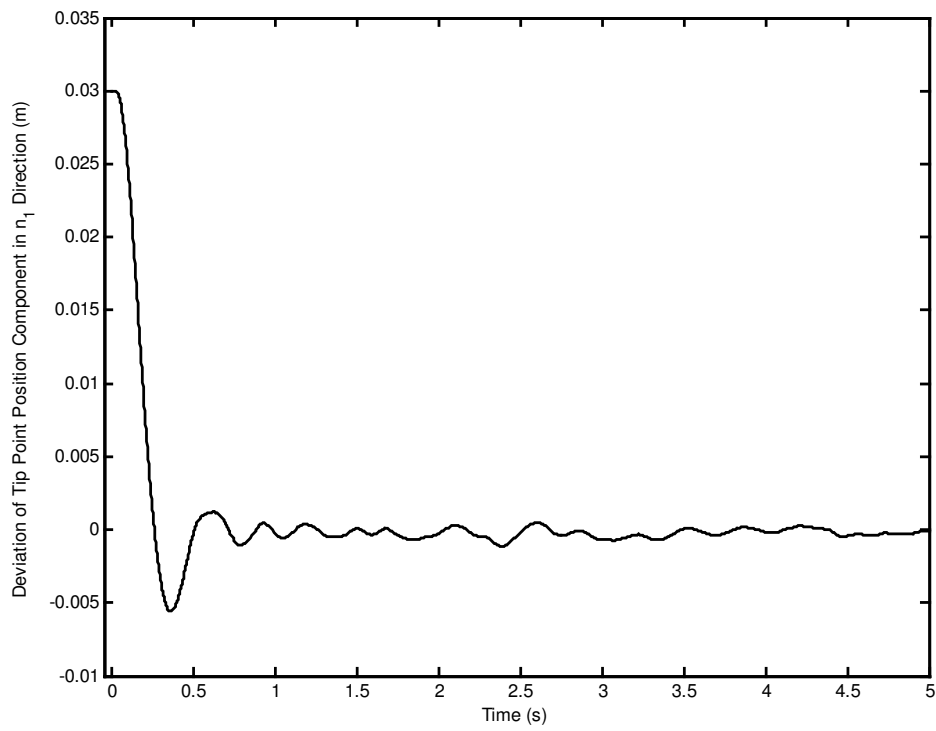


Figure 5.98 Deviation of tip point position component in n_1 direction.

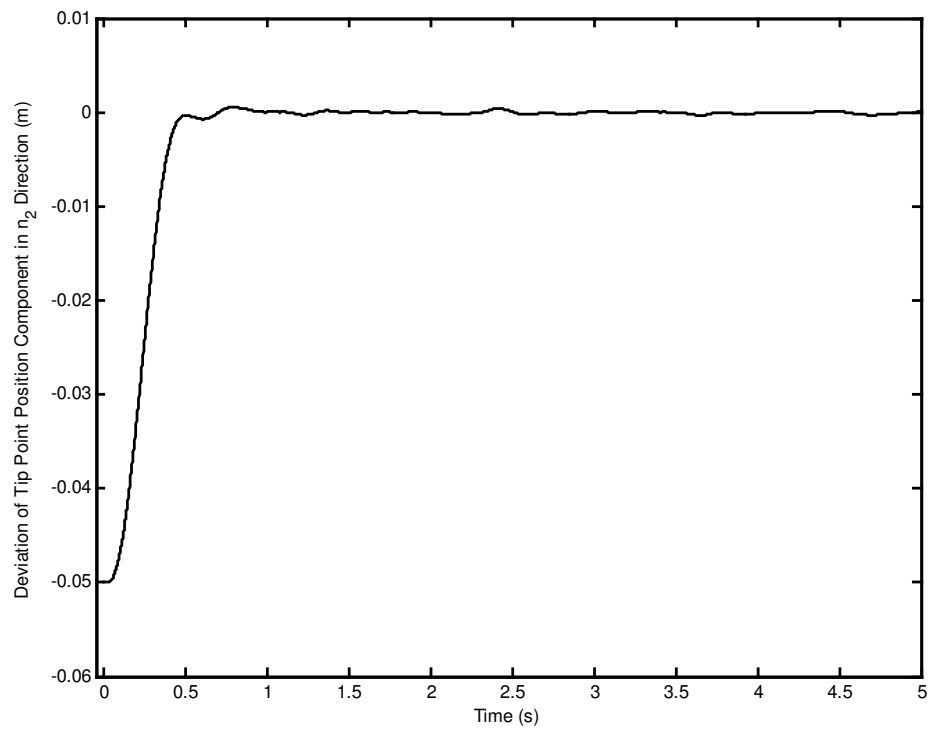


Figure 5.99 Deviation of tip point position component in n_2 direction.

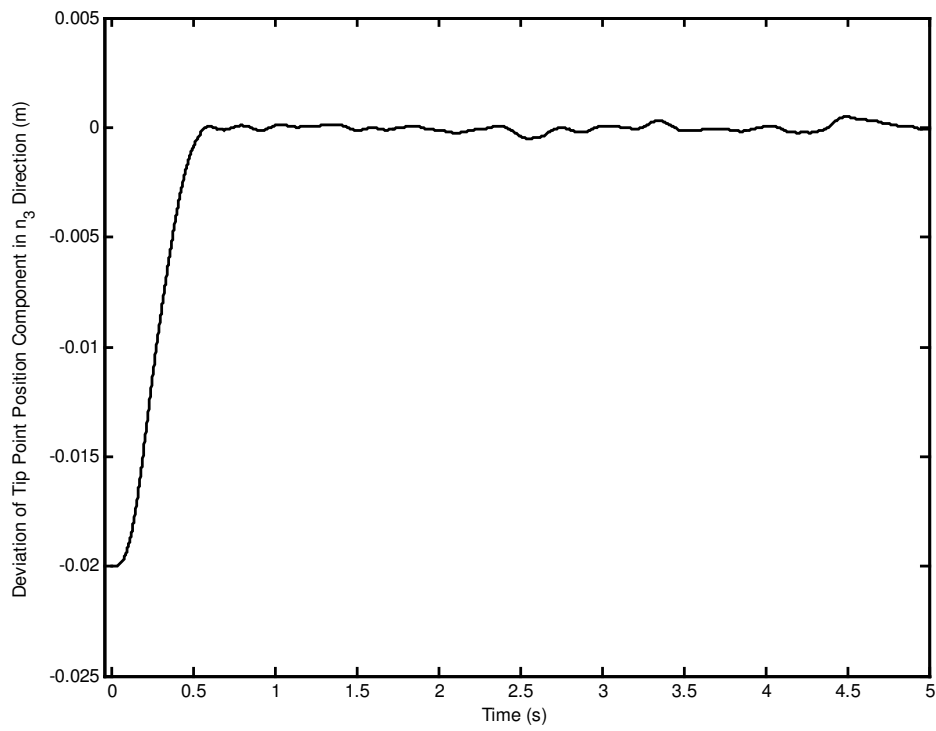


Figure 5.100 Deviation of tip point position component in n_3 direction.

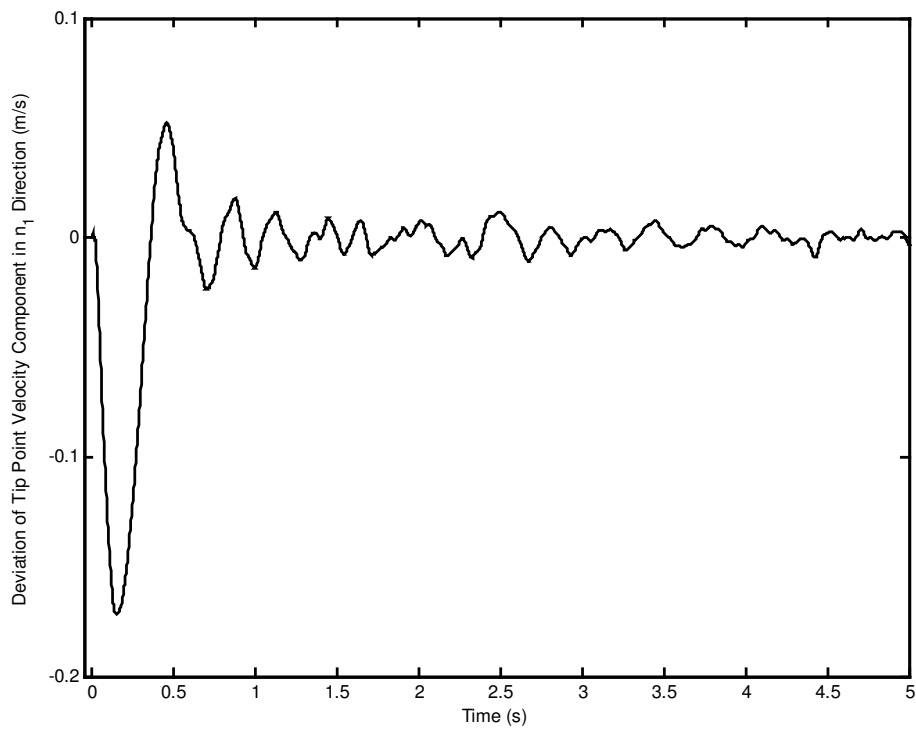


Figure 5.101 Deviation of tip point velocity component in n_1 direction.

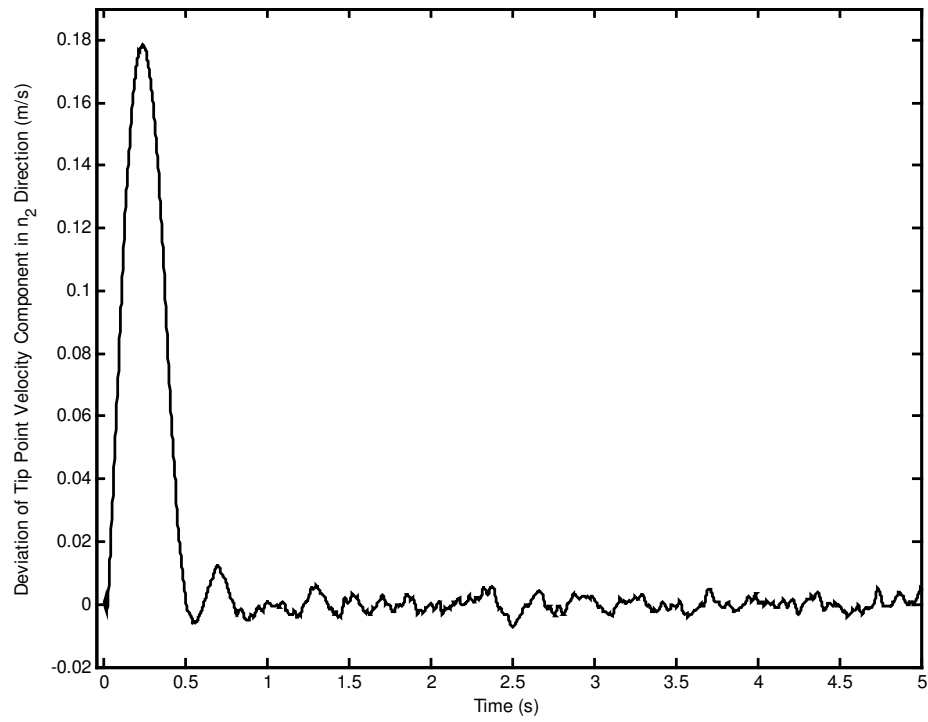


Figure 5.102 Deviation of tip point velocity component in n_2 direction.

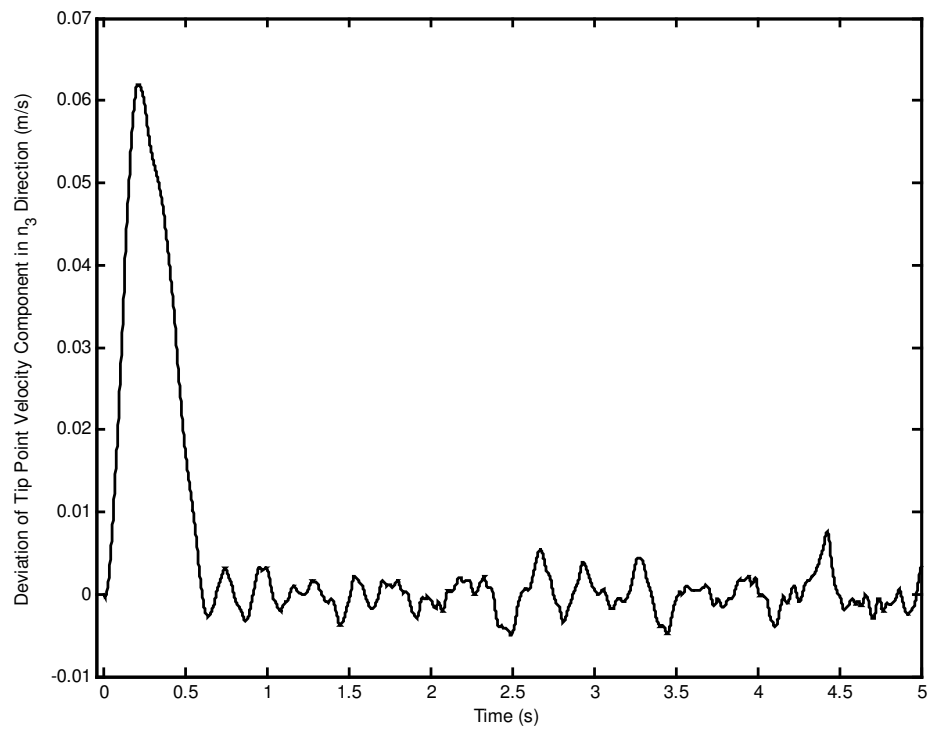


Figure 5.103 Deviation of tip point velocity component in n_3 direction.

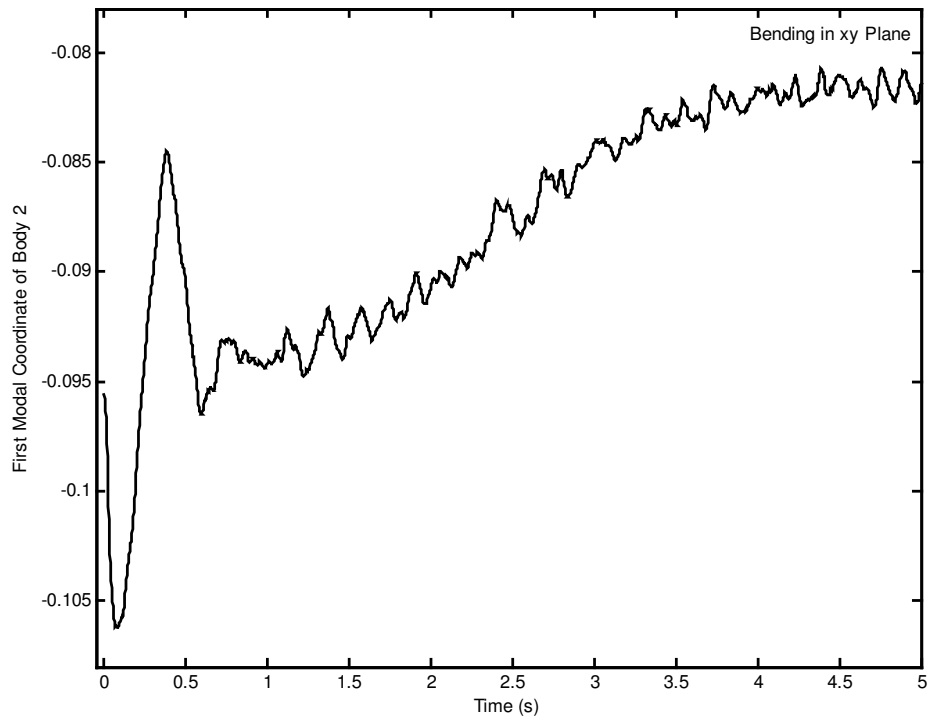


Figure 5.104 First modal coordinate of body 2 for bending in xy plane.

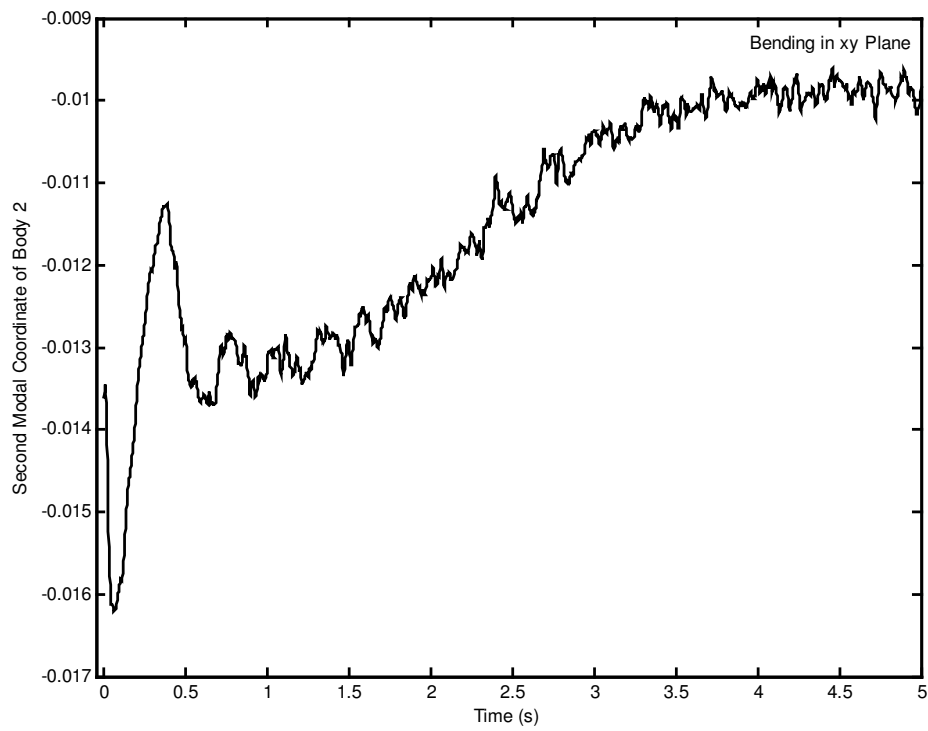


Figure 5.105 Second modal coordinate of body 2 for bending in xy plane.

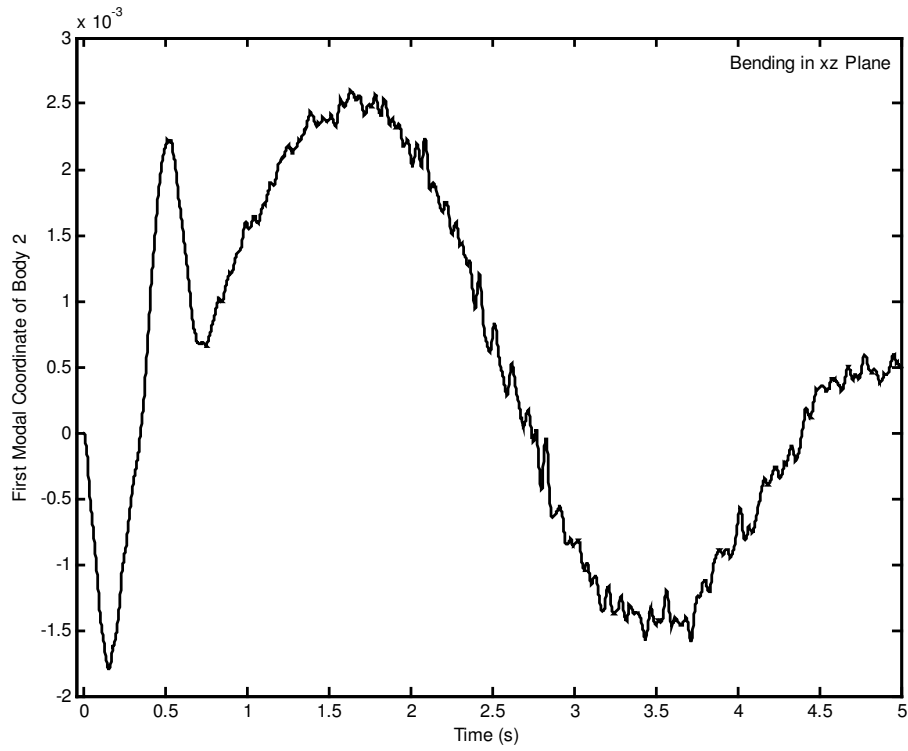


Figure 5.106 First modal coordinate of body 2 for bending in xz plane.

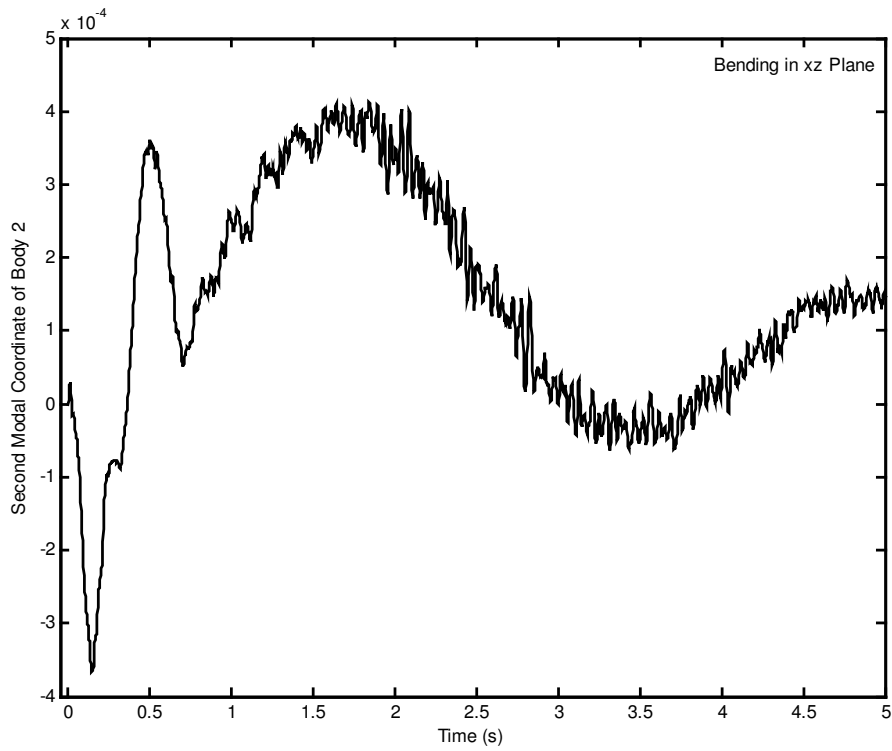


Figure 5.107 Second modal coordinate of body 2 for bending in xz plane.

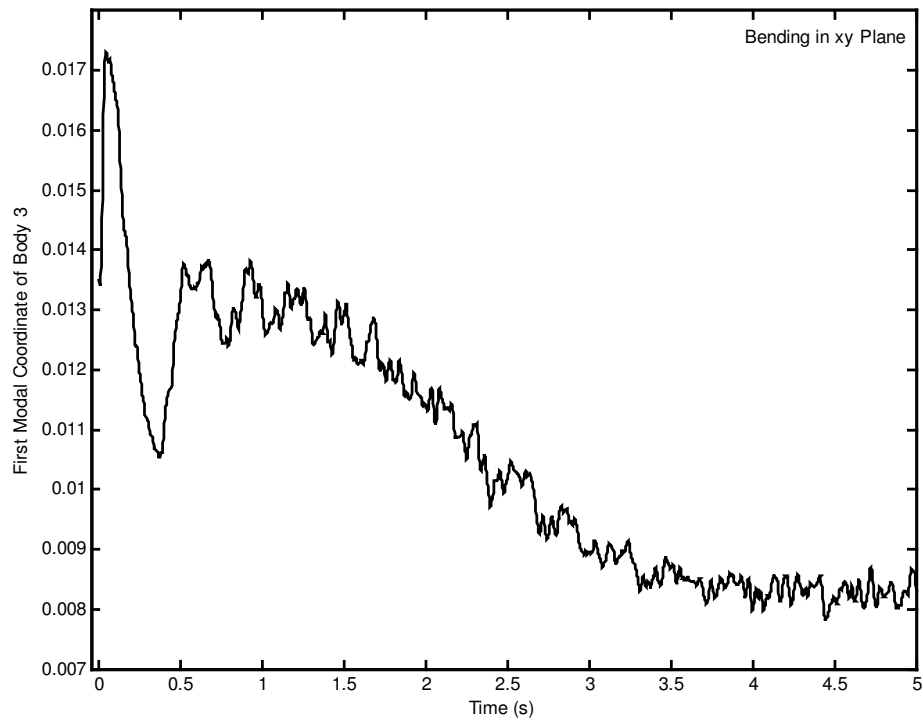


Figure 5.108 First modal coordinate of body 3 for bending in xy plane.

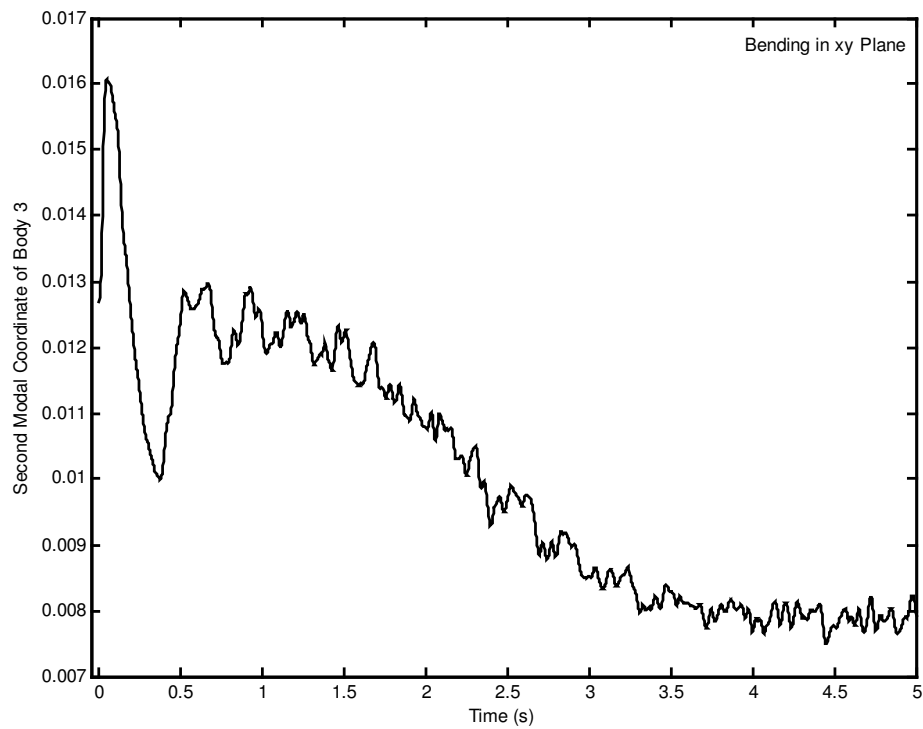


Figure 5.109 Second modal coordinate of body 3 for bending in xy plane.

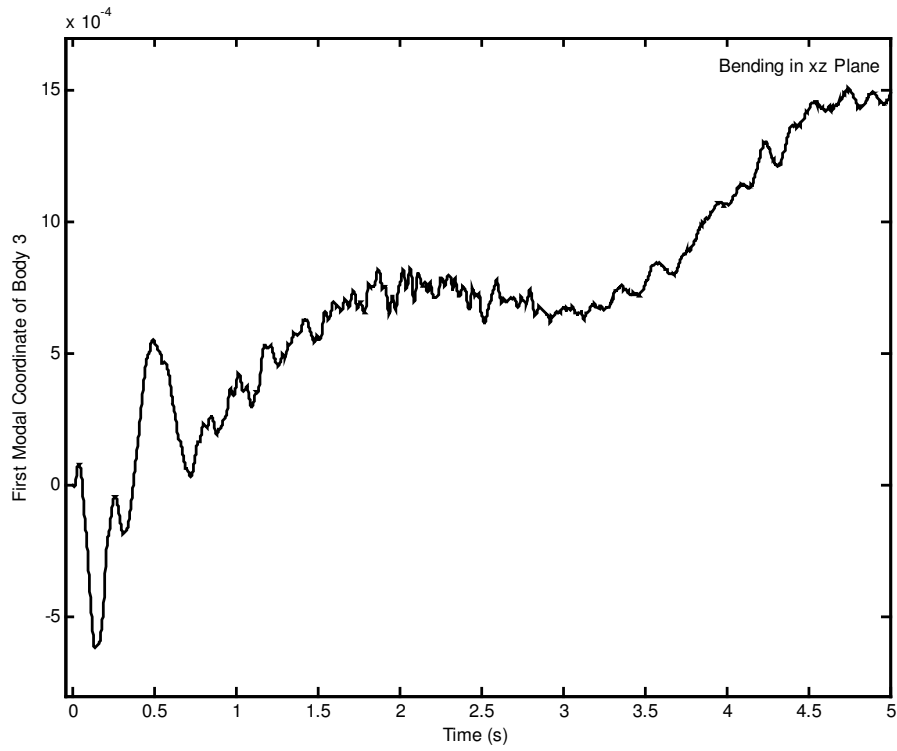


Figure 5.110 First modal coordinate of body 3 for bending in xz plane.

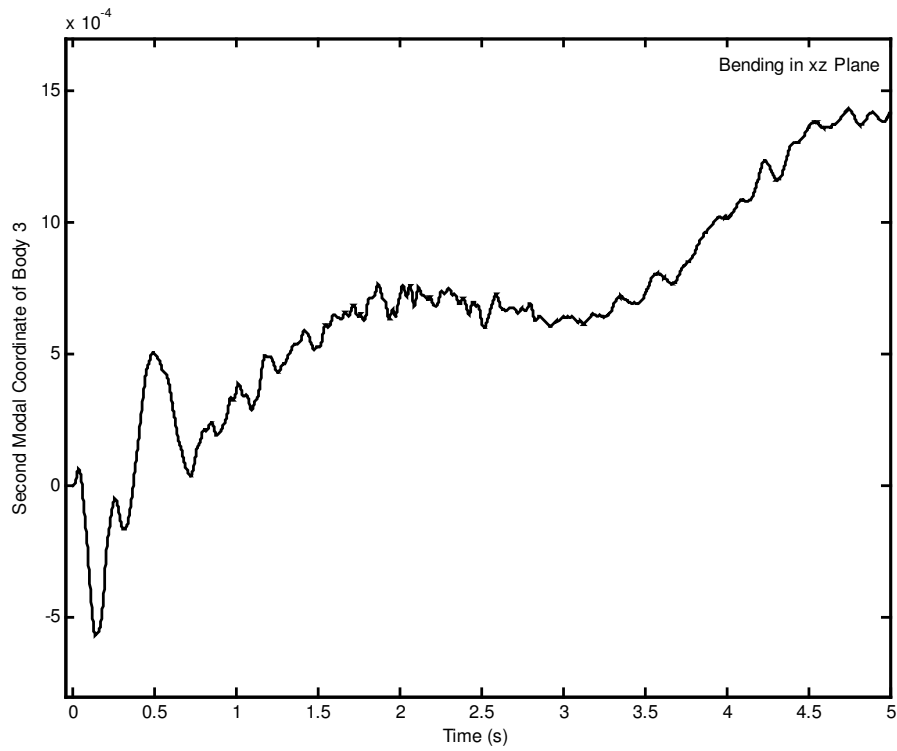


Figure 5.111 Second modal coordinate of body 3 for bending in xz plane.

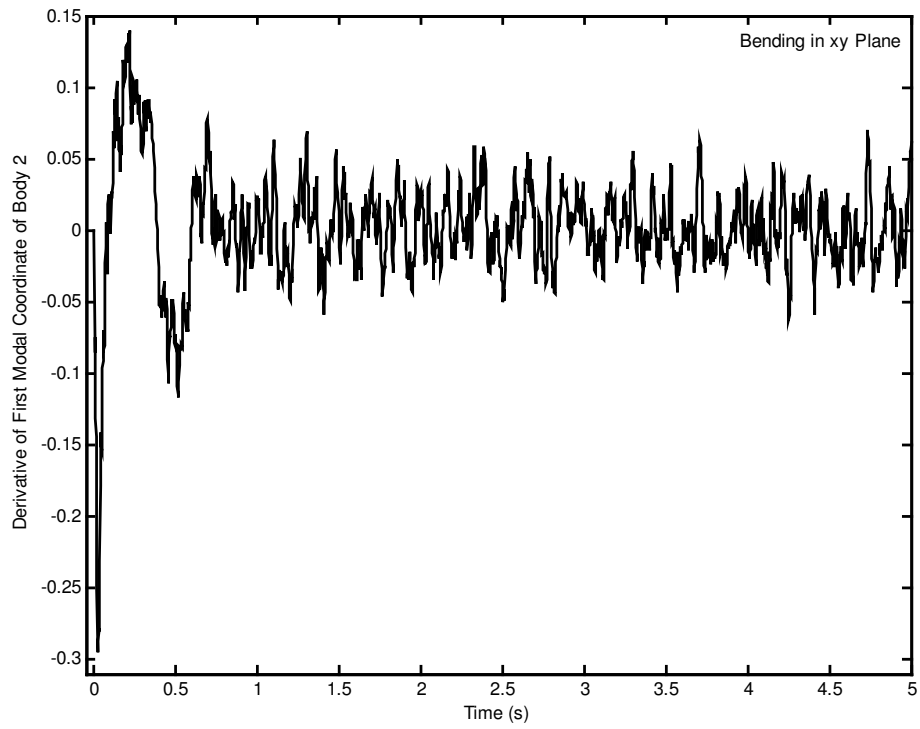


Figure 5.112 Derivative of first modal coordinate of body 2 for bending in xy plane.

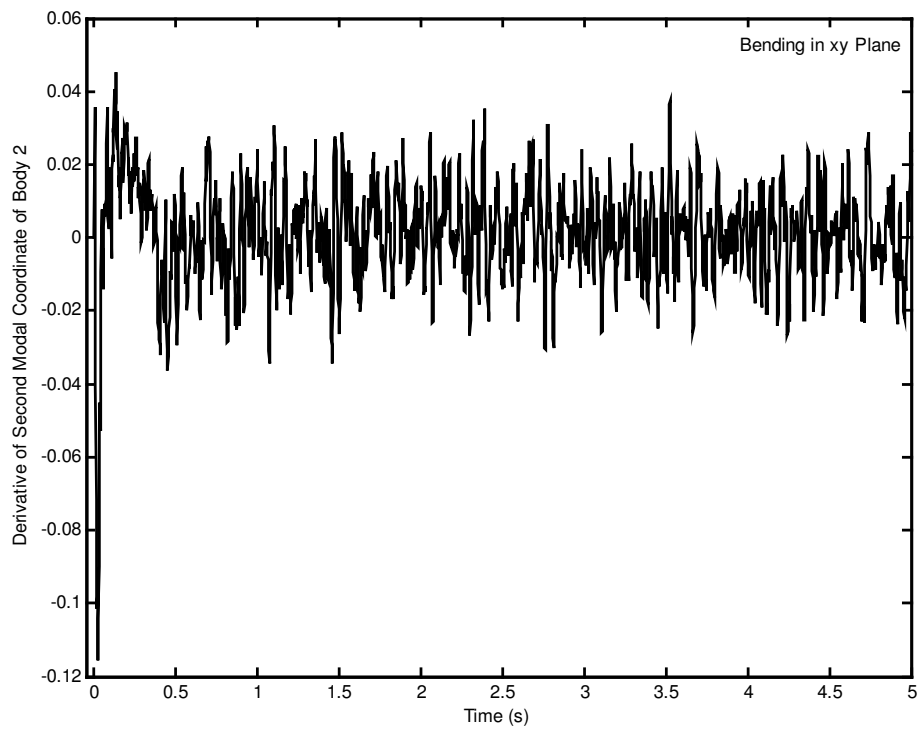


Figure 5.113 Derivative of second modal coordinate of body 2 for bending in xy plane.

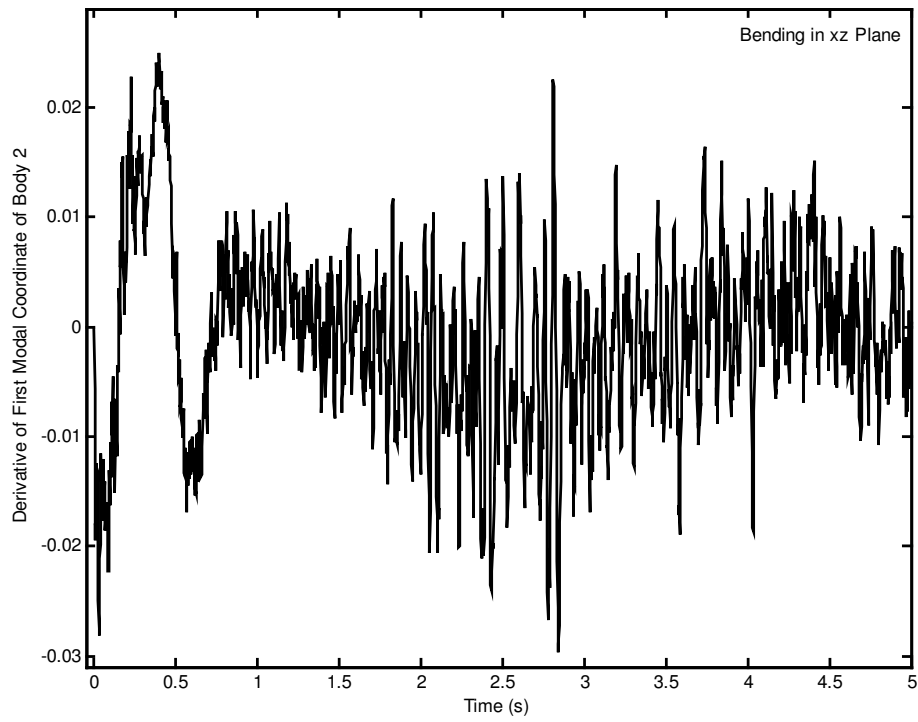


Figure 5.114 Derivative of first modal coordinate of body 2 for bending in xz plane.

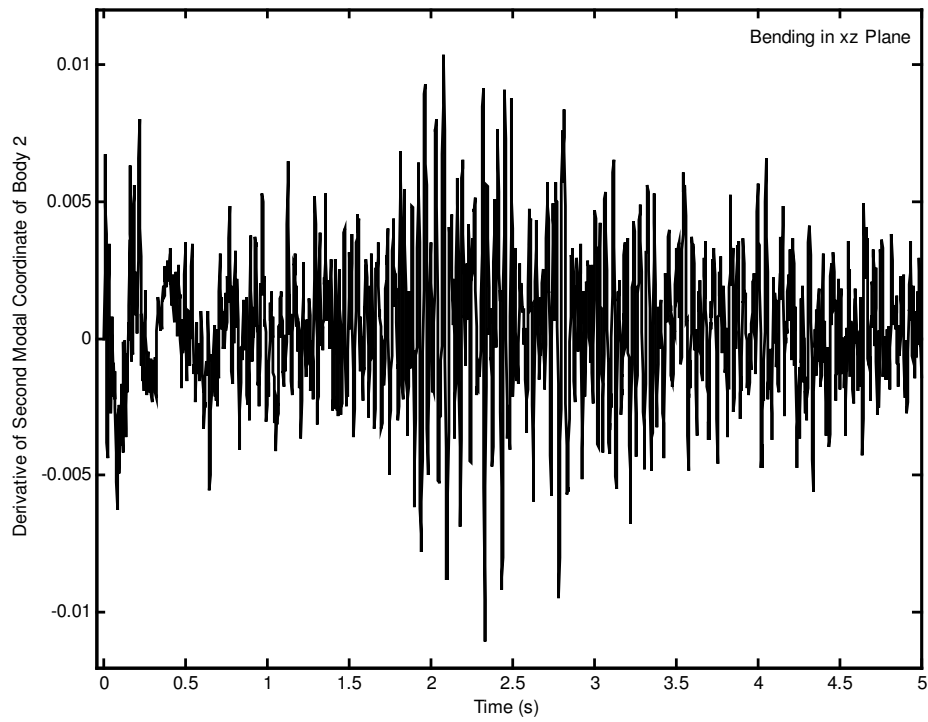


Figure 5.115 Derivative of second modal coordinate of body 2 for bending in xz plane.

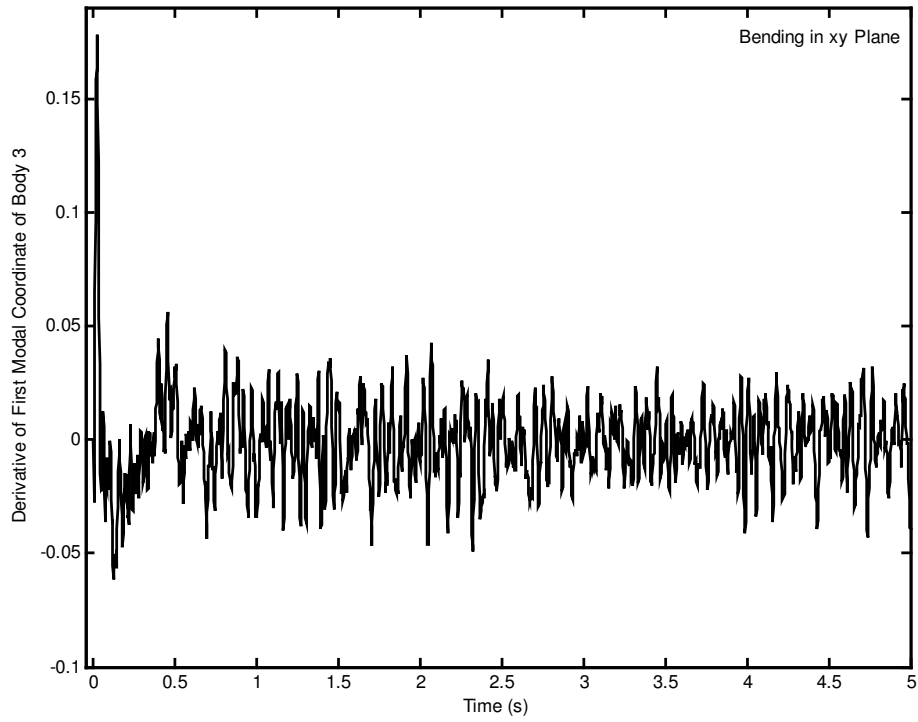


Figure 5.116 Derivative of first modal coordinate of body 3 for bending in xy plane.

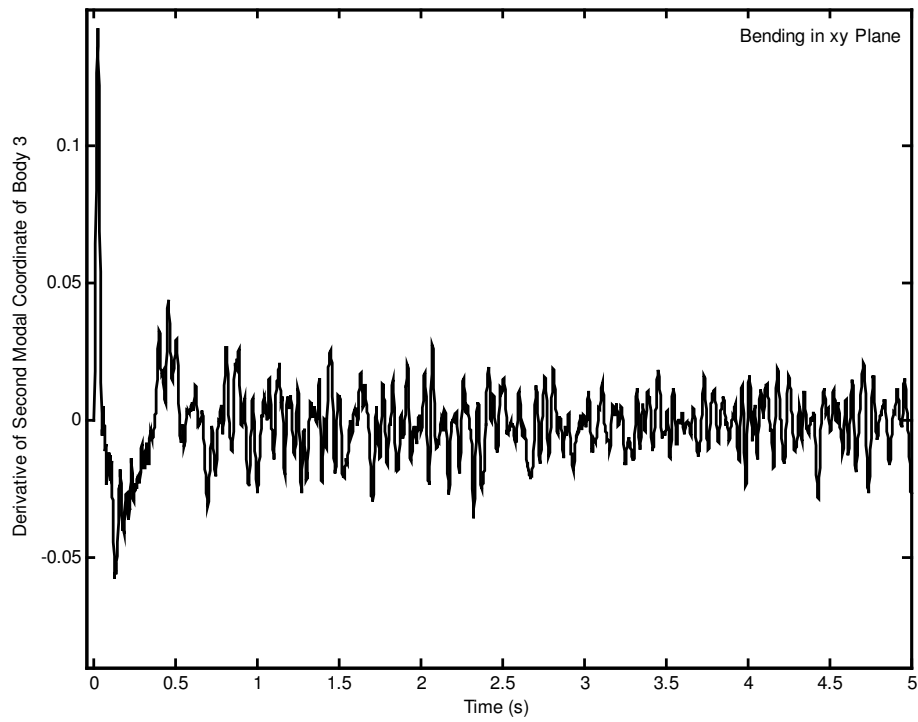


Figure 5.117 Derivative of second modal coordinate of body 3 for bending in xy plane.

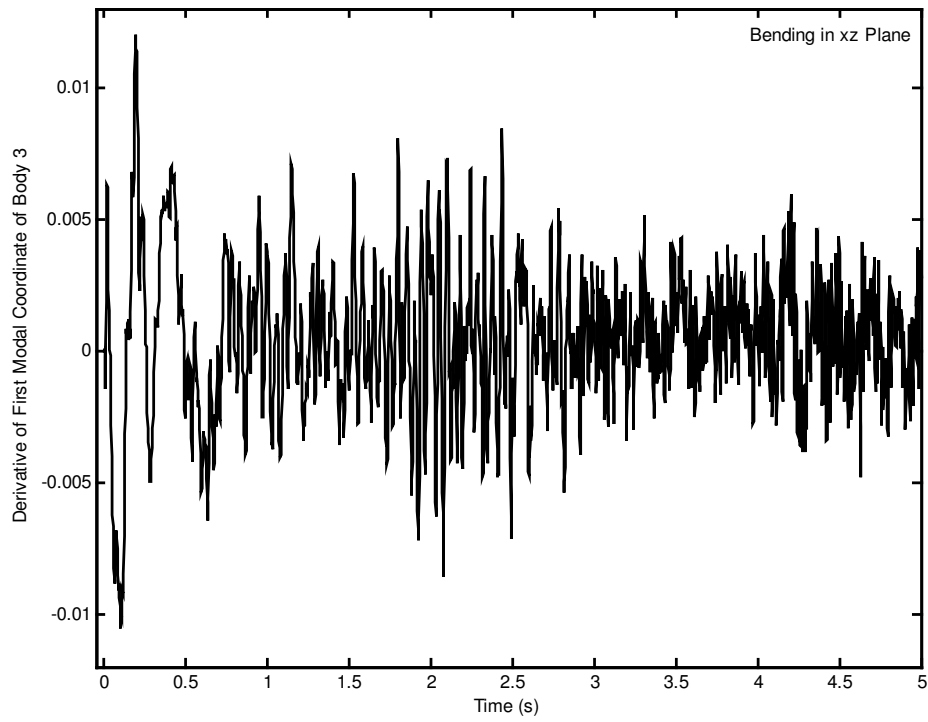


Figure 5.118 Derivative of first modal coordinate of body 3 for bending in xz plane.

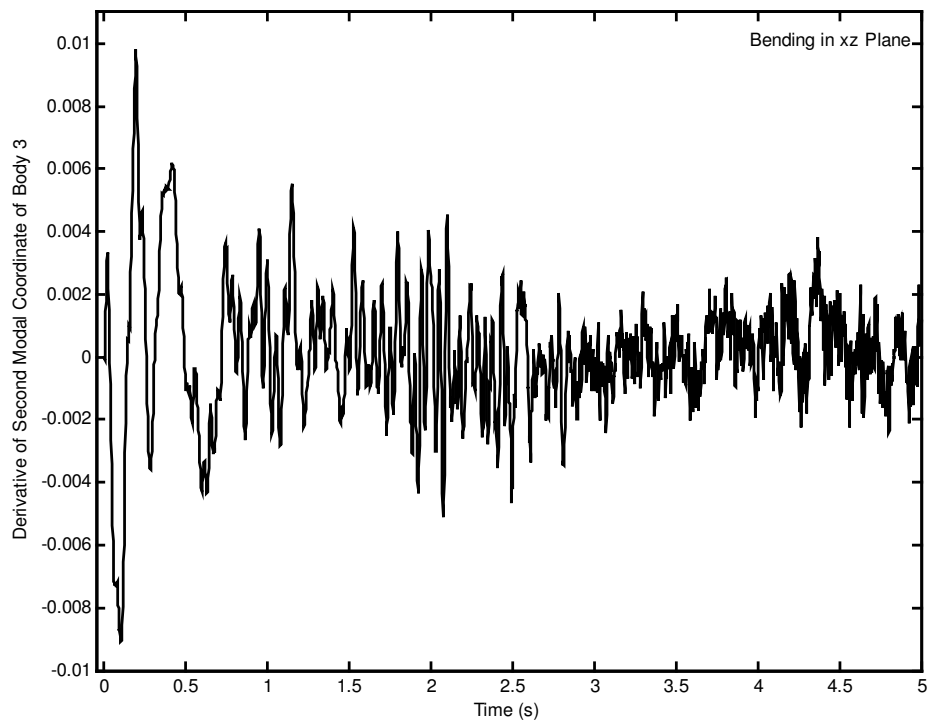


Figure 5.119 Derivative of second modal coordinate of body 3 for bending in xz plane.

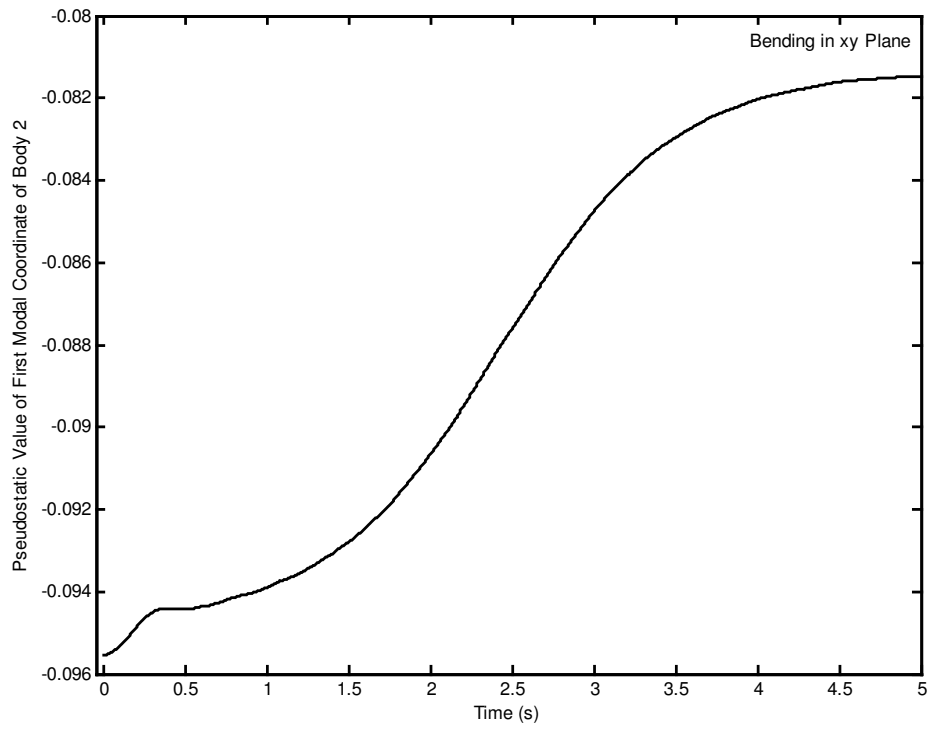


Figure 5.120 Pseudostatic value of first modal coordinate of body 2 for bending in xy plane.

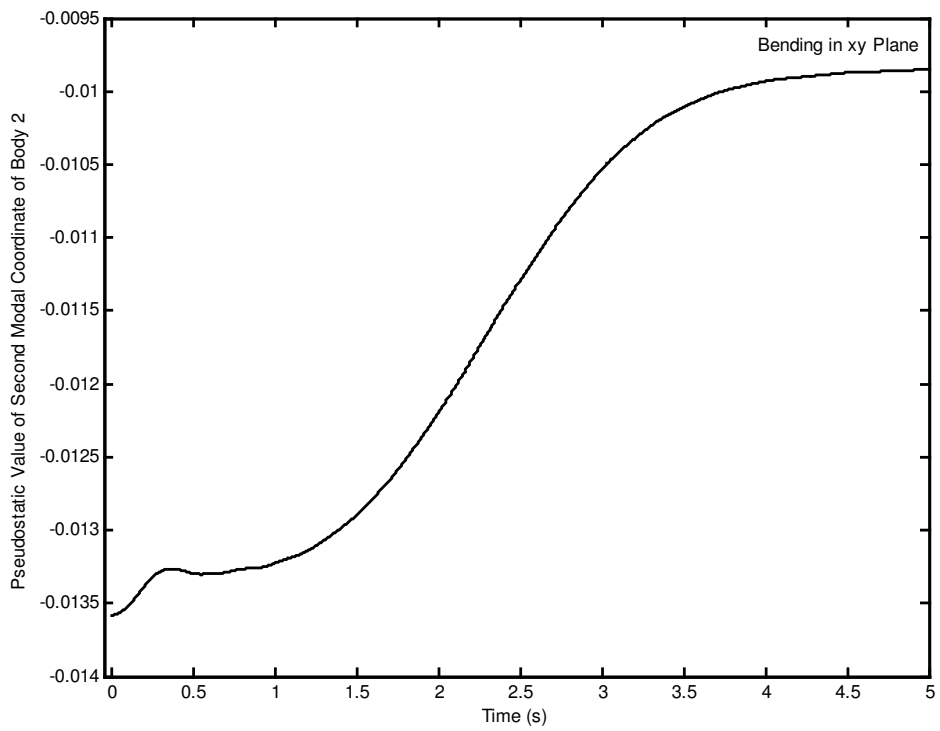


Figure 5.121 Pseudostatic value of second modal coordinate of body 2 for bending in xy plane.

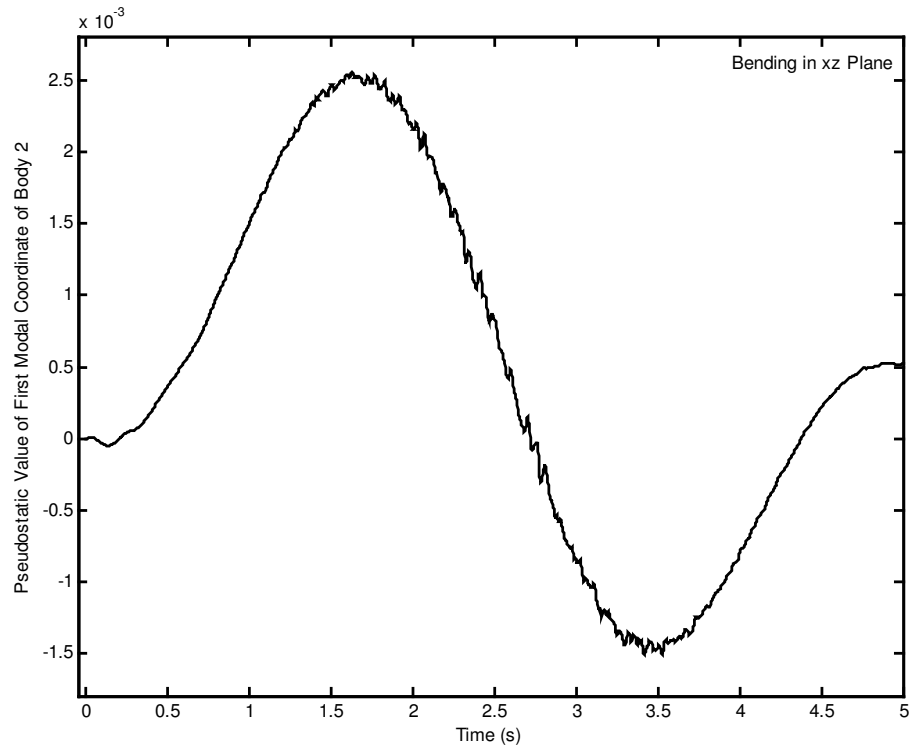


Figure 5.122 Pseudostatic value of first modal coordinate of body 2 for bending in xz plane.

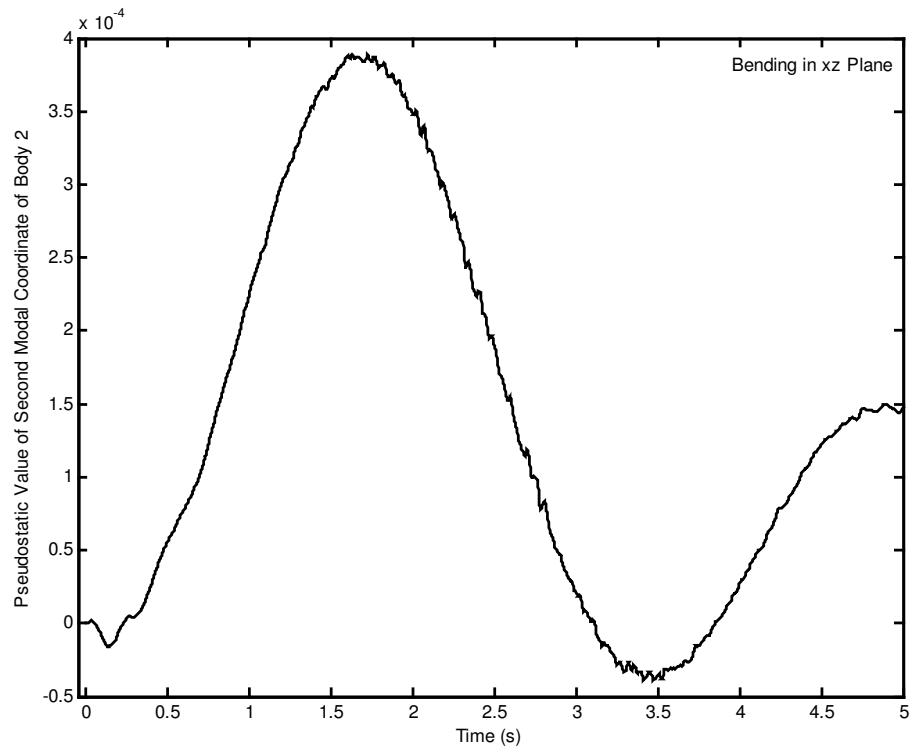


Figure 5.123 Pseudostatic value of second modal coordinate of body 2 for bending in xz plane.

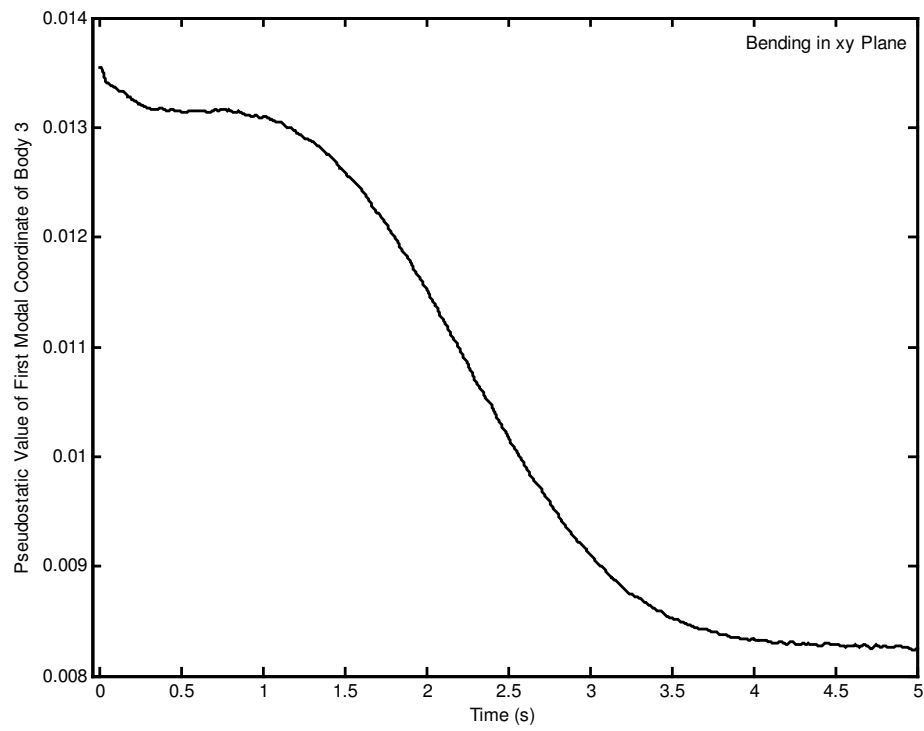


Figure 5.124 Pseudostatic value of first modal coordinate of body 3 for bending in xy plane.

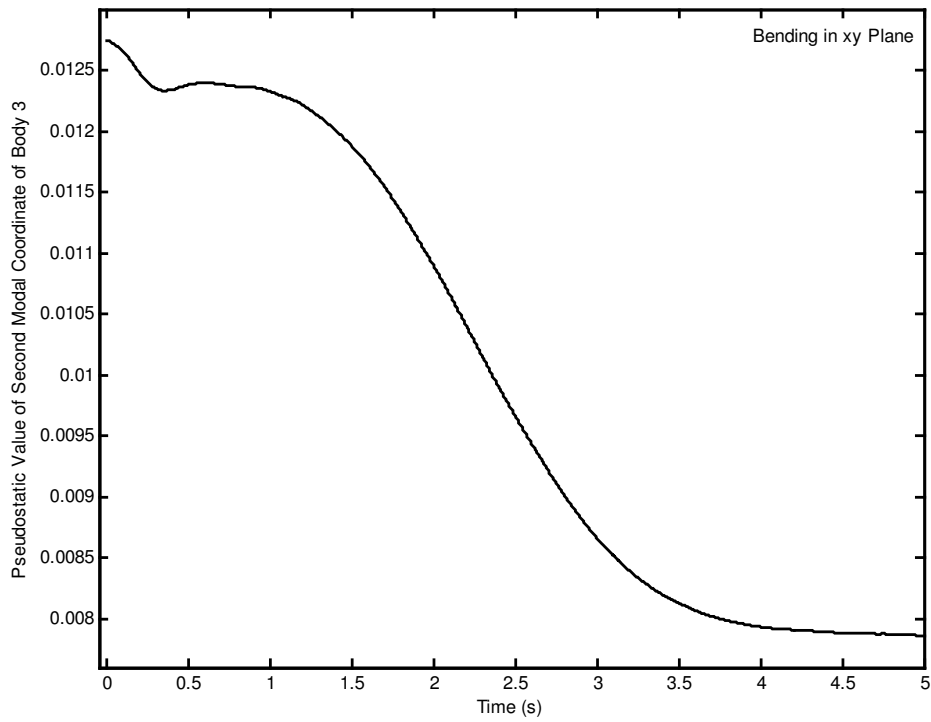


Figure 5.125 Pseudostatic value of second modal coordinate of body 3 for bending in xy plane.

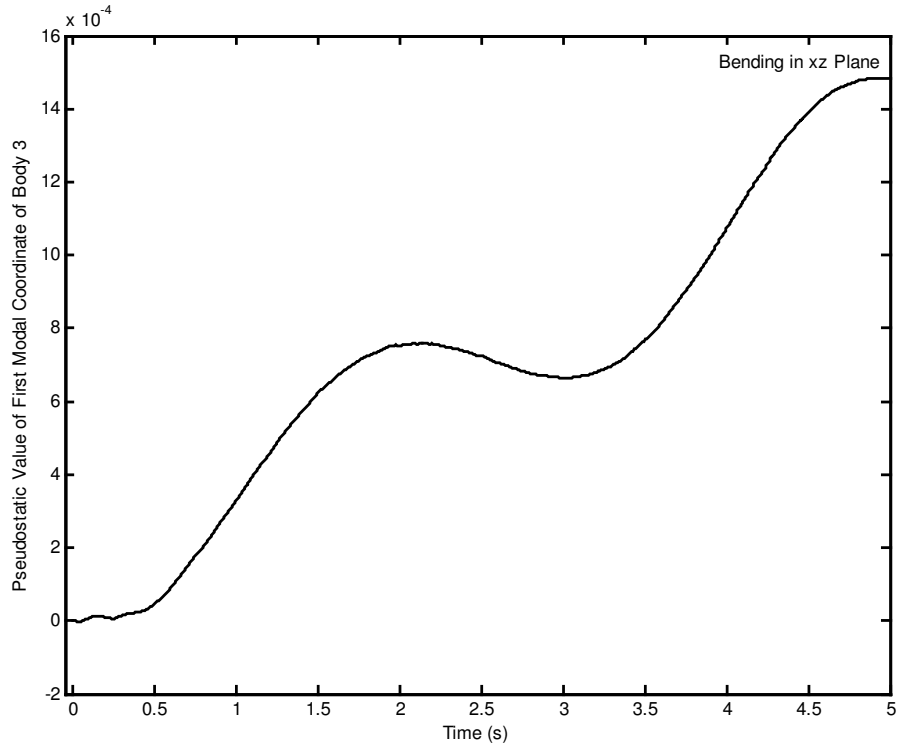


Figure 5.126 Pseudostatic value of first modal coordinate of body 3 for bending in xz plane.

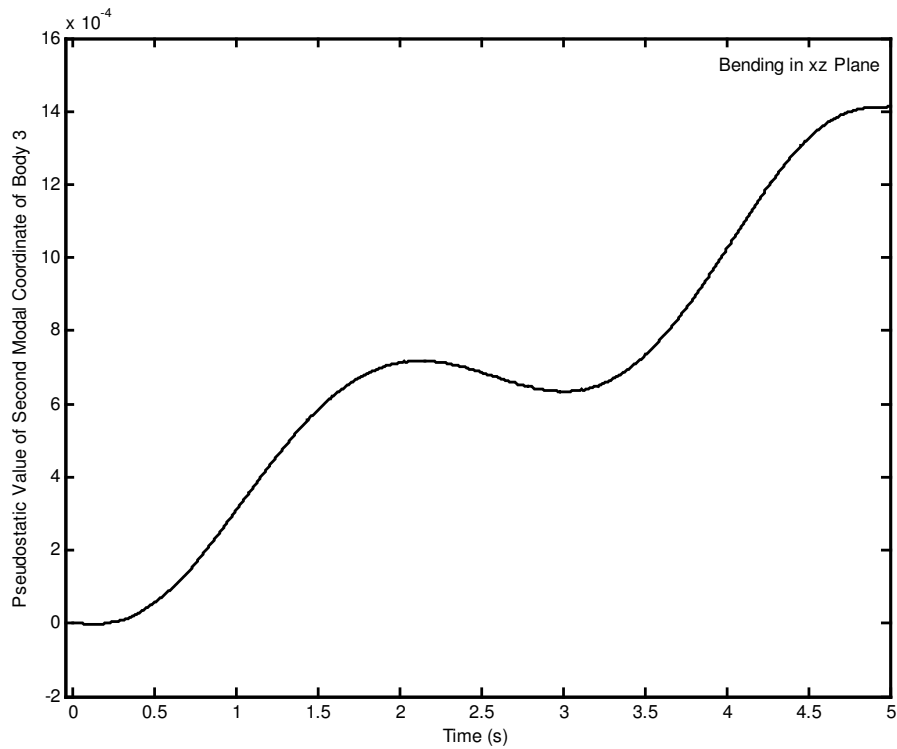


Figure 5.127 Pseudostatic value of second modal coordinate of body 3 for bending in xz plane.

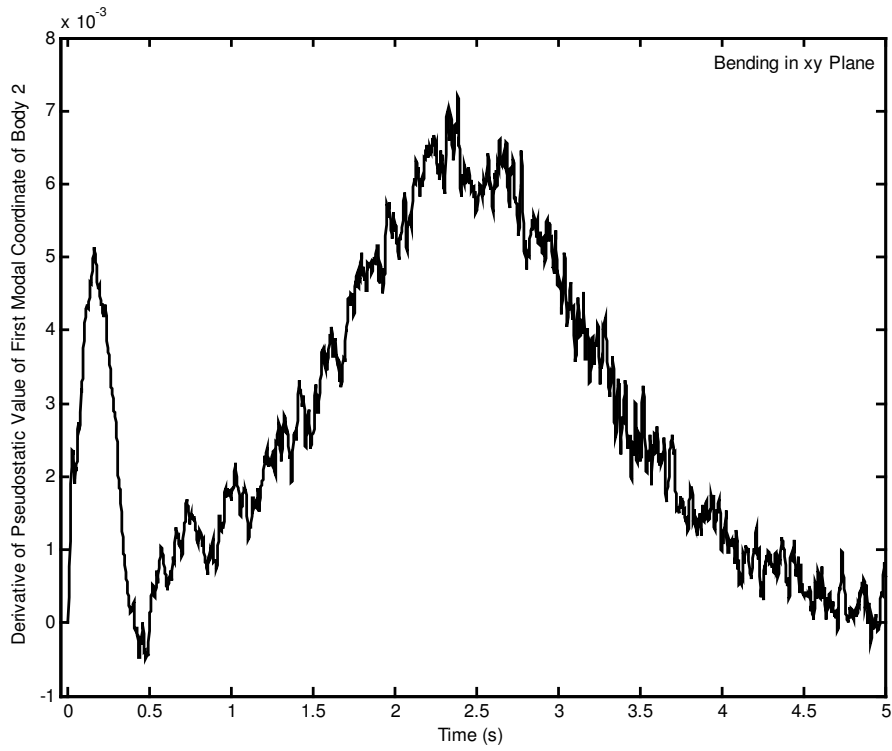


Figure 5.128 Derivative of pseudostatic value of first modal coordinate of body 2 for bending in xy plane.

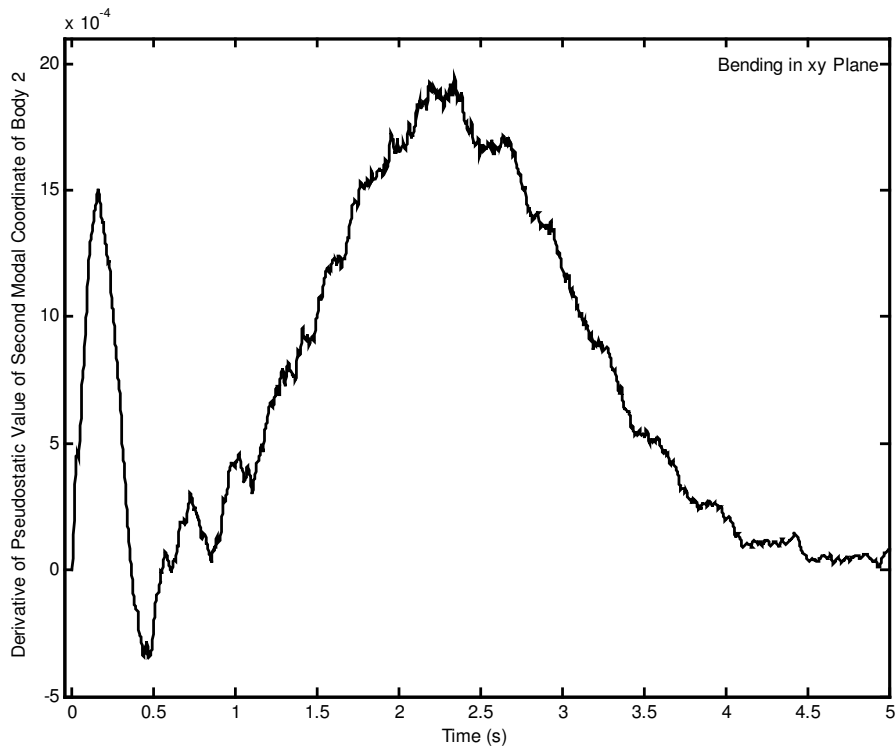


Figure 5.129 Derivative of pseudostatic value of second modal coordinate of body 2 for bending in xy plane.

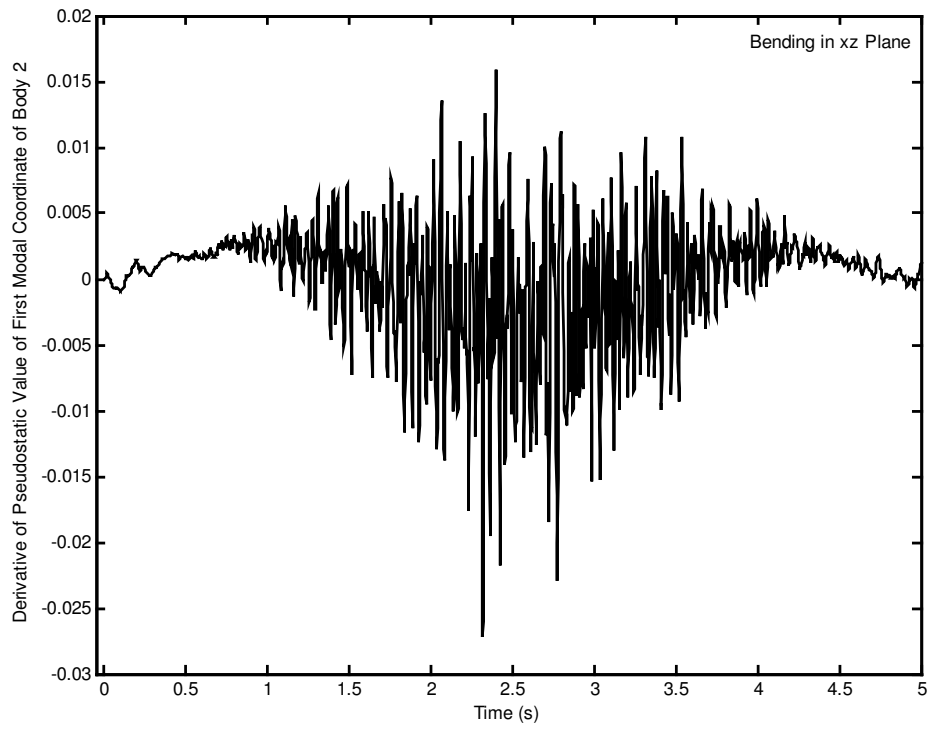


Figure 5.130 Derivative of pseudostatic value of first modal coordinate of body 2 for bending in xz plane.

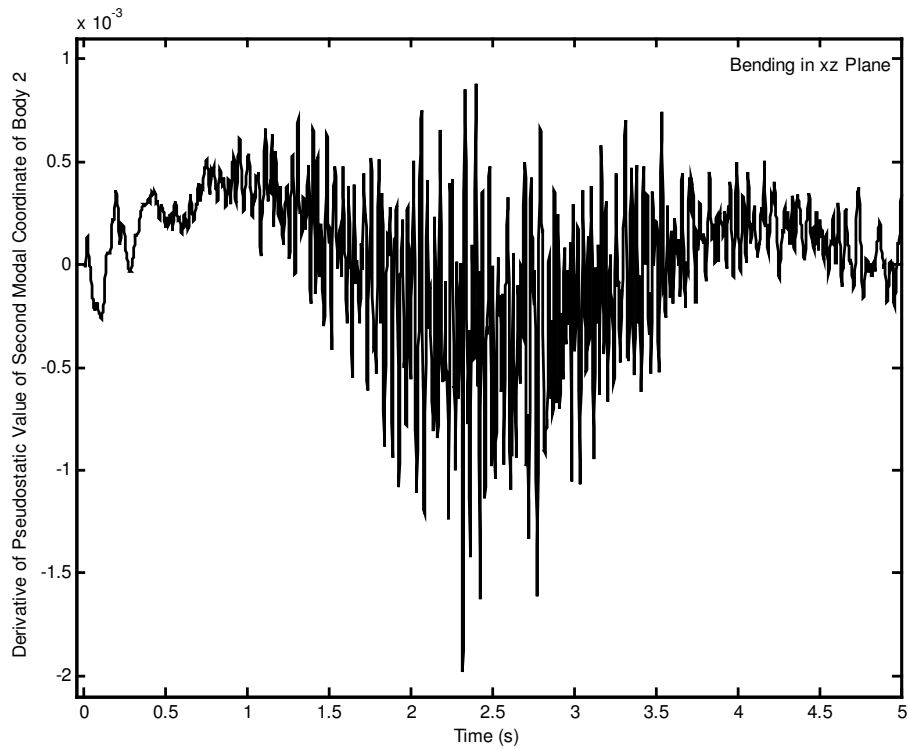


Figure 5.131 Derivative of pseudostatic value of second modal coordinate of body 2 for bending in xz plane.

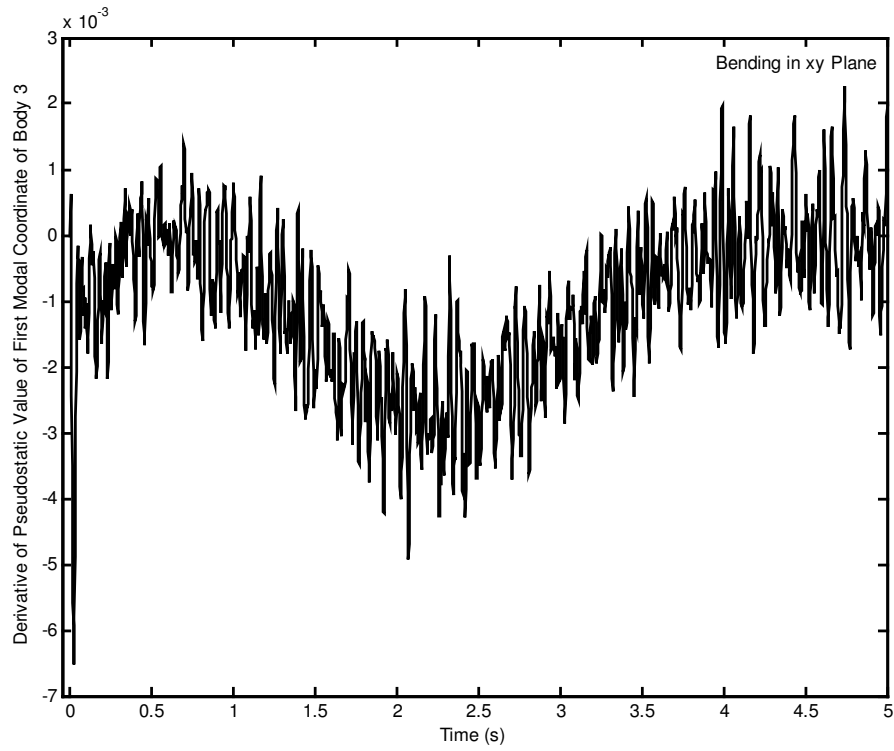


Figure 5.132 Derivative of pseudostatic value of first modal coordinate of body 3 for bending in xy plane.

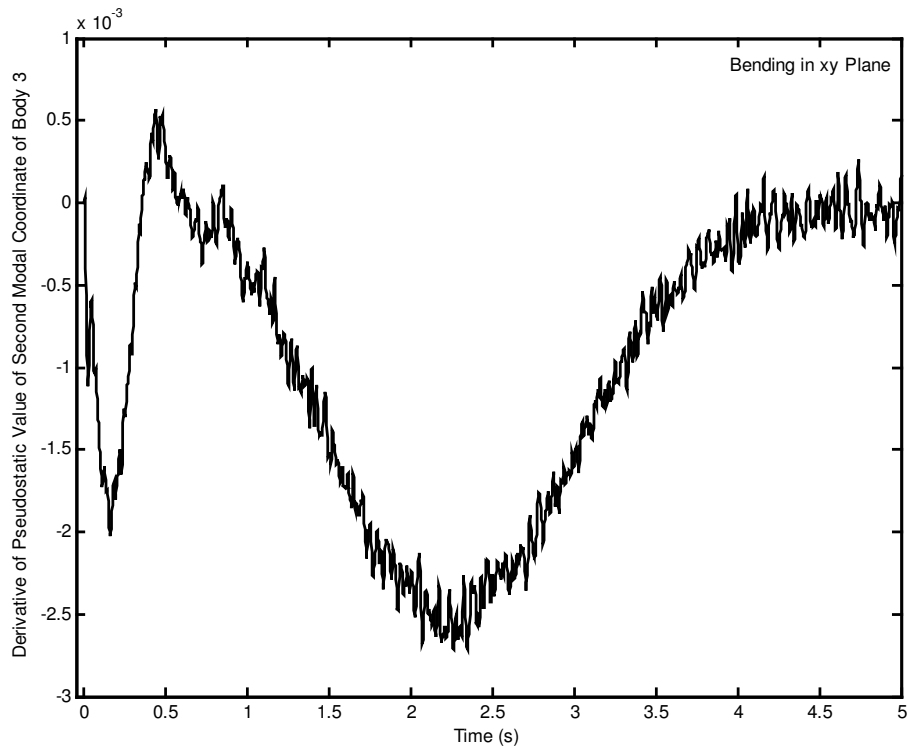


Figure 5.133 Derivative of pseudostatic value of second modal coordinate of body 3 for bending in xy plane.

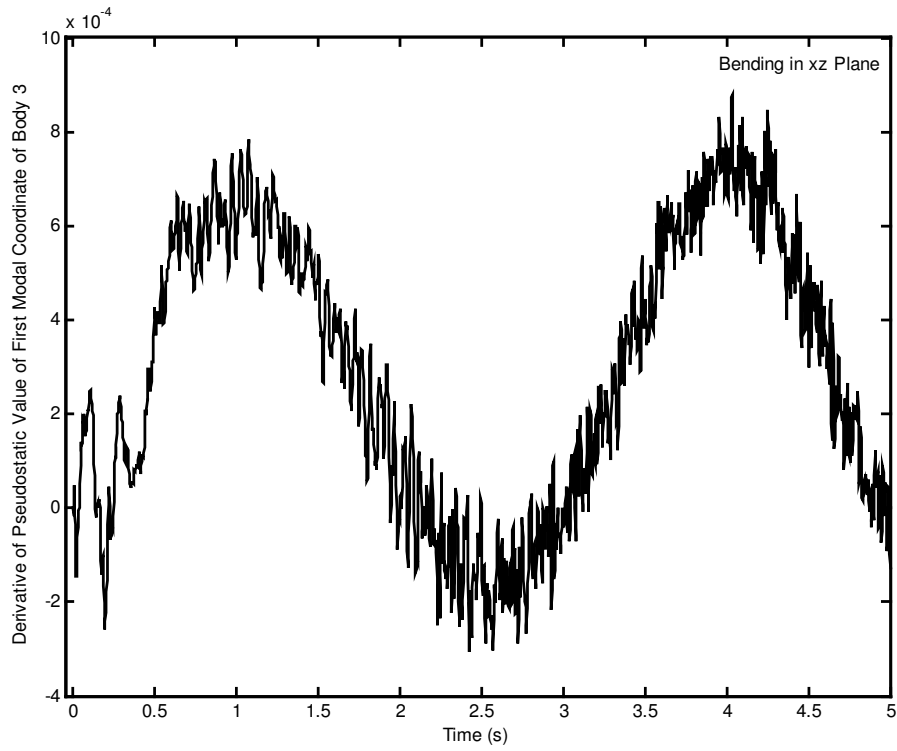


Figure 5.134 Derivative of pseudostatic value of first modal coordinate of body 3 for bending in xz plane.

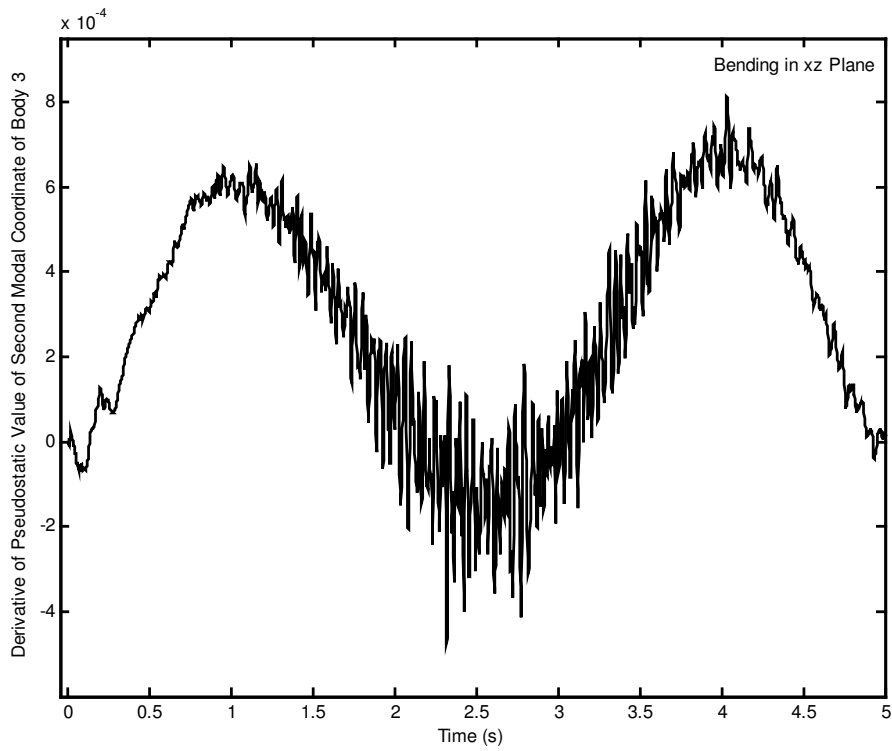


Figure 5.135 Derivative of pseudostatic value of second modal coordinate of body 3 for bending in xz plane.

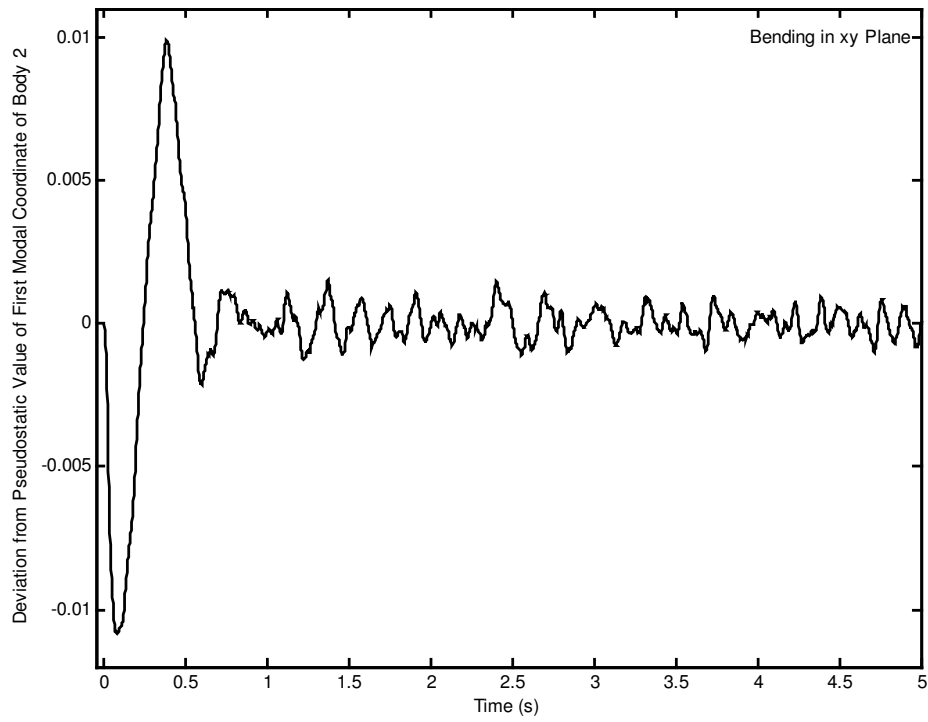


Figure 5.136 Deviation from pseudostatic value of first modal coordinate of body 2 for bending in xy plane.

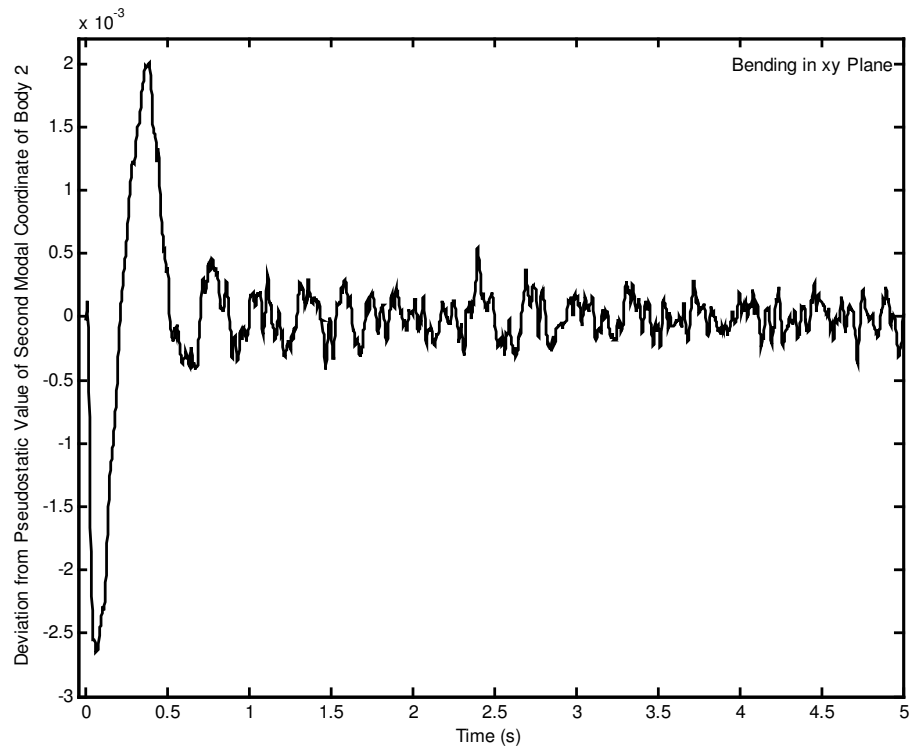


Figure 5.137 Deviation from pseudostatic value of second modal coordinate of body 2 for bending in xy plane.

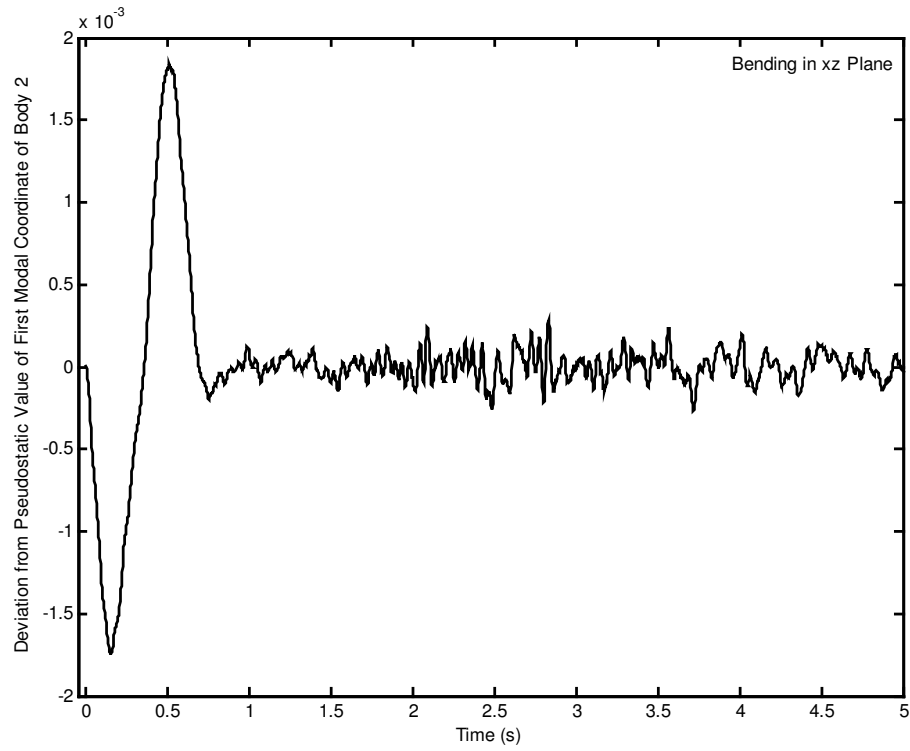


Figure 5.138 Deviation from pseudostatic value of first modal coordinate of body 2 for bending in xz plane.

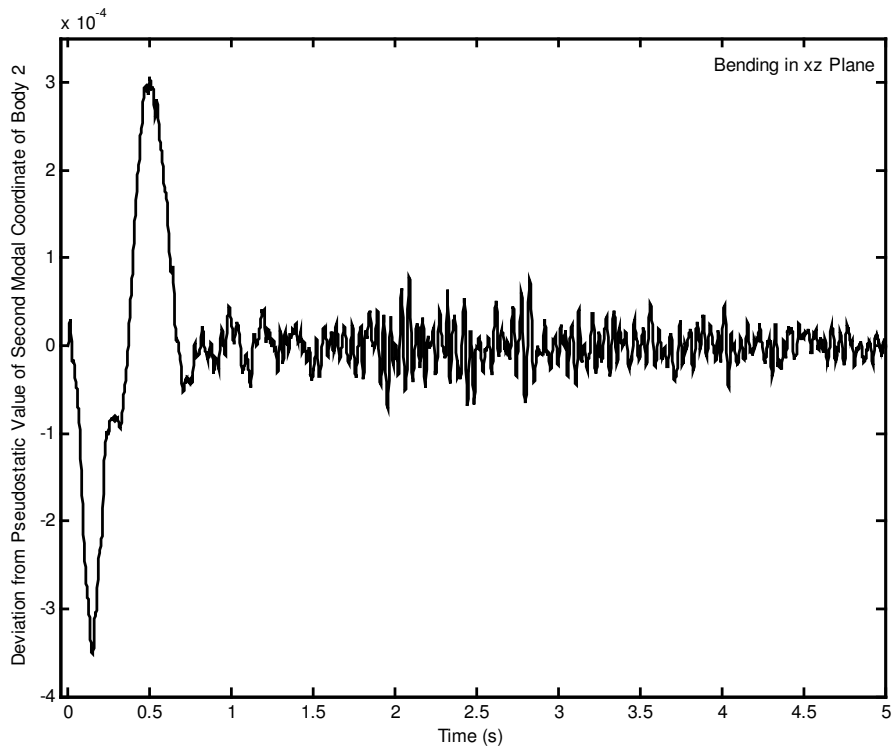


Figure 5.139 Deviation from pseudostatic value of second modal coordinate of body 2 for bending in xz plane.

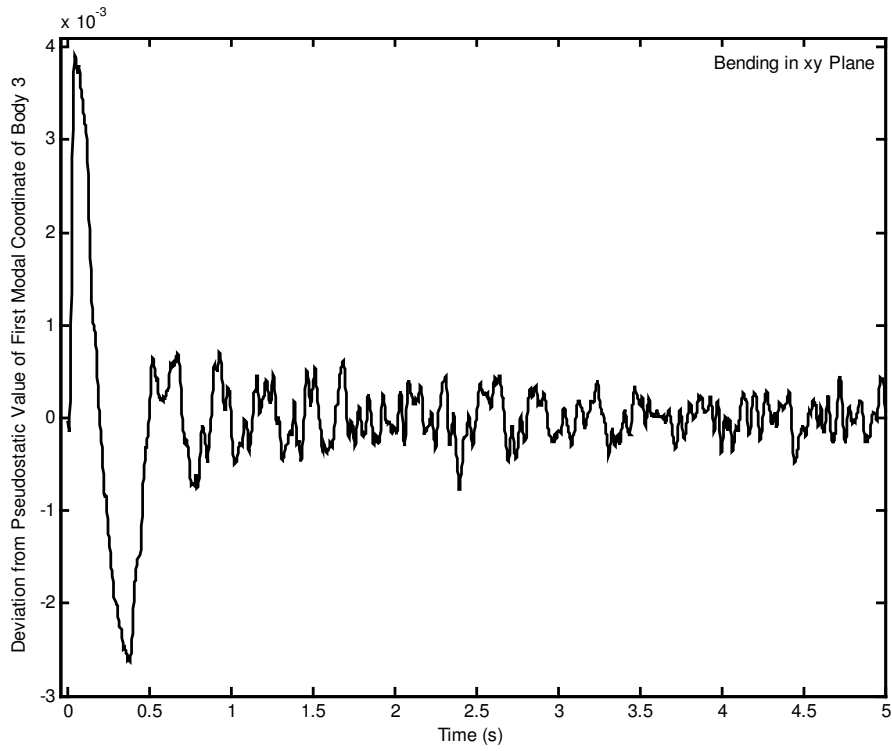


Figure 5.140 Deviation from pseudostatic value of first modal coordinate of body 3 for bending in xy plane.

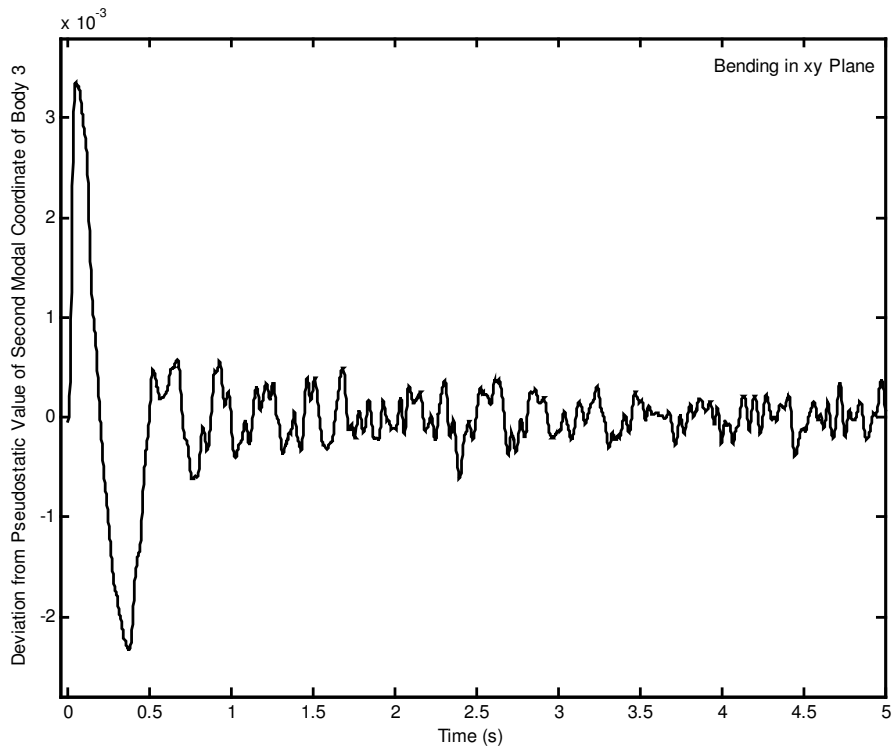


Figure 5.141 Deviation from pseudostatic value of second modal coordinate of body 3 for bending in xy plane.

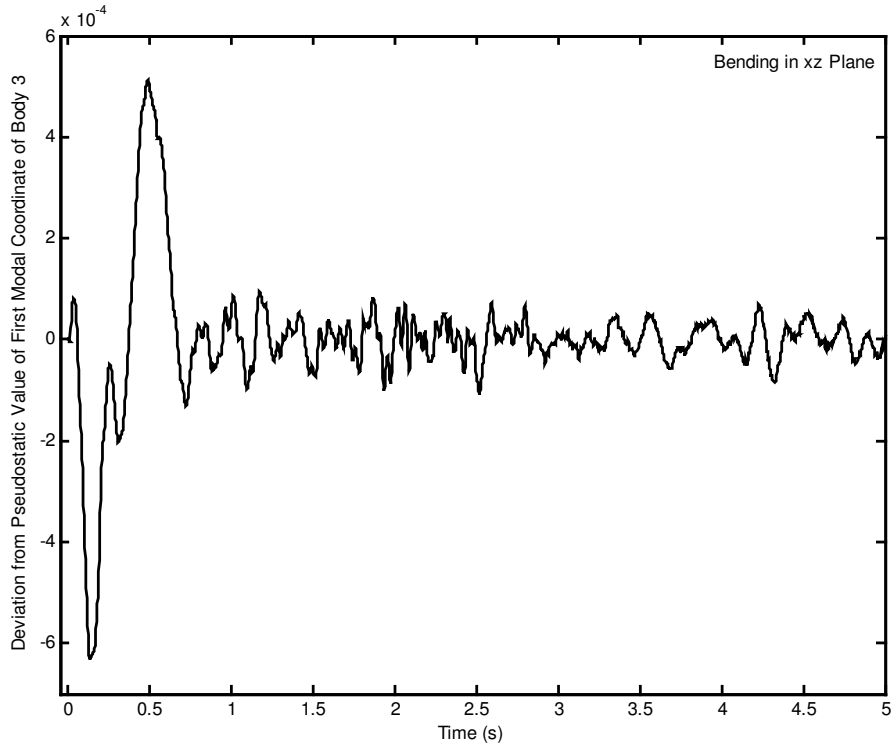


Figure 5.142 Deviation from pseudostatic value of first modal coordinate of body 3 for bending in xz plane.

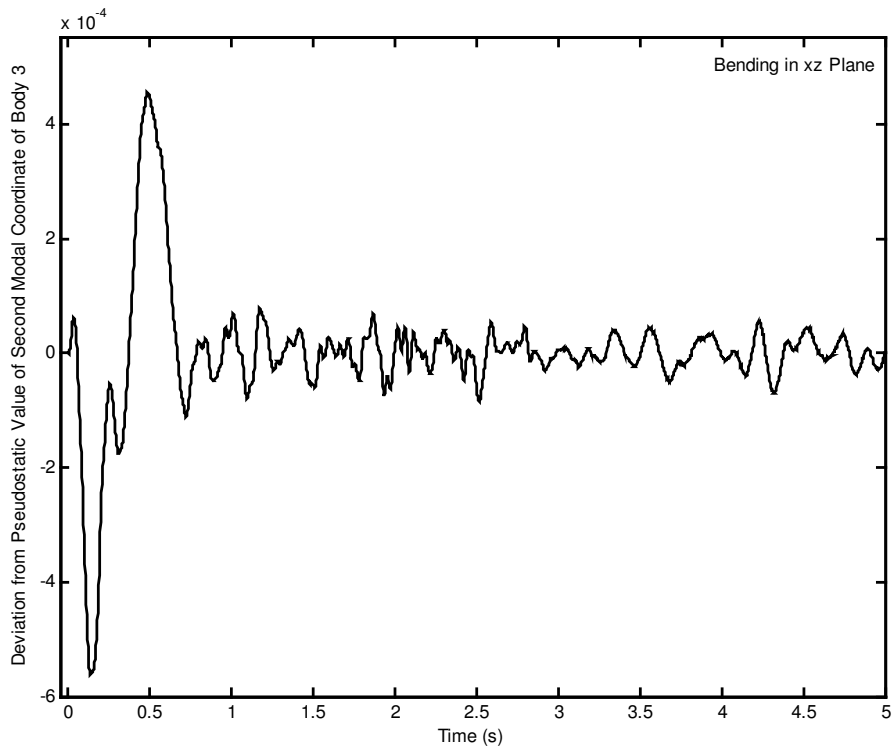


Figure 5.143 Deviation from pseudostatic value of second modal coordinate of body 3 for bending in xz plane.

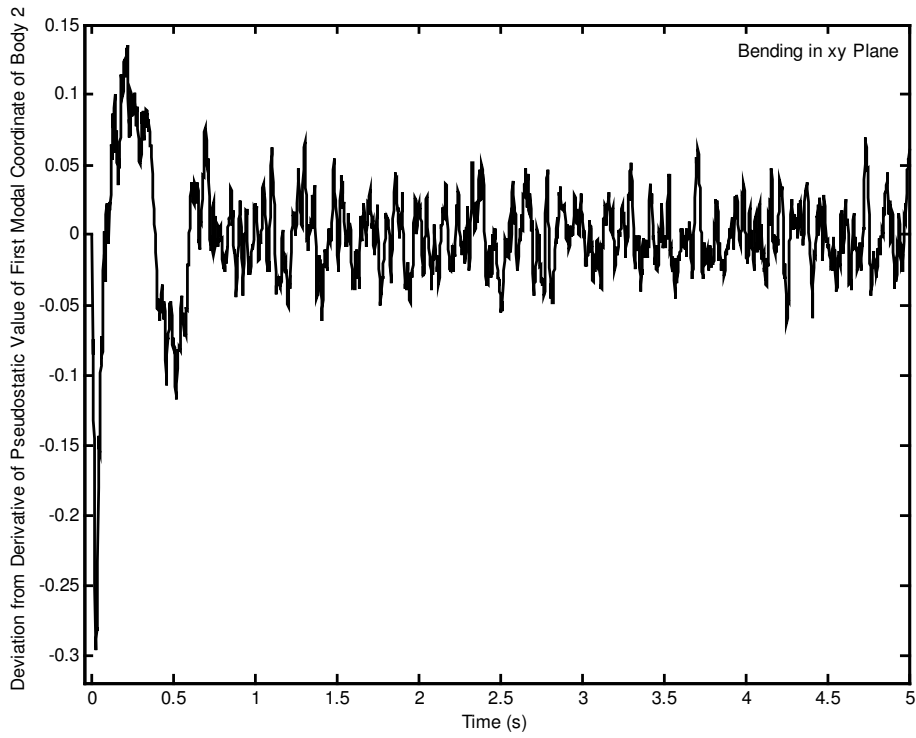


Figure 5.144 Deviation from derivative of pseudostatic value of first modal coordinate of body 2 for bending in xy plane.

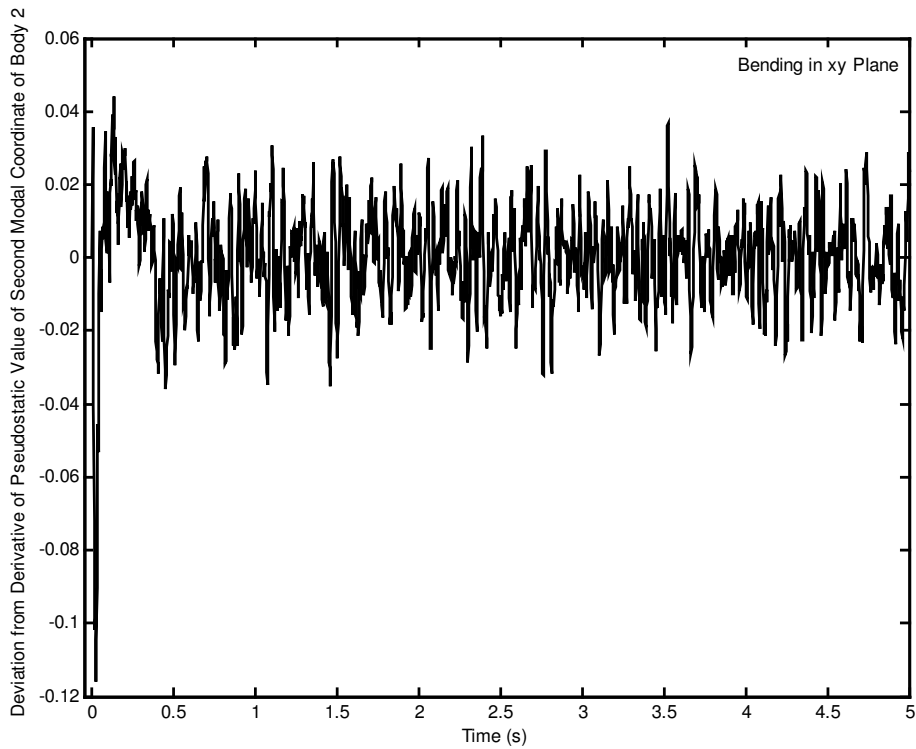


Figure 5.145 Deviation from derivative of pseudostatic value of second modal coordinate of body 2 for bending in xy plane.

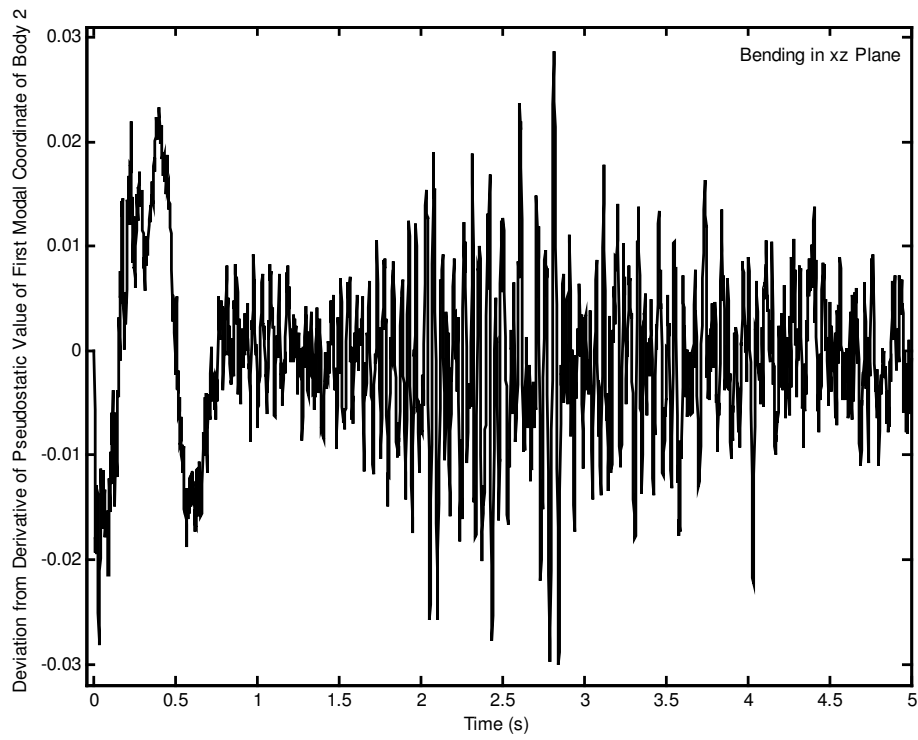


Figure 5.146 Deviation from derivative of pseudostatic value of first modal coordinate of body 2 for bending in xz plane.

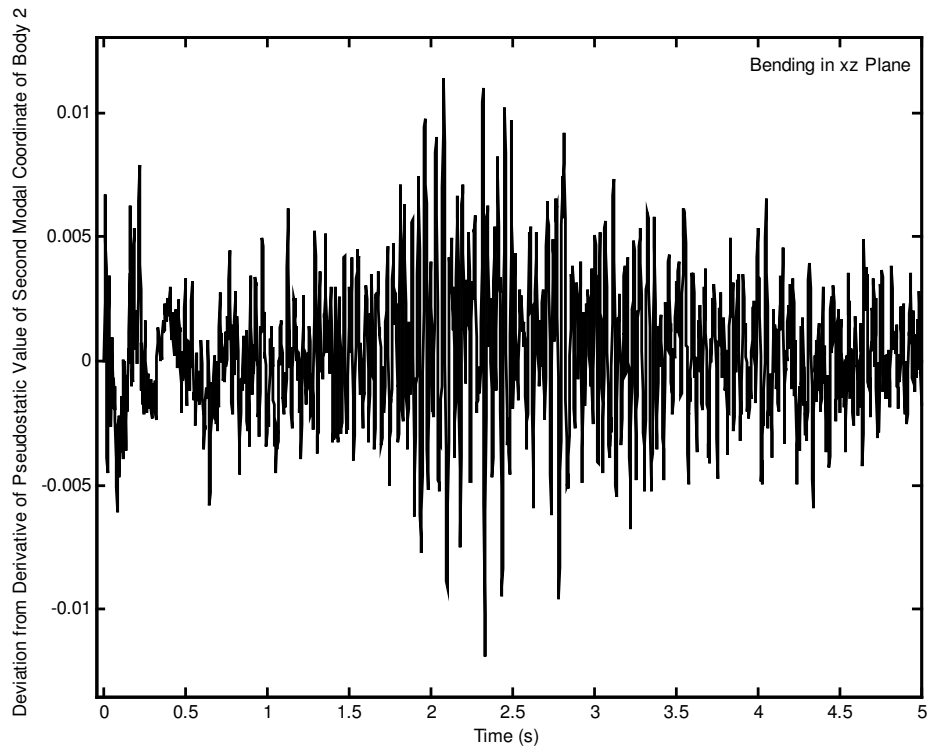


Figure 5.147 Deviation from derivative of pseudostatic value of second modal coordinate of body 2 for bending in xz plane.

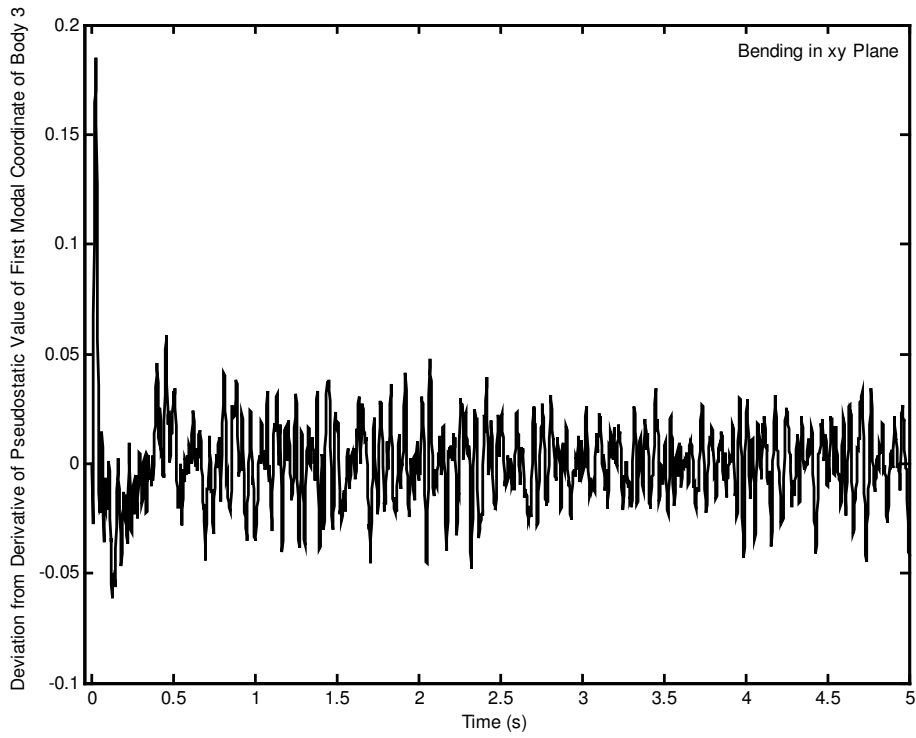


Figure 5.148 Deviation from derivative of pseudostatic value of first modal coordinate of body 3 for bending in xy plane.

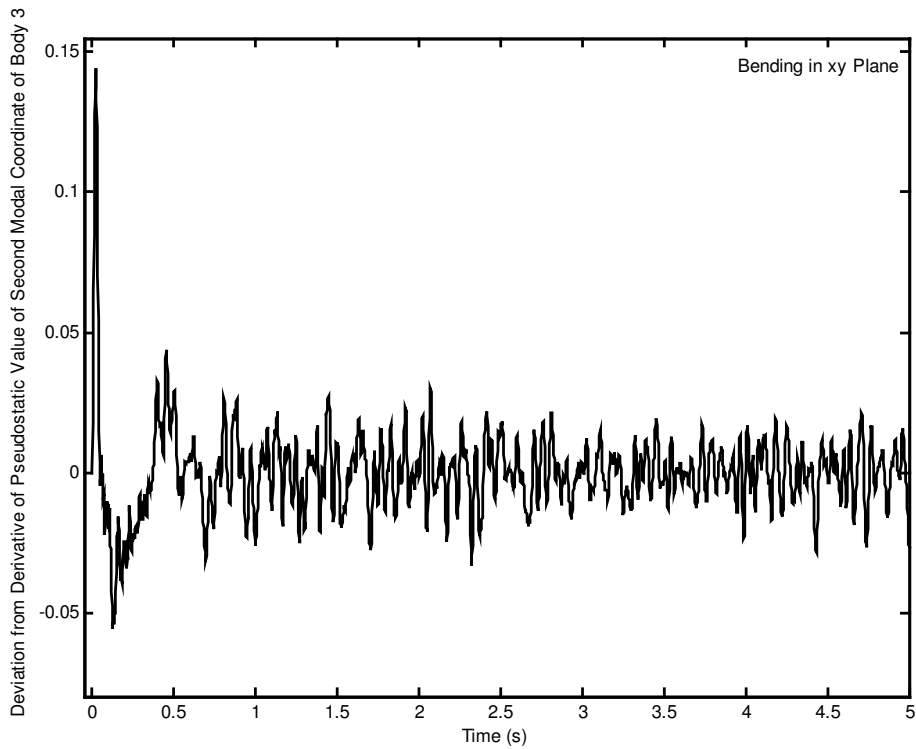


Figure 5.149 Deviation from derivative of pseudostatic value of second modal coordinate of body 3 for bending in xy plane.

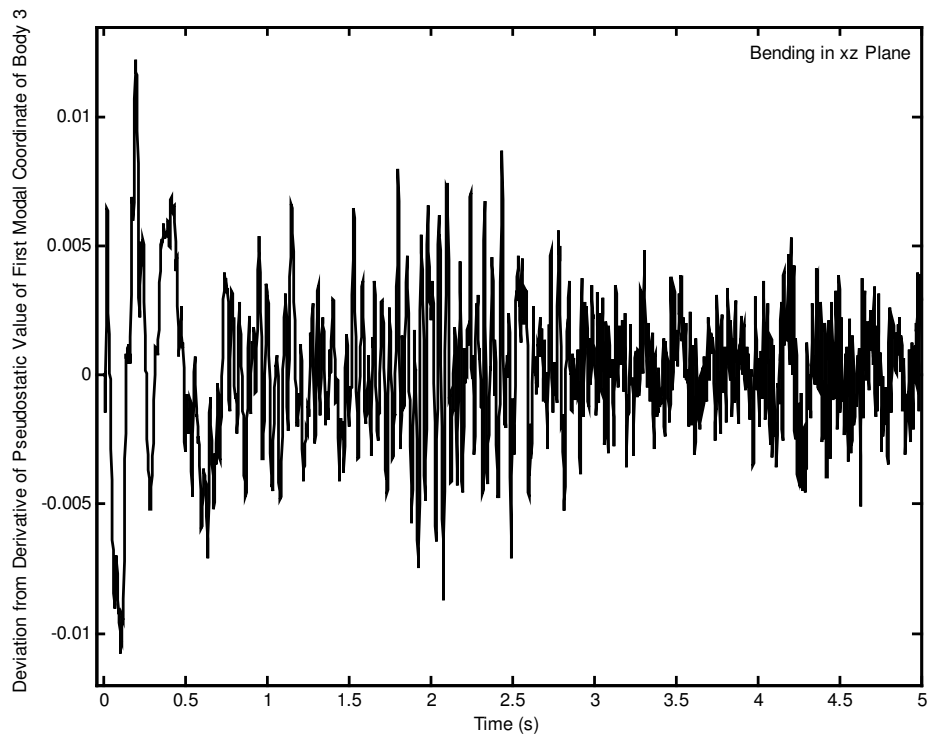


Figure 5.150 Deviation from derivative of pseudostatic value of first modal coordinate of body 3 for bending in xz plane.

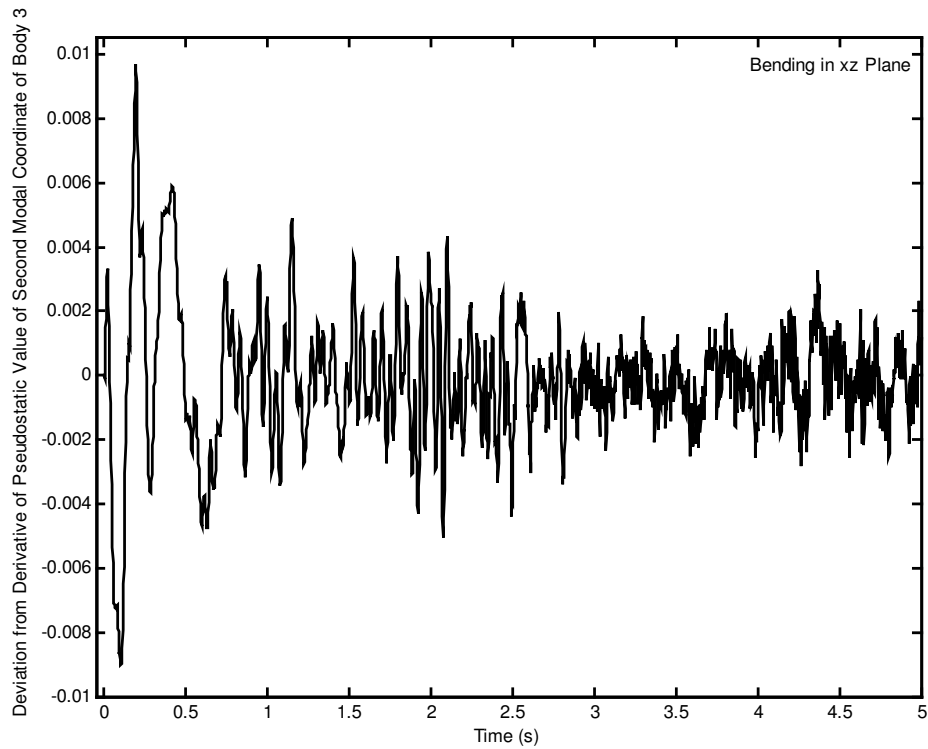


Figure 5.151 Deviation from derivative of pseudostatic value of second modal coordinate of body 3 for bending in xz plane.

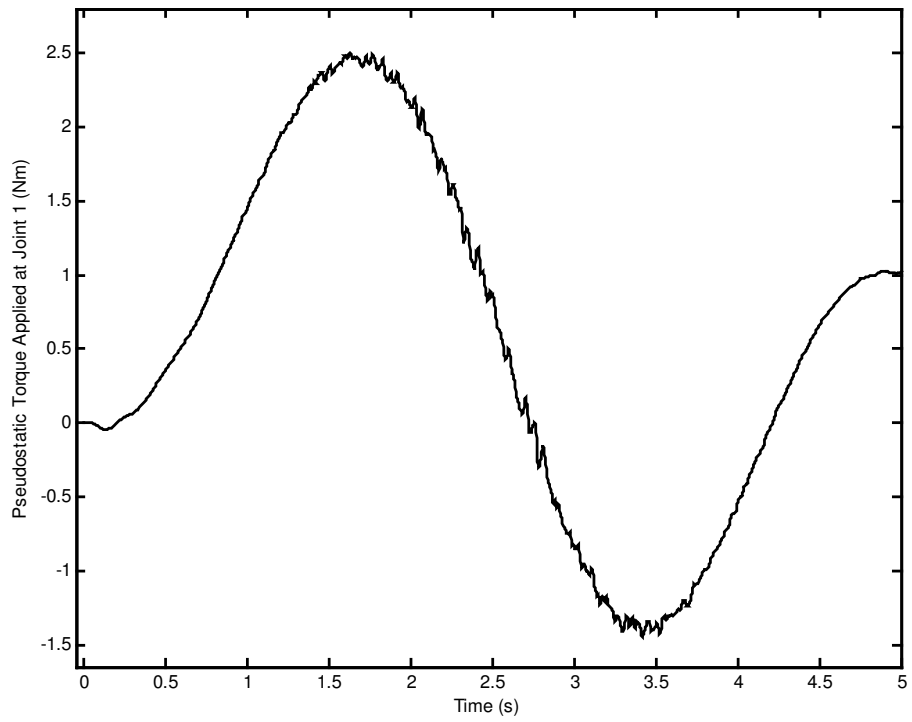


Figure 5.152 Pseudostatic torque applied at joint 1.

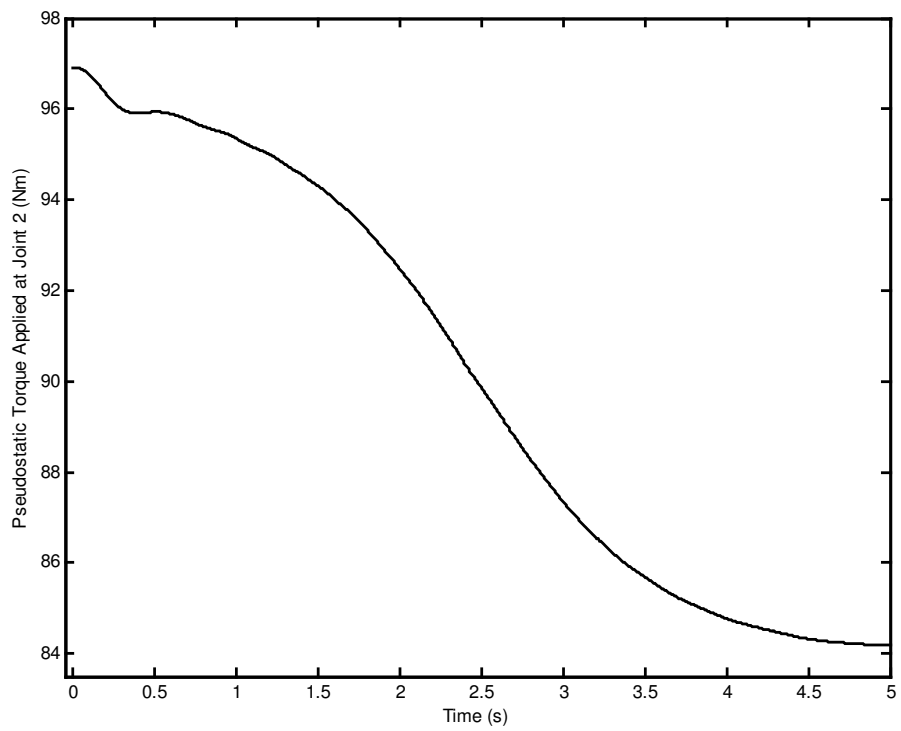


Figure 5.153 Pseudostatic torque applied at joint 2.

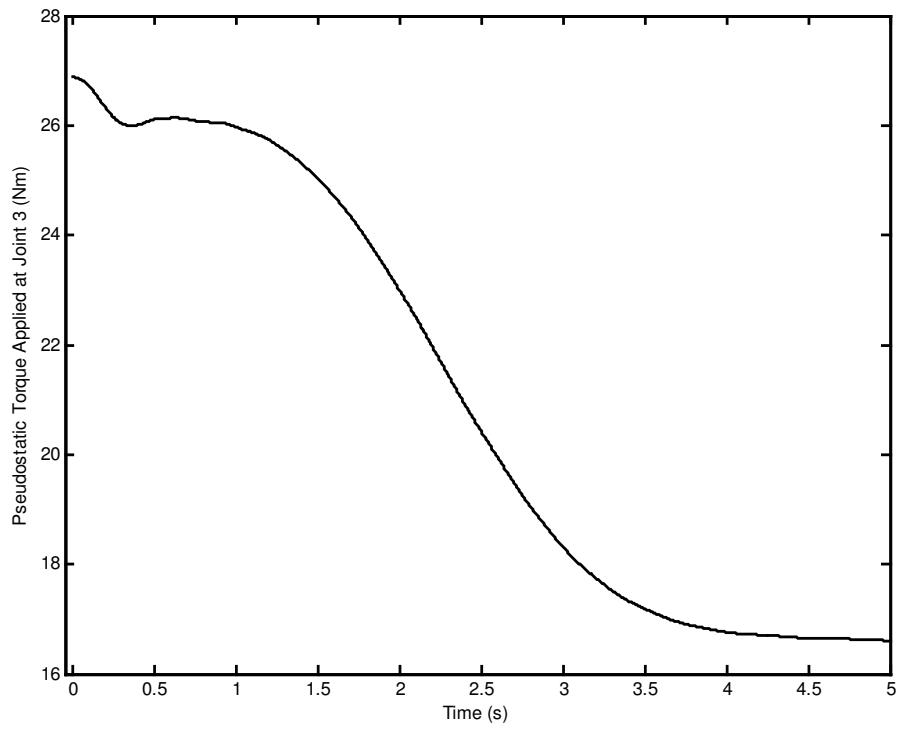


Figure 5.154 Pseudostatic torque applied at joint 3.

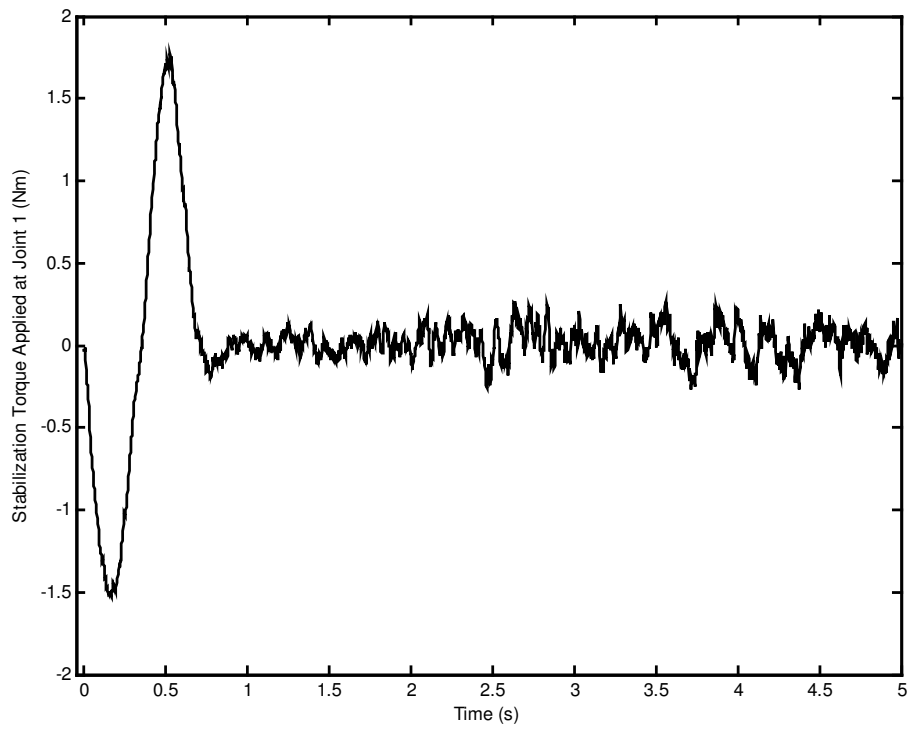


Figure 5.155 Stabilization torque applied at joint 1.

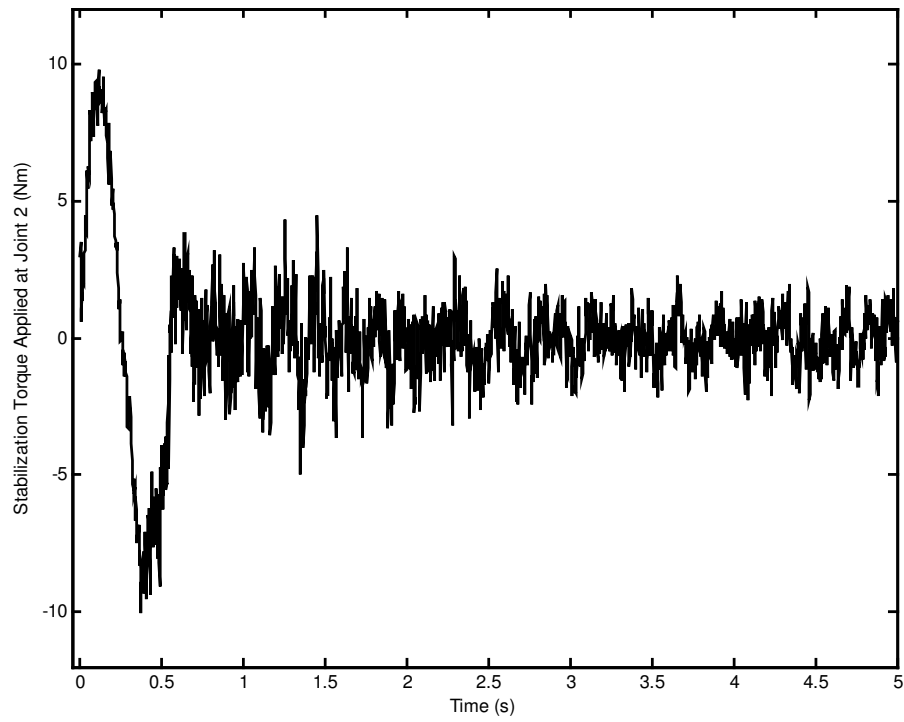


Figure 5.156 Stabilization torque applied at joint 2.

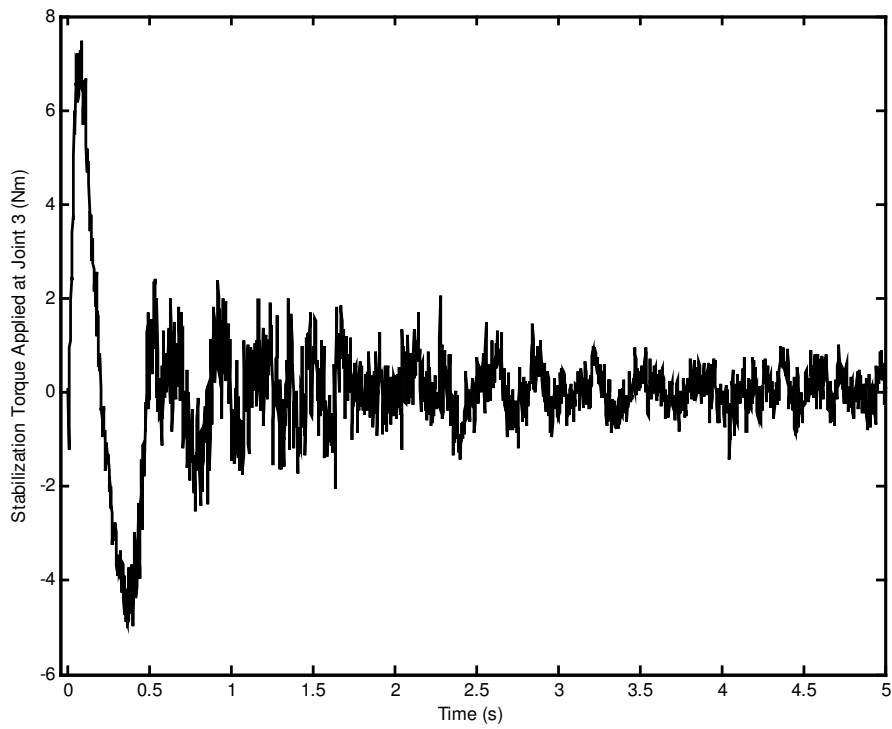


Figure 5.157 Stabilization torque applied at joint 3.

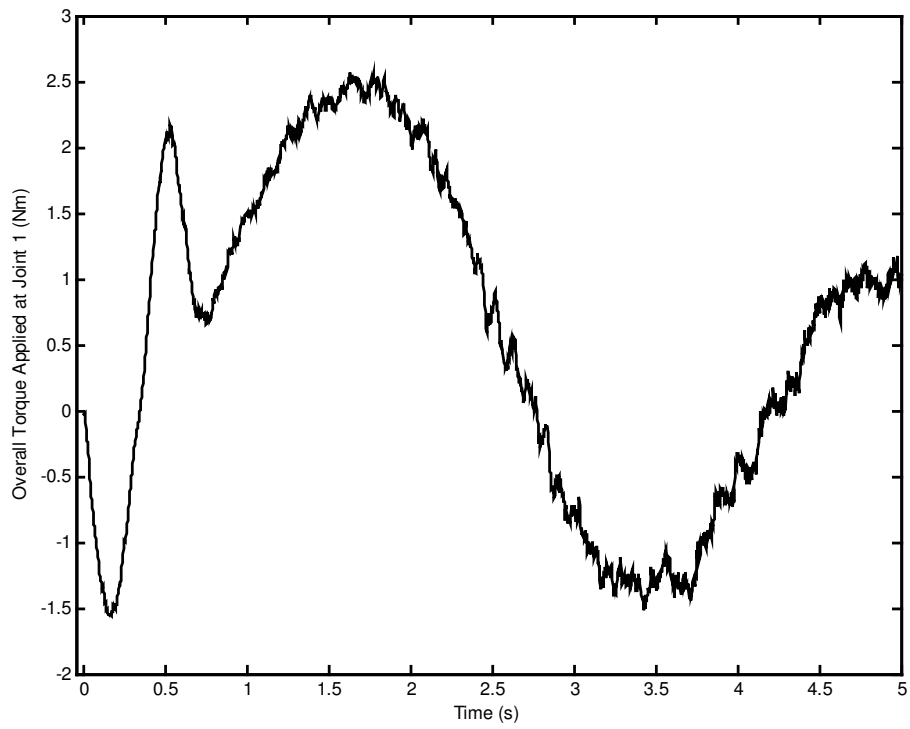


Figure 5.158 Overall torque applied at joint 1.

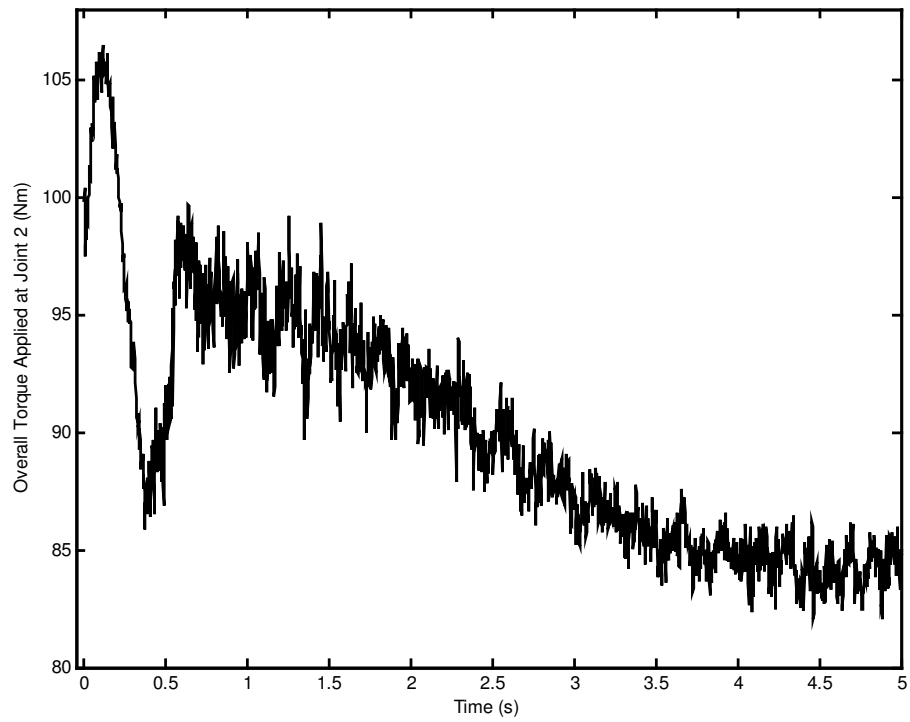


Figure 5.159 Overall torque applied at joint 2.

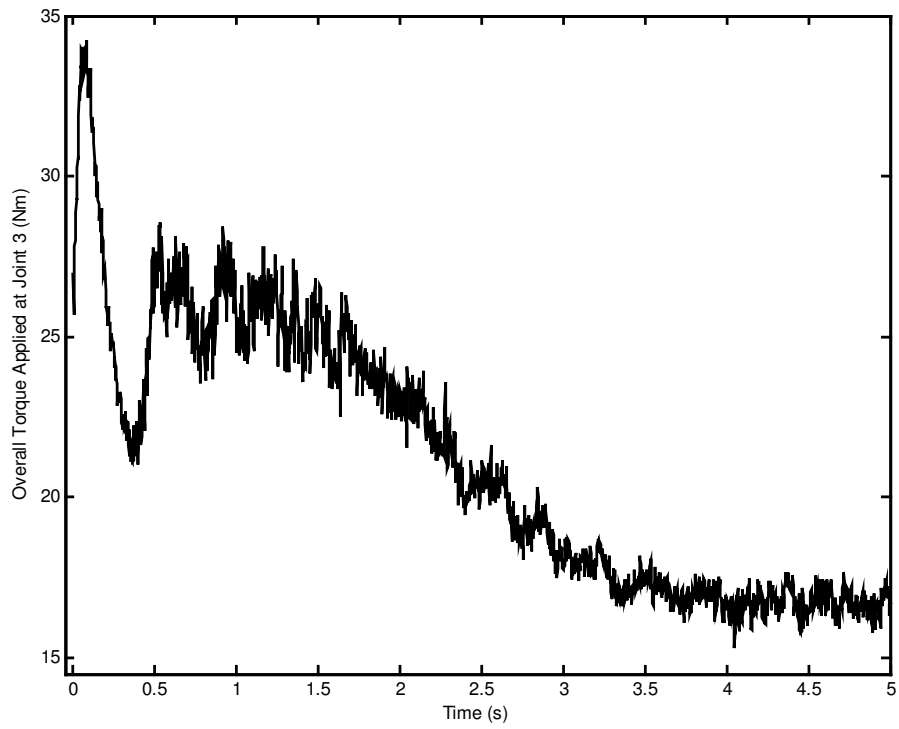


Figure 5.160 Overall torque applied at joint 3.

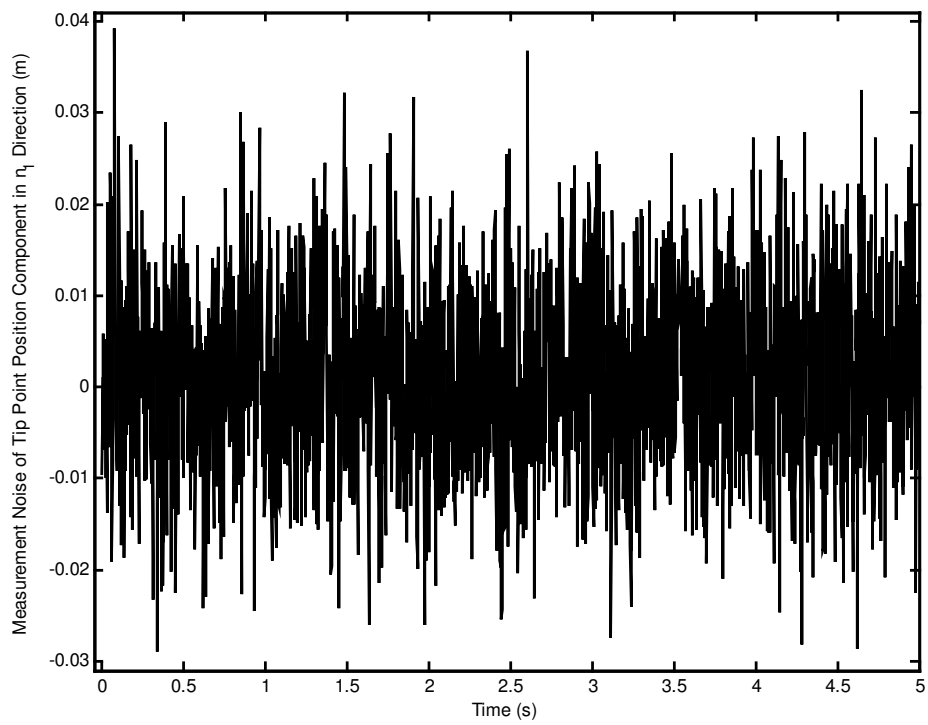


Figure 5.161 Measurement noise of tip point position component in n_1 direction.

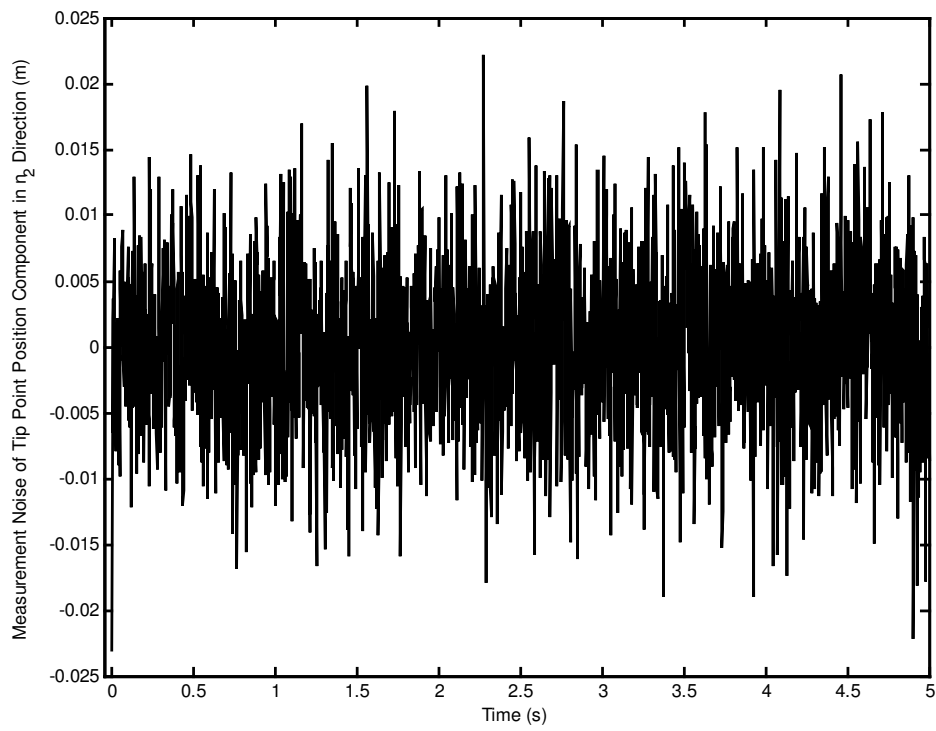


Figure 5.162 Measurement noise of tip point position component in n_2 direction.

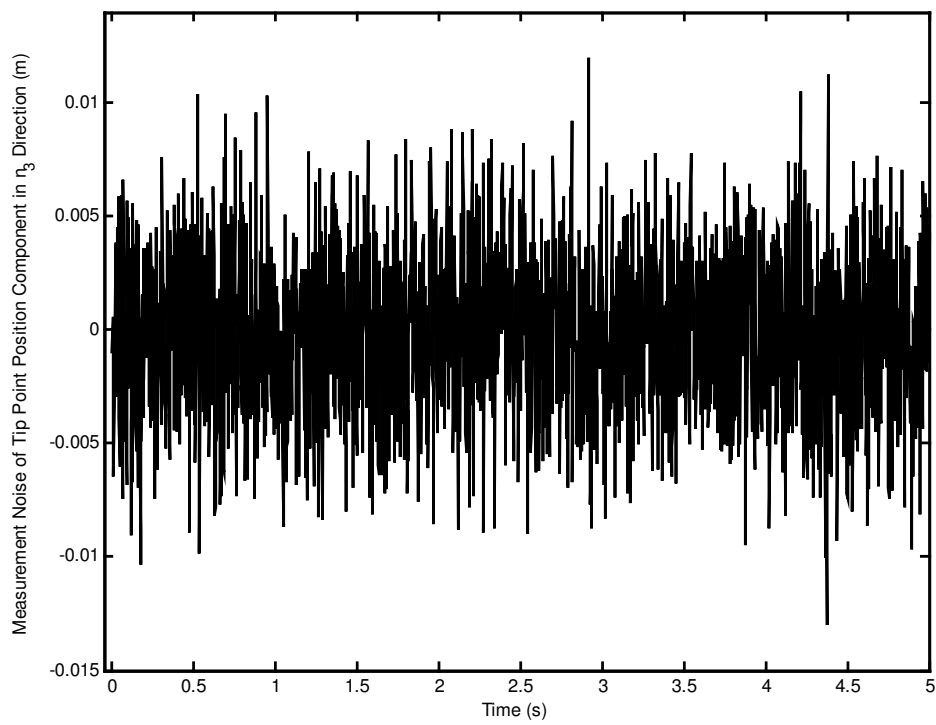


Figure 5.163 Measurement noise of tip point position component in n_3 direction.

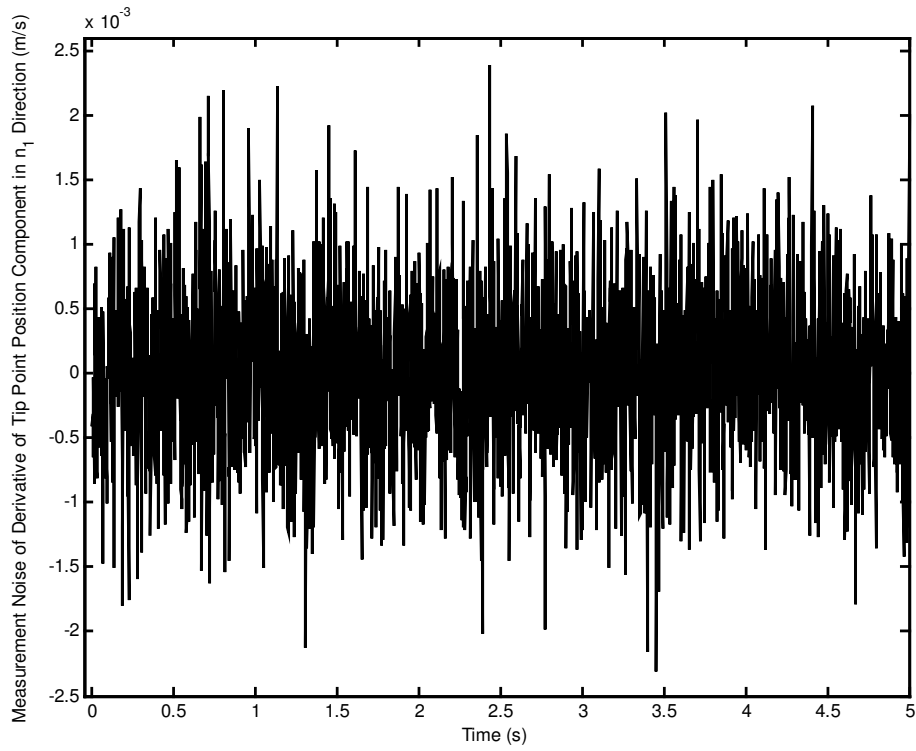


Figure 5.164 Measurement noise of tip point velocity component in n_1 direction.

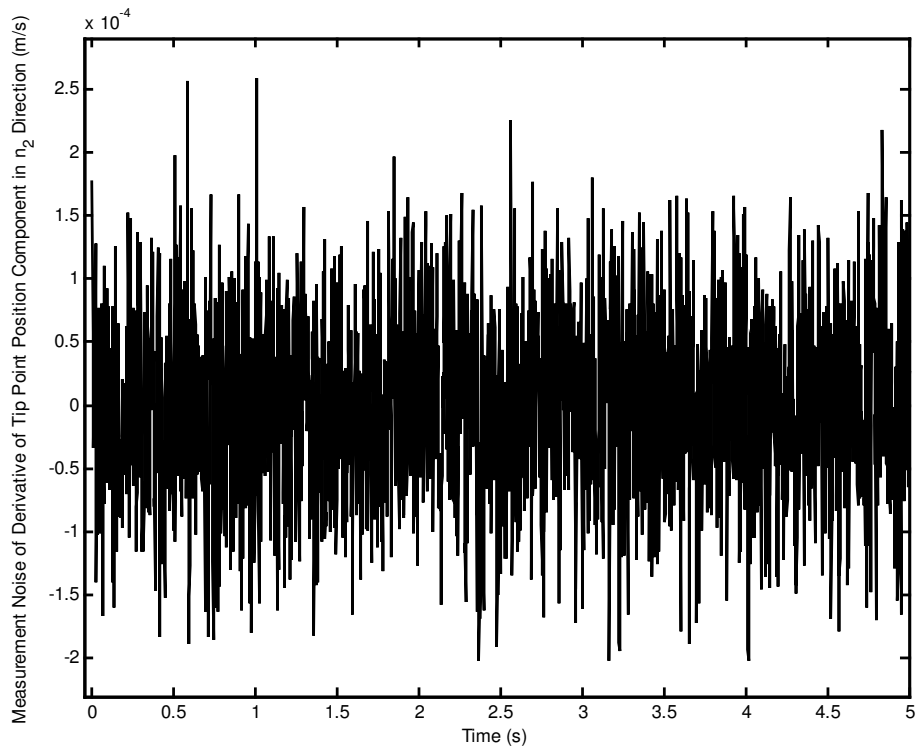


Figure 5.165 Measurement noise of tip point velocity component in n_2 direction.

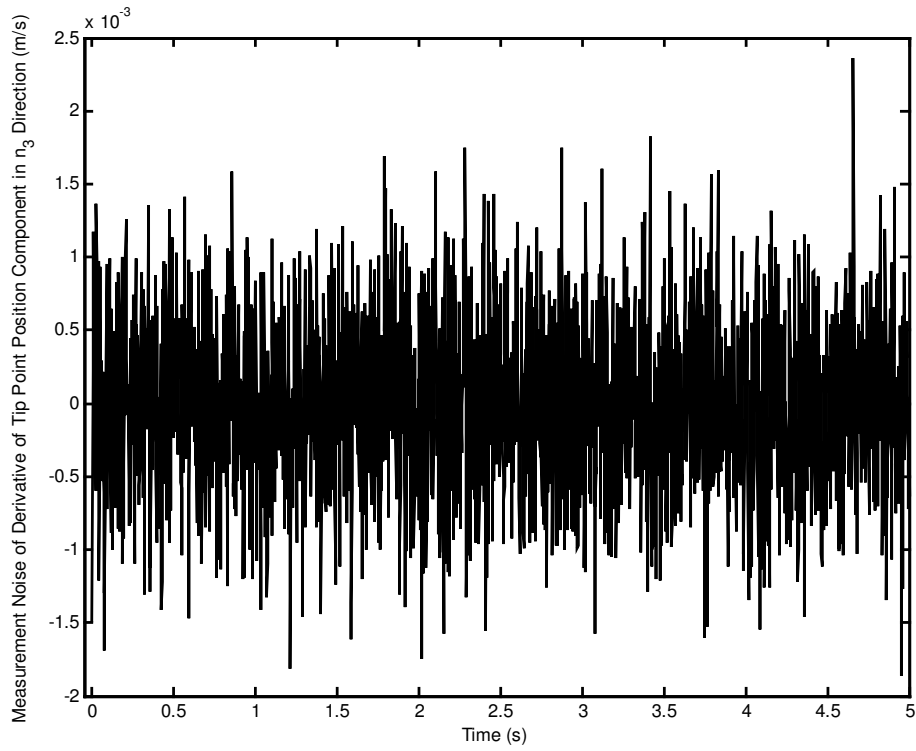


Figure 5.166 Measurement noise of tip point velocity component in n_3 direction.

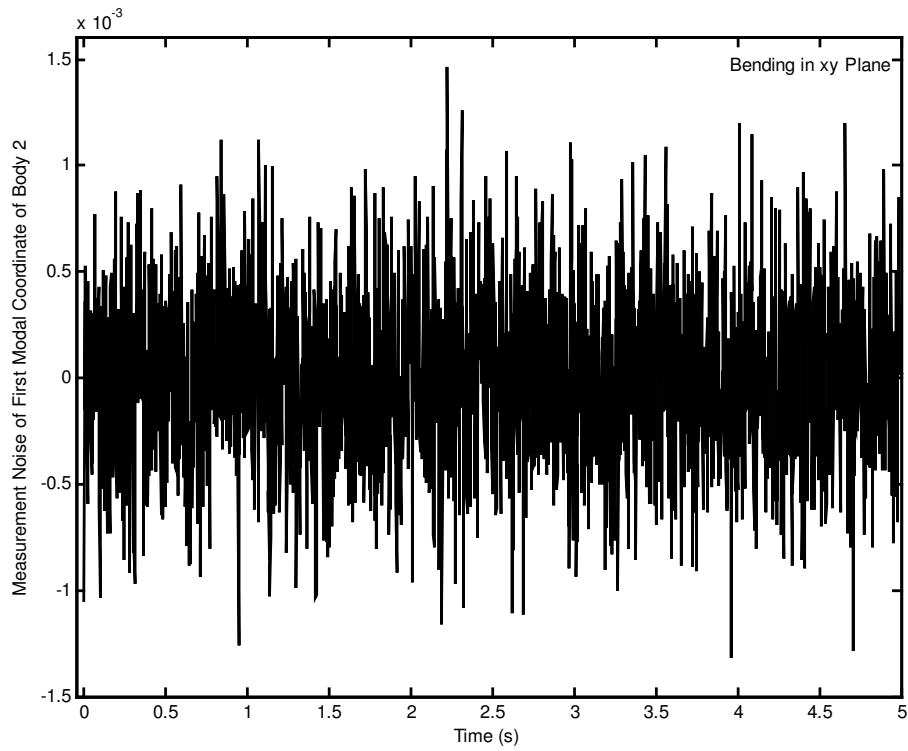


Figure 5.167 Measurement noise of first modal coordinate of body 2 for bending in xy plane.

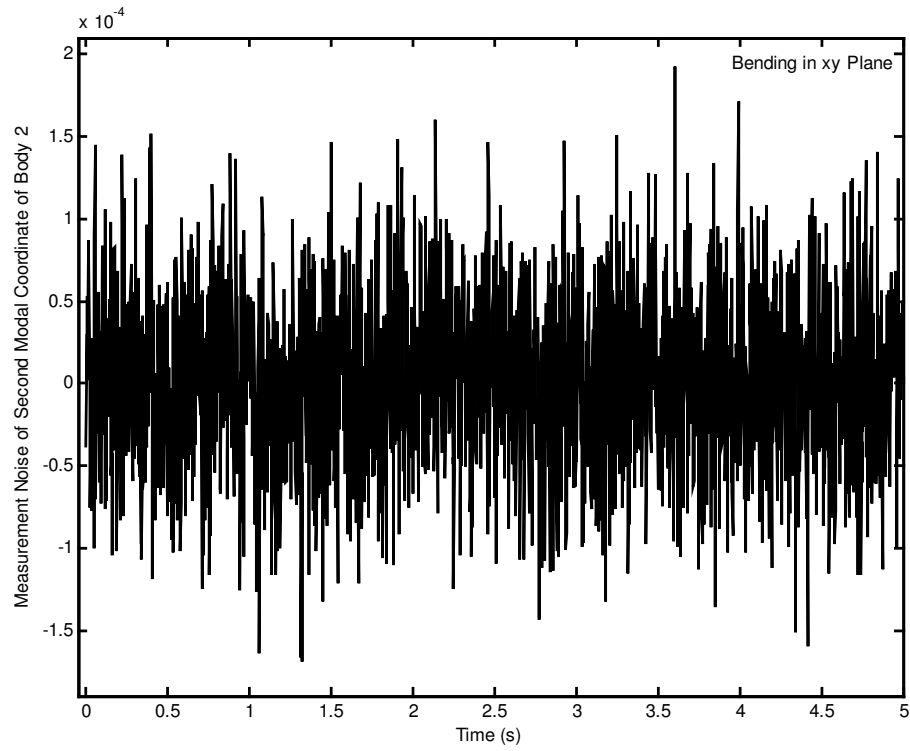


Figure 5.168 Measurement noise of second modal coordinate of body 2 for bending in xy plane.

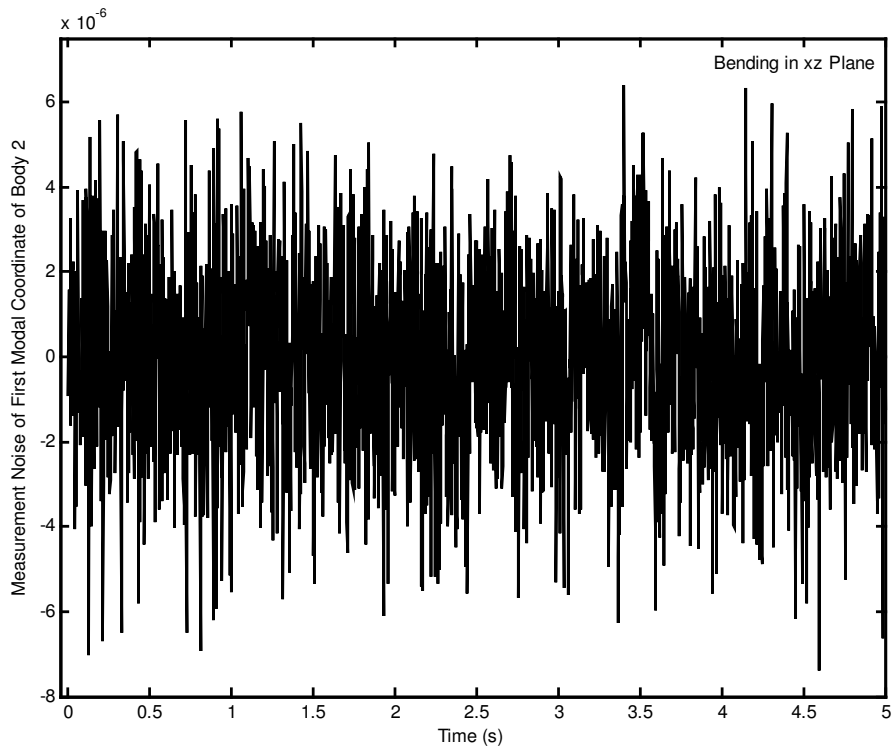


Figure 5.169 Measurement noise of first modal coordinate of body 2 for bending in xz plane.

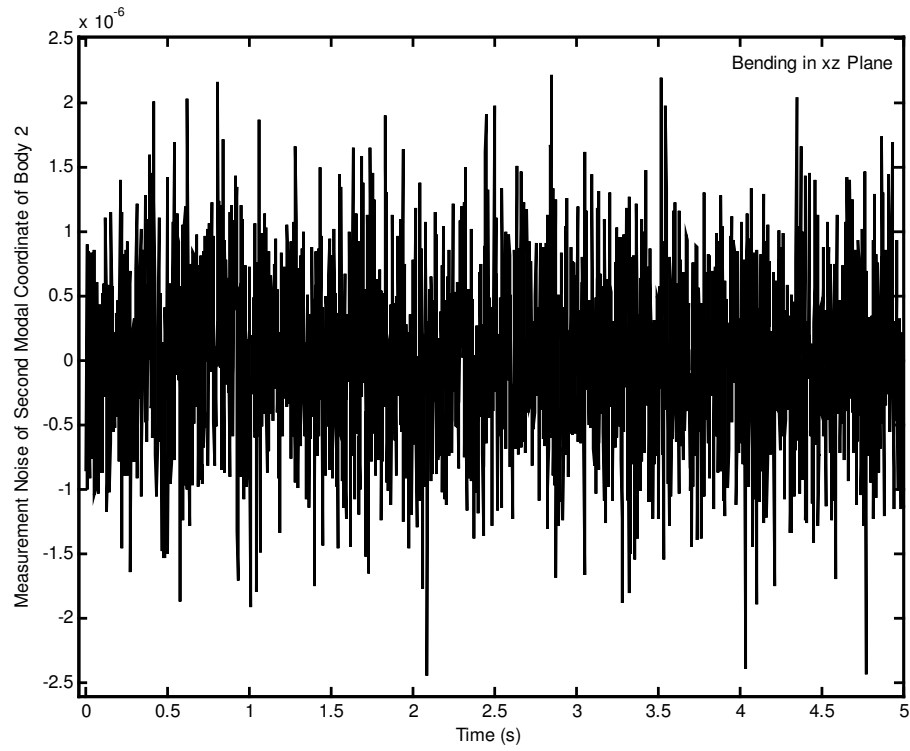


Figure 5.170 Measurement noise of second modal coordinate of body 2 for bending in xz plane.

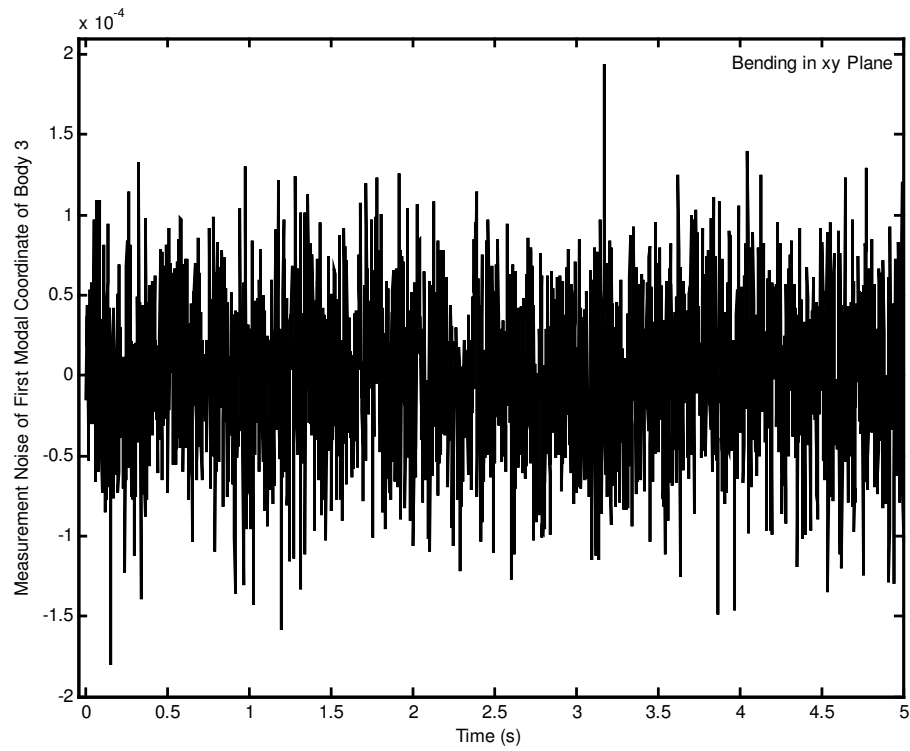


Figure 5.171 Measurement noise of first modal coordinate of body 3 for bending in xy plane.

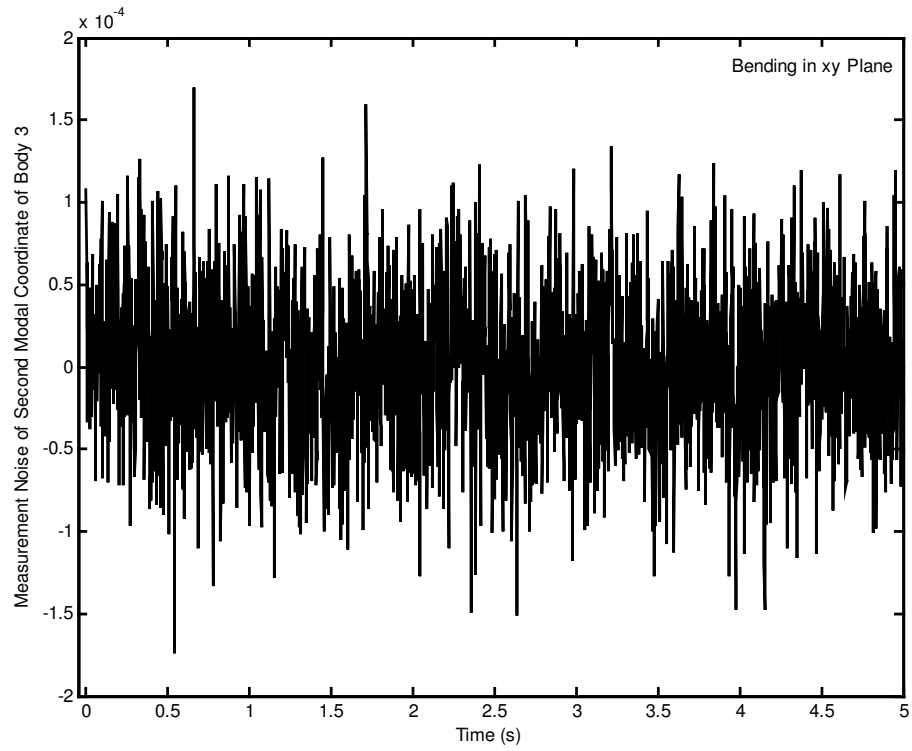


Figure 5.172 Measurement noise of second modal coordinate of body 3 for bending in xy plane.

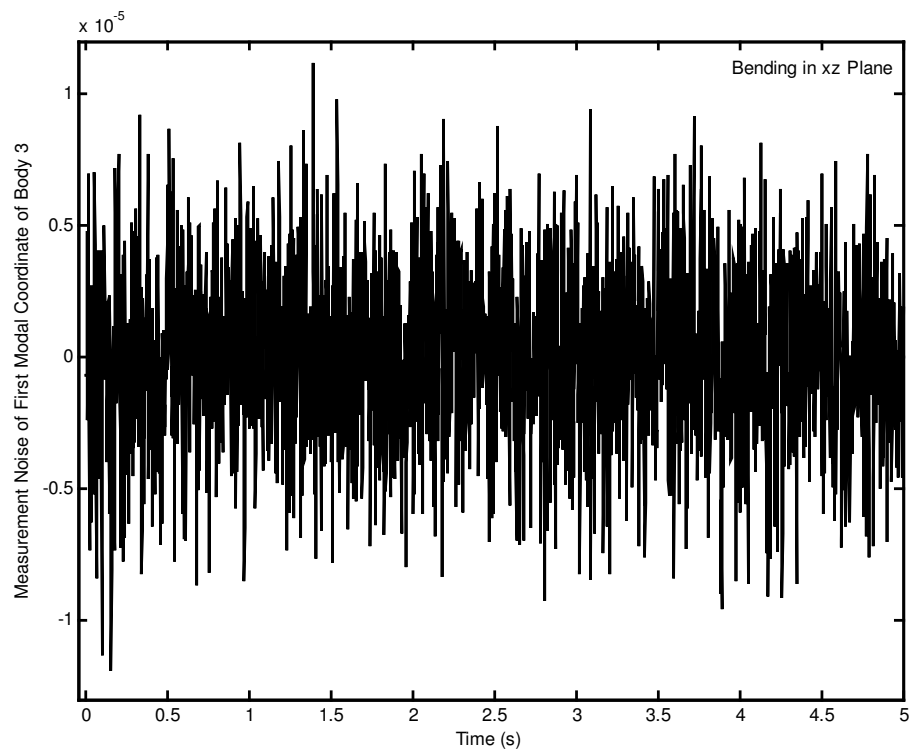


Figure 5.173 Measurement noise of first modal coordinate of body 3 for bending in xz plane.

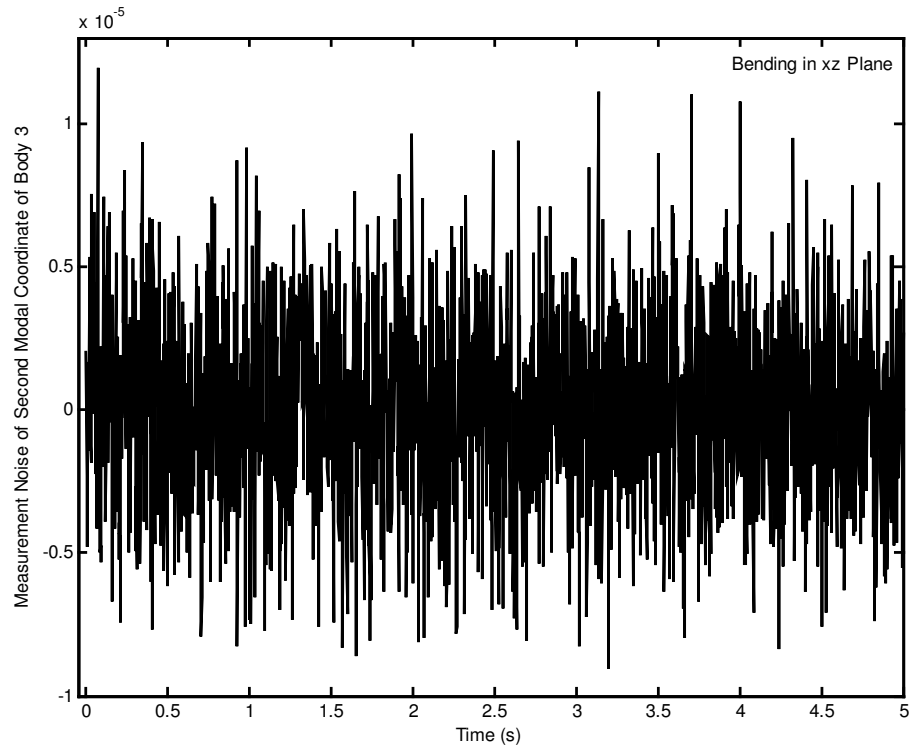


Figure 5.174 Measurement noise of second modal coordinate of body 3 for bending in xz plane.

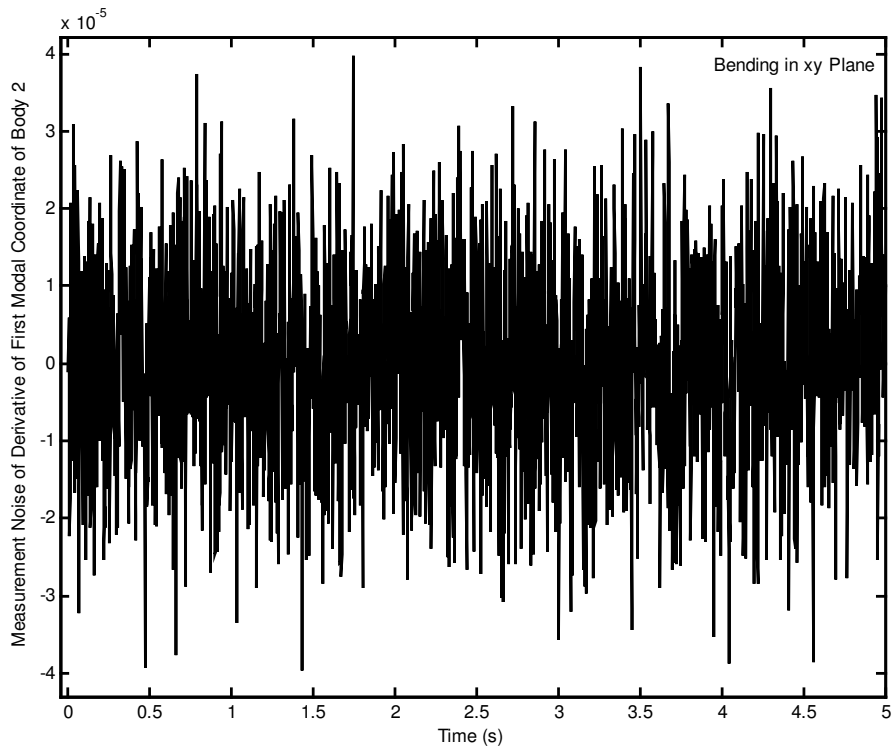


Figure 5.175 Measurement noise of derivative of first modal coordinate of body 2 for bending in xy plane.

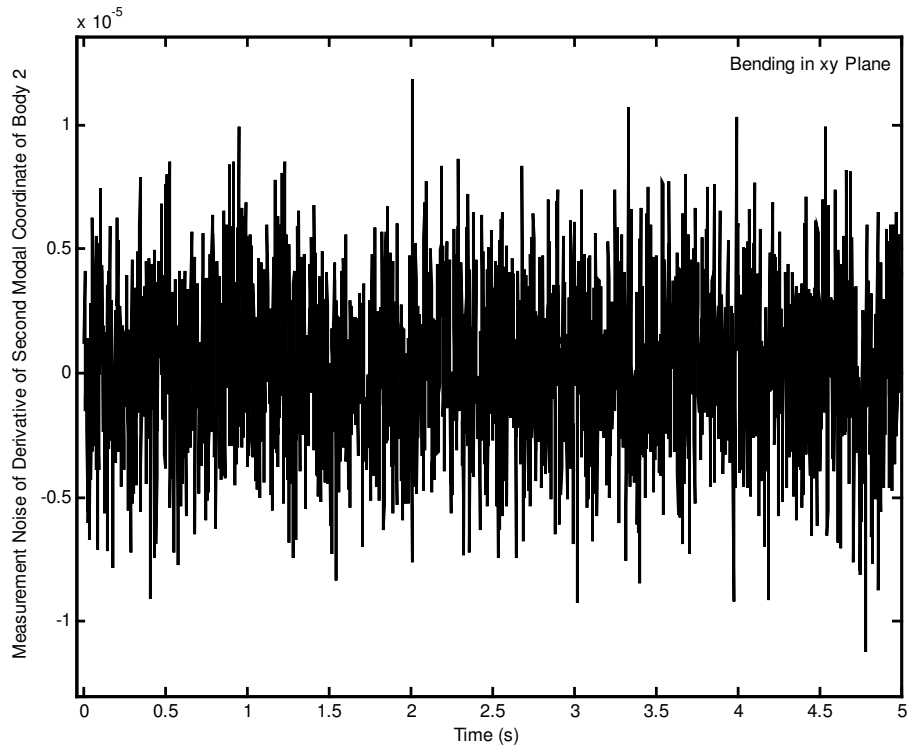


Figure 5.176 Measurement noise of derivative of second modal coordinate of body 2 for bending in xy plane.

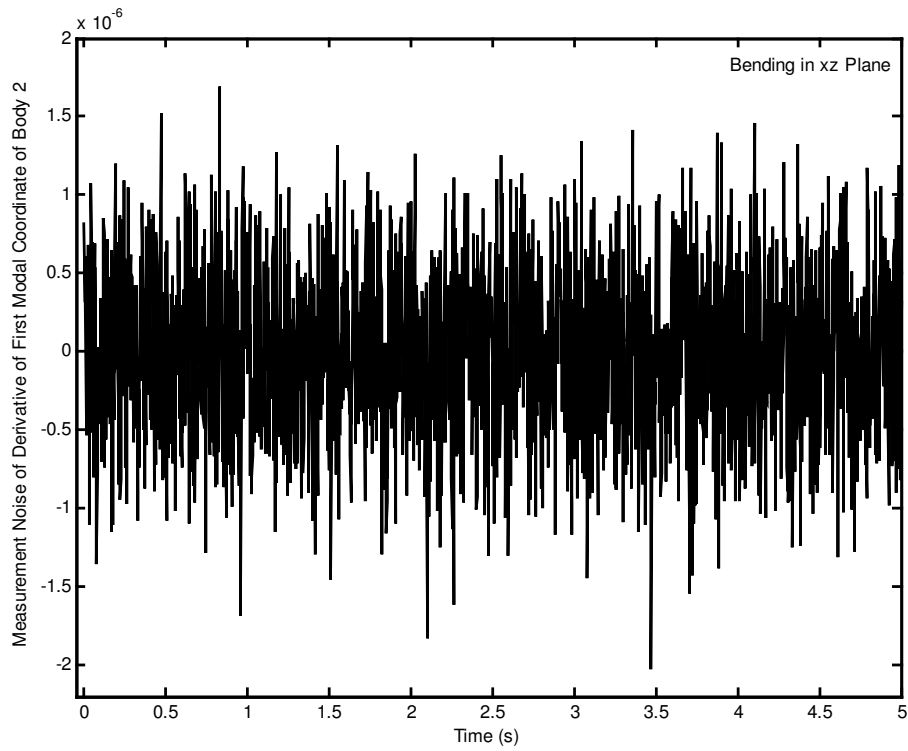


Figure 5.177 Measurement noise of derivative of first modal coordinate of body 2 for bending in xz plane.

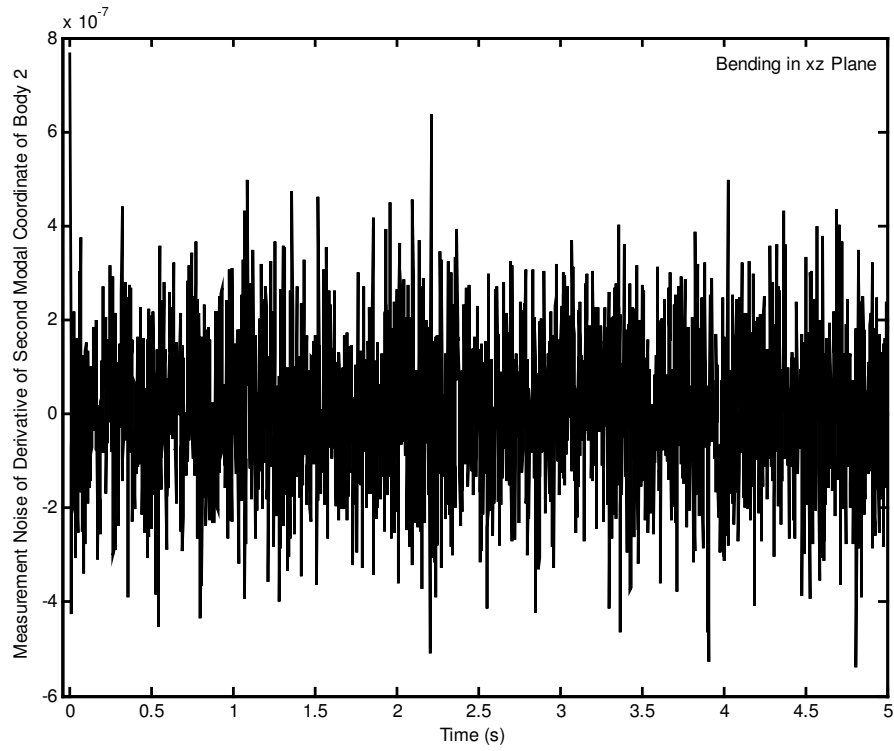


Figure 5.178 Measurement noise of derivative of second modal coordinate of body 2 for bending in xz plane.

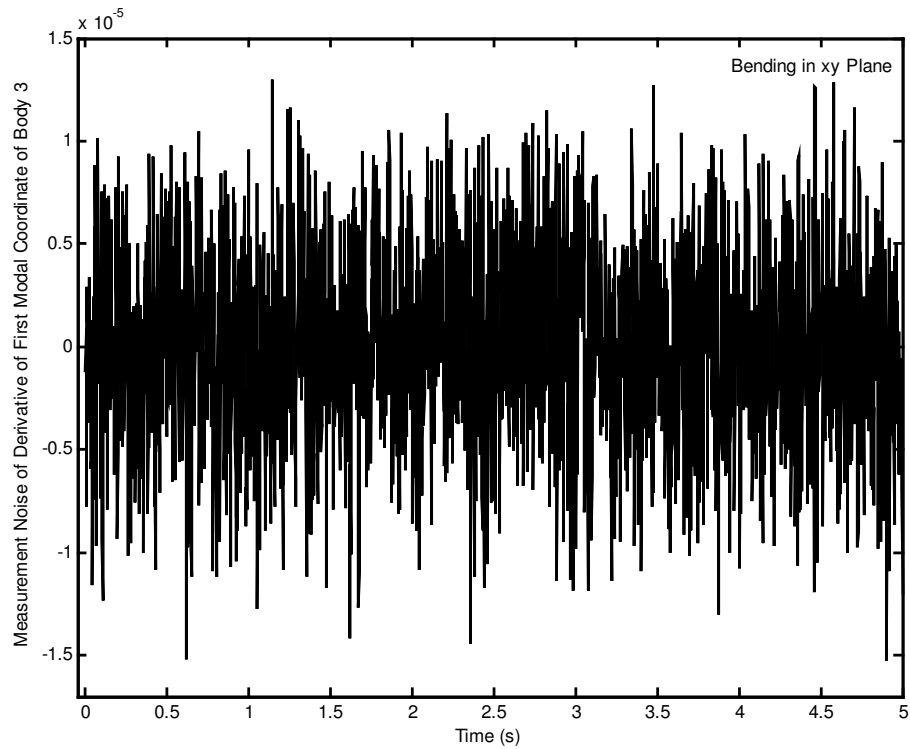


Figure 5.179 Measurement noise of derivative of first modal coordinate of body 3 for bending in xy plane.

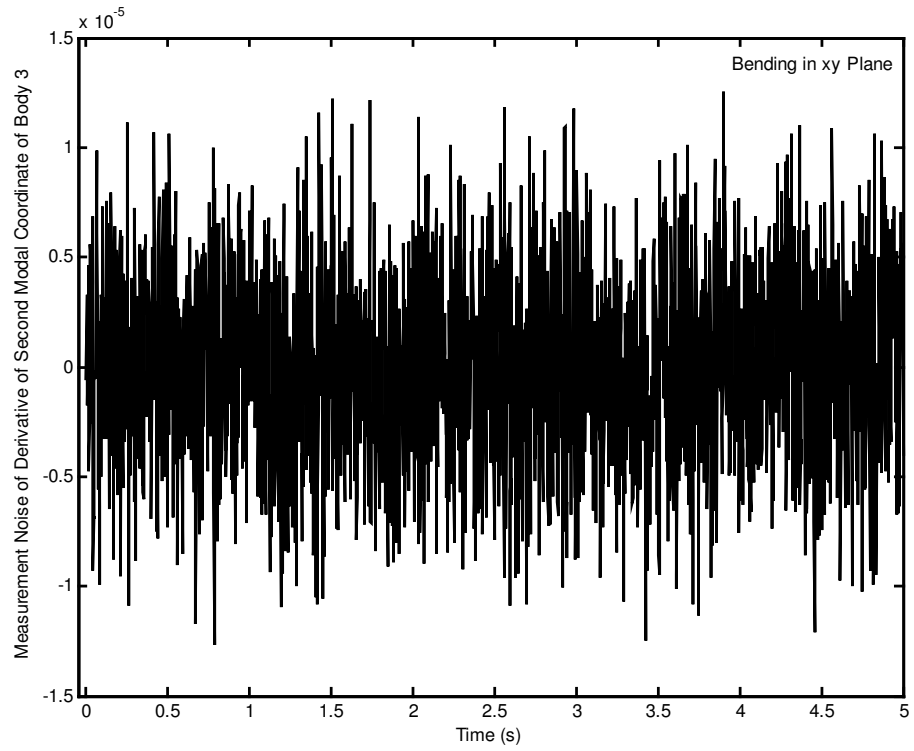


Figure 5.180 Measurement noise of derivative of second modal coordinate of body 3 for bending in xy plane.

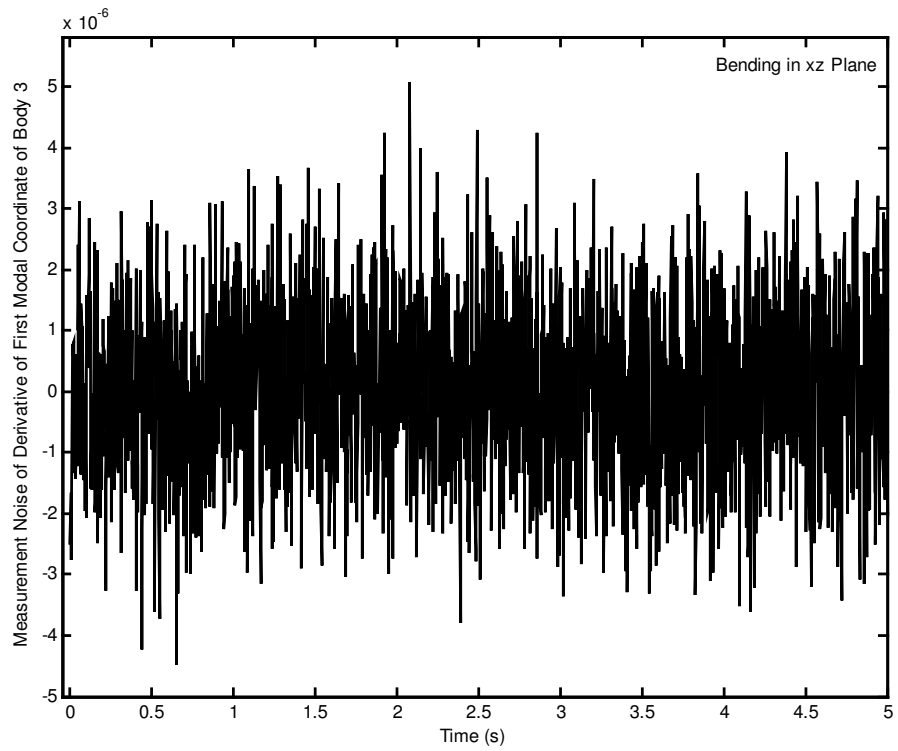


Figure 5.181 Measurement noise of derivative of first modal coordinate of body 3 for bending in xz plane.

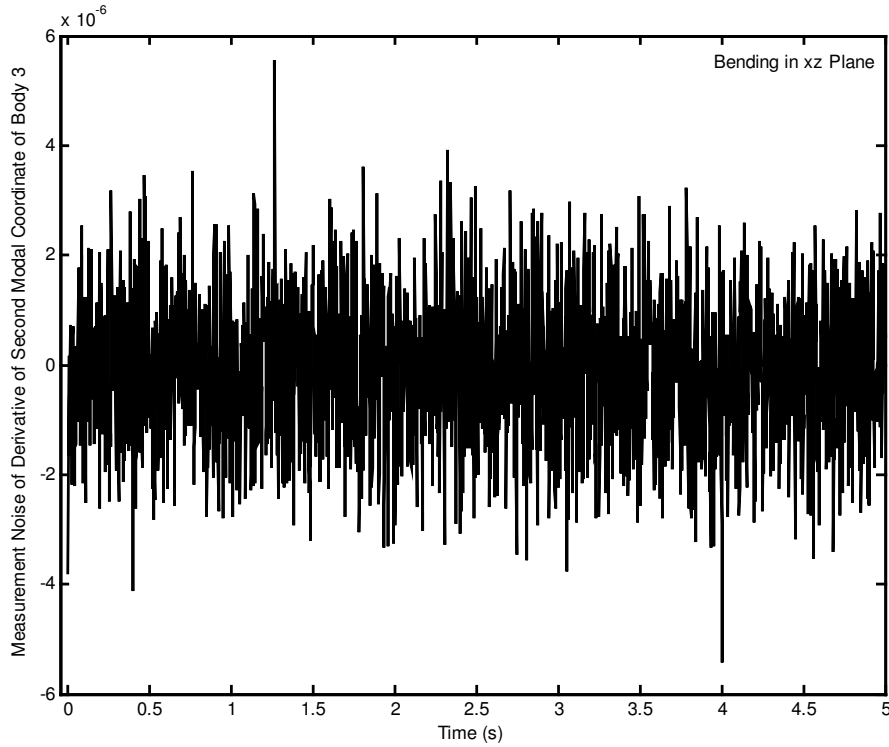


Figure 5.182 Measurement noise of derivative of second modal coordinate of body 3 for bending in xz plane.

As seen from Figures 5.98 - 5.100 the initial error due to the mispositioning of the tip point is 0.03 m, -0.05 m and -0.02 m in \mathbf{n}_1 , \mathbf{n}_2 and \mathbf{n}_3 directions, respectively. However, the effect of initial mispositioning can be compensated in about 1 s. There is a reverse action at the beginning of the motion as seen in the tip point velocity which is given in Figures 5.101 - 5.103. The maximum tip point position tracking error components along the trajectory after the tip point settles on the trajectory are -1.1436×10^{-3} m, 3.8068×10^{-4} m and -4.9839×10^{-4} m in \mathbf{n}_1 , \mathbf{n}_2 and \mathbf{n}_3 directions, respectively. The tip point position error components at the end of the motion are -1.0087×10^{-4} m, 1.1554×10^{-4} m and -4.9244×10^{-5} m in \mathbf{n}_1 , \mathbf{n}_2 and \mathbf{n}_3 directions, respectively. The maximum overall torques applied to the joints are in the order of 107 Nm as seen from Figures 5.158 - 5.160. Note that the measurement noises do not cause any noticeable increase in the control torques as compared to the case without noises.

As seen from the Figures 5.98 - 5.100, the errors in the tip point position components are all in acceptable levels considering the 1 % sensor uncertainty in the measured mean values of the variables. On this occasion, it is worth to point out that if the tip point coordinates are to be measured optically it is recommended that the optical sensor should be kept close to the tip point as much as possible in order to minimize measurement errors.

5.4 Numerical Simulation of Force and Motion Control of Spatial Robot

In this section, the numerical simulation of the force and motion control of the spatial robot with two flexible arms is presented by using the force and motion control method proposed at Chapter 2. The tip point is required to track a trajectory on a spherical surface. The constraint equation can be written in terms of the tip point coordinates as

$$\phi(P_1, P_2, P_3) = (P_1 - P_{1c})^2 + (P_2 - P_{2c})^2 + (P_3 - P_{3c})^2 - R^2 = 0 \quad (5.4)$$

which represents a motion on a spherical surface. P_{1c} , P_{2c} and P_{3c} represent the center coordinates of the sphere in P_1 , P_2 and P_3 directions, respectively with respect to the fixed frame and R is the radius of the sphere. Therefore, the tip point Cartesian coordinates in fixed frame and the spherical coordinates s_1 and s_2 can be related as

$$P_1 = P_{1c} + R \cos(s_2) \sin(s_1) \quad (5.5)$$

$$P_2 = P_{2c} + R \sin(s_2) \quad (5.6)$$

$$P_3 = P_{3c} - R \cos(s_2) \sin(s_1) \quad (5.7)$$

Here, s_1 and s_2 are known as the azimuth angle and the elevation angle coordinates of the tip point, respectively.

The same functions for the reference Lagrange multiplier and the reference tip point trajectory given in Chapter 4 are used.

After a few trials, proper closed loop natural frequencies and damping ratios are obtained as 10 rad/s, 20 rad/s, 30 rad/s, 43 rad/s, 43 rad/s, 44 rad/s, 44 rad/s, 268 rad/s, 268 rad/s, 276 rad/s, 276 rad/s, 0.85, 0.85, 0.85, 0.85, 0.85, 0.85, 0.85, 0.85, 0.85, 0.85, and 1. The corresponding closed loop poles are given in Table 5.5.

Table 5.5 Closed loop poles used in force and motion control of spatial robot.

Closed Loop Poles
$p_1 = -8.5000 + 5.2678j$
$p_2 = -8.5000 - 5.2678j$
$p_3 = -17.0000$
$p_4 = -17.0000 + 10.5357j$
$p_5 = -17.0000 - 10.5357j$
$p_{6,7} = -36.5500 + 22.6517j$
$p_{8,9} = -36.5500 - 22.6517j$
$p_{10,11} = -37.4000 + 23.1784j$
$p_{12,13} = -37.4000 - 23.1784j$
$p_{14,15} = -227.8000 + 141.1778j$
$p_{16,17} = -227.8000 - 141.1778j$
$p_{18,19} = -234.6000 + 145.3920j$
$p_{20,21} = -234.6000 - 145.3920j$

The sampling frequency is taken as 500 Hz. The simulation results are presented in Figures 5.183 - 5.251.

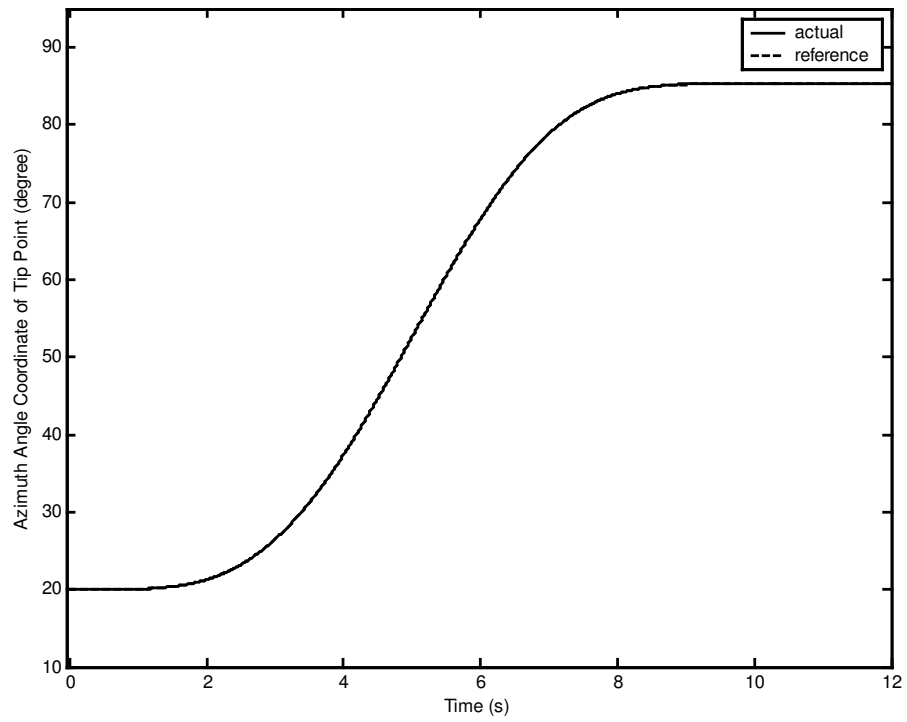


Figure 5.183 Azimuth angle coordinate of tip point.

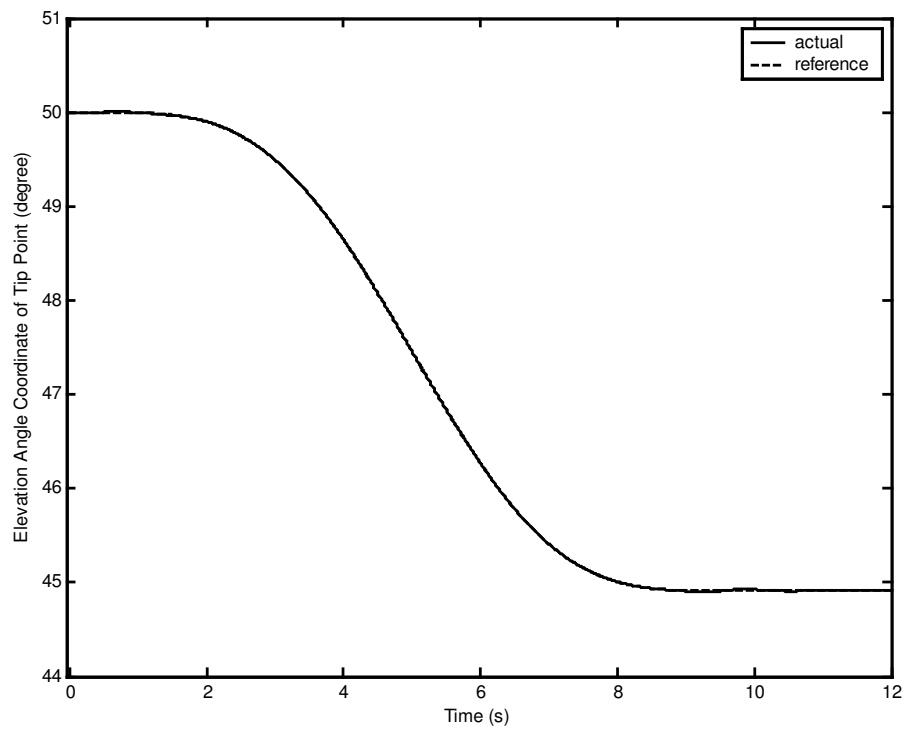


Figure 5.184 Elevation angle coordinate of tip point.

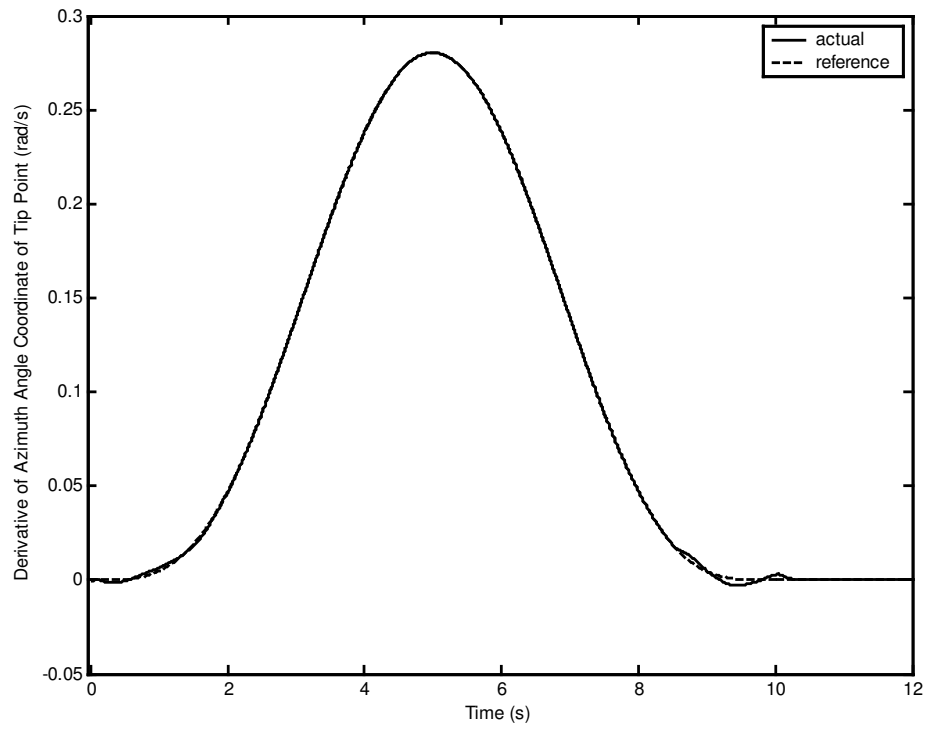


Figure 5.185 Derivative of azimuth angle coordinate of tip point.

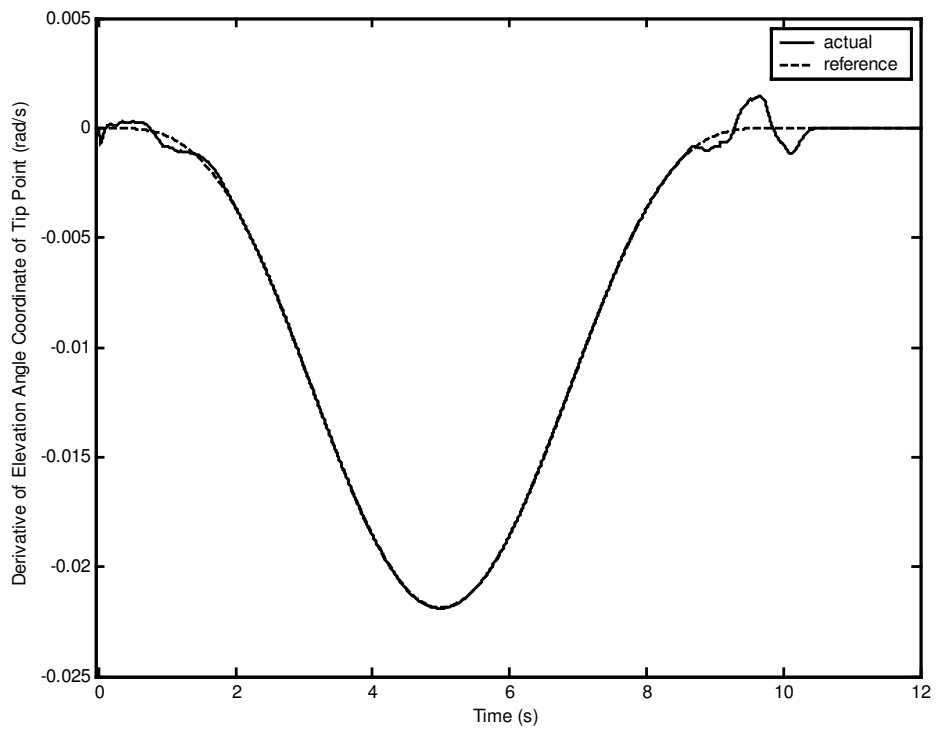


Figure 5.186 Derivative of elevation angle coordinate of tip point.

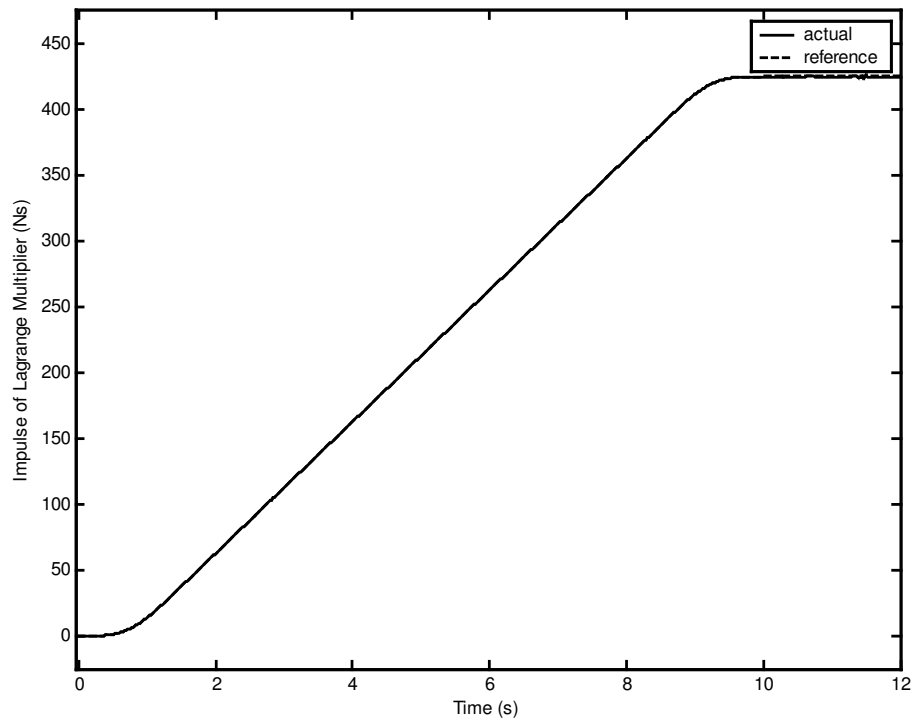


Figure 5.187 Impulse of Lagrange multiplier.

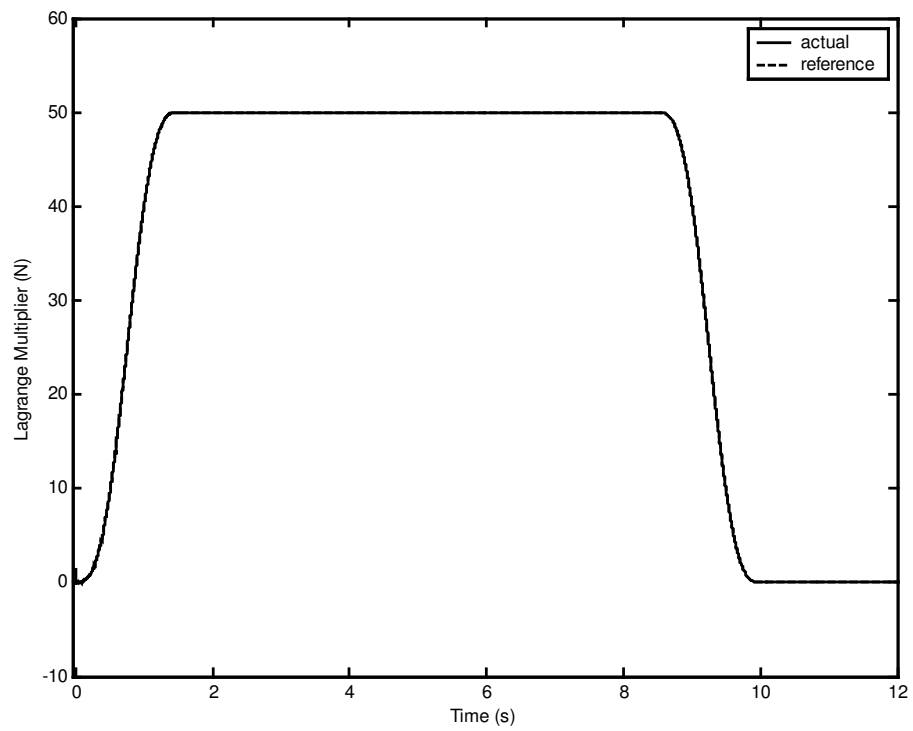


Figure 5.188 Lagrange multiplier.

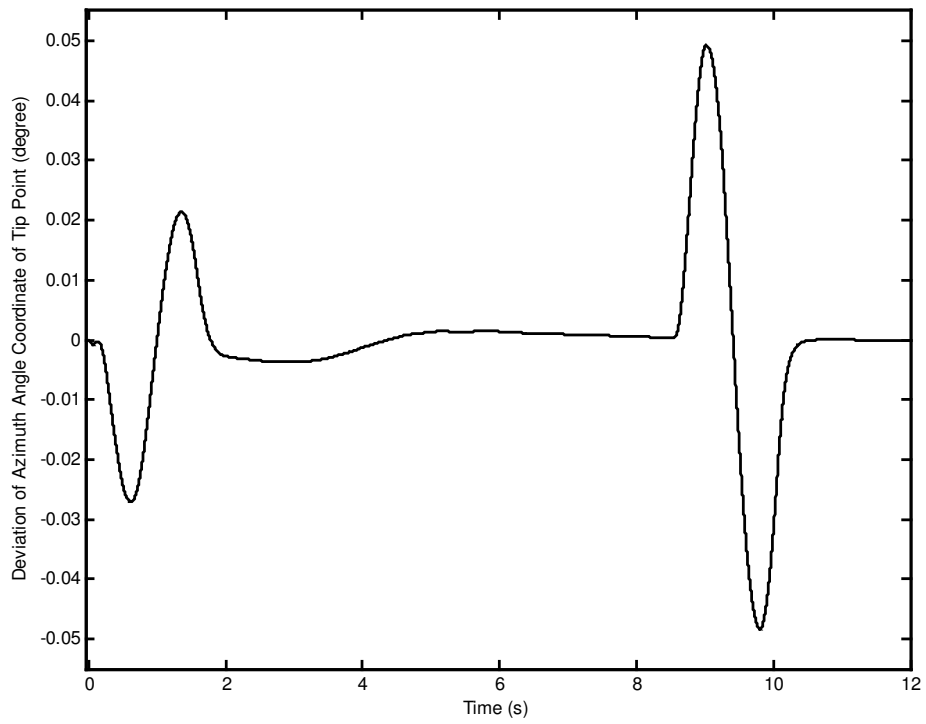


Figure 5.189 Deviation of azimuth angle coordinate of tip point.

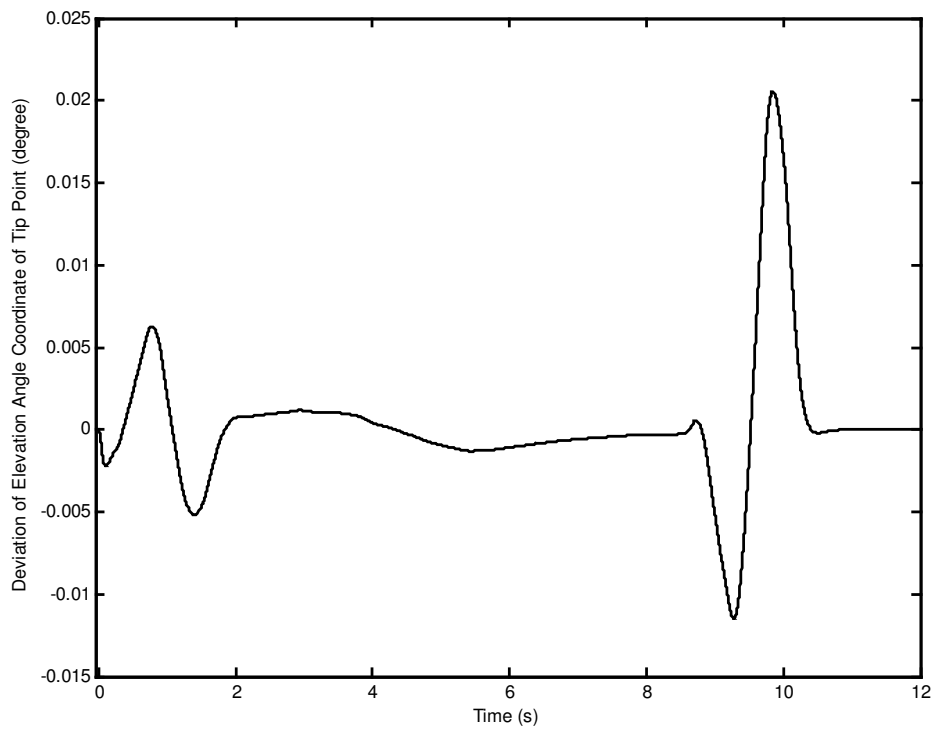


Figure 5.190 Deviation of elevation angle coordinate of tip point.

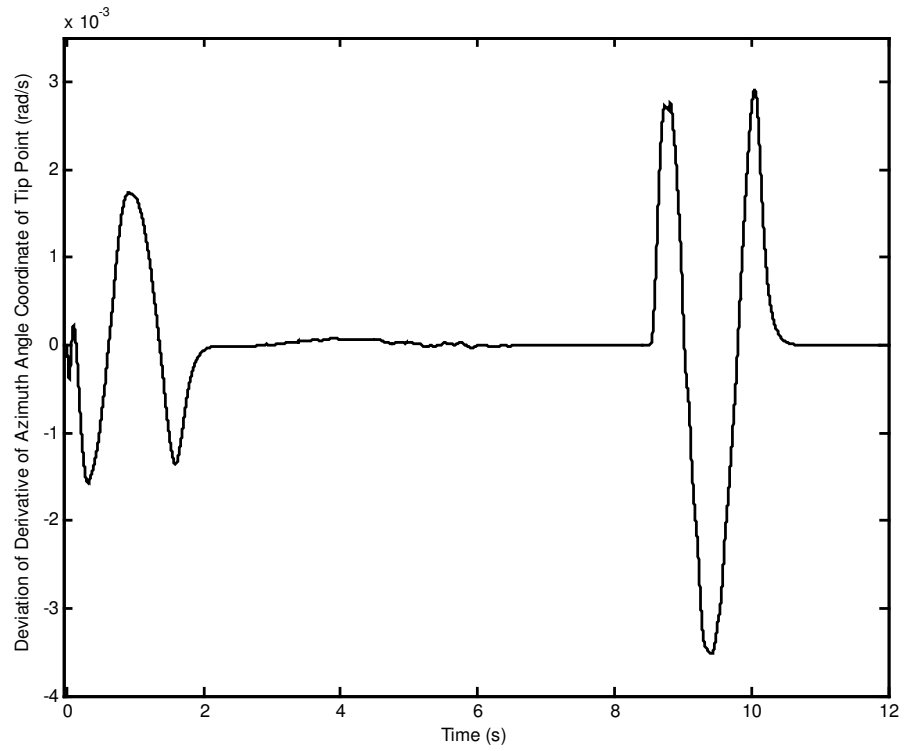


Figure 5.191 Deviation of derivative of azimuth angle coordinate of tip point.

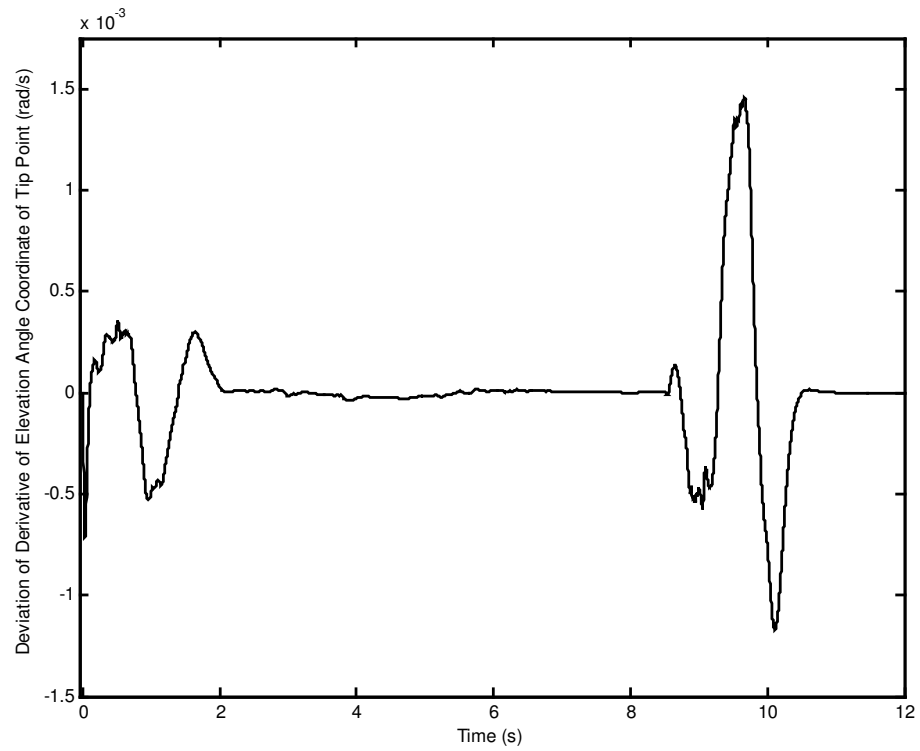


Figure 5.192 Deviation of derivative of elevation angle coordinate of tip point.

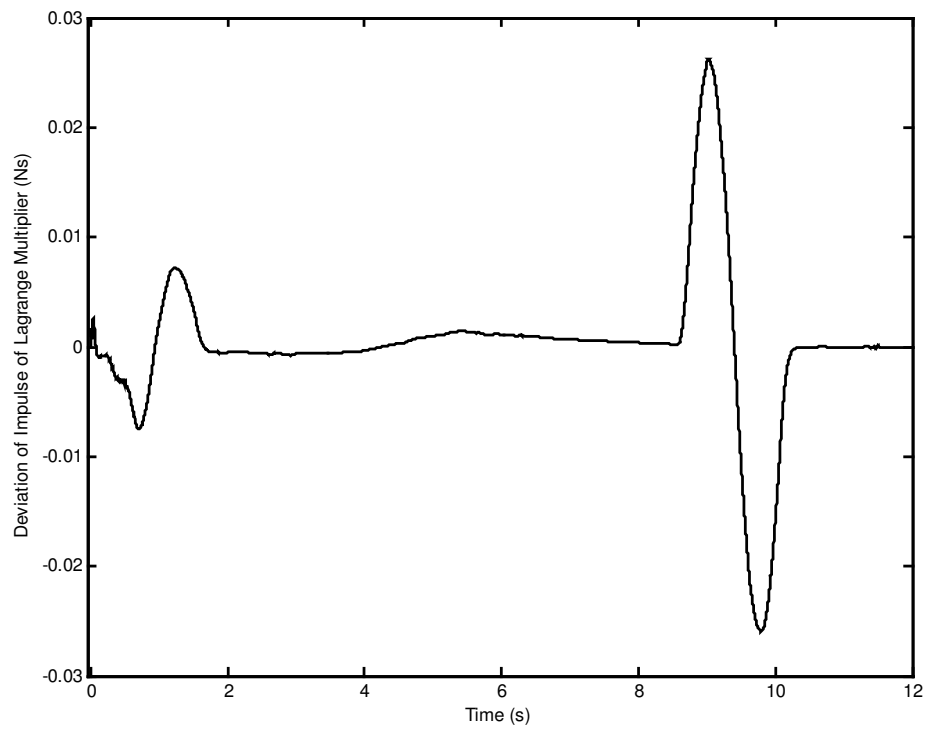


Figure 5.193 Deviation of impulse of Lagrange multiplier.

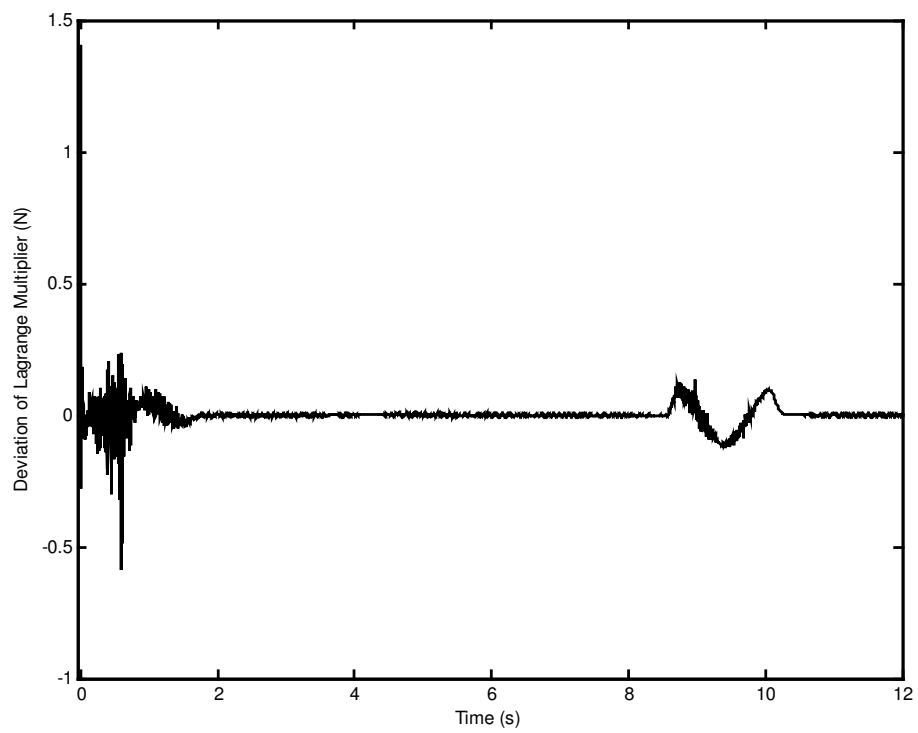


Figure 5.194 Deviation of Lagrange multiplier.

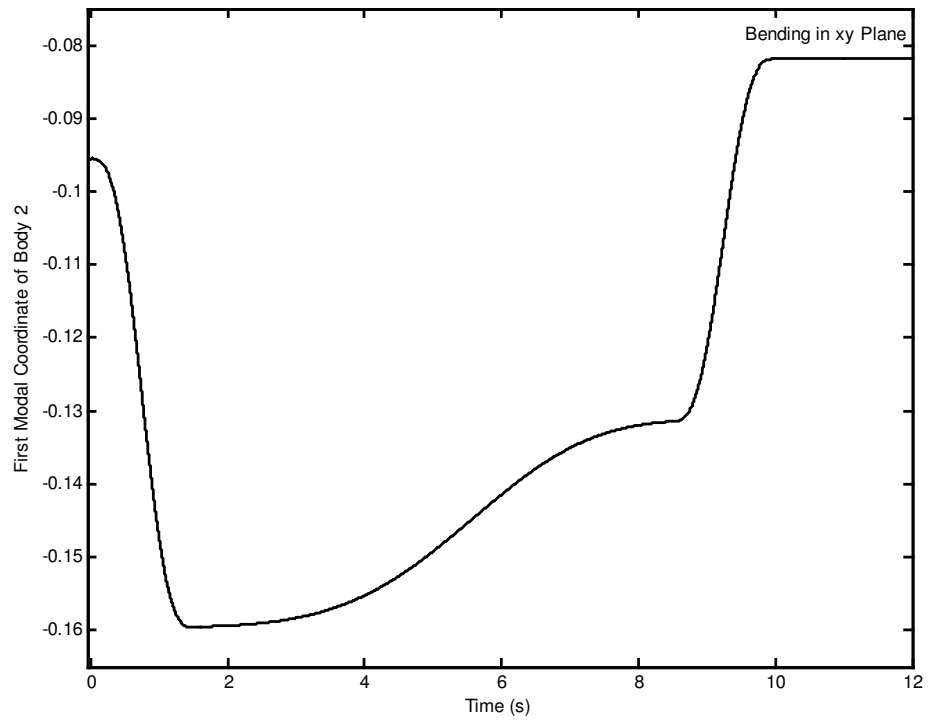


Figure 5.195 First modal coordinate of body 2 for bending in xy plane.

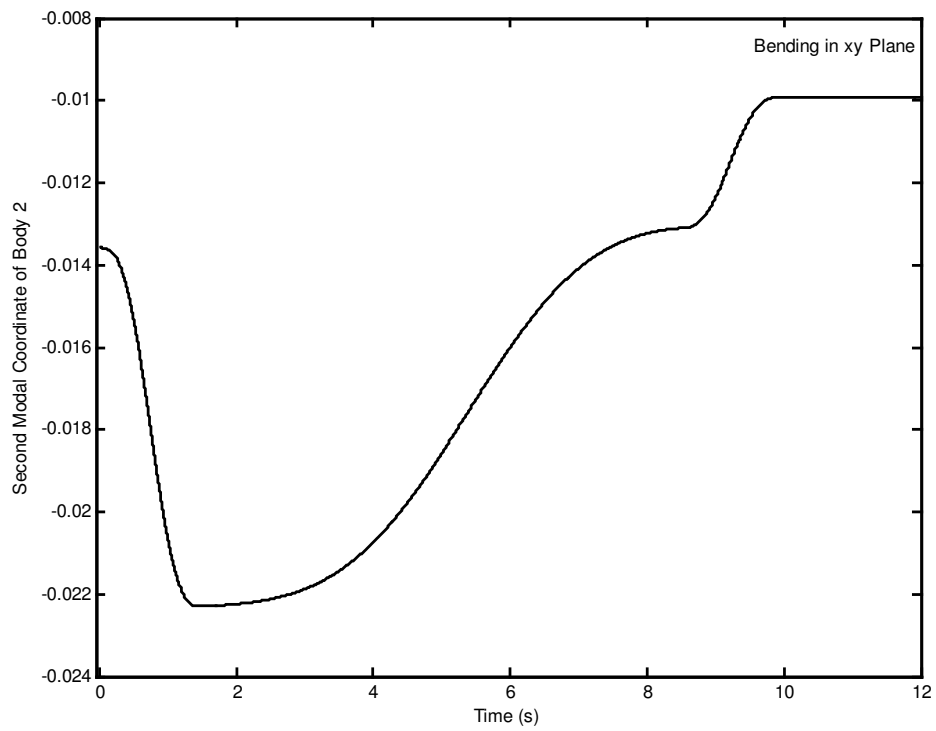


Figure 5.196 Second modal coordinate of body 2 for bending in xy plane.

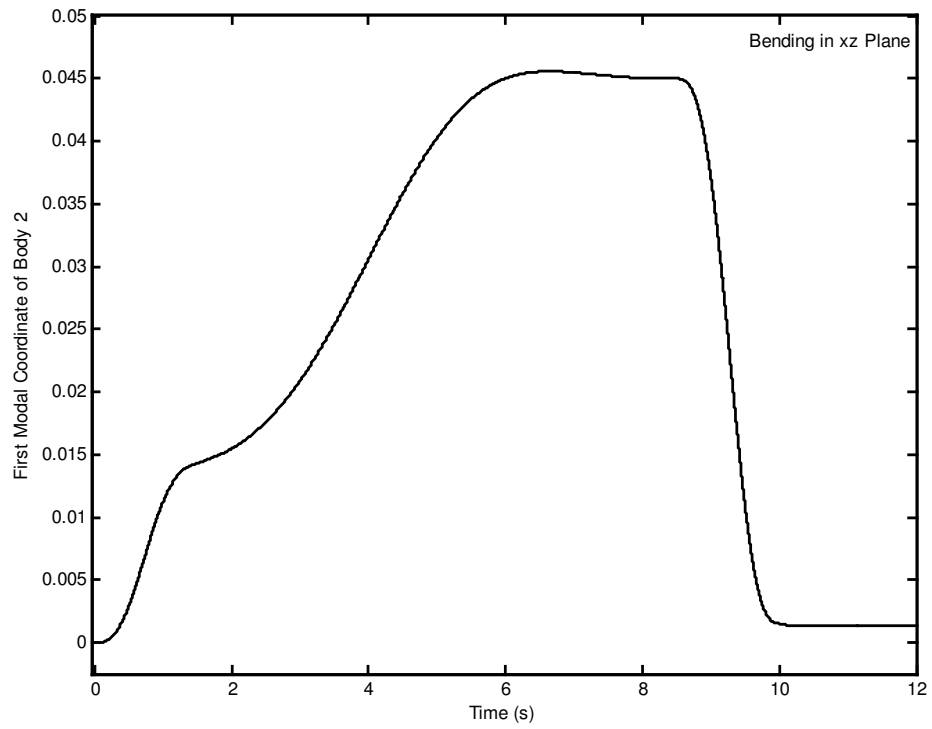


Figure 5.197 First modal coordinate of body 2 for bending in xz plane.

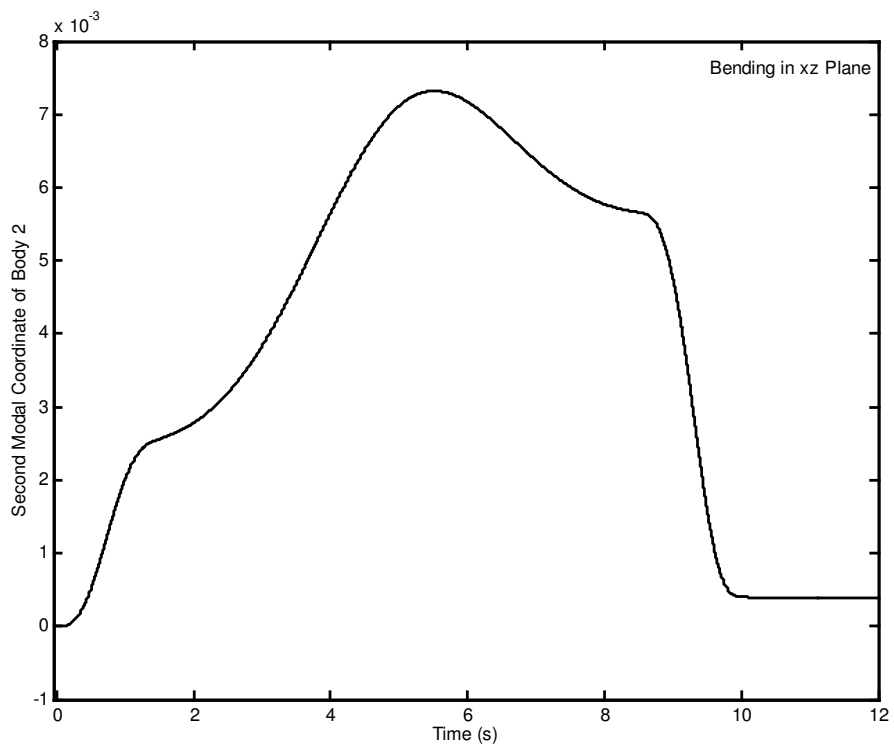


Figure 5.198 Second modal coordinate of body 2 for bending in xz plane.

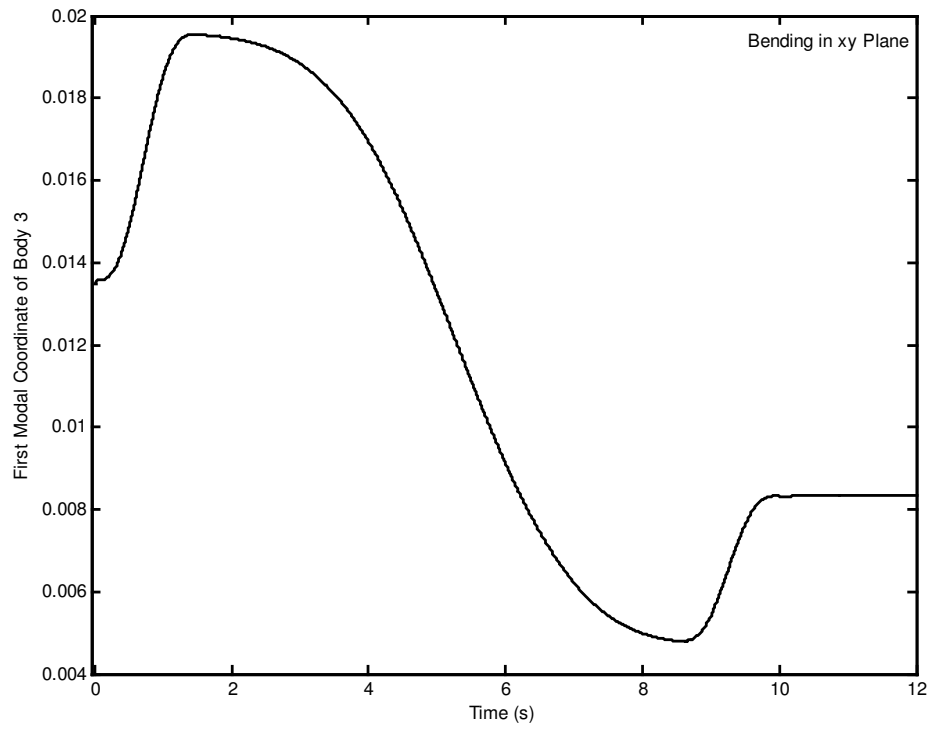


Figure 5.199 First modal coordinate of body 3 for bending in xy plane.

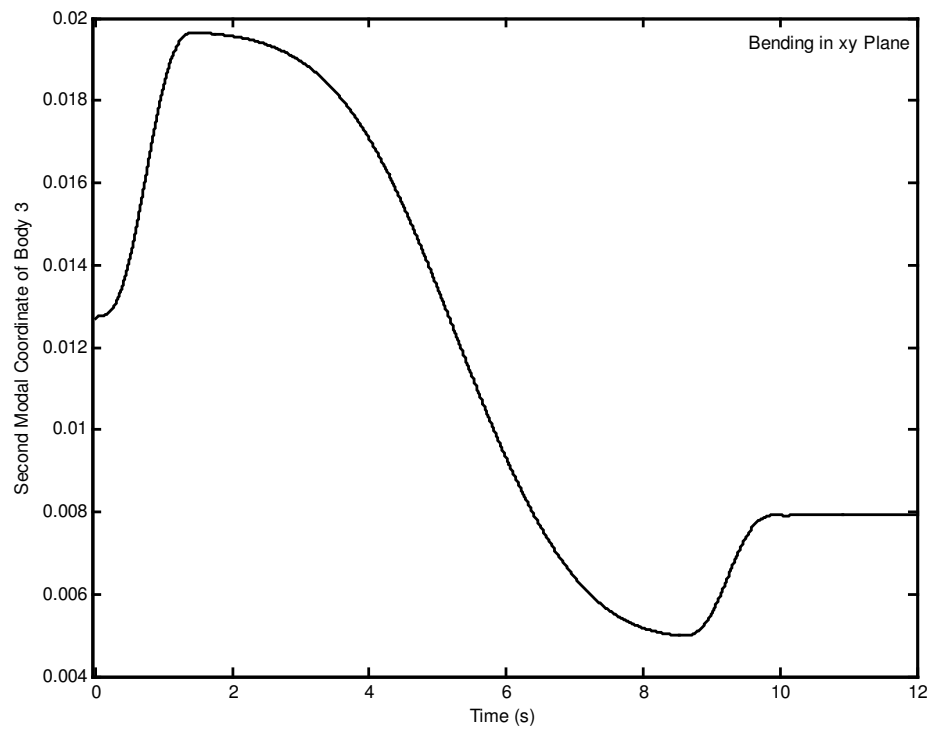


Figure 5.200 Second modal coordinate of body 3 for bending in xy plane.

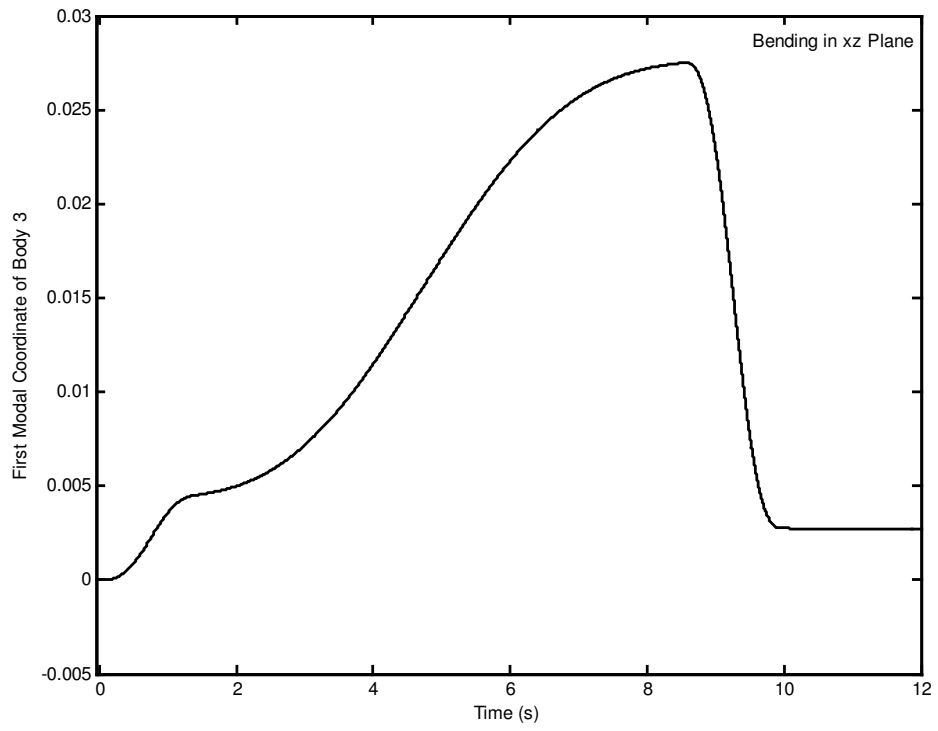


Figure 5.201 First modal coordinate of body 3 for bending in xz plane.

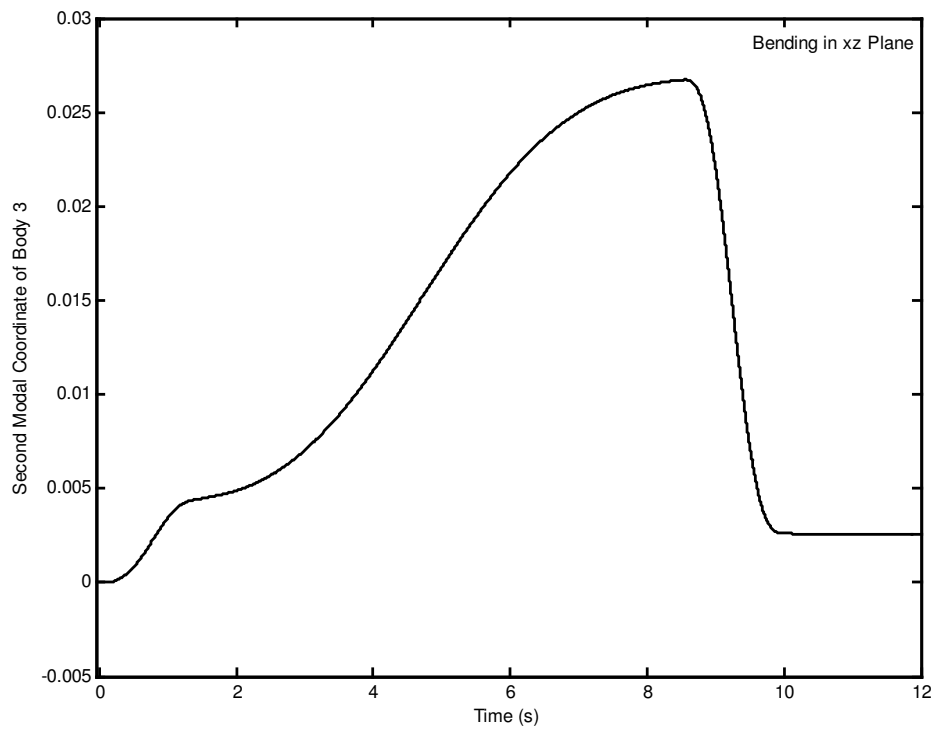


Figure 5.202 Second modal coordinate of body 3 for bending in xz plane.

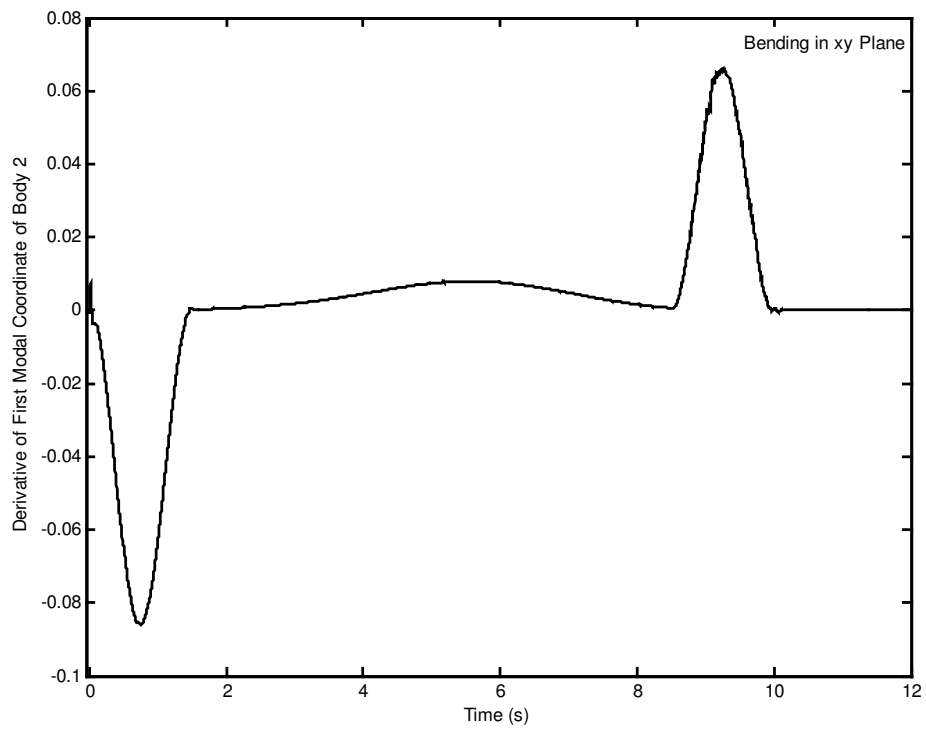


Figure 5.203 Derivative of first modal coordinate of body 2 for bending in xy plane.

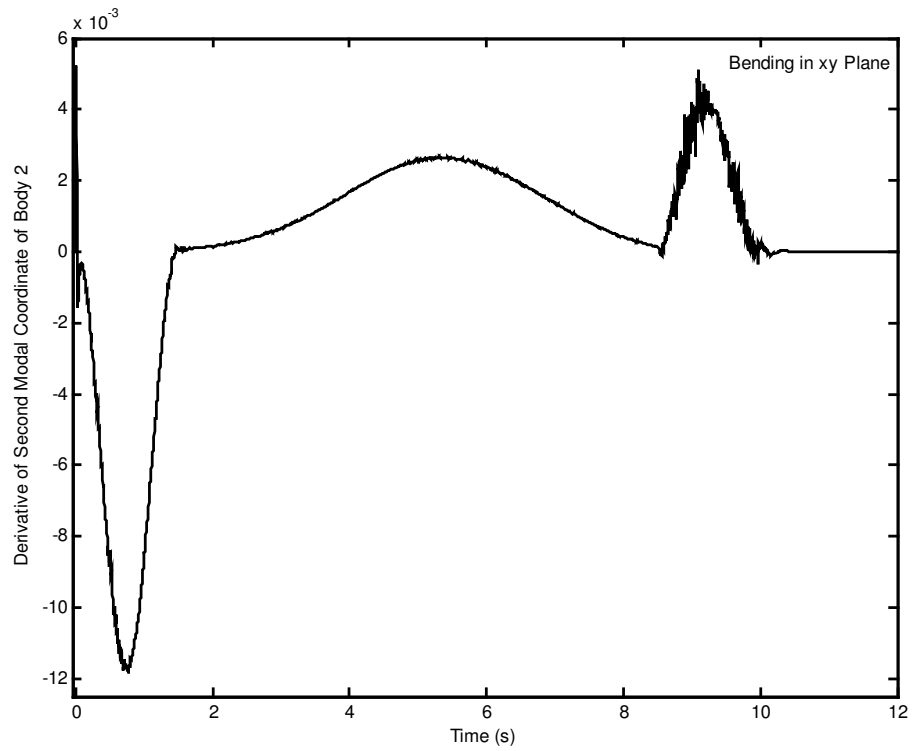


Figure 5.204 Derivative of second modal coordinate of body 2 for bending in xy plane.

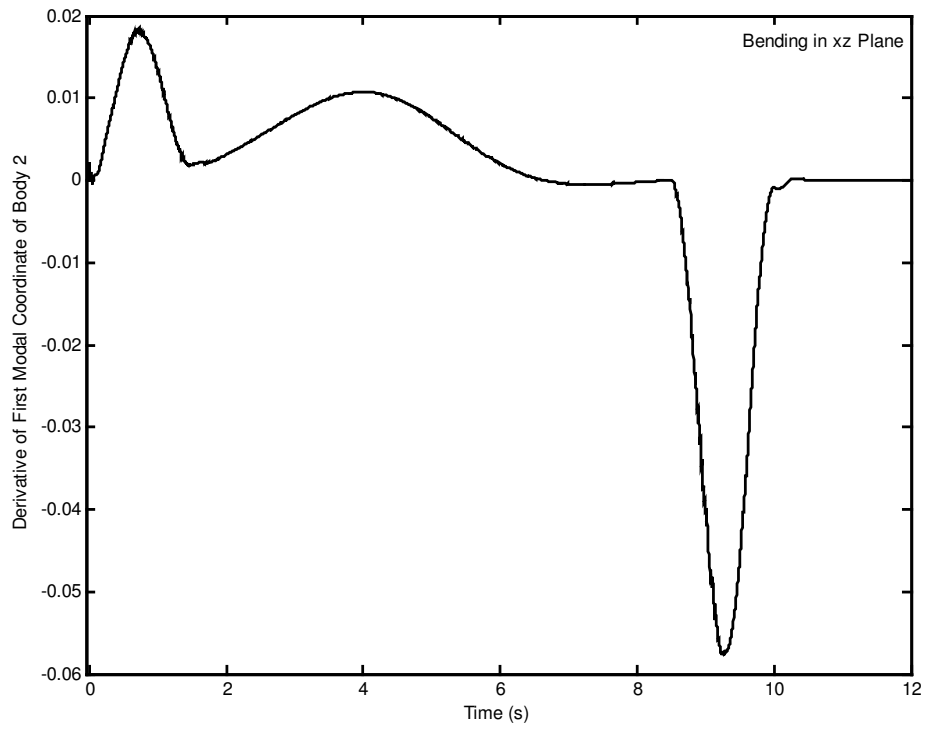


Figure 5.205 Derivative of first modal coordinate of body 2 for bending in xz plane.

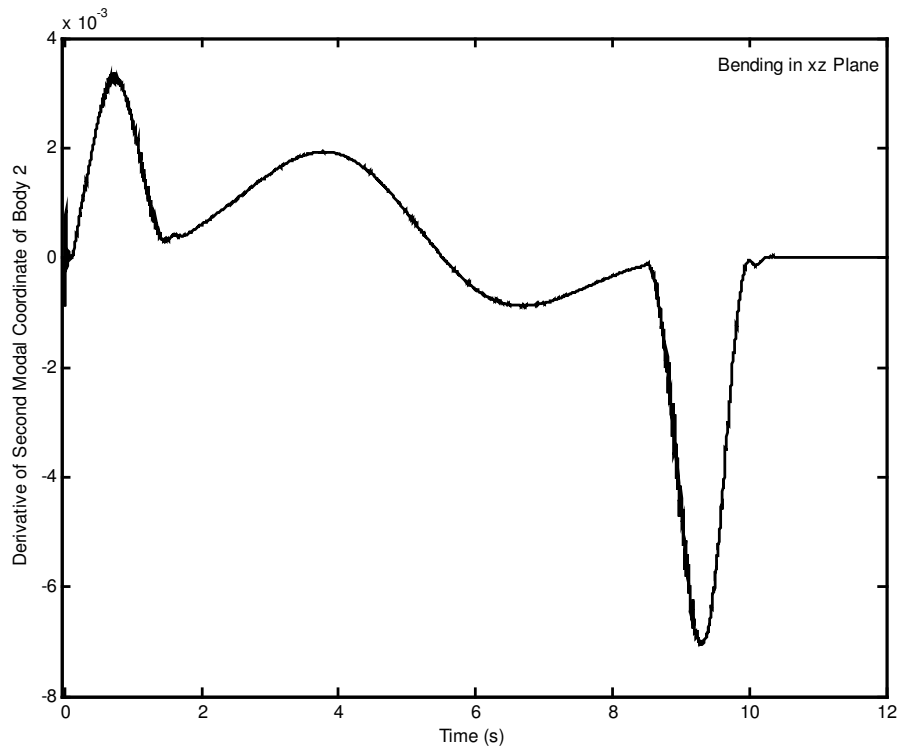


Figure 5.206 Derivative of second modal coordinate of body 2 for bending in xz plane.

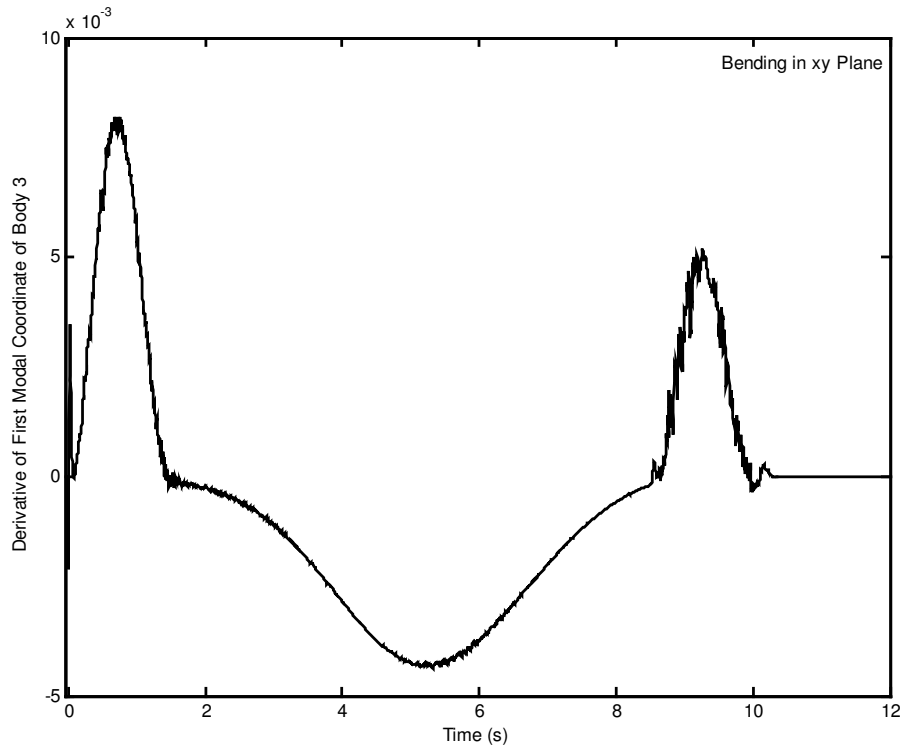


Figure 5.207 Derivative of first modal coordinate of body 3 for bending in xy plane.

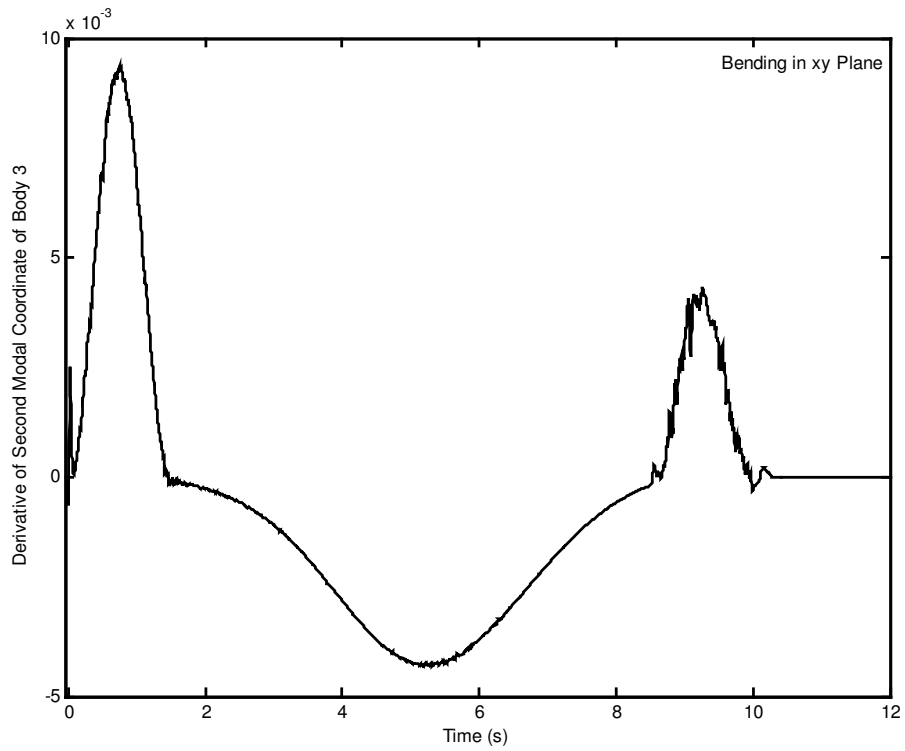


Figure 5.208 Derivative of second modal coordinate of body 3 for bending in xy plane.

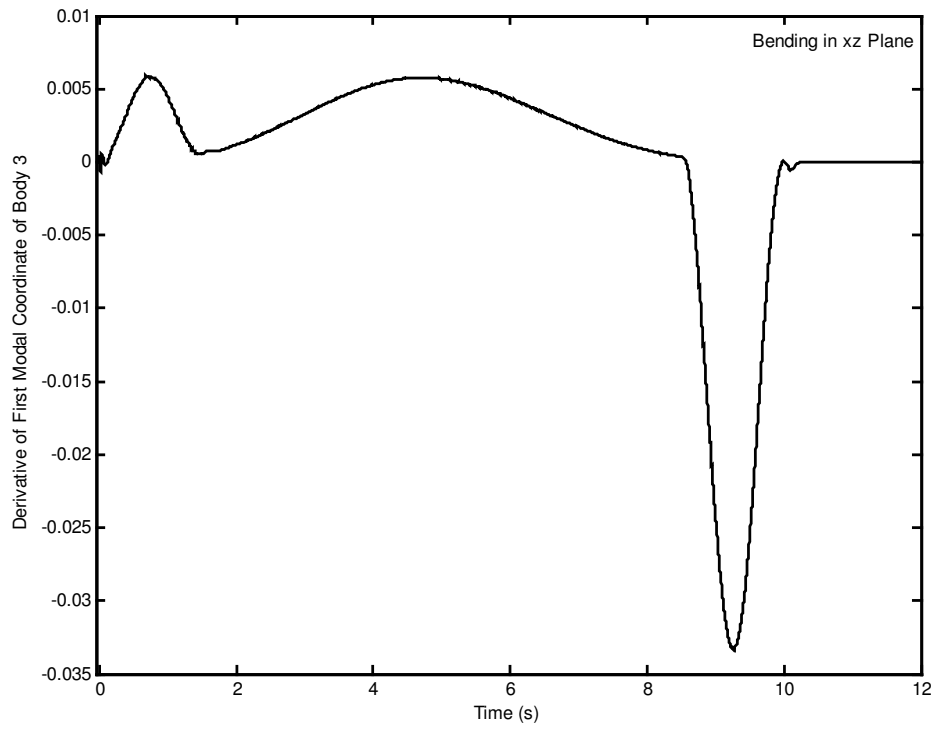


Figure 5.209 Derivative of first modal coordinate of body 3 for bending in xz plane.

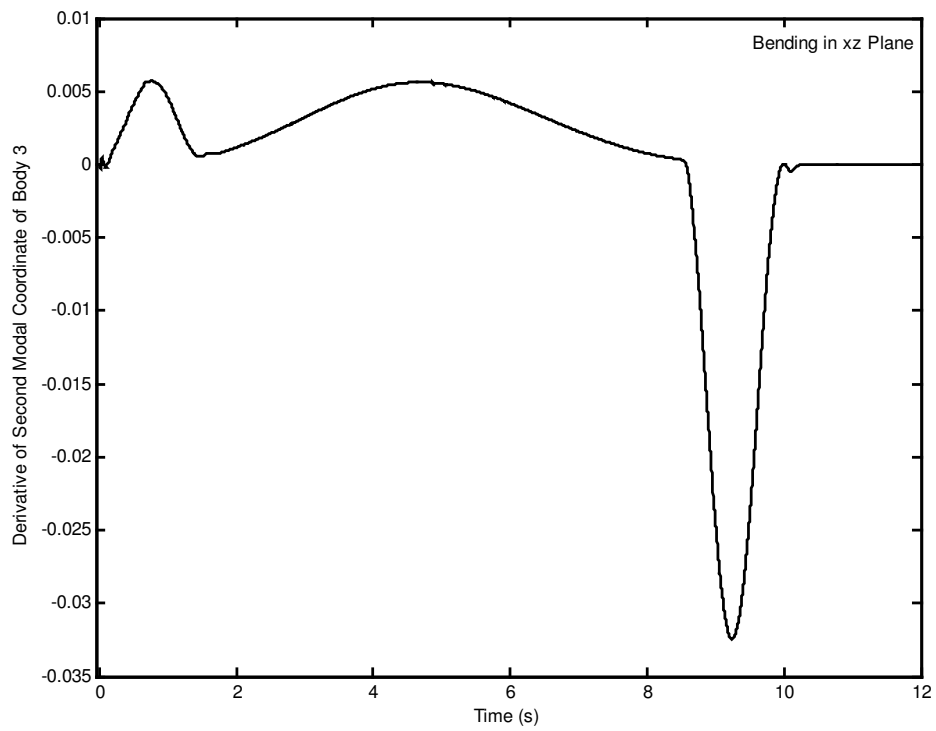


Figure 5.210 Derivative of second modal coordinate of body 3 for bending in xz plane.

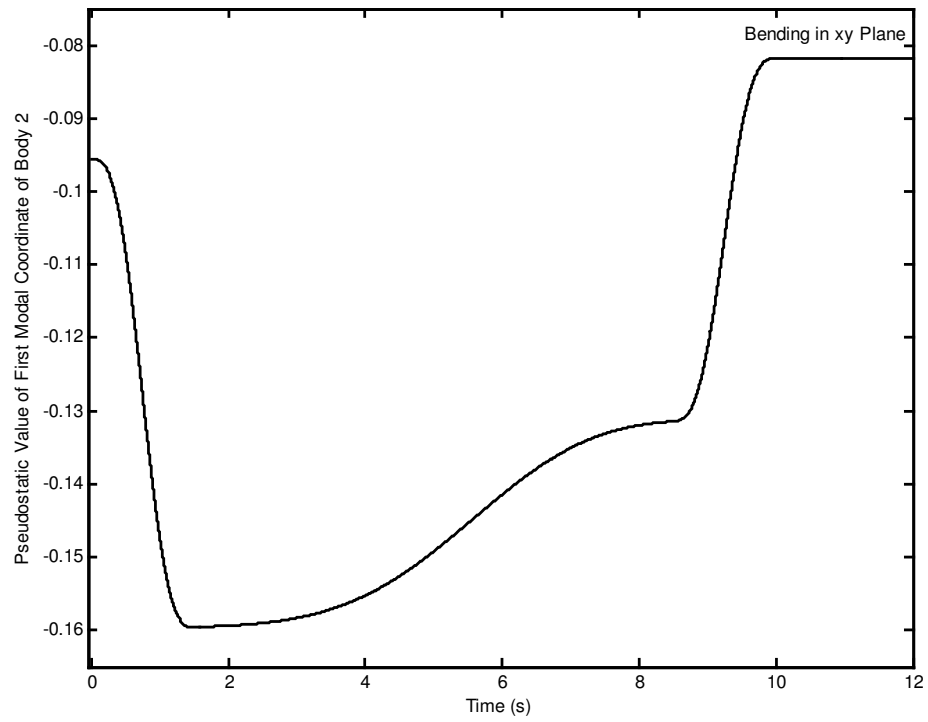


Figure 5.211 Pseudostatic value of first modal coordinate of body 2 for bending in xy plane.

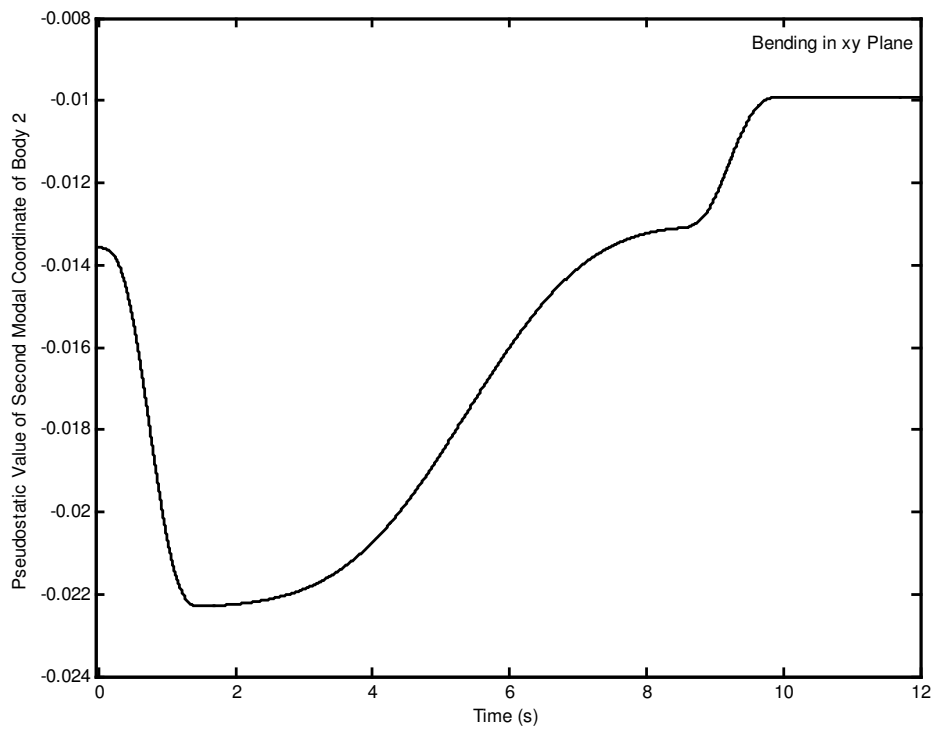


Figure 5.212 Pseudostatic value of second modal coordinate of body 2 for bending in xy plane.

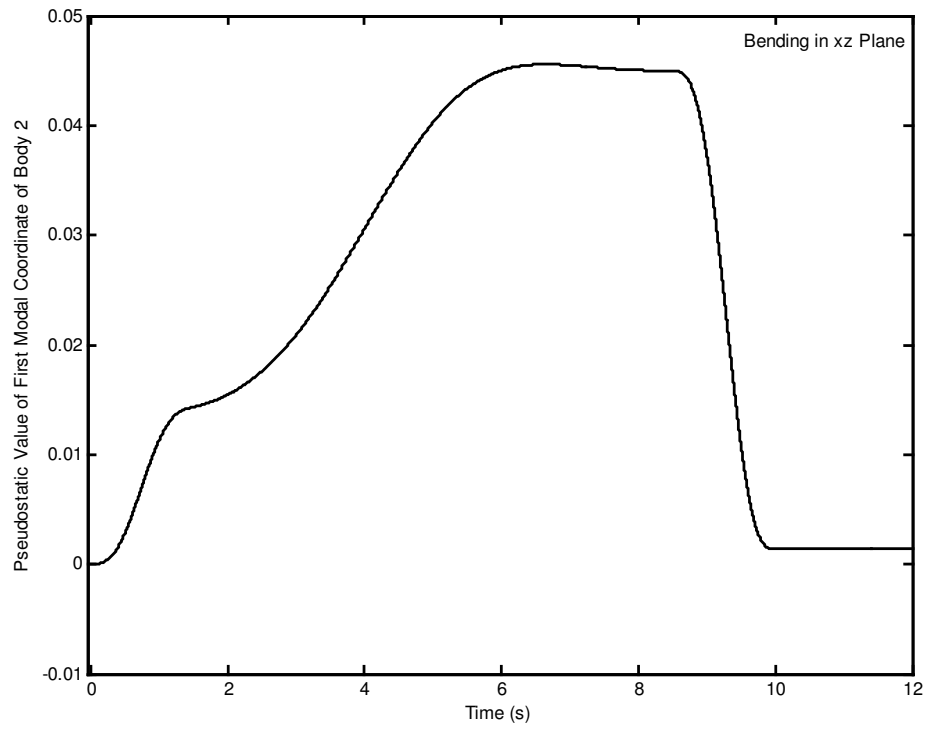


Figure 5.213 Pseudostatic value of first modal coordinate of body 2 for bending in xz plane.

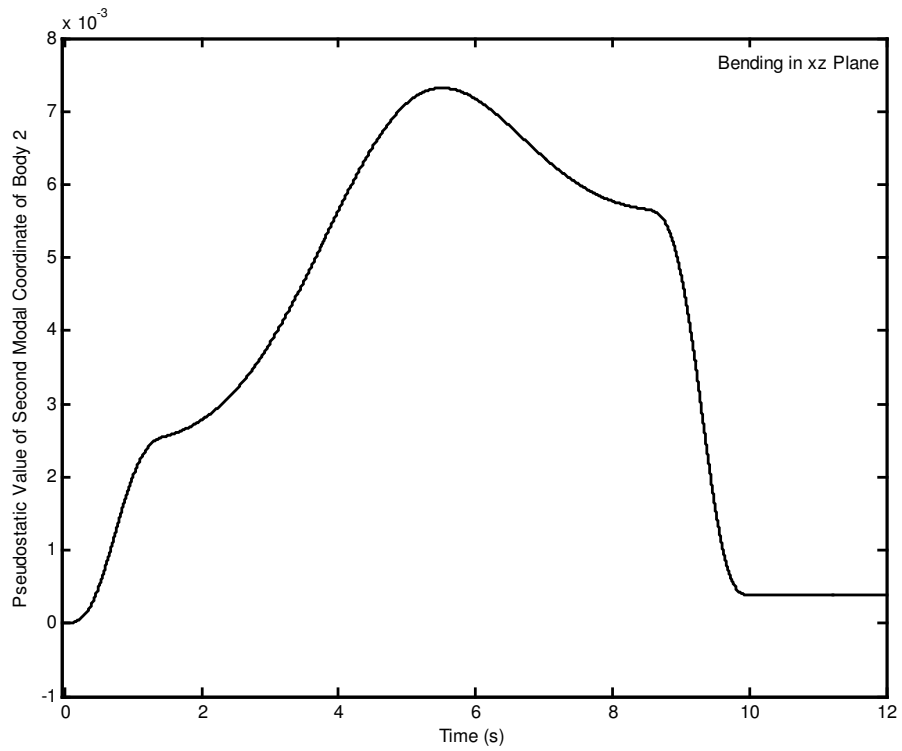


Figure 5.214 Pseudostatic value of second modal coordinate of body 2 for bending in xz plane.

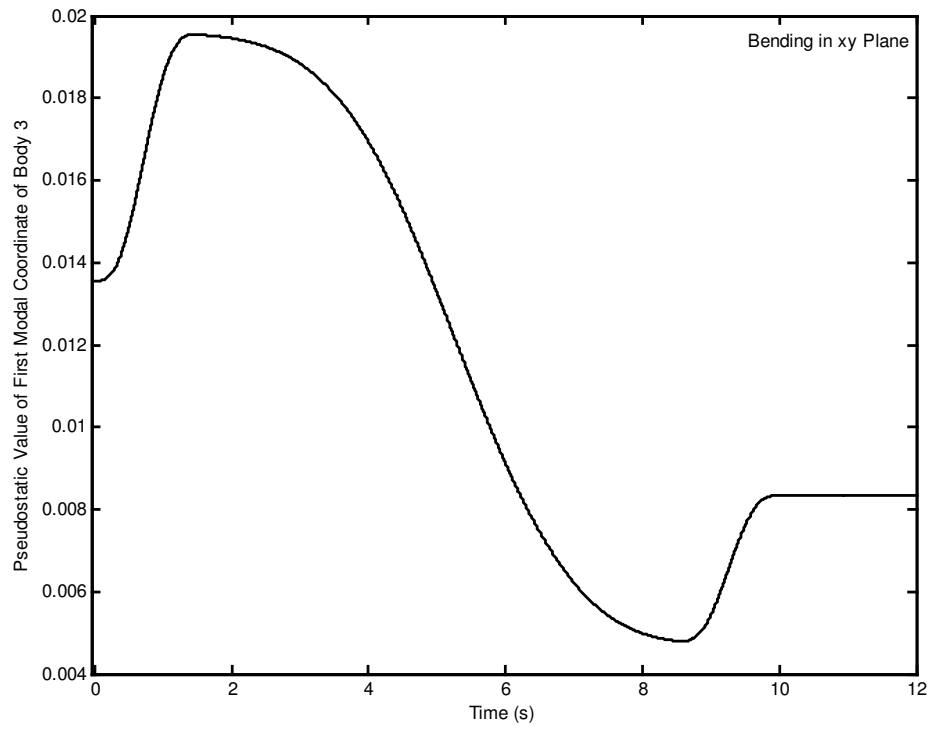


Figure 5.215 Pseudostatic value of first modal coordinate of body 3 for bending in xy plane.

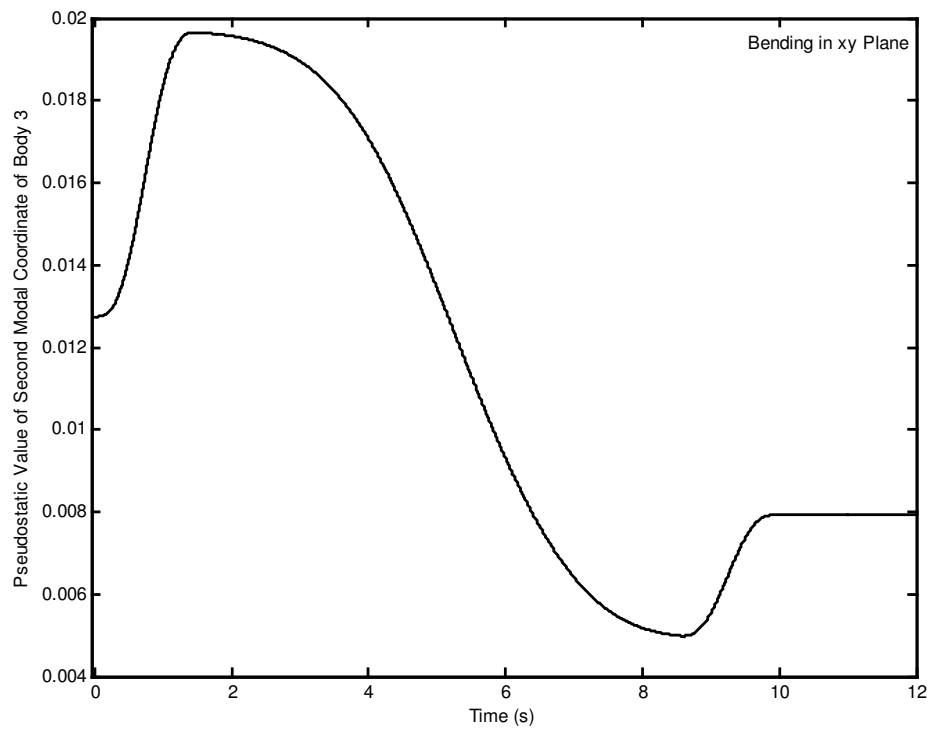


Figure 5.216 Pseudostatic value of second modal coordinate of body 3 for bending in xy plane.

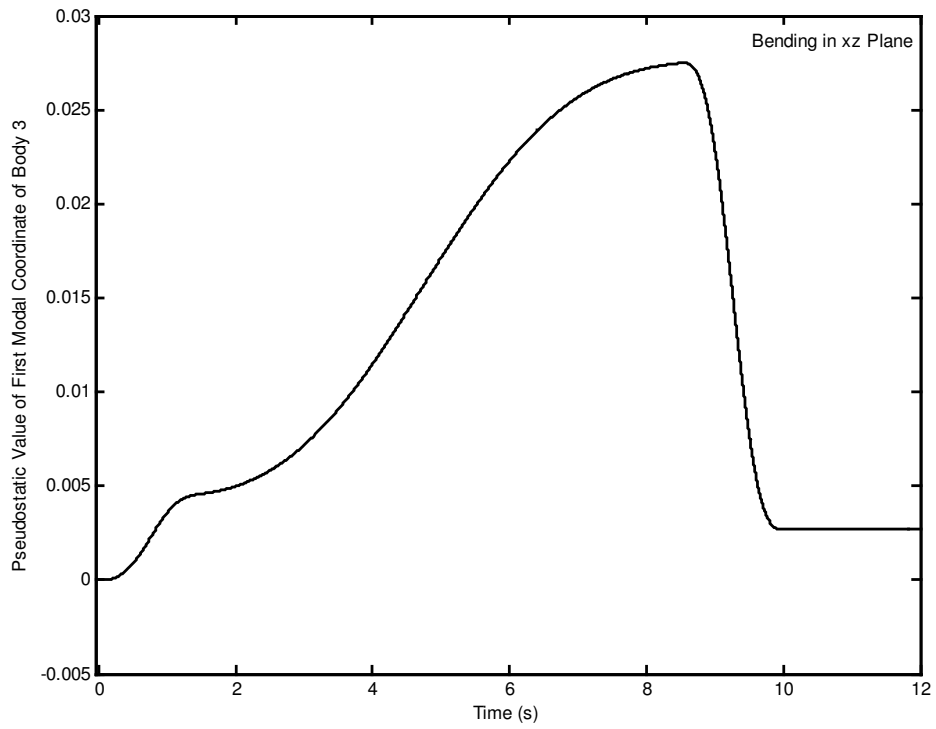


Figure 5.217 Pseudostatic value of first modal coordinate of body 3 for bending in xz plane.

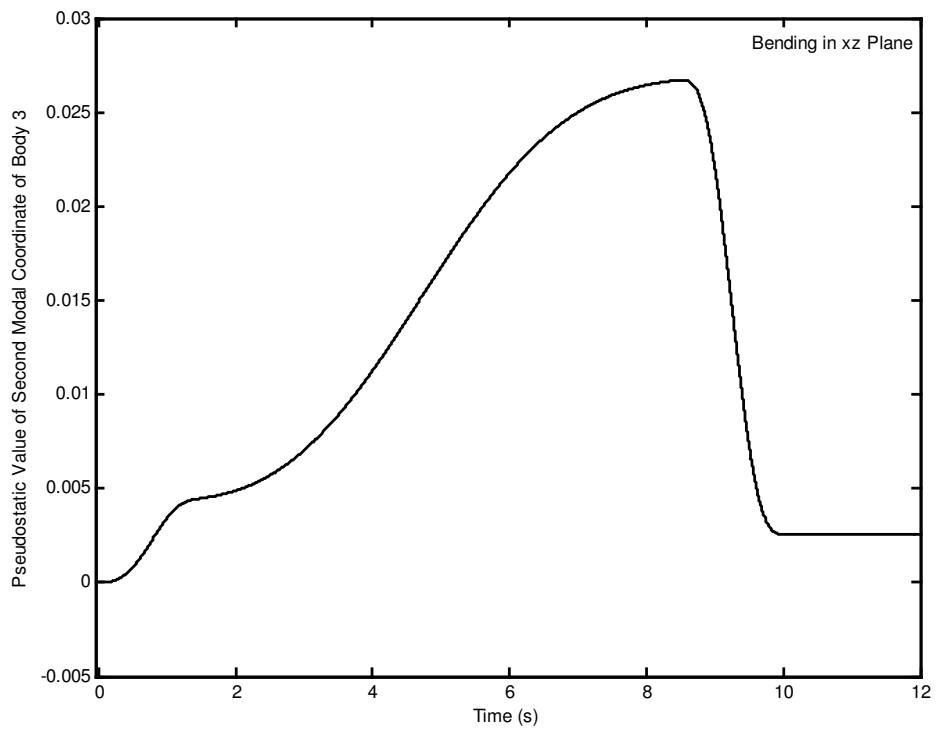


Figure 5.218 Pseudostatic value of second modal coordinate of body 3 for bending in xz plane.

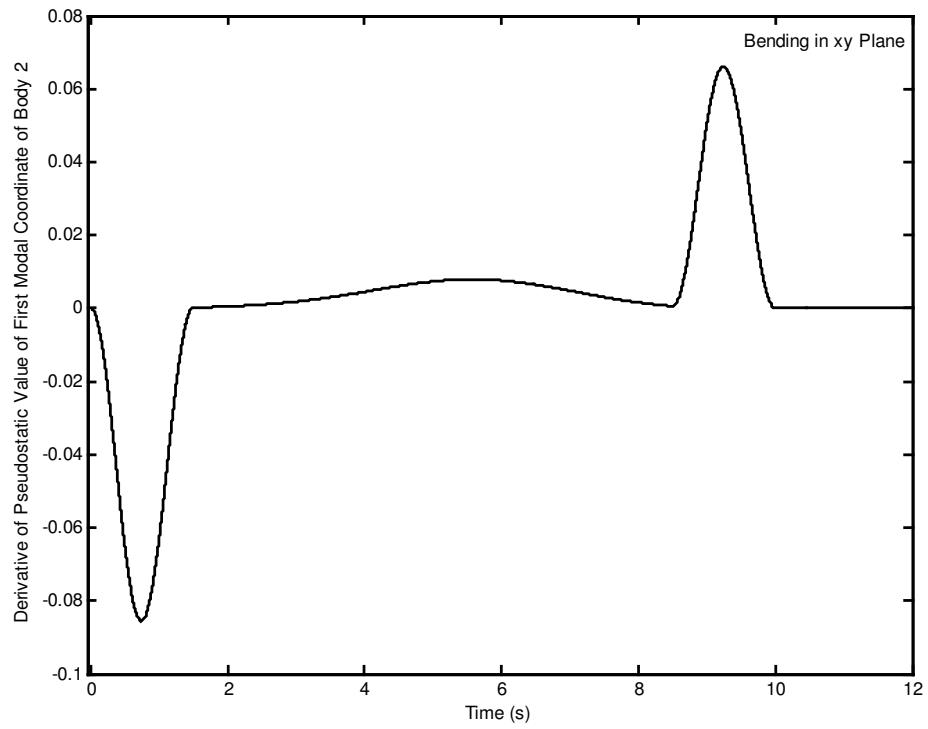


Figure 5.219 Derivative of pseudostatic value of first modal coordinate of body 2 for bending in xy plane.

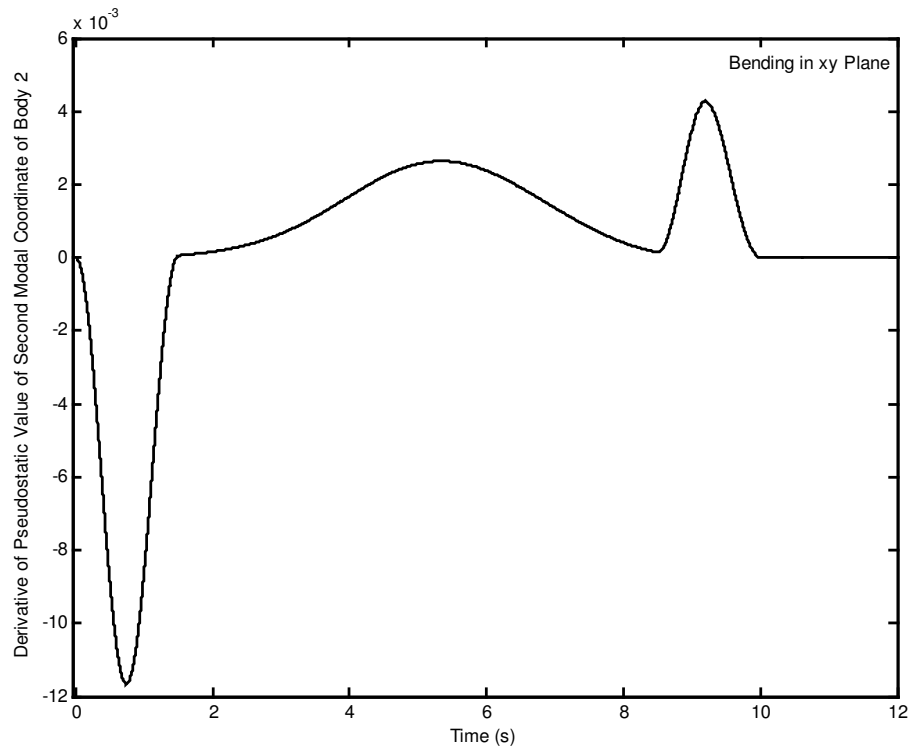


Figure 5.220 Derivative of pseudostatic value of second modal coordinate of body 2 for bending in xy plane.

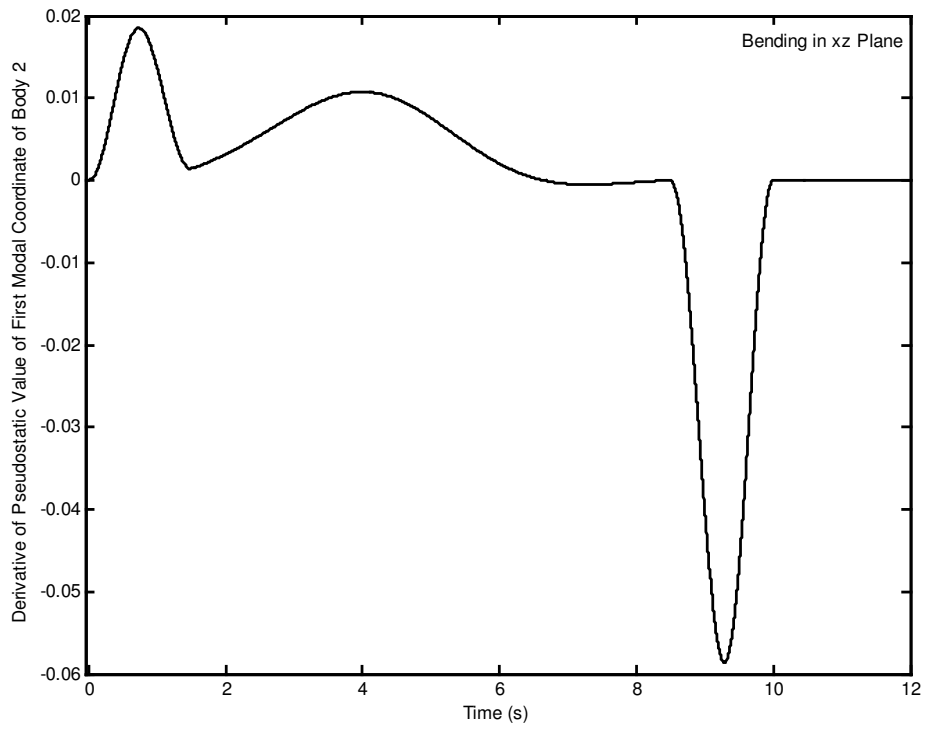


Figure 5.221 Derivative of pseudostatic value of first modal coordinate of body 2 for bending in xz plane.

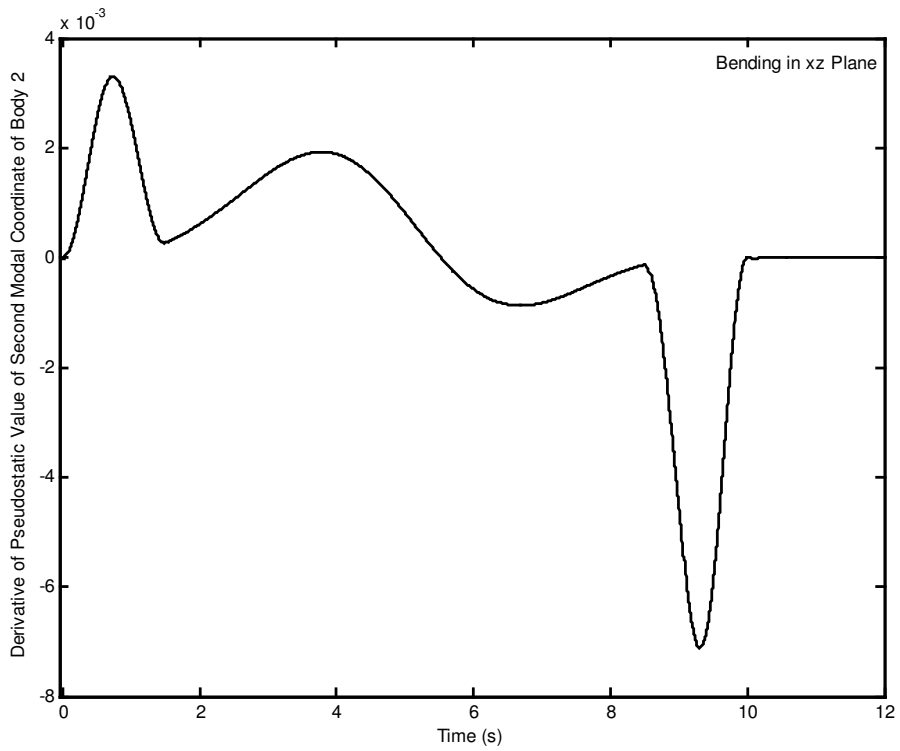


Figure 5.222 Derivative of pseudostatic value of second modal coordinate of body 2 for bending in xz plane.

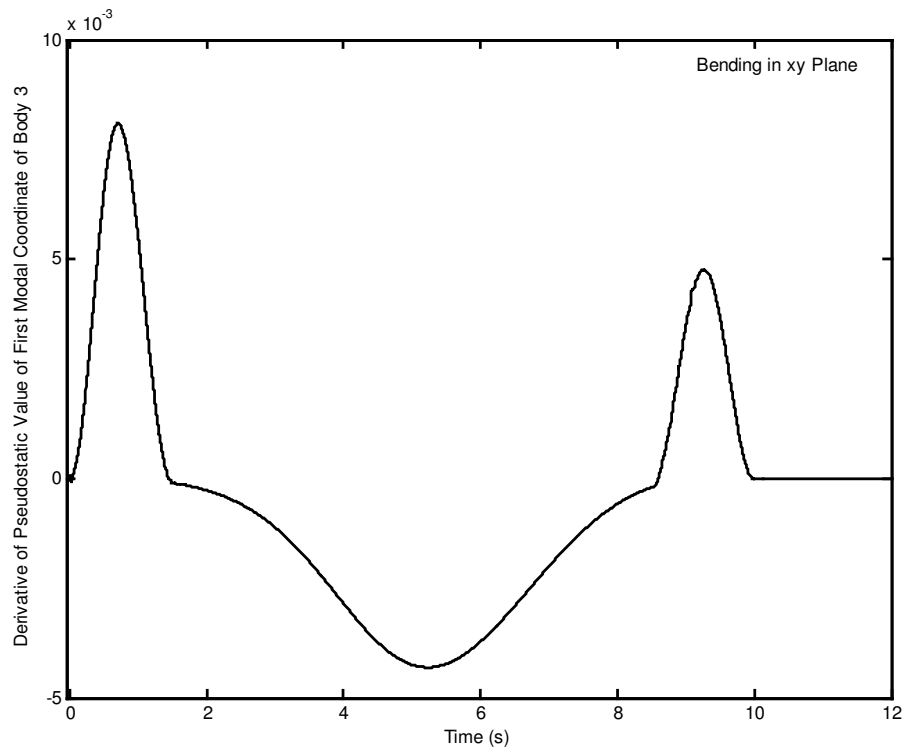


Figure 5.223 Derivative of pseudostatic value of first modal coordinate of body 3 for bending in xy plane.

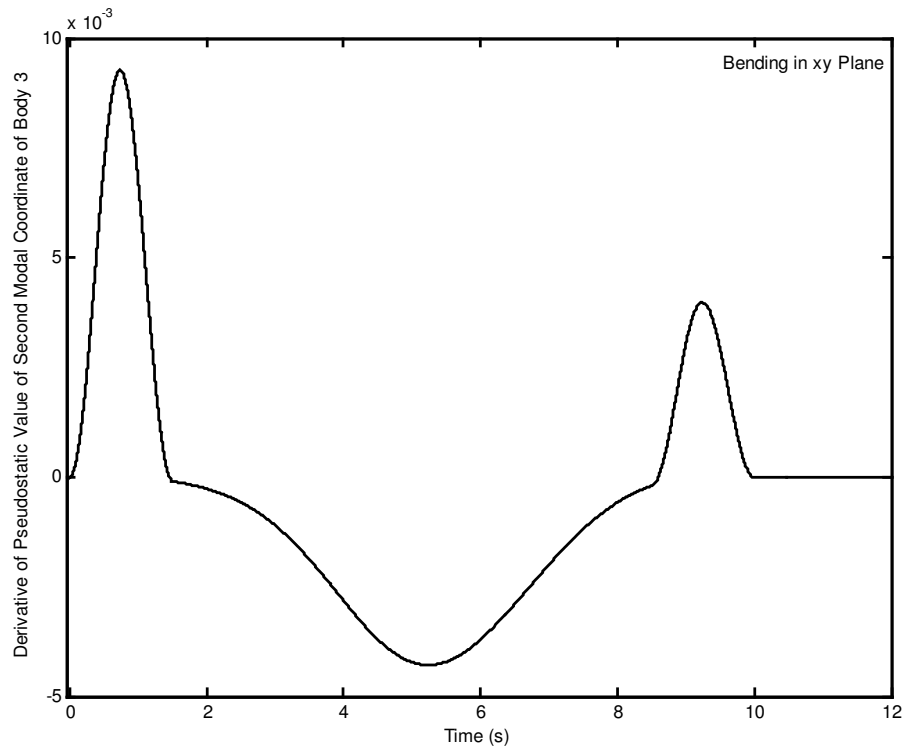


Figure 5.224 Derivative of pseudostatic value of second modal coordinate of body 3 for bending in xy plane.

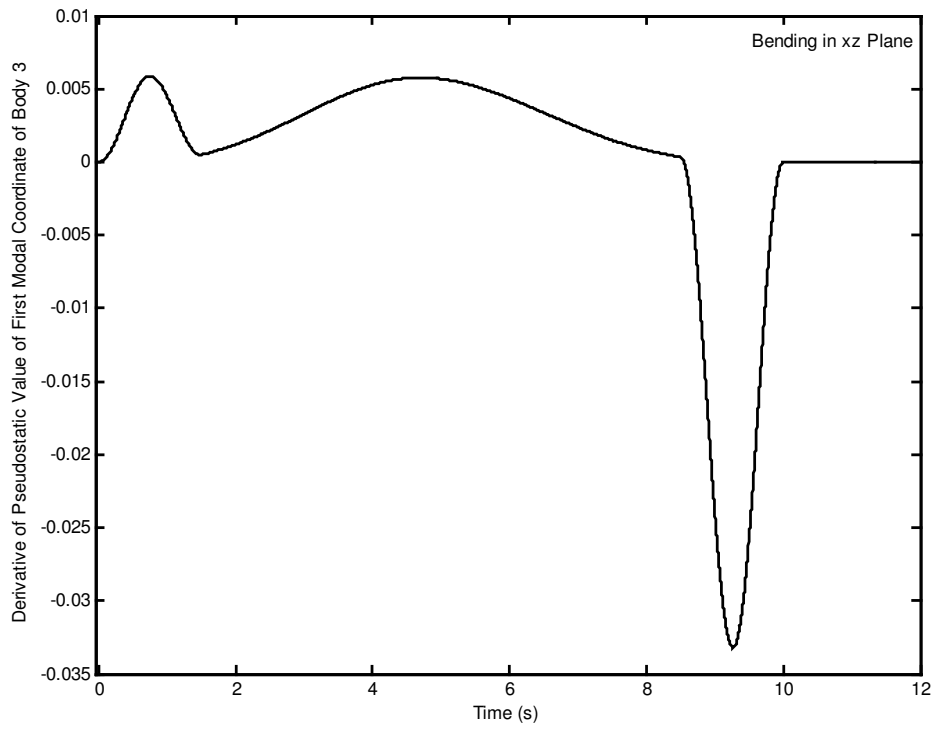


Figure 5.225 Derivative of pseudostatic value of first modal coordinate of body 3 for bending in xz plane.

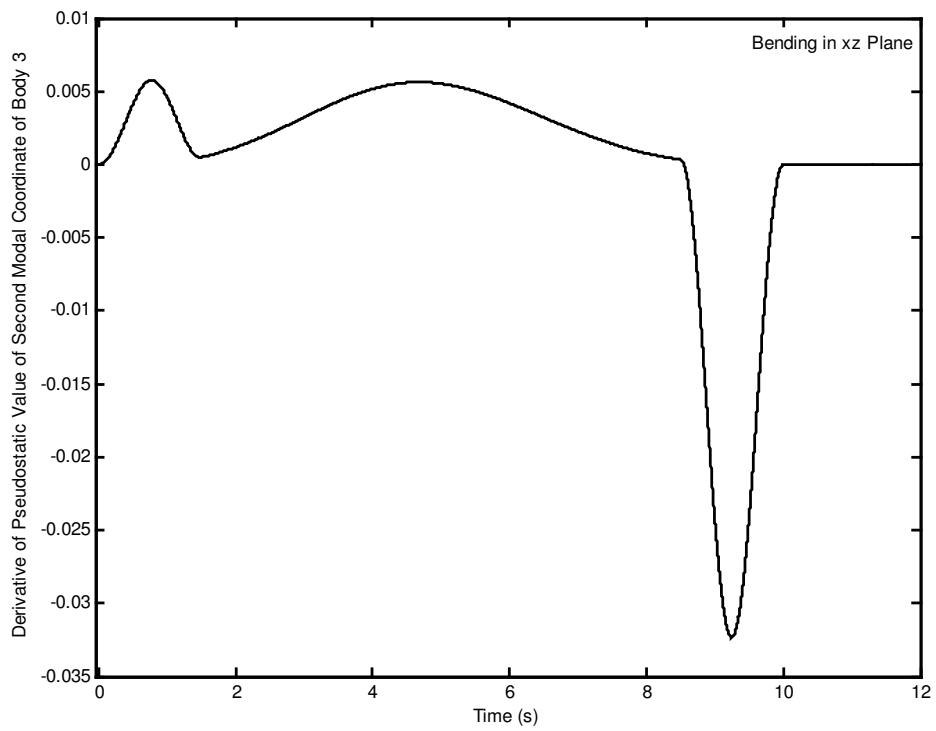


Figure 5.226 Derivative of pseudostatic value of second modal coordinate of body 3 for bending in xz plane.

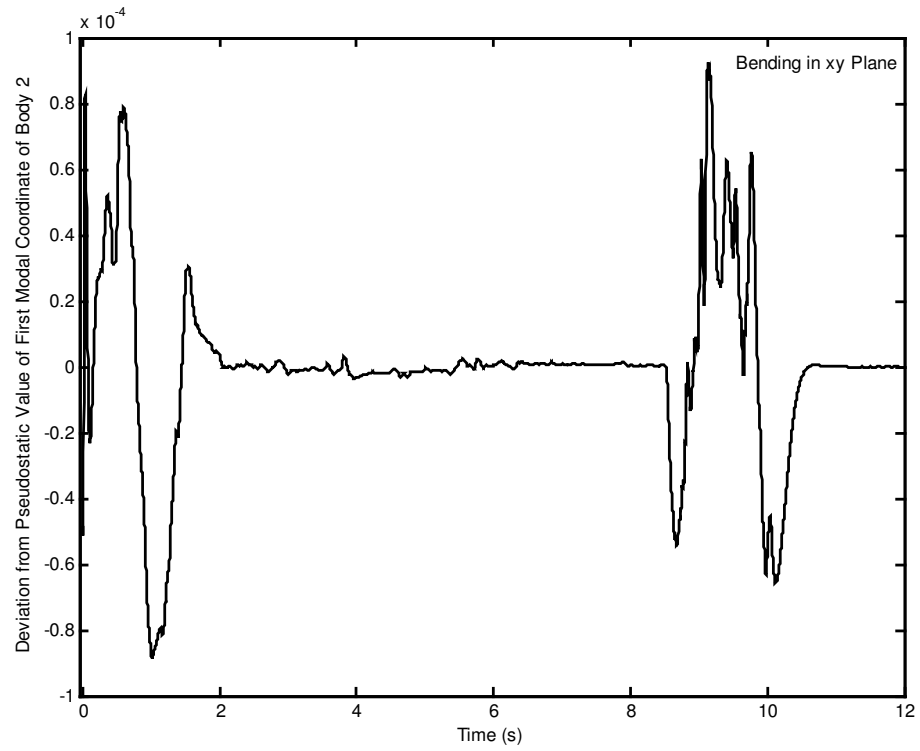


Figure 5.227 Deviation from pseudostatic value of first modal coordinate of body 2 for bending in xy plane.

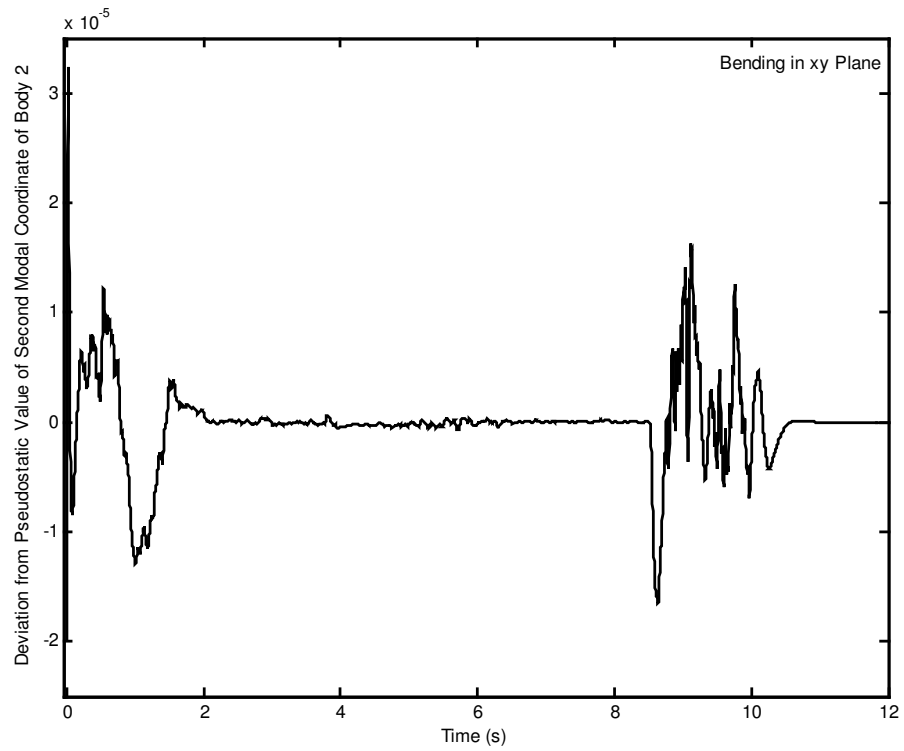


Figure 5.228 Deviation from pseudostatic value of second modal coordinate of body 2 for bending in xy plane.

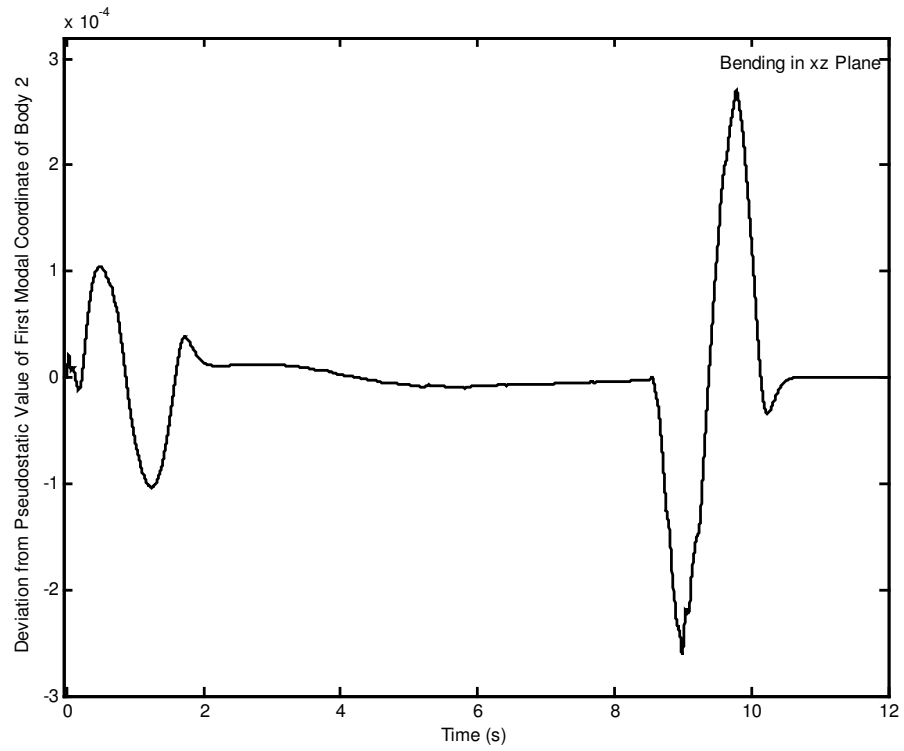


Figure 5.229 Deviation from pseudostatic value of first modal coordinate of body 2 for bending in xz plane.

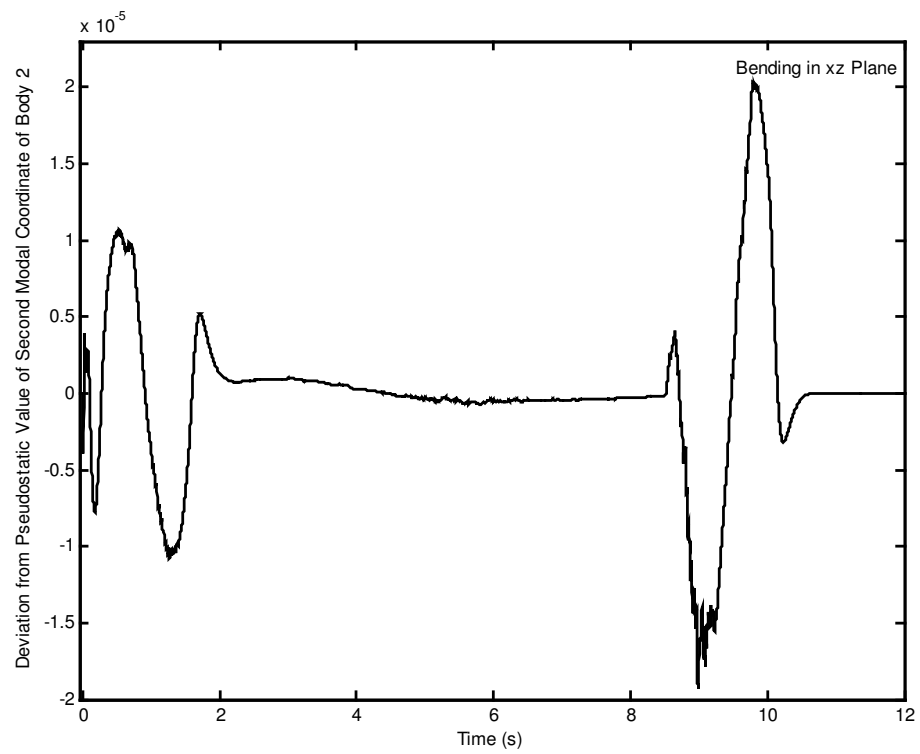


Figure 5.230 Deviation from pseudostatic value of second modal coordinate of body 2 for bending in xz plane.

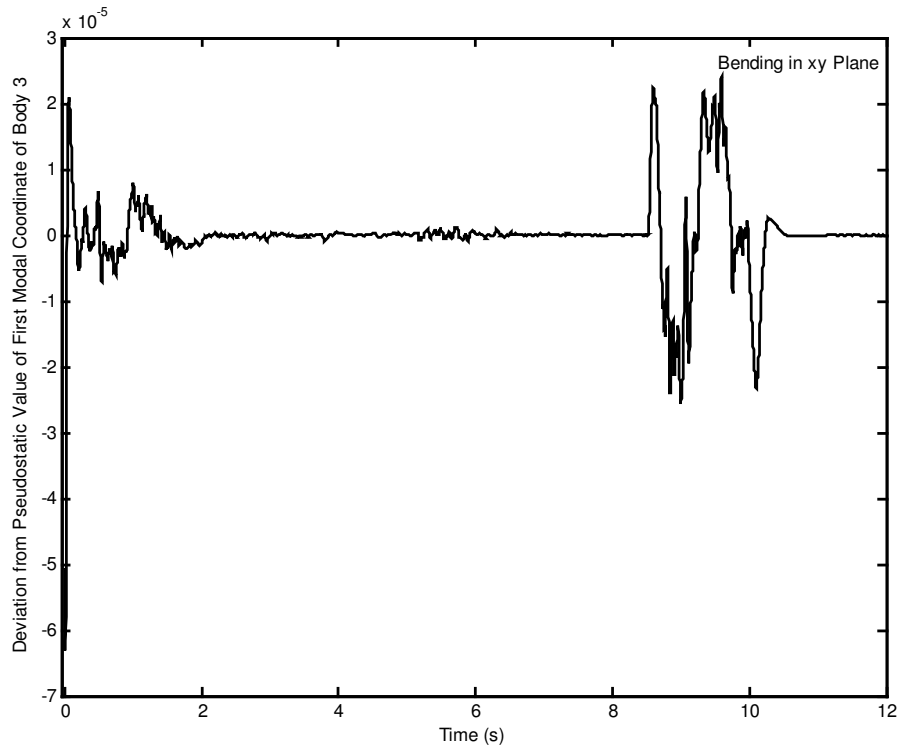


Figure 5.231 Deviation from pseudostatic value of first modal coordinate of body 3 for bending in xy plane.

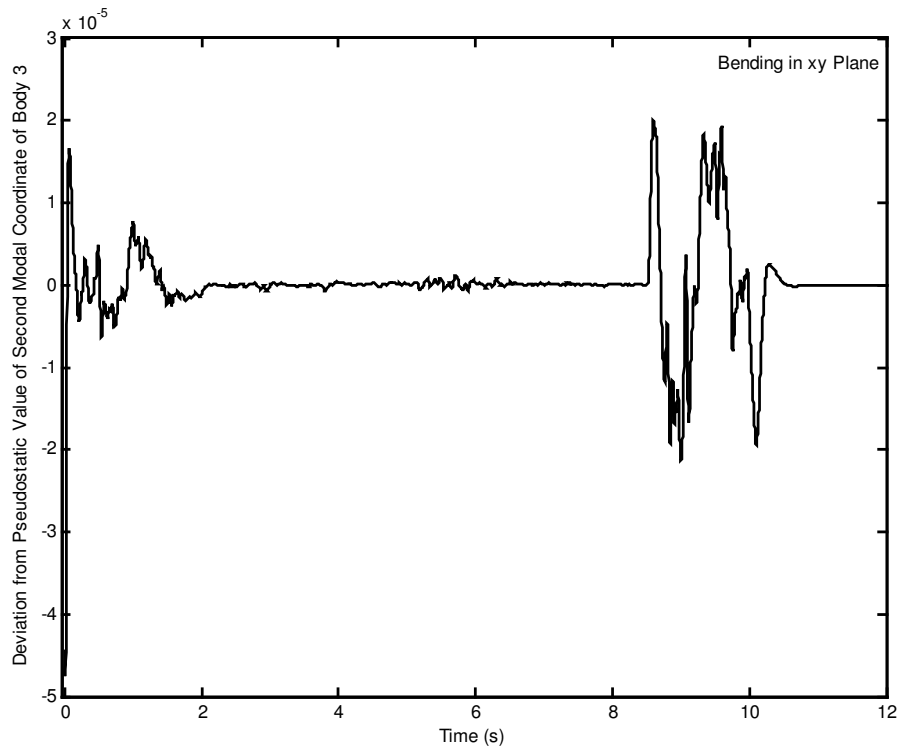


Figure 5.232 Deviation from pseudostatic value of second modal coordinate of body 3 for bending in xy plane.

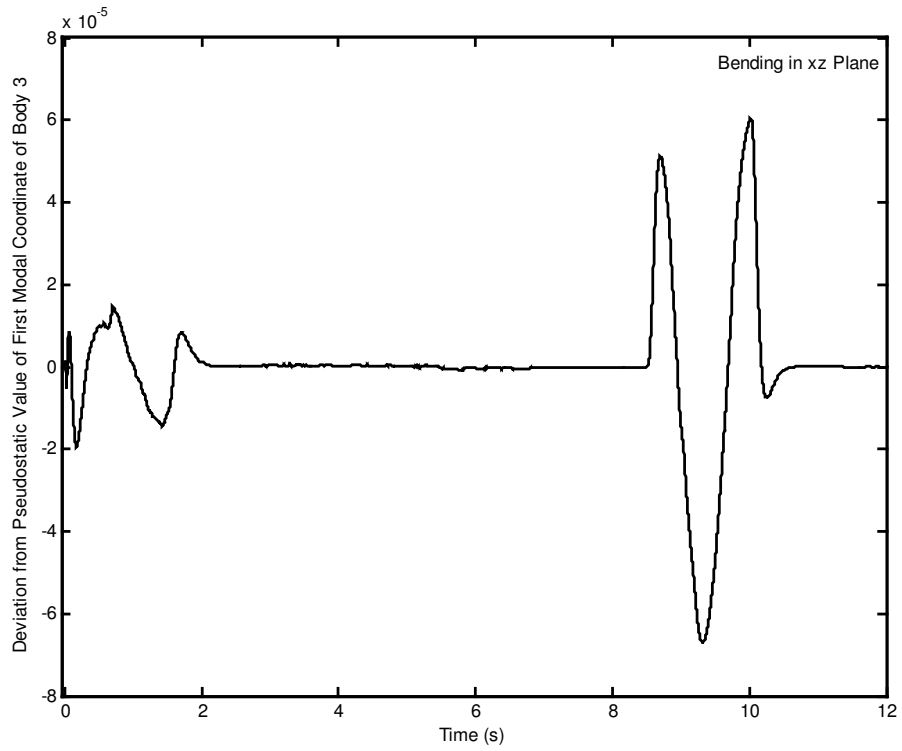


Figure 5.233 Deviation from pseudostatic value of first modal coordinate of body 3 for bending in xz plane.

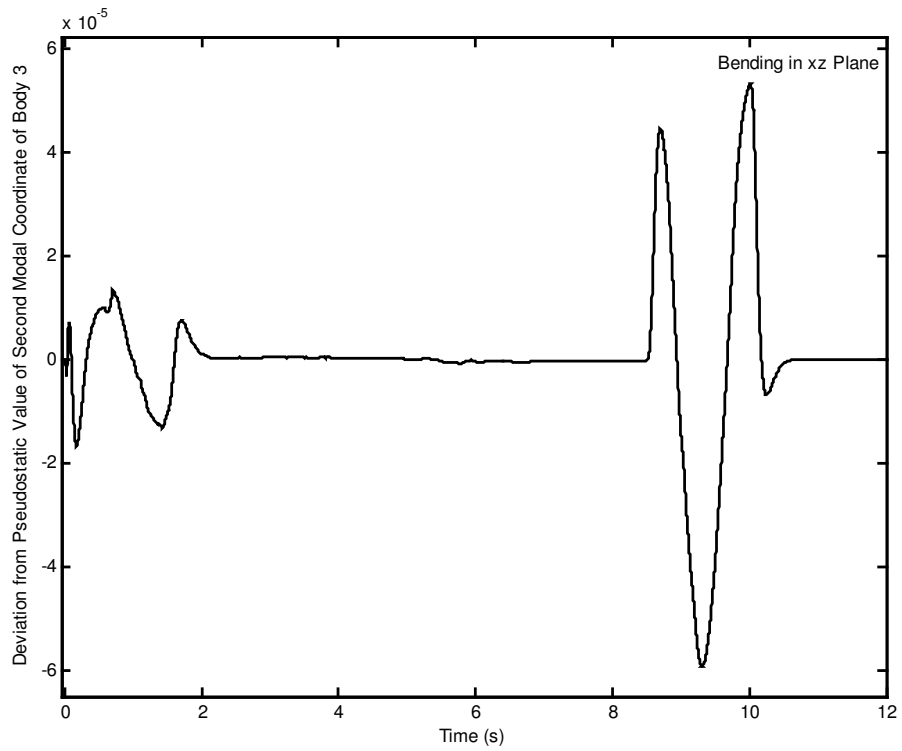


Figure 5.234 Deviation from pseudostatic value of second modal coordinate of body 3 for bending in xz plane.

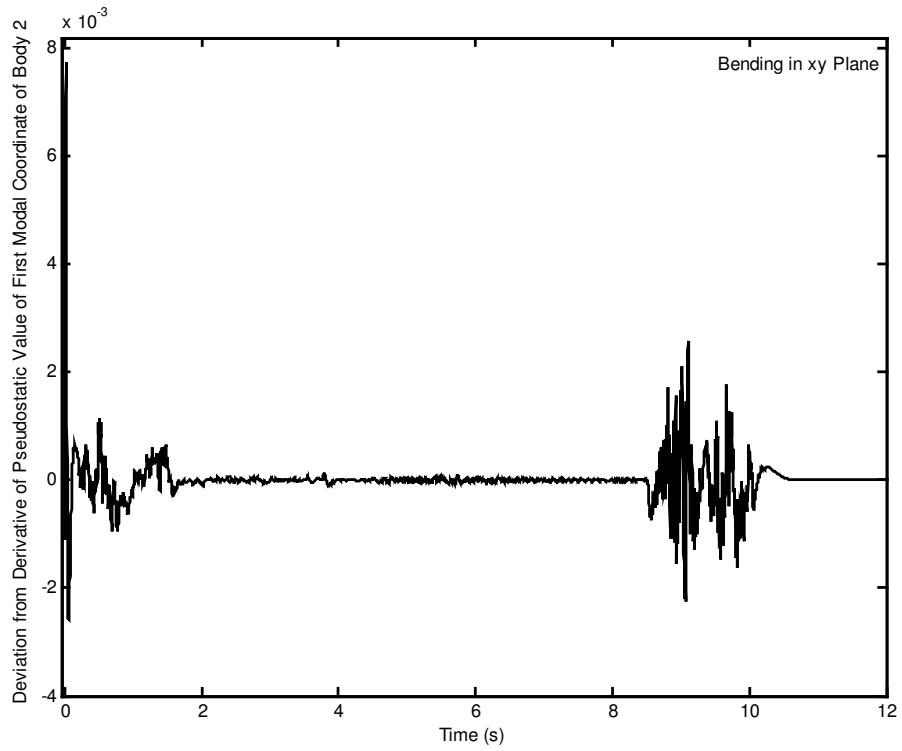


Figure 5.235 Deviation from derivative of pseudostatic value of first modal coordinate of body 2 for bending in xy plane.

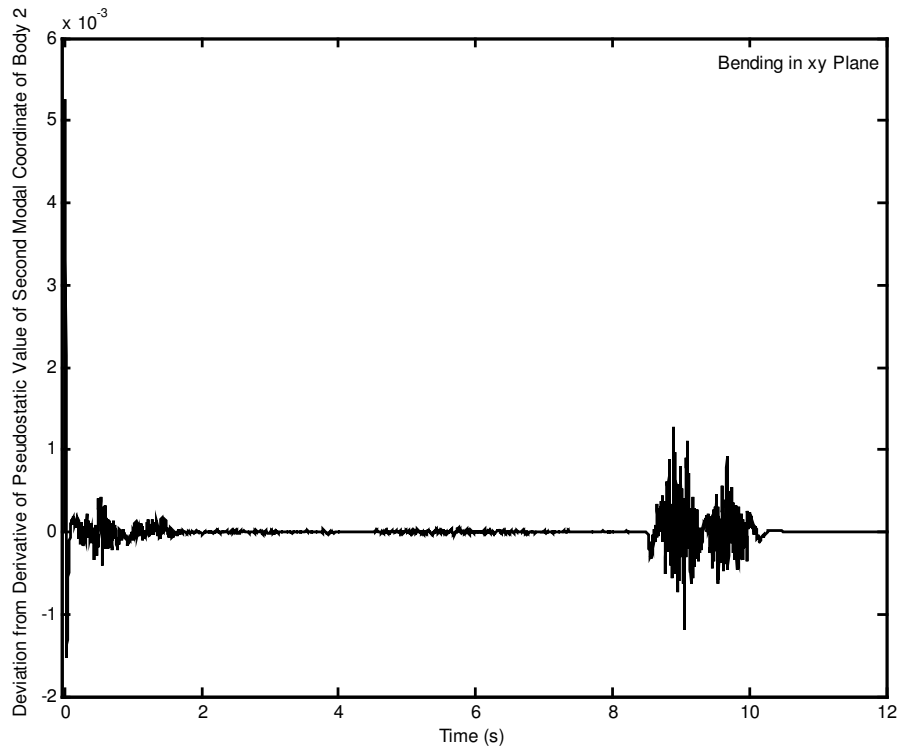


Figure 5.236 Deviation from derivative of pseudostatic value of second modal coordinate of body 2 for bending in xy plane.

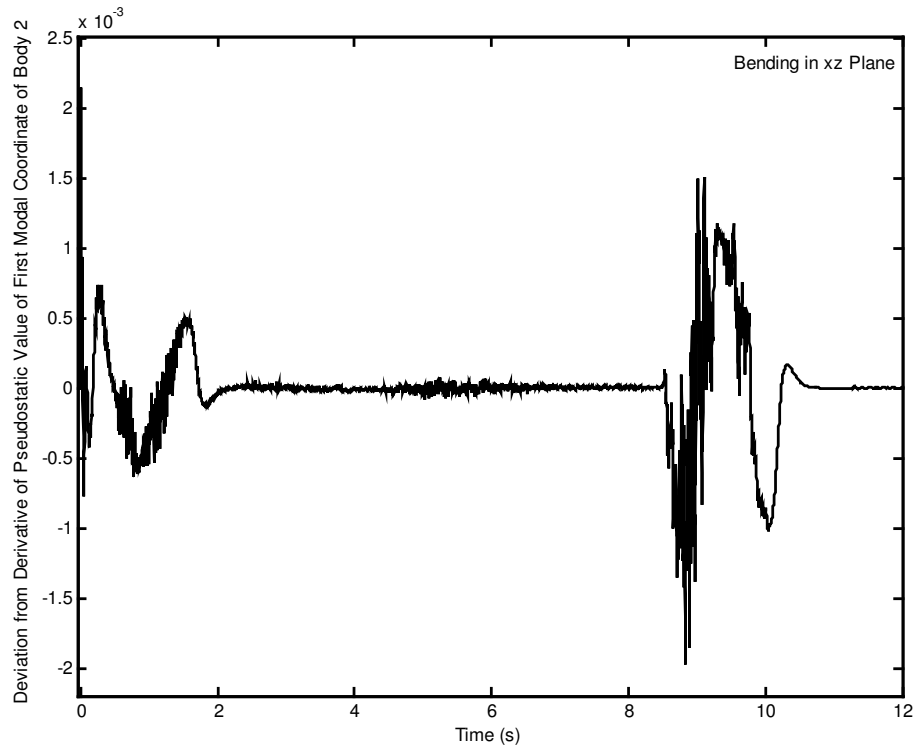


Figure 5.237 Deviation from derivative of pseudostatic value of first modal coordinate of body 2 for bending in xz plane.

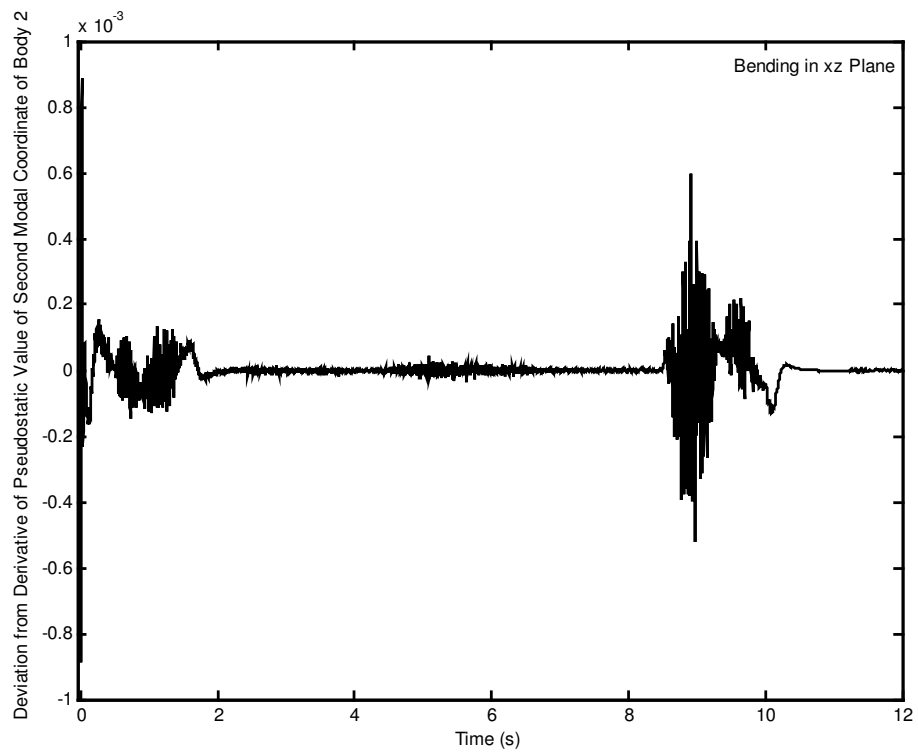


Figure 5.238 Deviation from derivative of pseudostatic value of second modal coordinate of body 2 for bending in xz plane.

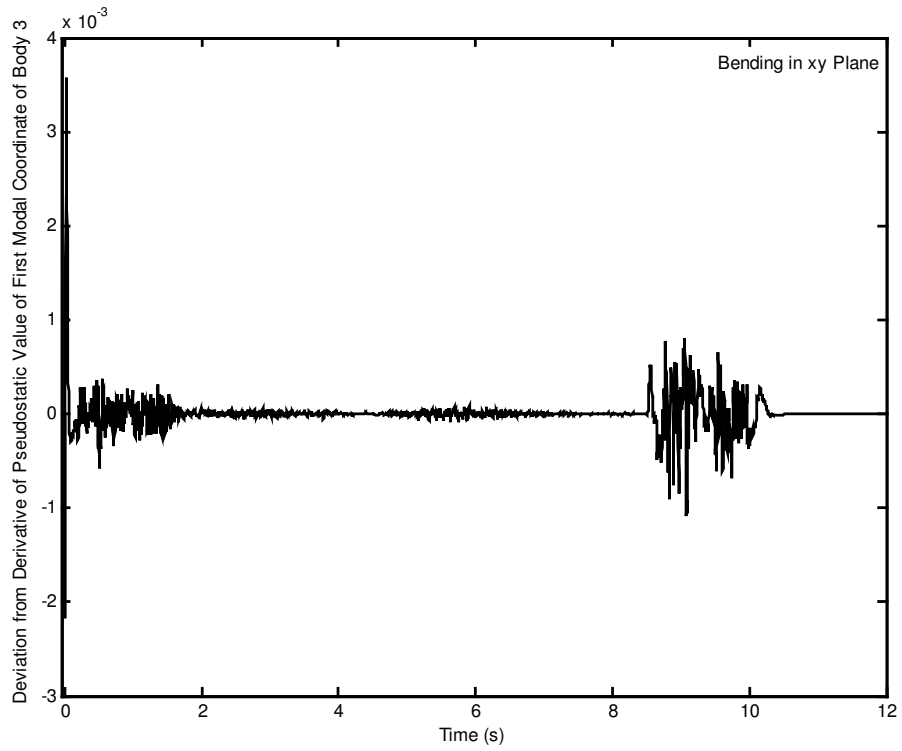


Figure 5.239 Deviation from derivative of pseudostatic value of first modal coordinate of body 3 for bending in xy plane.

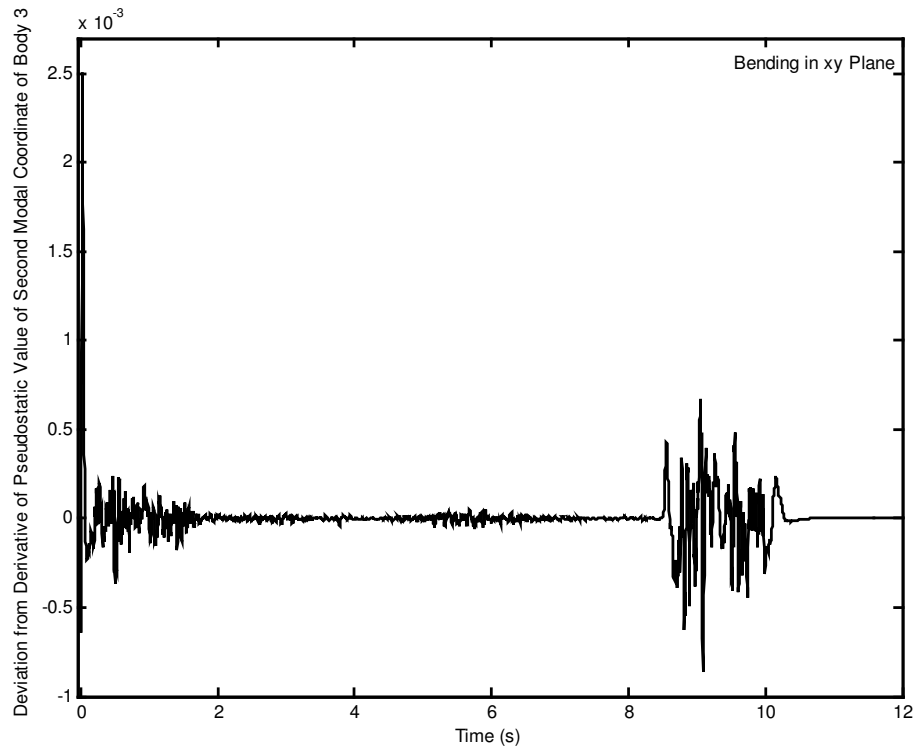


Figure 5.240 Deviation from derivative of pseudostatic value of second modal coordinate of body 3 for bending in xy plane.

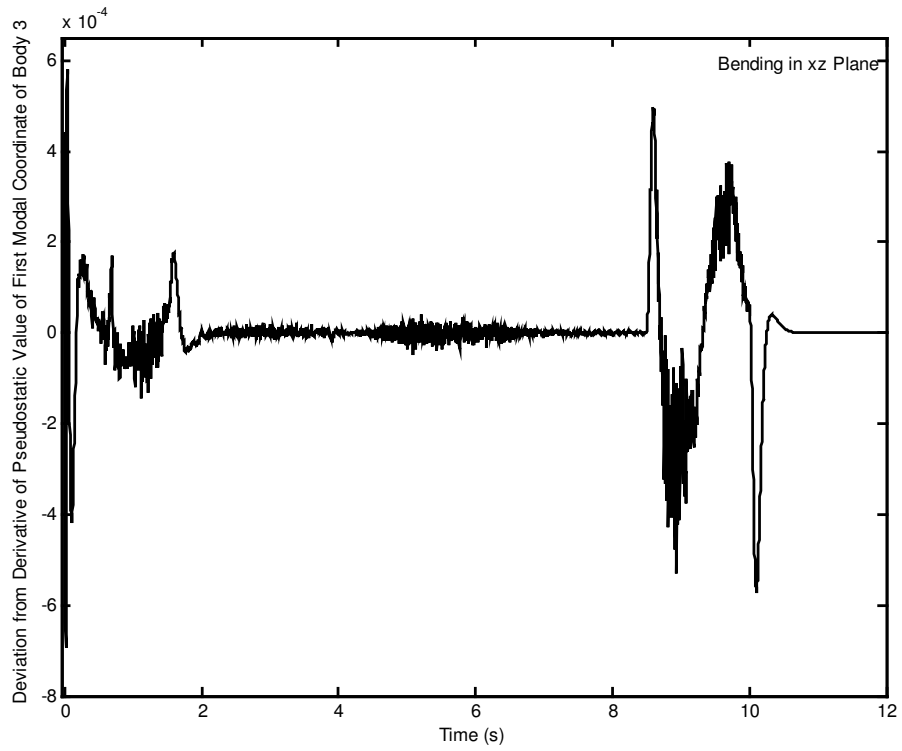


Figure 5.241 Deviation from derivative of pseudostatic value of first modal coordinate of body 3 for bending in xz plane.

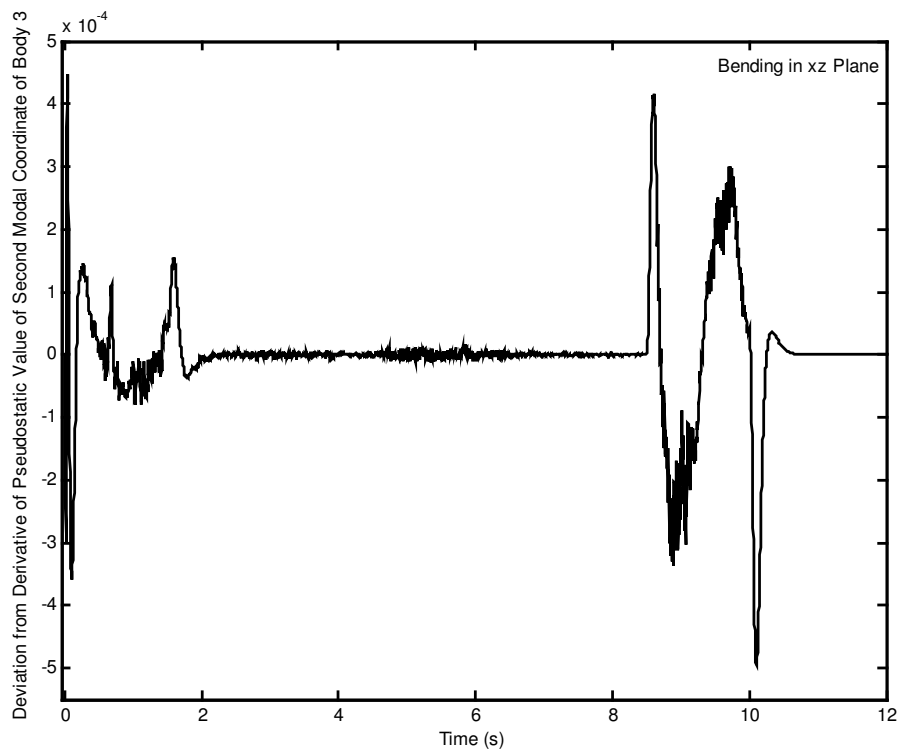


Figure 5.242 Deviation from derivative of pseudostatic value of second modal coordinate of body 3 for bending in xz plane.

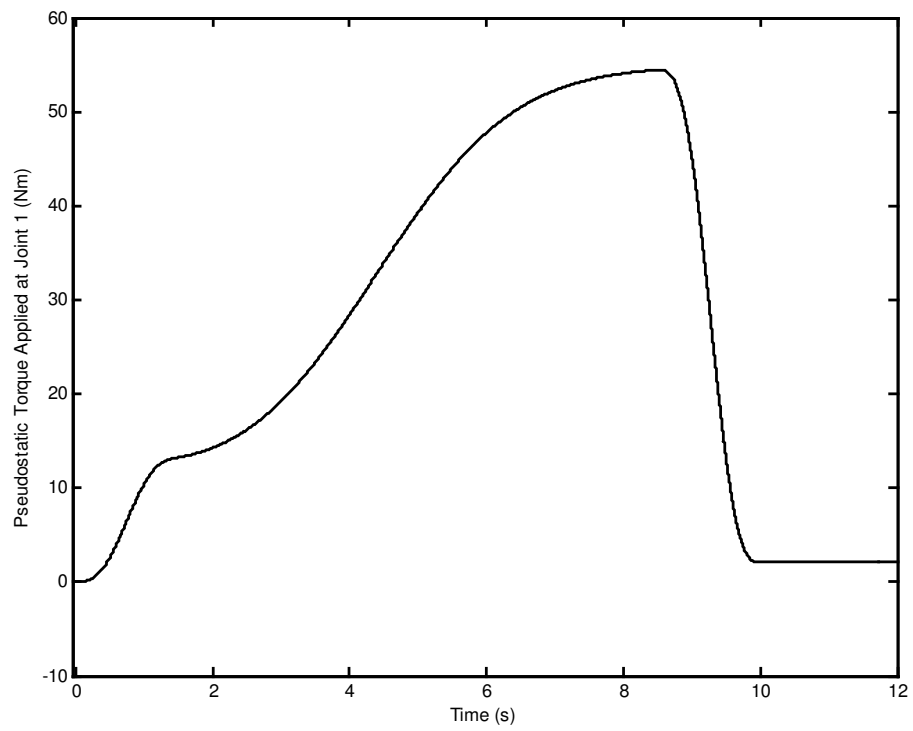


Figure 5.243 Pseudostatic torque applied at joint 1.

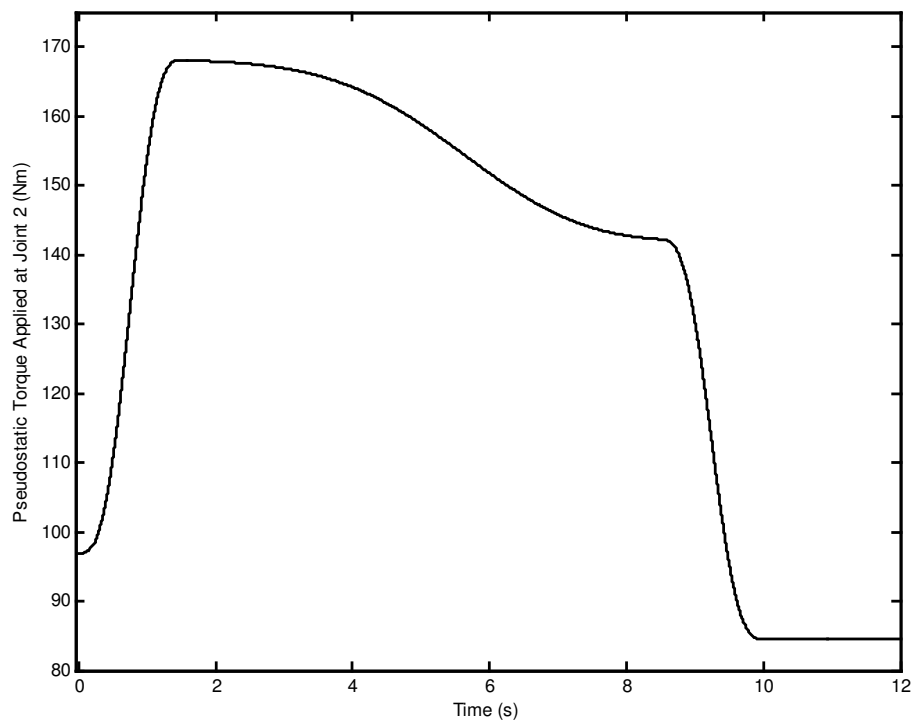


Figure 5.244 Pseudostatic torque applied at joint 2.

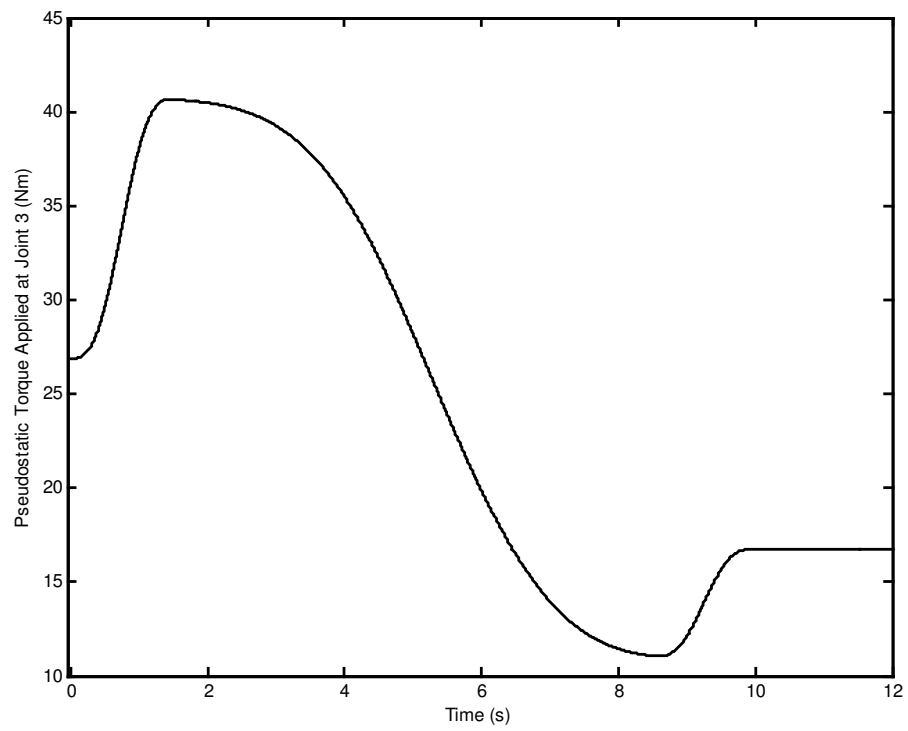


Figure 5.245 Pseudostatic torque applied at joint 3.

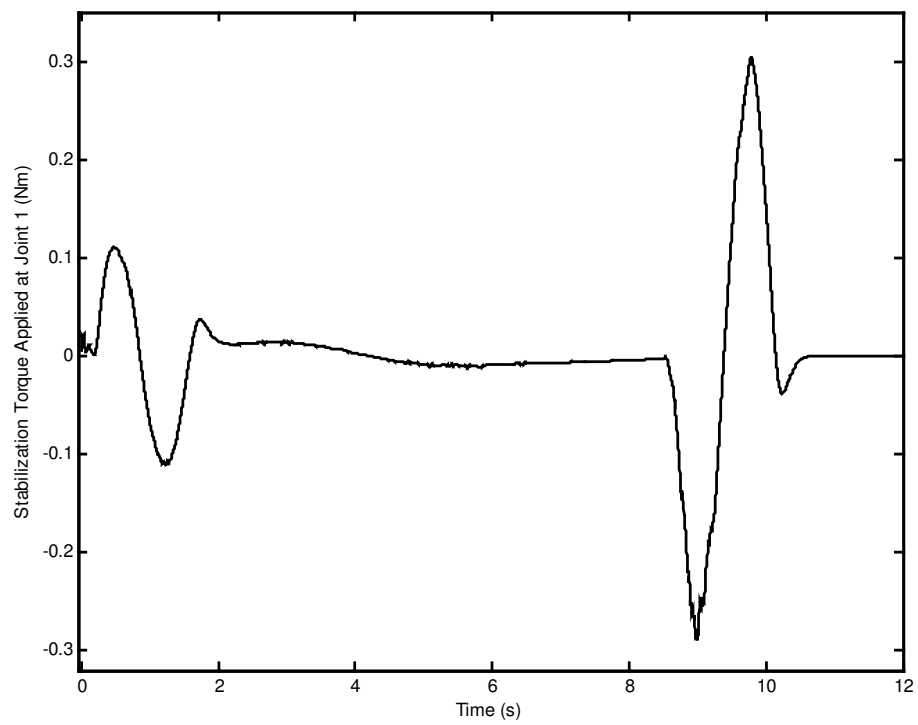


Figure 5.246 Stabilization torque applied at joint 1.

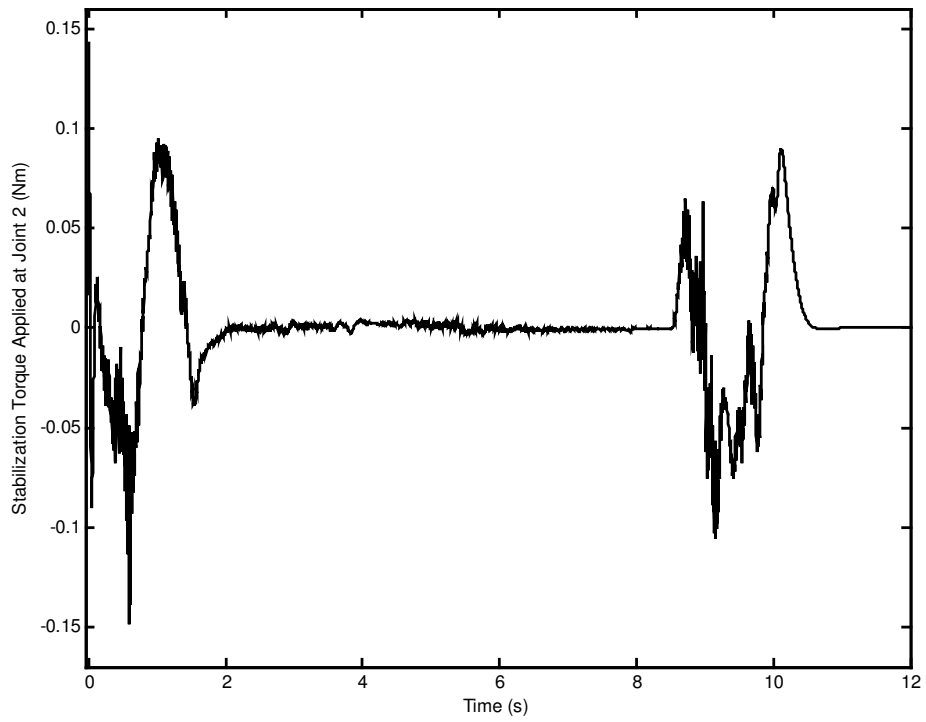


Figure 5.247 Stabilization torque applied at joint 2.

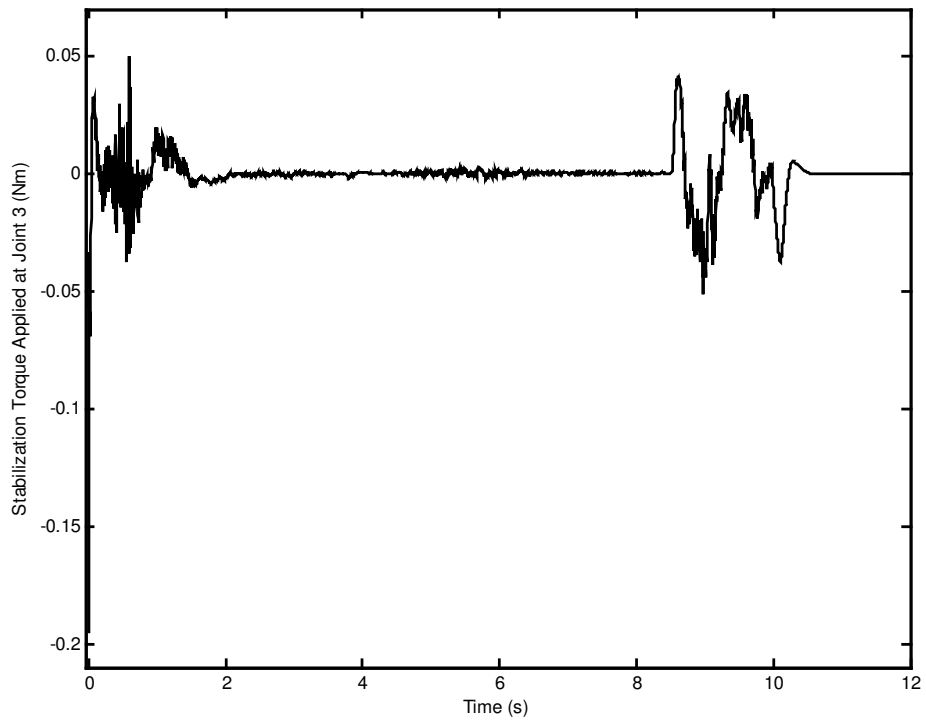


Figure 5.248 Stabilization torque applied at joint 3.

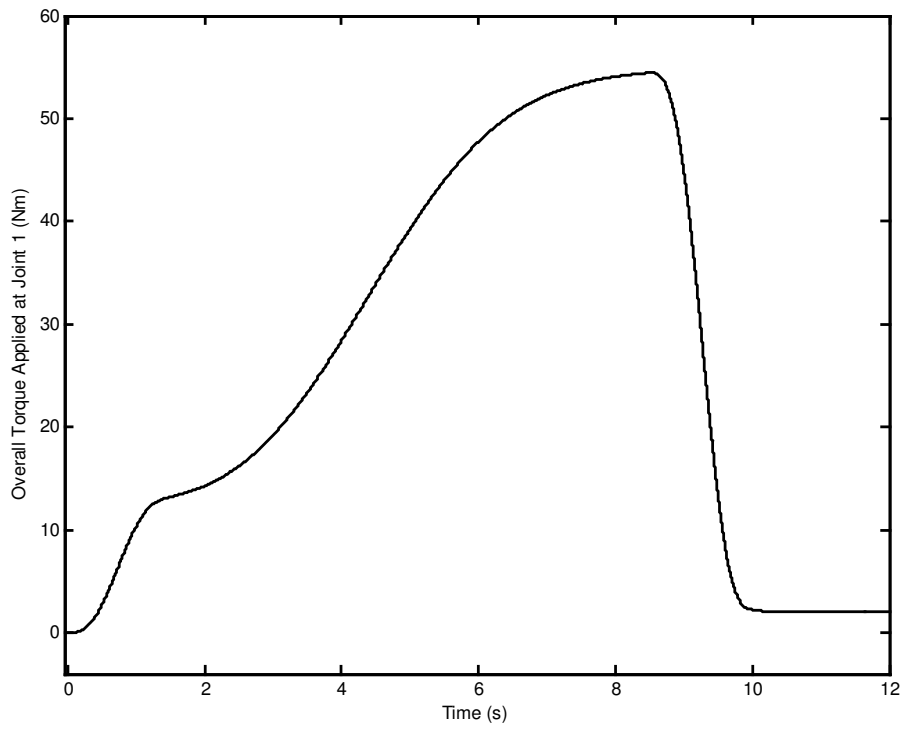


Figure 5.249 Overall torque applied at joint 1.

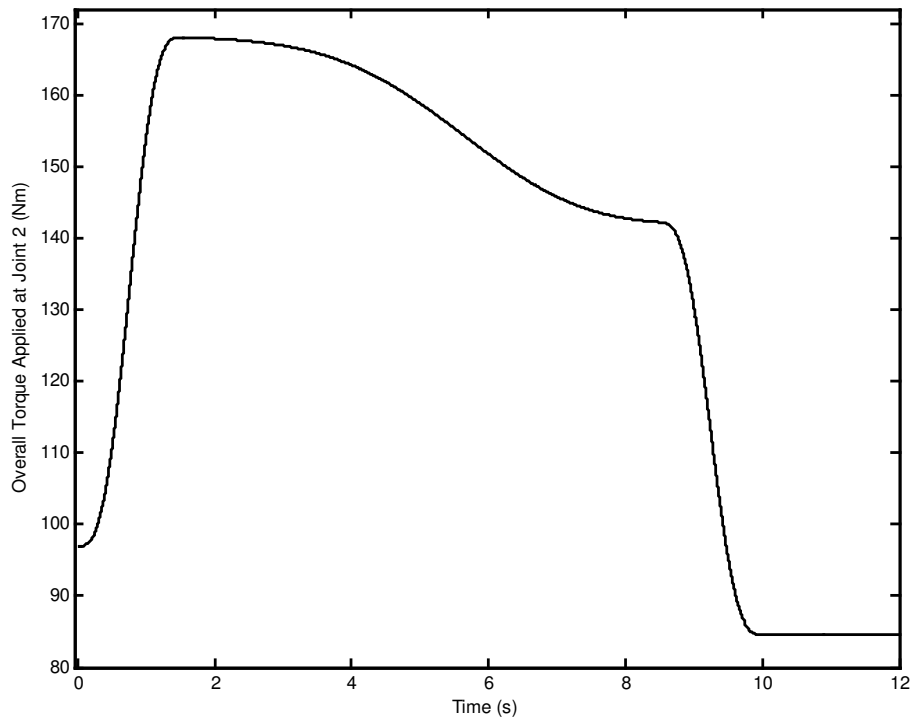


Figure 5.250 Overall torque applied at joint 2.

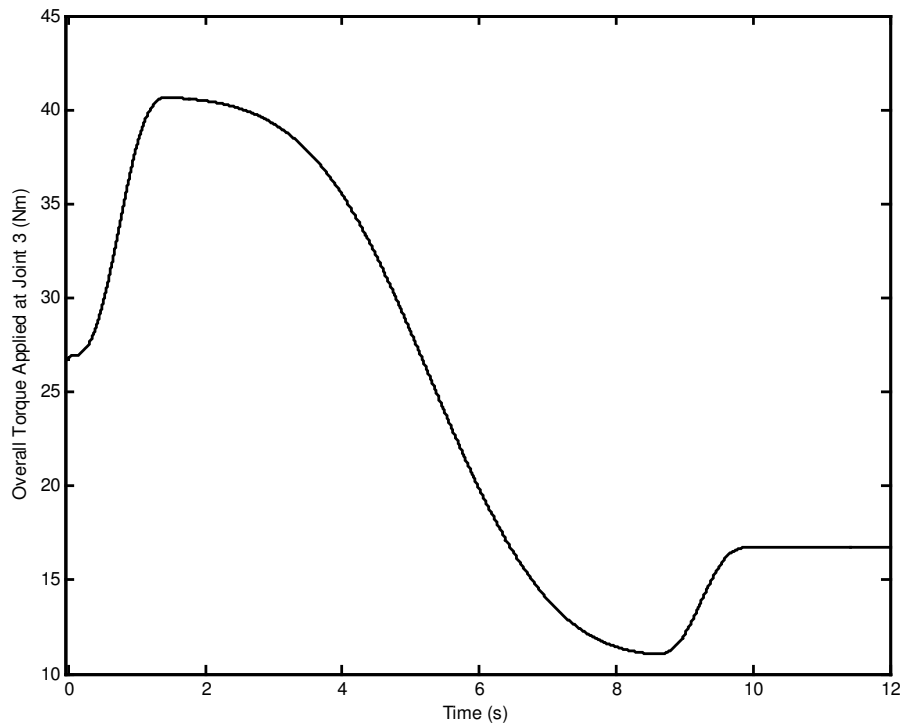


Figure 5.251 Overall torque applied at joint 3.

The maximum azimuth and elevation angle errors of the tip point along the trajectory after the settling time are 0.0493 degrees and 0.0206 degrees, respectively. The maximum Lagrange multiplier error after the settling time is – 0.588 N. The maximum overall torques applied to the joints are in the order of 168 Nm as seen from Figures 5.249 - 5.251.

5.5 Numerical Simulation of Force and Motion Control of Spatial Robot with Measurement Noises

In this section, the numerical simulation of the force and motion control of the spatial robot including measurement noises is presented by using the force and motion control method proposed at Chapter 2. The measurement noises are considered for the state variables that are used for the generation of the stabilization control torques (i.e., the measured variables). They are the azimuth and elevation angles and their rates, the modal variables of Body 2 and Body 3 and

their rates and the impulse of the Lagrange multiplier. In a real system, the Lagrange multiplier is measured instead of its impulse. Due to this reason, the measurement noise generated for the Lagrange multiplier is integrated before it is added to the impulse of the Lagrange multiplier.

The measurement noises are generated by using normally distributed random numbers with zero mean and specific standard deviation. 1 % deviation from the mean value of each variable is assumed to obtain the standard deviation for each variable.

The first order low pass filter whose transfer function given in Equation (5.3) is used again to filter the measured variables.

The same reference Lagrange multiplier, the same reference tip point trajectory and the same closed loop natural frequencies and damping ratios given in Section 5.4 are used. After a few trials, a proper crossover frequency for the filter is found as 276 rad/s. The sampling frequency is taken as 500 Hz. The simulation results are presented in Figures 5.252 - 5.341.

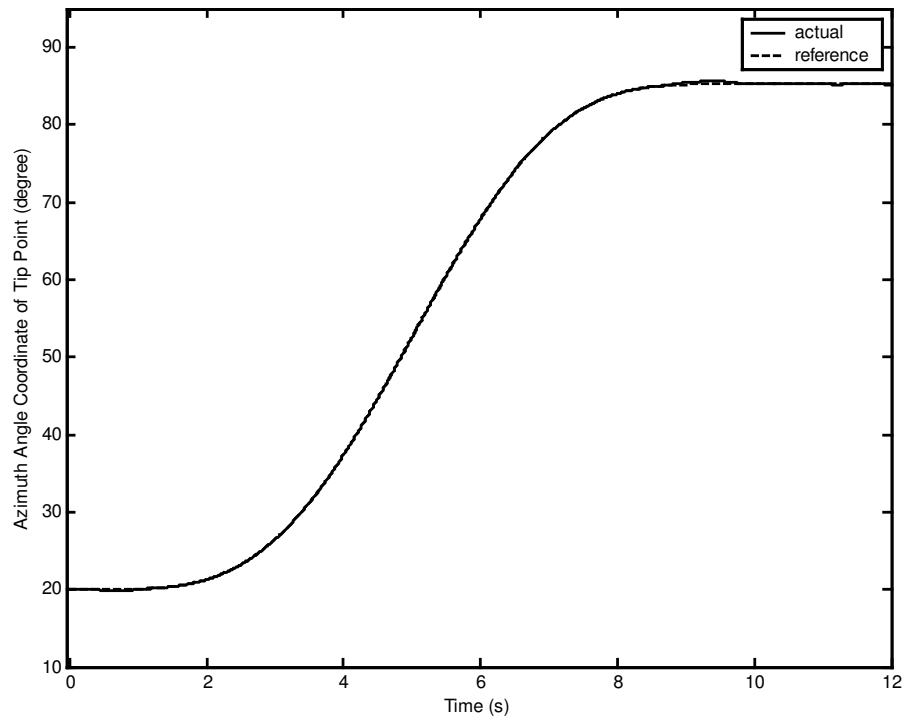


Figure 5.252 Azimuth angle coordinate of tip point.

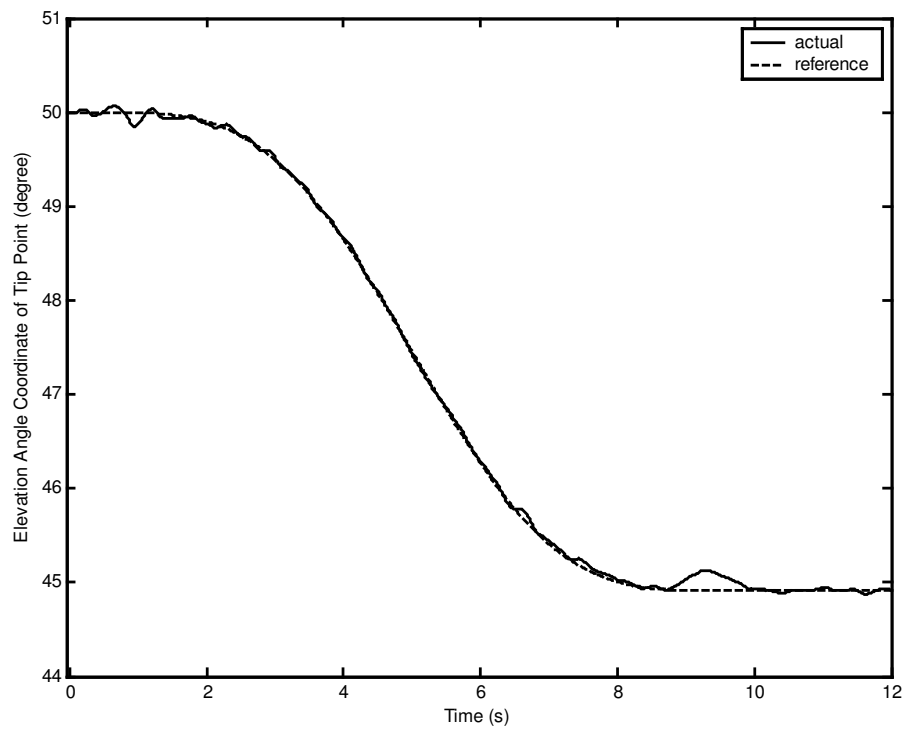


Figure 5.253 Elevation angle coordinate of tip point.

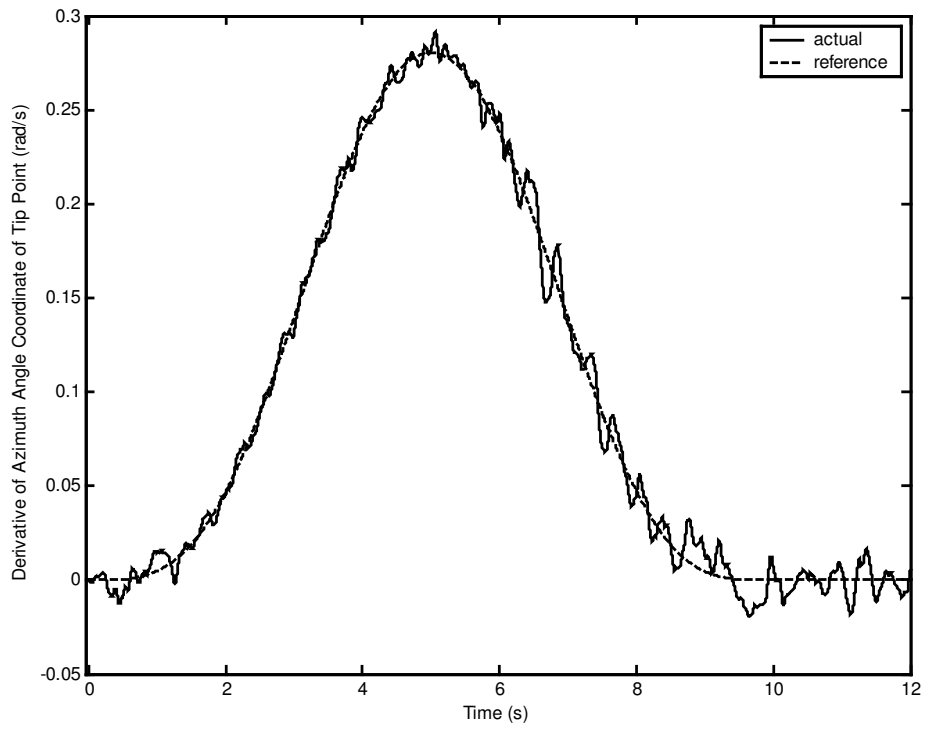


Figure 5.254 Derivative of azimuth angle coordinate of tip point.

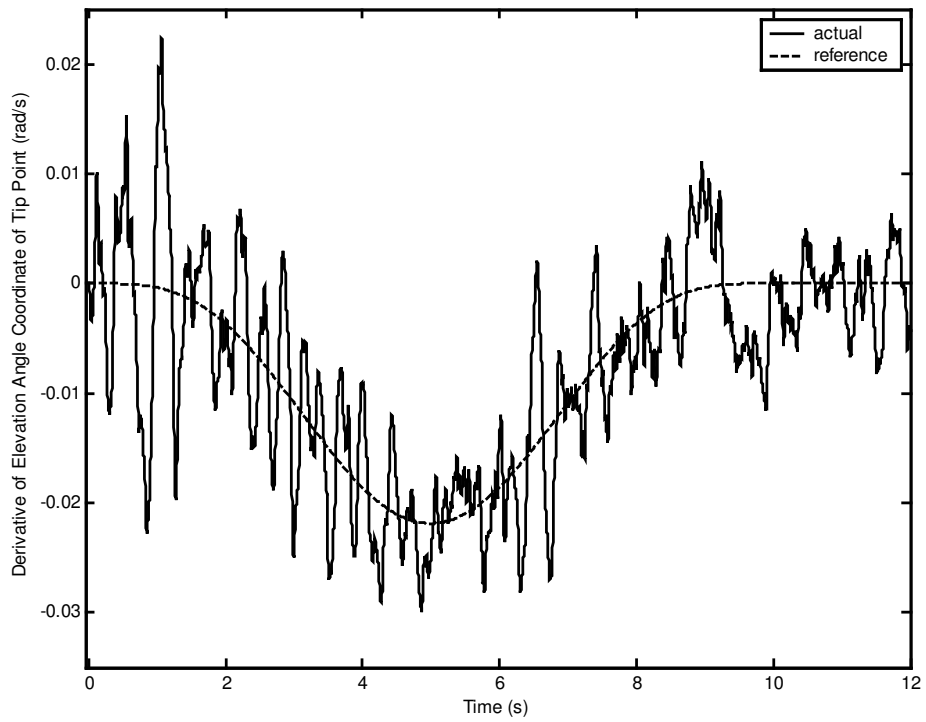


Figure 5.255 Derivative of elevation angle coordinate of tip point.

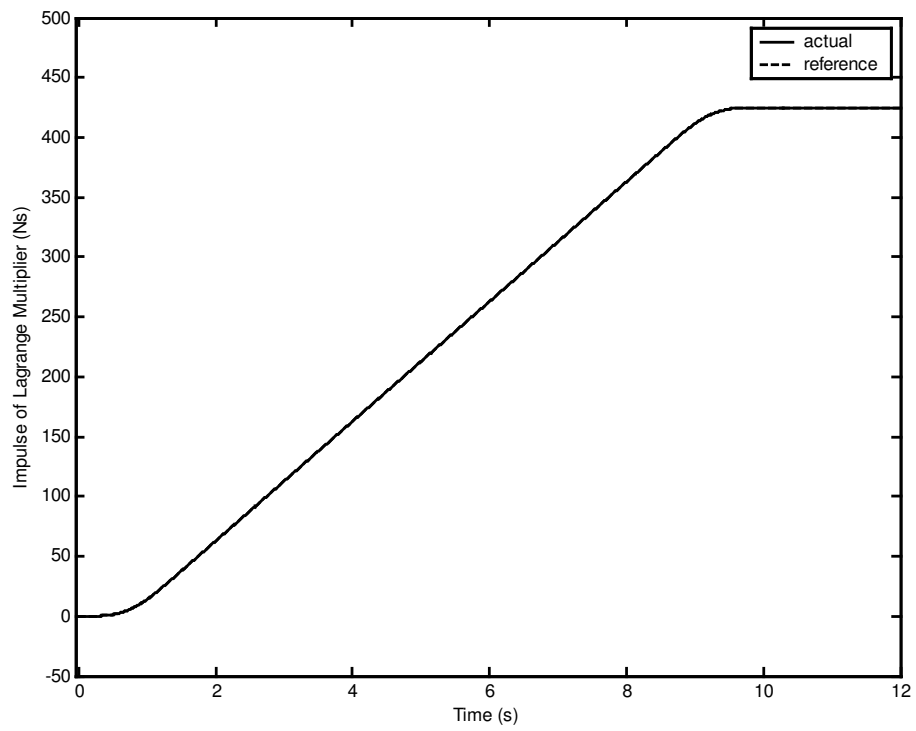


Figure 5.256 Impulse of Lagrange multiplier.

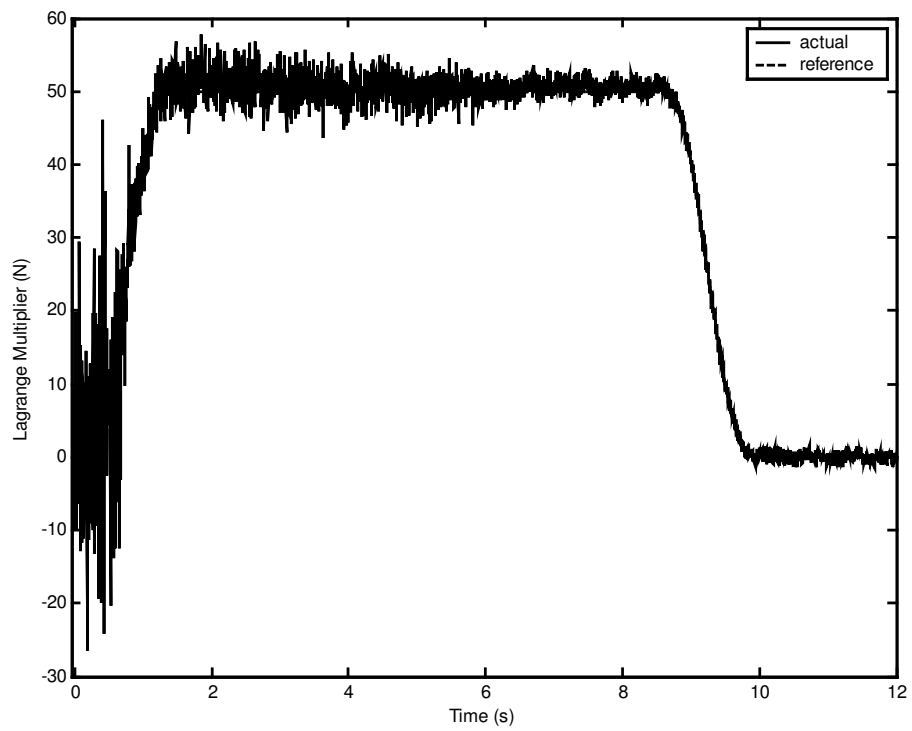


Figure 5.257 Lagrange multiplier.

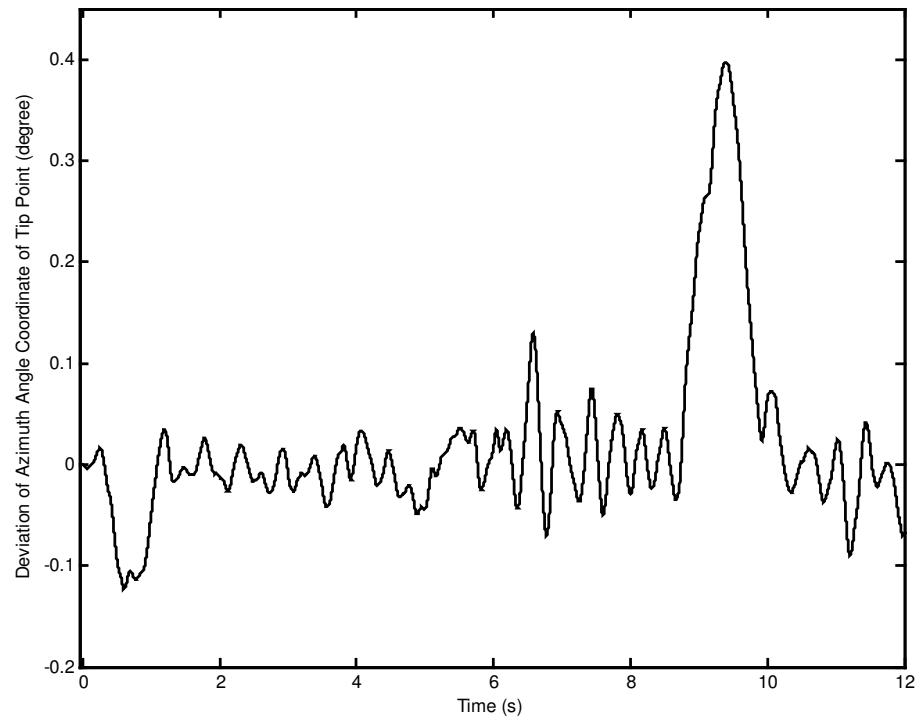


Figure 5.258 Deviation of azimuth angle coordinate of tip point.

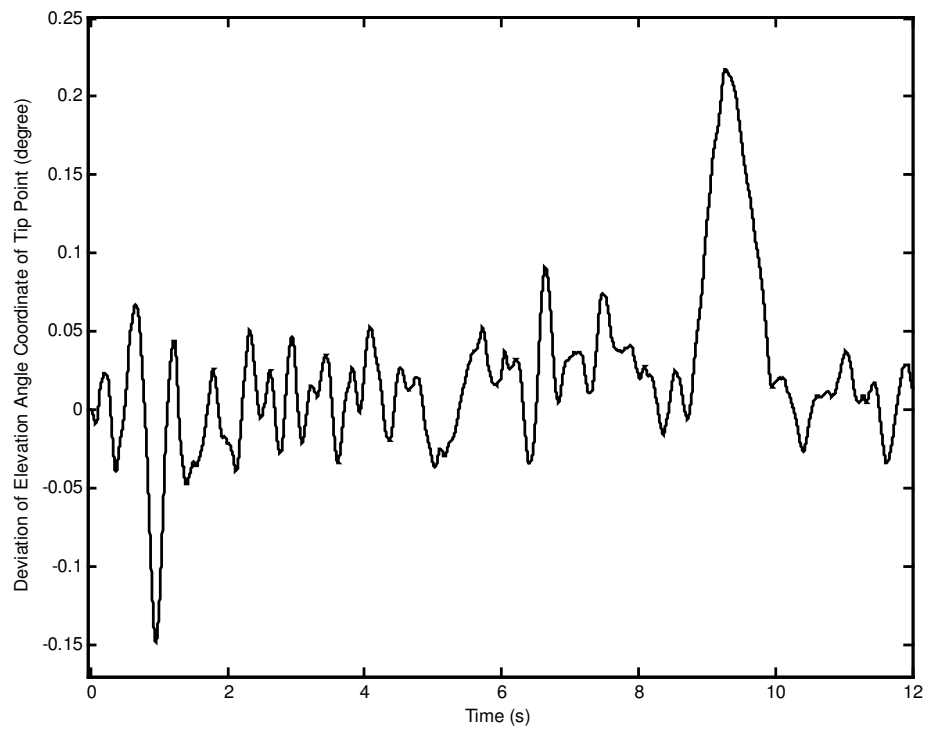


Figure 5.259 Deviation of elevation angle coordinate of tip point.

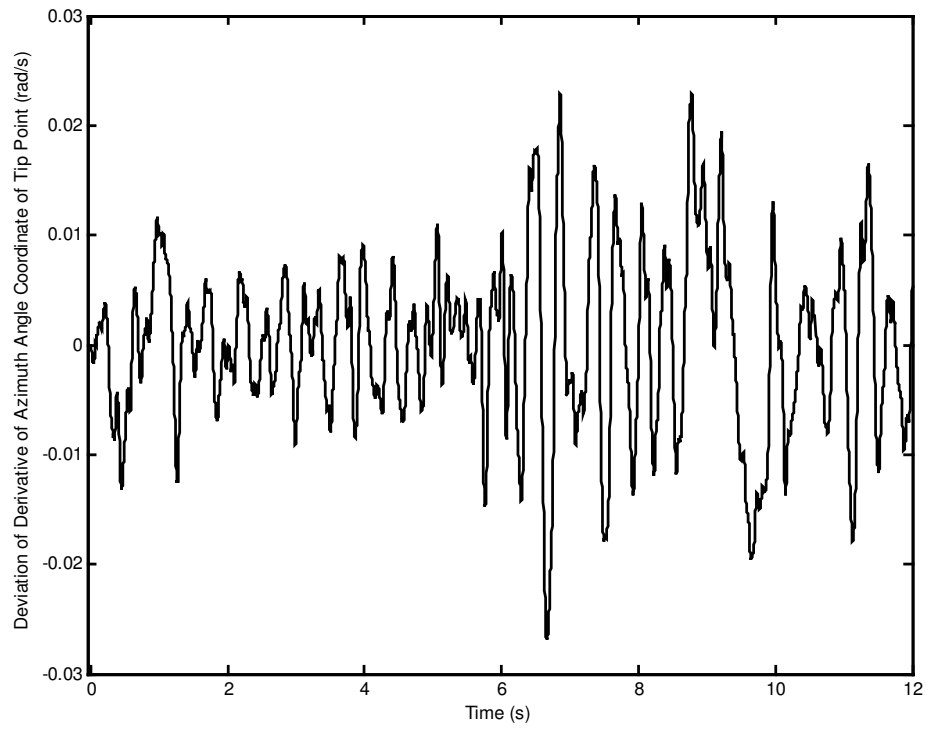


Figure 5.260 Deviation of derivative of azimuth angle coordinate of tip point.

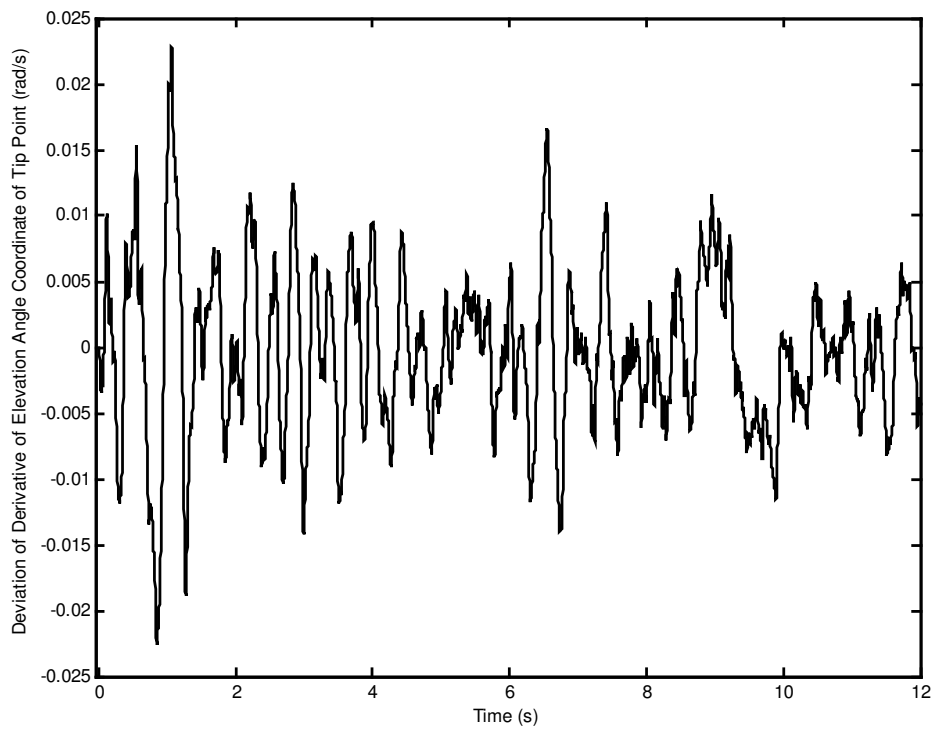


Figure 5.261 Deviation of derivative of elevation angle coordinate of tip point.

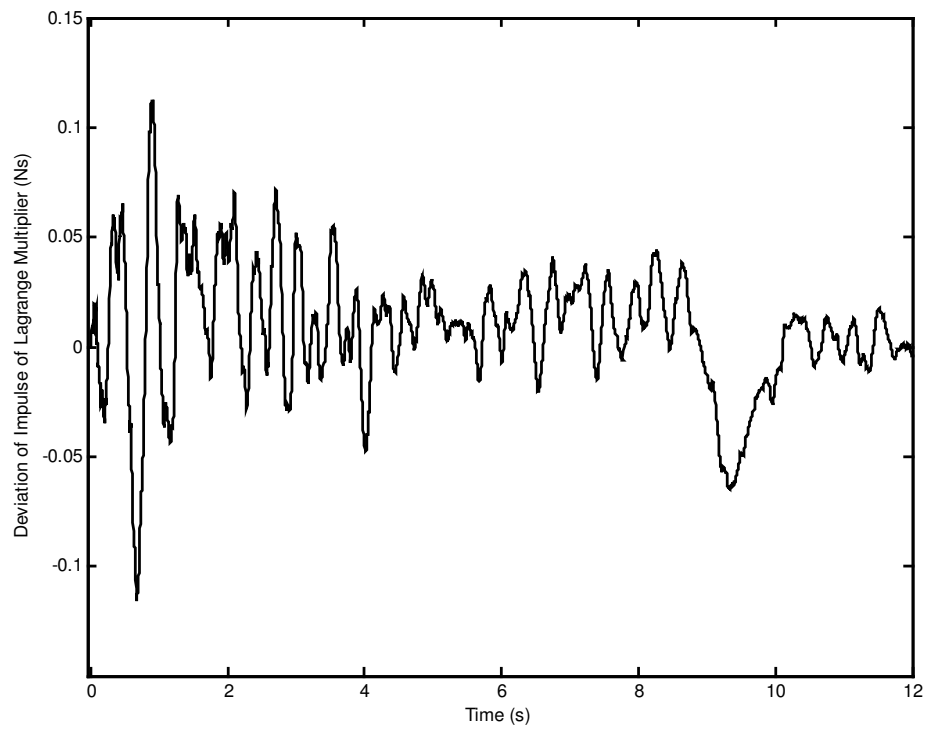


Figure 5.262 Deviation of impulse of Lagrange multiplier.

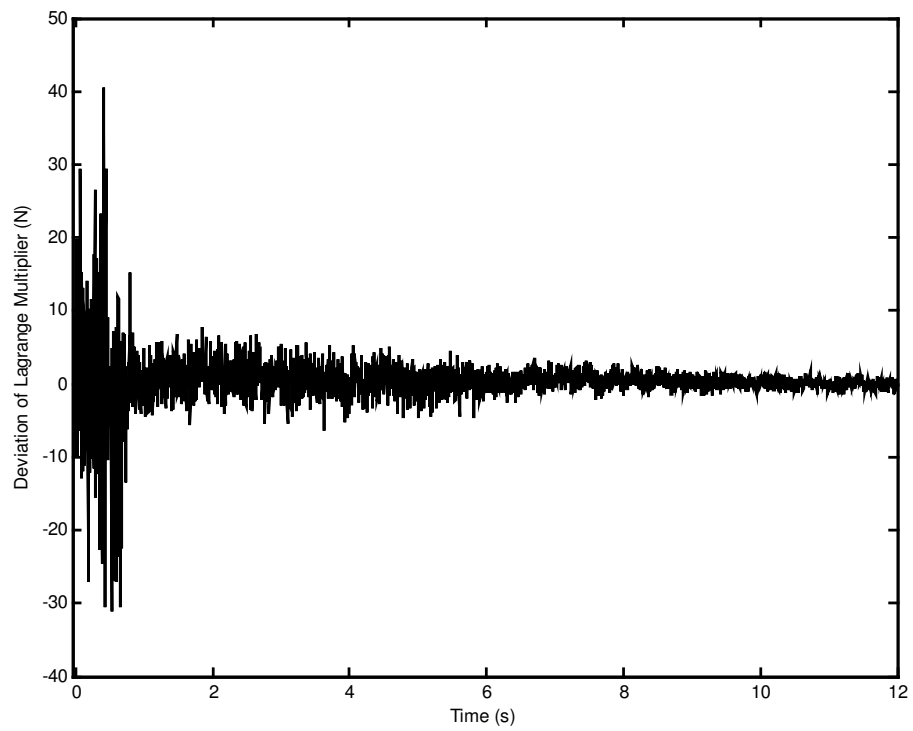


Figure 5.263 Deviation of Lagrange multiplier.

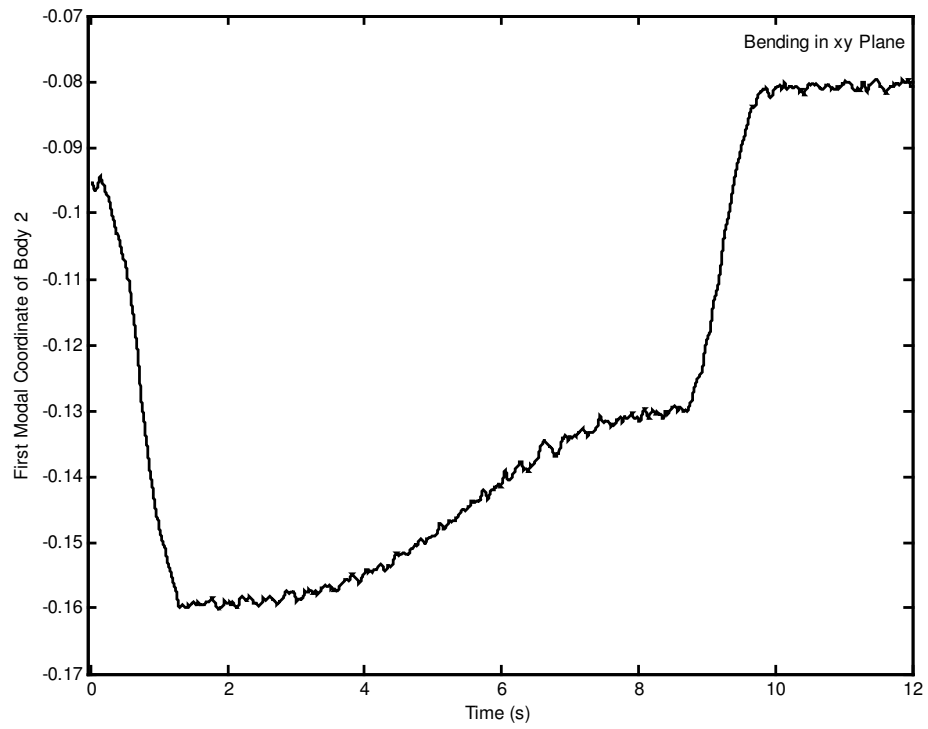


Figure 5.264 First modal coordinate of body 2 for bending in xy plane.

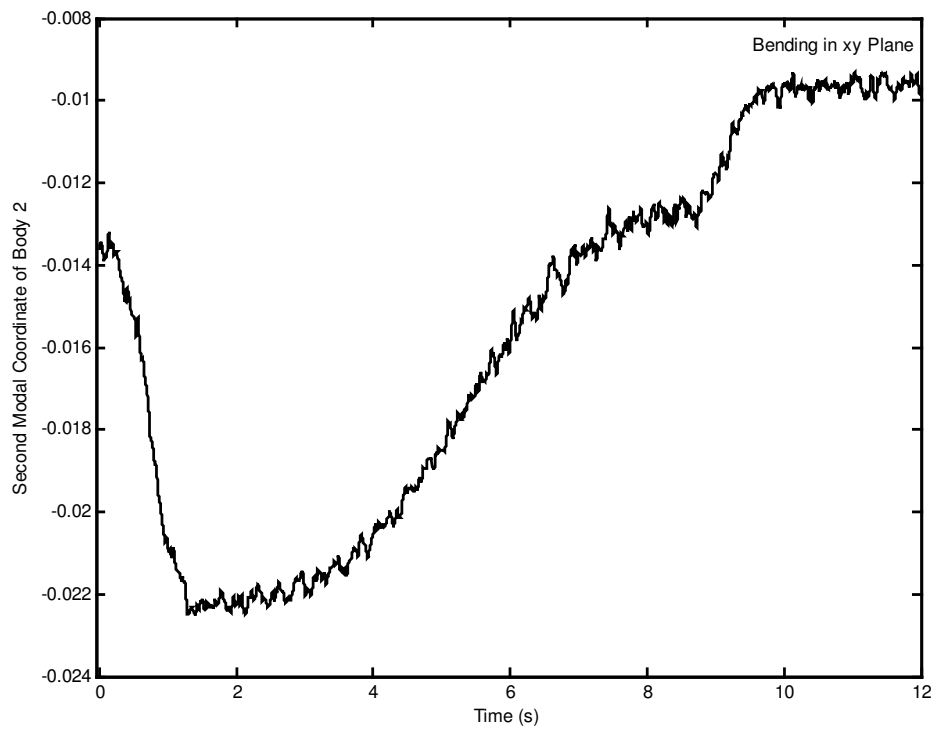


Figure 5.265 Second modal coordinate of body 2 for bending in xy plane.

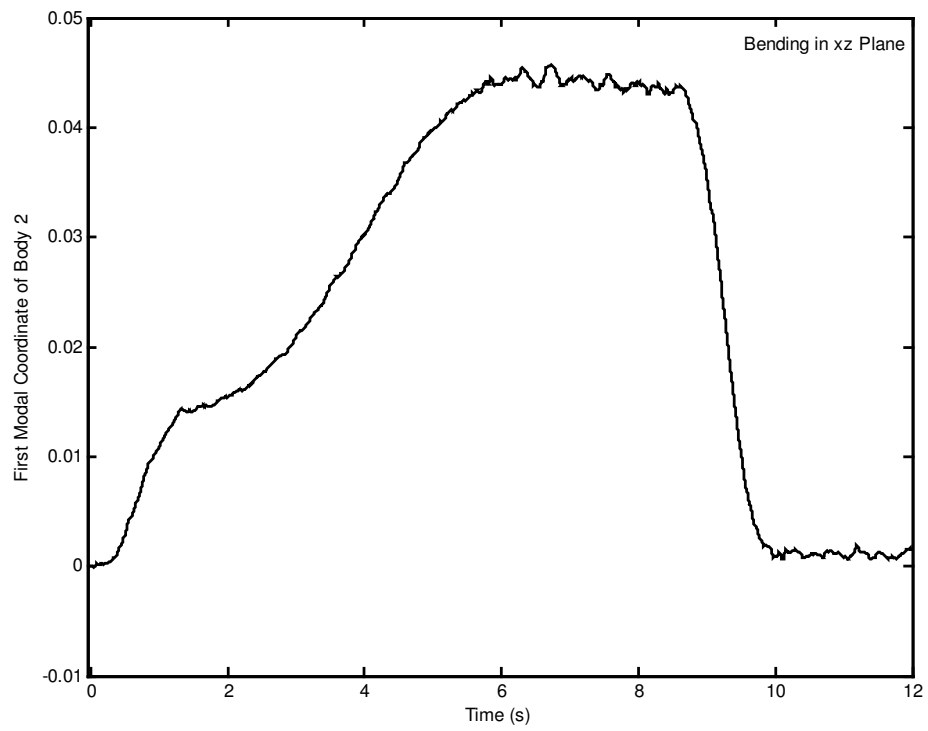


Figure 5.266 First modal coordinate of body 2 for bending in xz plane.

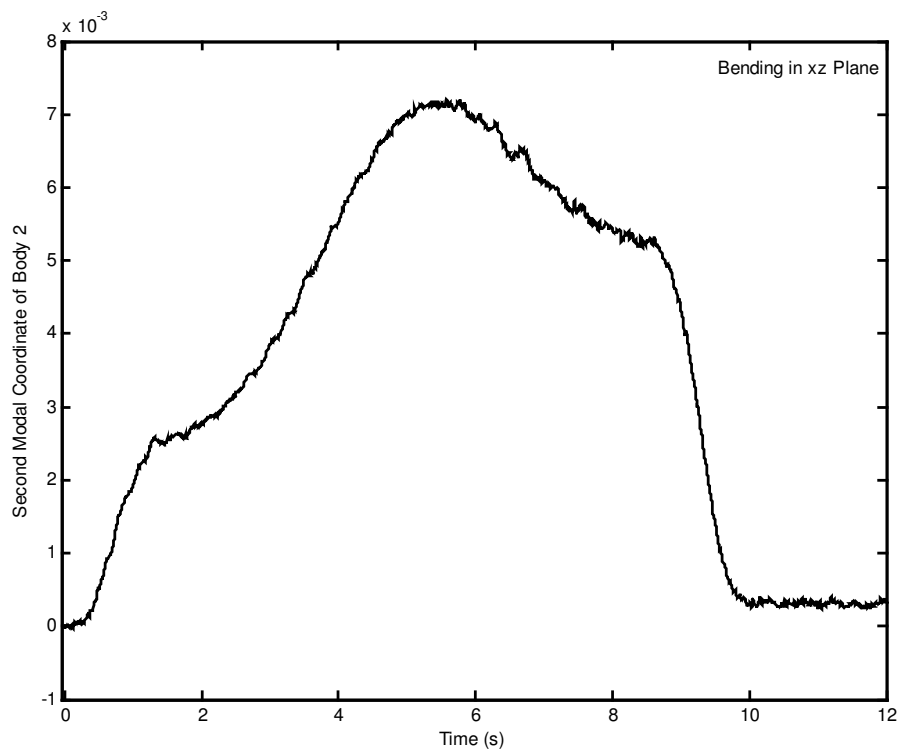


Figure 5.267 Second modal coordinate of body 2 for bending in xz plane.

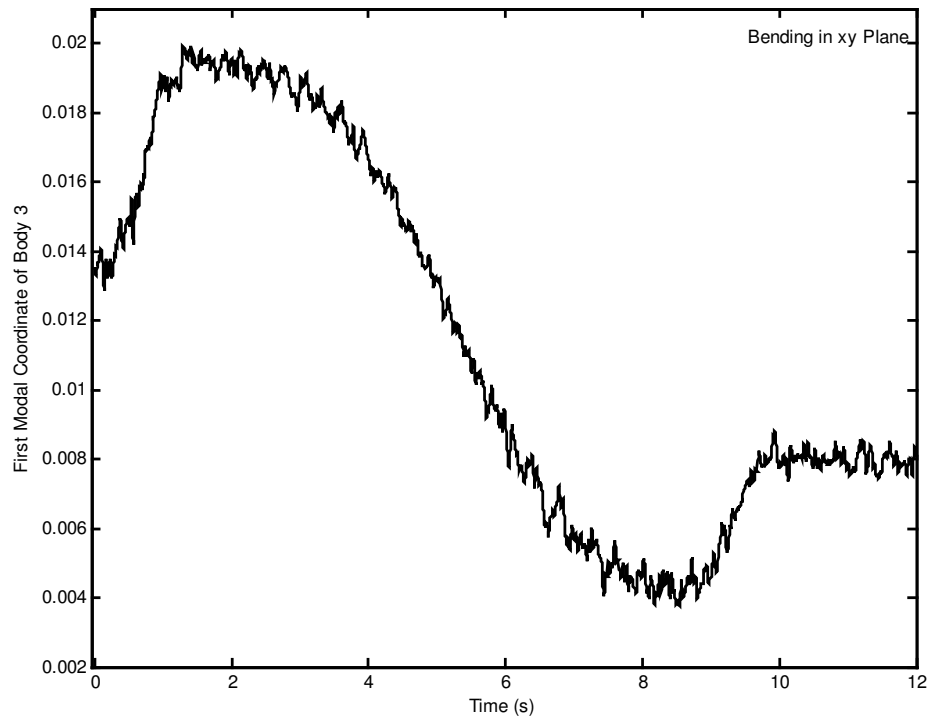


Figure 5.268 First modal coordinate of body 3 for bending in xy plane.

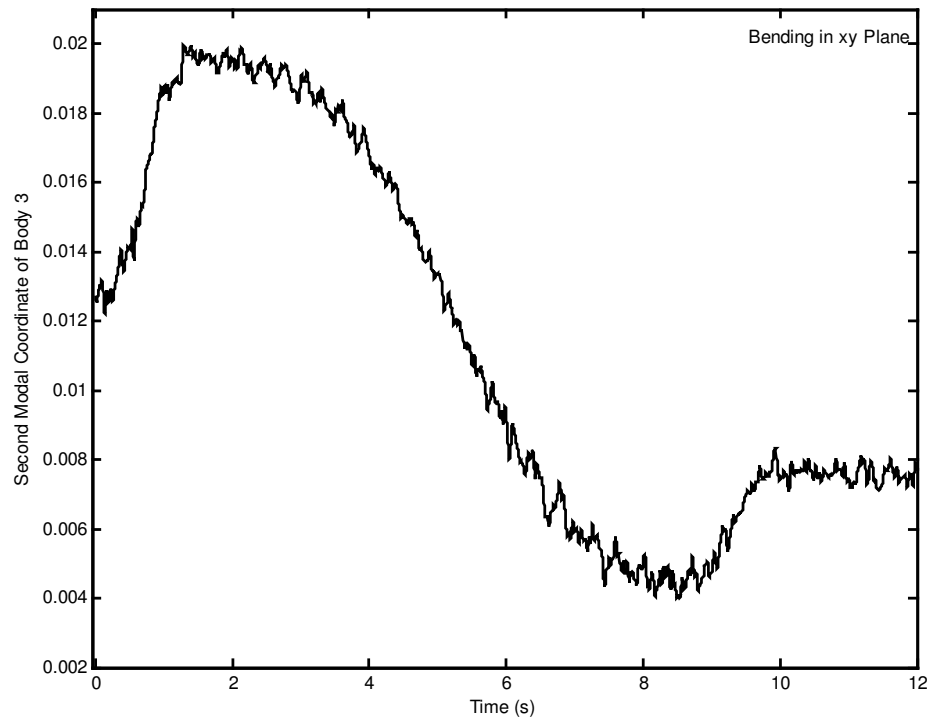


Figure 5.269 Second modal coordinate of body 3 for bending in xy plane.

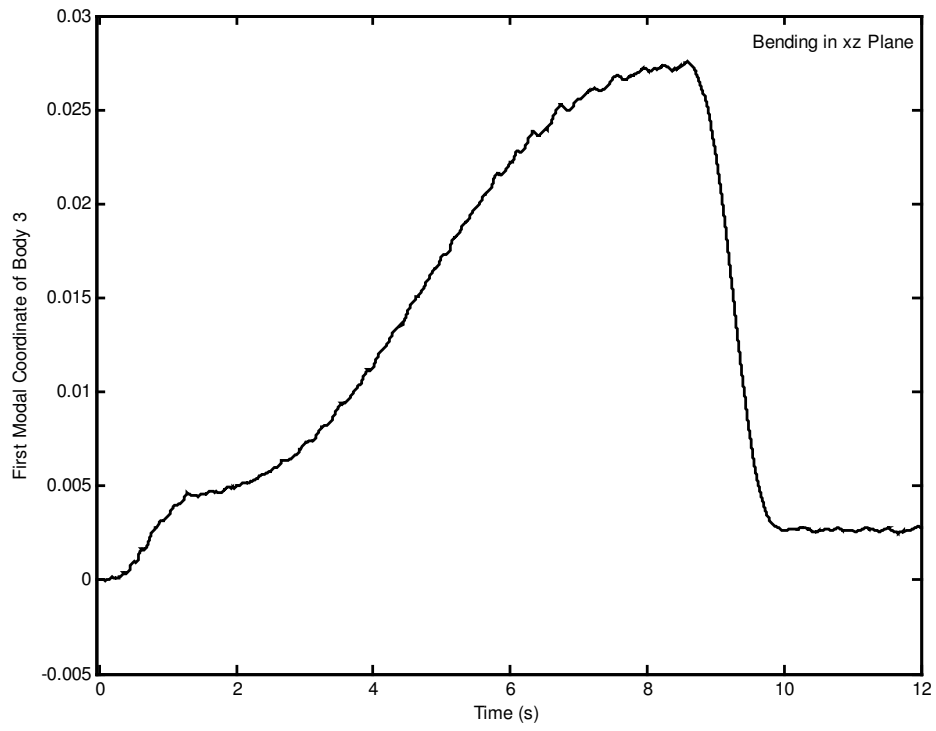


Figure 5.270 First modal coordinate of body 3 for bending in xz plane.

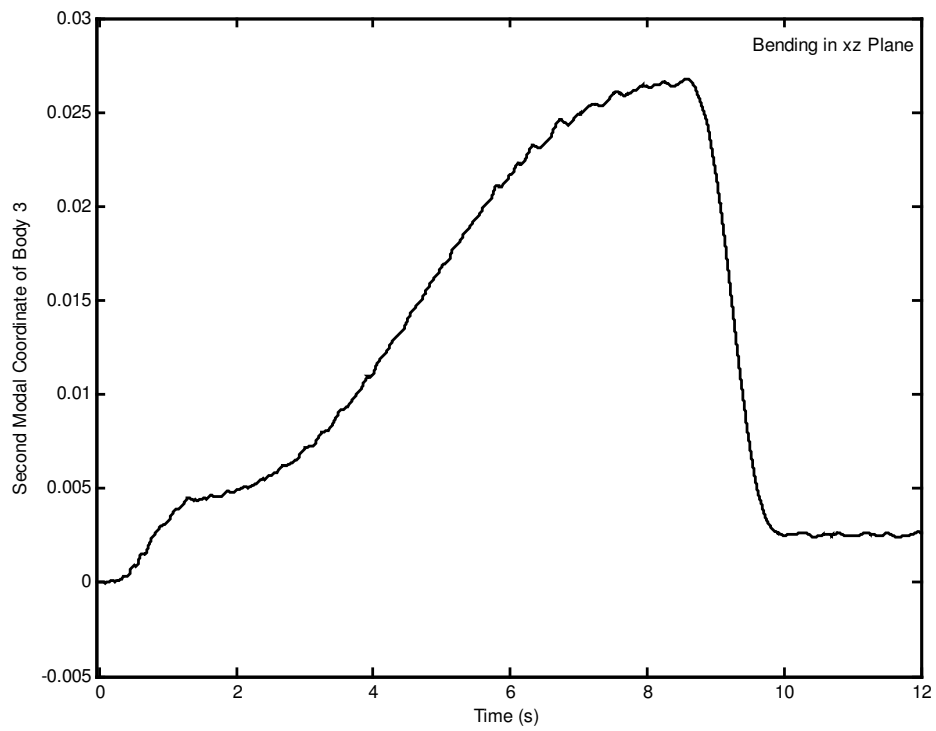


Figure 5.271 Second modal coordinate of body 3 for bending in xz plane.

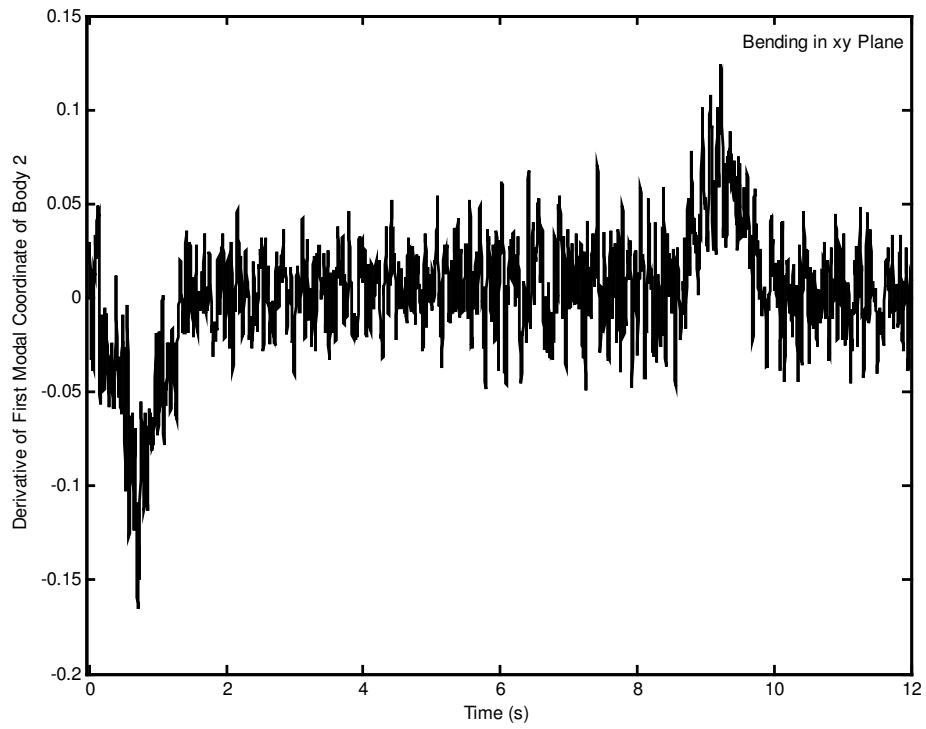


Figure 5.272 Derivative of first modal coordinate of body 2 for bending in xy plane.

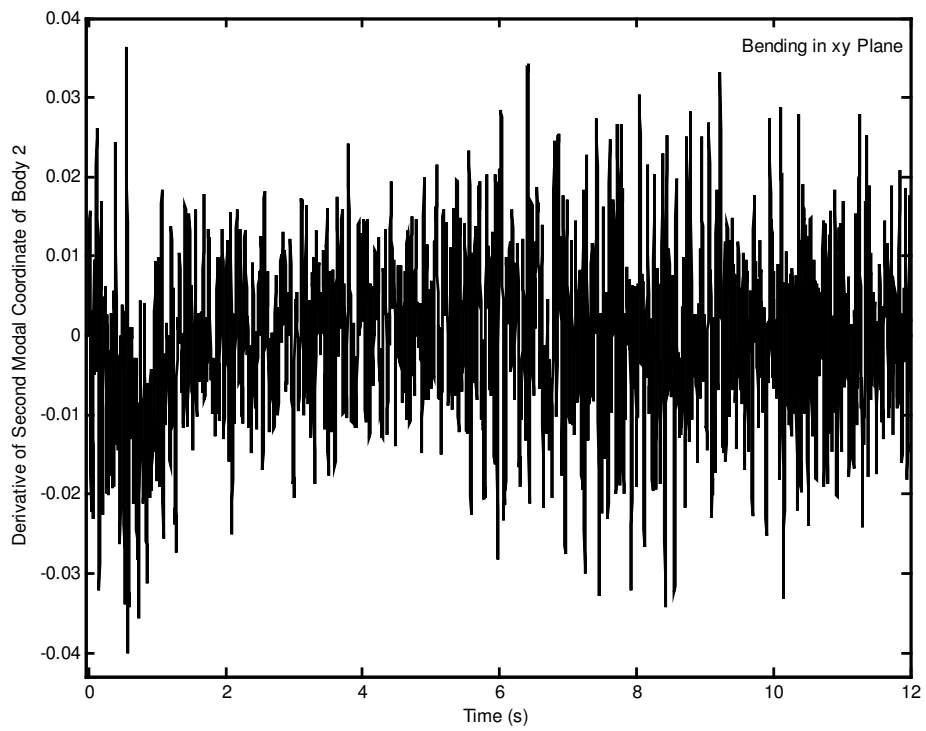


Figure 5.273 Derivative of second modal coordinate of body 2 for bending in xy plane.

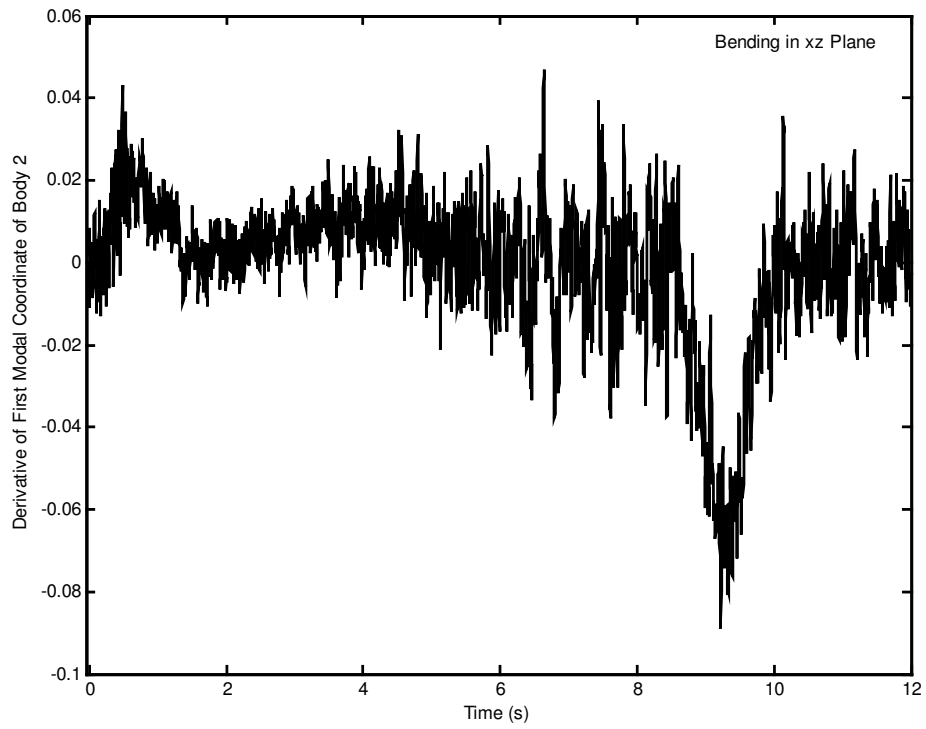


Figure 5.274 Derivative of first modal coordinate of body 2 for bending in xz plane.

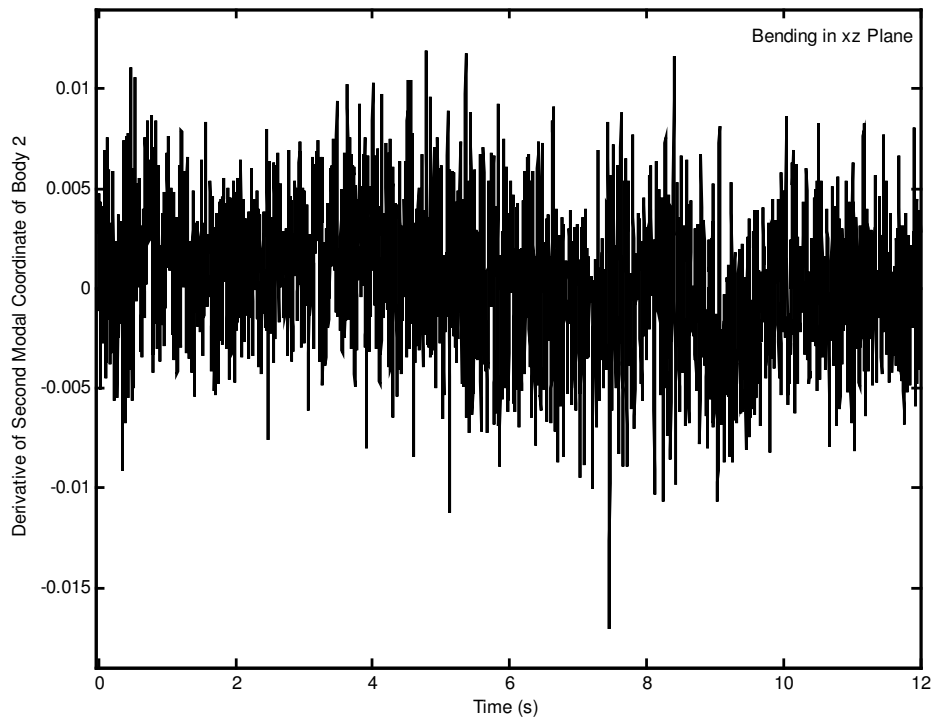


Figure 5.275 Derivative of second modal coordinate of body 2 for bending in xz plane.

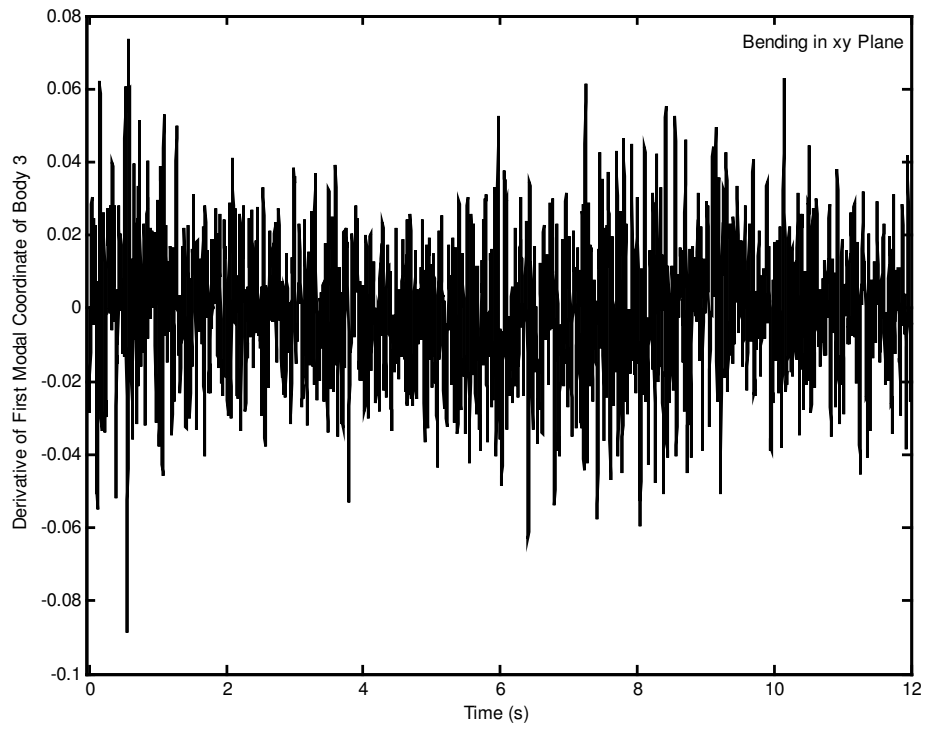


Figure 5.276 Derivative of first modal coordinate of body 3 for bending in xy plane.

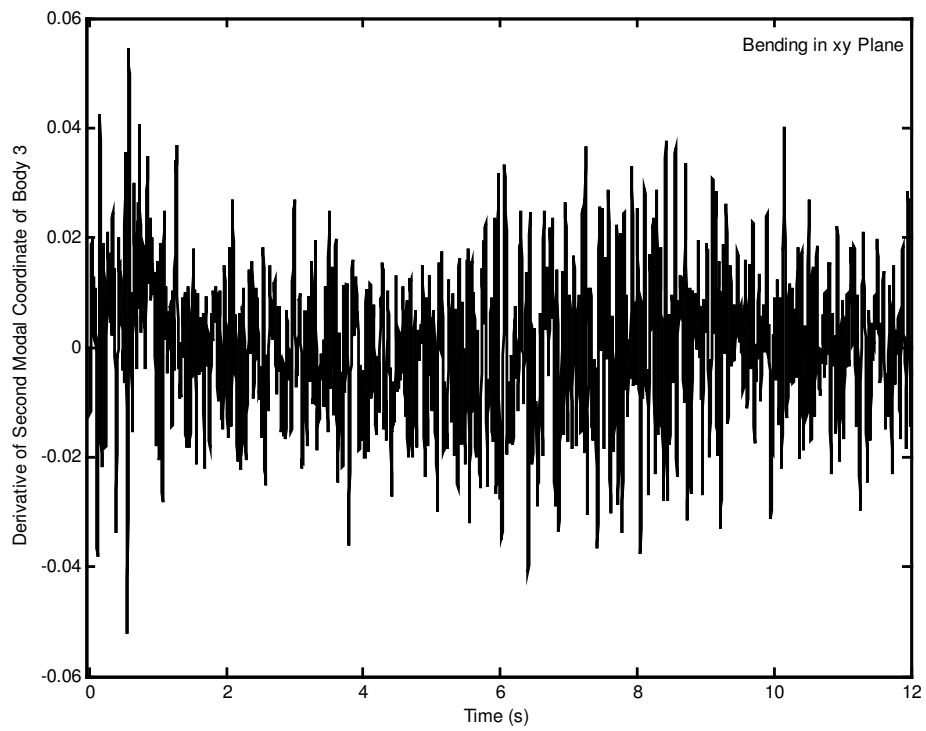


Figure 5.277 Derivative of second modal coordinate of body 3 for bending in xy plane.

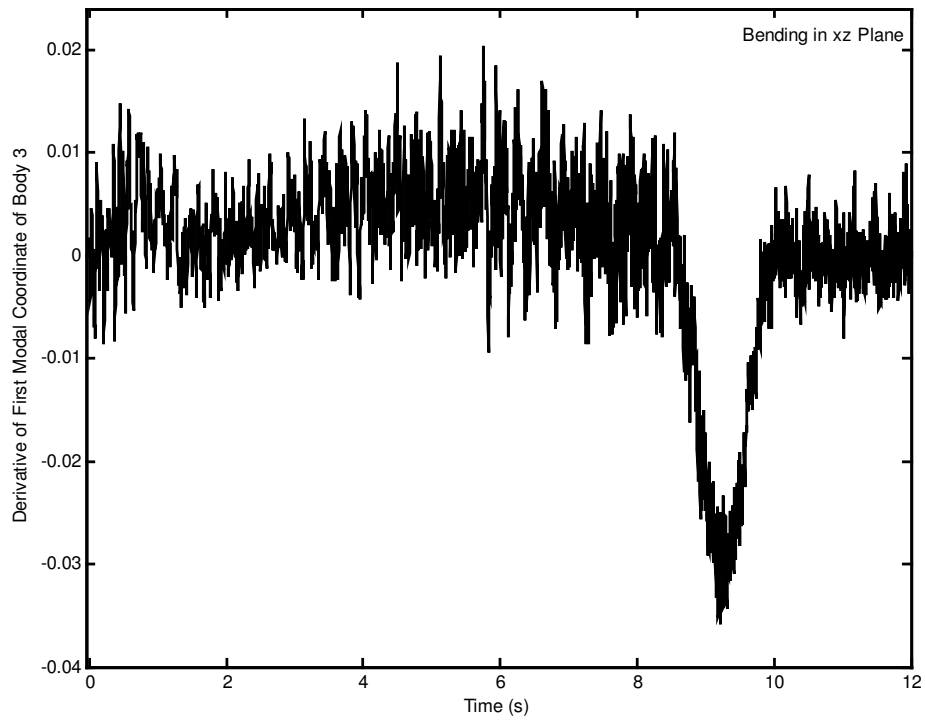


Figure 5.278 Derivative of first modal coordinate of body 3 for bending in xz plane.

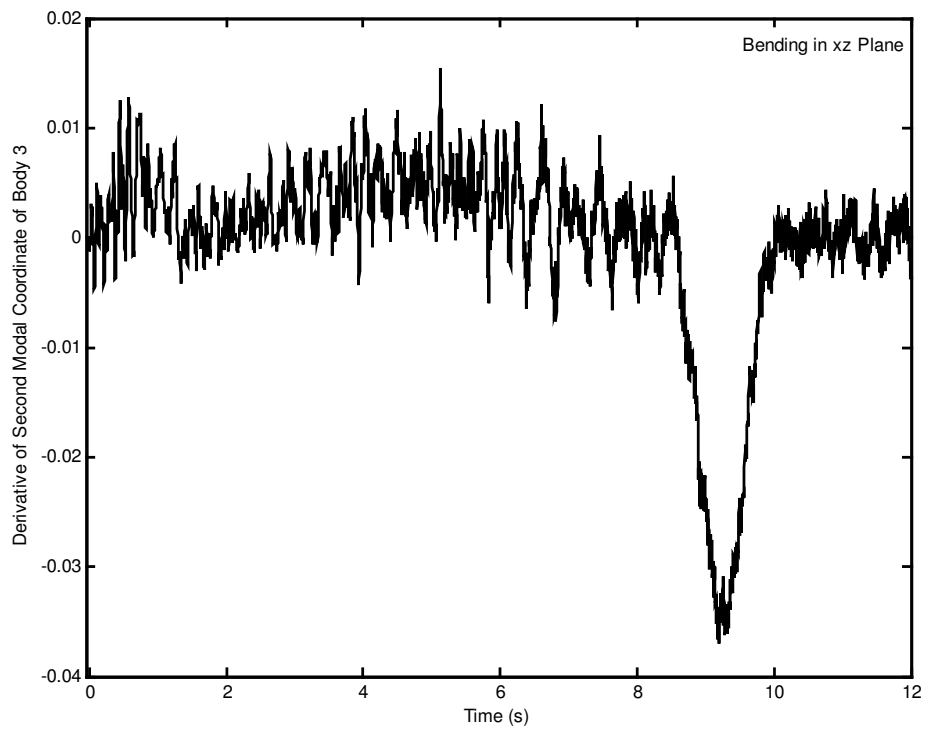


Figure 5.279 Derivative of second modal coordinate of body 3 for bending in xz plane.

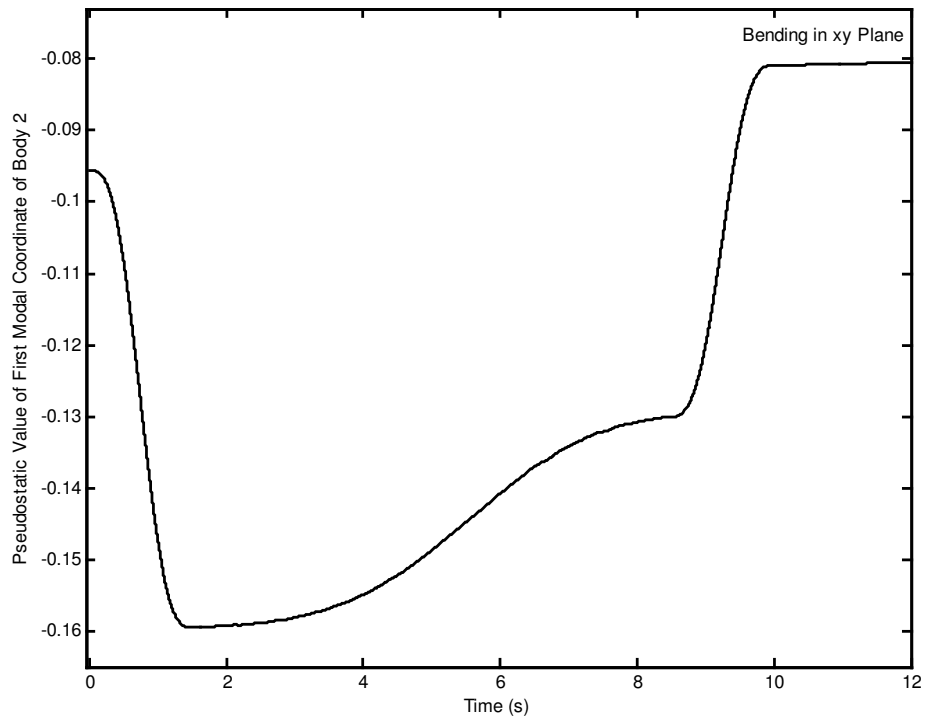


Figure 5.280 Pseudostatic value of first modal coordinate of body 2 for bending in xy plane.

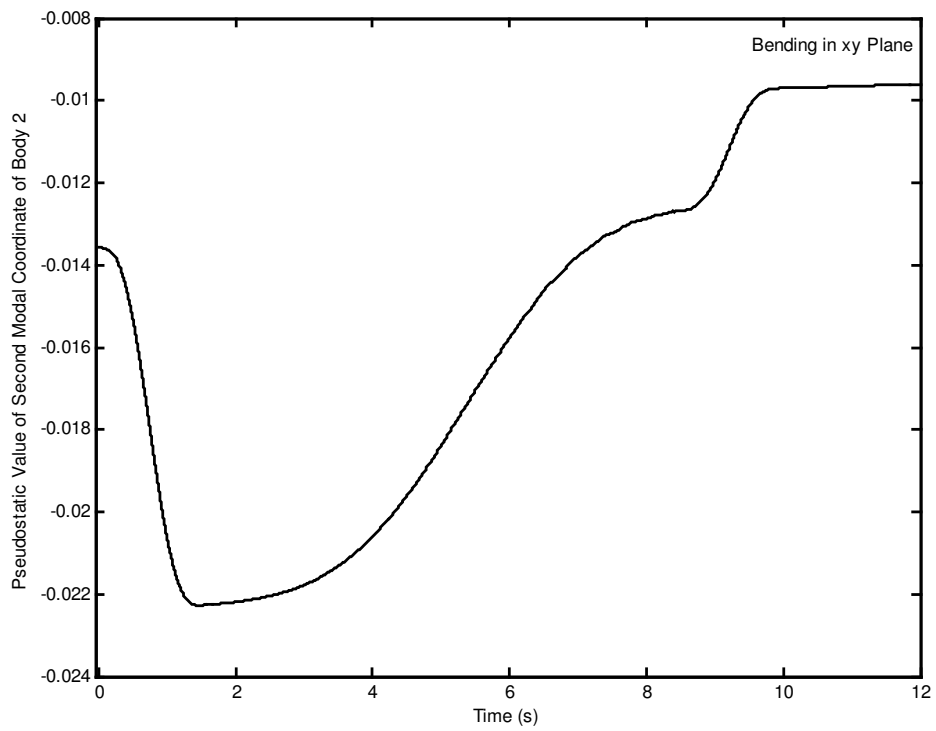


Figure 5.281 Pseudostatic value of second modal coordinate of body 2 for bending in xy plane.

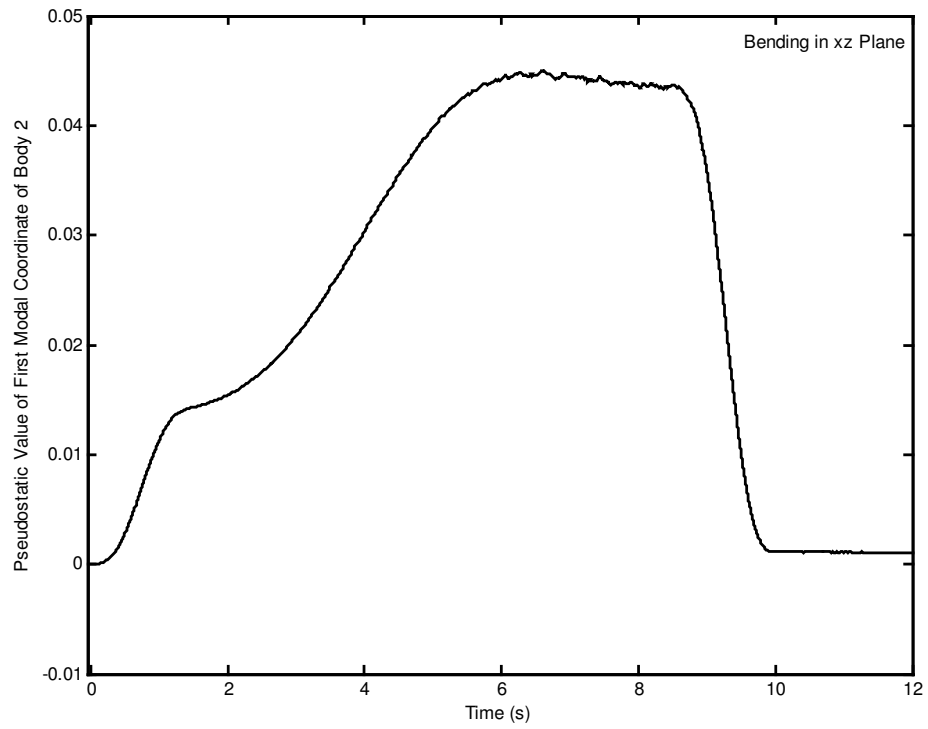


Figure 5.282 Pseudostatic value of first modal coordinate of body 2 for bending in xz plane.

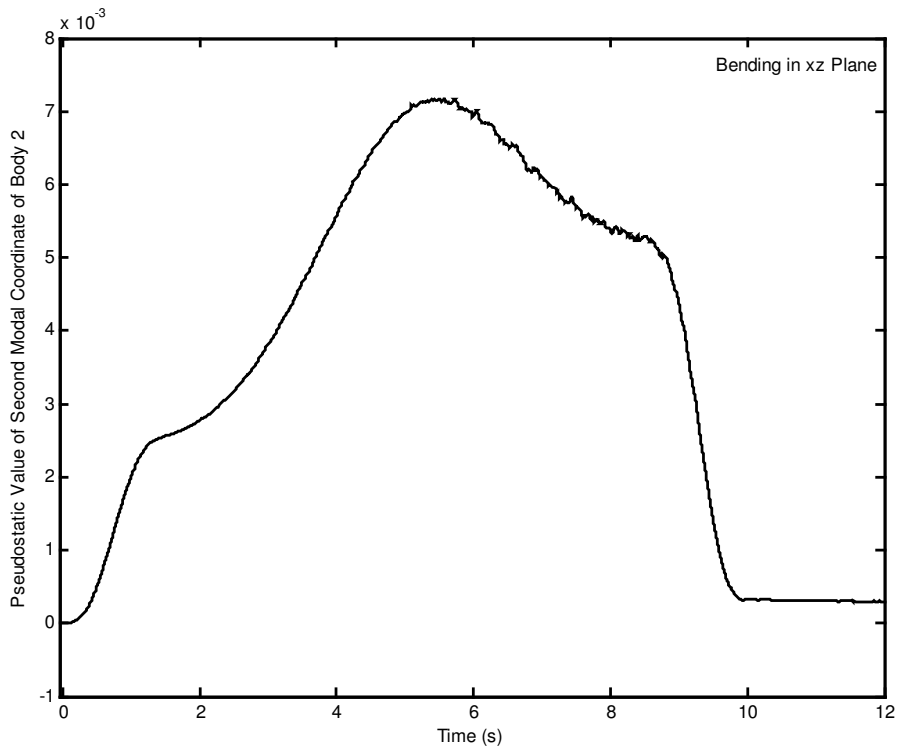


Figure 5.283 Pseudostatic value of second modal coordinate of body 2 for bending in xz plane.

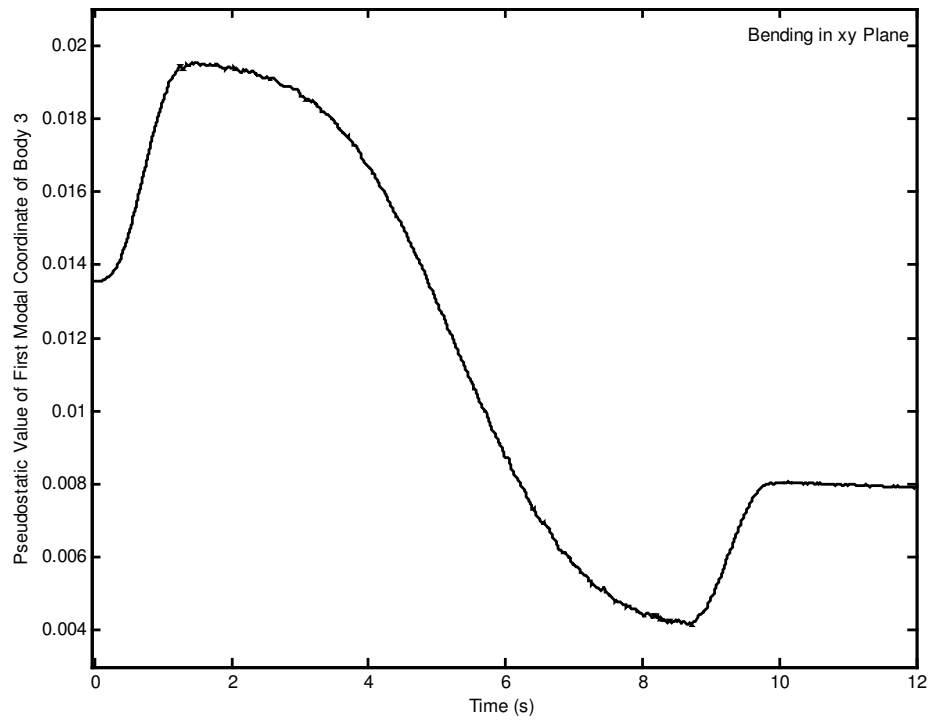


Figure 5.284 Pseudostatic value of first modal coordinate of body 3 for bending in xy plane.

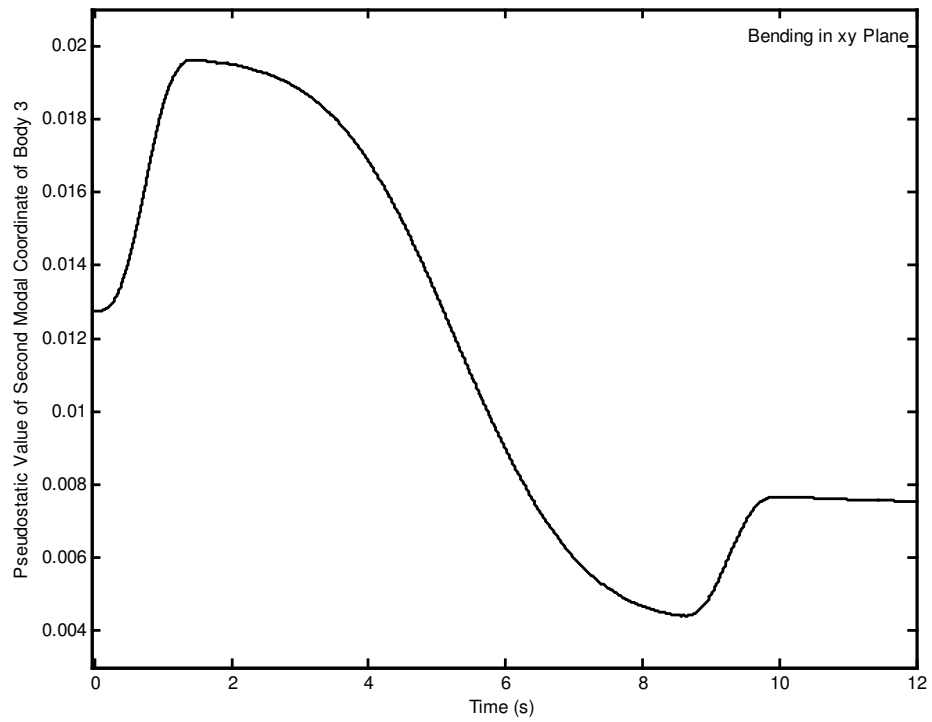


Figure 5.285 Pseudostatic value of second modal coordinate of body 3 for bending in xy plane.

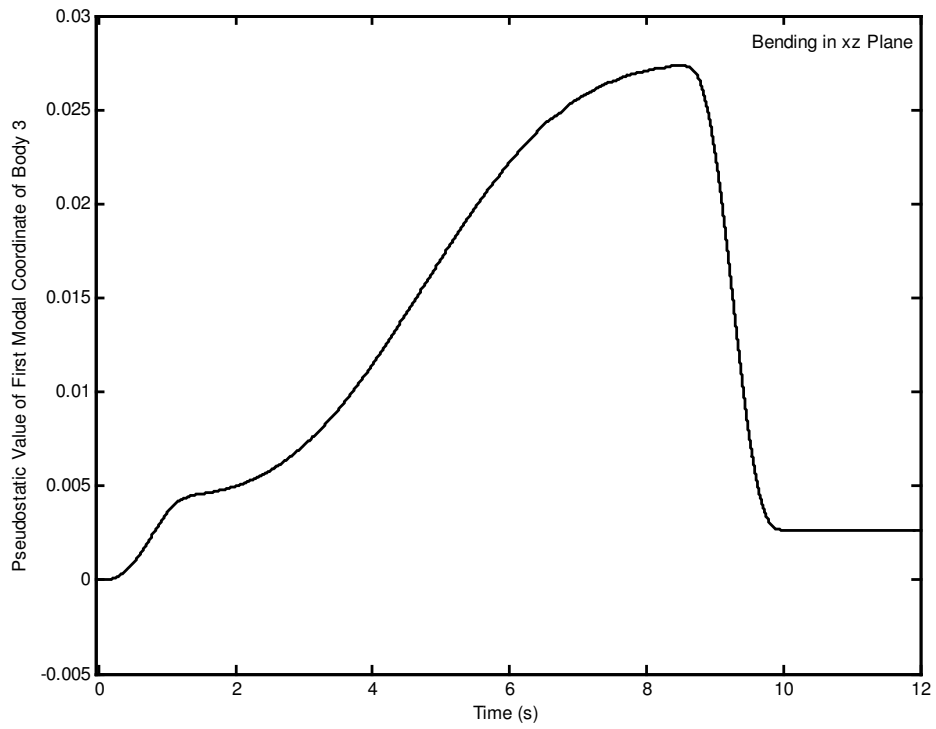


Figure 5.286 Pseudostatic value of first modal coordinate of body 3 for bending in xz plane.

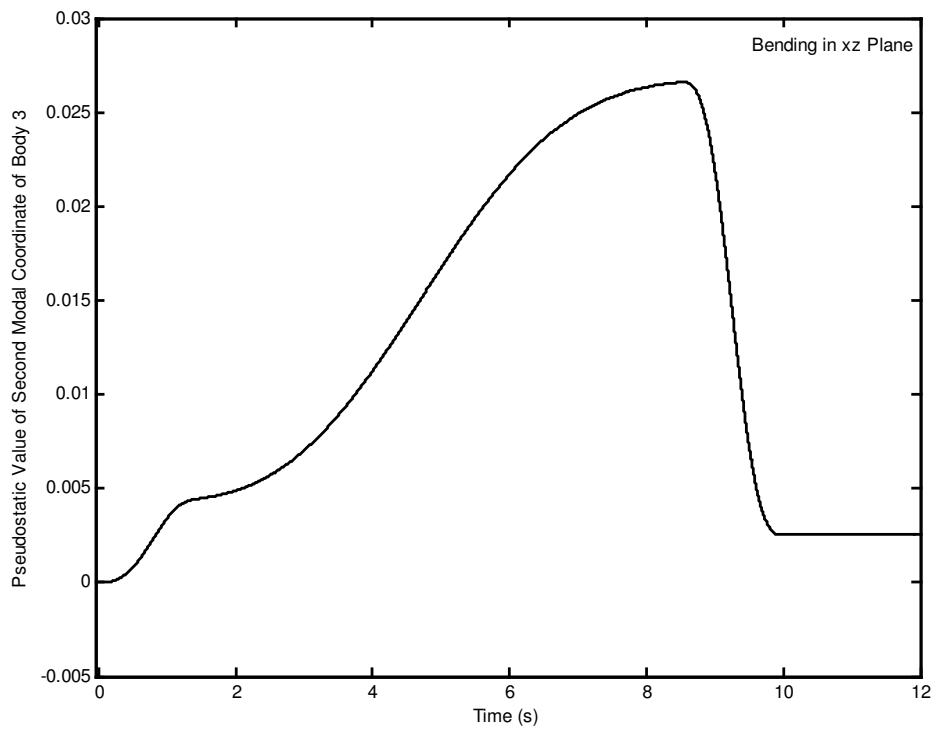


Figure 5.287 Pseudostatic value of second modal coordinate of body 3 for bending in xz plane.

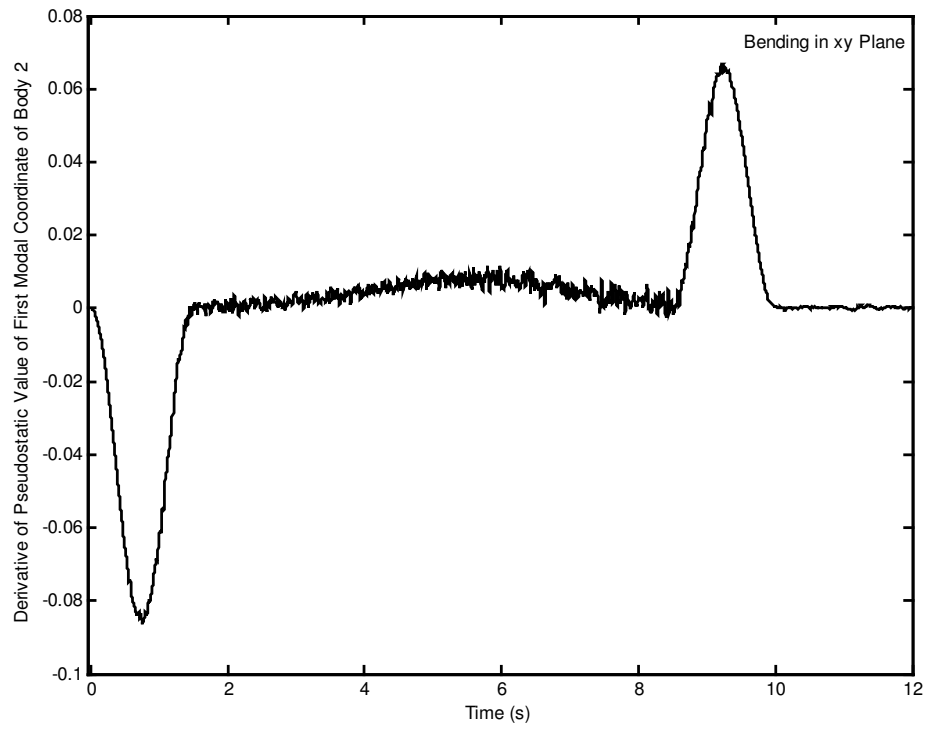


Figure 5.288 Derivative of pseudostatic value of first modal coordinate of body 2 for bending in xy plane.

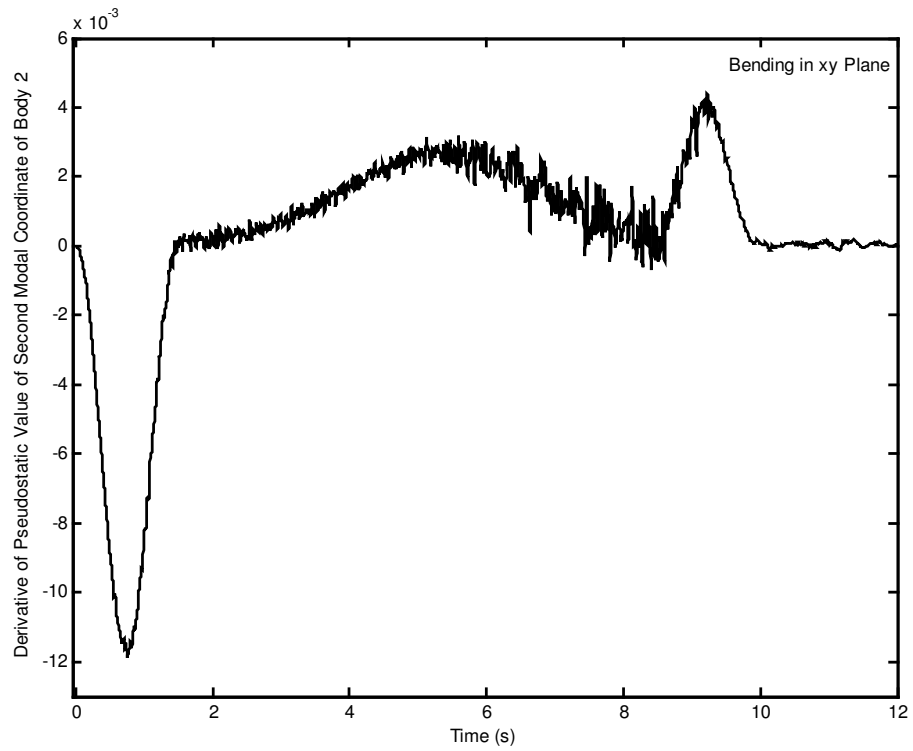


Figure 5.289 Derivative of pseudostatic value of second modal coordinate of body 2 for bending in xy plane.

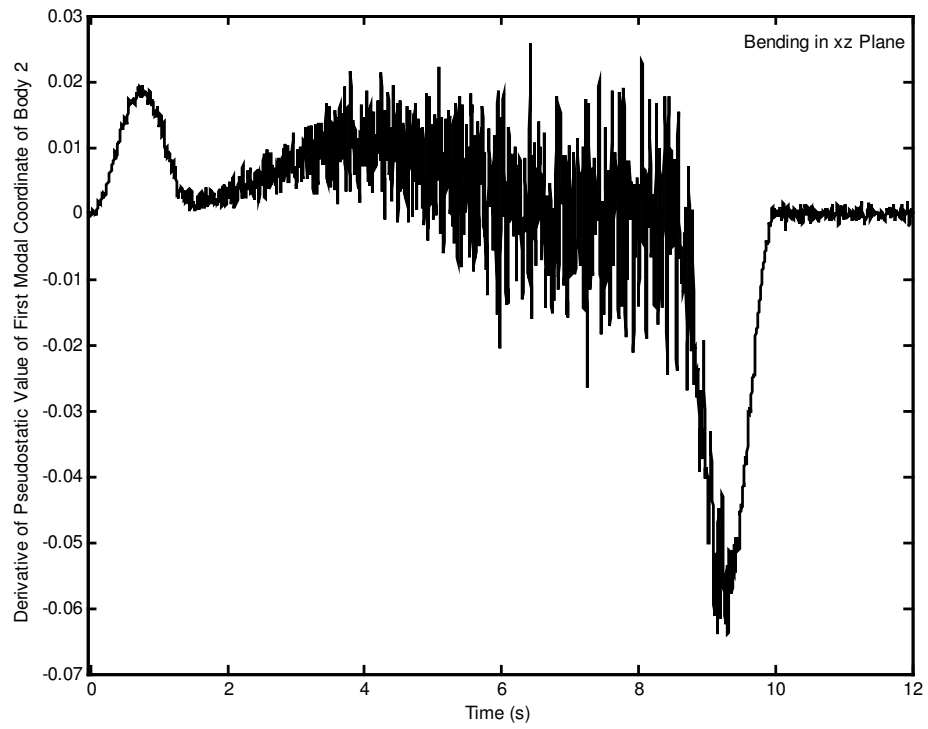


Figure 5.290 Derivative of pseudostatic value of first modal coordinate of body 2 for bending in xz plane.

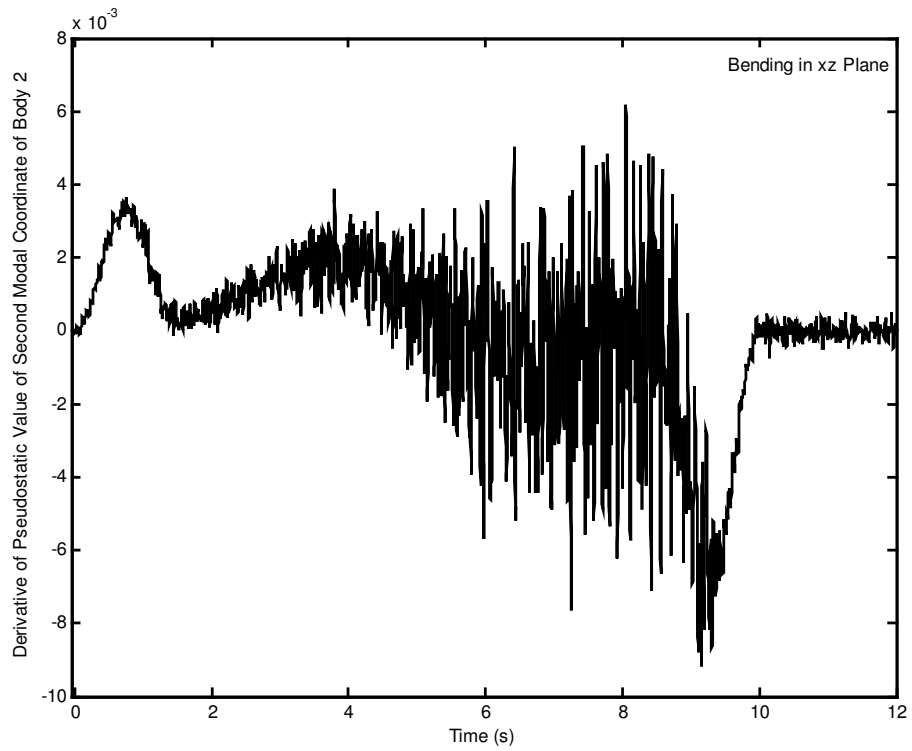


Figure 5.291 Derivative of pseudostatic value of second modal coordinate of body 2 for bending in xz plane.

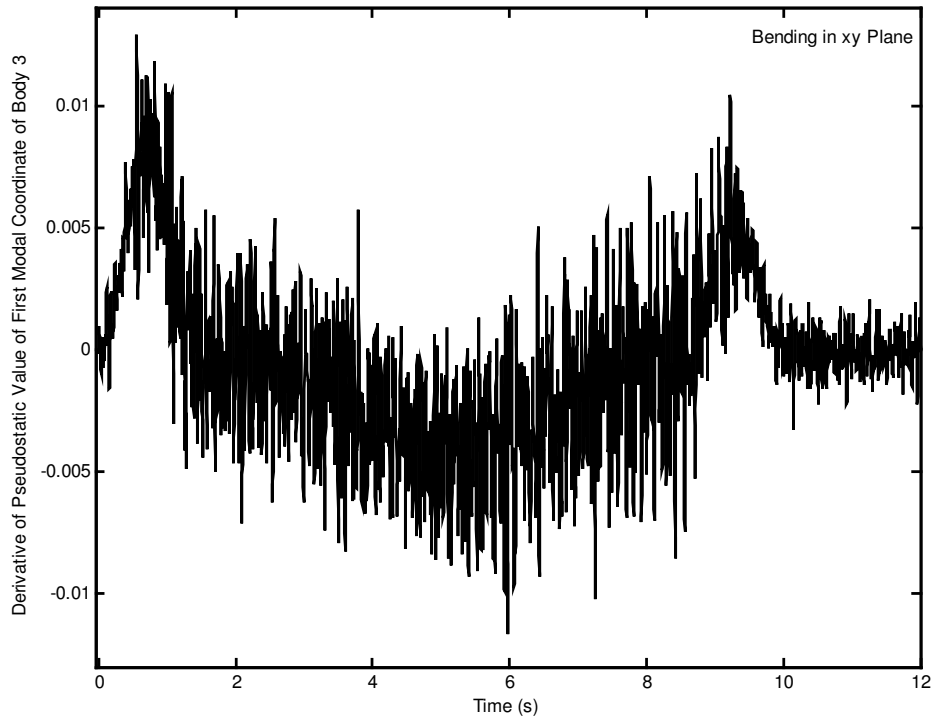


Figure 5.292 Derivative of pseudostatic value of first modal coordinate of body 3 for bending in xy plane.

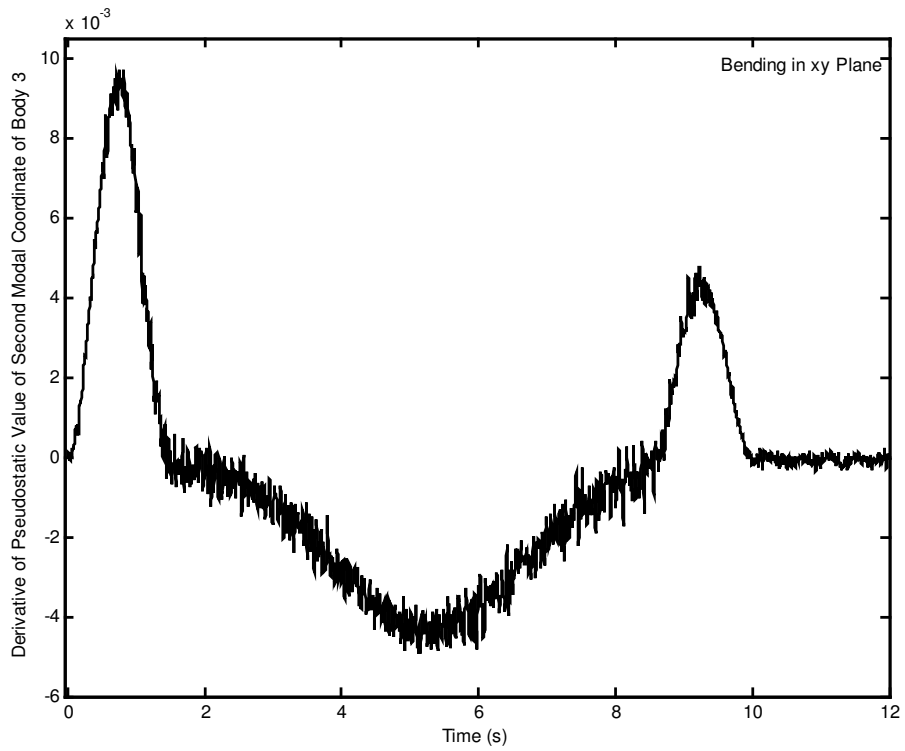


Figure 5.293 Derivative of pseudostatic value of second modal coordinate of body 3 for bending in xy plane.

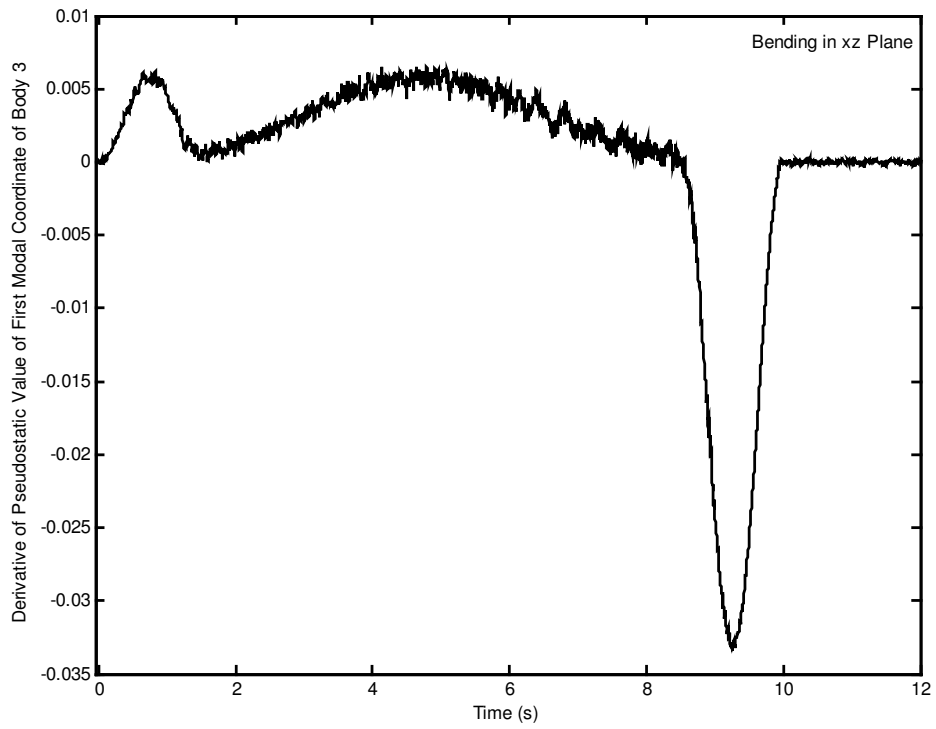


Figure 5.294 Derivative of pseudostatic value of first modal coordinate of body 3 for bending in xz plane.

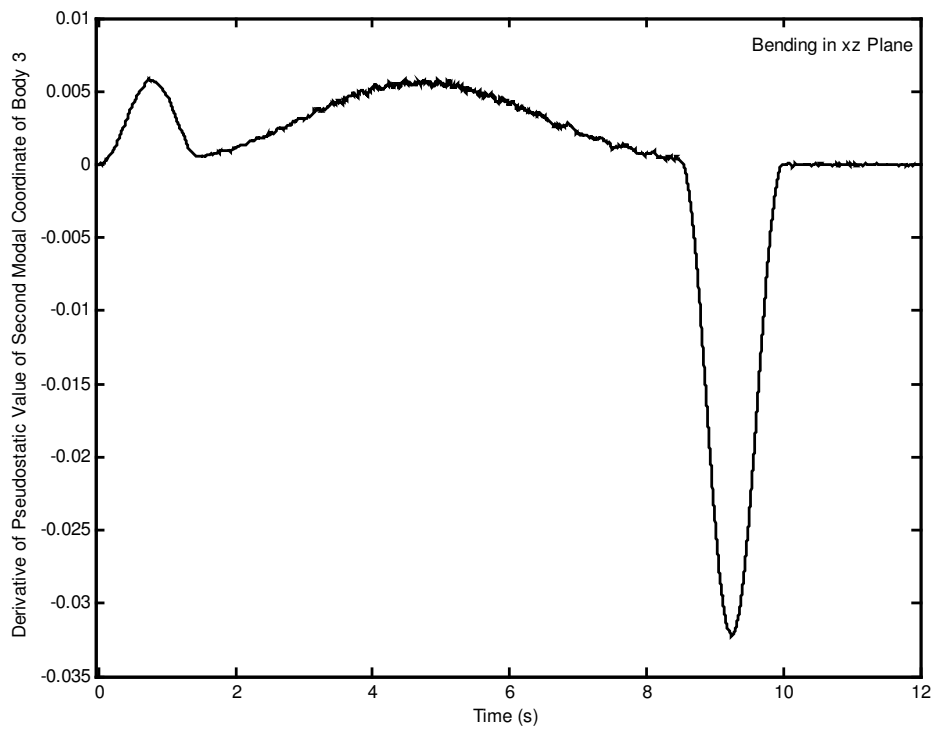


Figure 5.295 Derivative of pseudostatic value of second modal coordinate of body 3 for bending in xz plane.

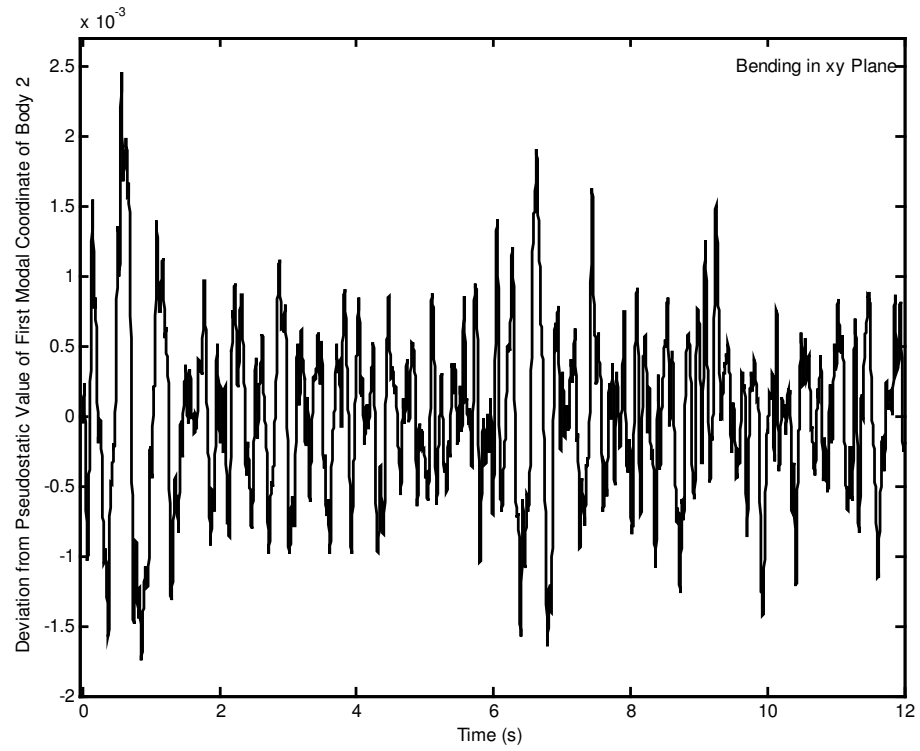


Figure 5.296 Deviation from pseudostatic value of first modal coordinate of body 2 for bending in xy plane.

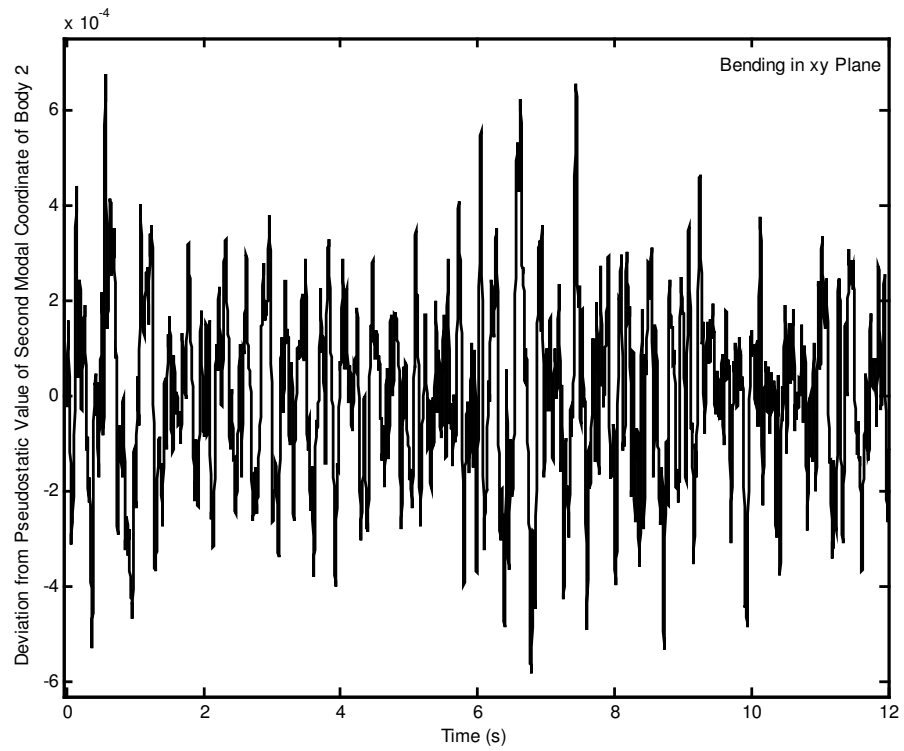


Figure 5.297 Deviation from pseudostatic value of second modal coordinate of body 2 for bending in xy plane.

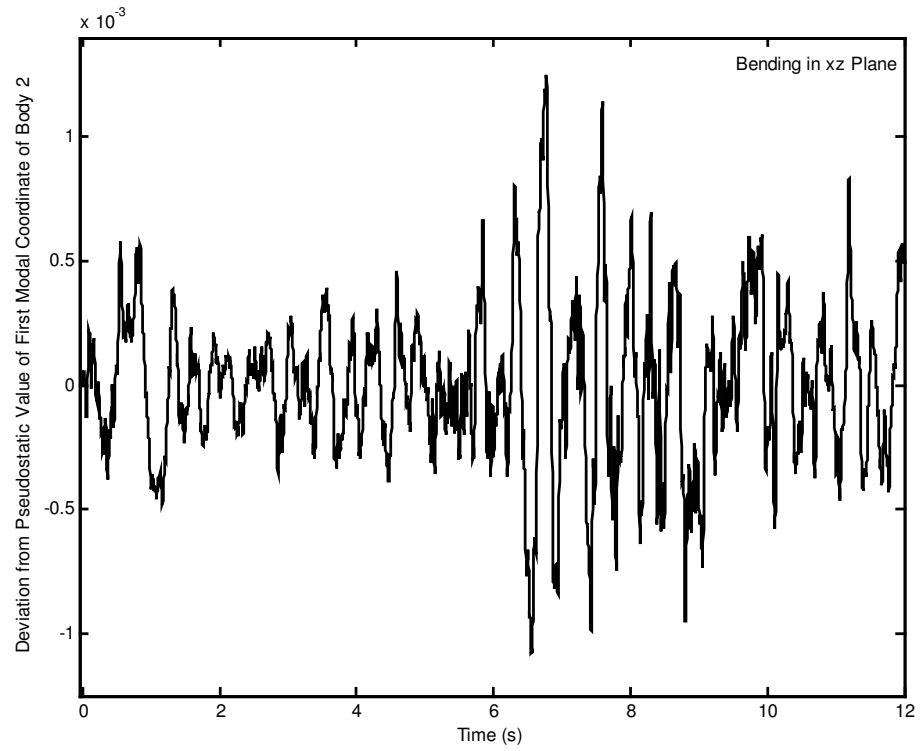


Figure 5.298 Deviation from pseudostatic value of first modal coordinate of body 2 for bending in xz plane.

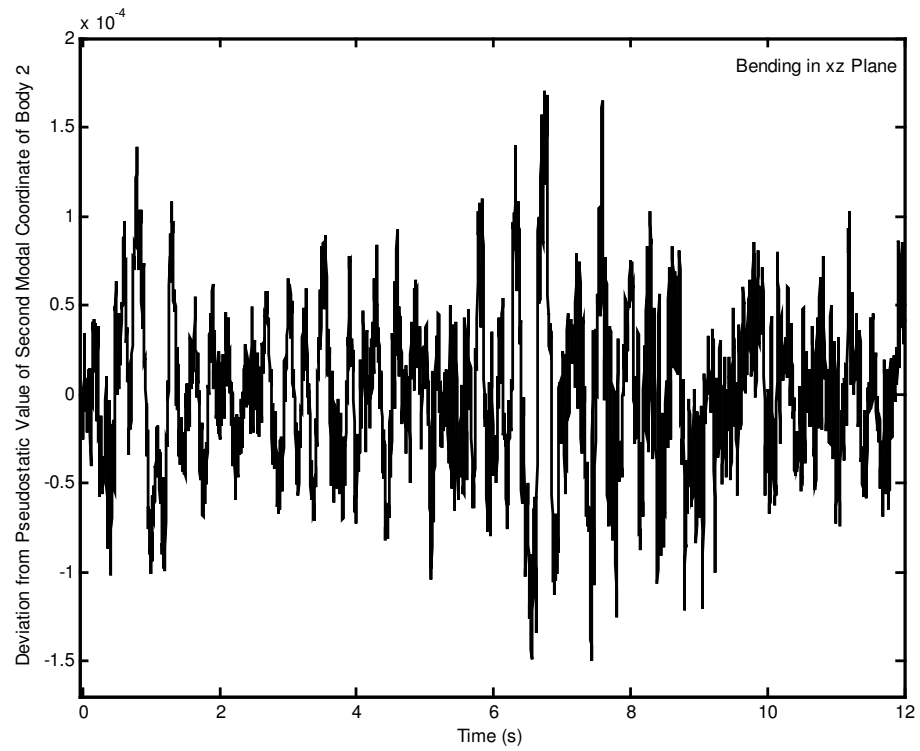


Figure 5.299 Deviation from pseudostatic value of second modal coordinate of body 2 for bending in xz plane.

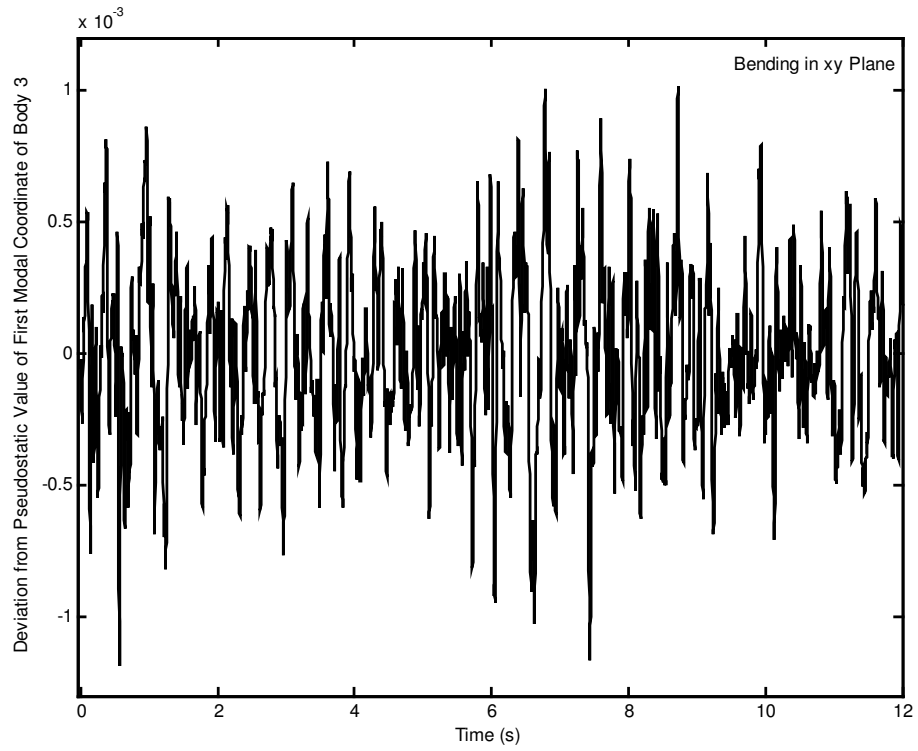


Figure 5.300 Deviation from pseudostatic value of first modal coordinate of body 3 for bending in xy plane.

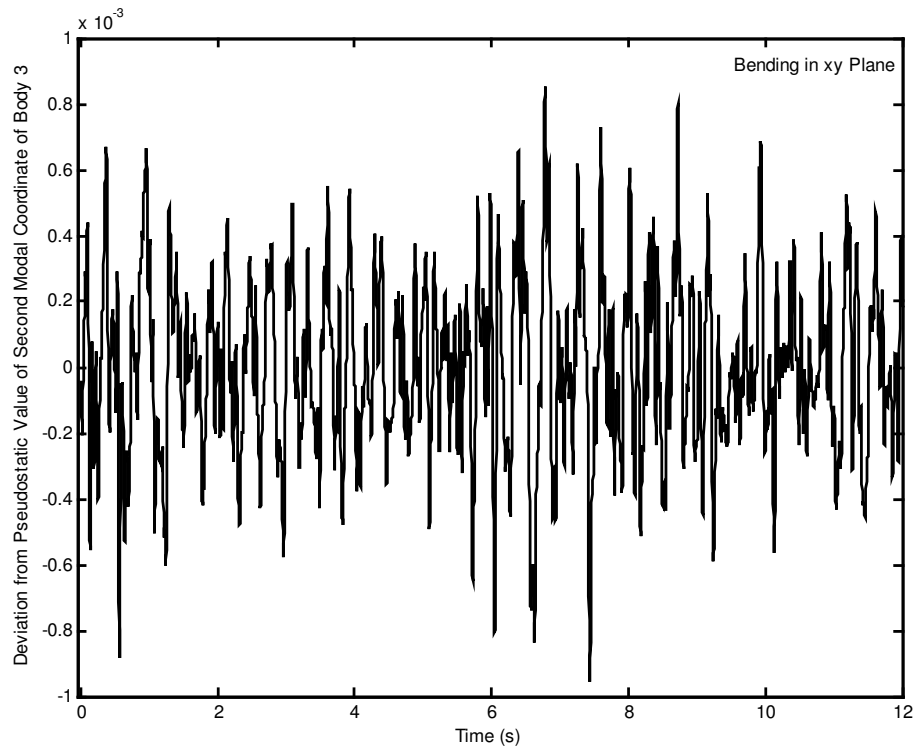


Figure 5.301 Deviation from pseudostatic value of second modal coordinate of body 3 for bending in xy plane.

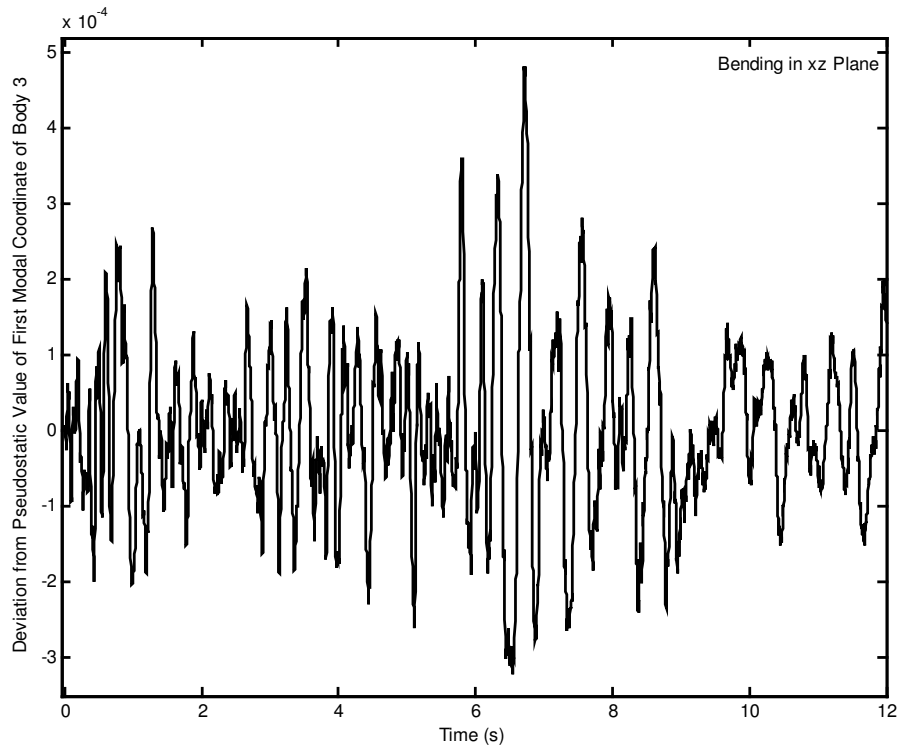


Figure 5.302 Deviation from pseudostatic value of first modal coordinate of body 3 for bending in xz plane.

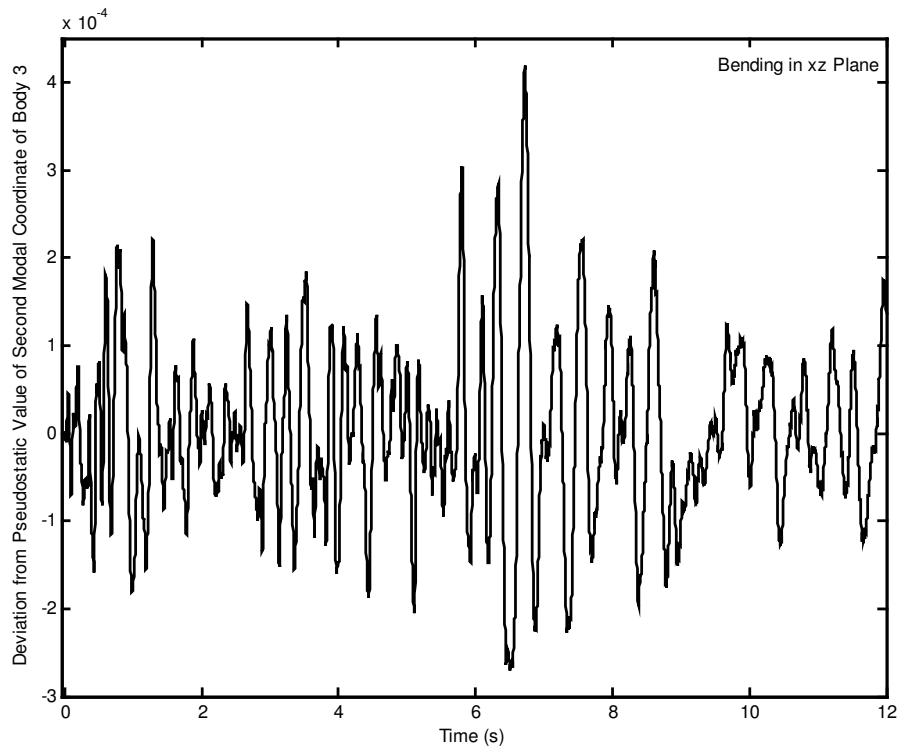


Figure 5.303 Deviation from pseudostatic value of second modal coordinate of body 3 for bending in xz plane.

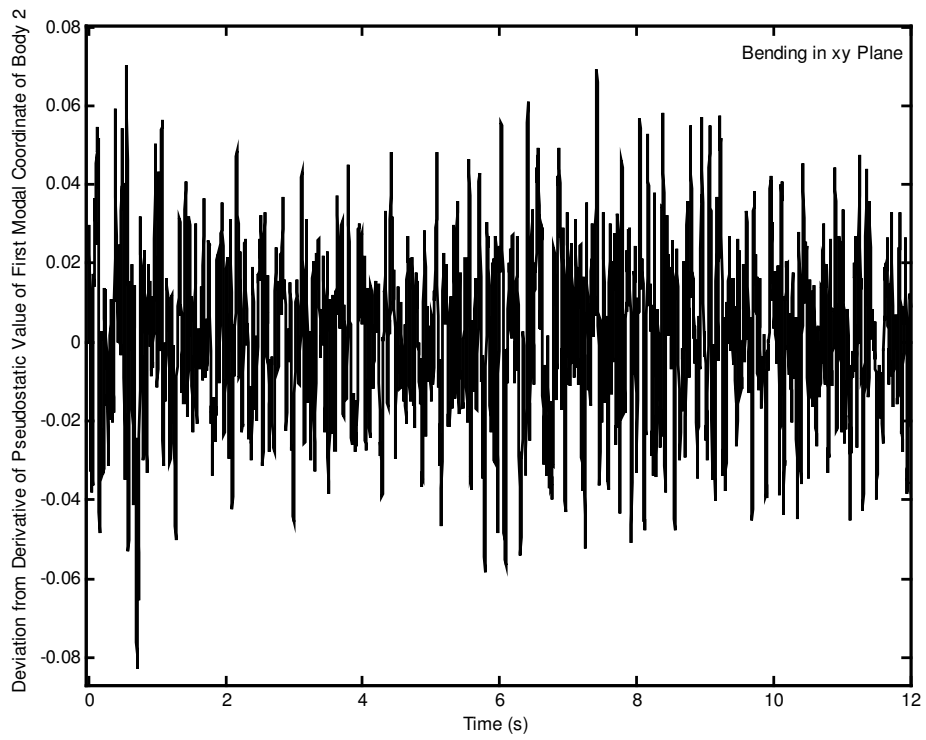


Figure 5.304 Deviation from derivative of pseudostatic value of first modal coordinate of body 2 for bending in xy plane.

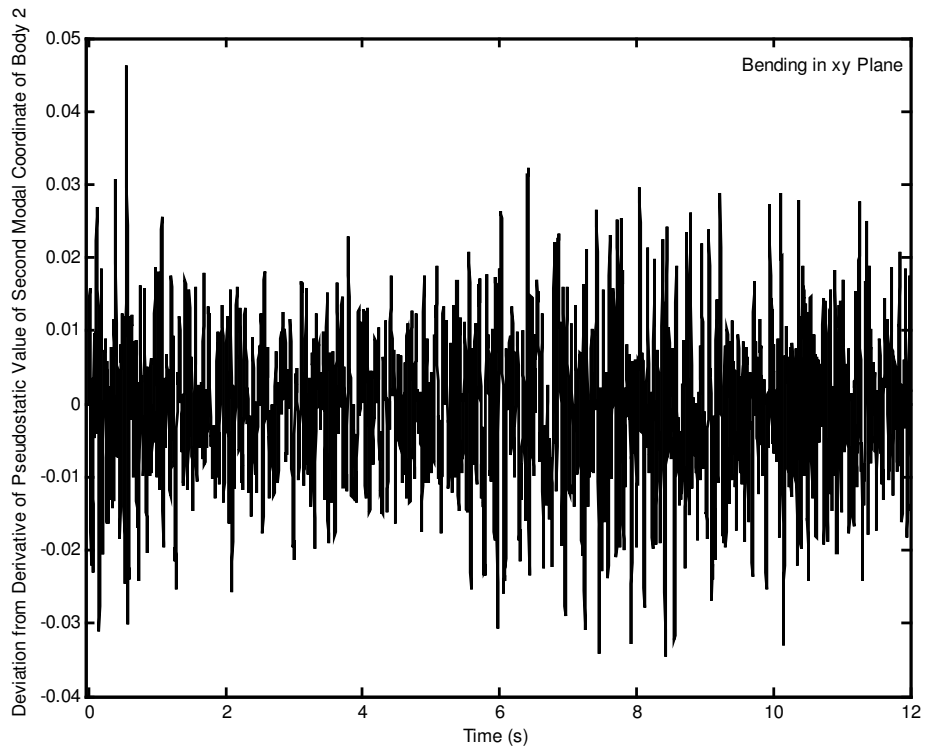


Figure 5.305 Deviation from derivative of pseudostatic value of second modal coordinate of body 2 for bending in xy plane.

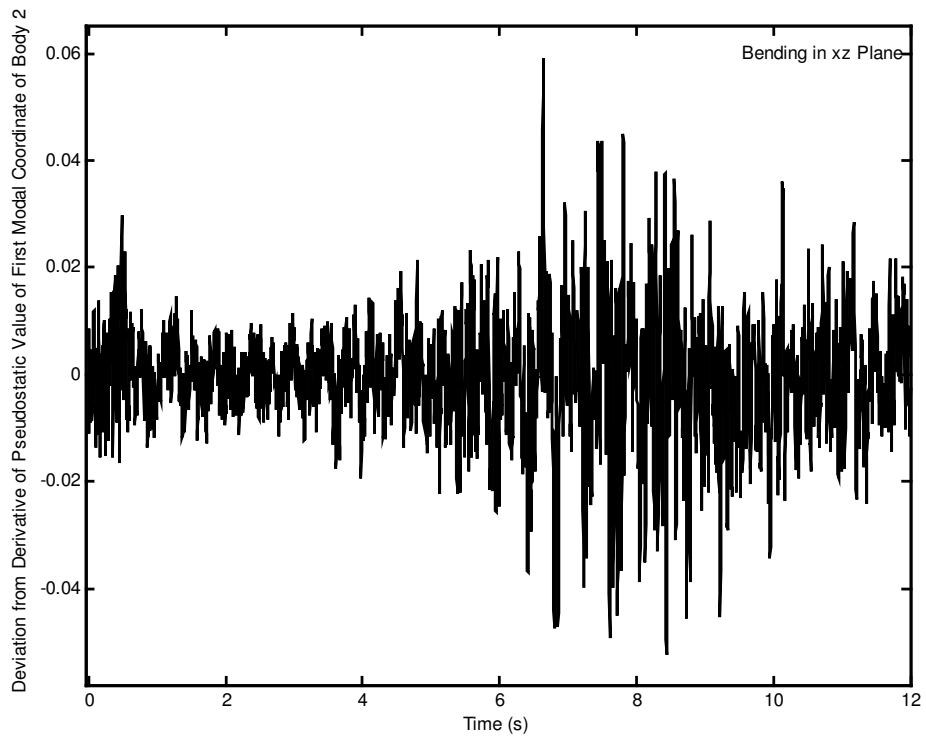


Figure 5.306 Deviation from derivative of pseudostatic value of first modal coordinate of body 2 for bending in xz plane.

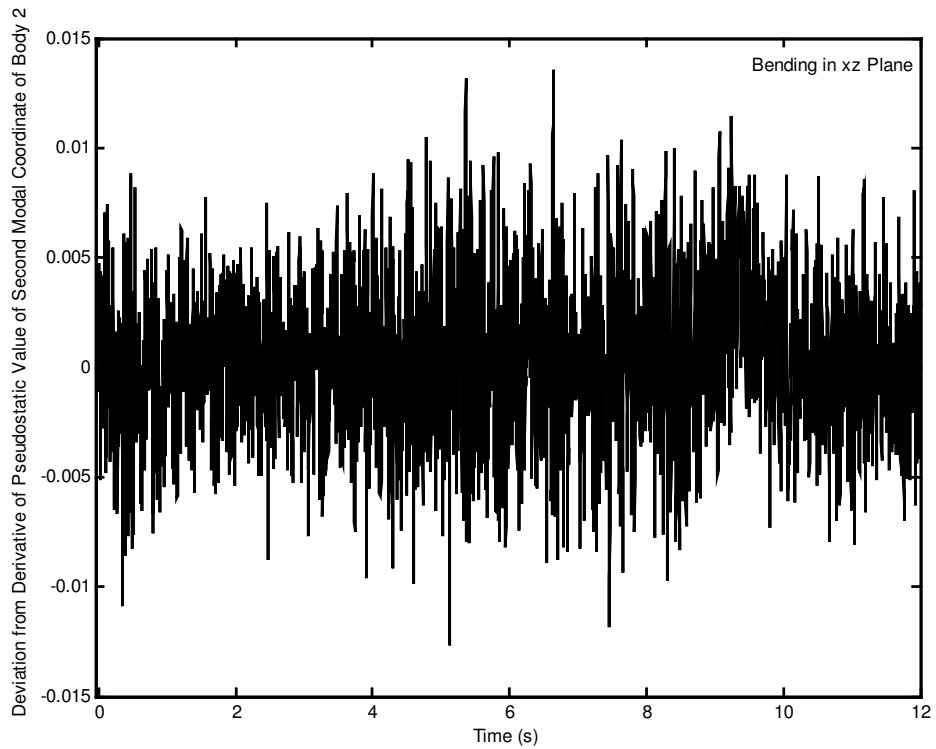


Figure 5.307 Deviation from derivative of pseudostatic value of second modal coordinate of body 2 for bending in xz plane.

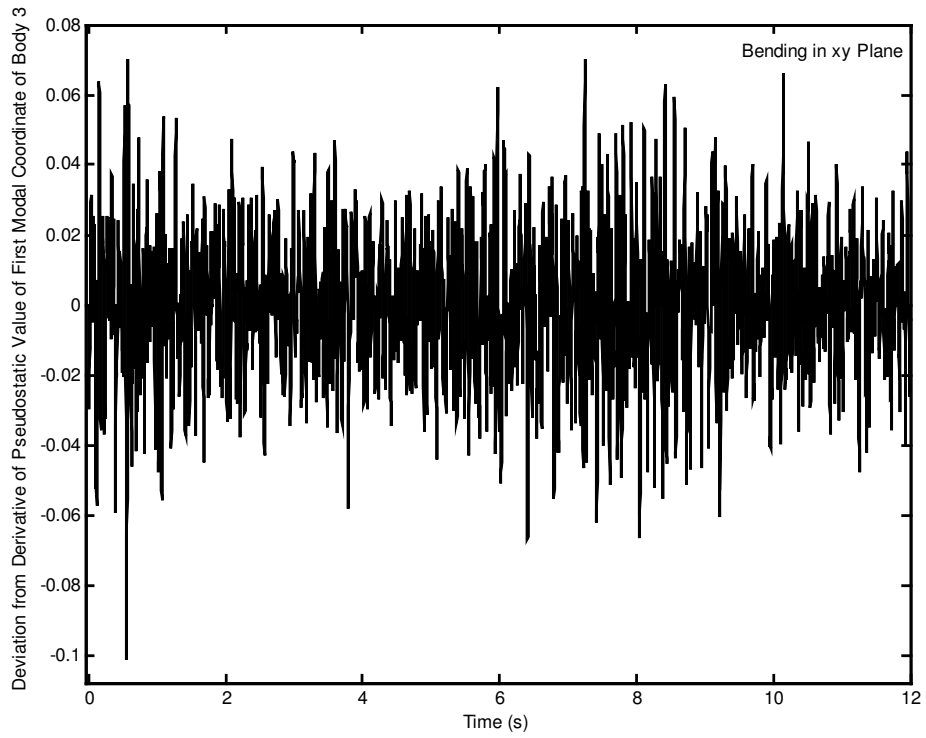


Figure 5.308 Deviation from derivative of pseudostatic value of first modal coordinate of body 3 for bending in xy plane.

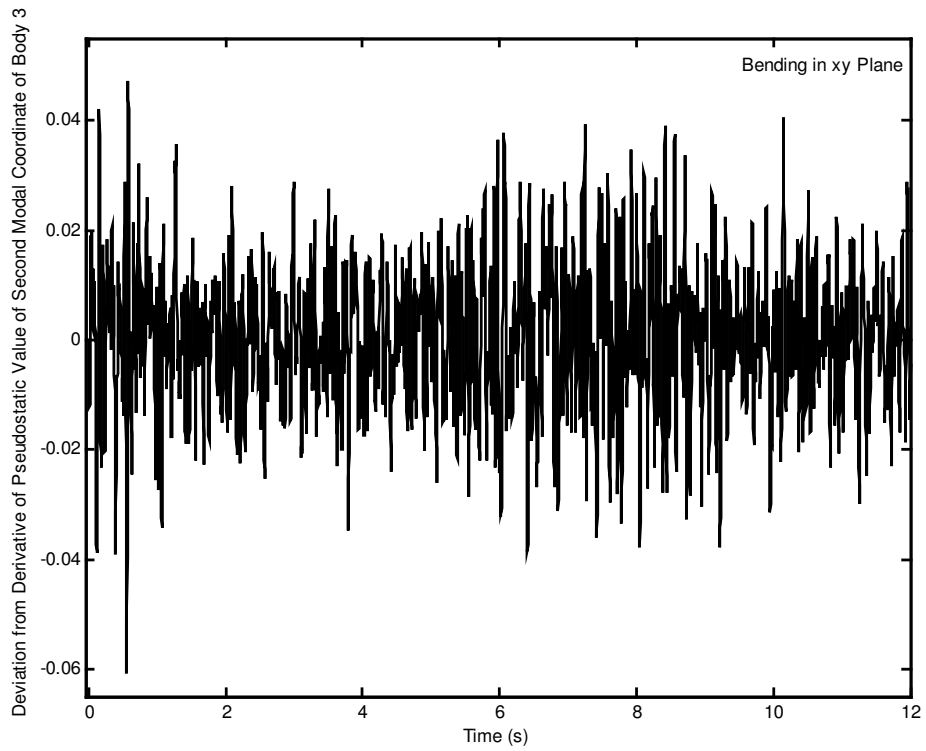


Figure 5.309 Deviation from derivative of pseudostatic value of second modal coordinate of body 3 for bending in xy plane.

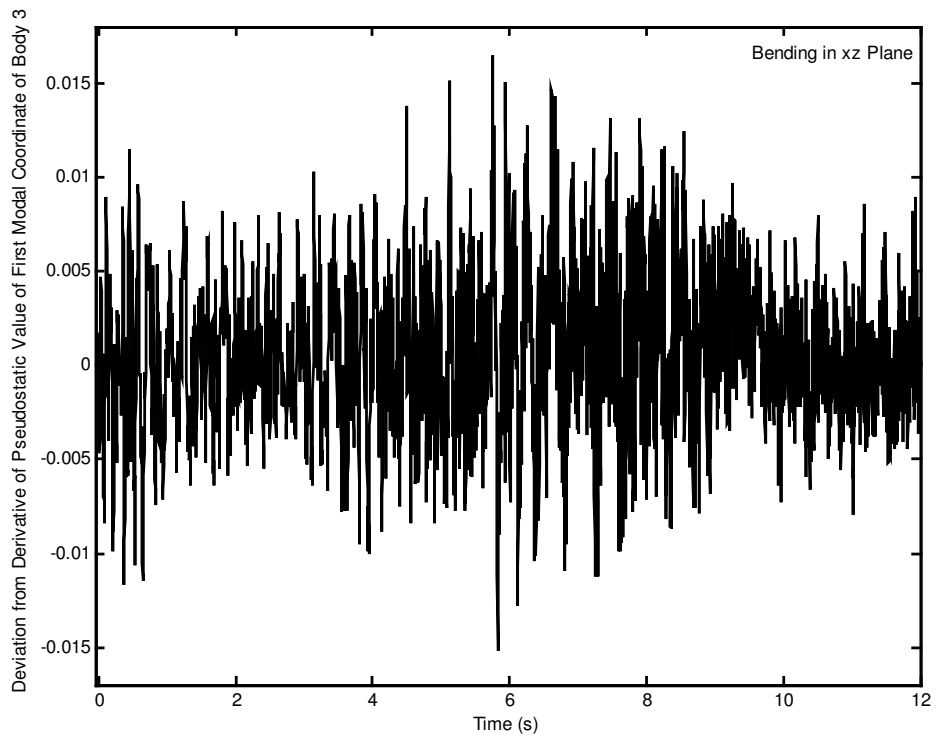


Figure 5.310 Deviation from derivative of pseudostatic value of first modal coordinate of body 3 for bending in xz plane.

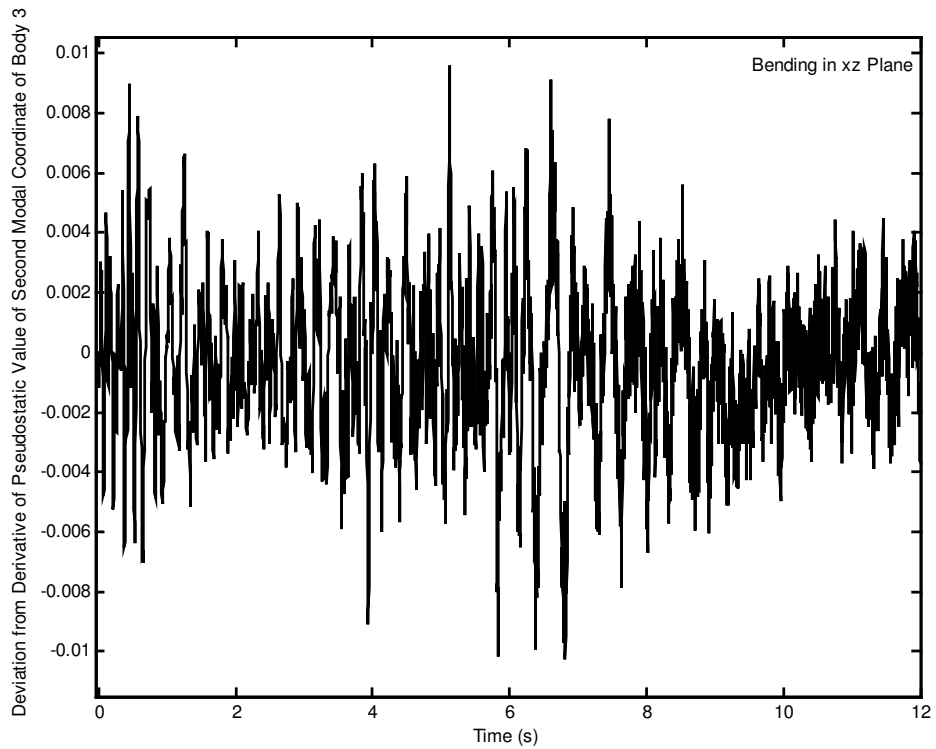


Figure 5.311 Deviation from derivative of pseudostatic value of second modal coordinate of body 3 for bending in xz plane.

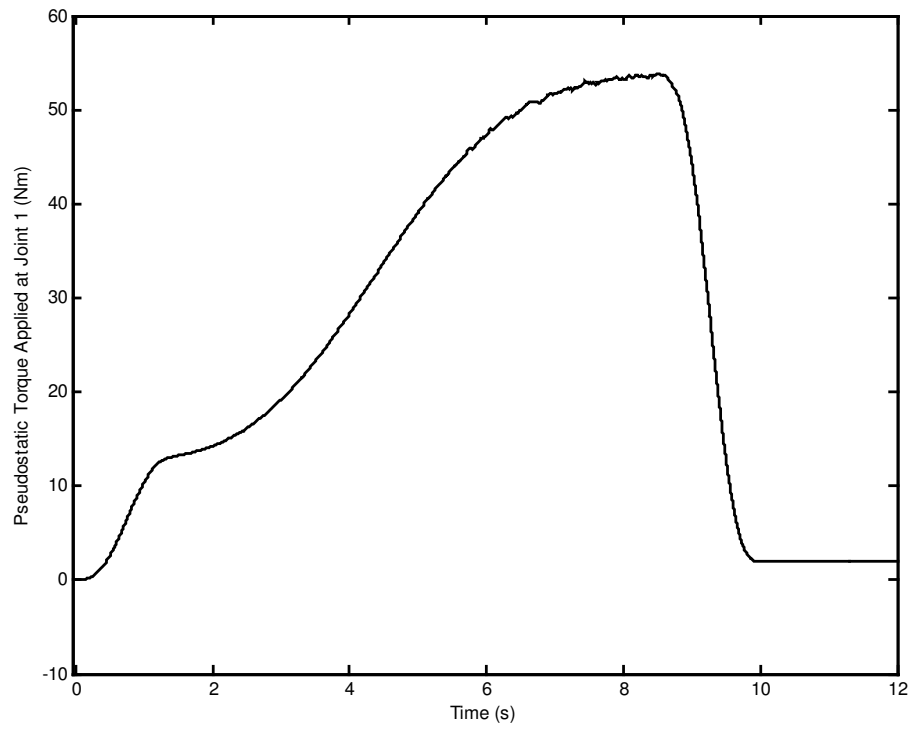


Figure 5.312 Pseudostatic torque applied at joint 1.

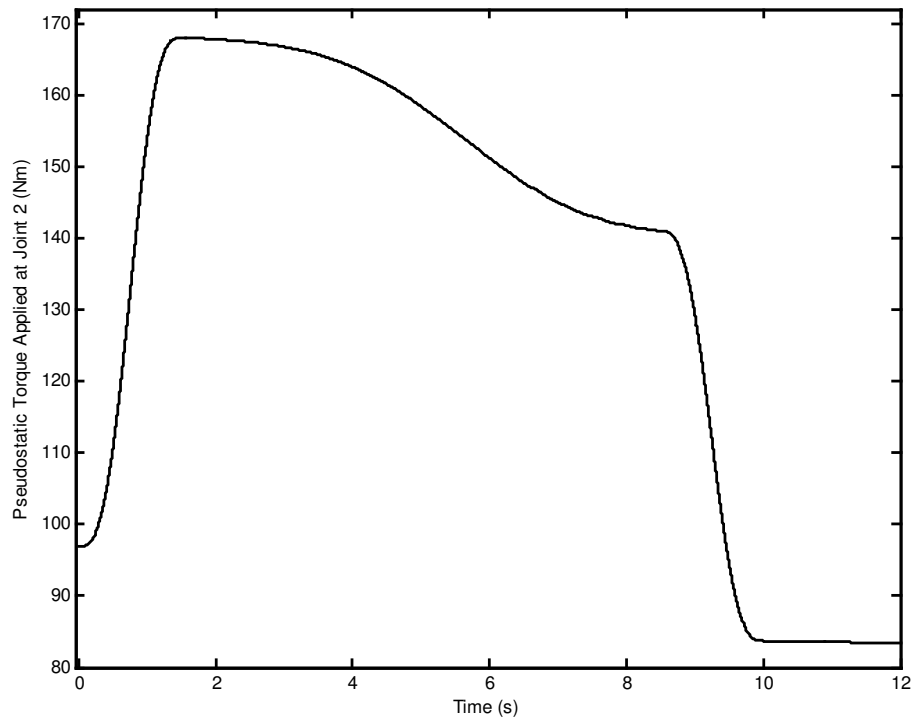


Figure 5.313 Pseudostatic torque applied at joint 2.

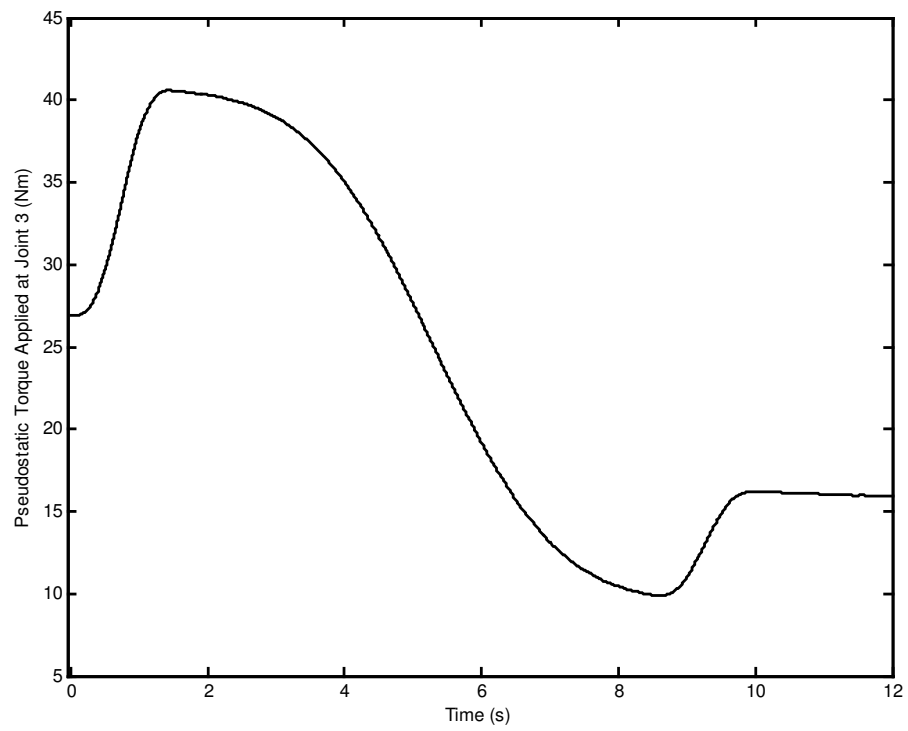


Figure 5.314 Pseudostatic torque applied at joint 3.

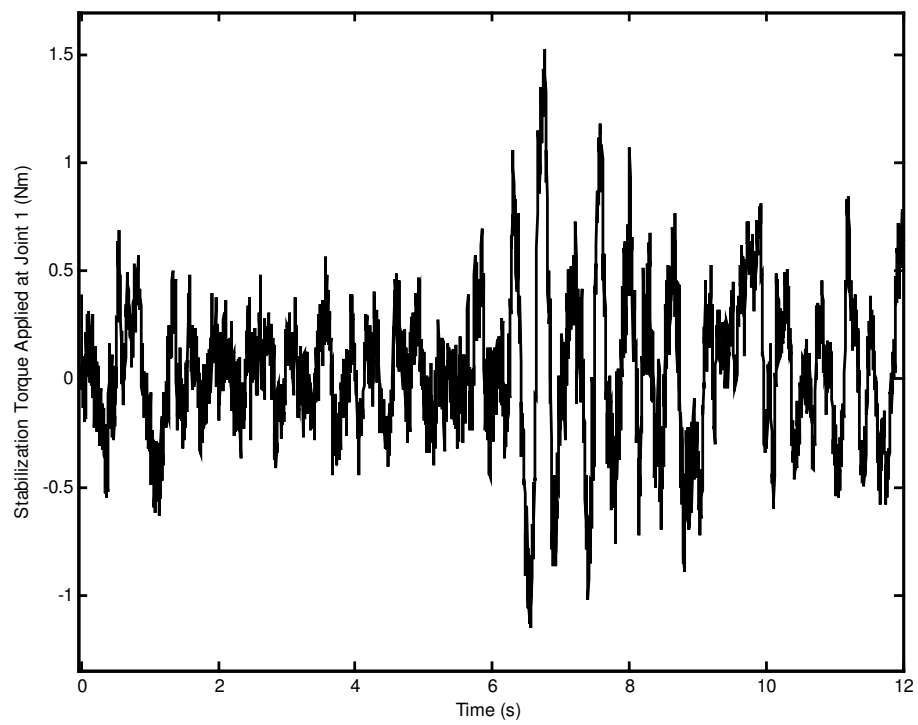


Figure 5.315 Stabilization torque applied at joint 1.

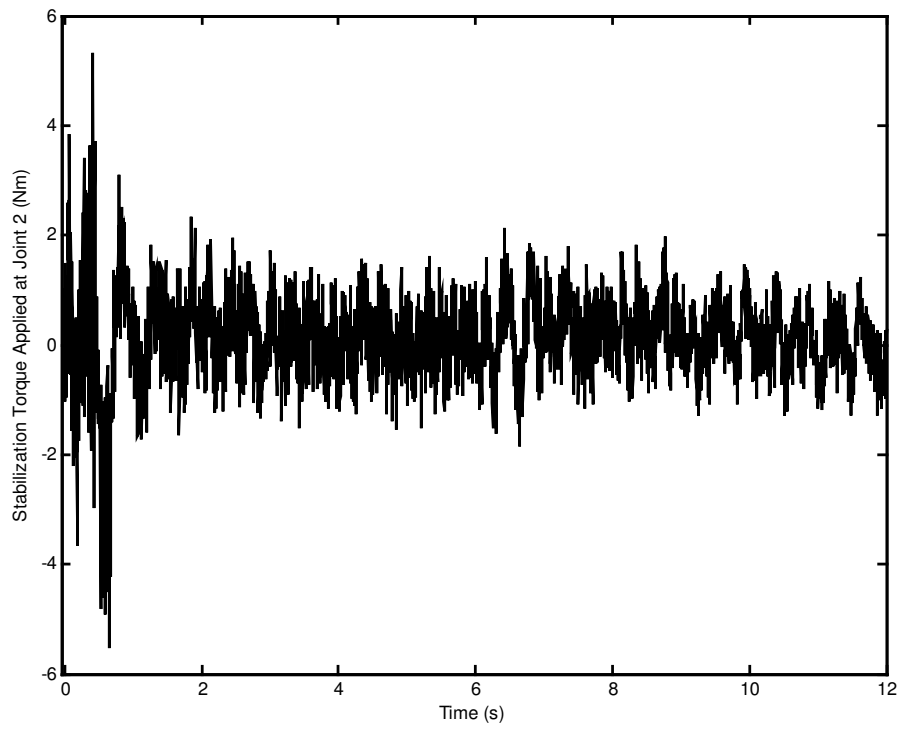


Figure 5.316 Stabilization torque applied at joint 2.

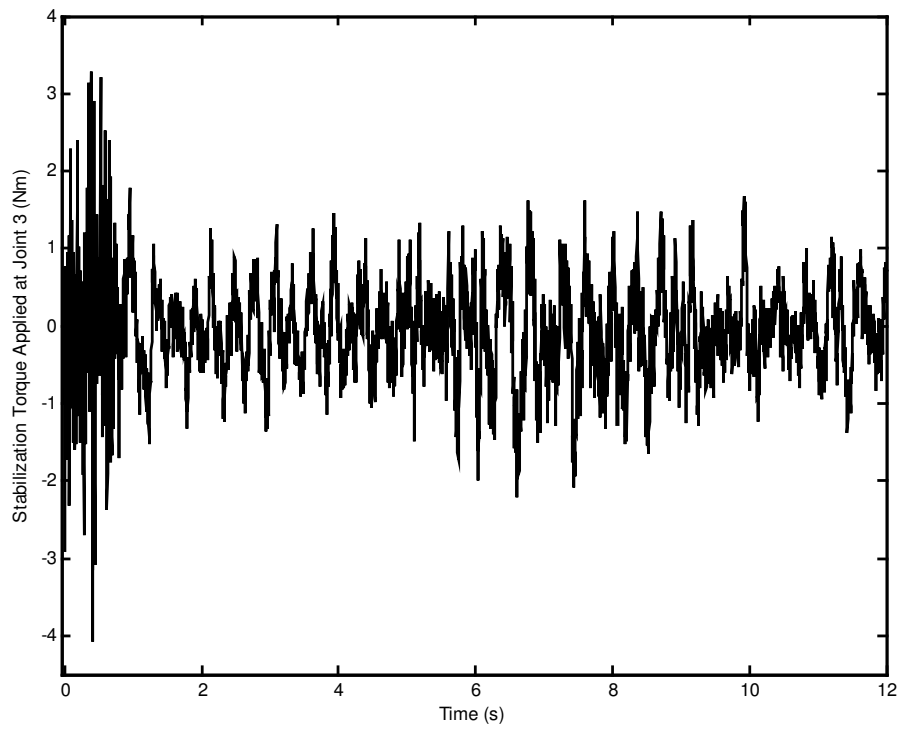


Figure 5.317 Stabilization torque applied at joint 3.

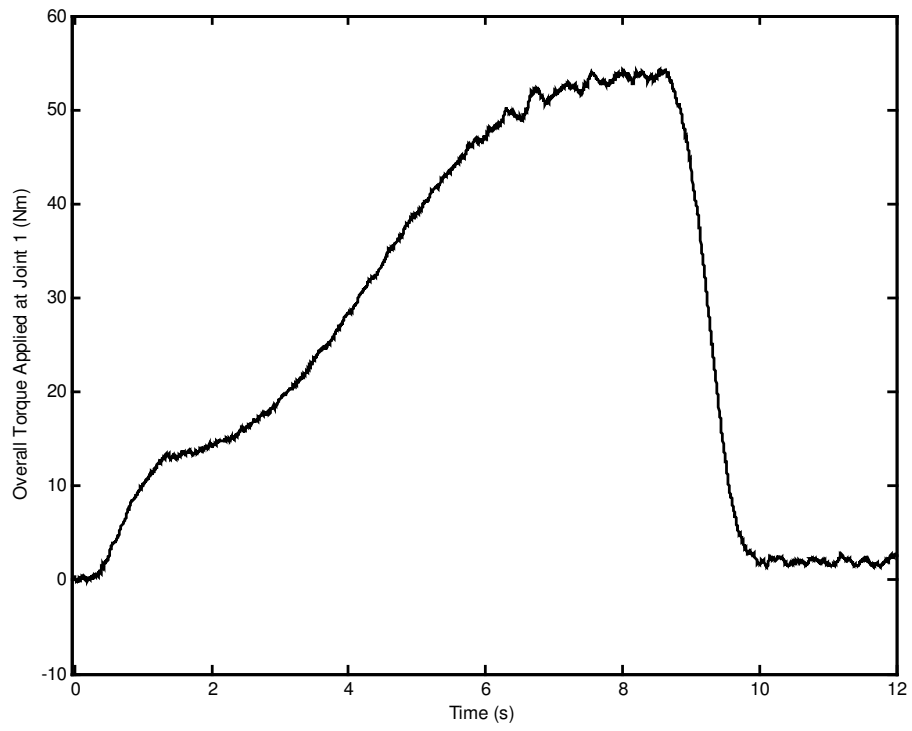


Figure 5.318 Overall torque applied at joint 1.

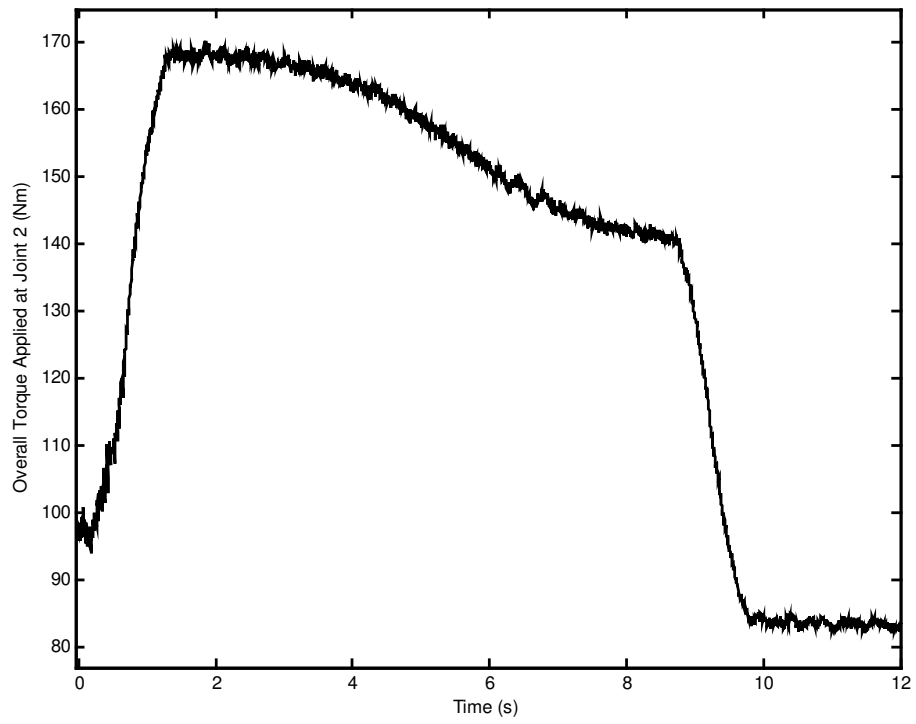


Figure 5.319 Overall torque applied at joint 2.

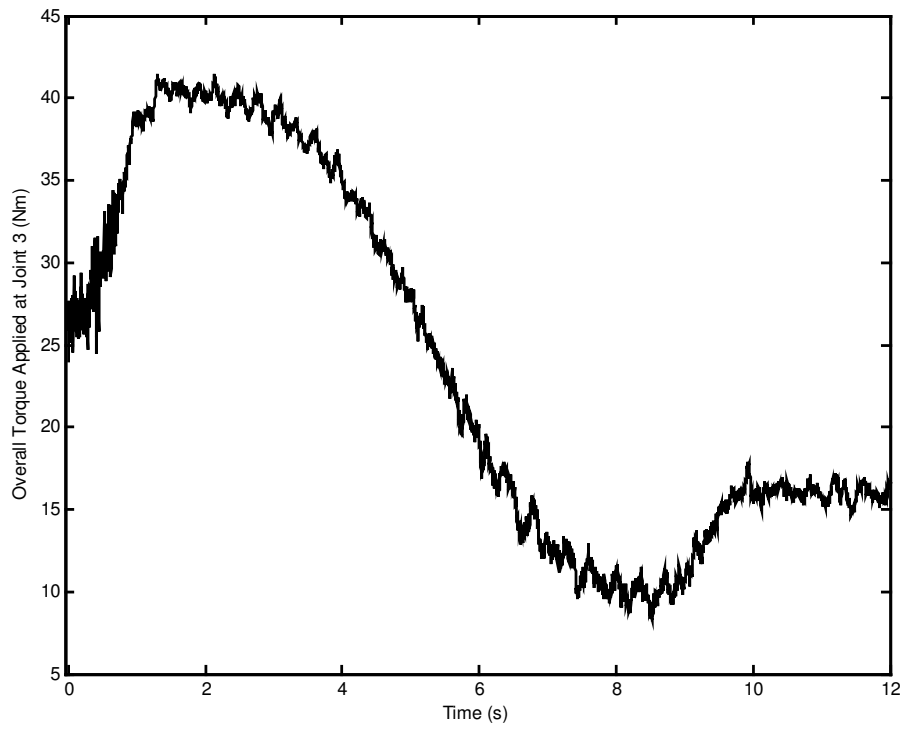


Figure 5.320 Overall torque applied at joint 3.

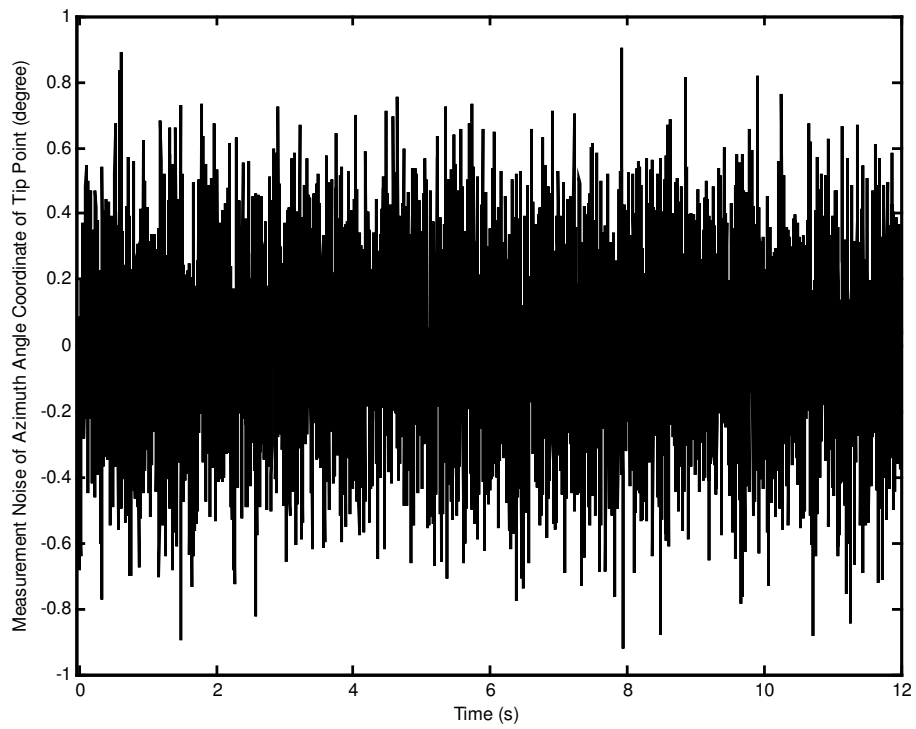


Figure 5.321 Measurement noise of azimuth angle coordinate of tip point.

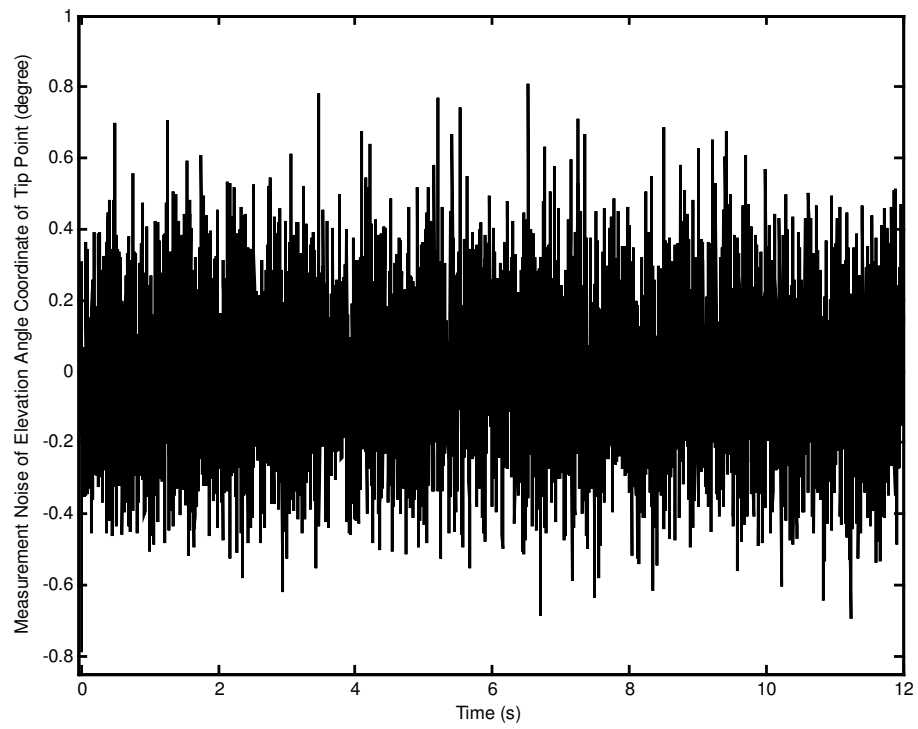


Figure 5.322 Measurement noise of elevation angle coordinate of tip point.

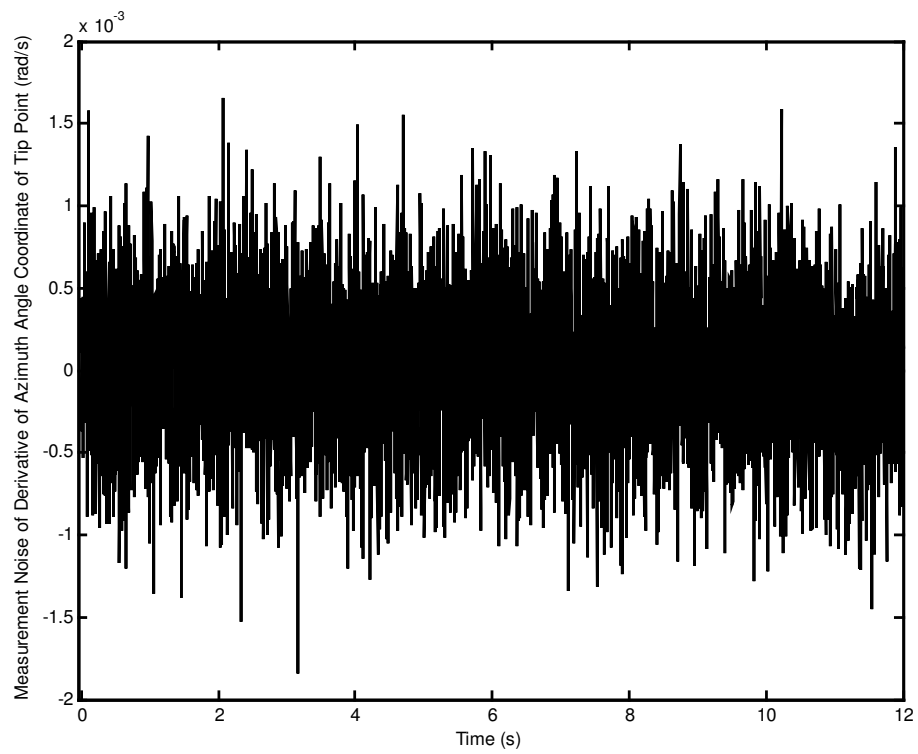


Figure 5.323 Measurement noise of derivative of azimuth angle coordinate of tip point.

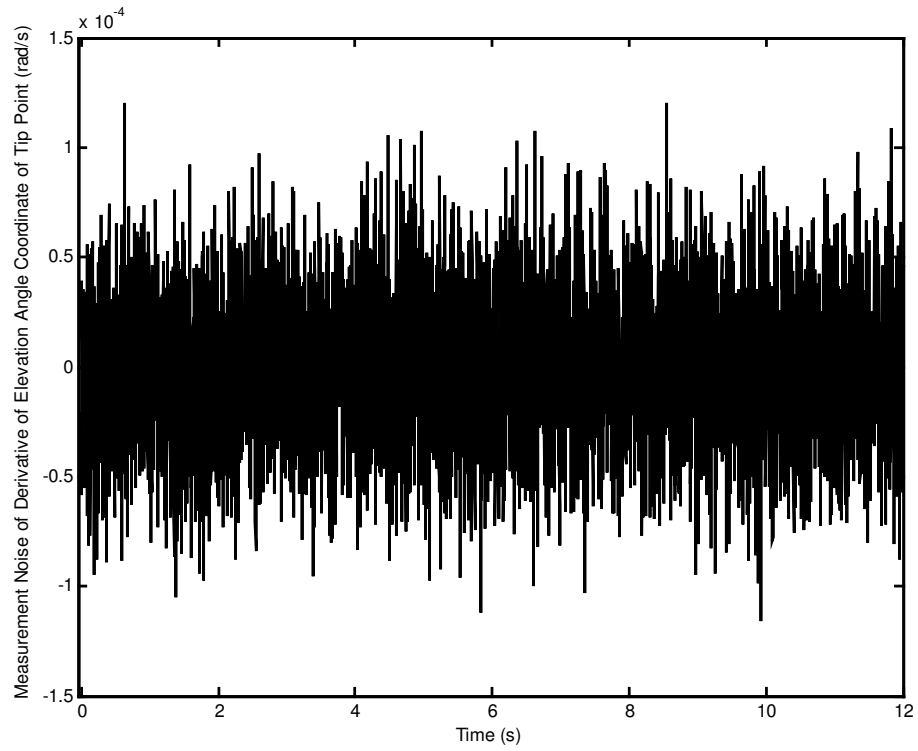


Figure 5.324 Measurement noise of derivative of elevation angle coordinate of tip point.

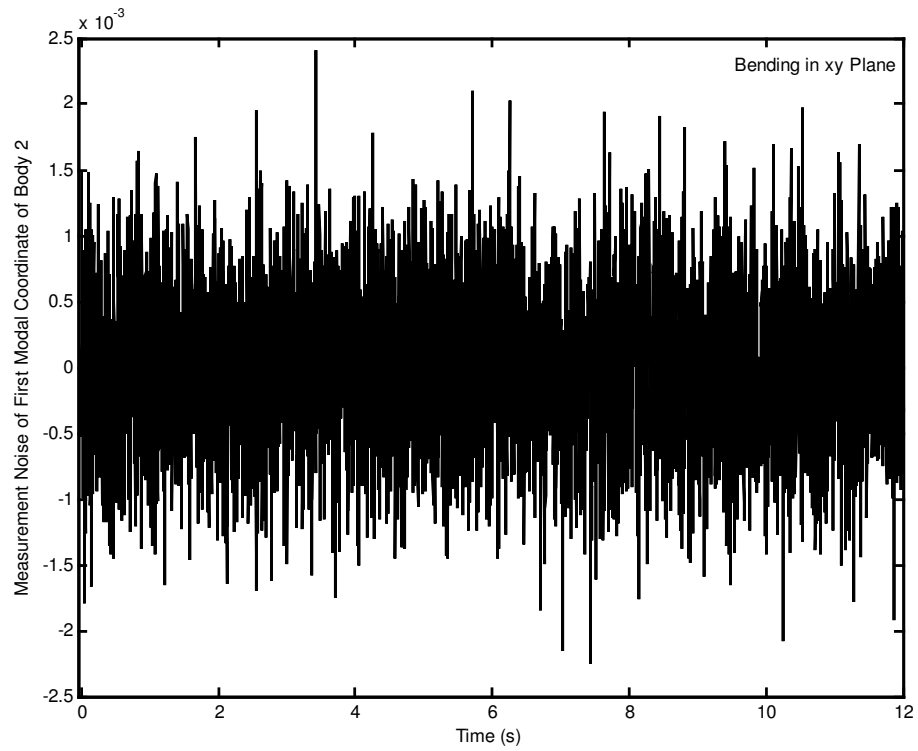


Figure 5.325 Measurement noise of first modal coordinate of body 2 for bending in xy plane.

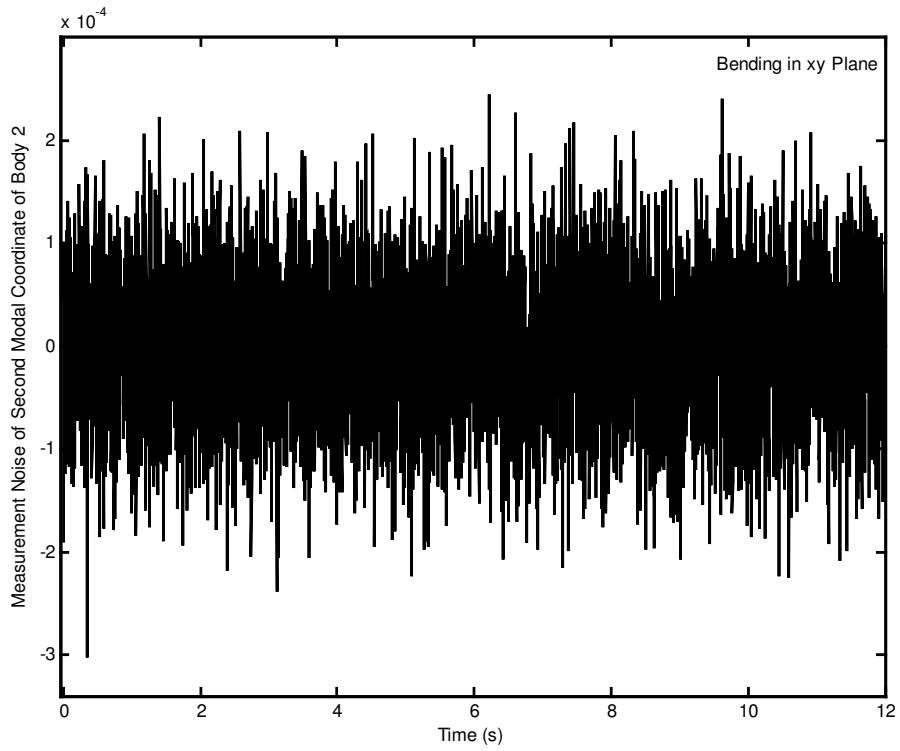


Figure 5.326 Measurement noise of second modal coordinate of body 2 for bending in xy plane.

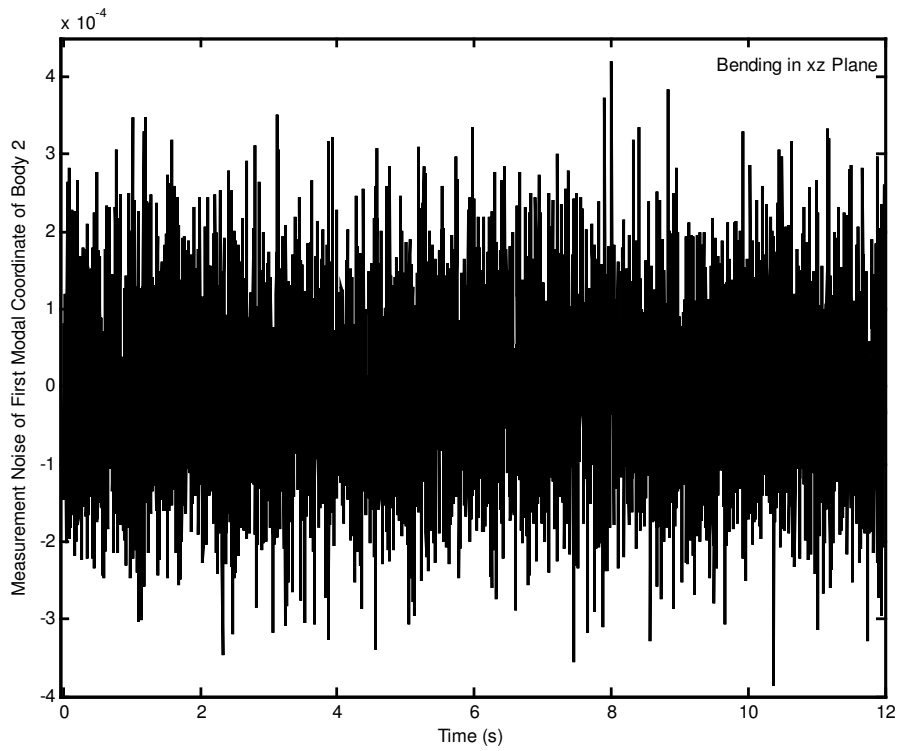


Figure 5.327 Measurement noise of first modal coordinate of body 2 for bending in xz plane.

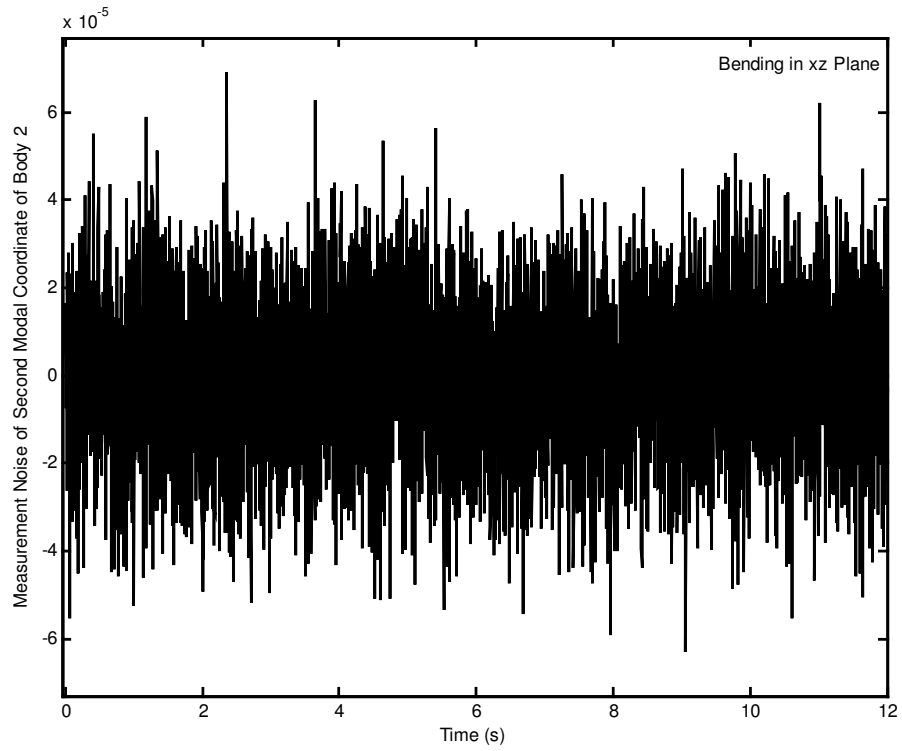


Figure 5.328 Measurement noise of second modal coordinate of body 2 for bending in xz plane.

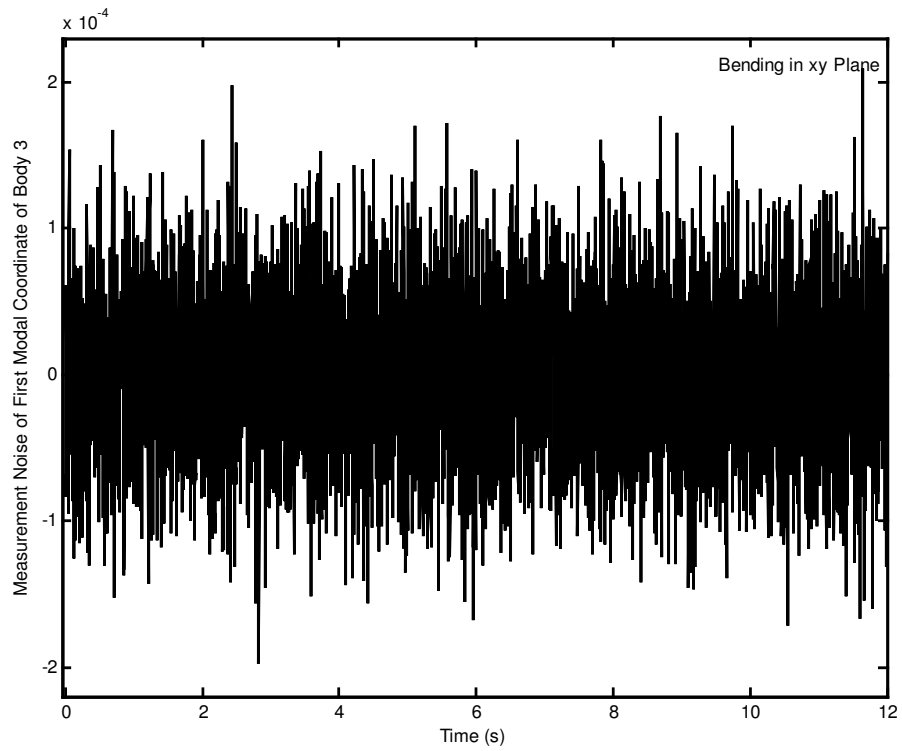


Figure 5.329 Measurement noise of first modal coordinate of body 3 for bending in xy plane.

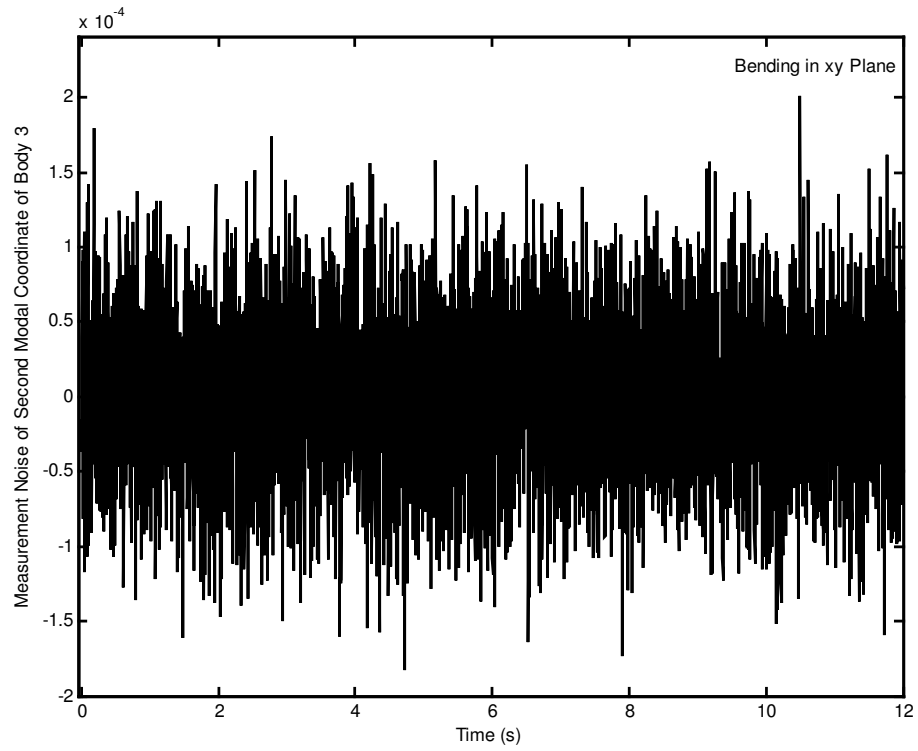


Figure 5.330 Measurement noise of second modal coordinate of body 3 for bending in xy plane.

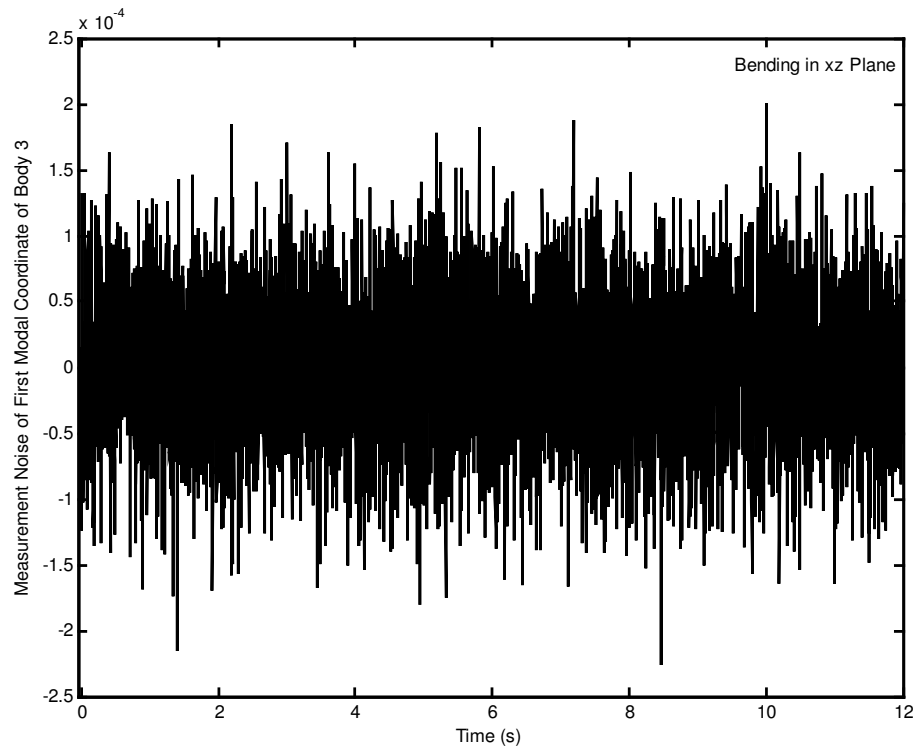


Figure 5.331 Measurement noise of first modal coordinate of body 3 for bending in xz plane.

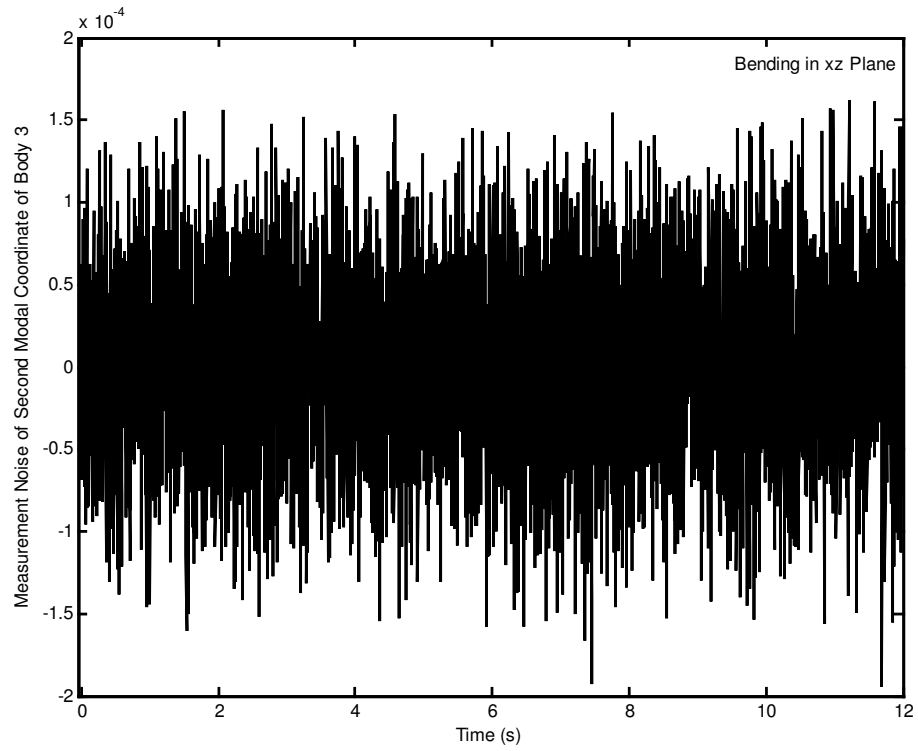


Figure 5.332 Measurement noise of second modal coordinate of body 3 for bending in xz plane.

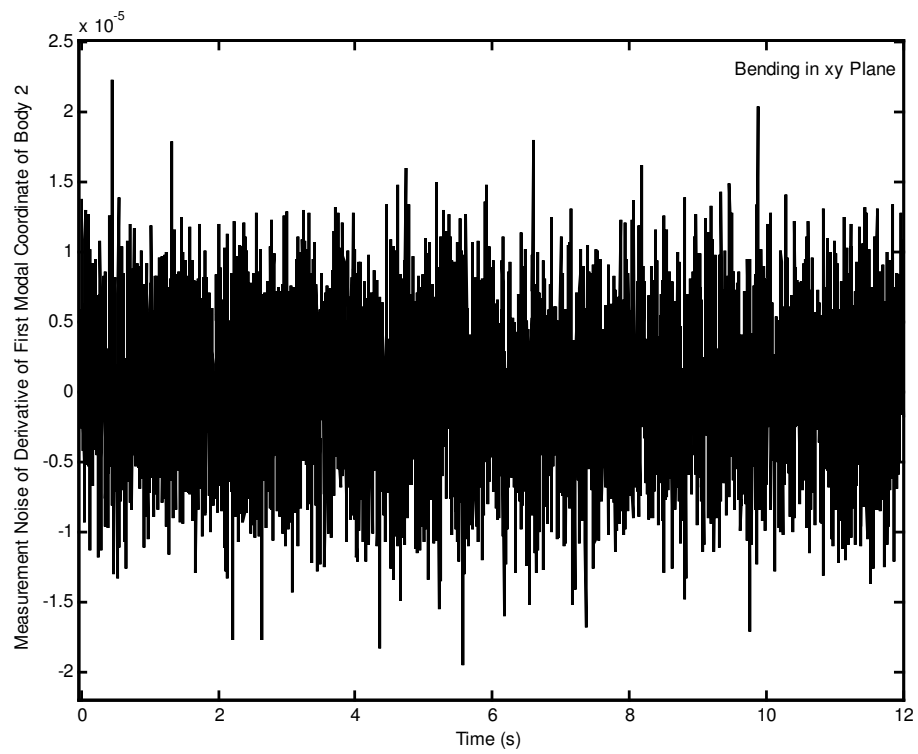


Figure 5.333 Measurement noise of derivative of first modal coordinate of body 2 for bending in xy plane.

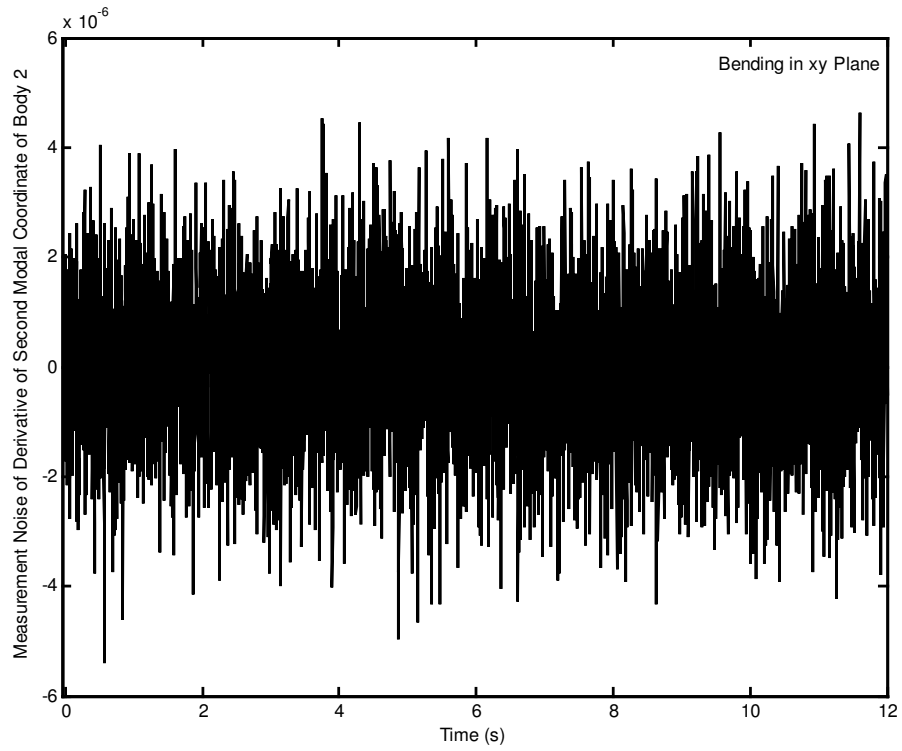


Figure 5.334 Measurement noise of derivative of second modal coordinate of body 2 for bending in xy plane.

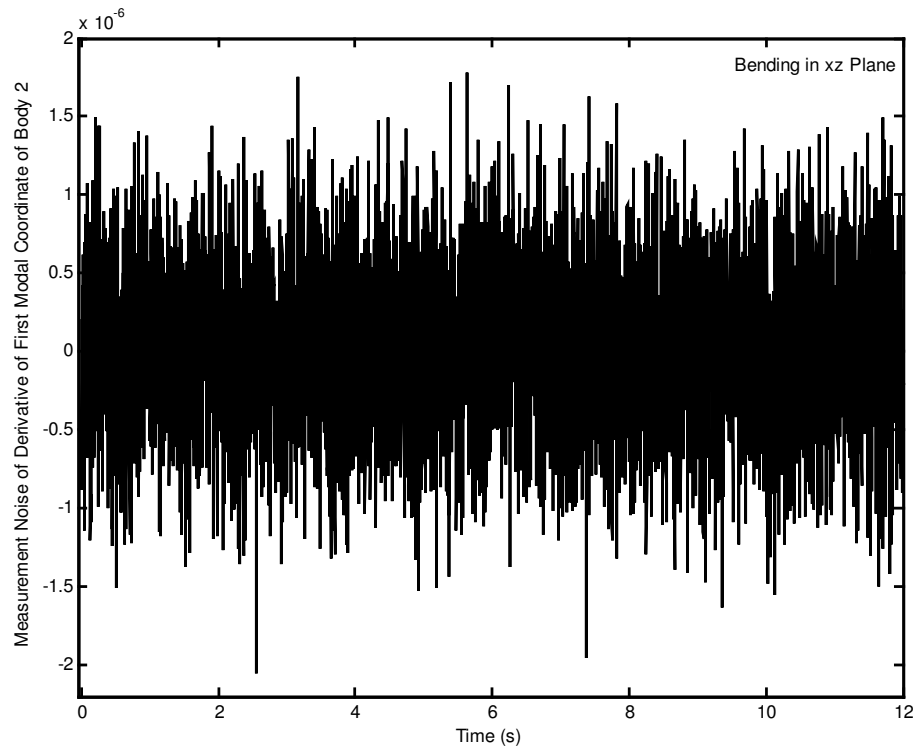


Figure 5.335 Measurement noise of derivative of first modal coordinate of body 2 for bending in xz plane.

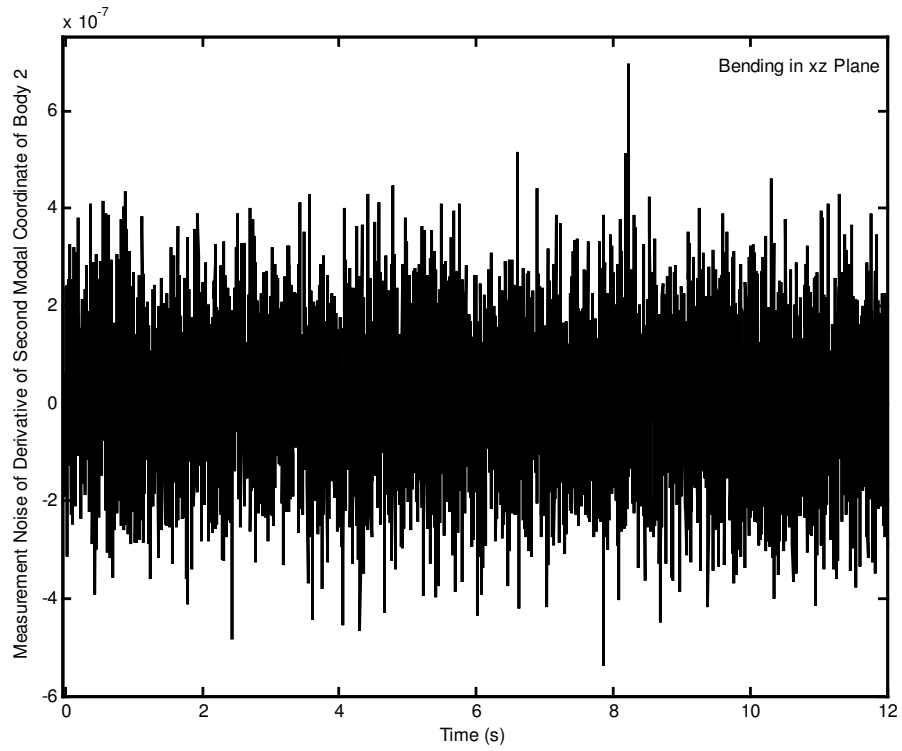


Figure 5.336 Measurement noise of derivative of second modal coordinate of body 2 for bending in xz plane.

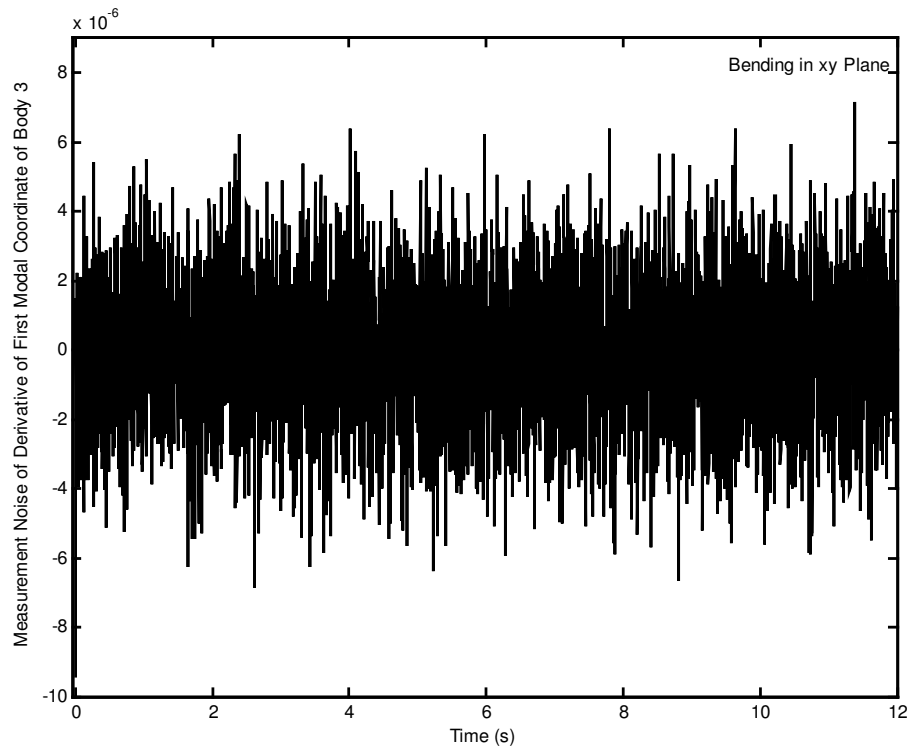


Figure 5.337 Measurement noise of derivative of first modal coordinate of body 3 for bending in xy plane.

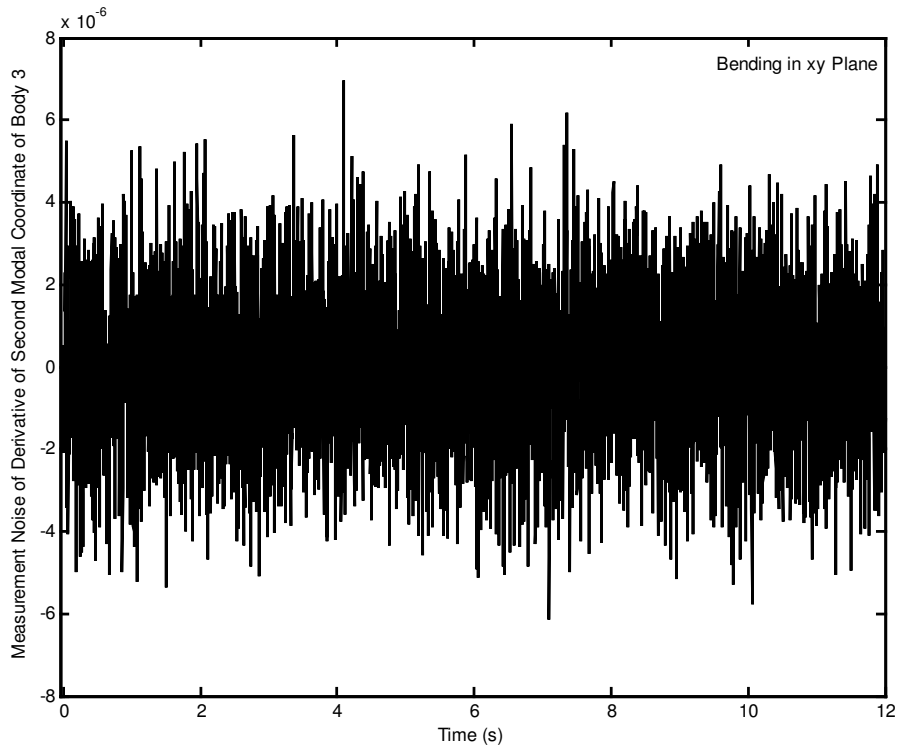


Figure 5.338 Measurement noise of derivative of second modal coordinate of body 3 for bending in xy plane.

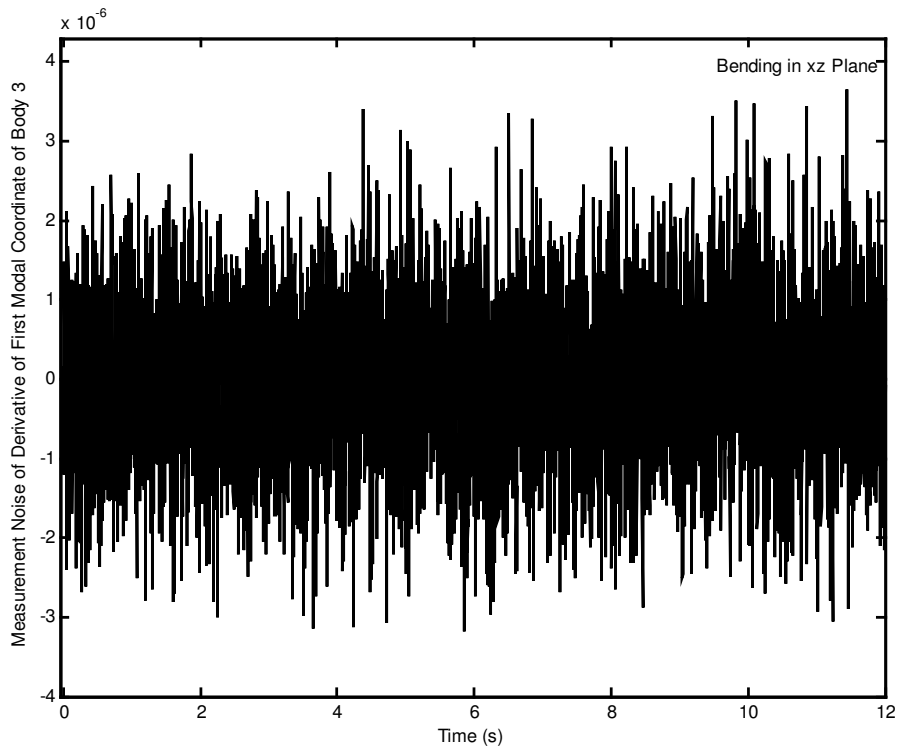


Figure 5.339 Measurement noise of derivative of first modal coordinate of body 3 for bending in xz plane.

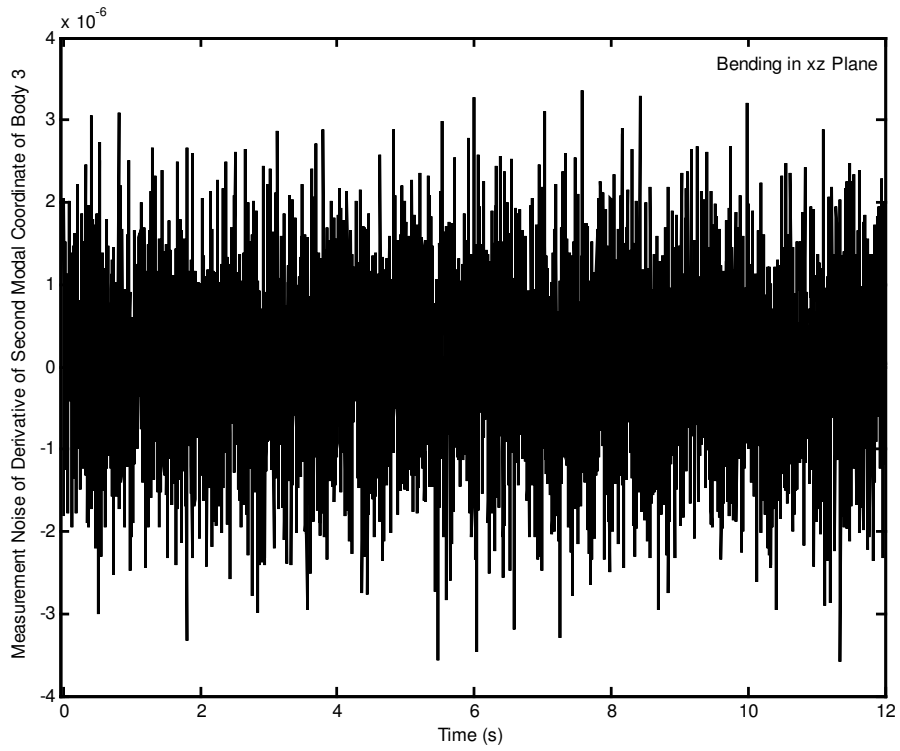


Figure 5.340 Measurement noise of derivative of second modal coordinate of body 3 for bending in xz plane.

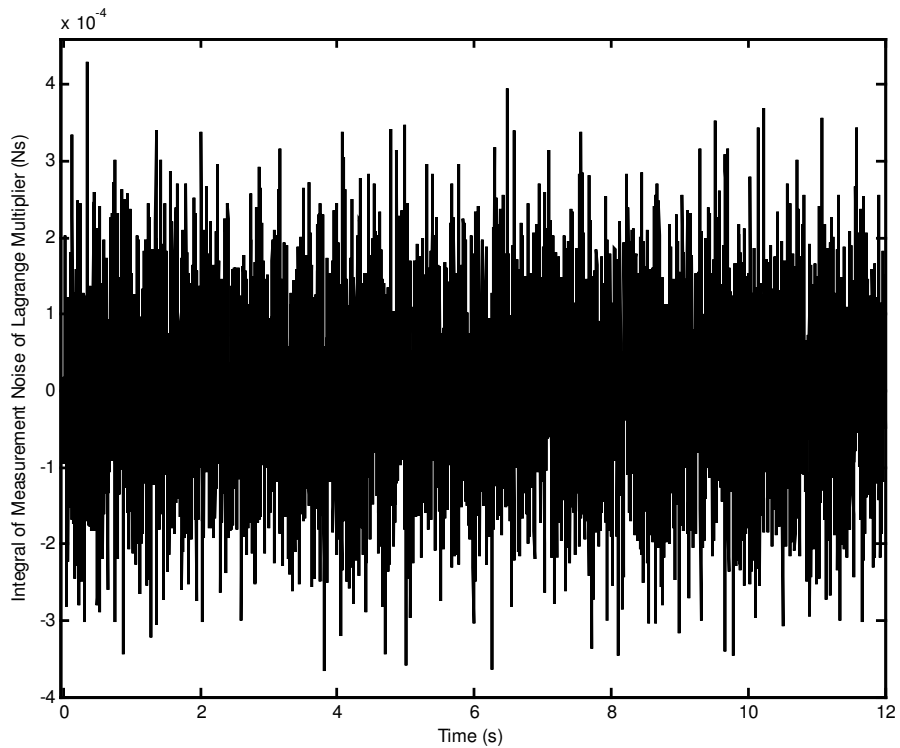


Figure 5.341 Integral of measurement noise of Lagrange multiplier.

The maximum azimuth and elevation angle errors of the tip point along the trajectory after the settling time are 0.3968 degrees and 0.2173 degrees, respectively. The maximum Lagrange multiplier error after the settling time is – 7.7696 N. The maximum overall torques applied to the joints are in the order of 170 Nm as seen from Figures 5.318 - 5.320. Note that the measurement noises do not cause any noticeable increase in the control torques as compared to the case without noises.

As seen from the Figures 5.258, 5.259 and 5.262 the errors in the azimuth and elevation angles of the tip point and the Lagrange multiplier are all in acceptable levels considering the 1 % sensor uncertainty in the measured mean values of the variables.

CHAPTER 6

CONCLUSIONS AND FURTHER WORKS

In this thesis, alternative control methods are proposed for the unconstrained motion and constrained force and motion control of flexible robots. The performances of the proposed methods are illustrated firstly on a planar two link robot with a flexible forearm. Then, a more complex example which is a spatial three link robot with two flexible arms are taken into consideration.

The main advantage of the proposed control methods is that no linearization of the dynamic equations is required but conventional linear control techniques are still used based on the fact that the system can be rendered “slowly varying” with proper placement of the closed loop poles [49], [50]. Therefore, implementation of the proposed control methods are easy which is especially important for high degree of freedom robots with flexible arms. The proposed control methods are designed based on the tip point variables, therefore better tracking quality is obtained compared to the control methods designed based on the joint variables assuming that the tip point variables are measured precisely.

In the application of the proposed methods, the dynamic equations of a flexible robot are partitioned as pseudostatic equilibrium equations and deviations from them. The pseudostatic equilibrium considered here is defined as a hypothetical state where the tip point variables have their desired values while the modal variables are instantaneously constant. Then, the control torques for the pseudostatic equilibrium and for the stabilization of the deviation equations are formed in terms of tip point coordinates, modal variables and the contact force components. In the constrained force and motion control method, the tip point

position variables are replaced with the contact surface coordinates by using the constraint equations before applying the control method.

In order to have asymptotic stability in the large, the closed-loop system must be slowly varying [49], [50]. It is shown that this stability condition is satisfied by placing the poles sufficiently away from the imaginary axis.

Avoiding from the singularities is a necessary condition to obtain a controllable system. However, it may not be sufficient alone. Actually, the necessary and sufficient condition is that the controllability matrix be of full rank, where the controllability matrix is defined based on the state space representation of the system.

An incremental rotary optical encoder is the most popular sensor to monitor a joint variable of a robot. Typically, encoder angular resolutions ranging from 1.44 degrees down to 0.0036 degrees are achievable [45]. Strains are measured to calculate the modal variables. Probably the most sensitive strain gauge is the semiconductor gauge for this aim. A $\pm 1\%$ accuracy is typical, and this is a fundamental limit on accuracy in stress analysis applications [46]. On a flexible link, strains can be measured at those locations where the maximum stresses occur for each mode. These locations can be determined from the mode shapes of the flexible link. Contact force sensors generally placed between the end effector and last joint of the manipulator. Such a sensor consists of a mechanical structure instrumented with strain gauges which can measure the forces and torques acting on the end effector. Typically, these sensors also have $\pm 1\%$ accuracy [47]. Optical devices may also be used to measure the position of the tip point [48], [10]. It is recommended that they should be kept close to the tip point as much as possible. New technologies continue to improve the sensitivities of the sensors. The rates of the position and modal variables can be obtained by numerically differentiating their measured values.

Different modeling approaches for the flexible multibody systems and different discretization methods for the flexible arms are used while modeling the planar

and spatial robots. Planar two link robot with flexible forearm is modeled by using the relative coordinates approach and its flexible arm is discretized by using the assumed modes method. On the other hand, spatial three link robot with two flexible arms is modeled by using the absolute coordinates approach and its flexible arms are discretized by using the finite element method. Then, an alternative form of the dynamic equations, which has necessary and sufficient number of generalized coordinates and equations, is given for the controller design.

A ninth order hermite polynomial is used for the reference motion trajectory and a profile that consists of a cycloidal rise, a constant level and a cycloidal return is used for the reference Lagrange multiplier. Simulations are performed by programs written in MATLAB[®].

Uncontrolled motion of the planar robot is simulated to verify the dynamic equations. In order to determine the effectiveness of the control methods, the unconstrained motion and constrained force and motion control simulations are presented firstly for the planar robot. Unmodeled dynamics is taken into consideration to illustrate the performance of the control method even in the case of unmodeled dynamics, then unconstrained motion and constrained force and motion control simulations are presented again. Motion control of the planar flexible robot by using the computed torque method with the rigidity assumption is also simulated for a comparison with the proposed method. After that, the uncontrolled motion of the spatial robot is simulated. The unconstrained motion and constrained force and motion control simulations are this time presented for the spatial robot. Measurement noises are also taken into consideration and the unconstrained motion and constrained force and motion control simulations are presented again by filtering the measured variables in order to illustrate the performance of the control method in the presence of measurement noises. It can be said from the simulation results that the proposed control methods work satisfactorily.

In some applications, the robot may pass from the unconstrained motion to the constrained force and motion and/or from the constrained force and motion to the unconstrained motion. While the motion type of the robot is changing, there may be an impact force. Therefore, the impact force is also taken into consideration in such combined motions. A very limited study is available on this type of problem. Thus, this type of problem can be considered as a further work.

Another subject to work on in future is the actuating singularity analysis that arises in determining the pseudostatic torques in association with the pseudostatic values of the modal variables.

REFERENCES

- [1] Goldenberg, A. A., and Rakhsha, F., 'Feedforward Control of a Single Link Flexible Robot,' *Mechanism and Machine Theory*, Vol. 21, No. 4, 1986, pp. 325-335.
- [2] Luca, A. D., and Siciliano, B., 'Trajectory Control of a Nonlinear One-Link Flexible Arm,' *International Journal of Control*, Vol. 50, No. 5, 1989, pp. 1699-1715.
- [3] Kwon, D.-S., and Book, W. J., 'A Time-Domain Inverse Dynamic Tracking Control of a Single-Link Flexible Manipulator,' *Journal of Dynamic Systems, Measurement, and Control*, Vol. 116, June 1994, pp. 193-200.
- [4] Zhu, G. Ge, S. S., and Lee, T. H., 'Simulation Studies of Tip Tracking Control of a Single-Link Flexible Robot Based on a Lumped Model,' *Robotica*, Vol. 17, 1999, pp. 71-78.
- [5] Feliu, V., and Rattan, K. S., 'Feedforward Control of Single-Link Flexible Manipulators by Discrete Model Inversion,' *Journal of Dynamic Systems, Measurement, and Control*, Vol. 121, December 1999, pp. 713-721.
- [6] Ge, S. S., Lee, T. H., and Zhu, G., 'A Nonlinear Feedback Controller for a Single Link Flexible Manipulator Based on a Finite Element Model,' *Journal of Robotic Systems*, Vol. 14, No. 3, 1997, pp. 165-178.
- [7] Yeung, K. S., and Chen, Y. P., 'Sliding Mode Controller Design of a Single Link Flexible Manipulator Under Gravity,' *International Journal of Control*, Vol. 52, No. 1, 1990, pp. 101-117.
- [8] Qian, W. T., and Ma, C. C. H., 'A New Controller Design for a Flexible One Link Manipulator,' *IEEE Transactions on Automatic Control*, Vol. 37, No. 1, January 1992, pp. 132-137.
- [9] Luca, A. D., Lucibello, P., and Ulivi, G., 'Inversion Techniques for Trajectory Control of Flexible Robot Arms,' *Journal of Robotic Systems*, Vol. 6, No. 4, 1989, pp. 325-344.
- [10] Bayo, E., Papadopoulos, P., Stubbe, J., and Serna, M. A., 'Inverse Dynamics and Kinematics of Multilink Elastic Robots: An Iterative Frequency Domain Approach,' *The International Journal of Robotics Research*, Vol. 8, No. 6, December 1989, pp. 49-62.
- [11] Asada, H., Ma, Z.-D., and Tokumaru, H., 'Inverse Dynamics of Flexible Robot Arms: Modeling and Computation for Trajectory Control,' *Journal of*

Dynamic Systems, Measurement, and Control, Vol. 112, June 1990, pp. 177-185.

- [12] Xi, F., 'Trajectory Tracking of a Spatial Flexible Link Manipulator Using an Inverse Dynamics Method,' *Mechanism and Machine Theory*, Vol. 30, No. 8, 1995, pp. 1113-1126.
- [13] Gawronski, W., Ih, C. H. C., and Wang, S. J., 'On Dynamics and Control of Multilink Flexible Manipulators,' *Journal of Dynamic Systems, Measurement, and Control*, Vol. 117, June 1995, pp. 134-142.
- [14] Moallem, M., Patel, R. V., and Khorasani, K., 'An Inverse Dynamics Control Strategy for Tip Position Tracking of Flexible Multilink Manipulators,' *Journal of Robotic Systems*, Vol. 14, No. 9, 1997, pp. 649-658.
- [15] Chalhoub, N. G., and Ulsoy, A. G., 'Control of a Flexible Robot Arm: Experimental and Theoretical Results,' *Journal of Dynamic Systems, Measurement, and Control*, Vol. 109, December 1987, pp. 299-309.
- [16] Baruh, H., and Tadikonda, S. S. K., 'Issues in the Dynamics and Control of Flexible Robot Manipulators,' *Journal of Guidance, Control, and Dynamics*, Vol. 12, No. 5, September-October 1989, pp.659-671.
- [17] Carusone, J., and D'Eleuterio, G. M. T., 'Tracking Control for End-Effector Position and Orientation of Structurally Flexible Manipulators,' *Journal of Robotic Systems*, Vol. 10, No. 6, 1993, pp. 847-870.
- [18] Ider, S. K., Ozgoren, M. K., and Ay, V., 'Trajectory Tracking Control of Robots with Flexible Links,' *Mechanism and Machine Theory*, Vol. 37, 2002, pp. 1377-1394.
- [19] Pfeiffer, F., 'A Feedforward Decoupling Concept for the Control of Elastic Robots,' *Journal of Robotic Systems*, Vol. 6, No. 4, 1989, pp. 407-416.
- [20] Luca, A. D., and Siciliano, B., 'Inversion-Based Nonlinear Control of Robot Arms with Flexible Links,' *Journal of Guidance, Control, and Dynamics*, Vol. 16, No. 6, November-December 1993, pp. 1169-1176.
- [21] Li, D., 'Nonlinear Control Design for Tip Position Tracking of a Flexible Manipulator Arm,' *International Journal of Control*, Vol. 60, No. 6, 1994, pp. 1065-1082.
- [22] Yim, W., 'Inverse Cartesian Trajectory Control and Stabilization of a Three Axis Flexible Manipulator,' *Journal of Robotic Systems*, Vol. 11, No., 4, 1994, pp. 311-326.
- [23] Zhao, H., and Chen, D., 'Tip Trajectory Tracking for Multilink Flexible Manipulators Using Stable Inversion,' *Journal of Guidance, Control, and Dynamics*, Vol. 21, No. 2, March-April 1998, pp.314-320.

- [24] Chen, Y. P., and Yeung, K. S., 'Sliding-Mode Control of Multilink Flexible Manipulators,' *International Journal of Control*, Vol. 54, No. 2, 1991, pp. 257-278.
- [25] Nathan, P. J., and Singh, S. N., 'Sliding Mode Control and Elastic Mode Stabilization of a Robotic Arm with Flexible Links,' *Journal of Dynamic Systems, Measurement, and Control*, Vol. 113, December 1991, pp. 669-676.
- [26] Moallem, M., Khorasani, K., and Patel, R. V., 'Inversion-Based Sliding Control of a Flexible-Link Manipulator,' *International Journal of Control*, Vol. 71, No. 3, 1998, pp. 477-490.
- [27] Vandegrift, M. W., Lewis, F. L., and Zhu, S. Q., 'Flexible Link Robot Arm Control by a Feedback Linearization/Singular Perturbation Approach,' *Journal of Robotic Systems*, Vol. 11, No. 7, 1994, pp. 591-603.
- [28] Morita, Y., Ukai, H., and Kando, H., 'Robust Trajectory Tracking Control of Elastic Robot Manipulators,' *Journal of Dynamic Systems, Measurement, and Control*, Vol. 119, December 1997, pp. 727-735.
- [29] Moallem, M., Khorasani, K., and Patel, R. V., 'An Integral Manifold Approach for Tip-Position Tracking of Flexible Multilink Manipulators,' *IEEE Transactions on Robotics and Automation*, Vol. 13, No. 6, December 1997, pp. 823-837.
- [30] Bodur, M., and Sezer, M. E., 'Adaptive Control of Flexible Multilink Manipulators,' *International Journal of Control*, Vol. 58, No. 3, 1993, pp. 519-536.
- [31] Pham, C. M., Khalil, W., and Chevallereau, C., 'A Nonlinear Model-Based Control of Flexible Robots,' *Robotica*, Vol. 11, 1993, pp 73-82.
- [32] Arteaga, M. A., and Siciliano, B., 'On Tracking Control of Flexible Robot Arms,' *IEEE Transactions on Automatic Control*, Vol. 45, No. 3, March 2000, pp. 520-527.
- [33] Morgul, O., 'On the Boundary Control of a Flexible Robot Arm,' *IEEE International Workshop on Intelligent Motion Control*, Istanbul, August 1990, pp. 519-522.
- [34] Morgul, O., 'Orientation and Stabilization of a Flexible Beam Attached to a Rigid Body: Planar Motion,' *IEEE Transactions on Automatic Control*, Vol. 36, No. 8, August 1991, pp. 953-962.
- [35] Choi, B.-O., and Krishnamurthy, K., 'Unconstrained and Constrained Motion Control of a Planar Two-Link Structurally Flexible Robotic Manipulator,' *Journal of Robotic Systems*, Vol. 11, No. 6, 1994, pp. 557-571.

- [36] Matsuno, F., Sakawa, Y., and Asano, T., 'Modeling and Quasi-Static Hybrid Position/Force Control of Constrained Planar Two-Link Flexible Manipulators,' *IEEE Transactions on Robotics and Automation*, Vol. 10, No. 3, 1994, pp. 287-297.
- [37] Borowiec, J., and Tzes, A., 'Linear Quadratic Frequency-Shaped Implicit Force Control of Flexible Link Manipulators,' *Journal of Dynamic Systems, Measurement, and Control*, Vol. 119, September 1997, pp. 405-411.
- [38] Shi, Z. X., Fung, E. H. K., and Li, Y. C., 'Dynamic Modelling of a Rigid-Flexible Manipulator for Constrained Motion Task Control,' *Applied Mathematical Modelling*, Vol. 23, 1999, pp. 509-525.
- [39] Siciliano, B., and Villani, L., 'An Inverse Kinematics Algorithm for Interaction Control of a Flexible Arm With a Compliant Surface,' *Control Engineering Practice*, Vol. 9, 2001, pp. 191-198.
- [40] Hu, F. L., and Ulsoy, A. G., 'Force and Motion Control of a Constrained Flexible Robot Arm,' *Journal of Dynamic Systems, Measurement, and Control*, Vol. 116, September 1994, pp. 336-343.
- [41] Yim, W., and Singh, S. N., 'Inverse Force and Motion Control of Constrained Elastic Robots,' *Journal of Dynamic Systems, Measurement, and Control*, Vol. 117, September 1995, pp. 374-383.
- [42] Choi, S.-B., Lee, H.-B., and Thompson, B. S., 'Compliant Control of a Two-Link Flexible Manipulator by Constraint Hamiltonian System,' *Mechanism and Machine Theory*, Vol. 33, No. 3, 1998, pp. 293-306.
- [43] Kim, H. K., Choi, S. B., and Thompson, B. S., 'Compliant Control of a Two-Link Flexible Manipulator Featuring Piezoelectric Actuators,' *Mechanism and Machine Theory*, Vol. 36, No. 3, 2001, pp. 411-424.
- [44] Matsuno, F., and Yamamoto, K., 'Dynamic Hybrid Position/Force Control of a Two Degree-of-Freedom Flexible Manipulator,' *Journal of Robotic Systems*, Vol. 11, No. 5, 1994, pp. 355-366.
- [45] Automation Consulting and Supply, Inc., *Industrial Encoder Specifications*, <http://www.oddparts.com/>, 1997.
- [46] Doebelin, E., O., *Measurement Systems: Application and Design*, Fifth Edition, McGraw-Hill Higher Education, New York, 2004.
- [47] GlobalSpec, Inc., *Force and Torque Sensors*, <http://www.globalspec.com/>, 2004.
- [48] Cannon, R., and Schmitz, E., 'Initial Experiments on End-Point Control of a Flexible One-Link Robot,' *The International Journal of Robotics Research*, Vol. 3, No. 3, 1984, pp. 62-75.

- [49] Rosenbrock, H. H., 'The Stability of Linear Time-Dependent Control Systems,' *Journal of Electronics and Control*, Vol. 15, July 1963, pp. 73-80.
- [50] Desoer, C. A., 'Slowly Varying Systems $\dot{x} = A(t)x$,' *IEEE Transactions on Automatic Control*, Vol. AC-14, December 1969, pp. 780-781.
- [51] Fortmann, T. E., and Hitz, K. L., *An Introduction to Linear Control Systems*, Marcel Dekker, New York, 1977.
- [52] Chen, C.-T., *Linear System Theory and Design*, Third Edition, Oxford University Press, Inc., New York, 1999.
- [53] Kane, T. R., and Levinson, D. A., *Dynamics: Theory and Applications*, McGraw-Hill, Inc., 1985.
- [54] MATLAB User Guide, Version 6, Revised for MATLAB 6.5, The MathWorks, Inc., Natick, MA, August 2002.
- [55] Meirovitch, L., *Analytical Methods in Vibrations*, The Macmillan Company, Collier-Macmillan Limited, London, 1967.
- [56] Jankowski, K. P., and Van Brussel, H., 'An Approach to Discrete Inverse Dynamics Control of Flexible Joint Robots,' *IEEE Transactions on Robotics and Automation*, Vol. 8, No. 5, 1992, pp. 651-658.
- [57] Przemieniecki, J. S., *Theory of Matrix Structural Analysis*, McGraw-Hill, Inc., New York, 1968.
- [58] Dym, C. L., and Shames, I. H., *Solid Mechanics: A Variational Approach*, McGraw-Hill, Inc., New York, 1973.

APPENDIX A

BEAM ELEMENT SHAPE FUNCTIONS

Let the beam B_k be modeled by one dimensional beam elements. Consider an element with nodes A and B. Let δ_i and γ_i , $i=1,2,3$ denote the deformation displacements and rotations respectively of axis frames fixed along the centroidal line of the element, and u_i denote the deformation displacements of arbitrary points in the element.

δ_i and γ_i are expressed in terms of the nodal variables α_j by utilizing polynomials of appropriate order [57] as

$$\delta_i = s_{ij} \alpha_j \quad i=1,2,3 \quad j=1,\dots,12 \quad (\text{A.1})$$

and

$$\gamma_i = s_{rotij} \alpha_j \quad (\text{A.2})$$

where α_j are the displacements of rotations at the nodes,

$$\boldsymbol{\alpha} = \left[\delta_1^A \quad \delta_2^A \quad \delta_3^A \quad \gamma_1^A \quad \gamma_2^A \quad \gamma_3^A \quad \delta_1^B \quad \delta_2^B \quad \delta_3^B \quad \gamma_1^B \quad \gamma_2^B \quad \gamma_3^B \right]^T \quad (\text{A.3})$$

and the element shape functions neglecting shear deformation are given by

$$\mathbf{s} = \begin{bmatrix} a_1 & 0 & 0 & 0 & 0 & 0 & a_2 & 0 & 0 & 0 & 0 & 0 \\ 0 & b_1 & 0 & 0 & 0 & b_2 & 0 & b_3 & 0 & 0 & 0 & b_4 \\ 0 & 0 & b_5 & 0 & b_6 & 0 & 0 & 0 & b_7 & 0 & b_8 & 0 \end{bmatrix} \quad (\text{A.4})$$

and

$$\mathbf{s}_{\text{rot}} = \begin{bmatrix} 0 & 0 & 0 & a_1 & 0 & 0 & 0 & 0 & 0 & a_2 & 0 & 0 \\ 0 & 0 & c_5 & 0 & c_6 & 0 & 0 & 0 & c_7 & 0 & c_8 & 0 \\ 0 & c_1 & 0 & 0 & 0 & c_2 & 0 & c_3 & 0 & 0 & 0 & c_4 \end{bmatrix} \quad (\text{A.5})$$

where

$$a_1 = 1 - \xi \quad (\text{A.6})$$

$$a_2 = \xi \quad (\text{A.7})$$

$$b_1 = 1 - 3\xi^2 + 2\xi^3 = b_5 \quad (\text{A.8})$$

$$b_2 = L(\xi - 2\xi^2 + \xi^3) = -b_6 \quad (\text{A.9})$$

$$b_3 = 3\xi^2 - 2\xi^3 = b_7 \quad (\text{A.10})$$

$$b_4 = L(-\xi^2 + \xi^3) = -b_8 \quad (\text{A.11})$$

$$c_1 = \frac{6}{L}(-\xi + \xi^2) = -c_3 = -c_5 = c_7 \quad (\text{A.12})$$

$$c_2 = 1 - 4\xi + 3\xi^2 = c_6 \quad (\text{A.13})$$

$$c_4 = -2\xi + 3\xi^2 = c_8 \quad (\text{A.14})$$

In Equations (A.6) to (A.14), $\xi = \frac{x}{L}$ where x is measured from the element axis fixed at node A and L is the length of the element.

Using δ_i and γ_i , the displacement field for arbitrary points in the beam element, $u_i(x, y, z, t)$ can be derived for small rotations, using references [57], [58] and extending its two dimensional representation to three dimensions, such that

$$u_1(x, y, z, t) = \delta_1(x, t) + z\gamma_2(x, t) - y\gamma_3(x, t) \quad (\text{A.15})$$

$$u_2(x, y, z, t) = \delta_2(x, t) - z\gamma_1(x, t) \quad (\text{A.16})$$

$$u_3(x, y, z, t) = \delta_3(x, t) + y\gamma_1(x, t) \quad (\text{A.17})$$

Using Equations (A.1) and (A.2) and the relations given by Equations (A.15), (A.16) and (A.17), u_i is obtained as

$$u_i = s_{ij} \alpha_j \quad i=1,2,3 \quad j=1,\dots,12 \quad (\text{A.18})$$

where the consistent mass shape function s becomes

$$s = \begin{bmatrix} a_1 & -yc_1 & -zc_1 & 0 & zc_2 & -yc_2 & a_2 & yc_1 & zc_1 & 0 & zc_4 & -yc_4 \\ 0 & b_1 & 0 & -za_1 & 0 & b_2 & 0 & b_3 & 0 & -za_2 & 0 & b_4 \\ 0 & 0 & b_1 & ya_1 & -b_2 & 0 & 0 & 0 & b_3 & ya_2 & -b_4 & 0 \end{bmatrix} \quad (\text{A.19})$$

If the cross section dimensions are small, then the terms involving y and z in Equation (A.19) can be neglected. Thus, the shape function matrix simplifies to Equation (A.4).

APPENDIX B

INERTIA PROPERTIES OF SPATIAL ROBOT

In this section, the inertia properties of the beam element used for the spatial robot can be obtained as

$$\int_{V_{ki}} \rho_{ki} \phi^{ki} dV = m_{ki} \begin{bmatrix} \frac{1}{2} & 0 & 0 & 0 & 0 & 0 & \frac{1}{2} & 0 & 0 & 0 & 0 & 0 \\ 0 & \frac{1}{2} & 0 & 0 & 0 & \frac{1}{12} L_{ki} & 0 & \frac{1}{2} & 0 & 0 & 0 & -\frac{1}{12} L_{ki} \\ 0 & 0 & \frac{1}{2} & 0 & -\frac{1}{12} L_{ki} & 0 & 0 & 0 & \frac{1}{2} & 0 & \frac{1}{12} L_{ki} & 0 \end{bmatrix} \quad (\text{B.1})$$

$$\int_{V_{ki}} \rho_{ki} X^{ki} \phi^{ki} dV = m_{ki} \begin{bmatrix} \frac{1}{6} L_{ki} & 0 & 0 & 0 & 0 & 0 & \frac{1}{3} L_{ki} & 0 & 0 & 0 & 0 & 0 \\ 0 & \frac{3}{20} L_{ki} & 0 & 0 & 0 & \frac{1}{30} L_{ki}^2 & 0 & \frac{7}{20} L_{ki} & 0 & 0 & 0 & -\frac{1}{20} L_{ki}^2 \\ 0 & 0 & \frac{3}{20} L_{ki} & 0 & -\frac{1}{30} L_{ki}^2 & 0 & 0 & 0 & \frac{7}{20} L_{ki} & 0 & \frac{1}{20} L_{ki}^2 & 0 \end{bmatrix} \quad (\text{B.2})$$

$$\int_{V_{ki}} \rho_{ki} \phi_1^{kiT} \phi_2^{ki} dV = m_{ki} \begin{bmatrix} 0 & 0 & 0 & 0 & 0 & 0 & 0 & 0 & 0 & 0 & 0 \\ \frac{7}{20} & 0 & 0 & 0 & 0 & 0 & \frac{3}{20} & 0 & 0 & 0 & 0 \\ 0 & 0 & 0 & 0 & 0 & 0 & 0 & 0 & 0 & 0 & 0 \\ 0 & 0 & 0 & 0 & 0 & 0 & 0 & 0 & 0 & 0 & 0 \\ 0 & 0 & 0 & 0 & 0 & 0 & 0 & 0 & 0 & 0 & 0 \\ \frac{1}{20} L_{ki} & 0 & 0 & 0 & 0 & 0 & \frac{1}{30} L_{ki} & 0 & 0 & 0 & 0 \\ 0 & 0 & 0 & 0 & 0 & 0 & 0 & 0 & 0 & 0 & 0 \\ \frac{3}{20} & 0 & 0 & 0 & 0 & 0 & \frac{7}{20} & 0 & 0 & 0 & 0 \\ 0 & 0 & 0 & 0 & 0 & 0 & 0 & 0 & 0 & 0 & 0 \\ 0 & 0 & 0 & 0 & 0 & 0 & 0 & 0 & 0 & 0 & 0 \\ 0 & 0 & 0 & 0 & 0 & 0 & 0 & 0 & 0 & 0 & 0 \\ -\frac{1}{30} L_{ki} & 0 & 0 & 0 & 0 & 0 & -\frac{1}{20} L_{ki} & 0 & 0 & 0 & 0 \end{bmatrix} \quad (\text{B.4})$$

$$\int_{V_{ki}} \rho_{ki} \phi_1^{kiT} \phi_3^{ki} dV = m_{ki} \begin{bmatrix} 0 & 0 & 0 & 0 & 0 & 0 & 0 & 0 & 0 & 0 & 0 & 0 \\ 0 & 0 & 0 & 0 & 0 & 0 & 0 & 0 & 0 & 0 & 0 & 0 \\ \frac{7}{20} & 0 & 0 & 0 & 0 & 0 & \frac{3}{20} & 0 & 0 & 0 & 0 & 0 \\ 0 & 0 & 0 & 0 & 0 & 0 & 0 & 0 & 0 & 0 & 0 & 0 \\ -\frac{1}{20}L_{ki} & 0 & 0 & 0 & 0 & 0 & -\frac{1}{30}L_{ki} & 0 & 0 & 0 & 0 & 0 \\ 0 & 0 & 0 & 0 & 0 & 0 & 0 & 0 & 0 & 0 & 0 & 0 \\ 0 & 0 & 0 & 0 & 0 & 0 & 0 & 0 & 0 & 0 & 0 & 0 \\ \frac{3}{20} & 0 & 0 & 0 & 0 & 0 & \frac{7}{20} & 0 & 0 & 0 & 0 & 0 \\ 0 & 0 & 0 & 0 & 0 & 0 & 0 & 0 & 0 & 0 & 0 & 0 \\ \frac{1}{30}L_{ki} & 0 & 0 & 0 & 0 & 0 & \frac{1}{20}L_{ki} & 0 & 0 & 0 & 0 & 0 \\ 0 & 0 & 0 & 0 & 0 & 0 & 0 & 0 & 0 & 0 & 0 & 0 \end{bmatrix} \quad (\text{B.5})$$

$$\int_{V_{ki}} \rho_{ki} \phi_2^{kiT} \phi_2^{ki} dV = m_{ki} \begin{bmatrix} 0 \\ 0 & \frac{13}{35} \\ 0 & 0 & 0 \\ 0 & 0 & 0 & 0 & \text{sym} \\ 0 & 0 & 0 & 0 & 0 \\ 0 & \frac{11}{210} L_{ki} & 0 & 0 & 0 & \frac{1}{105} L_{ki}^2 \\ 0 & 0 & 0 & 0 & 0 & 0 \\ 0 & \frac{9}{70} & 0 & 0 & 0 & \frac{13}{420} L_{ki} & 0 & \frac{13}{35} \\ 0 & 0 & 0 & 0 & 0 & 0 & 0 & 0 \\ 0 & 0 & 0 & 0 & 0 & 0 & 0 & 0 & 0 \\ 0 & 0 & 0 & 0 & 0 & 0 & 0 & 0 & 0 \\ 0 & -\frac{13}{420} L_{ki} & 0 & 0 & 0 & -\frac{1}{140} L_{ki}^2 & 0 & -\frac{11}{210} L_{ki} & 0 & 0 & 0 & \frac{1}{105} L_{ki}^2 \end{bmatrix} \quad (\text{B.6})$$

$$\int_{V_{ki}} \rho_{ki} \phi_2^{kiT} \phi_3^{ki} dV = m_{ki} \begin{bmatrix} 0 & 0 & 0 & 0 & 0 & 0 & 0 & 0 & 0 & 0 \\ 0 & 0 & 0 & 0 & 0 & 0 & 0 & 0 & 0 & 0 \\ 0 & \frac{13}{35} & 0 & 0 & \frac{11}{210} L_{ki} & 0 & \frac{7}{9} & 0 & 0 & -\frac{13}{420} L_{ki} \\ 0 & 0 & 0 & 0 & 0 & 0 & 0 & 0 & 0 & 0 \\ 0 & -\frac{11}{210} L_{ki} & 0 & 0 & -\frac{1}{105} L_{ki}^2 & 0 & -\frac{13}{420} L_{ki} & 0 & 0 & \frac{1}{140} L_{ki}^2 \\ 0 & 0 & 0 & 0 & 0 & 0 & 0 & 0 & 0 & 0 \\ 0 & 0 & 0 & 0 & 0 & 0 & 0 & 0 & 0 & 0 \\ 0 & \frac{9}{70} & 0 & 0 & \frac{13}{420} L_{ki} & 0 & \frac{13}{35} & 0 & 0 & -\frac{11}{210} L_{ki} \\ 0 & 0 & 0 & 0 & 0 & 0 & 0 & 0 & 0 & 0 \\ 0 & \frac{13}{420} L_{ki} & 0 & 0 & \frac{1}{140} L_{ki}^2 & 0 & \frac{11}{210} L_{ki} & 0 & 0 & -\frac{1}{105} L_{ki}^2 \\ 0 & 0 & 0 & 0 & 0 & 0 & 0 & 0 & 0 & 0 \end{bmatrix} \quad (\text{B.7})$$

$$\int_{V_{ki}} \rho_{ki} \phi_3^{kiT} \phi_3^{ki} dV = \mathbf{m}_{ki} \begin{bmatrix} 0 \\ 0 & 0 \\ 0 & 0 & \frac{13}{35} \\ 0 & 0 & 0 & 0 & \text{sym} \\ 0 & 0 & -\frac{11}{210} L_{ki} & 0 & \frac{1}{105} L_{ki}^2 \\ 0 & 0 & 0 & 0 & 0 & 0 \\ 0 & 0 & 0 & 0 & 0 & 0 & 0 \\ 0 & 0 & \frac{9}{70} & 0 & -\frac{13}{420} L_{ki} & 0 & 0 & 0 & \frac{13}{35} \\ 0 & 0 & 0 & 0 & 0 & 0 & 0 & 0 & 0 \\ 0 & 0 & \frac{13}{420} L_{ki} & 0 & -\frac{1}{140} L_{ki}^2 & 0 & 0 & 0 & \frac{11}{210} L_{ki} & 0 & \frac{1}{105} L_{ki}^2 \\ 0 & 0 & 0 & 0 & 0 & 0 & 0 & 0 & 0 & 0 & 0 \end{bmatrix} \quad (\text{B.8})$$

(B.10)

where L_{ki} is the length of element i of Body k , A_{ki} is the cross sectional area of element i of Body k , E_{ki} is the modulus of elasticity of element i of Body k , G_{ki} is the shear modulus of elasticity of Body k , I_{22}^{ki} is the second moment of area of element i of Body k about \mathbf{n}_2^{ki} axis, I_{33}^{ki} is the second moment of area of element i of Body k about \mathbf{n}_3^{ki} axis, J^{ki} is the area polar moment of inertia of element i of Body k .

APPENDIX C

INERTIA PROPERTIES OF PLANAR ROBOT

The necessary inertia properties for obtaining the dynamics of the planar robot can be obtained as

$$\mathbf{K}^{(2)} = \frac{\mathbf{E}^{(2)}\mathbf{I}_3^{(2)}}{L_2^3} \begin{bmatrix} 114.0579 & -1.5759 \\ -1.5759 & 1.4490 \times 10^6 \end{bmatrix} \quad (\text{C.1})$$

$$\int_{V_1} \rho_1 \bar{\mathbf{r}}^{(1)T} dV = \begin{bmatrix} \frac{m_1 L_1}{2} & 0 \end{bmatrix} \quad (\text{C.2})$$

where m_1 is the mass of Body 1

$$\int_{V_1} \rho_2 \bar{\mathbf{r}}^{(2)T} dV = \begin{bmatrix} \frac{m_2 L_2}{2} & 0 \end{bmatrix} \quad (\text{C.3})$$

where m_2 is the mass of Body 2

$$\int_{V_2} \rho_2 \boldsymbol{\phi}^{(2)} dV = m_2 \begin{bmatrix} 0 & 0 \\ -2.3783 & -23.7069 \end{bmatrix} \quad (\text{C.4})$$

$$\int_{V_1} \rho_2 \bar{\mathbf{r}}^{(1)T} \bar{\mathbf{r}}^{(1)} dV = \frac{1}{3} m_1 L_1^2 \quad (\text{C.5})$$

$$\int_{V_1} \rho_2 \bar{\mathbf{r}}^{(2)T} \bar{\mathbf{r}}^{(2)} dV = \frac{1}{3} m_2 L_2^2 \quad (\text{C.6})$$

$$\int_{V_2} \rho_2 \bar{\mathbf{r}}^{(2)T} \boldsymbol{\phi}^{(2)} dV = [0 \quad 0] \quad (\text{C.7})$$

$$\int_{V_2} \rho_2 \boldsymbol{\phi}^{(2)T} \boldsymbol{\phi}^{(2)} dV = m_2 \begin{bmatrix} 9.2262 & 4.6486 \times 10^{-4} \\ 4.6486 \times 10^{-4} & 2.9845 \times 10^3 \end{bmatrix} \quad (\text{C.8})$$

$$\int_{V_2} \rho_2 \bar{\mathbf{r}}^{(2)T} \tilde{\mathbf{I}} \boldsymbol{\phi}^{(2)} dV = m_2 L_2 [-1.7872 \quad -4.9593] \quad (\text{C.9})$$

where $\tilde{\mathbf{I}}$ is given as

$$\tilde{\mathbf{I}} = \begin{bmatrix} 0 & 1 \\ -1 & 0 \end{bmatrix} \quad (\text{C.10})$$

$$\int_{V_2} \rho_2 \boldsymbol{\phi}^{(2)T} \tilde{\mathbf{I}} \boldsymbol{\phi}^{(2)} dV = \begin{bmatrix} 0 & 0 \\ 0 & 0 \end{bmatrix} \quad (\text{C.11})$$

$$\int_{V_1} \rho_2 \bar{\mathbf{r}}^{(1)T} \tilde{\mathbf{I}} \bar{\mathbf{r}}^{(1)} dV = 0 \quad (\text{C.12})$$

$$\int_{V_1} \rho_2 \bar{\mathbf{r}}^{(2)T} \tilde{\mathbf{I}} \bar{\mathbf{r}}^{(2)} dV = 0 \quad (\text{C.13})$$

CURRICULUM VITAE

Sinan Kilicaslan was born in Istanbul, Turkey. He received his BSc degree in Mechanical Engineering from Gazi University. He received the MSc and PhD degrees in Mechanical Engineering from Middle East Technical University. He has been working as an assistant in Mechanical Engineering Department of Gazi University. His research interests include dynamics and control of rigid and structurally flexible robotic systems.